

**DISCOVERY AND DEVELOPMENT OF ANTI-INFECTIVES
WITH NOVEL MODES OF ACTION FOR THE TREATMENT
OF RESPIRATORY TRACT INFECTIONS**

DISSERTATION

zur Erlangung des Grades
des Doktors der Naturwissenschaften
der Naturwissenschaftlich-Technischen Fakultät
der Universität des Saarlandes

von

Apotheker & Dipl.-Pharm. Andreas Thomann

Saarbrücken

2016

Tag des Kolloquiums: 17.02.2017

Dekan: Prof. Dr. Guido Kickelbick

Berichterstatter: Prof. Dr. Rolf W. Hartmann
Prof. Dr. Dr. h. c. Hans H. Maurer

Vorsitz: Prof. Dr. Alexandra K. Kiemer

Akad. Mitarbeiter: Dr. Josef Zapp

Die vorliegende Arbeit wurde von Januar 2012 bis Dezember 2015 unter Anleitung von Herrn Univ.-Prof. Dr. Rolf W. Hartmann in der Fachrichtung 8.2 Pharmazeutische und Medizinische Chemie der Naturwissenschaftlich-Technischen Fakultät III der Universität des Saarlandes sowie am Helmholtz-Institut für Pharmazeutische Forschung Saarland (HIPS) in der Abteilung Drug Design and Optimization (DDOP) angefertigt.

“Je suis de ceux qui pensent que la science est d’une grande beauté. Un scientifique dans son laboratoire est non seulement un technicien: il est aussi un enfant placé devant des phénomènes naturels qui l’impressionnent comme des contes de fées.”

Marie Curie (1867 - 1934)

Abstract

Function of the lung is a prerequisite for human survival. Infection of the lung is therefore a life-threatening illness. Treatment is constantly losing its effectivity due to resistance development. Moreover, pathogens developed mechanisms to evade the immune response, e.g. biofilms. Hence, developing new antibiotic drugs with novel targets, restoring activity of old drugs or blocking pathogenicity is highly necessary. These concepts are the basis of this work focused on *Pseudomonas aeruginosa* (PA) and *Mycobacterium tuberculosis* (Mtb) both causing severe pulmonary infections.

The quorum sensing system of PA is a highly sophisticated network using small molecules for group coordinated release of virulence factors, biofilm formation and persistence. A key sensor is the Pseudomonas Quinolone Signal (PQS). Blocking the downstream effects of PQS can be achieved by interference with its receptor (PqsR) or synthases (e.g. PqsD). Targeting PqsR and PqsD is a promising goal to lower pathogenicity, restore antibiotic activity and - immune response while reducing risks for resistance.

Infections by extreme drug resistant Mtb are on the rise making discovery of novel anti-mycobacterial agents inevitable. Novel potential targets are cytochrome-P-450 enzymes. CYP125 & CYP121 are two representatives of which the first is essential during host infection and the latter for bacterial survival. Hence development of inhibitors for these enzymes is a promising strategy to fill the antibiotic gap.

Zusammenfassung

Die Funktion der Lunge ist essentiell für unser Überleben. Daher sind Infektionen lebensbedrohlich. Zusätzlich verlieren Antibiotika aufgrund steigender Resistenzentwicklungen ihre Wirkung. Weiterhin haben Pathogene Schutzmechanismen z.B. Biofilme entwickelt um dem Immunsystem zu entkommen. Daher ist die Entwicklung neuer-/ Reaktivierung alter Antibiotika oder Blockade der Pathogenität äußerst wichtig. Dies ist die Basis dieser Arbeit, welche sich auf die Bekämpfung der Keime *Pseudomonas aeruginosa* (PA) und *Mycobacterium tuberculosis* (Mtb) fokussiert.

Das Quorum Sensing System von PA nutzt kleine Moleküle als Regulatoren von Virulenz Faktoren, Biofilmen und der Persistenz. Ein Molekül ist das Pseudomonas Quinolone Signal (PQS). Die Blockierung der Effekte von PQS kann einerseits durch Blockade des Rezeptor PqsR oder durch Hemmung der Synthesen (z.B. PqsD) erfolgen. Interferenz mit PqsR und PqsD ist ein vielversprechender Ansatz die Pathogenität von PA zu verringern & die Wirksamkeit von Antibiotika und Immunzellen wiederherzustellen, bei verringertem Resistenzrisiko.

Infektionen mit resistenten Mtb steigen stetig, was eine Entwicklung neuer Antibiotika unumgänglich macht. Die Inhibierung der essentiellen Cytochrom-P450 Enzyme 125 & 121 ist ein neues Konzept um Mtb zu bekämpfen. Daher ist die Entwicklung von Hemmstoffen dieser CYP Enzyme eine vielversprechende Strategie die Antibiotika-Lücke zu füllen.

Publications & chapters included in this thesis

The results part of this thesis is divided into eight chapters, which are referred to in the text by their roman numerals (I-VIII). Seven have already been published in seven articles (I-V, VII, VIII), the work described in chapter 3.5 (V) and 3.7 (VII) has been accepted for publication recently.

I. Microwave-Assisted Synthesis of 4-Substituted 2-Methylthiopyrimidines
Andreas Thomann, Carsten Börger, Martin Empting, and Rolf W. Hartmann, *Synlett*, **2014**, *25*, 935 – 938.

II. Steering the Azido-Tetrazole Equilibrium of 4-Azidopyrimidines via Substituent Variation – Implications for Drug Design and Azide-Alkyne Cycloadditions
Andreas Thomann, Josef Zapp, Michael Hutter, Martin Empting, and Rolf W. Hartmann, *Organic & Biomolecular Chemistry* **2015**, *13*, 10620-10630.

III. Mild and Catalyst-free Microwave-assisted Synthesis of 4,6-Disubstituted 2-Methylthiopyrimidines – Exploiting Tetrazole as an Efficient Leaving Group
Andreas Thomann, Jens Eberhard, Giuseppe Allegretta, Martin Empting, and Rolf W. Hartmann, *Synlett* **2015**, *26*, 2606 – 2610.

IV. Application of Dual Inhibition Concept Within Looped Autoregulatory Systems Towards Anti-virulence Agents Against *Pseudomonas aeruginosa* Infections

Andreas Thomann^Δ, Antonio G. G. de M. Martins^Δ, Christian Brengel, Martin Empting, and Rolf W. Hartmann, *ACS Chemical Biology* **2016**, *11*, 1279–1286

^ΔThese authors have equally contributed to this work

V. Structure-activity Relationships of 2-Sufonylpyrimidines as Quorum Sensing Inhibitors to Tackle Biofilm Formation and eDNA Release of *Pseudomonas aeruginosa*

Andreas Thomann, Christian Brengel, Carsten Börger, Dagmar Kail, Anke Steinbach, Martin Empting and Rolf W. Hartmann, *ChemMedChem*, published online: 12.10.2016 , DOI: 10.1002/cmdc.201600419

VI. Biophysical Screening of a Focused Library for the Discovery of Novel Anti-mycobacterials Targeting CYP121

Chapter VI

VII. Discovery and Biophysical Evaluation of First Low Nanomolar Hits Targeting CYP125 of *M. tuberculosis*

Christian Brengel^Δ, Andreas Thomann^Δ, Jens Eberhard, Alexander Schifrin, and Rolf W. Hartmann, *ChemMedChem*, published online: 28.09.2016, DOI: 10.1002/cmdc.201600361

^ΔThese authors contributed equally to this work.

VIII. Crystal structure of 4-methylsulfanyl-2-(2*H*-tetrazol-2-yl)pyrimidine

Andreas Thomann, Volker Huch and Rolf W. Hartmann, *Acta Crystallographica*; **2015**; E71, o1051 – o1052.

Contribution report

The author wishes to clarify his contributions to the published work included in this thesis.

- I. The author developed the synthetic method, synthesized and characterized all compounds. He conceptualized and wrote the paper.
- II. The author developed the synthetic method, designed, synthesized, and characterized all compounds. Furthermore, he conducted all kinetic experiments and interpreted the results. He performed the *in silico* studies and was responsible for the biological assays. He conceptualized and wrote the paper.
- III. The author developed the synthetic method, synthesized, and characterized all compounds. He conceptualized and wrote the paper.
- IV. The author developed the synthetic method, designed, synthesized, and characterized all compounds. Furthermore, he interpreted the biological results and was responsible for the biological enzyme and receptor assays, as well as the pyocyanin experiments for his compound class. He conceptualized and wrote the paper.
- V. The author developed the synthetic method, designed, synthesized and characterized most of the compounds. He was responsible for the PqsR, PqsD and pyocyanin *in vitro* assays and interpreted the results. He determined the Hansch equations and calculated the Ligand efficiency indices. He performed the flexible alignments. He conceptualized and wrote the manuscript.
- VII. The author conceptualized the project and identified the target from literature. He expressed and purified the CYP125, Arh and etp proteins for biological

Contribution report

testing. He assisted in the SPR screening and performed the UV/VIS Heme assay. He wrote the manuscript.

- VIII.** The author synthesized, characterized the compound and developed the crystallization conditions. He crystallized the compound for X-ray crystallography. Furthermore, he conceptualized and wrote the paper.

Abbreviations

°C	Degree Celsius
μL	Microliter
μM	Micromolar
2-ABA	2-Aminobenzoylacetate
2-ABACoA	2-Aminobenzoylacetatyl coenzyme A
3D	Three-dimensional
Å	Angstrom
AA	Anthranilic acid
ACoA	Anthranoyl coenzyme A
AIDS	Acquired Immunodeficiency Syndrome
BCG	<i>Mycobacterium bovis Bacillus Calmette-Guérin</i>
BHL	<i>N</i> -Butanoyl-L-homoserine lactone
Brine chloride	Saturated aqueous solution of sodium
CDCl ₃	Deuterated chloroform
cLogD _{7.4}	Calculated octanol-water coefficient at pH 7.4
cLogP	Calculated octanol-water coefficient
cm ⁻¹	Wavenumber
CoA	Coenzyme A
CoMFA	Comperative Molecular Field Analysis
COPD	Chronic Obstructive Pulmonary Disease
COSY	COrelated Spectroscopy
Cryo-EM	Cryo-electron microscopy
CYP	Cytochrome P450
cYY	<i>cyclo</i> -di- _L -tyrosine

Abbreviations

d	Doublet
dd	Doublet of doublets
ddd	Doublet of doublet of doublets
DCM	Dichloromethane
DHQ	2,4-Dihydroxyquinolone
DMF	<i>N,N</i> -Dimethylformamid
DMSO	Dimethylsulfoxide
dt	Doublet of triplets
<i>E. coli</i>	<i>Escherichia coli</i>
EDG	Electron-donating group
eDNA	Extracellular DNA
EE	Ethylacetate
eq	Equivalents
ESI	Electrospray ionization
EWG	Electron-withdrawing group
FBDD	Fragment-based Drug Discovery
FDA	Food and Drug Administration
FT-IR	Fourier-Transform Infrared spectroscopy
g	Gramm
HE	Hexane
HEK	Human Embryonic Kidney 293 cells
HHQ	2-Heptyl-4-HydroxyQuinolone
HMQC	Heteronuclear Multiple-Quantum Correlation
hrs	Hours
HSQC	Heteronuclear Single Quantum Coherence
Hz	Hertz
IC ₅₀	Drug concentration required for 50% inhibition

Abbreviations

IQS	Integrated Quorum Sensing Signal
J	Coupling constant
K_D	Dissociation constant
L	Liter
LC-MS	High pressure liquid chromatography mass spectrometry
LE	Ligand Efficiency
LLE	Ligand Lipophilicity Efficiency
M	Molar (mol/L)
MDR	Multi drug resistant
mg	Milligram
MIC ₅₀	Concentration at 50% growth inhibition
MIC ₉₀	Concentration at 90% growth inhibition
min	Minutes
mL	Milliliter
mp	Melting point
MS	Mass spectrometry
Mtb	<i>Mycobacterium tuberculosis</i>
MW	Molecular Weight
nM	Nanomolar
NMR	Nuclear Magnetic Resonance
OD ₆₀₀	Optical density at $\lambda= 600$ nm
OdDHL	<i>N</i> -(3-oxododecanoyl)-L-homoserine lactone
PA	<i>Pseudomonas aeruginosa</i>
PE	Petrolether
ppm	Parts per million
PQS	<i>Pseudomonas</i> Quinolone Signal
q	Quartet

Abbreviations

QS	Quorum Sensing
QSAR	Quantitative Structure Activity Relationship
quin	Quintet
r.t.	Room Temperature
rpm	Rounds per minute
s	Singulet
<i>S. aureus</i>	<i>Staphylococcus aureus</i>
SAR	Structure Activity Relationship
SDG	Sterically Demanding Group
SPR	Surface Plasmon Resonance
t	Triplet
td	Triplet of doublets
UV-VIS	Ultraviolet-Visible Light
WHO	World Health Organization
XDR	Extensively Drug Resistant
δ	Chemical shift

Table of contents

1	Introduction	1
1.1	Bacterial infections and resistance development	1
1.2	Rational strategies in drug discovery	2
1.2.1	Ligand-based design	2
1.2.2	Structure-based design.....	4
1.3	<i>Pseudomonas aeruginosa</i>	6
1.4	Quorum Sensing in <i>Pseudomonas aeruginosa</i> – A novel drug-target	6
1.5	Targeting PqsD and PqsR to block pathogenicity of <i>Pseudomonas aeruginosa</i>	8
1.6	Chemical synthesis of substituted pyrimidines.....	11
1.7	<i>Mycobacterium tuberculosis</i>	12
1.8	The cytochrome P450 family – enzymatic reaction and types of inhibition	13
1.9	CYP121 and CYP125 as anti-mycobacterial drug-targets	15
2	Aims of the thesis	19
3	Results.....	21
3.1	Microwave-Assisted Synthesis of 4-Substituted 2-Methylthiopyrimidines	21
3.2	Steering the Azido-Tetrazole Equilibrium of 4-Azidopyrimidines via Substituent Variation – Implications for Drug Design and Azide-Alkyne Cycloadditions.....	26
3.3	Mild and Catalyst-free Microwave-assisted Synthesis of 4,6-Disubstituted 2-Methylthiopyrimidines – Exploiting Tetrazole as an Efficient Leaving Group	38
3.4	Application of Dual Inhibition Concept Within Looped Autoregulatory Systems Towards Anti-virulence Agents Against <i>Pseudomonas aeruginosa</i>	44
3.5	Structure-activity Relationships 2-Sulfonylpyrimidines as Quorum sensing inhibitors to Tackle Biofilm Formation and eDNA Release of <i>Pseudomonas aeruginosa</i>	54
3.6	Biophysical Screening of a Focused Library for the Discovery of Novel Anti-mycobacterials Targeting CYP121.....	67

Table of contents

3.7	Discovery and Biophysical Evaluation of First Low Nanomolar Hits Targeting CYP125 of <i>M. tuberculosis</i>	87
3.8	Crystal structure of 4-methylsulfanyl-2-(2 <i>H</i> -tetrazol-2-yl)pyrimidine.....	95
4	Concluding discussion and perspectives	98
4.1	Novel synthetic methods to access substituted pyrimidines	98
4.2	Two approaches - one goal: fighting treatment-resistant bacterial infections of the respiratory tract.....	101
4.2.1	Addressing PqsD and PqsR to reduce pathogenicity of <i>Pseudomonas aeruginosa</i>	101
4.2.2	The cytochrome P450 enzymes 121 and 125 as novel drug targets for the treatment of mycobacterial infections	107
5	References.....	108
6	Supporting information	112
6.1	Supporting information for Publication I	112
6.2	Supporting information for Publication II	119
6.3	Supporting information for Publication III	232
6.4	Supporting information for Publication IV.....	248
6.5	Supporting information for Publication V.....	266
6.6	Supporting information for Chapter VI.....	287
6.7	Supporting information for Publication VII.....	322
6.8	Supporting information for Publication VIII.....	331
6.9	Supporting information for Posters.....	338
7	Appendices.....	347
7.1	Curriculum vitae	347
7.2	Conference contributions	348
7.2.1	Oral presentations	348
7.2.2	Poster presentations.....	348
7.4	Publications	350
8	Acknowledgements	352

1 Introduction

1.1 Bacterial infections and resistance development

Bacteria are the oldest life-form on earth and without them no higher organisms could have been evolved. Prime examples of this dependency are humans. Health of e.g. the skin, the gut as well as the immune system highly depends on a balanced multispecies flora of bacteria living in total symbiosis with us. However, besides the positive effects of these microorganisms, there are also other strains that can either cause minor infections or deadly diseases. Till the discovery of these bacteria in 1673 by Leewenhoeck *et al.*^[1] and the concept by Koch^[2] that these microorganisms are the origin of the symptoms of infection, a rational search for medicines to fight these diseases was not possible. Fortunately, in the 1930s the first antibacterial compounds, the sulfonamides, were introduced into the clinic ultimately leading to the cure of the bacterial infection which is, till today, an outstanding characteristic of successful antibiotic treatment. This was the beginning of an era which is today often referred to as “the golden age of antibiotic drug discovery” as many of these compounds with different modes of action were found in between 1940 and 1960 (Figure 1). As a result, these agents were rapidly used throughout the globe to fight bacterial infections. Unfortunately, mankind was not aware of the evolutionary power of bacteria. Only a few years after the approval and clinical usage, resistance began to spread making treatment more and more ineffective (Figure 1, red marks). This is a general trend also observed for antibiotics that were introduced later.

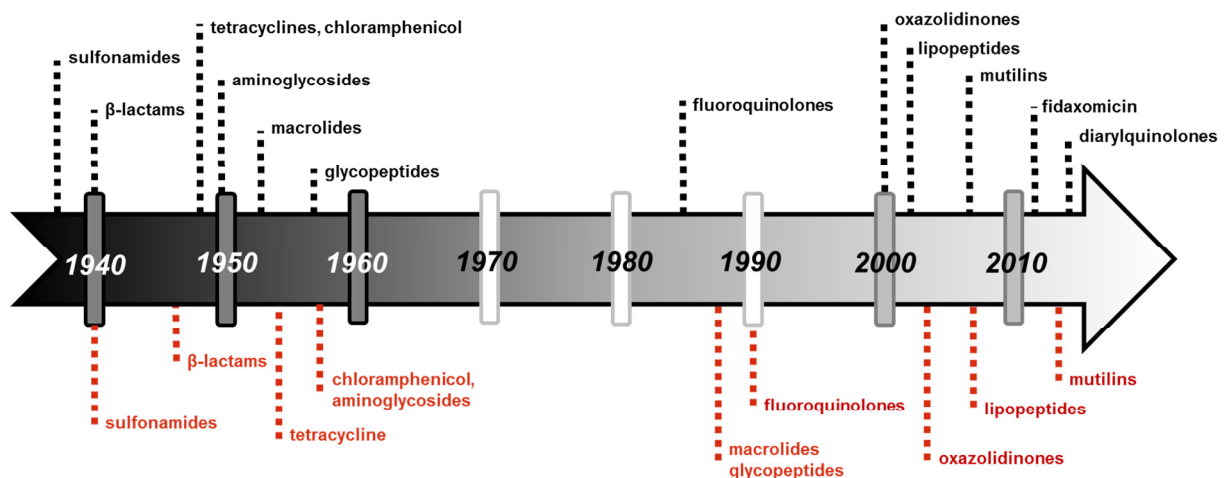


Figure 1. Approval of a collection of antibiotics for human use (black, depicted above the timeline) and first appearance of resistance in the clinic against the respective class (red, below the timeline).^[3]

1 Introduction

Hence, we have to identify novel drug targets and, discover new sites of action to develop new drugs against these pathogens.

1.2 Rational strategies in drug discovery

To understand the meaning of the wording “rational drug design” itself, a look into the dictionary aids to decipher this phrase (from Oxford English Dictionary, Copyright © 2015 Oxford University Press). *Rational*: Based on or derived from reason or reasoning, esp. as opposed to emotion, intuition, instinct, etc. *Drug*: a natural or synthetic substance used in the prevention or treatment of disease, a medicine; (also) a substance that has a physiological effect on a living organism. *Design*: a plan or scheme conceived in the mind and intended for subsequent execution; the preliminary conception of an idea that is to be carried into effect by action; a project. To sum up and combine these definitions, rational drug design is the reasonable approach for the structured development of a medicine. Alternatively, one can also define the process as the development of a small molecule compound interfering with a critical step in a disease-related pathophysiological process represented by a molecular target. In terms of function, this could imply intervening at essential metabolic steps or perturbing of a specific receptor system by stimulation or inhibition. Furthermore, this molecule should be ideally non-toxic and specific for one (or more) target(s) to reduce side-effects.

To rationalize the development of a compound towards a drug, there are basically two major approaches in medicinal chemistry: ligand-based and structure-based design. These two strategies are outlined in the following chapters.

1.2.1 Ligand-based design

This approach is usually applied when there is no structural information about the target available or when the target is unknown. The starting point of the drug optimization process is a compound that can either be a known substrate of the target or a described ligand.^[4] The shape and structure of the target’s pocket defines the position and character of the functional groups of the ligand. The three-dimensional (3D) arrangement of these hot-spots for ligand-target interaction is defined as “pharmacophore”.^[5] An example of a pharmacophore of FDA-approved

fluoroquinolones is given in Figure 2A. The colored spheres represent a common functional group feature shared by the compounds (e.g. red sphere as an anionic feature (F4) placed on the carboxylic acid moiety, Figure 2A). This three-dimensional model can then be used to search for molecules that fit into the latter blueprint. This can be achieved by screening an *in silico* library of millions of compounds leading to the discovery of novel scaffolds for the inhibition of the fluoroquinolone target. By derivatization of a compound class and subsequent study of its *in vitro* and/or *in vivo* effects it is possible to directly connect the observed results to the structure of the molecule. Such a qualitative relationship is referred to as “structure activity relationship”, in short SAR. An example is given in Figure 2B where distinct structural prerequisites for e.g. activity or pharmacokinetic properties are directly related to the residues of the fluoroquinolone core. With such a pattern in hand, medicinal chemists are able to rationally design inhibitors based on experimental knowledge. For quantifying these

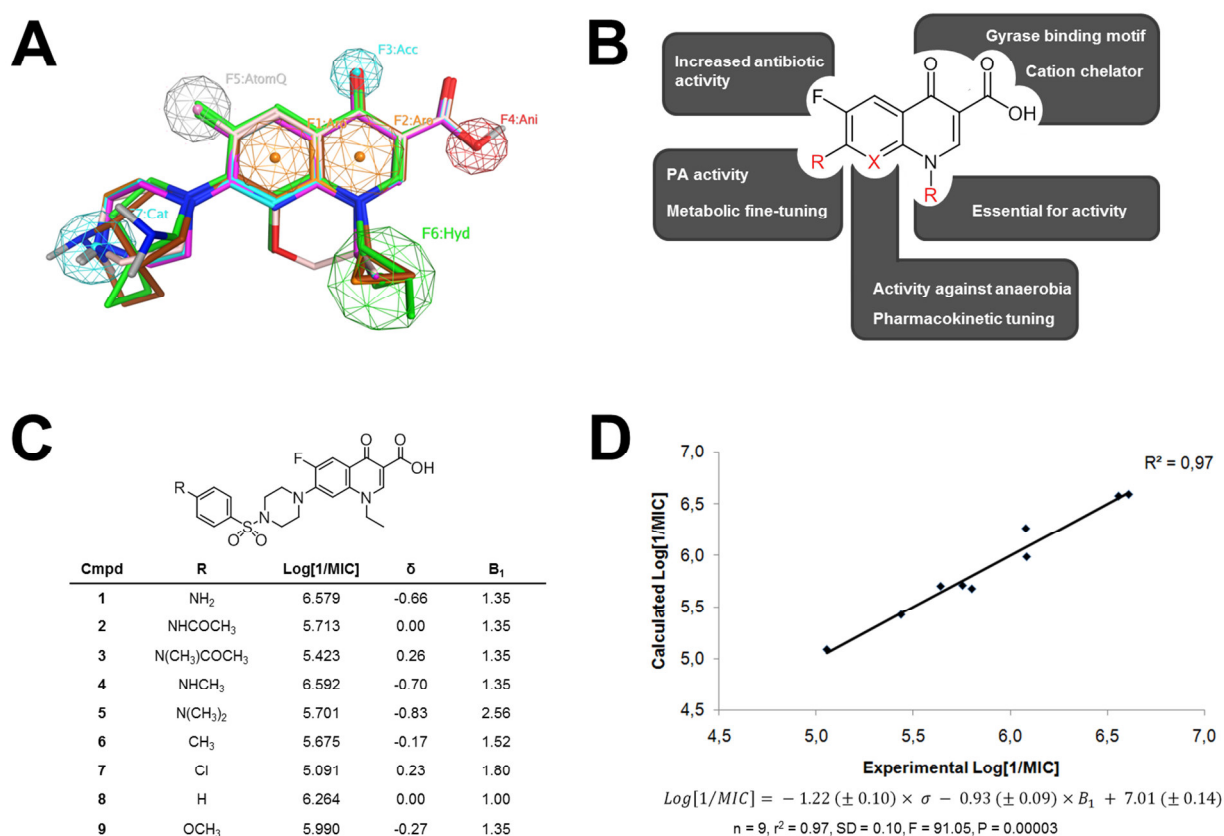


Figure 2. Assembly of different methods for ligand-based design: pharmacophore modelling based on a flexible alignment search of fluoroquinolone derivatives (A),^[6] structure activity relationship (SAR) of *in vivo* properties (B),^[7] quantitative structure activity relationship (QSAR, here Hansch analysis) of a subset of fluoroquinolone derivatives correlating *in vitro* activity with two physicochemical properties: Hammett constant δ and STERIMOL parameter B_1 (C). The correlation of calculated and empirical IC_{50} is striking providing evidence for a quantitative relationship of molecular properties and activity (D).^[8]

1 Introduction

effects and making predictions for novel compounds in terms of biological activity, a “quantitative structure activity relationship” (QSAR) can be set up as mathematical expression. Figure 2C shows such a 2D QSAR model, a so-called Hansch analysis,^[9] where steric as well as electronic properties at the phenyl ring of a substituted fluoroquinolone are correlated with the biological activity expressed as 1/MIC.^[8] Moreover, the calculated IC₅₀ values correlate with the experimentally determined ones very well, underlining the good predictivity of the model (Figure 2D). With the resulting equation, medicinal chemists can estimate, which group is the most reasonable choice to be introduced in order to obtain higher activity. However, besides those classical approaches, more sophisticated 3D QSAR methods have been developed as well, including 3D properties (e.g. conformation) of the compounds. In such a model, every grid point in the 3D matrix around the molecule is represented by physicochemical properties. This approach is referred to as CoMFA and relies on extensive *in silico* calculation times limited by current computer power and consumption for the respective calculations.^[10]

1.2.2 Structure-based design

Making use of 3D protein structures for drug development is, compared to ligand-based approaches, a relatively novel field introduced in the mid 1980s. Already in the beginning of the 1990s, first success stories have been published making use of structural information for drug design.^[11] The first and, today still, the method of choice to is protein crystallography with subsequent X-ray structure elucidation. However in the last decade, novel approaches like NMR and Cryo-EM have evolved accelerating research and elucidation of the new structures. CryoEM has been proven to be exceptionally useful for poorly crystallizable membrane proteins.^[12] Even in case of unknown protein structures, computational methods became available allowing creation of a model of the drug target based on a highly identical or homologous protein with known structure. This method is referred to as homology modelling and was applied to identify and optimize hits into lead structures.^[13] Applying *in silico* methodology for effective drug optimization is not limited to protein homology modeling. It can also be used for binding pose prediction, giving the medicinal chemist the opportunity to examine his ideas for drug development at the site of action. This process is generally described by the term “docking”.^[14] However,

structural information gathered today by X-ray crystallography is, in most cases, still lacking the understanding of movement and conformational changes in protein structures, which can be of crucial interest for protein function and by this means for drug development.^[15] Nevertheless, computational efforts in the field of molecular dynamics simulations have been undertaken to close this gap.^[16] Based on the growing information regarding protein structure and co-crystallized ligands, a novel field has been developed in the past decade to accelerate drug discovery with more efficient molecules by using smaller libraries: the fragment-based design approach. The idea is to use compounds small in size (< 300 Da) to cover a wide range of chemical space with a minimum of compounds (normally between 100-1000 fragments) compared to high-throughput screening methods employing millions of lead-like molecules.^[17] The combination of this approach with X-ray crystallography had a tremendous impact on the field of medicinal chemistry. Having access to the co-crystal structure of ligand and target protein, one can basically follow two different strategies: fragment linking (Figure 3, orange boxes) or fragment growing (Figure 3, grey boxes). For fragment-linking, at least the structures of two fragments in close proximity in the binding pocket have to be elucidated to successfully link them to one structure. This ideally results in a compound that is much more affine because the entropy terms for translational and rotational energy costs for binding to a protein are

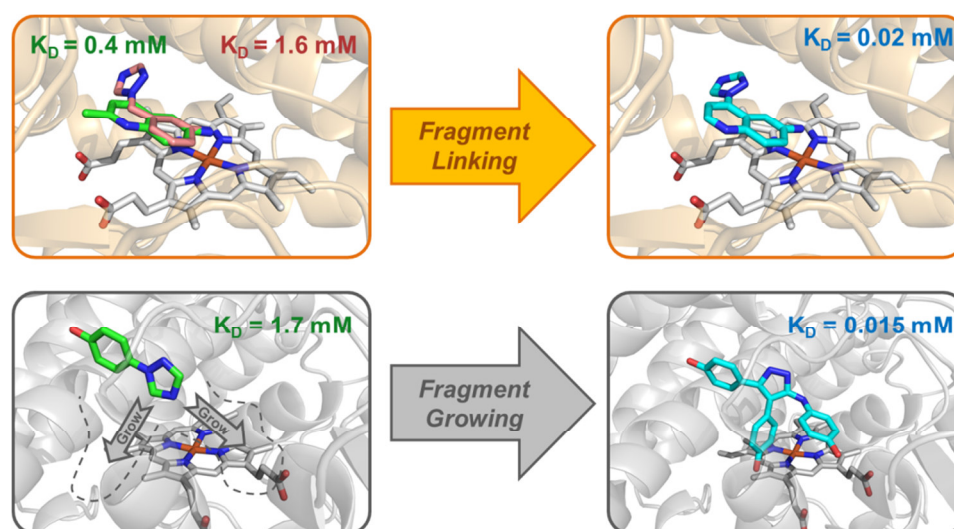


Figure 3. Examples for two strategies in structure-based design for the discovery and optimization of CYP121 inhibitors: fragment linking (upper scheme, orange, PDB-IDs: 4G45 (green structure), 4G44 (red structure), 4G1X (cyan structure)) and fragment growing (lower scheme, gray, PDB-IDs: 4G47 (green structure), 4KTL (cyan structure)). Activity was subsequently increased by rational enlargement of the molecule based on overlapping fragments (upper left structures, green and red molecule) or careful study of the binding-site's properties and spacing for fragment growing (lower left structure, green).^[18,19]

1 Introduction

then only accounted once.^[20] If only one fragment is solved or others are not accessible via linking, the fragment-growing approach can be applied. Therefore, the surrounding pocket has to be carefully studied to generate ideas - usually supported by docking - on how to enlarge the fragment into neighboring cavities to pick up additional interactions with the target. These strategies were successfully applied in generation of more hydrophilic and efficient drugs and have become one standard approach in the past decade.^[21]

1.3 *Pseudomonas aeruginosa*

Pseudomonas aeruginosa (PA) is a rod-shaped, ubiquitous, gram-negative, opportunistic bacterial pathogen that causes severe nosocomial pulmonary infections, especially in immunocompromised patients.^[22] Treatment of diseases in such patients is heavily complicated by PA's ability to shield itself against the human immune system, to inactivate antibiotics, and to remain as a dormant, persisting bacterium with down-regulated metabolism in the lung.^[22,23] In chronic PA infections, lungs drastically lose their functionality, and, finally leading to death of e.g. cystic fibrosis, COPD or AIDS patients.^[24,25] The loss of lung function is connected to PA's ability to form biofilms, a heterogeneous hydrogel which is a barrier for the immune system but also a resistance mechanism against different antibiotics.^[26,27] Besides biofilm-production, PA has an arsenal of numerous virulence factors to harm the epithelium of the lung and, as a result, manifest at the site of infection.^[28-30] Thus, novel therapies to reduce the pathogenicity of PA and to restore the efficiency of antibiotics as well as host defensive mechanisms is of great importance to maintain pulmonary function and by this means, to increase survival of patients.

1.4 Quorum sensing in *Pseudomonas aeruginosa* – A novel drug-target

Quorum sensing (QS) is a cell-density-dependent communication system of bacteria employing small molecule sensors to alter gene expression, coordinate group behavior and regulate phenotypes in the bacterial community.^[31] In PA, four hierarchically organized systems (*las*, *rhl*, *iqs* and *pqs*) which are interconnected and dependent on each other, are the key players of the QS network (Figure 4).^[31] Regarding druggability of QS *per se*, it was shown that QS gene mutations or treatment with QS inhibitors, resulted in strains being heavily impaired in their virulence and pathogenicity *in vitro* and *in vivo*.^[32] As antibiotic resistance is on the

rise (see chapter 1.1) QS inhibition is a promising new concept compared to classic antibiotic treatment because of its non-essentiality for bacterial survival. Consequently, selection pressure should be low.^[33]

The class of *N*-acyl-L-homoserine lactones (BHL and OdDHL) are the chemical signals of the *las* and *rhl* systems which are widespread in Gram-negative bacteria and also found in PA.^[34] However, the Pseudomonas Quinolone Signal (PQS) system and the Integrated Quorum Sensing System (IQS) Signal is to present date, exclusively found in *Pseudomonas* and, in case of the PQS system, also in *Burkholderia* species.^[35] Mutational studies designed to diminish the QS activity in PA confirmed reduction of virulence and pathogenicity *in vivo* together with lower risk to resistance development.^[36] Targeting the pqs-systems has several advantages, as the human beneficial microbiome will be not impaired by a selective approach and if resistance arises it will not be useful for bacteria other than PA *via* horizontal gene transfer

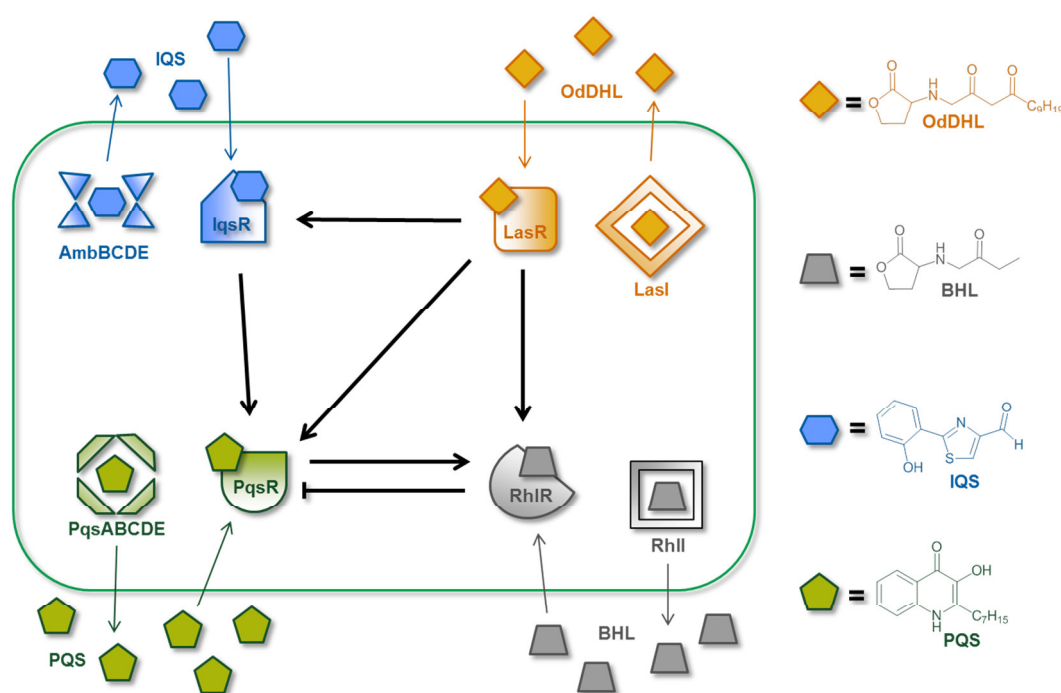


Figure 4. Schematic presentation of the interplay of the four quorum sensing networks in PA, namely *las* (orange), *rhl* (grey), *iqs* (blue) and *pqs* (green), their biosynthetic enzyme(s), signaling molecule structures and corresponding receptors. Arrows indicate activation, blunt-end lines inhibition of the respective system. The *iqs* receptor still remains elusive.^[31]

1 Introduction

1.5 Targeting PqsD and PqsR to block pathogenicity of *Pseudomonas aeruginosa*

Synthesis of the signaling molecules (HHQ and PQS) of the *pqs* system starts with anthranilic acid which is subsequently modified by the synthases of the *pqs* operon, namely *pqsABCDE* (Figure 5). The last oxidation step from HHQ to PQS is catalyzed by PqsH, the only required enzyme outside the PQS operon. In addition to their signaling character, HHQ and PQS have also virulence factor characteristics which is, for example, interfering with NF- κ B function, inhibiting T-cell proliferation, inducing biofilm formation, and increasing HIF-1a degradation.^[39] Additionally, during synthesis of HHQ and PQS two products of the biosynthetic intermediates 2-ABACoA and 2-ABA are spontaneously formed: DHQ and 2-AA. DHQ is known to impair viability of lung epithelial cells and 2-AA for its ability to induce persister cell formation and antibiotic tolerance.^[30,40] Therefore, blocking the production of the signaling molecules HHQ and PQS as well as the two degradation products DHQ and 2-AA is of high interest in order to reduce pathogenicity and virulence of PA. Interfering with the key synthase PqsD being responsible for the synthesis of the intermediate 2-ABACoA, one could accomplish the aforementioned goal.^[37]

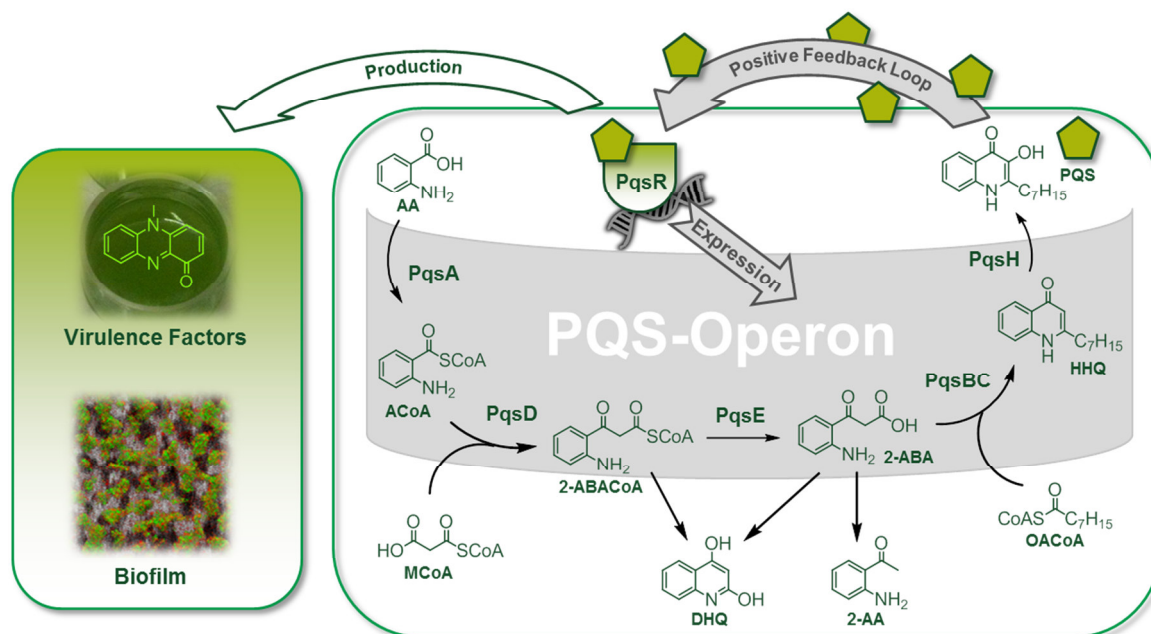


Figure 5. Representation of PQS biosynthesis and the auto-inductive positive feedback loop employing PqsR as the transcriptional regulator of the *pqsABCDE* operon. Activation of PqsR by HHQ and PQS leads to biofilm formation, virulence factor production and PQS biosynthesis. 2-AA = 2-aminoacetophenone, 2-ABA = 2-aminobenzoylacetate, 2-ABACoA = 2-aminobenzoylacyl-CoenzymeA, AA = anthranilic acid, ACoA = anthraniloyl-CoenzymeA, DHQ = 2,4-dihydroxyquinoline, HHQ = 2-heptyl-4(1H)-quinolone, MCoA = malonyl-CoenzymeA, OCoA = octanoyl-CoenzymeA, PQS = Pseudomonas Quinolone Signal.^[37,38]

By blocking PqsD's function none of the latter mentioned signaling and virulence determining molecules should be produced. Thus, a promising strategy is to develop PqsD inhibitors. It has been shown previously that inhibitors designed for this purpose are able to strongly impair signal molecule production and interfere with biofilm formation.^[41–43] Examples for such PqsD inhibitors are depicted in Figure 6 (5 – 8). However, most of them lack favorable physicochemical properties either for oral bioavailability or activity in Gram-negative bacteria.^[44] Thus, compounds addressing PqsD *in cellulo* are of high demand. Besides inhibition of biosynthesis, another strategy to reduce PQS-associated virulence is to antagonize its receptor PqsR, also known as multiple virulence factor regeulator (MvfR).^[45] PqsR was validated *in vivo* by a HHQ related small molecule antagonist **1** as well as *in vitro* by several other compound classes (**2 – 4**, Figure 6). By antagonizing PqsR, it is possible to reduce the production of one of the major virulence factors of PA: pyocyanin (Figure 5, light green structure in upper left corner).^[46,49,51] This redox-active molecule has been shown to be essential for full virulence of PA. In detail, administration of pyocyanin causes a cystic fibrosis-like lung, induces mucin production as well as inflammation, and harms epithelial cells by an increase of reactive oxygen species.^[28,29,54] Additionally, PqsR mutant strains of PA showed impaired production of several other virulence factors and toxins, e.g., hydrogen cyanide, lecA, lecB, and rhamnolipids.^[45] As for the PqsD inhibitors, an antagonism of PqsR also leads to significant reduction of biofilm volume.^[47] Hence, the development of PqsR antagonists is a worthwhile endeavor to reduce pathogenicity of PA. Ideally, a dual inhibition of both PqsR and PqsD might lead to a superior compound acting additively or synergistically on virulence reduction.

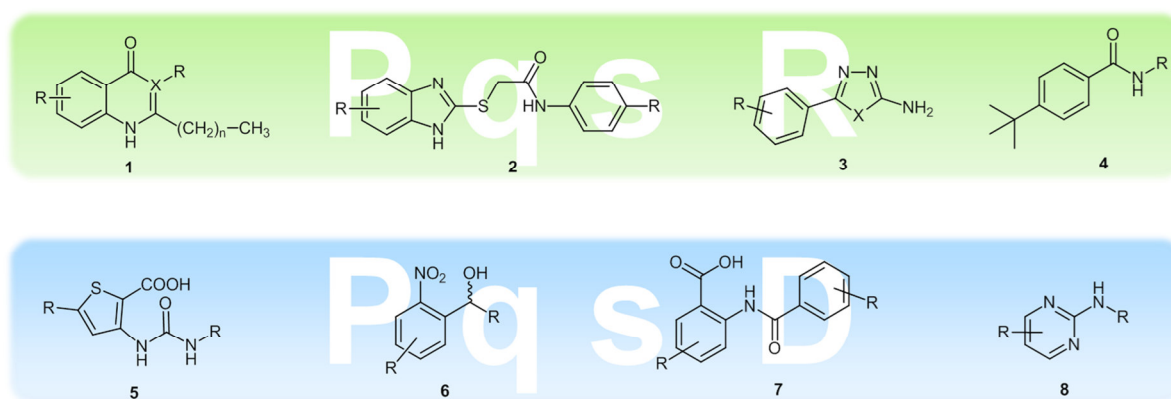


Figure 6. Examples for classes of reported PqsR antagonists (compounds **1-4**, green background) and PqsD inhibitors (compounds **5-8**, blue background).^[41,42,46,47,48,49–53]

1 Introduction

Regarding drug design, both aforementioned drug discovery strategies can be applied to these targets, as the crystal structure of the proteins has been determined and their natural substrates/ligands have been identified (Figure 7).

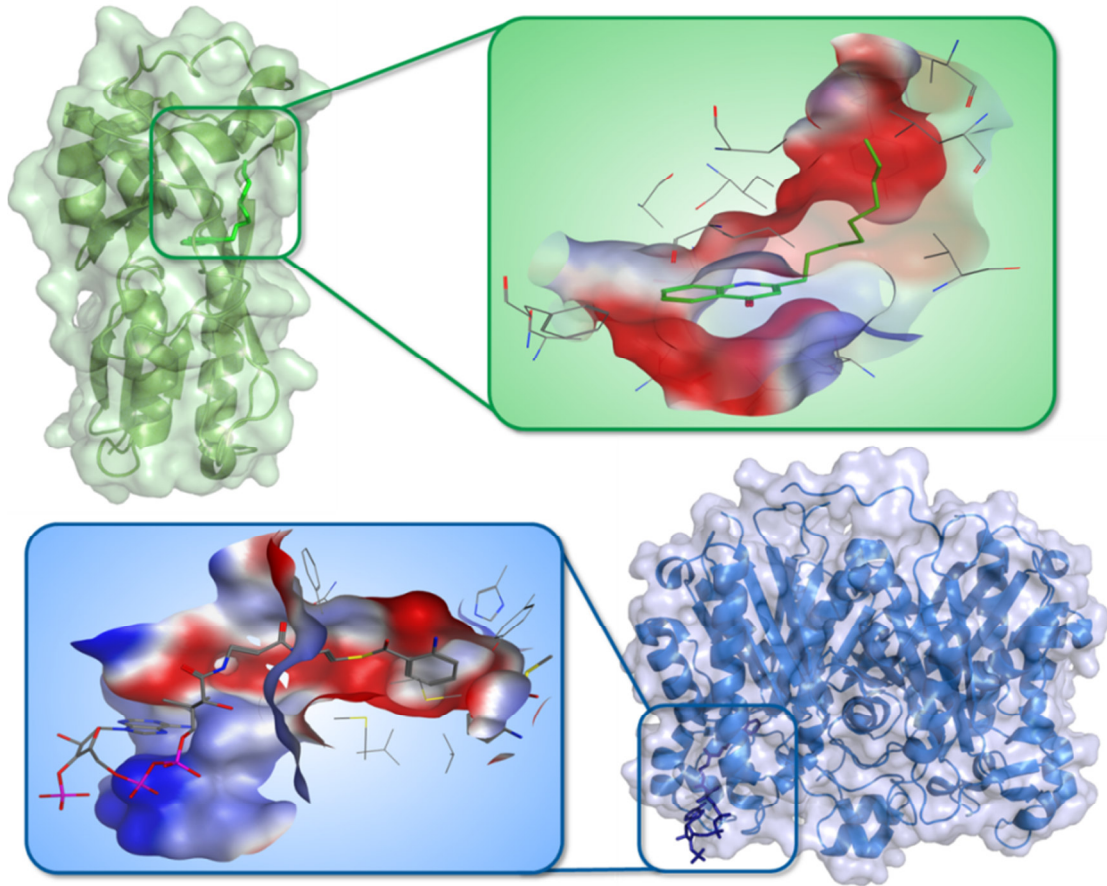


Figure 7. X-ray cocrystalstructures of PqsR's ligand-binding domain with ligand NHQ (green, PDB-ID: 4JVD) and PqsD with its substrate anthraniloyl-CoenzymeA (blue, PDB-ID: 3H77). Binding-site architectures of both proteins are displayed in the colored boxes each. The surfaces of the binding sites were colored with regard to the lipophilicity (red = lipophilic, blue = hydrophilic) of the corresponding amino acids.

1.6 Chemical synthesis of substituted pyrimidines

Substituted pyrimidines are important scaffolds in many bioactive small molecules and, moreover, are present in numerous FDA-approved drugs, e.g., aronixil, buspirone, enazadrem, minoxidil, sulfamethoxydiazine (Figure 8). Additionally, pyrimidine-based compounds have been identified by us to inhibit PqsD (Figure 6, Cmpd 8).^[53] Thus, a chemical synthesis to gain access to this desirable motif is highly interesting for researchers in general and for those working in the field of medicinal chemistry in particular. In small molecule drug discovery, usually, synthetic routes are employed which grant fast access to the structure, are cost efficient, highly robust and ideally allow introduction of a broad range of functional groups or fragments. These requirements are key criteria for in-time library generation in a combinatorial chemistry fashion in order to rapidly acquire SAR information. Hence, the development of methods to accomplish the latter mentioned requirements is an ambitious aim. A general route for the synthesis of substituted pyrimidines often starts from the (poly-)chlorinated pyrimidine as precursor. However, these traditional approaches have several drawbacks, as they can take between several hours and days of reaction time per step and are restricted to sophisticated laboratory equipment and cost-intensive chemicals.

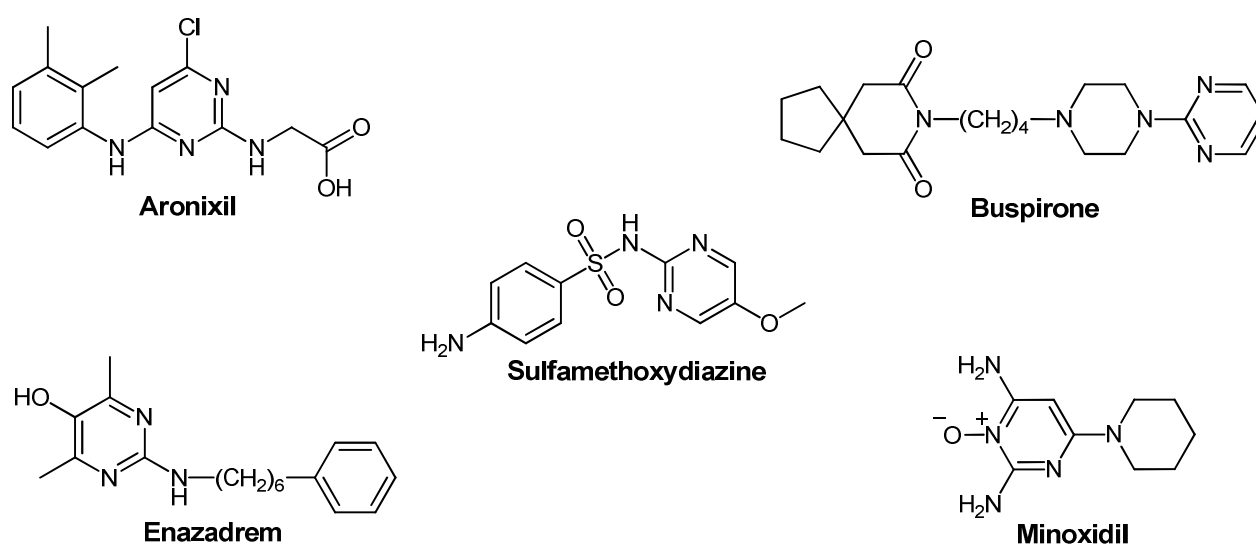


Figure 8. Five examples of pyrimidine-containing FDA-approved drugs for various kinds of diseases.

1 Introduction

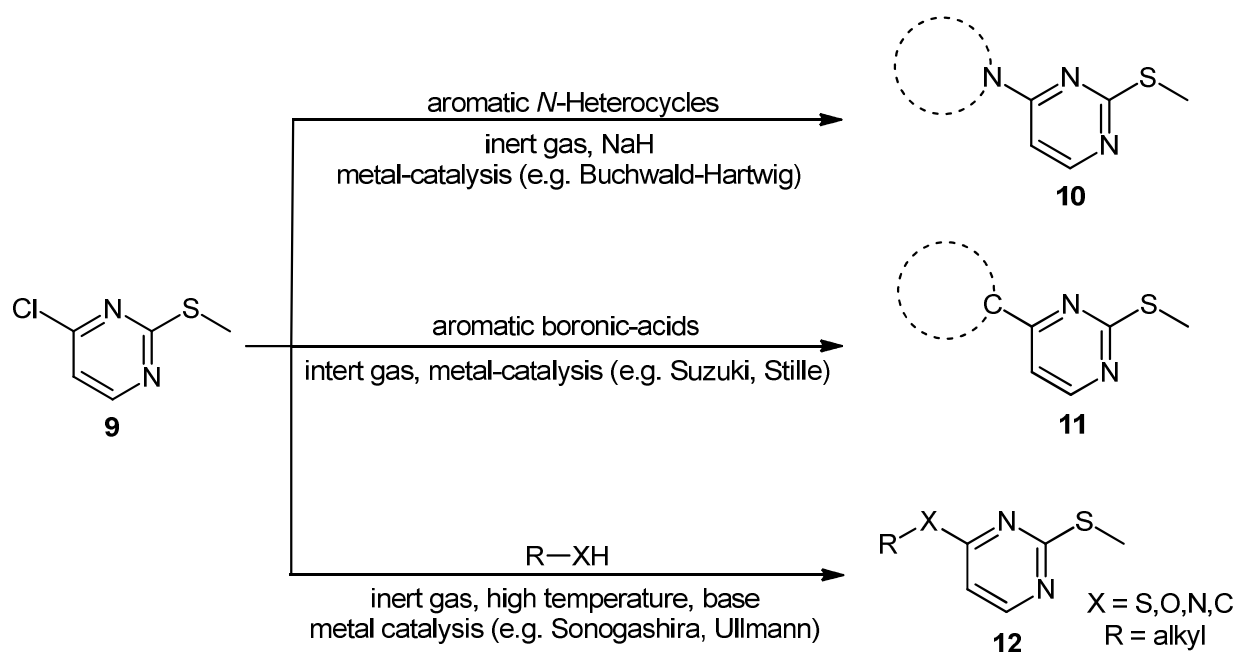


Figure 9. Examples for reaction types routinely used by medicinal chemists to decorate the 2-thiomethylpyrimidine core with different substituents starting from chlorinated precursor **1**. Most of the reactions rely on metal catalysis (e.g., Buchwald-Hartwig) or harsh reaction conditions (e.g., sodium hydride and/or high temperature).

These include for example, Schlenk lines, dry solvents and expensive and/or toxic catalysts (Figure 9). These prerequisites make them less attractive for medicinal chemists. Thus, novel methods are needed that meet the criteria of medicinal chemistry driven drug discovery and circumvent the limitations of traditional approaches.

1.7 *Mycobacterium tuberculosis*

Mycobacterium tuberculosis (Mtb) is a rod-shaped, Gram-positive, obligate human pathogen and causes one of the most deadly diseases worldwide claiming about 1.5 million lives per year in 2014.^[55] Mtb primarily infects the lungs through transmission by aerosol.^[56] After arrival in the lung, Mtb is incorporated by phagocytic cells, i.e., macrophages or neutrophils.^[57] Although many drugs against tuberculosis have been approved or are at a late stage clinical development, the need for novel strategies is undisputed.^[58] A problematic issue of treating Mtb infections arises from the pathogen's ability to change from an actively replicating bacillus to a dormant, non-replicating persister inside the phagosome of human macrophages.^[59] In the latter life cycle, Mtb's metabolic activity is strongly reduced resulting in increased tolerance to antibiotics targeting active metabolism (e.g., cell wall synthesis or protein

biosynthesis).^[56] Thus, novel antibiotics are of high demand, which ideally address targets required for Mtb's survival in the dormant state. Such a strategy would presumably reduce treatment time, which is one of the major cost factors, and failure. Besides the naturally occurring behavior of Mtb to form persister cells, there is a raising number of extremely drug resistant tuberculosis strains (XDR TB) which does not respond to any available antibiotic treatment.^[60] For these reasons, developing new treatment options with alternate mode of action against tuberculosis is of urgent need to counter resistance development and prolonged treatment.

1.8 The cytochrome P450 family – enzymatic reaction and types of inhibition

Since their first discovery by Omura in 1962 in liver microsomes, cytochrome P450 (CYP, CY = cytochrome and P = pigment) enzymes have been found in all classes of living organisms.^[61] The name corresponds to the characteristic spectral absorbance peak at 450 nm when carbon monoxide binds to the reduced ferric-heme in the active site of the enzyme.^[62] The substrate scope of these oxidoreductases can either be narrow for specific conversions (e.g., CYP11B1) or broad for modification of e.g. xenobiotics (e.g., CYP3A4).^[63] The oxidative cycle of CYP enzymes requires electron transfer involving reductases and ferredoxins to generate superoxide anions, which are inserted into a C-H bond of a substrate in a second step (Figure 10).^[64,65]

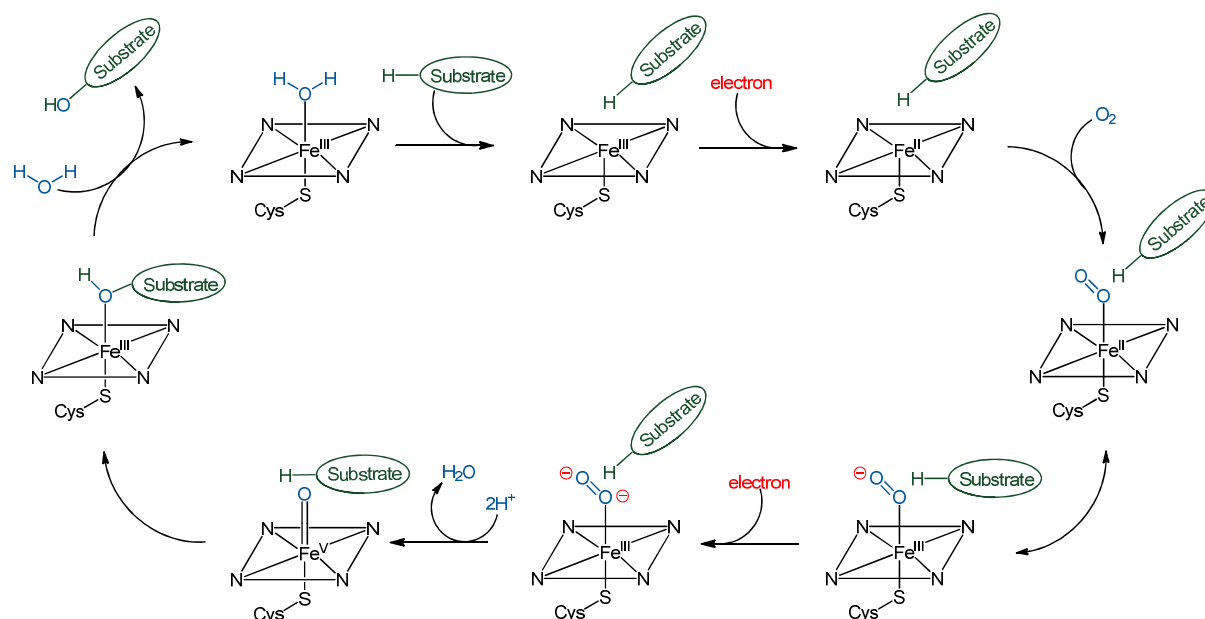


Figure 10. Catalytic cycle and mechanism of the oxidation of a generic substrate by P450 enzyme at the heme iron via the intermediate formation of an O_2^{2-} anion at the iron(III) center.^[64,65]

1 Introduction

Targeting CYP enzymes in drug discovery was proven to be a success story for various kinds of diseases (e.g., CYP17 in prostate cancer or CYP19 in breast cancer) and led to the approval of several drugs such as Abiraterone and Letrozol. Besides human targets, CYP enzymes also represent interesting structures to be addressed in bacteria for the discovery of novel antibiotics.^[66] Based on the unique spectral characteristics of CYP enzymes, different binding modes can be observed for ligands interacting with the ferric-heme. A compound that directly coordinates to the iron(II) center shifts the so-called Soret-band at 420 nm to higher wavelengths, whereas a ligand interacting through coordinated water molecule(s), a so-called water-bridge, induces a shift to lower wavelengths.^[67] These two types of ligation are referred to as type II (direct interaction) and type I (water-bridged interaction) and can be distinguished by difference spectroscopy *versus* non-bound protein (Figure 11). This information can then be used to determine the K_D of the ligand *via* titration experiments while the binding type itself can be exploited for structure-based design strategies.

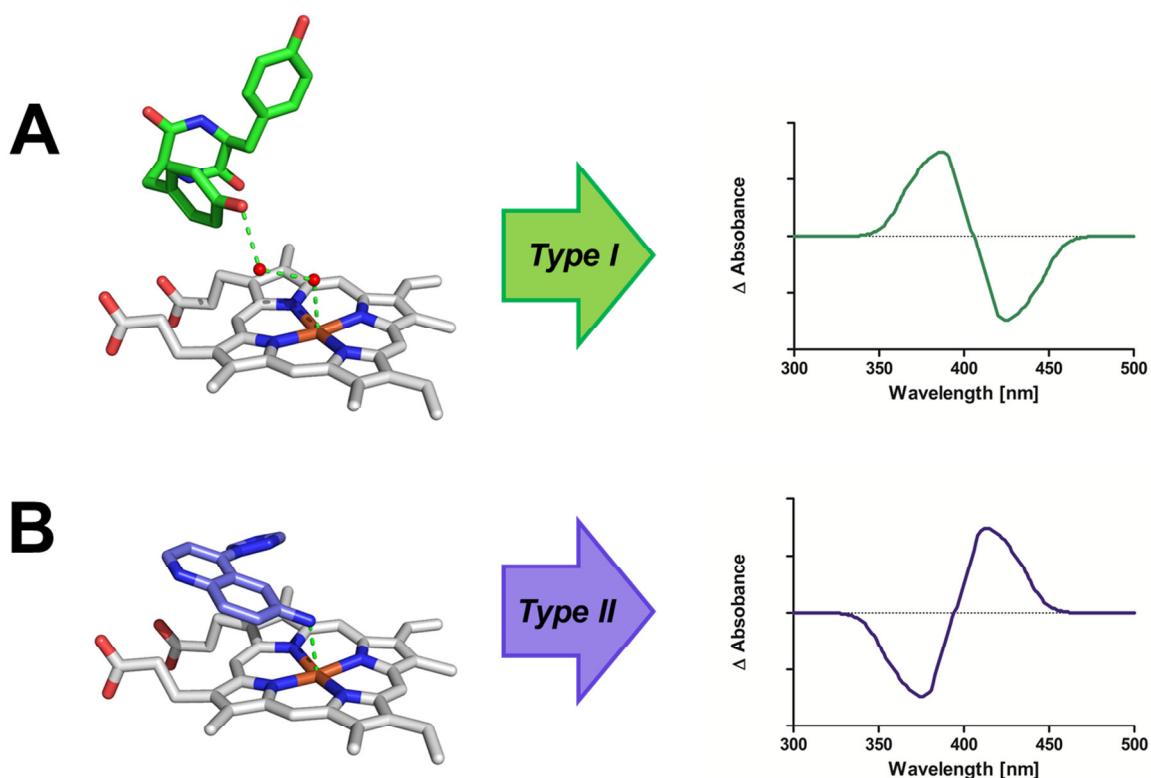


Figure 11. Schematic representations of UV-VIS difference spectra of a type I (A, substrate cYY, PDB-ID: 3G5H) and a type II ligand binding to CYP121 (B, inhibitor of CYP121, PDB-ID: 4G1X).^[18,68]

1.9 CYP121 and CYP125 as anti-mycobacterial drug targets

The discovery of CYP enzymes for anti-mycobacterial drug discovery started with the study on azole antifungals for antibacterial properties against *Mtb*.^[69] First, CYP51, a mycobacterial CYP enzyme closely related to the fungal CYP target of the azoles, was suspected to be the primary target of these compounds and a X-ray co-crystal structure with fluconazole was derived.^[70] However, recent results suggested that CYP121 might be the more relevant target, as it has been shown to be essential for growth of *Mtb*, and in addition, the latter mentioned azoles bind also more strongly to CYP121 than to CYP51.^[69,71] Moreover, CYP51 is not essential for mycobacterial growth *in vitro*.^[72] CYP121 catalyzes an unusual C-C bond formation of the C-2 positions of the tyrosine residues of the cyclic-dipeptide cyclo-di-L-tyrosine (cYY) with high substrate specificity (Figure 12).^[68] Also the exact function of the reaction product, mycocyclosine or its predecessor for mycobacterial survival is unknown. However, the vital necessity of the enzyme itself is undisputed.^[71] Thus, essentiality and novelty of the target renders CYP121 an excellent starting point for anti-tuberculosis drug discovery.

Another essential mycobacterial CYP enzyme is CYP125, which is involved in the sidechain oxidation of cholest-3-en-4-one at C-26 (Figure 12) in order to detoxify this cholesterol-derived metabolite for *Mtb*.^[73]

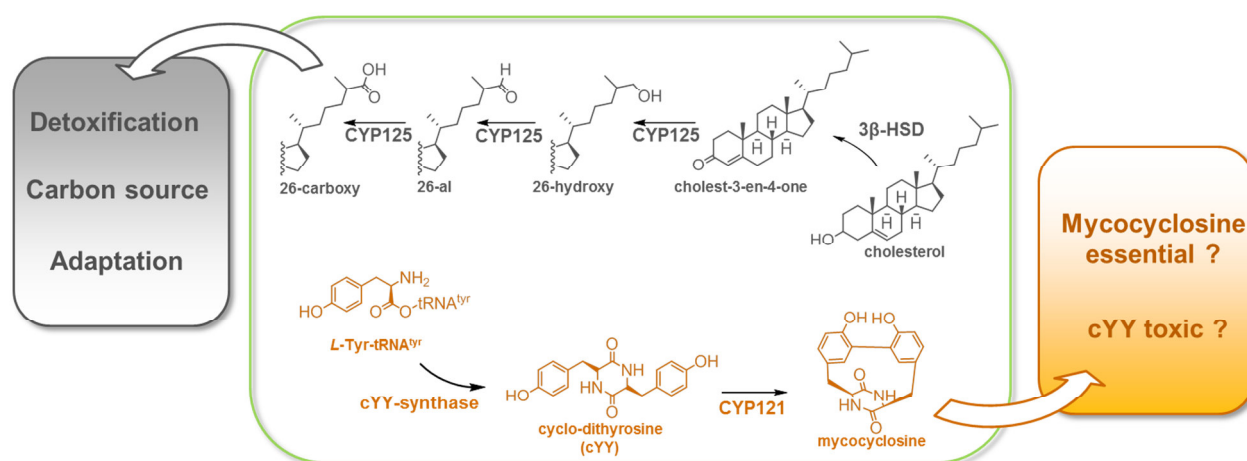


Figure 12. Schematics of the first steps of cholesterol/cholest-3-en-4-one metabolism by 3β-HSD/CYP125 (grey pathway) and the synthesis of mycocyclosine by CYP121 (orange pathway). The role of mycocyclosine or its precursor is still not elucidated to present date. In contrast, the products of CYP125 reaction are known to serve as carbon source during adaptation to the site of infection.^[68,73,74]

1 Introduction

Cholest-3-en-4-one is primarily generated upon infection of the host, when Mtb faces a cholesterol-rich environment, e.g., in the phagosome of macrophages.^[74] Consequently, the expression of CYP125 is induced and enables survival of Mtb upon infection of the host. Essentiality of CYP125 could be shown *in vitro* using a CYP125 defective strain which was unable to grow on cholesterol or cholest-3-en-4-one enriched media.^[75] But, more importantly, this was also confirmed *in vivo* by the use of defective mutants in mouse infection models.^[76] The biological role of CYP125 makes it an ideal target candidate for the development of anti-infective agents against Mtb exploiting a novel mode of action. More importantly, regarding selectivity towards human CYP enzymes, especially hepatic CYPs, none of the two targets has a high degree of homology. In addition to that, this strategy should not induce cross resistance with existing, approved Mtb drugs which opens up the possibility of a combination to increase treatment efficiency against resistant strains of Mtb.

Besides the azole-antifungals (e.g., compounds **14**, **16**, **19**) which, by chance, inhibit both targets, CYP121 and CYP125 have already attracted the attention of medicinal chemists and drug developers in order to develop specific inhibitors (Figure 13). These discovery campaigns were driven by either random screening (compound **13**), ligand-based (compound **20**), or structure-guided fragment-based approaches (compounds **17**, **18**).^[18,19,77,78]

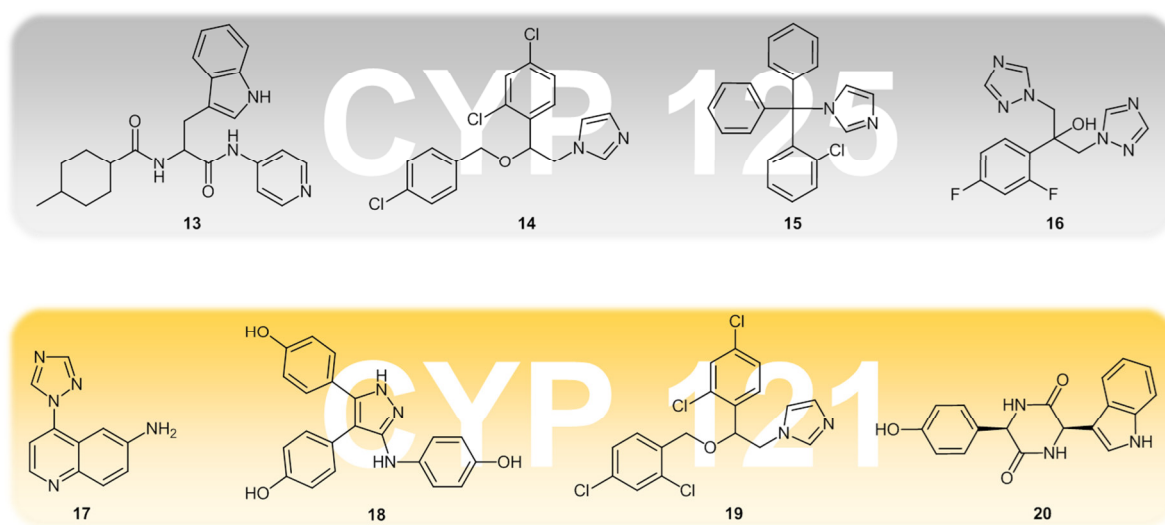


Figure 13. Examples of CYP125 (compounds **13-16**, gray) and CYP121 inhibitors (compounds **17-20**, orange).^[18,19,71,77-79]

Nevertheless, none of the developed compounds was shown to have cellular activity on Mtb. Additionally, the reported compounds lack convincing on-target activity, as they have affinities in the triple to double digit micromolar range. Thus, for target validation and proof of drugability, further studies showing effects on the bacterium and in *in vivo* models are of high demand to rationalize further drug discovery attempts. As mentioned before, first drug discovery campaigns were based on the crystal structure of CYP121 (Figure 14, orange). From this approach, several structures with co-crystallized ligands were derived, making structure-based drug design even more applicable. Besides those studies, the natural substrate of CYP121 is also known and several different synthetic analogues of cYY were tested for their ability to serve as substrates and inhibitors.^[68]

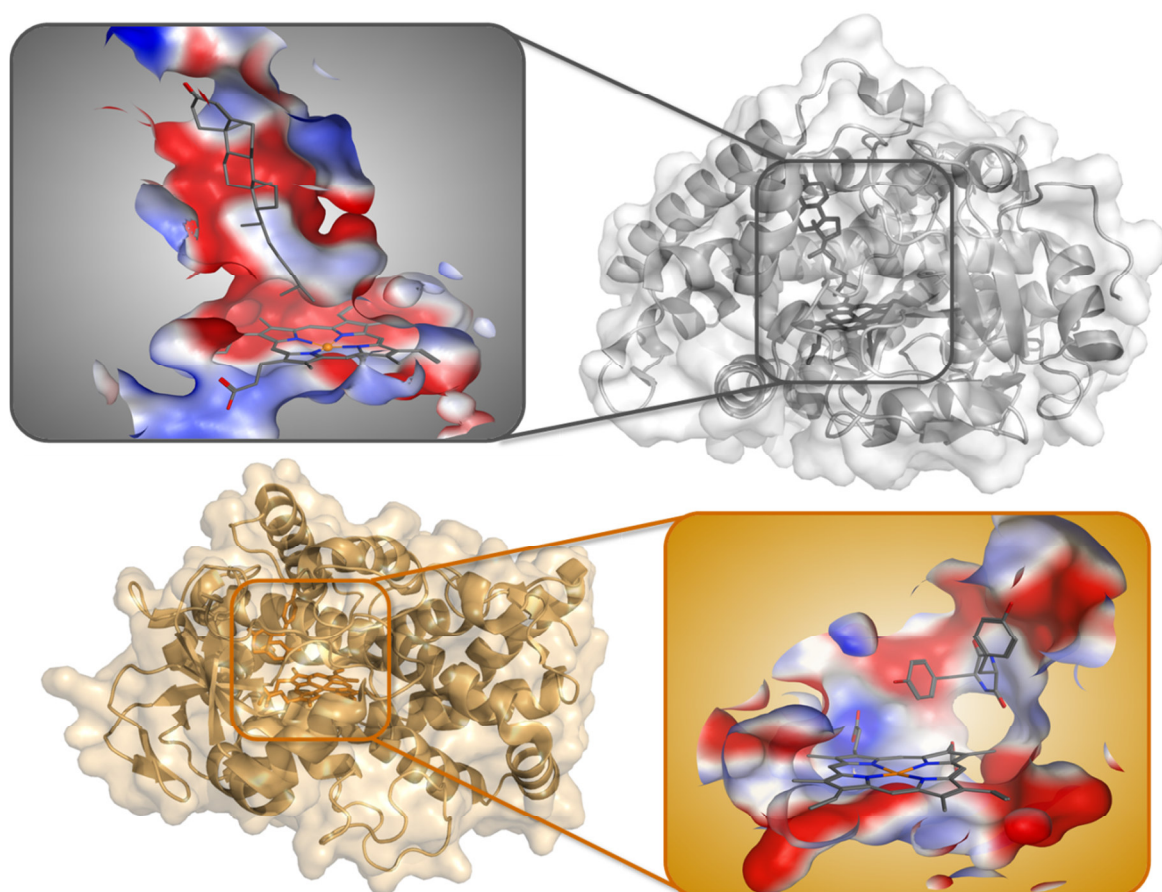


Figure 14. X-ray co-crystal structures of CYP121 with natural substrate cYY bound to heme (orange, PDB-ID: 3G5H) and CYP125 with its substrate cholst-4-en-3-one coordinating the iron (II) centre of the heme (gray, PDB-ID: 2X5W). The binding-site architectures of both proteins are displayed in the colored boxes each. The surfaces of the binding sites were colored with regard to the lipophilicity of the substrate surrounding amino acids in 6 Å proximity.

1 Introduction

Thus, a ligand-based approach in drug discovery using cYY as a template seems also plausible. With regard to CYP125, almost the same starting conditions for rational drug discovery hold true. The substrate and the protein X-ray crystal structure (Figure 14, grey) is known and first inhibitors have been published. Thus, both ligand- and structure-based design are possible which provides, for both targets, an excellent starting point for medicinal chemists to rationally develop potent but selective compounds for both enzymes.

2 Aims of the thesis

Upcoming resistance is a major problem for the treatment of respiratory tract infections by PA and Mtb. Therefore, in this thesis, two different approaches were followed to maximize the success of anti-infective drug development. For PA a novel, innovative concept was chosen: combating pathogenicity without effecting growth to circumvent resistance development by selection pressure. Regarding Mtb, a classic antibiotic strategy was followed by targeting an essential process to eradicate the pathogens at the site of infection. The discovered inhibitors should not show any cross resistance to existing anti-mycobacterial drugs and hence may counter the resistance problem in tuberculosis treatment.

Development of PQS quorum sensing inhibitors against PA infections

- I. Identification, biological evaluation and optimization of novel drug-like inhibitors targeting the PQS cell-to-cell communication system. To accomplish this goal, previous work by Storz and Lu served as the basis for the development of inhibitors of PqsD and antagonists of PqsR.^[41,51] The herein developed compounds should have improved physicochemical properties and biological activities to overcome the limitations of the previously developed inhibitors and provide more drug-like compounds and further proof for the drugability of the two targets.

- II. Development of a robust, fast, and economic synthetic route allowing the introduction of a broad scope of substituents into the identified compound is essential for library generation and to subsequently derive structure activity relationship information. Therefore, it was a key objective to develop a robust and rapid synthetic route for the in-time generation of drug-like compounds to address the latter requirements in a medicinal chemistry environment.

2 Aim of the thesis

Discovery of Cytochrom-P450 inhibitors against Mtb infections

- III. Identification and biological evaluation of first anti-mycobacterial hits against CYP121 and CYP125 from Mtb was the major goal of this part of the thesis. To achieve this aim a focused CYP-inhibitor library composed of in-house available compounds from human CYP projects should be compiled. This library would then be the basis for a subsequent biophysical screening procedure for the discovery of first binders to the mycobacterial CYP enzymes. The most promising inhibitors from this *in vitro* screening are then prime candidates for further evaluation in several cellular models (e.g., M. bovis BCG, Mtb, HEK Cells, HEP Cells) to identify frontrunner compounds with a promising biological and physicochemical profile. As crystallographic data is available on both targets, a goal is to predict the binding modes of the front runner compounds for a structure-guided design approach towards novel anti-tuberculosis drug candidates.

3 Results

3.1 Microwave-Assisted Synthesis of 4-Substituted 2-Methylthiopyrimidines

Andreas Thomann, Carsten Börger, Martin Empting, and Rolf W. Hartmann

Synlett; **2014**; 25; 935–938; DOI: 10.1055/s-0033-1340860

Reprinted with permission from Georg Thieme Verlag Stuttgart • New York
(Copyright 2014)

Publication I

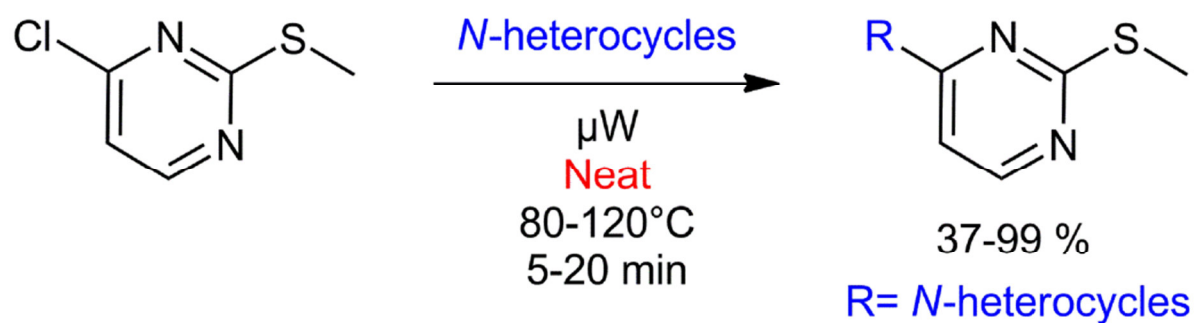


Figure 15. Graphical abstract of publication I.

Microwave-Assisted Synthesis of 4-Substituted 2-Methylthiopyrimidines

Andreas Thomann,^a Carsten Börger,^b Martin Empting,^a Rolf W. Hartmann^{*a,c}

^a Helmholtz-Institute for Pharmaceutical Research Saarland, Saarland University, Campus C2.3, 66123 Saarbrücken, Germany
Fax +49(681)30270308; E-mail: rolf.hartmann@helmholtz-hzi.de

^b PharmBioTec GmbH, Saarland University, Science Park 1, 66123 Saarbrücken, Germany

^c Pharmaceutical and Medicinal Chemistry, Saarland University, Campus C2.3, 66123 Saarbrücken, Germany

Received: 06.01.2014; Accepted after revision: 04.02.2014

Abstract: Typically, S_NAr reactions at 4-chloro-2-methylthiopyrimidine are carried out employing DMF and sodium hydride under inert gas as well as prolonged reaction times. Herein, we describe a mild and rapid microwave-assisted synthesis to achieve 4-substituted 2-methylthiopyrimidines from the corresponding chlorine precursor. Moderate to excellent yields were obtained in a green chemistry fashion requiring only few minutes of reaction time.

Key words: green chemistry, pyrimidine, combinatorial chemistry, medicinal chemistry, nucleophilic aromatic substitution

The family of 4-substituted pyrimidines is a prominent class of chemical scaffolds for the design of kinase modulators,¹ inhibitors,^{2–5} 5-HT_{2A} receptor antagonists,⁶ gastric cytoprotective agents,⁷ inducers of cancer cell apoptosis,⁸ and derivatives with antiproliferative activity against melanoma cells.⁹ A well-reported route^{3,4} to synthesize these desirable target compounds proceeds via S_NAr reaction conditions employing 4-chloro-2-methylthiopyrimidine as a commercially available starting material. However, in order to decorate the pyrimidine core with an additional N-heterocycle, relatively harsh conditions using sodium hydride in anhydrous DMF under inert atmosphere are typically used. Anhydrous DMF is expensive and well-known to be toxic.^{10a,b} Furthermore, these reactions take between several hours and days, making them less attractive for combinatorial approaches in a medicinal chemistry environment.^{1,2}

Additionally, our attempts to generate a benzotriazole derivative (compound **9**, Scheme 1) via this route did not yield the desired product. Thus, we investigated whether it is possible to broaden the scope of this reaction and to simplify the synthetic procedure itself. Interestingly, we observed a direct and clean conversion of a neat 1:1 mix-

Table 1 Conditions Used to Obtain 4-(1-Benzotriazolyl)-2-methylthiopyrimidine

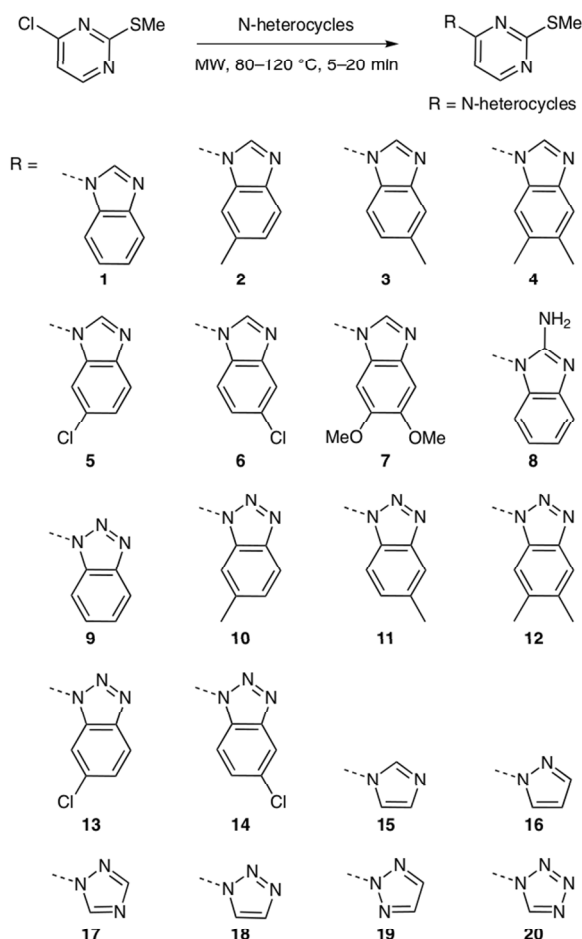
Method	Conditions	Yield (%)
heating	DMF, NaH, 0–90 °C, inert gas, 1 d	0
MW	neat, 80 °C, 50 Watt, 5 min, MW	99
heating	neat, 80 °C, 5 min, sealed tube	99

SYNLETT 2014, 25, 0935–0938

Advanced online publication: 24.03.2014

DOI: 10.1055/s-0033-1340860; Art ID: ST-2014-B0015-L

© Georg Thieme Verlag Stuttgart · New York



Scheme 1 Reaction conditions to achieve 4-substituted methylthiopyrimidines

ture of 4-chloro-2-methylthiopyrimidine and 1H-benzotriazole under microwave irradiation (Table 1).

A similar procedure has already been described for the substitution of chloro-substituted pyridines with benzotriazoles to achieve natural product analogues of α -carboline by Vera-Luque et al.¹¹ However, to the best of our knowledge, this method has not been reported for 4-chloro-2-methylthiopyrimidine, yet. Corroborating the results

published by Vera-Luque et al., we observed that conventional thermal heating is sufficient to drive the reaction to completion, indicating that here is no ‘microwave effect’^{12,13} involved (Table 1). However, the use of microwave irradiation provides a simple and homogenous energy input into the sample for effective temperature control and facilitates straightforward automation of the process. Thus, we conducted all subsequent reactions in an automated microwave synthesizer demonstrating the applicability to combinatorial chemistry approaches.

Macroscopically, we observed two stages of the reaction: (1) The suspension of benzotriazole (white solid) and 4-chloro-2-methylthiopyrimidine turned into a colorless solution (1 min), with the pyrimidine being the solvent as well as the reactant. (2) The product precipitates as white solid (4–5 min, Figure 1).



Figure 1 Stages of the reaction of 1*H*-benzotriazole and 4-chloro-2-methylthiopyrimidine over time: 0 min suspension, 1 min clear solution, 5 min white solid (final product)

To further investigate the scope of the method, we chose 1*H*-tetrazol as a model for an unstable ring system which is usually generated starting from an amino-substituted aryl precursor.¹⁴ Interestingly, under these conditions which include orthoformate and sodium azide in acetic acid,¹⁴ we were not able to obtain the desired compound using 4-amino-2-methylthiopyrimidine (data not shown). Even employing a reported catalyst¹⁵ [ytterbium(III)trifluoromethanesulfonate] did not yield the tetrazolyl-substituted product. Using our developed protocol, however, we were able to achieve the desired compound **20** in moderate yield, emphasizing robustness of the presented approach.

Encouraged by these findings, we completed the series of unsubstituted five-membered N-heterocycles by testing pyrrol, imidazol, pyrazol, 1,2,3-triazol, and 1,2,4-triazol as possible reactants. Except for pyrrol, all of these N-pentacycles were successfully attached to the 2-methylthiopyrimidine core (products **15–19**). In the case of 1,2,3-triazole a mixture of 1- (**18**) and 2-substituted (**19**) isomers was obtained as reported before.¹⁶

Finally, we further investigated the regioselectivity of the reaction using five-substituted benzimidazoles and benzotriazoles as coupling partners. As expected, the final products were a mixture of regioisomers (**2, 3, 5, 6, 10, 11, 13, 14**). The crude product could easily be purified by simple filtration and washing with methanol. Hence, a mixture of regioisomers was obtained in moderate to good yields and

high purity as indicated by HPLC and NMR analysis (Table 2). The lack of regioselectivity can be easily explained due to the tautomeric nature of benzimidazoles¹⁷ and benzotriazoles¹⁸ as well as the above-mentioned 1,2,3-triazoles, leading to different substitution patterns when substituted at N-1 as shown before.^{19–21}

In summary, the presented method provides a facile and rapid access to a variety of 4-N-heterocycle-substituted 2-methylthiopyrimidines. This has been demonstrated for unsubstituted aromatic systems and heterocycles containing electron-withdrawing as well as electron-donating groups. However, the presence of at least two nitrogen centers within the ring is a prerequisite for a successful S_NAr reaction at least in the set of tested compounds. Hence, pyrrols and indols fall outside the scope of this method (Table 2). This observation might be due to the lowered basicity of pyrrol and indol as compared to the other heterocycles used, or the lack of a free electron pair to carry out the nucleophilic attack.

We have developed a fast, cheap, and environmental friendly microwave-assisted synthesis to achieve a broad spectrum of 4-substituted methylthiopyrimidines. The reaction proceeds without the need for solvents, catalysts, inert gas conditions, or reactive agents like sodium hydride. Due to these features and a good overall atom economy at 1:1 stoichiometry this resembles a green-chemistry-like method. The conditions used enable easy scale up and are suitable for automated combinatorial chemistry approaches. Furthermore, the synthesized scaffolds are of high interest in medicinal chemistry as they can routinely be substituted at the 2-position of pyrimidine by simple oxidation of the methylthio group to the corresponding sulfone,²² which is a well-known leaving group to couple a variety of nucleophiles such as thiols,²³ alcohols,²³ or amines,²⁴ allowing fast generation of molecule libraries.

Experimental Procedure for the Synthesis of Compound 9

1*H*-Benzotriazole (119 mg, 1 mmol) was given to 4-chloro-2-methylthiopyrimidine (161 mg, 1 mmol) and stirred for 5 min in a CEM Discover SP microwave oven connected to a CEM Explorer SP 12S autosampler at 80 °C and 50 W to achieve the corresponding hydrochloride salt as a white solid (yield 278 mg, 99%); mp 178 °C. UV-vis (MeOH): 203, 242, 263, 311 (sh), 320 nm. FTIR: 3097, 2156, 2017, 1893, 1596, 1564, 1552, 1506, 1486, 1463, 1428, 1347, 1324, 1306, 1288, 1242, 1205, 1144, 1121, 1090, 1065, 1039, 1009, 976, 917, 864, 841, 826, 801 cm⁻¹. ¹H NMR (300 MHz, CHCl₃-*d*): δ = 2.82 (s, 3 H), 7.55 (t, *J* = 8.3 Hz, 1 H), 7.70 (t, *J* = 8.9 Hz, 1 H), 8.06 (d, *J* = 5.9 Hz, 1 H), 8.18 (d, *J* = 8.3 Hz, 1 H), 8.57 (d, *J* = 8.3 Hz, 1 H), 8.72 (d, *J* = 5.9 Hz, 1 H), 9.19 (br s, 1 H). ¹³C NMR (75 MHz, CHCl₃-*d*): δ = 14.3, 103.2, 115.6, 116.4, 122.0, 131.6, 135.1, 157.9, 159.3, 161.0, 174.1. ESI-MS: 244.1 [M + H]⁺. HRMS: *m/z* calcd for [M + H]⁺: 244.06514; found: 244.06501.

Acknowledgment

We thank Michael Hoffmann for recording HRMS spectra of compound **9** and Joseph Zapp for recording 2-D NMR spectra of the regioisomers.

Table 2 Microwave-Assisted Synthesis of 4 Substituted 2-Methylthiopyrimidines^a

N-Heterocycle	Method	Compound number	Isolated yield (%)
benzotriazol	A	9	99
benzimidazol	B	1	99
imidazol	B	15	68
pyrazol	B	16	65
1,2,3-triazol	B	18 + 19	67 (mixture of regioisomers) ^b
1,2,4-triazol	B	17	72
tetrazol	B	20	53
5,6-dimethoxybenzimidazol	C	7	60
5,6-dimethylbenzimidazol	C	4	37
5,6-dimethylbenzotriazol	C	12	48
2-aminobenzimidazol	C	8	51
5-chlorobenzimidazol	C	13 + 14	62 (mixture of regioisomers) ^c
5-methylbenzimidazol	C	2 + 3	55 (mixture of regioisomers) ^d
5-chlorobenzotriazol	C	5 + 6	71 (mixture of regioisomers) ^e
5-methylbenzotriazol	C	10 + 11	55 (mixture of regioisomers) ^f
pyrrol	B, C		0
indol	B, C		0

^a Reagents and conditions: in all methods: 4-chloro-2-methylthiopyrimidine (1 equiv), of N-heterocycle (1 equiv); method A: 80 °C, 50 Wt, 5 min, MW; method B: Et₃N (1 mmol), 80 °C, 50 W, 10 min, MW; method C: Et₃N (1 mmol), 120 °C, 150 W, 20 min, MW.

^b 1,2,3-Triazol-1-yl/1,2,3-triazol-2-yl (3:1)

^c 5-Chloro-benzimidazolyl/6-chloro-benzimidazolyl (4:3)

^d 5-Methyl-benzimidazolyl/6-methyl-benzimidazolyl (4:3)

^e 5-Chloro-benzotriazolyl/6-chloro-benzotriazolyl (1:1)

^f 5-Methyl-benzotriazolyl/6-methyl-benzotriazolyl (1:1)

Supporting Information for this article is available online at <http://www.thieme-connect.com/ejournals/toc/synlett>.

References

- (1) Goldstein, D. M.; Gong, L.; Michoud, C.; Palmer, W. S.; Sidduri, A. US Patent WO 2008028860 (A1), **2008**.
- (2) Goulet Joung, L.; Holmes, M. A.; Hunt, J. A.; Mills, S. G.; Parsons, W. H.; Sinclair, P. J.; Zaller, D. US Patent WO 0100207 (A1), **2001**.
- (3) Beresis, R. T.; Goulet, J. L.; Hermes, J. D.; Holmes, M. A.; Hong, X. J.; Hunt, J. A.; Kovacs, E.; Mills, S. G.; Park, Y.-W.; Ruzek, R. D.; Salowe, S. P.; Sinclair, P. J.; Sonatore, L. M.; Wong, F.; Woods, A.; Wu, L.; Zaller, D. M. *Bioorg. Med. Chem. Lett.* **2009**, *19*, 5440.
- (4) Balitza, A. E.; Bilodeau, M. T.; Coll, K. E.; Hartman, G. D.; Manley, P. J.; McFall, R. C.; Rickert, K. W.; Rodman, L. D.; Thomas, K. A. *Bioorg. Med. Chem. Lett.* **2003**, *13*, 1673.
- (5) Kim, M.-H.; Lee, J.; Jung, K.; Kim, M.; Park, Y.-J.; Ahn, H.; Kwon, Y.; Hah, J.-M. *Bioorg. Med. Chem.* **2013**, *21*, 2271.
- (6) Borowski, T.; Mokrosz, M. J.; Krol, M.; Broclawik, E.; Baranowski, T. C.; Strekowski, L. *J. Med. Chem.* **2000**, *43*, 1901.
- (7) Ikeda, M.; Maruyama, K.; Okabe, S.; Nobuhara, Y.; Yamada, T. *Chem. Pharm. Bull.* **1997**, *45*, 549.
- (8) Lukasik, P. M.; Elabar, S.; Lam, F.; Shao, H.; Liu, X.; Abbas, A. Y.; Wang, S.; Lam, F.; Wang, S. *Eur. J. Med. Chem.* **2012**, *57*, 311.
- (9) Chung, J. Y.; Hah, J.-M.; Kim, H.; Lee, J.; Oh, C.-H.; Sim, T.; Yoo, K. H.; Yu, H. *Bioorg. Med. Chem. Lett.* **2010**, *20*, 1573.
- (10) (a) Kennedy, G. L. *Drug Chem. Toxicol.* **1986**, *9*, 147.
(b) Massmann, W. *Brit. J. Ind. Med.* **1956**, *13*, 51.
- (11) Vera-Luque, P.; Alajarin, R.; Alvarez-Builla, J.; Vaquero, J. *J. Org. Lett.* **2006**, *8*, 415.
- (12) Kappe, C. O. *Angew. Chem. Int. Ed.* **2004**, *43*, 6250.
- (13) de la Hoz, A.; Diaz-Ortiz A. Moreno A. *Chem. Soc. Rev.* **2005**, 164.
- (14) Vorobiov, A. N.; Gaponik, P. N.; Petrov, P. T.; Ivashkevich, O. A. *Synthesis* **2006**, 1307.
- (15) Su, W.-K.; Hong, Z.; Shan, W.-G.; Zhang, X.-X. *Eur. J. Org. Chem.* **2006**, 2723.

- (16) Ouali, A.; Taillefer, M.; Xia, N. *Angew. Chem. Int. Ed.* **2007**, *46*, 934.
- (17) Wright, J. B. *Chem. Rev.* **1951**, *48*, 397.
- (18) Larinaa, L. I.; Milatab, V. *Magn. Reson. Chem.* **2009**, *47*, 142.
- (19) Jouvin, K.; Coste, A.; Bayle, A.; Legrand, F.; Karthikeyan, G.; Tadiparthi, K.; Evano, G. *Organometallics* **2012**, *31*, 7933.
- (20) Bentin, T.; Hamzavi, R.; Salomonsson, J.; Roy, H.; Ibba, M.; Nielsen, P. E. *J. Biol. Chem.* **2004**, *279*, 19839.
- (21) Barlin, G. B.; Batterham, T. F. *J. Chem. Soc. B* **1967**, 516.
- (22) Hurst, D. T.; Johnson, M. *Heterocycles* **1985**, *23*, 611.
- (23) He, H.; Jin, C.; Fu, L.; Liang, Y.-J. *Eur. J. Med. Chem.* **2011**, *46*, 429.
- (24) List, B.; Castello, C. *Synlett* **2001**, 1687.

3 Results

3.2 Steering the Azido-Tetrazole Equilibrium of 4-Azidopyrimidines via Substituent Variation – Implications for Drug Design and Azide-Alkyne Cycloadditions

Andreas Thomann, Josef Zapp, Michael Hutter, Martin Empting, and Rolf W. Hartmann

Reproduced with permission from *Organic and Biomolecular Chemistry*, **2015**; 13; 10620-30; DOI: 10.1039/C5OB01006C.

Copyright 2015 The Royal Chemical Society.

Publication II

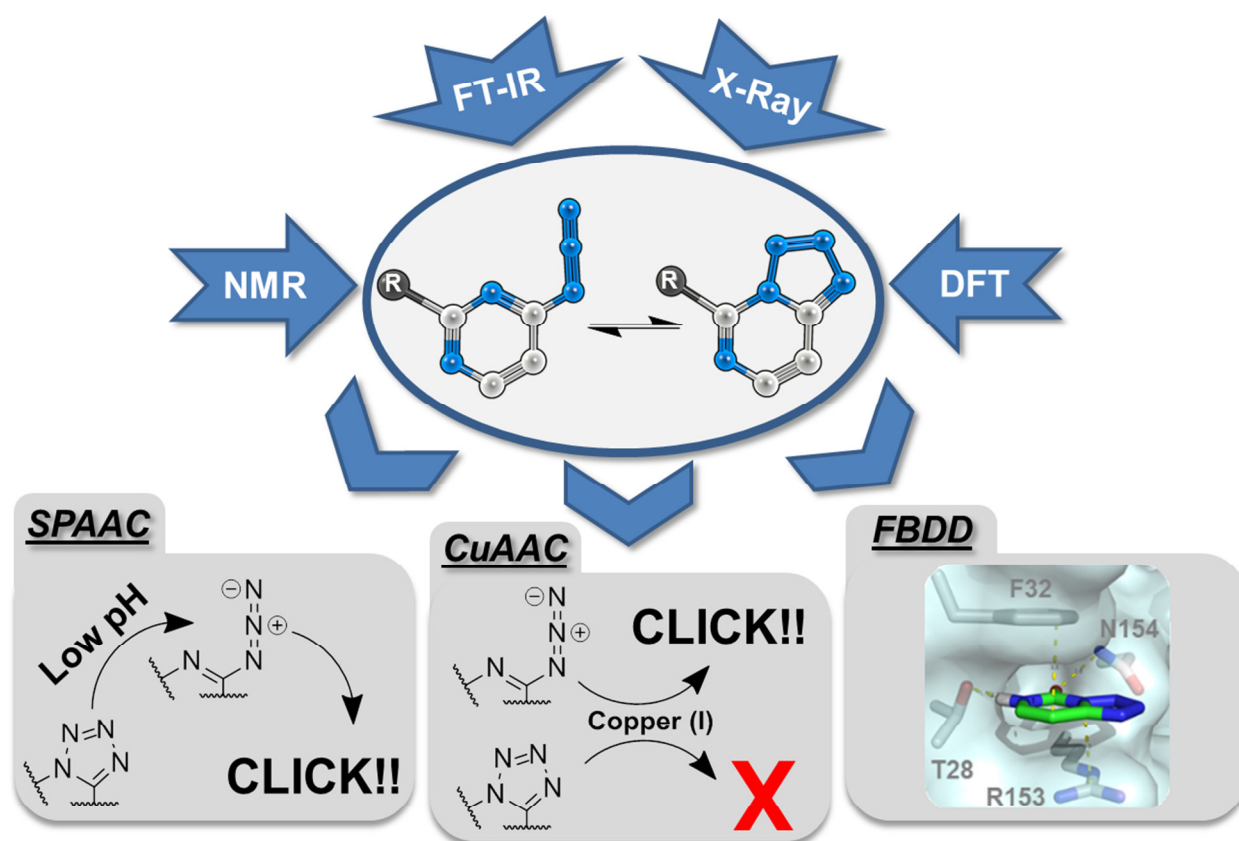


Figure 16. Graphical abstract of publication II.



Cite this: DOI: 10.1039/c5ob01006c

Steering the azido–tetrazole equilibrium of 4-azidopyrimidines *via* substituent variation – implications for drug design and azide–alkyne cycloadditions†

A. Thomann,^a J. Zapp,^b M. Hutter,^c M. Empting^{*a} and R. W. Hartmann^{*a,d}

This paper focuses on an interesting constitutional isomerism called azido–tetrazole equilibrium which is observed in azido-substituted N-heterocycles. We present a systematic investigation of substituent effects on the isomer ratio within a 2-substituted 4-azidopyrimidine model scaffold. NMR- and IR-spectroscopy as well as X-ray crystallography were employed for thorough analysis and characterization of synthesized derivatives. On the basis of this data, we demonstrate the possibility to steer this valence tautomerism towards the isomer of choice by means of substituent variation. We show that the tetrazole form can act as an efficient disguise for the corresponding azido group masking its well known reactivity in azide–alkyne cycloadditions (ACCs). In copper(i)-catalyzed AAC reactions, substituent-stabilized tetrazoles displayed a highly decreased or even abolished reactivity whereas azides and compounds in the equilibrium were directly converted. By use of an acid sensitive derivative, we provide, to our knowledge, the first experimental basis for a possible exploitation of this dynamic isomerism as a pH-dependent azide-protecting motif for selective SPAAC conjugations in aqueous media. Finally, we demonstrate the applicability and efficiency of stabilized tetrazolo[1,5-c]pyrimidines for Fragment-Based Drug Design (FBDD) in the field of quorum sensing inhibitors.

Received 18th May 2015,
Accepted 25th August 2015

DOI: 10.1039/c5ob01006c

www.rsc.org/obc

Introduction

Substituted pyrimidines represent important molecular scaffolds in the fields of biologically active entities,¹ synthetic chemistry,² coordination chemistry,³ and materials science.⁴ The azide functionality, on the other hand, is a highly useful, readily reactive, and easily prepared chemical moiety for bioorthogonal click chemistry,⁵ polymer research,⁶ and medicinal chemistry.⁷

By the linkage of the azide group at the 2, 4 and/or 6 position of pyrimidines, a phenomenon which is referred to as azido–tetrazole equilibrium, can be observed.^{8–14} This constitutional isomerism is characterized by a ring closure of the azide with *ortho*-nitrogen of the pyrimidine core, resulting in the corresponding tetrazole (Scheme 1) and has drawn enormous attention of NMR- and IR-analysts,^{8–18} synthetic chemists,^{17–25} researchers in drug discovery,^{26–28} and scientists from the field of computational chemistry.^{29–31} In 1979, Könnecke *et al.* provided a detailed analysis of substituent-dependent effects on this valence tautomerism and suggested that besides solvent and temperature, electronic as well as steric effects should be considered when investigating the position of the equilibrium.⁹ They demonstrated that the electron density at the imino nitrogen ion pair is of particular importance for driving the ratio of isomers towards the cyclic tetrazole form. Although their studies were based on a molecular scaffold possessing a different substitution pattern, we concluded that this is the parameter of choice to enforce either of the constitutional states.

In the presented study, we systematically investigated the possibility to steer the equilibrium towards azide or tetrazole isomers by variations of the substituents at the 2 position of 4-azidopyrimidine. To facilitate the establishment of a decent

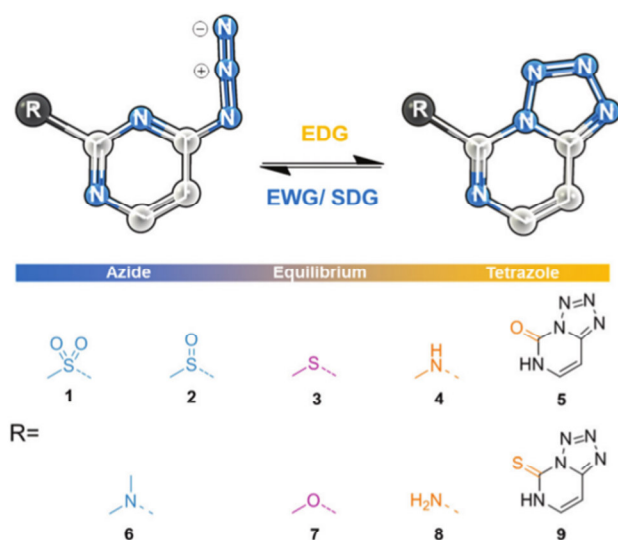
^aHelmholtz Institute for Pharmaceutical Research Saarland (HIPS), Department for Drug Design and Optimization (DDOP), Campus C2.3, 66123 Saarbrücken, Germany. E-mail: rolf.hartmann@helmholtz-hzi.de, martin.empting@helmholtz-hzi.de

^bSaarland University, Department of Pharmaceutical Biology, Campus C2.2, 66123 Saarbrücken, Germany

^cSaarland University, Center for Bioinformatics, Campus E2.1, 66123 Saarbrücken, Germany

^dSaarland University, Department for Pharmaceutical and Medicinal Chemistry, Campus C2.3, 66123 Saarbrücken, Germany

†Electronic supplementary information (ESI) available: Full experimental details, molecular modelling, pK_a determination, LC-MS kinetic analysis, characterization data including ¹H-NMR, ¹³C-NMR, FT-IR, ¹⁵N-NMR, X-ray crystallography, HRMS are provided. CCDC 1045217–1045219. For ESI and crystallographic data in CIF or other electronic format see DOI: 10.1039/c5ob01006c



Scheme 1 Depiction of azido–tetrazole equilibrium at 2-substituted 4-azidopyrimidines showing defined substituent effects to steer the equilibrium. Blue substituents fully steer the equilibrium towards the azide tautomer whereas orange groups steer to the tetrazole isomer. Residues which show both isomers are colored accordingly. EDG = electron-donating group, EWG = electron-withdrawing group, and SDG = sterically demanding group.

relationship between the chemical structure and the position of the equilibrium, we selected different substituents covering a wide range of electronic properties and steric demand. To gather further insight, we conducted density functional theory calculations including a solvation model using the structures of synthesized derivatives.³² Such an isomerism should have an impact on the reactivity of the azide group.²³ In order to study this effect with our scaffold, we conducted model azide–alkyne cycloaddition (AAC) reactions with selected derivatives resembling both isomers as well as compounds in thermal equilibrium. Finally, such small compounds containing stabilized tetrazoles give rise to fragment-like structures which might be suitable for Fragment-Based Drug Design (FBDD). In a rational approach, we investigated whether these structural features could be exploited for FBDD.

Results and discussion

Structure elucidation and substituent effects

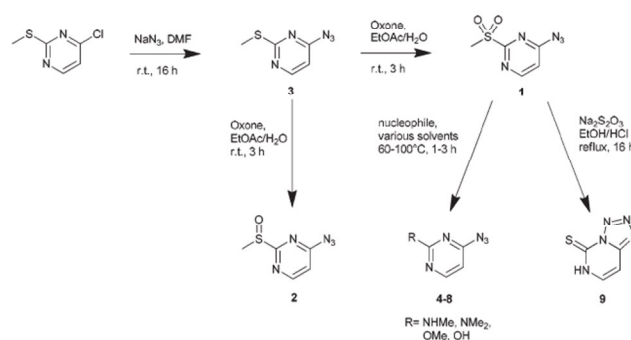
The effect of substituents on the azido–tetrazole equilibrium of 4-azidopyrimidines has been described for a small subset of a heterogeneously substituted series.^{8,13,33} In contrast to more intensely studied 2-azidopyrimidines^{10,11,14} this molecular scaffold displays only one possible cyclization geometry and, hence, just one tetrazole isomer. Notably, derivatives of 4-substituted pyrimidines have recently moved into the focus of our research³⁴ emphasizing their relevance as starting points for the design and synthesis of biologically active entities. The occurrence of the described constitutional isomerism in azido-

pyrimidines added another level of structural complexity and variability to the compounds which we wanted to investigate in more detail. To the best of our knowledge, no rational approach to steer the equilibrium in this system towards the desired connectivity and, hence, activity by substituent variation has been described to date. Therefore, we chose nine functional groups, different in electronic and steric properties, as substituents at the 2-position to study the effect on the equilibrium (Schemes 1 and 2).

As shown before, the equilibrium can be directly monitored by ¹H-NMR and ¹⁵N-NMR.^{8–10,13,15–18,35,36} According to ¹H-NMR spectral data the doublets for the two protons at C-5 and C-6 of the pyrimidine rings are distant to each other for the azide ($\Delta\text{ppm} = 1.0\text{--}1.9$) and are closer and downfield shifted for the tetrazole-form ($\Delta\text{ppm} = 0.2\text{--}0.8$) (Fig. 1A).^{8,10,12}

In the case of compound **1**, bearing a sulfomethyl-group at the 2-position, ¹H- and ¹⁵N-NMR spectra provided a signal set of only one isomer with chemical shifts resembling the monocyclic variant (Fig. 1A, ESI section II.e†). This finding was supported by IR data, as we observed the characteristic absorption band at 2100 cm^{-1} (Fig. 1B).³⁷ Hence, under the conditions used (ambient temperature, DMSO as the solvent) only the azide form of compound **1** is detectable.

The complete absence of the tetrazole valence tautomer is quite notable, as this cyclic isomer is considered to be the favored low temperature structure in the case of pyridine, pyrazine, and pyrimidine cores.³⁸ Both steric as well as electronic effects induced by the bulky, electron-withdrawing sulfomethyl moiety might be responsible for this result. To further investigate this, we synthesized compound **2** bearing a sulfoxide, which possesses a lower steric demand but has almost equal electron-withdrawing properties (Hammett constants are $\sigma_{\text{m,SOMe}} = 0.52$ and $\sigma_{\text{m,SO}_2\text{Me}} = 0.60$).³⁹ Interestingly, we observed a signal subset of very low intensity within the ¹H-NMR-spectrum belonging to the tetrazole form, while the main isomer for **2** was showing chemical shifts of the azide (Table 1). This finding suggests that bulky substituents at the 2 position may favor the azide. The sulfomethyl group of **1** might cause steric clashes upon the formation of tetrazole which impairs the degree of rotational freedom at the substituent site. This penalty would be less pronounced in the case of sulfoxide **2**



Scheme 2 Synthesis of compounds **1–9**.

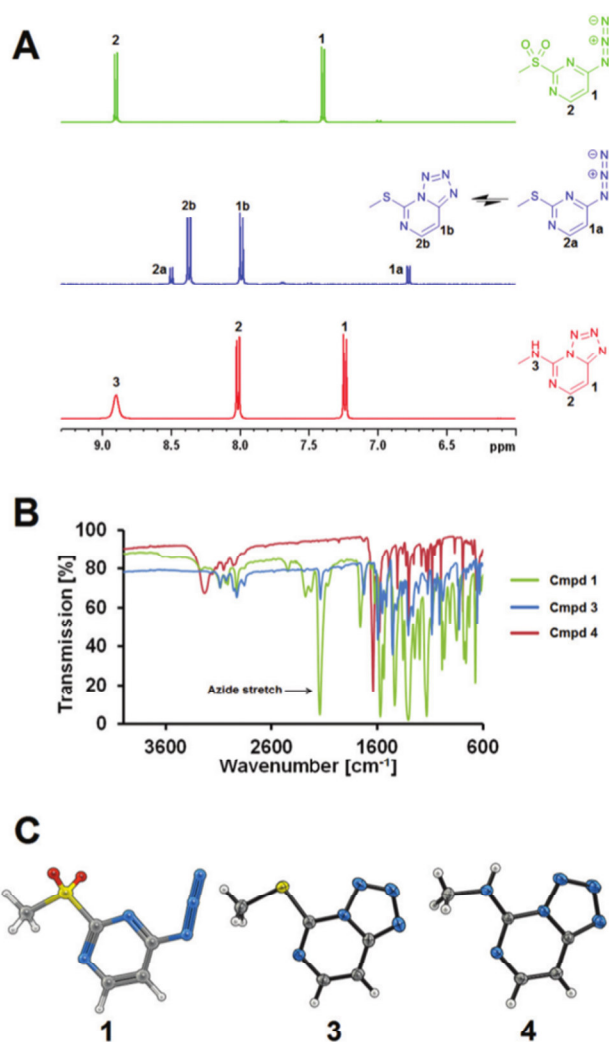


Fig. 1 Analytical data of compounds **1** (green), **3** (blue) and **4** (red) allowing for the determination of azide and tetrazole isomers. $^1\text{H-NMR}$ (A), IR (B), X-ray crystallography (**3** and **4**) and modeling of compound **1** (energy optimized using the MM2 semi-empirical method) (C). $^1\text{H-NMR}$ chemical shifts for protons at C5 and C6 of tetrazole tautomers are significantly closer to each other (**3**: $\Delta\text{ppm} = 0.4$, **4**: $\Delta\text{ppm} = 0.8$) than the respective signals for azide isomers (**1**: $\Delta\text{ppm} = 1.5$, **3**: $\Delta\text{ppm} = 1.7$) (A). $^{15}\text{N-NMR}$ chemical shifts (B) and azide-band appearance at $\sim 2100\text{ cm}^{-1}$ in IR (B) support the structural proposals (**4** only tetrazole, **3** both isomers, **1** only azide) shown in Table 1. In the crystal form only tetrazole tautomers were observed as determined by X-ray crystallography for compounds **3** and **4** (C).

providing a possible explanation for the presence of the tetrazole at detectable levels.

To investigate the effect of electron-donating groups (EDGs) we introduced thiomethyl (**3**) and methoxy (**7**) substituents. Interestingly, both compounds were in the equilibrium state whereas the thiomethyl derivative showed more tetrazole character (Fig. 1A, Table 1, ESI section II.a†). Comparing the Hammett constants³⁹ of both groups, the methoxy-substituent ($\sigma_m = 0.15$) is less electron donating compared to its thio isostere ($\sigma_m = 0.12$). These results are consistent with the hypothesis that EWGs at the 2-position favor the azide over the

tetrazole (Table 1). This trend can also be witnessed by comparing the IR-spectra as compounds **3** and **7** show weaker azide bands than **1** (Fig. 1B, ESI section II.g†). In addition to NMR and IR, we performed X-ray structural analysis with selected compounds that were readily crystallizable (Table 1). However, even for compound **3** only the tetrazole form was observed in the elucidated structure (Fig. 1C). This might be a result of the crystallization procedure favoring those isomers which pack more densely. Notably, no crystals were obtained for compounds showing the most pronounced azide characteristics (**1**, **2**, **6**, and **7**).

With the aim to further investigate the influence of EDGs, we decorated the 2-position with a series of substituents possessing ascending electron-donating properties by the introduction of an amine (**8**), a methylamine (**4**) and a dimethylamine group (**6**).³⁹ Again we collected $^1\text{H-NMR}$ and IR data for these compounds and, additionally, elucidated the structure of compound **4** by $^{15}\text{N-NMR}$ and X-ray crystallography. We found the equilibrium to be fully shifted towards the tetrazole in the case of compounds **4** (Fig. 1, Table 1, ESI section II.e†) and **8** (Table 1). Interestingly, dimethyl derivative **6** was found to exist mainly in the azido state as indicated by $^1\text{H-NMR}$ and IR analyses (Table 1, ESI section II.a.g†) although it is the group with the strongest electron-donating properties within this subset of compounds (**4**, **6**, and **8**). As hypothesized before (in the case of compounds **1** and **2**, *vide supra*), the space demanding properties of the two methyl groups of compound **6** may force the equilibrium towards the azide. We found the proton at the amine within the crystal structure of closely related tetrazole **4** to be in proximity to the neighboring nitrogen of the tetrazole-ring (Fig. 1C). Upon replacing this proton by a methyl group *in silico* (yielding the tetrazolo isomer of **6**), intramolecular steric clashes occur between the newly introduced group and the tetrazole nitrogen (ESI section I.d†). These results might explain the shift of the thermal equilibrium towards the azide form underlining the impact of steric factors in the likelihood of the cyclic valence tautomer. The involvement of an intramolecular hydrogen bond for stabilization of the tetrazole over the azide-isomer in **4** was ruled out by monitoring of the N–H shift in CDCl_3 under DMSO titration as described before (ESI section II.b†).⁴⁰

As we were also interested in the thiol and hydroxy derivatives, we synthesized compounds **5** and **9**. However, as reported before,⁴¹ these structures could not be obtained as the free hydroxy or thiol compounds but “trapped” in urea-like tautomers. For both compounds the equilibrium was fully shifted towards the tetrazole as indicated by $^1\text{H-NMR}$ (Table 1) and X-ray crystallography (ESI section I.b†). Previous studies on the structure of **5** were based on its UV spectrum and Fox *et al.* could, therefore, only speculate that it might be the tetrazole derivative.⁴¹ As the structures of **5** and **9** are similar to 2-hydroxypyrimidine, which was reported to be NH acidic ($\text{pK}_a = 2.9$),⁴² we hypothesized that **5** and **9** could also be acids.

To check this hypothesis, we determined pK_a values for compounds **5** and **9**. Interestingly, **9** turned out to be even as

Table 1 Substitution pattern of compounds 1–9 and the observed effect on the equilibrium determined by ¹H-NMR in DMSO, IR and X-ray crystallography

Cmpd	Group	Effect ^a	¹ H-NMR ^b	IR	X-Ray ^b
1	SO ₂ Me	EWG/SDG	A	Strong azide	—
2	SOMe	EWG	$K_T = 33.3$	Strong azide	—
3	SMe	EDG	$K_T = 0.20$	Intermediate azide	T
4	NHMe	EDG	T	No azide	T
5	Carbonyl	EDG	T	Weak azide	T
6	NMe ₂	EDG/SDG	$K_T = 10.0$	Strong azide	—
7	OMe	EDG	$K_T = 1.5$	Intermediate azide	—
8	NH ₂	EDG	T	No azide	—
9	Thionyl	EDG	T	No azide	—

^a EDG = electron-donating group, EWG = electron-withdrawing group, and SDG = sterically demanding group. ^b A = azide, T = tetrazole, and K_T = equilibrium constant.¹¹

acidic as acetic acid with a pK_a of 4.6. Compound 5 ($pK_a = 6.8$) is two orders of magnitude less acidic than 9. Furthermore, we concluded from these findings that the polarization of hydrogen at N6 could lead to an increased electron density in the ring system, resulting in the preference for the tetrazole.

In summary, we have shown that EDGs favor the tetrazole while electron-withdrawing-groups (EWGs) shift the equilibrium towards the azide (Scheme 1). However, sterically demanding substituents may suppress the formation of the cyclic isomer even with strong EDGs being present.

To further investigate the influence of substituents at the 2-position on the electronic properties and, hence, the stability of the corresponding constitutional isomers, we performed hybrid density functional theory (DFT) calculations including a continuum solvation model. Previous molecular modeling experiments in this field applied gas-phase DFT calculations to evaluate azido-pyridines and their tetrazolo analogues *in silico*.^{29–31} As mentioned above, solvent effects may significantly contribute to the state of the equilibrium.^{8,10} In the present study, we used the COnductor-like Screening Model (COSMO) solvation methodology³² as implemented in NWChem (version 6.1) to predict the contributions of water, DMSO and CHCl₃. This procedure provides a high numerical efficiency for facilitating fast calculations while retaining sufficient accuracy especially in solvents with high permittivity (*e.g.* water).⁴³ For energy optimization we chose the B3LYP/aug-cc-pVDZ level of theory.

For the accurate computation of similar isomerization energies *in vacuo*, Grimme *et al.* showed that coupled-cluster methods are most reliable and pointed out some flaws of the popular B3LYP density functional for the determination of kinetic and thermodynamic energy terms.⁴⁴ In particular the transformation of π into σ bonds shows substantial errors.⁴⁵ Likewise, Grimme and co-workers found that only triple- ζ basis sets such as the here applied aug-cc-pVDZ basis set are necessary for obtaining precise results. On the other hand, the mentioned drawbacks of the B3LYP functional do not affect the prediction of molecular structures that are required for subsequent single-point energy computations, using for example other density functionals, higher-level methods, or solvent models.

As a result, our computations suggested that the tetrazole form is mostly energetically favored except for derivative 1 (Table 2). Hence, the absolute position of the equilibrium differed from that observed in our NMR and IR experiments.

We attribute the systematic over-estimation of the stability of the tetrazole form to the fact that hydrogen-bonding and any other directional interactions with the solvent are not considered because the solvent is treated as continuum, whereby its dielectric constant is the decisive parameter. Thus, these kinds of interactions, which are likely to shift the tautomeric equilibrium, are beyond the scope of conventional density functional methods and continuum solvation models.

Nevertheless, several qualitative aspects of the constitutional isomerism could be reproduced *in silico* quite well. For example, our experimental data (ESI section II.b†) and the literature suggested^{8,10} that less polar solvents favor the azide form in contrast to polar ones. In the case of compound 1 the predictions perfectly matched the experimental results with the azide being the predominant species. Additionally, for 5 and 9 a rather high preference for the cyclic form was predicted with an energy difference of -8.57 kcal mol⁻¹ and -10.27 kcal mol⁻¹, respectively. Hence, the calculations

Table 2 Calculated differences in solvation energy obtained by the COSMO solvent model. Library compounds 1–9 were energetically minimized at the B3LYP/aug-cc-pVDZ level of theory. Units are given in kcal mol⁻¹

Cmpd	Water		DMSO		Chloroform	
	A	T	A	T	A	T
1	-2.48	0	-2.14	0.0	—	—
2	0	-1.04	0	-1.02	0	-0.88
3	0	-5.14	0	-5.88	0	-4.93
7	0	-4.16	0	-4.14	0	-3.70
6	0	-2.96	0	-3.26	—	—
4	0	-2.96	0	-3.62	—	—
8	0	-5.99	0	-6.77	—	—
5	0	-8.57	0	-10.48	—	—
9	0	-10.27	0	-8.68	—	—

A = azide, T = tetrazole.

suggest that according to the Boltzmann distribution only one ppm or less of the compounds exists in the azide form at room temperature.⁴⁶ In accordance with that, no signals for the azide-isomer have been observed for **5** and **9** by NMR characterization (*vide supra*). For compounds **3** and **7** we observed both isomers in our experiments. The former favors the tetrazole and the latter the azide form under the conditions used (Table 1). Our computational results, however, suggest that both forms preferably adopt the cyclic constitution. Nevertheless, the calculated energy difference for thiomethyl **3** was higher than for its methoxy congener **7** which describes the general trend correctly.

In the case of amines **6**, **4**, and **8**, all derivatives were predicted to favor the tetrazole form. While primary amine **8** displayed the strongest preference for the cyclic isomer in this subset, the secondary (**4**) and tertiary (**6**) variants both yielded similar values regarding the calculated energy difference. Experimentally, we determined a ten-fold excess of the azide form for the latter while the secondary amine was confirmed to be a tetrazole as predicted. We assume that the observed discrepancy between computational and experimental results is caused by a steric effect of the bulky dimethyl functionality attenuating cyclisation propensity which is not appropriately accounted for by the DFT method.

For compound **2** only a small difference between the azide and the tetrazole isomer of about 1 kcal mol⁻¹ was predicted indicating that both forms are suggested to exist in a near equal ratio with a slight preference for the cyclic one. Our experiments, however, clearly show a strong shift of the equilibrium towards the azide. Nevertheless, in comparison with the other compounds predicted to be tetrazoles (**3–9**) sulfoxide **2** displays the lowest preference for the cyclic isomer. Hence, although the overall outcome of our calculations is biased towards the tetrazole, the general trend is described quite well.

Implications for copper-catalyzed azide–alkyne cycloaddition (CuAAC)

The copper-catalyzed azide–alkyne cycloaddition (CuAAC) is the method of choice for the synthesis of 1,4-disubstituted 1,2,3-triazoles and is known to proceed under mild conditions (*e.g.* in water at ambient temperature).⁴⁷ Since its first appearance in the literature in 2002,⁴⁸ it has had a huge impact in all fields of synthetic chemistry. Notably, a variety of applications in the drug design and medicinal chemistry including fast compound library generation, bioconjugation, or bioisosteric replacements has been developed in the last decade.

The effects of the constitutional isomerism on triazole formation were investigated for pyridine compounds,^{17,23,25} quinazoline derivatives,⁴⁹ as well as azidopurines.^{18,24,35,36,50} Furthermore, in a computational study the effect of copper(I) species (in this case CuCl) on the azido–tetrazole equilibrium in pyridine and imidazole test systems was investigated.⁵¹ Depending on the scaffold, the coordination of the transition metal can have a stabilizing effect not only on the tetrazole isomer (pyridine) but also on the azide form (imidazole). Hence, a possible shift of the equilibrium under CuAAC con-

ditions in the pyrimidine system described herein cannot be excluded.

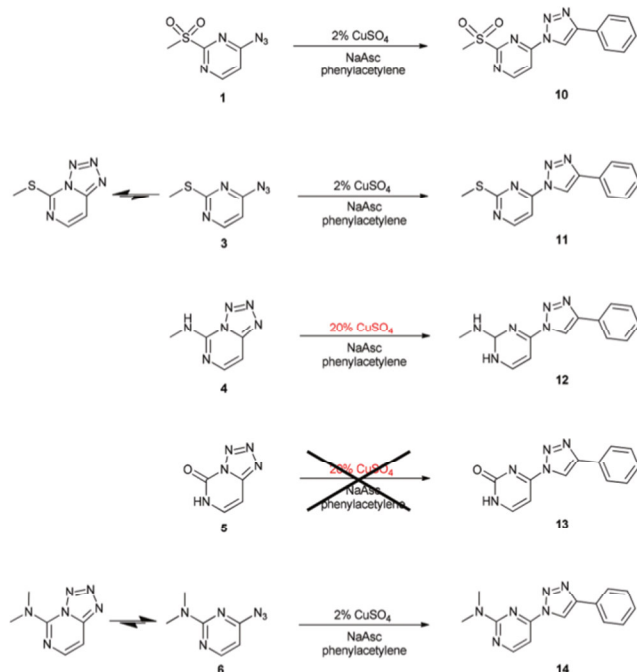
These results demonstrated that tetrazole formation has a detrimental effect on the yield of this reaction type. For pyrimidines, especially 2-azidopyrimidines, the impact of the tautomerization on CuAAC has not been investigated, yet. Only a few reports about the transformation of 2-azidopyrimidines¹⁹ and 4-azidopyrimidines^{20–22} into the corresponding triazoles have been published to date. However, in the aforementioned studies usage of Huisgen conditions (high temperature, no catalyst) resulting in a mixture of 1,4- and 1,5-disubstituted regioisomers (for terminal alkynes) or trisubstituted triazoles (for internal alkynes) is described. To address the impact of heat on the equilibrium, we conducted a temperature gradient ¹H-NMR experiment and observed a shift from tetrazole to the azide species for compound **3** (ESI section II.f†) upon raising temperature. This is in accordance with the literature as the azide is described to be the high-temperature species.⁹ Hence, Huisgen conditions intrinsically favor the open form directly facilitating thermal AAC. As ambient temperature is applicable for routine CuAAC reactions, we expected that the impact of the tautomerism and the state of the equilibrium would be more pronounced under these mild conditions. It has been reported that electronic as well as steric features of substituents at the azide group may influence the reaction rate of the CuAAC reaction.⁵² We were curious to know how our “stabilized” azide (compound **1**), the equilibrium state (compound **3**) and the “stabilized” tetrazole (compounds **4** and **5**) behave in the click reaction. Therefore, we used phenylacetylene, CuSO₄·5H₂O, and sodium ascorbate in *tert*BuOH:water (1:1) as a model system and monitored the reactions *via* LC-MS analysis.

Sulfone-containing compound **1**, although being fully shifted towards the azide, gave lower isolated yield than its thiomethyl analogue **3**. A possible explanation might be the different electronic properties of both groups which could influence the azide reactivity (*vide supra*). Whether the azide group of **3** is more activated or not, it seems that as long as there is the open species present in a significant amount, the CuAAC reaction proceeds (Scheme 3, Table 3).

To corroborate these results, we employed **6** in the same reaction. Analogous to **1** and **3**, compound **6**, mainly existing as azide, was directly convertible to triazole product **14** (Table 3, Scheme 3, ESI section I.a†) using a 2% copper(I) catalyst.

For the stabilized tetrazoles **4** and **5** no product was found in our LC-MS analysis. Hence, tetrazole formation suppressed the CuAAC reaction under the used conditions. To increase the reaction speed and yield, we increased the amount of copper(I) catalyst by a factor of ten (Scheme 3, Table 3).

Indeed, we were able to obtain triazole compound **12** using aminomethyl **4** as an adduct. Interestingly, derivative **5** did not react even under these conditions indicating that tetrazole formation successfully abolished CuAAC reactivity of this compound (Scheme 3, Table 3). Nevertheless, access to the carbonyl-derivative decorated with a triazole at the 4-position



Scheme 3 Model CuACC reaction for the synthesis of triazoles **10–14**, employing phenylacetylene, CuSO_4 and sodium ascorbate (NaAsc). Compounds **1**, **3** and **6** readily undergo the reaction while compound **4** only reacts upon high catalyst load. Compound **5** remained “unclickable” under the applied conditions.

Table 3 Isolated yields of model CuACC reactions for the synthesis of triazoles **10–15** employing phenylacetylene, CuSO_4 and sodium ascorbate. Compounds **1**, **3** and **6** readily undergo the reaction while compound **4** only reacts upon high catalyst load. Compound **5** remained “unclickable” under the applied conditions

Compound	2% ^a	20% ^a
1	55%	—
3	81%	—
4	0%	51%
5	0%	0%
6	68%	—

^a mol% of $\text{CuSO}_4 \cdot 5\text{H}_2\text{O}$.

could be gained through treatment of **10** with sodium hydroxide in a dioxane/water mixture to transform the sulfomethyl group into the mentioned carbonyl compound.

Implications for strain-promoted azide–alkyne cycloaddition (SPAAC)

Strain-promoted azide–alkyne cycloaddition has drawn enormous attention of the biological and chemical community because of its ability to be directly used in cellular systems⁵³ without the need of cytotoxic copper or ruthenium catalysts.

It was described that acidic conditions lead to a ring opening of the tetrazole shifting the equilibrium towards the azide.^{9,12} To investigate the effect of acidic, basic, and neutral

conditions on our stabilized tetrazoles we chose compounds **4** and **5** to determine the equilibrium under the influence of TFA and sodium hydroxide. Under neutral and basic conditions, the compound remained in its tetrazole form. It is noteworthy that under harsh basic conditions (1 M NaOH) an additional minor signal set occurred that was due to compound degradation (ESI section II.c†). As expected, signals of **4** shifted under acidic treatment indicating a ring opening and formation of the azide. This was confirmed by the appearance of the characteristic band in the IR spectrum for the hydrochloric salt of **4** (Fig. 2A, ESI section II.g†).

Interestingly, **5** was not convertible to the azide through TFA treatment. Under neutral and acidic conditions only NMR signals assigned to the tetrazole form were detected (Fig. 2B).

Motivated by these results, we used compounds **4**, **5**, and **3** in a pH-dependent SPAAC reaction with dibenzocyclooctyneamine to see whether the pH sensitivity of the equilibrium

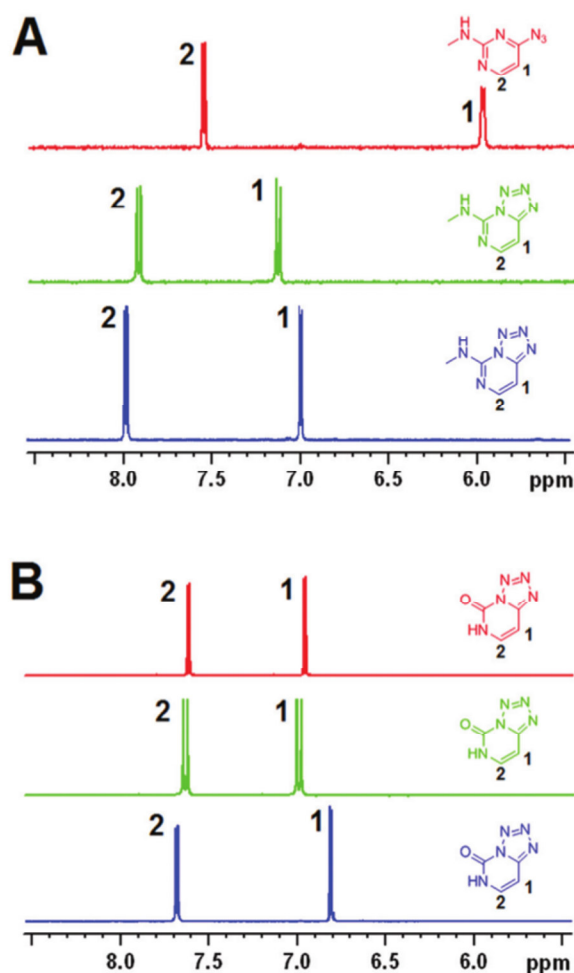
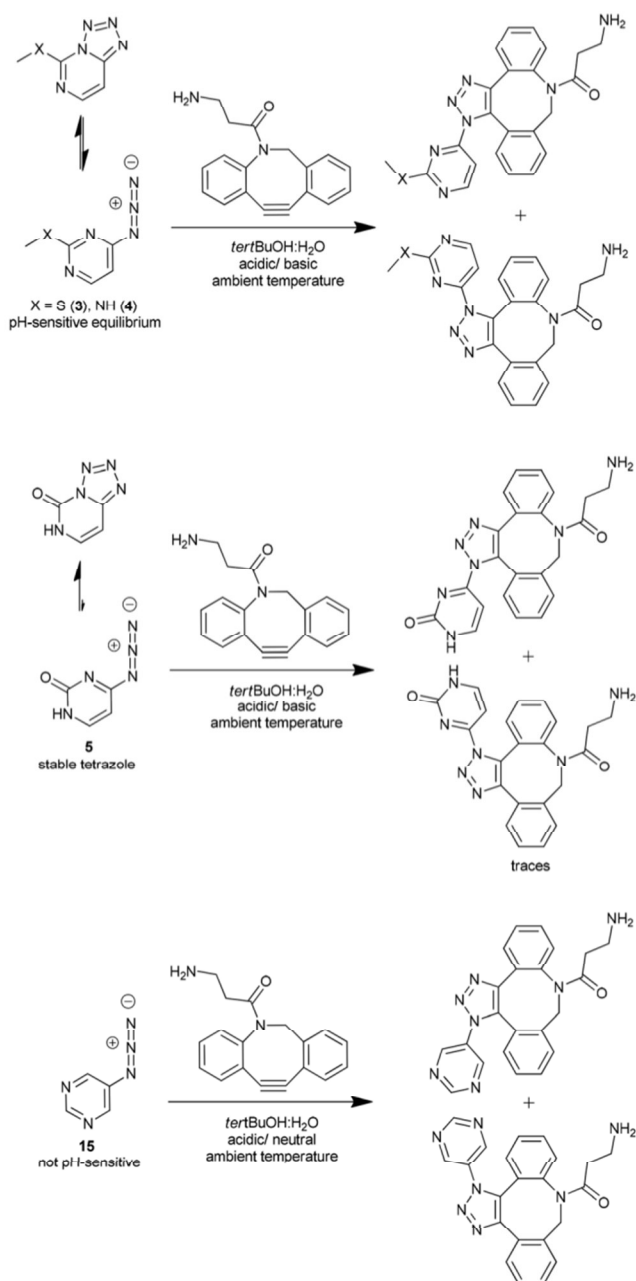


Fig. 2 pH dependency of the azido–tetrazole equilibrium of compounds **4** (A, green spectrum D_2O , red spectrum D_2O + TFA, blue spectrum D_2O + NaOH) and **5** (B, green spectrum D_2O , red spectrum D_2O + TFA, blue spectrum: D_2O + NaOH) monitored by ^1H -NMR. Results indicate a tetrazole ring opening under acidic treatment of **4** whereas **5** remains as the tetrazole isomer.

effects reactivity (Scheme 4). As expected, **3** reacted under all conditions with the SPAAC reagent but with a significantly higher reaction rate in the acidic environment (Table 4, ESI section I.h†).

As suggested by the $^1\text{H-NMR}$ results, compound **4** readily reacted in 0.1 M HCl or 0.2% TFA but was almost unreactive under neutral or basic conditions (0.1 M NaOH) as indicated by LC-MS experiments. Moreover, stronger acidic conditions (0.1 M HCl) resulted in a higher reaction rate compared to the less acidic one (0.2% TFA), suggesting a clear pH dependency



Scheme 4 SPAAC of pH-sensitive 4-azidopyrimidines **3**, **4**, **5** and pH-non-sensitive 5-azidopyrimidine (**15**) and dibenzylcyclooctyne-amine under varying pH environments in aqueous media.

Table 4 LC-MS conversions of model pH dependent SPAAC reactions employing dibenzylcyclooctyneamine with **3**, **4** and **5** after 1.5 hours of the reaction time in 0.1 M HCl, 0.2% TFA and 0.1 M NaOH in *tert*BuOH : water (1 : 1). **4** showed increased click-reactivity upon decreasing pH whereas pure azide **15** was equally reactive at pH 1.4 and 7.0 after 3 hours at ambient temperature

Cmpd	HCl _{aq} 0.1 M	TFA _{aq} 0.2%	NaOH _{aq} 0.1 M	pH 7.0 ^d	pH 4.1 ^b	pH 2.5 ^c	pH 1.4 ^d
3	32%	28%	4%	—	—	—	—
4	51%	23%	1%	—	3%	8%	36%
5	<1%	<1%	<1%	—	—	—	—
15	—	—	—	77%	—	—	77%

^a Aqueous phosphate buffer + *tert*BuOH (1 : 1). ^b Aqueous acetate buffer + *tert*BuOH (1 : 1). ^c 0.01 M HCl_{aq} (*tert*BuOH : H₂O, 1 : 1). ^d 0.1 M HCl_{aq} (*tert*BuOH : H₂O, 1 : 1), conversions were monitored by LC-UV₂₅₄-MS.

of the reactivity (ESI section I.h†). To confirm this hypothesis, we monitored the reaction of compound **4** and dibenzylcyclooctyne-amine under different acidic pH conditions (Fig. 3, Table 4). These results clearly demonstrate the pH-dependent acceleration of the reaction when shifting the milieu towards higher acidity. Finally, compound **5** was only able to undergo SPAAC in traces in the acidic or neutral environment but remained unreacted under basic conditions (ESI section I.h†). However, differences in conversion could potentially also arise from a protonation leading to altered reactivity of the azide-group. To evaluate whether low pH has a direct effect on azide reactivity we synthesized 5-azidopyrimidine (**15**, Scheme 4, ESI section I.a†). Compound **15** is not able to form a tetrazole and was used in a SPAAC reaction with dibenzylcyclooctyne-amine at pH 1.4 and pH 7.0 (Table 4, ESI section I.i†). For these two environments no difference in product formation over time and the total conversion after 3 hours was found. Hence, a direct influence of acidic pH on azide reactivity, *e.g.* via protonation of the pyrimidine core, can be excluded in this case.

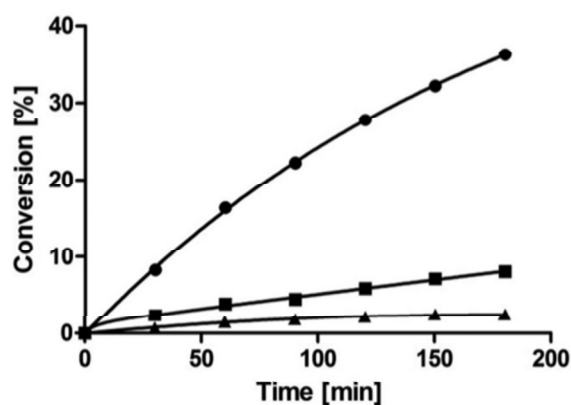


Fig. 3 Kinetic analysis of the SPAAC of compound **4** and dibenzylcyclooctyne-amine at pH 1.5 (●), 2.5 (■) and 4.1 (▲) at room temperature. Conversion was monitored by LC-UV₂₅₄ and products were identified by mass spectrometry.

Moreover, these results indicate that the improved reactivity of **4** at low pH mainly depends on tetrazole ring opening. These results are in good accordance with our data on the “unclickability” of compound **5** in CuAAC reactions (Table 3). More importantly, our results gathered for compound **4** hint at the possibility to exploit this tautomerism effect as a pH-dependent atom-economical protection method for the azide group. This would allow us to regioselectively address different azides within the same molecule simply by reversibly capping one of them as a tetrazole *via* simple pH adjustments. In light of the fact that CuAAC reactions are routinely carried out in the presence of a tertiary amino base (e.g. Hünig's base)⁵⁴ a regioselective sequence of CuAAC and SPAAC might be achieved.

Implications for fragment-based drug design (FBDD)

FBDD has attracted huge attention in the past decade.⁵⁵ The advantages of fragments lie in their low molecular weight and the possibility to generate high structural diversity by the use of rather small libraries. In general, all ligands need to overcome the translational and rotational rigid body entropy barrier⁵⁶ to attractively interact with a protein target. As fragment-like compounds possess only a few pharmacophore features due to their small size, they are supposed to display near optimal binding modes to be able to overcompensate the entropy term of the freely diffusing solute. As a result, fragment-sized binders usually display high ligand efficiencies, a metric used to evaluate inhibitors with regard to their molecular weight.⁵⁷ This, in combination with favorable physicochemical properties, renders such fragment hits as ideal starting points for further drug development.⁵⁸ Several molecular parameters have been defined as guideposts for the straightforward design of fragment libraries and are usually referred to as the Astex ‘rule of 3’.⁵⁹

With these concepts in mind, we hypothesized that our substituent-stabilized tetrazolopyrimidines might be suitable candidates for FBDD. It is noteworthy that such molecular scaffolds can be found as substructures in pharmaceutically relevant entities^{26,28} and they share some similarity with purine nucleobases present in many biologically active compounds. Coenzyme A (CoA), for example, is a molecule which incorporates an adenosyl moiety and is involved in many cellular processes.⁶⁰ It is employed by nature as an acyl carrier to provide thioester-activated substrates for a large variety of enzymes. One acetylase that is in the focus of our research and uses such CoA-linked structures is called PqsD.^{61,62} It is a bacterial signal molecule synthase found in the opportunistic human pathogen *Pseudomonas aeruginosa*. PqsD is essential for the production of the so-called *Pseudomonas* Quinolone Signal (PQS).⁶² This autoinducer is the eponymous molecule driving the PQS quorum sensing (QS) system – a cell-to-cell communication apparatus regulating pathogenicity-determining factors of *P. aeruginosa*. In this regard, we have shown before that blocking PqsD by small molecule inhibitors leads to reduction of biofilm formation rendering this enzyme a potential novel target for anti-infective agents.⁶¹ Both substrates of this enzyme, anthraniloyl-CoA and malonyl-CoA,

carry the adenosyl moiety.⁶² Guided by the above-mentioned rationale that our fragments have a high degree of similarity towards this residue (Fig. 4, Scheme 1), we assumed that these compounds may bind to PqsD and could potentially inhibit the enzyme reaction. Indeed, two of our tetrazole fragments (**5** and **9**) displayed IC₅₀ values in the lower micromolar range resulting in high ligand efficiencies (Fig. 4B and C). The optimal starting point for FBDD is a LE score of at least 0.3^{58,64} whereas our fragments possess LE's which are at least two-fold higher than this proposed mark (Fig. 4B and C).

A comparison of the IC₅₀s of **5** and **9** (Fig. 4B and C) revealed the carbonyl to be slightly advantageous for activity. Having in mind our working hypothesis that the fragments might occupy the adenosyl site at the surface of PqsD, we modeled the fragments into that pocket using the X-ray cocrystal structure of PqsD and anthraniloyl-CoA (PDB-ID: 3H77).

The modeling results suggest that the carbonyl and thionyl moieties of **5** and **9** form a hydrogen bond with N154 (Fig. 4). This interaction might be weaker for the thionyl pendant **9** which is known to be a less potent hydrogen bond acceptor.⁶⁵ Additionally, the protonated nitrogen of the pyrimidine core may act as a hydrogen bond donor to T28 (Fig. 4B and C). With regard to acidic characteristics of **5** and **9** it is also plausible that the compounds are deprotonated at the nitrogen in the 6-position and, hence, could interact as hydrogen bond acceptors for the side chain of T28 like the adenosyl moiety in the crystal structure. Moreover, the electron-enriched tetrazolopyrimidines could form stronger pi interactions with R153 and

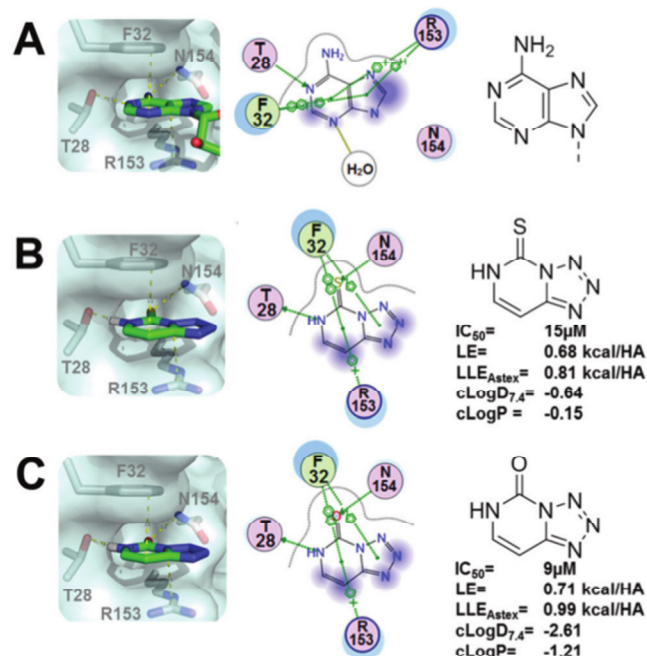


Fig. 4 cLogD_{7.4}, cLogP, IC₅₀s, ligand efficiency indices and predicted interactions of **9** (B) and **5** (C) in comparison with the natural substrate anthraniloyl-CoA (A) in the adenosyl-pocket of PqsD (PDB-ID: 3H77). Both LE⁶³ and LLE_{Astex} were calculated based on IC₅₀s. HA = heavy atom count.

F32. To derive further SAR (structure–activity relationship) information regarding the structural prerequisites for activity we also tested hypoxanthine and adenine for PqsD inhibition. Although being quite similar to **5** and **9**, hypoxanthine showed only 9% enzyme inhibition at 50 μM while adenine was inactive at this concentration (see the ESI section I.†). These findings underline the values of **5** and **9** as fragment-inhibitors of PqsD, but also shed light on the tight SAR at the tetrazolo substructure which demonstrates higher potency than the tested imidazolo congeners.

It is well known that during a drug optimization campaign compounds tend to become larger and more lipophilic.⁶⁶

Therefore, it is of great importance to start from a core molecule with low $\text{cLog } P$ and $\text{cLog } D_{7,4}$ values. As lipophilicity is of great importance for solubility and passive diffusion over the plasma cellular membrane a new metric has been introduced: ligand lipophilicity efficiency (LLE).⁶⁷ This metric evaluates compounds not only on their activity and molecular weight but also on their lipophilicity. Notably, our fragments perform even better with regard to this novel efficiency index than in the traditional ligand efficiency rating (Fig. 4B and C).

Accordingly, both metrics suggest that these fragment inhibitors could be ideal starting points for further FBDD efforts towards novel drug-like inhibitors of PqsD and, hence, potential anti-biofilm agents.

Conclusions

In summary, the data presented in this paper provides the basis for a rational approach towards steering the azido–tetrazole equilibrium within 4-azidopyrimidines. By choice of the substituent at the 2-position either the azide or the tetrazole isomer can be efficiently stabilized. These findings provided insights into substituent effects like the electronic and steric parameters influencing this phenomenon. This information was used to evaluate azide-based compounds which are readily “clickable”, “poorly clickable” and “unclickable” in a model copper-catalyzed click reaction. In additional experiments, we demonstrated a pH-dependent protecting group characteristic of the acid-sensitive tetrazole in SPAAC reactions. These results may motivate the application of azidopyrimidine moieties for the regio-control of multi-step AAC reactions. Such a strategy could be exploited for the facile generation of heterovalent bioconjugates or may pave the way towards pH-selective labeling in acidic cellular environments like lysosomes⁶⁸ as well as cancerous⁶⁹ or inflammatory tissue⁷⁰ via bioorthogonal click chemistry.

Despite the limitations of the applied solvent model in our DFT calculations general trends could be described quite well and experimental data for further optimization of these models towards better predictive power were provided. Finally, the analytical results were used for a FBDD approach towards inhibitors of PqsD, a reported anti-biofilm target. The usefulness of these fragments as potential analogues of adenosyl motifs has been demonstrated and may lead to further fragment-based drug development campaigns.

Acknowledgements

We like to thank Michael Hoffmann for recording HRMS spectra, Giuseppe Allegretta for the determination of the $\text{p}K_{\text{a}}$ of compounds **5** and **9**, and Volker Huch for recording the X-ray crystal structures of compounds **3**, **4** and **5**. This project was funded by BMBF through grant 1616038B.

References

- (a) S. Fujii, T. Kobayashi, A. Nakatsu, H. Miyazawa and H. Kagechika, *Chem. Pharm. Bull.*, 2014, **62**, 700–708; (b) A. McCluskey, P. A. Keller, J. Morgan and J. Garner, *Org. Biomol. Chem.*, 2003, **1**, 3353; (c) P. B. Mohite, R. B. Pandhare and S. G. Khanage, *Biointerface Res. Appl. Chem.*, 2012, **2**, 258–263; (d) T. Nagata, K. Masuda, S. Maeno and I. Miura, *Pest Manage. Sci.*, 2004, **60**, 399–407.
- (a) D. Meyer, M. A. Taige, A. Zeller, K. Hohlfeld, S. Ahrens and T. Strassner, *Organometallics*, 2009, **28**, 2142–2149; (b) G.-L. Wu, S.-L. Cao, J. Chen and Z. Chen, *Eur. J. Org. Chem.*, 2012, 6777–6784; (c) J. L. Schuchardt and L. Jonathan, *Patent WO*, 02/098931 A1, 2002.
- (a) T. D. Nixon, A. J. Gamble, R. J. Thatcher, A. C. Whitwood and J. M. Lynam, *Inorg. Chim. Acta*, 2012, **380**, 252–260; (b) S. Roy, T. N. Mandal, A. K. Barik, S. Pal, S. Gupta, A. Hazra, R. J. Butcher, A. D. Hunter, M. Zeller and S. K. Kar, *Polyhedron*, 2007, **26**, 2603–2611; (c) A. Rodríguez, A. Sousa-Pedrares, J. A. García-Vázquez, J. Romero and A. Sousa, *Polyhedron*, 2009, **28**, 2240–2248.
- (a) S. S. Gunathilake, H. D. Magurudeniya, P. Huang, H. Nguyen, E. A. Rainbolt, M. C. Stefan and M. C. Biewer, *Polym. Chem.*, 2013, **4**, 5216; (b) A. Slaczka and J. Lubczak, *Polimery*, 2010, **55**, 681–684; (c) A. Gallego, O. Castillo, C. J. Gómez-García, F. Zamora and S. Delgado, *Inorg. Chem.*, 2012, **51**, 718–727.
- (a) C. Besanceney-Webler, H. Jiang, T. Zheng, L. Feng, D. S. del Amo, W. Wang, L. M. Klivansky, F. L. Marlow, Y. Liu and P. Wu, *Angew. Chem., Int. Ed.*, 2011, **50**, 8051–8056; (b) P. Shieh, M. S. Siegrist, A. J. Cullen and C. R. Bertozzi, *Proc. Natl. Acad. Sci. U. S. A.*, 2014, **111**, 5456–5461.
- (a) L. Billiet, X. K. Hillewaere, Du Prez and E. Filip, *Eur. Polym. J.*, 2012, **48**, 2085–2096; (b) S. K. Reshmi, K. P. Vijayalakshmi, D. Thomas, E. Arunan and C. P. Reghunadhan Nair, *Propellants, Explos., Pyrotech.*, 2013, **38**, 525–532; (c) H.-k. Li, J.-z. Sun, A.-j. Qin and B. Z. Tang, *Chin. J. Polym. Sci.*, 2012, **30**, 1–15.
- P. Thirumurugan, D. Matosiuk and K. Jozwiak, *Chem. Rev.*, 2013, **113**, 4905–4979.
- C. Wentrup, *Tetrahedron*, 1970, **26**, 4969–4983.
- A. Könnecke, R. Dörre, E. Kleinpeter and E. Lippmann, *Tetrahedron*, 1979, **35**, 1957–1963.
- W. E. Hull, M. Künstlinger and E. Breitmaier, *Angew. Chem., Int. Ed. Engl.*, 1980, **19**, 924–926.

- 11 C. Temple and J. A. Montgomery, *J. Org. Chem.*, 1965, **30**, 826–829.
- 12 S. L. Deev, Z. O. Shenkarev, T. S. Shestakova, O. N. Chupakhin, V. L. Rusinov and A. S. Arseniev, *J. Org. Chem.*, 2010, **75**, 8487–8497.
- 13 C. Thétaz, F. W. Wehrli and C. Wentrup, *Helv. Chim. Acta*, 1976, **59**, 259–264.
- 14 I. A. Khalymbadzha, T. S. Shestakova, S. L. Deev, V. L. Rusinov, O. N. Chupakhin, Z. O. Shenkarev and A. S. Arseniev, *Russ. Chem. Bull.*, 2013, **62**, 521–528.
- 15 C. Temple, M. C. Thorpe, W. C. Coburn and J. A. Montgomery, *J. Org. Chem.*, 1966, **31**, 935–938.
- 16 J. A. Montgomery, K. Hewson, S. J. Clayton and H. J. Thomas, *J. Org. Chem.*, 1966, **31**, 2202–2210.
- 17 Q. Zhang, X. Wang, C. Cheng, R. Zhu, N. Liu and Y. Hu, *Org. Biomol. Chem.*, 2012, **10**, 2847–2854.
- 18 M. K. Lakshman, M. K. Singh, D. Parrish, R. Balachandran and B. W. Day, *J. Org. Chem.*, 2010, **75**, 2461–2473.
- 19 E. R. El-Sawy, M. S. Ebaid, H. M. Abo-Salem, A. G. Al-Sehemi and A. H. Mandour, *Arabian J. Chem.*, 2014, **7**, 914–923.
- 20 V. P. Krivopalov, E. B. Nikolaenkova, V. F. Sedova and V. P. Mamaev, *Chem. Heterocycl. Compd.*, 1983, **19**, 1116–1120.
- 21 V. P. Krivopalov, E. B. Nikolaenkova, V. F. Sedova and V. P. Mamaev, *Chem. Heterocycl. Compd.*, 1983, **19**, 977–981.
- 22 R. Huisgen, K. v. Fraunberg and H. J. Sturm, *Tetrahedron Lett.*, 1969, **10**, 2589–2594.
- 23 R. Sun, H. Wang, J. Hu, J. Zhao and H. Zhang, *Org. Biomol. Chem.*, 2014, **12**, 5954–5963.
- 24 L. Cosyn, K. K. Palaniappan, S.-K. Kim, H. T. Duong, Z.-G. Gao, K. A. Jacobson and S. van Calenbergh, *J. Med. Chem.*, 2006, **49**, 7373–7383.
- 25 B. Chattopadhyay, C. I. Rivera Vera, S. Chuprakov and V. Gevorgyan, *Org. Lett.*, 2010, **12**, 2166–2169.
- 26 A. M. Alanazi, A. A.-M. Abdel-Aziz, I. A. Al-Suwaidan, S. G. Abdel-Hamide, T. Z. Shower and A. S. El-Azab, *Eur. J. Med. Chem.*, 2014, **79**, 446–454.
- 27 (a) M. M. Ghorab, M. S. Alsaïd, M. Ceruso, Y. M. Nissan and C. T. Supuran, *Bioorg. Med. Chem.*, 2014, **22**, 3684–3695; (b) F. I. Hanafy, *Eur. J. Chem.*, 2011, **2**, 65–69; (c) M. S. Mohamed, M. M. Youns and N. M. Ahmed, *Eur. J. Med. Chem.*, 2013, **69**, 591–600; (d) S.-B. Wang, X.-Q. Deng, D.-C. Liu, H.-J. Zhang and Z.-S. Quan, *Med. Chem. Res.*, 2014, **23**, 4619–4626.
- 28 C. de Graaf, A. J. Kooistra, H. F. Vischer, V. Katritch, M. Kuijter, M. Shiroishi, S. Iwata, T. Shimamura, R. C. Stevens, I. J. P. de Esch and R. Leurs, *J. Med. Chem.*, 2011, **54**, 8195–8206.
- 29 W. A. Zordok, *IJAST*, 2012, **2**, 339–357.
- 30 M. Kanyalkar and E. C. Coutinho, *Tetrahedron*, 2000, **56**, 8775–8777.
- 31 M. Monajjemi, H. Bahareh and M. Hadieh, *J. Mex. Chem. Soc.*, 2006, **50**, 143–148.
- 32 A. Klamt and G. Schüürmann, *J. Chem. Soc., Perkin Trans. 2*, 1993, 799.
- 33 V. P. Krivopalov, V. I. Mamatyuk and E. B. Nikolaenkova, *Russ. Chem. Bull.*, 1995, **44**, 1435–1443.
- 34 (a) A. Thomann, C. Börger, M. Empting and R. Hartmann, *Synlett*, 2014, 935–938; (b) E. Weidel, M. Negri, M. Empting, S. Hinsberger and R. W. Hartmann, *Future Med. Chem.*, 2014, **6**, 2057–2072.
- 35 T. Wada, A. Mochizuki, S. Higashiya, H. Tsuruoka, S.-i. Kawahara, M. Ishikawa and M. Sekine, *Tetrahedron Lett.*, 2001, **42**, 9215–9219.
- 36 A. Masternak, B. Skalski and J. Milecki, *J. Labelled Compd. Radiopharm.*, 2007, **50**, 43–46.
- 37 M. Empting, O. Avrutina, R. Meusinger, S. Fabritz, M. Reinwarth, M. Biesalski, S. Voigt, G. Buntkowsky and H. Kolmar, *Angew. Chem., Int. Ed.*, 2011, **50**, 5207–5211.
- 38 V. Y. Pochinok, L. F. Avramenko, P. S. Grigorenko and V. N. Skopenko, *Russ. Chem. Rev.*, 1975, **44**, 481–492.
- 39 C. Hansch, A. Leo and R. W. Taft, *Chem. Rev.*, 1991, **91**, 165–195.
- 40 A. Jansma, Q. Zhang, B. Li, Q. Ding, T. Uno, B. Bursulaya, Y. Liu, P. Furet, N. S. Gray and B. H. Geierstanger, *J. Med. Chem.*, 2007, **50**, 5875–5877.
- 41 J. J. Fox, D. van Praag, I. Wempen, I. L. Doerr, L. Cheong, J. E. Knoll, M. L. Eidinoff, A. Bendich and G. B. Brown, *J. Am. Chem. Soc.*, 1959, **81**, 178–187.
- 42 D. J. Brown, *Nature*, 1950, **165**, 1010.
- 43 *Computational medicinal chemistry for drug discovery*, ed. P. Bultinck, H. de Winter, W. Langenaeker and J. P. Tollenaere, Marcel Dekker, New York, 2004.
- 44 S. Grimme, M. Steinmetz and M. Korth, *J. Org. Chem.*, 2007, **72**, 2118–2126.
- 45 S. N. Pieniazek, F. R. Clemente and K. N. Houk, *Angew. Chem., Int. Ed.*, 2008, **47**, 7746–7749.
- 46 J. W. Gibbs, *Elementary principles in statistical mechanics. Developed with especial reference to the rational foundation of thermodynamics*, Ox Bow Press, Woodbridge, Conn., 1981.
- 47 H. C. Kolb, M. G. Finn and K. B. Sharpless, *Angew. Chem., Int. Ed.*, 2001, **40**, 2004–2021.
- 48 (a) V. V. Rostovtsev, L. G. Green, V. V. Fokin and K. B. Sharpless, *Angew. Chem., Int. Ed.*, 2002, **41**, 2596–2599; (b) C. W. Tornøe, C. Christensen and M. Meldal, *J. Org. Chem.*, 2002, **67**, 3057–3064.
- 49 A. Kalniņa, Ē. Bizdēna, G. Kiselovs, A. Mishnev and M. Turks, *Chem. Heterocycl. Compd.*, 2014, **49**, 1667–1673.
- 50 A. Kovalovs, I. Novosjolova, Ē. Bizdēna, I. Bižāne, L. Skardziute, K. Kazlauskas, S. Jursenas and M. Turks, *Tetrahedron Lett.*, 2013, **54**, 850–853.
- 51 F. Blanco, I. Alkorta and J. Elguero, *Tetrahedron*, 2011, **67**, 8724–8730.
- 52 P. L. Golas, N. V. Tsarevsky and K. Matyjaszewski, *Macromol. Rapid Commun.*, 2008, **29**, 1167–1171.
- 53 E. M. Sletten and C. R. Bertozzi, *Angew. Chem., Int. Ed.*, 2009, **48**, 6974–6998.
- 54 H. Fittler, O. Avrutina, B. Glotzbach, M. Empting and H. Kolmar, *Org. Biomol. Chem.*, 2013, **11**, 1848–1857.
- 55 D. E. Scott, A. G. Coyne, S. A. Hudson and C. Abell, *Biochemistry*, 2012, **51**, 4990–5003.
- 56 C. W. Murray and M. L. Verdonk, *J. Comput. Aided Mol. Des.*, 2002, **16**, 741–753.

- 57 A. L. Hopkins, C. R. Groom and A. Alex, *Drug Discovery Today*, 2004, **9**, 430–431.
- 58 C. Abad-Zapatero, *Expert Opin. Drug Discovery*, 2007, **2**, 469–488.
- 59 M. Congreve, R. Carr, C. Murray and H. Jhoti, *Drug Discovery Today*, 2003, **8**, 876–877.
- 60 R. Leonardi, Y.-M. Zhang, C. O. Rock and S. Jackowski, *Prog. Lipid Res.*, 2005, **44**, 125–153.
- 61 M. P. Storz, C. K. Maurer, C. Zimmer, N. Wagner, C. Brengel, C. J. de Jong, S. Lucas, M. Müsken, S. Häussler, A. Steinbach and R. W. Hartmann, *J. Am. Chem. Soc.*, 2012, **134**, 16143–16146.
- 62 C. E. Dulcey, V. Dekimpe, D.-A. Fauvelle, S. Milot, M.-C. Groleau, N. Doucet, L. G. Rahme, F. Lépine and E. Déziel, *Chem. Biol.*, 2013, **20**, 1481–1491.
- 63 M. D. Shultz, *Bioorg. Med. Chem. Lett.*, 2013, **23**, 5980–5991.
- 64 S. Schultes, C. de Graaf, E. E. Haaksma, I. J. P. de Esch, R. L. Leurs and O. Krämer, *Drug Discovery Today*, 2010, **7**, e147–e202.
- 65 F. H. Allen, C. M. Bird, R. S. Rowland and P. R. Raithby, *Acta Crystallogr., Sect. B: Struct. Sci.*, 1997, **53**, 696–701.
- 66 A. L. Hopkins, G. M. Keserü, P. D. Leeson, D. C. Rees and C. H. Reynolds, *Nat. Rev. Drug Discovery*, 2014, **13**, 105–121.
- 67 P. N. Mortenson and C. W. Murray, *J. Comput. Aided Mol. Des.*, 2011, **25**, 663–667.
- 68 J. A. Mindell, *Annu. Rev. Physiol.*, 2012, **74**, 69–86.
- 69 Y. Kato, S. Ozawa, C. Miyamoto, Y. Maehata, A. Suzuki, T. Maeda and Y. Baba, *Cancer Cell Int.*, 2013, **13**, 89.
- 70 D. E. Becker and K. L. Reed, *Anesth. Prog.*, 2006, **53**, 98–109.

3 Results

3.3 Mild and Catalyst-free Microwave-assisted Synthesis of 4,6-Disubstituted 2-Methylthiopyrimidines – Exploiting Tetrazole as an Efficient Leaving Group

Andreas Thomann, Jens Eberhard, Giuseppe Allegretta, Martin Empting, and Rolf W. Hartmann

Reprinted with permission from *Synlett*; **2015**; 26, 2606-2610, DOI: 10.1055/s-0035-1560577

Copyright 2015 Georg Thieme Verlag Stuttgart • New York

Publication III

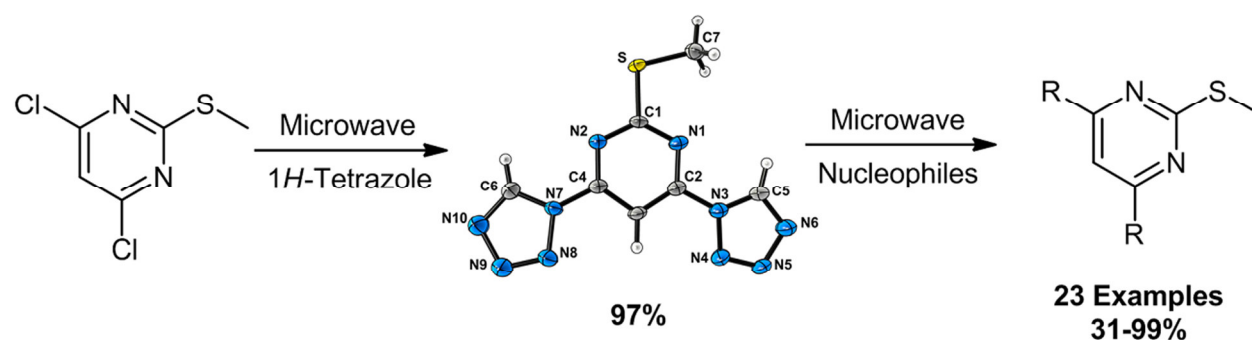


Figure 17. Graphical abstract of publication III.

Mild and Catalyst-Free Microwave-Assisted Synthesis of 4,6-Disubstituted 2-Methylthiopyrimidines – Exploiting Tetrazole as an Efficient Leaving Group

Andreas Thomann^a

Jens Eberhard^a

Giuseppe Allegretta^a

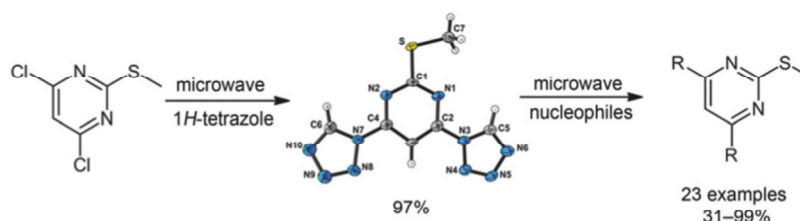
Martin Empting^a

Rolf W. Hartmann^{a,b}

^a Helmholtz-Institute for Pharmaceutical Research Saarland, Saarland University, Campus E8.1, 66123 Saarbrücken, Germany

rolf.hartmann@helmholtz-hzi.de

^b Department of Pharmacy, Pharmaceutical and Medicinal Chemistry, Saarland University, Campus C2.3, 66123 Saarbrücken, Germany



Received: 15.06.2015

Accepted after revision: 03.09.2015

Published online: 21.10.2015

DOI: 10.1055/s-0035-1560577; Art ID: st-2015-b0444-I

Abstract Typically, 4,6-disubstituted 2-thiomethylpyrimidines are synthesized starting from 4,6-dichloro-2-thiomethylpyrimidine or an amino-substituted precursor. However, these reactions take several hours up to days and require multiple steps. Herein, we report a novel, easy, and quick-to-prepare synthetic intermediate, namely 2-(methylthio)-4,6-di(1*H*-tetrazol-1-yl)pyrimidine, for the synthesis of these interesting target compounds. The intermediate can be transformed within minutes into desired substituted pyrimidines under mild conditions with moderate to excellent yields. The reaction can be conducted in an automated microwave system, at room temperature or by conventional heating. Furthermore, we demonstrate the robustness of the method in a one-pot procedure.

Keywords tetrazole, pyrimidine, combinatorial chemistry, medicinal chemistry, nucleophilic aromatic substitution

Tetrazole moieties have drawn increasing attention by medicinal chemists as they can be exploited for the generation of bioactive small molecules.¹ In addition to their desirable physicochemical properties, these azoles display reasonable metabolic stability and can serve as bioisosteric replacements of carboxylic acids.² The family of 4,6-disubstituted pyrimidines and tetrazolyl-substituted pyrimidines is a prominent class of chemical scaffolds for the design of kynurenine-3-monooxygenase inhibitors,^{3,4} c-Kit modulators,⁵ herbicides,⁶ Bmi-1 inhibitors,⁷ kinase inhibitors,^{8–10} cell protective agents,¹¹ antibacterials,^{12–14} inhibitors of NF_κB DNA binding,¹⁵ and corticotropin releasing hormone type 1 antagonists.¹⁶ One well-reported step for the synthesis of these interesting target compounds proceeds via S_NAr reaction conditions employing 4,6-dichloro-2-methylthiopyrimidine as a commercially available starting material. These conditions generally require reaction times between

several hours and days to couple different nucleophiles to the 4- and 6-position of pyrimidine.^{8,10,11,15–17} Interestingly, to directly decorate the pyrimidine core with a tetrazole substituent a novel method can be employed, which has recently been published by us.¹⁸ Unfortunately, the developed protocol using different conditions failed to introduce a tetrazole moiety into the 6-chloro-*N,N*-dimethyl-2-(methylthio)pyrimidin-4-amine scaffold (see Table 1 in Supporting Information). We hypothesized that the electron-donating properties of the dimethylamine substituent in the 6-position drastically reduced the leaving-group properties of the chloro substituent at the 4-position. Consequently, we tried to synthesize 4-chloro-2-(methylthio)-6-(1*H*-tetrazol-1-yl)pyrimidine, but to our surprise the major product was compound **1**, substituted with two tetrazoles. NMR analysis revealed both tetrazoles to be attached in the same regioselectivity to the 2-thiomethylpyrimidine core. However, an unambiguous clarification of the structure was achieved by X-ray crystallography. The structure coordinates of compound **1** revealed that the tetrazole substituents were linked via N1 of the tetrazole scaffold (viz. N3 and N7 in Figure 1) to the 4- and 6-position of 2-thiomethylpyrimidine (C4 and C2 in Figure 1).

Moreover, when applying four equivalents of tetrazole instead of one, the reaction can be completed with almost quantitative yield (97%) within 10 minutes at 60 °C under microwave irradiation.¹⁹ With regard to product yield, we could not determine any differences between thermal heating and microwave conditions (Table 1).

As microwave irradiation ensures a homogeneous and fast energy input, we consider this procedure the method-of-choice for facile and rapid generation of intermediate **1** (Scheme 1).

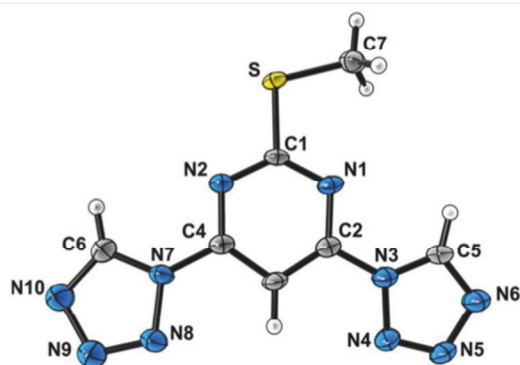
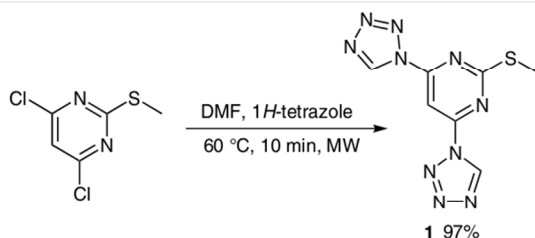


Figure 1 X-ray crystal structure of **1** revealing the regiochemistry of attached tetrazol-1-yl substituents; blue = nitrogen, grey = carbon, yellow = sulfur, white = hydrogen

Table 1 Conditions Used To Obtain 2-(Methylthio)-4,6-di(1*H*-tetrazol-1-yl)pyrimidine (**1**)^a

Method	Conditions	Yield (%)
Heating	DMF, 60 °C, Et ₃ N, 1 <i>H</i> -tetrazole, 10 min	95
Microwave	DMF, 60 °C, Et ₃ N, 1 <i>H</i> -tetrazole, 10 min	97

^a Conditions: 1 equiv of 4,6-dichloro-2-methylthiopyrimidine and 4 equiv of 1*H*-tetrazole were employed.



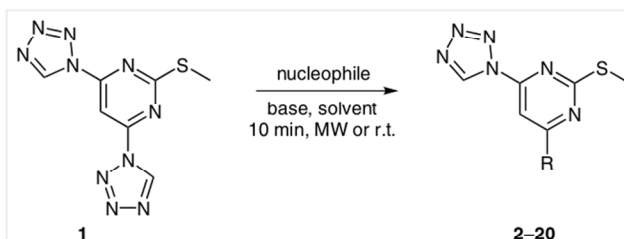
Scheme 1 Reaction conditions to obtain compound **1**

Moreover, to investigate the applicability of our novel synthetic route for automated combinatorial synthesis we performed all reactions in an automated microwave system (Tables 2 and 3).

Inspired by a previously observed side reaction, we tested whether compound **1** could be an appropriate precursor for the synthesis of further 4,6-disubstituted target compounds. Indeed, di-tetrazolyl intermediate **1** could be successfully transformed into compound **2** under microwave irradiation by usage of one equivalent dimethylamine. In addition to the clean conversion, the reaction only needs 10 minutes for completion and, hence, is much faster than traditional approaches.^{8,10,11,15–17} Moreover, due to its acidity,²⁰ the cleaved tetrazole can be directly removed from the reaction mixture by simple aqueous workup, making it a con-

venient leaving group. Thus, this method may be easily implemented in automated combinatorial chemistry approaches.

To test the scope of the reaction, we used different nitrogen-, oxygen-, and sulfur-containing nucleophiles (Scheme 2). For instance, alkyl (**2**, **3**), saturated and unsaturated heterocyclic amines (**6–9**), benzylamine (**5**), and unsubstituted amine (**4**) were successfully attached to the pyrimidine core yielding the substituted pyrimidines in moderate to excellent yields (Table 2) within minutes. Preliminary tests with aromatic amines, such as aniline, showed no conversion and are not suitable to be used in this reaction.



Scheme 2 Generic reaction scheme for the generation of 6-substituted 4-(1*H*-tetrazol-1-yl)-2-thiomethylpyrimidines

The subset of oxygen-containing nucleophiles consisted of methanol, sodium hydroxide, sodium ethoxide, and phenol. With no exception, all hydroxyderivatives readily reacted with **1** to achieve the corresponding 6-substituted 4-(1*H*-tetrazol-1-yl)-2-thiomethylpyrimidines (**10–13**, Table 2). Notably, the methoxy group can be conveniently attached at room temperature under treatment with potassium carbonate in a methanol–THF mixture. 4-Hydroxypyrimidine is known to be a very weak acid ($pK_a = 8.59$).²¹ Thus, we were curious whether **10** also shows acidic character and conducted titration experiments to determine its pK_a . Indeed, **10** showed a pK_a of 3.17 ± 0.05 which is about five orders of magnitude lower than the unsubstituted 4-hydroxypyrimidine. A plausible explanation for the increase in acidity could be the electron-withdrawing properties of the tetrazole and thiomethyl substituent with respective Hammett constants of $\sigma_{meta}^{tetrazole} = 0.52$ and $\sigma_{meta}^{thiomethyl} = 0.15$.²²

To study the reactivity of **1** towards thiols, we used alkylmercaptans, benzylmercaptan, and thiophenols as reactants. All sulfur-containing nucleophiles were successfully introduced into the 2-thiomethylpyrimidine core in good to excellent yields (**13–19**, Table 2).

Notably, these results show that **1** is also able to react with sterically hindered (**15**, **20**), electron-poor (**18**), and electron-rich (**19**) nucleophiles demonstrating that the procedure can be used in automated robotic systems for one-pot combinatorial approaches. Furthermore, this protocol is a convenient approach for the synthesis of 6-substituted 4-(1*H*-tetrazol-1-yl)-2-thiomethylpyrimidines which we

Table 2 Microwave-Assisted Synthesis of 6-Substituted 4-(1*H*-tetrazol-1-yl)-2-thiomethylpyrimidines **2–20**^a

Nucleophile	Product	R	Method	Yield (%)
dimethylamine	2	NMe ₂	DMF, Et ₃ N, 60 °C	66
methylamine	3	NHMe	DMF, Et ₃ N, 60 °C	53
ammonia ^b	4	NH ₂	DMF, Et ₃ N, 60 °C	60
benzylamine	5	NHBn	DMF, Et ₃ N, 60 °C	80
pyrrolidine	6	pyrrolidin-1-yl	DMF, Et ₃ N, 60 °C	88
morpholine	7	morpholin-1-yl	DMF, Et ₃ N, 60 °C	95
piperidine	8	piperidin-1-yl	DMF, Et ₃ N, 60 °C	94
imidazole	9	imidazol-1-yl	DMF, Et ₃ N, 60 °C	63
sodium hydroxide	10	OH	THF, H ₂ O, 60 °C	70
methanol (excess)	11	OMe	THF, K ₂ CO ₃ , r.t.	85
sodium ethoxide	12	OEt	EtOH, r.t.	88
phenol	13	OPh	DMF, Et ₃ N, 60 °C	68
ethylmercaptan	14	SEt	DMF, K ₂ CO ₃ , r.t.	83
<i>tert</i> -butylmercaptan	15	S <i>t</i> -Bu	DMF, K ₂ CO ₃ , r.t.	82
benzylthiol	16	SBn	DMF, K ₂ CO ₃ , r.t.	79
thiophenol	17	SPh	DMF, K ₂ CO ₃ , r.t.	96
4-chlorothiophenol	18	S(4-ClC ₆ H ₄)	DMF, K ₂ CO ₃ , r.t.	99
4-methoxythiophenol	19	S(4-MeOC ₆ H ₄)	DMF, K ₂ CO ₃ , r.t.	84
2-methylthiophenol	20	S(2-MeC ₆ H ₄)	DMF, K ₂ CO ₃ , r.t.	85

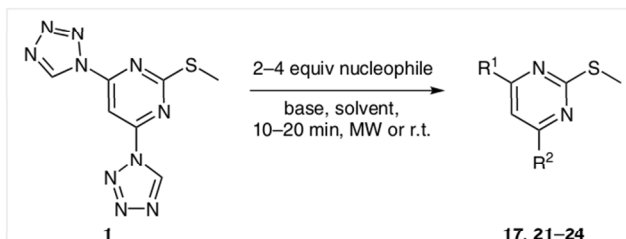
^a Except noted otherwise, a 1:1 stoichiometry of reactant and compound **1** was used. Reactions were carried out under microwave irradiation for 10 min.

^b As a 7 N solution in MeOH.

could not obtain using a substituted chloro-substituted precursor (compare Table 1 and Table 1 in Supporting Information).

To investigate whether both tetrazole substituents can also be replaced in one pot, we used thiophenol, imidazole, and sodium methanolate as representative reactants (Scheme 3, Table 3).

In all three cases, the corresponding 4,6-homo-disubstituted 2-thiomethylpyrimidine compounds (**21–23**) were obtained within 10–20 minutes in near quantitative yields (except **24**, vide supra) which underlines the good leaving-



Scheme 3 Reaction conditions of the one-pot procedure to replace both tetrazole substituents in **1** to obtain 4,6-homo- or 4,6-hetero-disubstituted 2-thiomethylpyrimidines

Table 3 Microwave-Assisted One-Pot Synthesis of 4,6-Disubstituted 2-Thiomethylpyrimidines **17** and **21–24**^a

Nucleophile (equiv)	Product	R ¹	R ²	Method	Yield (%)
thiophenol (1)	17 ^b	1 <i>H</i> -tetrazol-1-yl	SPh	DMF, Et ₃ N, 20 min, 60 °C to r.t., 'one-pot'	83
methanolate (3)	21	MeO	MeO	MeOH, 60 °C	96
thiophenol (2)	22	SPh	SPh	DMF, K ₂ CO ₃ , 10 min, r.t.	95
imidazole (4)	23	imidazol-1-yl	imidazol-1-yl	DMF, Et ₃ N, 20 min, 80–100 °C	99
benzylamine (1) + thiophenol (1)	24	NBn	SPh	DMF, Et ₃ N, K ₂ CO ₃ , 20 min, 60–120 °C	31

^a Compound **1** was used as a starting material unless otherwise noted. In all reactions 1 equiv of starting material was treated with the equivalents of nucleophile indicated in brackets.

^b For compound **17**, 4,6-dichloro-2-thiomethylpyrimidine was employed as starting material.

group properties of the tetrazolyl group (Scheme 3 and Table 3).

To study the robustness and broaden its applicability for combinatorial chemistry and with regard to the good overall yields we investigated if the reaction could also be used as a one-pot sequence to introduce two different substituents using intermediate **1** as starting material. Consequently, we used one equivalent of benzylamine and after 10 minutes of reaction time, we added one equivalent of thiophenol to replace the remaining tetrazole substituent from in situ prepared **5**. The hetero-4,6-disubstituted product **24** was successfully obtained in this one-pot, two-step reaction (Scheme 3 and Table 3).

To demonstrate the applicability for library synthesis and with respect to the excellent yield of **1**, we speculated whether the method could be also exploited for another one-pot procedure which directly starts from the commercially available chlorinated starting material. The idea was to charge the reaction with a nucleophile after **1** was formed in situ and apply 10 additional minutes of microwave irradiation to yield the final product. For this reaction, we chose thiophenol as a model reactant, and as expected, the two-step one-pot sequence showed complete conversion within 20 minutes, and **17** was isolated in high yield (Table 3). These model reactions clearly demonstrate the good leaving-group characteristics of the tetrazole group (fast to replace by nucleophiles and easy to remove from the reaction mixture) for S_NAr reactions at 2-thiomethylpyrimidine cores. By this means, homo- and hetero-disubstituted compounds were easily prepared.

In this study, we have discovered a novel synthetic intermediate **1** for the rapid synthesis of 4,6-disubstituted 2-thiomethylpyrimidines which accepts a broad range of nucleophiles under microwave irradiation. Next to the wide scope of nucleophilic additions, precursor **1** is accessible via the same route in excellent yields and short time, therefore enabling one-pot generation of this ditetrazole intermediate and subsequent coupling of nucleophiles. A further advantage of our protocol is that the reactions can be carried out without the need of highly demanding experimental setups (no inert gas, no reactive reagents, no catalysts) in automated systems, thus making it an ideal candidate for chemical library synthesis of biologically relevant scaffolds. As the 2-position of the pyrimidines synthesized is substituted with thiomethyl moiety, all of the herein displayed compounds can be easily further modified towards the sulfone by simple oxidation using established general methods (i.e., oxone,²³ MCPBA,²⁴ or hydrogen peroxide²⁵). In a subsequent reaction these 2-methylsulfones might then be reacted with various nucleophiles (i.e., amino,²⁶ thio,²⁷ and hydroxyl²⁸ derivatives) allowing access to an even broader chemical diversity.²⁹

Acknowledgment

We thank Michael Hoffmann for recording HRMS spectra and Volker Huch for the determination of the X-ray crystal structure of compound **1**. Many thanks go to Nadja Klippel for synthetic support.

Supporting Information

Supporting information for this article is available online at <http://dx.doi.org/10.1055/s-0035-1560577>.

References and Notes

- (1) (a) Mohite, P. B.; Bhaskar, V. H. *Adv. Pharm. Bull.* **2012**, *2*, 31. (b) Upadhyaya, R. S.; Jain, S.; Sinha, N.; Kishore, N.; Chandra, R.; Arora, S. K. *Eur. J. Med. Chem.* **2004**, *39*, 579.
- (2) (a) Herr, R. *Bioorg. Med. Chem.* **2002**, *10*, 3379. (b) Myznikov, L. V.; Hrabalek, A.; Koldobskii, G. I. *Chem. Heterocycl. Compd.* **2007**, *43*, 1. (c) Ostrovskii, V. A.; Trifonov, R. E.; Popova, E. A. *Russ. Chem. Bull.* **2012**, *61*, 768.
- (3) Dominguez, C.; Toledo-Sherman, L. M.; Winkler, D.; Brookfield, F.; De Aguiar Pena, P. C. WO 2011091153A1, **2011**.
- (4) Dominguez, C.; Toledo-Sherman, L. M.; Courtney, S. M.; Prime, M.; Mitchell, W.; Brown, C. J.; De Aguiar Pena, P. C.; Johnson, P. WO 2013016488A1, **2013**.
- (5) Cheng, W.; Co, E. W.; Kim, M. H.; Klein, R. R.; Le, D. T.; Lew, A.; Nuss, J. M.; Xu, W.; Bajjalieh, W. WO 2005020921A2, **2005**.
- (6) (a) Gates, P. S. WO 9211763, **1992**. (b) Goto, T.; Ito, S.; Minegishi, N.; Yamaoka, T.; Ueno, C.; Moriya, K.; Maurer, F.; Watanabe, R. EP0771797A1, **1997**.
- (7) Lee, C.-S.; Balazitov, R.; Caso, L.; Davis, T. W.; Du, W.; Liu, R.; Moon, Y.-c.; Paget, S. D.; Ren, H.; Sydorenko, N.; Wilde, R. G. WO 2014081906A2, **2014**.
- (8) Murphy, E. A.; Cheresch, D. A.; Arnord, L. D. WO 2011097594A2, **2011**.
- (9) (a) Tong, Y.; Penning, T. D.; Florjancic, A. S.; Miyashiro, J.; Woods, K. W. US 020120220572A1, **2012**. (b) Trani, G.; Barker, J. J.; Bromidge, S. M.; Brookfield, F. A.; Burch, J. D.; Chen, Y.; Eigenbrot, C.; Heifetz, A.; Ismaili, M.; Hicham, A.; Johnson, A.; Krülle, T. M.; MacKinnon, C. H.; Maghames, R.; McEwan, P. A.; Montalbetti, C. A. G. N.; Ortwine, D. F.; Pérez-Fuertes, Y.; Vaidya, D. G.; Wang, X.; Zarrin, A. A.; Pei, Z. *Bioorg. Med. Chem. Lett.* **2014**, *24*, 5818.
- (10) Seganish, W. M.; Brumfield, S. N.; Lim, J.; Matasi, J. J.; McElroy, W. T.; Tulshian, D. B.; Lavey, B. J.; Altman, M. D.; Gibeau, C. R.; Lampe, J. W.; Methot, J.; Zhu, L. WO 2013066729A1, **2013**.
- (11) Nagata, T.; Suzuki, T.; Yoshimura, A.; Tadano, N.; Toshiyuki, M.; Satoh, H.; Saitoh, K.; Ohta, S. US 20110152519A1, **2011**.
- (12) Rose, F. L.; Tuey, G. A. P. *J. Chem. Soc.* **1946**, 81.
- (13) Walker, S. R.; Williams, R. T. *Xenobiotica* **1972**, *2*, 69.
- (14) Mohite, P. B.; Pandhare, R. B.; Khanage, S. G. *Biointerface Res. Appl. Chem.* **2012**, *2*, 258.
- (15) Fujii, S.; Kobayashi, T.; Nakatsu, A.; Miyazawa, H.; Kagechika, H. *Chem. Pharm. Bull.* **2014**, *62*, 700.
- (16) McCluskey, A.; Keller, P. A.; Morgan, J.; Garner, J. *Org. Biomol. Chem.* **2003**, *1*, 3353.
- (17) Packiarajan, M. WO 2004034967A2, **2004**.
- (18) Thomann, A.; Börger, C.; Empting, M.; Hartmann, R. W. *Synlett* **2014**, 25, 935.

- (19) **Experimental Procedure for the Synthesis of 2-(Methylthio)-4,6-di(1H-tetrazol-1-yl)pyrimidine (1)**
 4,6-Dichloro-2-methylthiopyrimidine (195 mg, 1 equiv, 1.0 mmol) and 1H-tetrazole (280 mg, 4 equiv, 4.0 mmol) was dissolved in anhydrous DMF (3 mL). To the orange solution Et₃N (580 μL, 4 equiv, 4.0 mmol) was given, and the mixture was stirred in a capped vial for 10 min in a CEM Discover SP microwave at 60 °C and 50 W power. The reaction mixture was poured into H₂O, filtered, and washed with H₂O to yield an off-white solid (yield: 255 mg, 0.97 mmol, 97%); mp 193 ± 3 °C (decomp.). UV-Vis (MeOH): 221, 236, 269, 320 nm. FT-IR: 3168, 3138, 3098, 2161, 1704, 1597, 1563, 1539, 1466, 1446, 1432, 1416, 1403, 1330, 1316, 1307, 1284, 1248, 1189, 1170, 1101, 1092, 1073, 1004, 990, 951, 937, 881, 846, 824, 791, 758, 710, 681, 659 cm⁻¹. ¹H NMR (300 MHz, DMSO-*d*₆): δ = 10.51 (s, 2 H), 8.24 (s, 1 H), 2.77 (s, 3 H) ppm. ¹³C NMR (75 MHz, DMSO-*d*₆): δ = 174.1, 154.9, 142.5, 142.4, 95.8, 14.2 ppm. ESI-MS: *m/z* = 235.1 [M + H - N₂]⁺, 207.1 [M + H - 2N₂]⁺. HRMS: *m/z* calcd: 263.05704; found: 263.05688 [M + H]⁺. CCDC 1052351 contains the supplementary crystallographic data for this paper. These data can be obtained free of charge from the Cambridge Crystallographic Data Centre via www.ccdc.cam.ac.uk/data_request/cif.
- (20) Lieber, E.; Patinkin, S. H.; Tao, H. H. *J. Am. Chem. Soc.* **1951**, *73*, 1792.
- (21) Brown, D. J.; Mason, S. F. *Chem. Heterocycl. Compd.* **1962**, *16*, 475.
- (22) Hansch, C.; Leo, A.; Taft, R. W. *Chem. Rev.* **1991**, *91*, 165.
- (23) Nagata, T.; Masuda, K.; Maeno, S.; Miura, I. *Pest Manage. Sci.* **2004**, *60*, 399.
- (24) Arukwe, J.; Benneche, T.; Undheim, K. J. *Chem. Soc., Perkin Trans. 1* **1989**, 255.
- (25) Liang, Y.-m.; Luo, S.-j.; Zhang, Z.-x.; Ma, Y.-x. *Synth. Commun.* **2002**, *32*, 153.
- (26) Hurst, D. T.; Johnson, M. *Heterocycles* **1985**, *23*, 611.
- (27) Jin, C.; Liang, Y.-J.; He, H.; Fu, L. *Eur. J. Med. Chem.* **2011**, *46*, 429.
- (28) List, B.; Castello, C. *Synlett* **2001**, 1687.
- (29) *Caution: High-nitrogen-content compounds are known to be unstable. Although we experienced no difficulties in handling these compounds, all experiments were performed on a small scale (0.4–1.0 mmol) and with best safety precautions (e.g., gloves, protective eyewear, shield).*

3 Results

3.4 Application of Dual Inhibition Concept Within Looped Autoregulatory Systems Towards Anti-virulence Agents Against *Pseudomonas aeruginosa*

Andreas Thomann,⁺ Antonio de M. Martins,⁺ Christian Brengel, Martin Empting and Rolf W. Hartmann

⁺ both authors contributed equally to this work

Reproduced with permission from *ACS Chemical Biology*; **2016**, 11, 1279–1286, DOI: 10.1021/acscchembio.6b00117.

Copyright 2016 American Chemical Society.

Publication IV

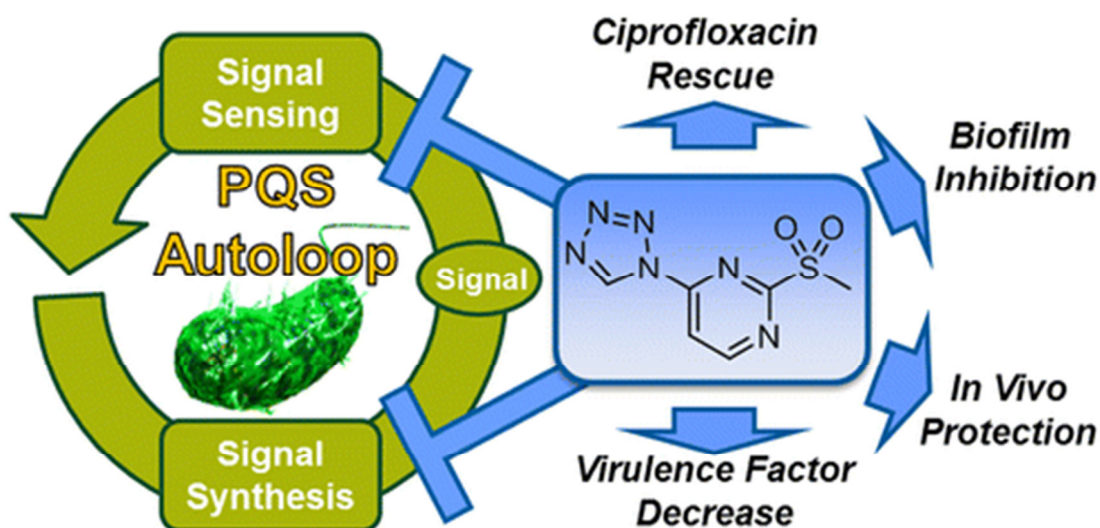
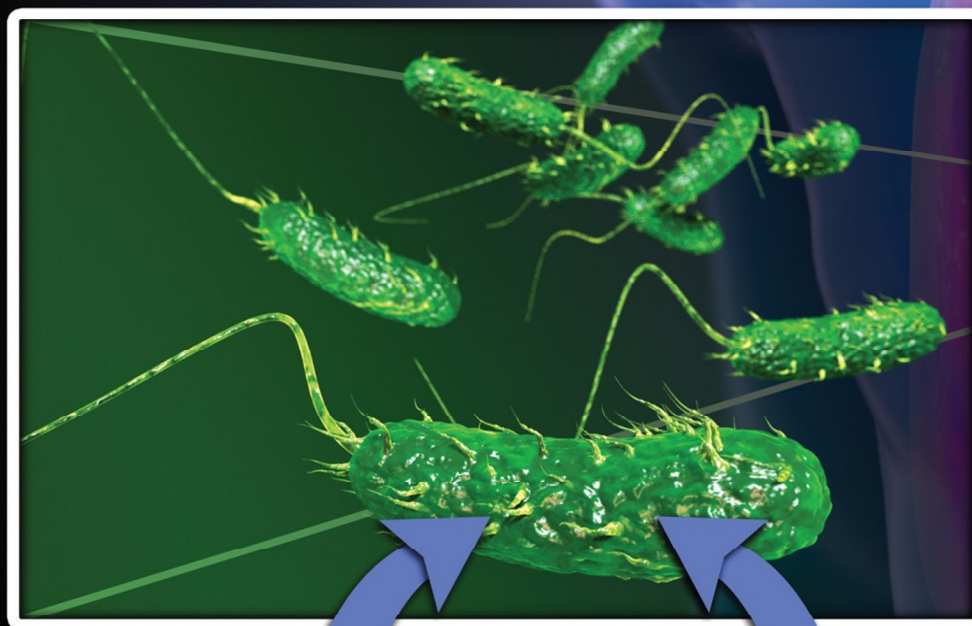


Figure 18. Graphical abstract of publication IV.

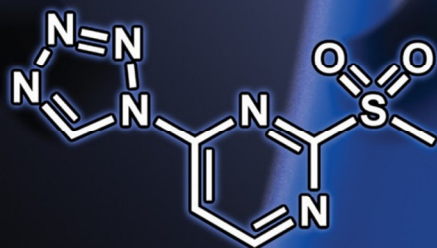
ACS chemical biology

MAY 2016
VOLUME 11, NUMBER 5
pubs.acs.org/acschemicalbiology

The Community of
Chemical Biologists



Dual-Target
Pathoblocker



Two in One :
A Dual-Target
Antivirulence Strategy



ACS Publications
Most Trusted. Most Cited. Most Read.

www.acs.org

Application of Dual Inhibition Concept within Looped Autoregulatory Systems toward Antivirulence Agents against *Pseudomonas aeruginosa* Infections

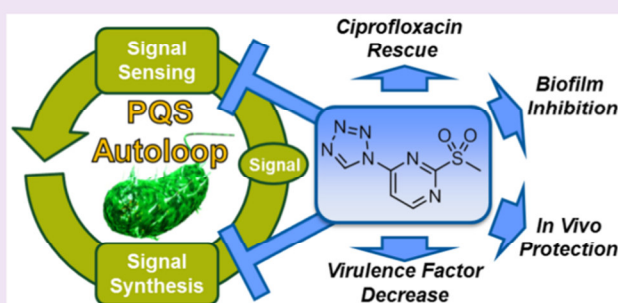
Andreas Thomann,^{S,†} Antonio G. G. de Mello Martins,^{S,†} Christian Brengel,[†] Martin Empting,^{*,†} and Rolf W. Hartmann^{*,†,‡}

[†]Helmholtz Institute for Pharmaceutical Research Saarland (HIPS), Department for Drug Design and Optimization, Campus E8.1, 66123 Saarbrücken, Germany

[‡]Department of Pharmacy, Pharmaceutical and Medicinal Chemistry, Saarland University, Campus C2.3, 66123 Saarbrücken, Germany

Supporting Information

ABSTRACT: *Pseudomonas aeruginosa* quorum-sensing (QS) is a sophisticated network of genome-wide regulation triggered in response to population density. A major component is the self-inducing pseudomonas quinolone signal (PQS) QS system that regulates the production of several nonvital virulence- and biofilm-related determinants. Hence, QS circuitry is an attractive target for antivirulence agents with lowered resistance development potential and a good model to study the concept of polypharmacology in autoloop-regulated systems *per se*. Based on the finding that a combination of PqsR antagonist and PqsD inhibitor synergistically lowers pyocyanin, we have developed a dual-inhibitor compound of low molecular weight and high solubility that targets PQS transcriptional regulator (PqsR) and PqsD, a key enzyme in the biosynthesis of PQS-QS signal molecules (HHQ and PQS). *In vitro*, this compound markedly reduced virulence factor production and biofilm formation accompanied by a diminished content of extracellular DNA (eDNA). Additionally, coadministration with ciprofloxacin increased susceptibility of PA14 to antibiotic treatment under biofilm conditions. Finally, disruption of pathogenicity mechanisms was also assessed *in vivo*, with significantly increased survival of challenged larvae in a *Galleria mellonella* infection model. Favorable physicochemical properties and effects on virulence/biofilm establish a promising starting point for further optimization. In particular, the ability to address two targets of the PQS autoinduction cycle at the same time with a single compound holds great promise in achieving enhanced synergistic cellular effects while potentially lowering rates of resistance development.



Polypharmacology, or addressing two or more disease-related targets at the same time, has proven to have a significant impact on the treatment efficacy of, e.g., cancer,^{1,2} bacterial^{3,4} and viral infections,⁵ high blood pressure,⁶ asthma,⁷ and hormone-related diseases⁸ in clinical setups. These multitarget effects are in most cases achieved by a combination of selective single target agents. Drug combinations can either act synergistically, whereby the combined effect is greater than the sum of their separate responses, or additively, when the resulting activity is the outcome of their combined individual effects, both of which are shown to have favorable outcomes on lowered resistance development in cancer⁹ and microbial¹⁰ infections.¹¹ Unfortunately, such multidrug cocktails may incur several drawbacks, such as undesired drug–drug interactions and increasingly complex dosing schemes resulting in a lesser compliance of patients to follow the prescribed intake schedules.¹² To reduce those problems, development of multitarget drugs is a worthwhile endeavor. In many of the

above-mentioned intricate systems, self-inducing autoloop cycles can be found. In this study, we describe the concept of such a multitarget approach in positively regulated autoloop systems to achieve beneficial and synergistic inhibitory effects against *Pseudomonas aeruginosa* (PA) infections. Autoinducing pathways are widely spread in mammalian,¹³ plant,¹⁴ and bacterial kingdoms¹⁵ and regulate vital functions in a variety of organisms.

As a model system to provide proof of this concept, we chose the cell-density-dependent¹⁶ *Pseudomonas* quinolone signal quorum-sensing system (PQS-QS) of *Pseudomonas aeruginosa*, which was intensively studied by us in the past.^{17–19} In PA, PQS and 2-heptyl-4-quinolone (HHQ) are the natural agonists of PqsR, which is the transcriptional regulator of the *pqsABCDE*

Received: February 5, 2016

Accepted: February 16, 2016

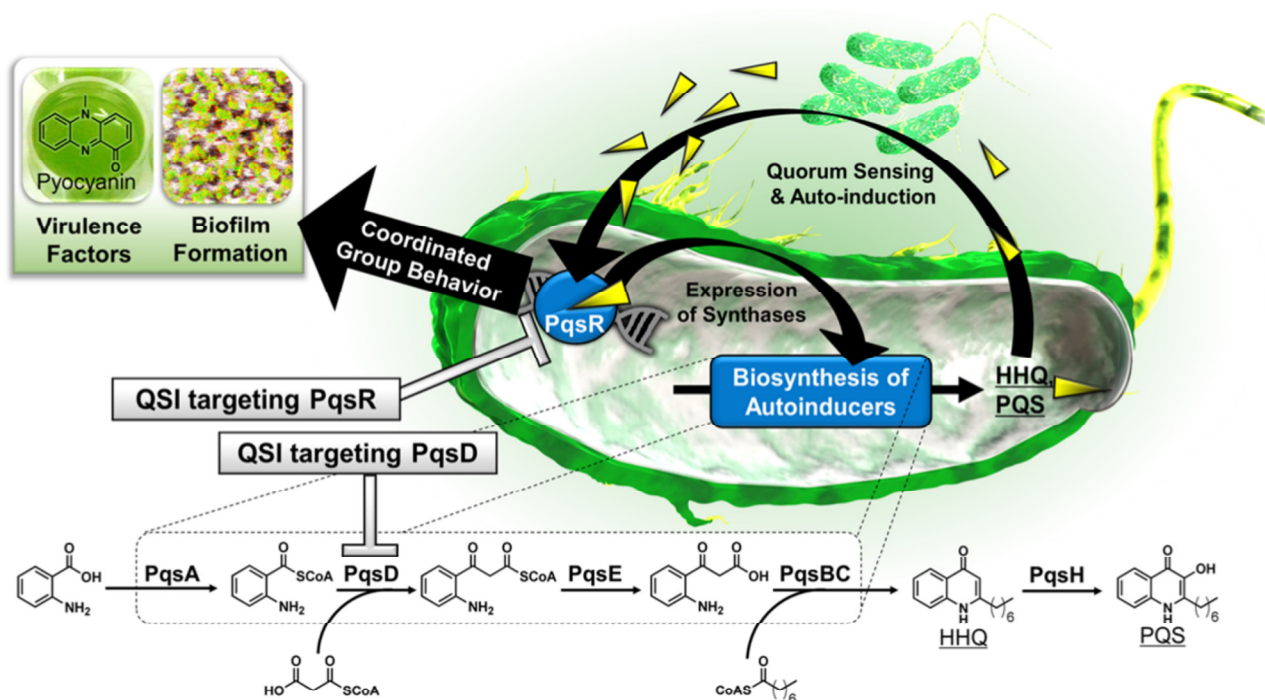


Figure 1. Schematic representation of the *Pseudomonas* quinolone signal (PQS) quorum-sensing system, involved in virulence factor production and biofilm formation. Anthranilate is converted by the *pqsABCDE* gene products into 2-heptyl-4-quinolone (HHQ), which can be converted intracellularly into PQS by the action of PqsH. HHQ and PQS are ligands of the Pqs Receptor (PqsR). Simultaneous inhibition of PQS synthesis (e.g., through PqsD) and interference with the autoloop transcriptional regulator PqsR lead to increased reduction of pathogenicity-associated biomarkers.

operon (Figure 1).²⁰ This operon harbors the genes encoding for the synthases responsible for PQS production. Thus, as soon as PQS and/or HHQ activate PqsR, they induce their own production and the concentration of signal molecules rises exponentially (Figure 1).²¹ Interference experiments, combined with mutational analysis, revealed PqsR and PqsD to be attractive drug targets for reducing pathogenicity of PA *in vivo*.^{17,22} Thus, PQS-QS displays an ideal and relevant model to study the concept of polypharmacology in such positive feedback loops with the possibility to directly transfer the results herein toward other similarly controlled biological systems. Furthermore, we directly put the lessons learned from drug combination experiments to an application for the straightforward rational design of the first drug-like dual-target PqsD/R inhibitors. Additionally, an optimized compound was achieved that shows promising reduction of two major virulence factors and biofilm inhibition *in vitro*. Finally, this optimized dual inhibitor displayed convincing activity in an *in vivo* acute PA infection model.

RESULTS AND DISCUSSION

Combination of PqsD Inhibitor and PqsR Antagonist Prominently Reduces Relevant Marker Pyocyanin through Synergistic Activity. As proof of principle to assess the amenability of the PQS-QS system to dual-target inhibition with improved outcome, we initially investigated the combinatorial effect of a PqsD inhibitor and a PqsR antagonist on a QS-dependent PA-exclusive secondary metabolite, pyocyanin.^{23,24} Pyocyanin is one of PA's most prominent virulence factors with distinct roles in acute infection establishment and biofilm formation. Pyocyanin also substantially contributes to the generation of reactive oxygen species

(ROS) by inhibiting the activity of catalase in eukaryotic cells. ROS is one of pseudomonas' adaptations to environmental competition against other microbes and is the cause for its cytotoxicity toward eukaryotic cells.²⁵ As a consequence, pyocyanin production is linked to increased inflammation, modulation of iron metabolism, and tissue necrosis.²⁶ Its important physiological role in diseased states and correlation with the QS system suggest that by monitoring pyocyanin levels we may gain relevant insights into the suitability of dual inhibition that efficiently targets PA virulence.

We cultured *P. aeruginosa* (PA14) wild type in the presence of different concentrations of a PqsD inhibitor **1**¹⁹ and PqsR antagonist **2**,¹⁷ as a single treatment or combination therapy. As seen in Figure 2, 500 μM of **1** alone does not influence the production of pyocyanin, but interestingly, when added in combination with 15 μM of **2**, we observed a dose-dependent decrease in pyocyanin production. Notably, the decrease from 38% (**2** alone) to 34%, 23%, and 18% (**2** added of 100 μM , 300 μM , and 500 μM of **1**, respectively) is highly significant at higher concentrations of **1**, corroborating the synergistic activity of two PQS-QS inhibitors with different modes of action. These results further demonstrate that a biomarker negative synthase inhibitor (e.g., compound **1**) can indirectly increase the potency of a receptor antagonist (e.g., **2**) presumably by decreasing the natural ligand concentration and thus lowering competition to the receptor's binding site. However, when extending the exposure of PA14 to PqsD inhibitor **1**, we observed a slight, yet significant, reduction of pyocyanin after 48 h of incubation (see Supporting Information, section IIc). Obviously, a continuous attenuation of PQS/HHQ production through PqsD inhibition can result in an antivirulence effect.

B

DOI: 10.1021/acschembio.6b00117
ACS Chem. Biol. XXXX, XXX, XXX–XXX

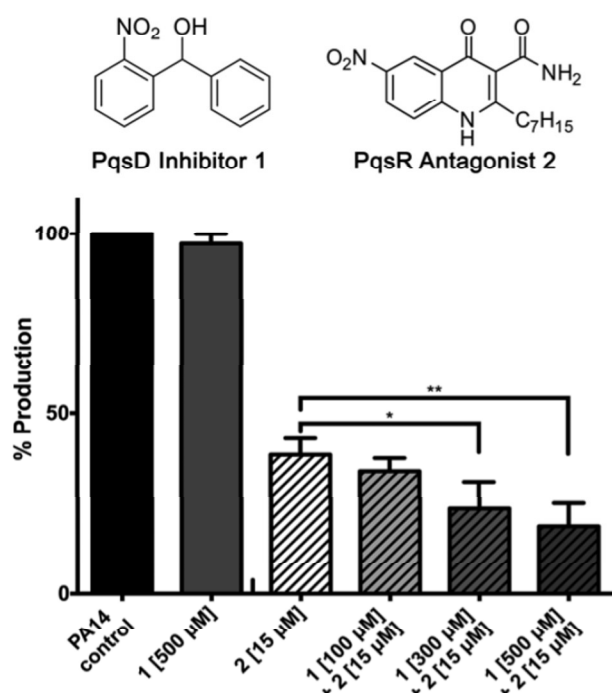


Figure 2. Synergistic activity of PqsD inhibitor 1 and PqsR antagonist 2 on pyocyanin inhibition in PA14 wild type. Treatment with 500 μM of 1 alone did not alter pyocyanin production. However, basal pyocyanin production under inhibition with 15 μM of 2 is significantly increased upon combinatorial titrated administration of 1 (100 μM , 300 μM , and 500 μM , respectively), indicative of synergistic activity. All values are relative to a control without inhibitors. Error bars represent the standard deviation of three independent experiments ($n = 3$). * = $p < 0.05$, ** = $p < 0.005$.

Application of Concept Study toward the Rational Design of Dual PqsD/R Inhibitors. Having demonstrated the potential of combining synthase inhibition and receptor antagonism, we searched through our in-house inhibitor library with regard to structural similarity of selective PqsD and PqsR

inhibitors. From this search, we found compound 3, which was designed as a PqsR antagonist ($\text{IC}_{50} = 26 \mu\text{M}$) with good activity on PA's virulence factor pyocyanin (Figure 3) and a quite similar compound, 4, which was designed to target PqsD ($\text{IC}_{50} = 1.7 \mu\text{M}$) based on SPR screening results recently reported by us (Figure 3).²⁷ As for 1, compound 4 displayed no inhibitory activity on pyocyanin even at the maximum soluble concentration.

Although, both compounds are selective for their respective targets, they share the same molecular scaffold: a pyrimidine core decorated with a triazole and a sulfone moiety (Figure 3). Thus, we decided to synthesize compound 5 and assess its biological activity, as it represents a simplified molecule consisting only of the shared structural features. Notably, the obtained compound 5 showed inhibition of both targets. Moreover, in very good accordance to our conceptual studies (*vide supra*), compound 5 showed a stronger reduction of pyocyanin compared to the equipotent PqsR selective precursor 3 (Figure 3). These results indicate that the concept of dual inhibition with combination experiments and the observed synergism can be directly combined in one compound. With regard to ligand lipophilicity efficiency (LLE), a metric used in medicinal chemistry to evaluate the activity of a compound based on its molecular weight and lipophilicity for further drug design, 5 showed a LLE = 0.56 on both targets which is above the suggested minimum score of 0.3.²⁸ To further improve the potential of 5 based on its LLE, we decided to modify it *via* a bioisosteric replacement of C4 at the triazole substituent. Introducing a nitrogen at this site yielded the tetrazole congener 6 (Figure 3). To confirm the regiochemistry of the introduced tetrazole moiety, we crystalized intermediate 6a²⁹ and verified the structure by X-ray analysis (CCDC-No.: 1432241, Supporting Information, section Ib.). As expected for the tetrazole substituent, lipophilicity of 6 dropped compared to 5, leading to an increase of the LLE score (PqsR = 0.67; PqsD = 0.66) and better solubility. Notably, activity on PqsR was slightly increased, while activity on PqsD was retained, resulting in an overall IC_{50} on pyocyanin of 86 μM (Figure 3).

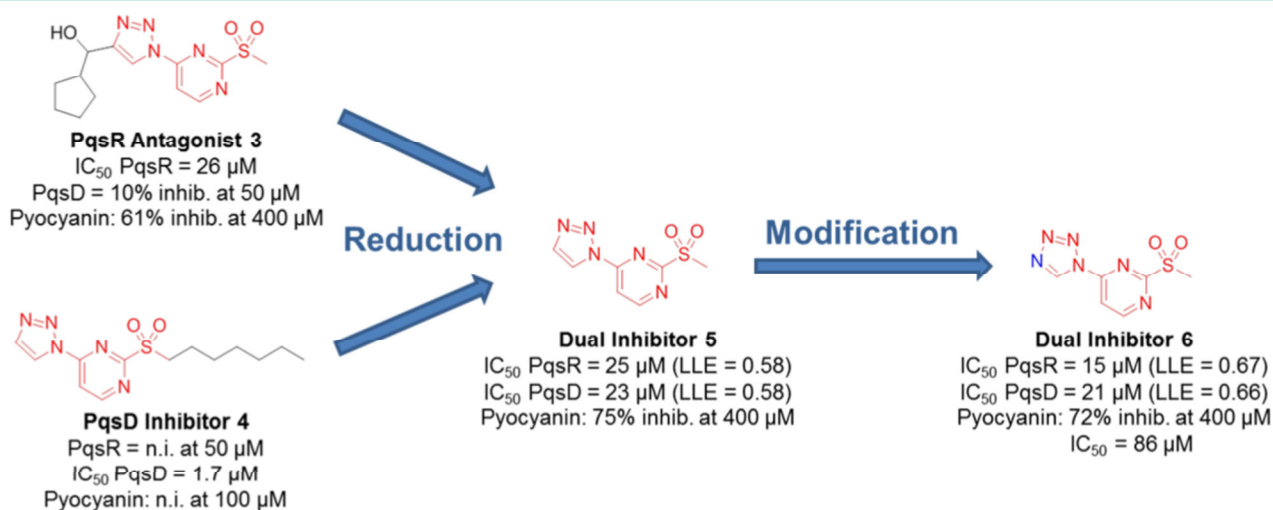


Figure 3. Reduction of structurally related PqsR antagonist 3 and PqsD inhibitor 4 to the common molecular core resulting in the first dual-active compound 5 (red). In comparison to 3, 5 shows higher activity on pyocyanin, although being similarly active on PqsR, corroborating the findings of the combination experiments (Figure 2). Bioisosteric modification (blue) led to dual inhibitor 6 with improved physicochemical properties as shown by its increased ligand lipophilicity efficiency (LLE).

Dual Inhibitor Not Only Affects Pyocyanin Production but Also Modulates the Generation of a Second Virulence Factor, Pyoverdine (PVD). Pyoverdines are *Pseudomonas*' primary siderophores. These fluorescent signaling molecules are used by the bacterium in iron scavenging and metabolism and are closely related to the production of other virulence factors in acute infections, as well as the correct architectural construction of biofilms.^{30,31} Since the absence of PVD in deficient mutants has shown to drastically reduce infection ability,³² and iron acquisition *in vitro* is linked to biofilm formation,³³ PVD metabolism provides a connection between acute pathogenicity and biofilm-related severe infections. The intrinsic relationship of PQS and PVD signaling pathways in iron metabolism and virulence has been shown to be mutual: on one hand, PQS induces the expression of genes involved in the biosynthesis of PVD,³⁴ on the other, PvdS, one of the major regulators in the biosynthesis of PVD, controls the expression of PqsR.^{35,36} Hence, we investigated whether our PQS dual inhibitor would have a beneficial effect on PVD inhibition by targeting PQS biosynthesis. We grew PA14 wild-type cultures in the presence of increasing concentrations of **6** (Figure 4). In accordance with our assumption, **6** was able to

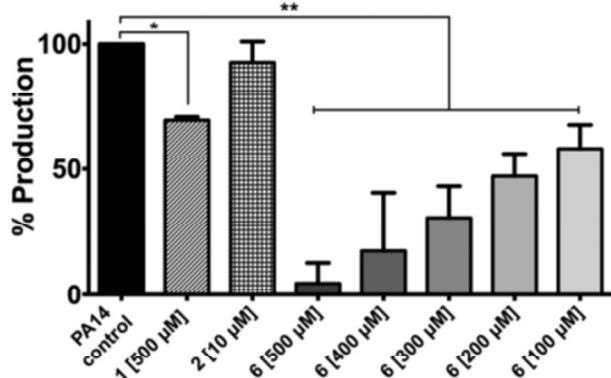


Figure 4. Effects of compounds **1**, **2**, and **6** on pyoverdine production. Compound **6** showed a prominent, significant decrease in pyoverdine levels in a concentration-dependent manner. At the highest concentration of 500 μM , pyoverdine production was almost completely arrested ($5\% \pm 8$), and halved at the lowest inhibitor concentration of 100 μM ($58\% \pm 10$). All values are relative to a control without inhibitors. Error bars represent standard deviation of three independent experiments ($n = 3$). * = $p < 0.05$, ** = $p < 0.005$.

decrease PVD significantly in all tested concentrations (500 μM to 100 μM). Production of the siderophore was essentially blocked at the highest tested concentration of **6**, while compounds **1** and **2** had only moderate or low effects in this assay ($69.7\% \pm 1.3$ and $92.8\% \pm 8.2$, respectively). Thus, dual inhibitor **6** is not only able to target pyocyanin biosynthesis, but also addresses PVD production, disrupting iron metabolism, and virulence factor production, ultimately reducing the environmental competitive advantage of PA, as well as its pathogenicity to lower levels that better respond to treatment. These beneficial cellular effects may contribute to attenuation of biofilm formation and establishment—a scenario that we further investigated in our next experiments.

Compound 6 Reduces Biofilm Formation and Restores Antibiotic Efficacy. Biofilms are one of the major clinically relevant resistance mechanisms of PA against antibiotic treatment,³⁷ immune responses,³⁸ and antimicrobial peptides³⁹ in particular. Thus, reduction of biofilm mass holds the potential to enable immunological clearance of the pathogen and restore antibiotic activity, features of undoubtedly high interest. The development of biofilms is dependent on the PQS Quorum sensing network, as shown in previous knockout studies.⁴⁰ Recently, we showed that PqsD inhibitor **1** reduces PA biofilms at high concentrations (reduction of biofilm volume to 62% at 500 μM).¹⁹ Furthermore, antibiofilm activities have been reported for PqsR antagonists designed on the basis of the natural ligand HHQ,⁴¹ the biological precursor of PQS (Figure 1), and we observed a reduction in biofilm volume by compound **2** to $84.8\% \pm 4.7$ at 15 μM (see supplementary Figure 5). These target-related effects and the reduction of the biofilm-associated virulence factor PVD (*vide supra*) motivated us to test whether our dual target compound **6** was also active on preventing biofilm formation. Indeed, **6** displayed prominent effects on biofilm development with an IC_{50} of 100 μM (Figure 5A, circles). This is in good accordance with previously obtained data regarding biofilm inhibition targeting either PqsR or PqsD.^{19,41,42}

We concluded that the dual inhibition concept might not only pronouncedly reduce pyocyanin formation but also result in stronger inhibition of PA biofilm. To further validate the target of **6** under biofilm-conditions, we assessed whether the dual inhibitor is still active on a PqsR deficient mutant strain of PA. We observed a reduced activity of about 1 log unit of the $\Delta pqsR$ mutant strain compared to wild type PA. This result, on the one hand, underlines the target-related activity but also shows that the compound has an additional target involved in

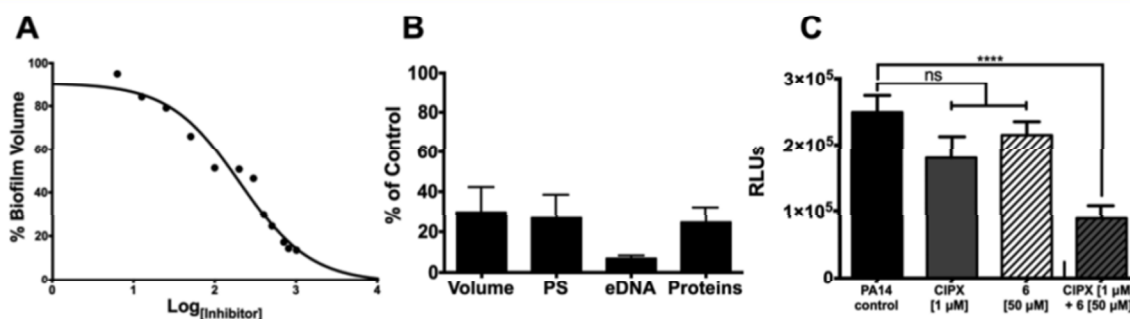


Figure 5. Dose-dependent reduction of biofilm in PA14 wild type cultures treated with compound **6** (A). Pronounced reduction of extracellular DNA (eDNA), polysaccharides (PS), and proteins of the biofilm matrix (Volume) was found at 400 μM of **6** (B). Activity of 1 μM ciprofloxacin (CIPX) was increased by a combination of the antibiotic with 50 μM of **6** under biofilm conditions (C). Error bars represent standard error of at least two independent experiments. ns = not significant, **** = $p < 0.0001$.

biofilm formation. A biofilm is a heterogeneous matrix composed of different components, e.g., polysaccharides (PS), proteins, lipopolysaccharides (LPS), and extracellular DNA (eDNA).⁴³ The latter has been described as responsible for resistance development against aminoglycoside⁴⁴ and fluoroquinolone antibiotics⁴⁵ as well as increased tolerance against host defensins.⁴⁶ Moreover, release of eDNA is directly regulated by the presence of pyocyanin⁴⁷ and PQS.⁴⁸ Hence, we were curious how **6** affects the components of the biofilm (Figure 5B). Our results demonstrate that **6** significantly inhibited eDNA release under biofilm conditions ($7\% \pm 2$ residual eDNA detected), which is in good accordance with the previous findings described above. Moreover, we observed a marked attenuation of PS and protein BF constituents down to $27\% \pm 20$ and $25\% \pm 13$, respectively. As a targeted decrease of eDNA might lead to higher efficacy of antibiotics on biofilm cultures of PA, we tested the susceptibility of PA14 against the fluoroquinolone-based antibiotic ciprofloxacin, the activity of which has been described to be hindered in the presence of eDNA.⁴⁵ Under biofilm conditions, no significant inhibition of PA viability by ciprofloxacin was observed (Figure 5C). However, in combination with **6**, which alone had no effect on the viability of PA, antibiotic activity could be restored under biofilm conditions that mimic a chronic infection *in vitro*. Furthermore, these findings complement published data regarding the application of PqsR antagonists in acute infection models.⁴² Thus, therapy of QSIs in combination with antibiotic treatment in acute and chronic PA infections holds great promise for future anti-infective drug discovery focusing on quorum sensing inhibition.

Compound **6** Reduces Pathogenicity of PA14 *in Vivo*.

Until today, a variety of *in vivo* models to assess the pathogenicity of PA were developed. We chose an animal infection model employing *Galleria mellonella* larvae which has been previously shown to have a high correlation with mouse PA infection models⁴⁹ and was also used by us to validate a PqsR antagonist *in vivo*.¹⁷ To determine efficacy of our dual-target compound **6**, *G. mellonella* larvae were inoculated with the agent in the presence and absence of PA. Interestingly, **6** was able to increase the survival rate of larvae in a dose-dependent manner with 53% survival at 1.25 nmol and 29% survival at 0.5 nmol applied dose (Figure 6). The susceptibility of larvae was described to be 50% if infected by one cell of PA.⁴⁹ Notably, in our experiments one larva was challenged with 10–13 PA cells, resulting in a very high bacterial load and hurdle to be taken by an anti-infective treatment. Regarding the average hemolymph and body weight ($450 \mu\text{L}$ and 450 mg)¹⁷ of each larvae, the most beneficial protective effect was observed at a dosage of 1.25 nmol, correspondent to a final *in vivo* concentration of $2.7 \mu\text{M}$ or 0.63 mg kg^{-1} .

Most interestingly, when assessing toxicity of **6** in *G. mellonella* we could show that even a 4 times higher concentration (5 nmol) than the effective dose was well tolerated with no observable disparity with PBS control.

CONCLUSION

In this study, we demonstrated the applicability of dual synergistic inhibition within the frame of positive feedback autoloop systems as a novel concept for the development of quorum sensing inhibitors. We chose the model PQS-QS system of *Pseudomonas aeruginosa* to demonstrate that an enzyme inhibitor **1** can increase the potency of the associated receptor antagonist **2** regarding virulence factor production.

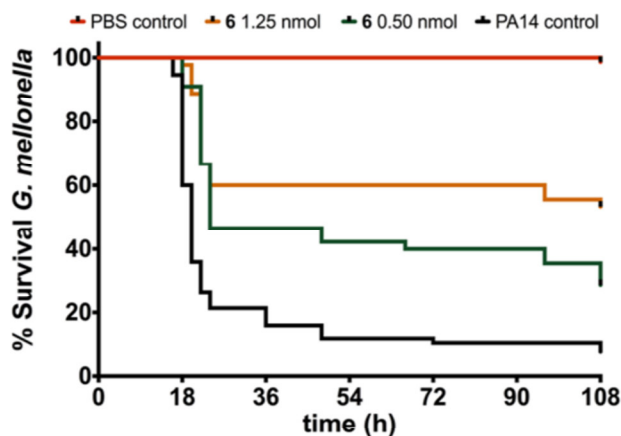


Figure 6. Dose-dependent *in vivo* protective effect of **6** on the survival of *Pseudomonas aeruginosa* PA14-challenged larvae of *Galleria mellonella*. Survival rate was significantly higher for treated larvae (0.5 nmol or 1.25 nmol) compared to the untreated control (0.5 and 1.25 nmol applied doses: $p < 0.0001$; log-rank test).

Presumably, this beneficial effect is due to lowered signal molecule levels and, therefore, less competition at the receptor's binding site. We successfully exploited this concept of dual inhibition in a rational design strategy to achieve the first dual-active inhibitor **5** targeting the PQS-QS system. This compound was further improved by bioisosteric replacement, culminating in inhibitor **6** with an enhanced efficiency/lipophilicity profile. This compound effectively reduced pyocyanin and pyoverdine, two major virulence factors of PA, in a dose-dependent manner without affecting bacterial growth. Importantly, **6** had a strong effect on PA biofilm assembly and restored the efficacy of ciprofloxacin, presumably due to hindrance of eDNA release. Finally, dual inhibitor **6** was also active *in vivo*, protecting *G. mellonella* larvae from lethal PA infections. Taken together, the presented dual inhibition strategy holds great potential to effectively interfere with intricate cellular systems. Via this promising approach, we achieved an enhanced bioactivity profile through synergistic action at two points-of-intervention (PqsD and PqsR) within a positive feedback loop (the PQS-QS system). Hence, this strategy might be a powerful tool for devising new treatment options for diseases related to complex or compensatory metabolic pathways similar to the one investigated in this study.

METHODS

Pyocyanin Assay. Pyocyanin formation was assessed as previously described^{18,23,50} with minor modifications. A single colony was removed from agar plates after 16 h of growth at 37°C and transferred into 25 mL Erlenmeyer flasks with 10 mL of PPGAS medium. Following 19 h of aerobic growth with shaking at 200 rpm and 37°C , cultures were centrifuged at $7.450g$, washed once with 10 mL of fresh PPGAS medium, and resuspended to a final volume of 5 mL. Cultures were then diluted to a final OD_{600} of 0.02 and distributed into test tubes in 1.2 mL aliquots. Compounds **1** and **2** were added in 1:100 dilutions with a final DMSO concentration of 1% (v/v). Treated and untreated cultures were incubated for an additional 17 h under aerobic conditions as mentioned above. Pyocyanin was extracted by adding $900 \mu\text{L}$ of chloroform to $900 \mu\text{L}$ of overnight culture and subsequently re-extracted with $250 \mu\text{L}$ of 0.2 M HCl from the organic phase. OD_{520} was measured in the aqueous phase. Pyocyanin formation values were normalized to a corresponding OD_{600} of the respective sample.

Pyoverdine Assay. For the analysis of pyoverdine formation, culture workup and stock solution of compounds **1**, **2**, and **6** were performed as described above (Pyocyanin Assay). Treated and untreated cultures were incubated in 200 μL of PPGAS medium for 8 h under aerobic conditions in black 96-well plates with glass bottoms. This allowed for the simultaneous measurements of pyoverdine (fluorescent light units with excitation at 400 ± 10 and emission at 460 ± 10) and bacterial growth at OD_{600} . Inhibition of pyoverdine was normalized to OD_{600} values.

Galleria mellonella Virulence Assay. An infection model of *G. mellonella* was used to determine disruption of virulence mechanisms *in vivo* as described in the works of Lu *et al.*¹⁷ Treatment conditions of larvae included (a) sterile PBS solution, (b) PA14 suspension, (c) 0.50 nmol of compound **6** in "b," and (d) 1.25 nmol of compound **6** in "b." For each treatment, data from at least three independent experiments were combined.

Biofilm Assay. Commonly used crystal violet (CV) assay procedures^{51–53} were adapted for determination of biofilm mass. For the cultivation of biofilm in 96-well plates, the protocol described by Frei *et al.*⁵³ was slightly modified by replacement of the medium and the *Pseudomonas* strain used. The experiment was performed using the *P. aeruginosa* PA14 strain (including ΔpqsR mutant, kindly provided by S. Häussler) and M63 medium.⁵⁴ CV staining was used to detect compound effects on the overall biofilm biomass. The impact on eDNA was assessed by incubation of biofilm with propidium iodide solution (0.05 mg mL^{-1}) for 3 h and detection of specific fluorescence at 620 nm after a thorough washing step with 18M Ω H_2O .⁵⁵ Polysaccharide levels in biofilm were specified by congo red staining described by Ghafoor *et al.*⁵⁶ For this purpose, a 20 mg mL^{-1} congo red solution was incubated with the matured biofilm for 3 h, followed by a washing step with water and the concentration measurement at 490 nm. For the detection of protein levels, Bradford reagent was diluted 1:5 (Roti-Quant, Carl Roth) and incubated with the washed biofilm for 5 min.⁵⁷ Next, 18M Ω H_2O was used to remove unbound dye. The amount of proteins was determined by absorbance measurement at 595 nm. To investigate the killing efficacy of ciprofloxacin in combination with QS inhibitor on biofilm-encapsulated bacteria, biofilm was grown under the same conditions used for CV assay. At first, biofilm growth was initiated under QS inhibitor treatment (50 μM) or DMSO control. After washing steps, matured biofilm was incubated with 4 $\mu\text{g mL}^{-1}$ ciprofloxacin dissolved in M63 medium and grown for a further 24 h. Viability of bacteria in the biofilm was determined by BacTiter-Glo Assay using black plates.⁵⁸

Chemical Synthesis and Analytical Characterization. NMR spectra were recorded on an Avance AV 300 or a Bruker DRX 500. The residual proton, ^1H , or carbon, ^{13}C , resonances of the >99% deuterated solvents were used for internal reference of all spectra acquired (CDCl₃ ^1H 7.260 ppm, ^{13}C 77.16 ppm; DMSO-*d*₆ ^1H 2.500 ppm, ^{13}C 39.52 ppm). Electrospray ionization (ESI) mass spectrometry and LC-UV purity determination were recorded with a Surveyor LC system MSQ electrospray mass spectrometer (ThermoFisher) LC-MS couple and acetonitrile/water gradient in positive mode (+), if not indicated otherwise. Then, 1% TFA was added if necessary. Compound **6** was analyzed using a setup produced by Waters Corporation containing a 2767 Sample Manager, a 2545 binary gradient pump, a 2998 PDA detector, and a 3100 electron spray mass spectrometer. Water containing 0.1% formic acid and acetonitrile containing 0.1% formic acid were used as solvents for the analysis. A Waters X-Bridge column (C18, 150 \times 4.6 mm, 5 μM) has been used with a flow of 1 mL min^{-1} starting with 10% acid containing acetonitrile to 95% acid containing acetonitrile. All final compounds were of $\geq 95\%$ purity. Unless otherwise stated, all reagents used were purchased from commercial vendors and used without further purification.

■ ASSOCIATED CONTENT

Supporting Information

The Supporting Information is available free of charge on the ACS Publications website at DOI: 10.1021/acscchembio.6b00117.

Spectra (^1H COSY, ^{13}C NMR, LC-MS, X-ray crystallography); synthetic procedures of described new compounds and details on PqsD and PqsR assays; growth curves, IC50 determination on Pyocyanin with **6**, LLE calculations, and antibiofilm effects of **2** (PDF)

■ AUTHOR INFORMATION

Corresponding Authors

*E-mail: martin.cmpting@helmholtz-hzi.de.

*E-mail: rolf.hartmann@helmholtz-hzi.de.

Author Contributions

[§]These authors contributed equally.

Funding

This project was funded by BMBF through grant 1616038B.

Notes

The authors declare no competing financial interest.

■ ACKNOWLEDGMENTS

We thank C. Maurer, S. Amann, and C. Scheidt for performing and supervising the PqsD, PqsR, and pyocyanin assays. Many thanks go to V. Huch for recording the X-ray structure of compound **6a** and B. Kirsch for helpful discussions and introduction to the *Galleria mellonella* assay. We thank C. Börger for LC-MS analysis of compound **6**.

■ ABBREVIATIONS

PQS, *Pseudomonas* Quinolone Signal; QS, Quorum Sensing; PA, *Pseudomonas aeruginosa*

■ REFERENCES

- (1) Tolaney, S. M.; Barry, W. T.; Dang, C. T.; Yardley, D. A.; Moy, B.; Marcom, P. K.; Albain, K. S.; Rugo, H. S.; Ellis, M.; Shapira, I.; Wolff, A. C.; Carey, L. A.; Overmoyer, B. A.; Partridge, A. H.; Guo, H.; Hudis, C. A.; Krop, I. E.; Burstein, H. J.; and Winer, E. P. (2015) Adjuvant paclitaxel and trastuzumab for node-negative, HER2-positive breast cancer. *N. Engl. J. Med.* 372, 134–141.
- (2) Robert, C.; Karaszewska, B.; Schachter, J.; Rutkowski, P.; Mackiewicz, A.; Stroiakovski, D.; Lichinitser, M.; Dummer, R.; Grange, F.; Mortier, L.; Chiarion-Sileni, V.; Drucis, K.; Krajsova, I.; Hauschild, A.; Lorigan, P.; Wolter, P.; Long, G. V.; Flaherty, K.; Nathan, P.; Ribas, A.; Martin, A.-M.; Sun, P.; Crist, W.; Legos, J.; Rubin, S. D.; Little, S. M.; and Schadendorf, D. (2015) Improved overall survival in melanoma with combined dabrafenib and trametinib. *N. Engl. J. Med.* 372, 30–39.
- (3) Diacon, A. H.; Pym, A.; Grobusch, M.; Patientia, R.; Rustomjee, R.; Page-Shipp, L.; Pistorius, C.; Krause, R.; Bogoshi, M.; Churchyard, G.; Venter, A.; Allen, J.; Palomino, J. C.; de Marez, T.; van Heeswijk, R. P. G.; Lounis, N.; Meyvisch, P.; Verbeeck, J.; Parys, W.; de Beule, K.; Andries, K.; and McNeeley, D. F. (2009) The diarylquinoline TMC207 for multidrug-resistant tuberculosis. *N. Engl. J. Med.* 360, 2397–2405.
- (4) Hilf, M.; Yu, V. L.; Sharp, J.; Zuravleff, J. J.; Korvick, J. A.; and Muder, R. R. (1989) Antibiotic therapy for *Pseudomonas aeruginosa* bacteremia: Outcome correlations in a prospective study of 200 patients. *Am. J. Med.* 87, 540–546.
- (5) Jarcho, J. A.; Gandhi, R. T.; and Gandhi, M. (2014) Single-pill combination regimens for treatment of HIV-1 infection. *N. Engl. J. Med.* 371, 248–259.

- (6) Sever, P. S., and Messerli, F. H. (2011) Hypertension management 2011: optimal combination therapy. *Eur. Heart J.* 32, 2499–2506.
- (7) Kerstjens, H. A. M., Engel, M., Dahl, R., Paggiaro, P., Beck, E., Vandewalker, M., Sigmund, R., Seibold, W., Moroni-Zentgraf, P., and Bateman, E. D. (2012) Tiotropium in asthma poorly controlled with standard combination therapy. *N. Engl. J. Med.* 367, 1198–1207.
- (8) Vilar, L., Naves, L. A., Machado, M. C., and Bronstein, M. D. (2015) Medical combination therapies in Cushing's disease. *Pituitary* 18, 253–262.
- (9) Samanta, D., Gilkes, D. M., Chaturvedi, P., Xiang, L., and Semenza, G. L. (2014) Hypoxia-inducible factors are required for chemotherapy resistance of breast cancer stem cells. *Proc. Natl. Acad. Sci. U. S. A.* 111, E5429–38.
- (10) Worthington, R. J., and Melander, C. (2013) Combination approaches to combat multidrug-resistant bacteria. *Trends Biotechnol.* 31, 177–184.
- (11) E. Buirra, A. Jaen (2015) Impact of Fixed-Dose Combinations of Antiretrovirals on Prevalence Trends of HIV Resistance: A 7 Year Follow-Up Study. *J. AIDS Clin. Res.* 06, 10.4172/2155-6113.1000416.
- (12) Anighoro, A., Bajorath, J., and Rastelli, G. (2014) Polypharmacology: challenges and opportunities in drug discovery. *J. Med. Chem.* 57, 7874–7887.
- (13) Bombeli, T., and Spahn, D. R. (2004) Updates in perioperative coagulation: physiology and management of thromboembolism and haemorrhage. *Br. J. Anaesth.* 93, 275–287.
- (14) Petruzzelli, L., Coraggio, I., and Leubner-Metzger, G. (2000) Ethylene promotes ethylene biosynthesis during pea seed germination by positive feedback regulation of 1-aminocyclo-propane-1-carboxylic acid oxidase. *Planta* 211, 144–149.
- (15) van Hoek, M., and Hogeweg, P. (2007) The effect of stochasticity on the lac operon: an evolutionary perspective. *PLoS Comput. Biol.* 3, e111.
- (16) Swift, S., Allan Downie, J., Whitehead, N. A., Barnard, A. M., Salmond, G. P., and Williams, P. (2001) Quorum sensing as a population-density-dependent determinant of bacterial physiology. *Adv. Microb. Physiol.* 45, 199–270.
- (17) Lu, C., Maurer, C. K., Kirsch, B., Steinbach, A., and Hartmann, R. W. (2014) Overcoming the unexpected functional inversion of a PqsR antagonist in *Pseudomonas aeruginosa*: an in vivo potent antivirulence agent targeting pqs quorum sensing: An In Vivo Potent Antivirulence Agent Targeting pqs Quorum Sensing. *Angew. Chem., Int. Ed.* 53, 1109–1112.
- (18) Klein, T., Henn, C., de Jong, J. C., Zimmer, C., Kirsch, B., Maurer, C. K., Pistorius, D., Müller, R., Steinbach, A., and Hartmann, R. W. (2012) Identification of small-molecule antagonists of the *Pseudomonas aeruginosa* transcriptional regulator PqsR: biophysically guided hit discovery and optimization. *ACS Chem. Biol.* 7, 1496–1501.
- (19) Storz, M. P., Maurer, C. K., Zimmer, C., Wagner, N., Brenzel, C., de Jong, J. C., Lucas, S., Müsken, M., Häussler, S., Steinbach, A., and Hartmann, R. W. (2012) Validation of PqsD as an anti-biofilm target in *Pseudomonas aeruginosa* by development of small-molecule inhibitors. *J. Am. Chem. Soc.* 134, 16143–16146.
- (20) Rutherford, S. T., and Bassler, B. L. (2012) Bacterial quorum sensing: its role in virulence and possibilities for its control. *Cold Spring Harbor Perspect. Med.* 2, a012427.
- (21) Déziel, E., Gopalan, S., Tampakaki, A. P., Lépine, F., Padfield, K. E., Saucier, M., Xiao, G., and Rahme, L. G. (2005) The contribution of MvfR to *Pseudomonas aeruginosa* pathogenesis and quorum sensing circuitry regulation: multiple quorum sensing-regulated genes are modulated without affecting lasRI, rhlRI or the production of N-acyl-L-homoserine lactones. *Mol. Microbiol.* 55, 998–1014.
- (22) Gallagher, L. A., McKnight, S. L., Kuznetsova, M. S., Pesci, E. C., and Manoil, C. (2002) Functions Required for Extracellular Quinolone Signaling by *Pseudomonas aeruginosa*. *J. Bacteriol.* 184, 6472–6480.
- (23) O'Loughlin, C. T., Miller, L. C., Siryaporn, A., Drescher, K., Semmelhack, M. F., and Bassler, B. L. (2013) A quorum-sensing inhibitor blocks *Pseudomonas aeruginosa* virulence and biofilm formation. *Proc. Natl. Acad. Sci. U. S. A.* 110, 17981–17986.
- (24) Recinos, D. A., Sekedat, M. D., Hernandez, A., Cohen, T. S., Saklitali, H., Prince, A. S., Price-Whelan, A., and Dietrich, L. E. P. (2012) Redundant phenazine operons in *Pseudomonas aeruginosa* exhibit environment-dependent expression and differential roles in pathogenicity. *Proc. Natl. Acad. Sci. U. S. A.* 109, 19420–19425.
- (25) Mavrodi, D. V., Parejko, J. A., Mavrodi, O. V., Kwak, Y.-S., Weller, D. M., Blankenfeldt, W., and Thomashow, L. S. (2013) Recent insights into the diversity, frequency and ecological roles of phenazines in fluorescent *Pseudomonas* spp. *Environ. Microbiol.* 15, 675–686.
- (26) Priyaja, P., Jayesh, P., Philip, R., and Bright Singh, I. S. (2016) Pyocyanin induced in vitro oxidative damage and its toxicity level in human, fish and insect cell lines for its selective biological applications. *Cytotechnology* 68, 143.
- (27) Weidel, E., Negri, M., Empting, M., Hinsberger, S., and Hartmann, R. W. (2014) Composing compound libraries for hit discovery—rationality-driven preselection or random choice by structural diversity? *Future Med. Chem.* 6, 2057–2072.
- (28) Mortenson, P. N., and Murray, C. W. (2011) Assessing the lipophilicity of fragments and early hits. *J. Comput.-Aided Mol. Des.* 25, 663–667.
- (29) Thomann, A., Börger, C., Empting, M., and Hartmann, R. (2014) Microwave-Assisted Synthesis of 4-Substituted 2-Methylthio-pyrimidines. *Synlett* 25, 935–938.
- (30) Banin, E., Vasil, M. L., and Greenberg, E. P. (2005) Iron and *Pseudomonas aeruginosa* biofilm formation. *Proc. Natl. Acad. Sci. U. S. A.* 102, 11076–11081.
- (31) Cézard, C., Farvacques, N., and Sonnet, P. (2015) Chemistry and biology of pyoverdines, *Pseudomonas* primary siderophores. *Curr. Med. Chem.* 22, 165–186.
- (32) Stanners, C. P., and Goldberg, V. J. (1975) On the mechanism of neurotropism of vesicular stomatitis virus in newborn hamsters. Studies with temperature-sensitive mutants. *J. Gen. Virol.* 29, 281–296.
- (33) Visca, P., Imperi, F., and Lamont, I. L. (2007) Pyoverdine siderophores: from biogenesis to biosignificance. *Trends Microbiol.* 15, 22–30.
- (34) Diggle, S. P., Matthijs, S., Wright, V. J., Fletcher, M. P., Chhabra, S. R., Lamont, I. L., Kong, X., Hider, R. C., Cornelis, P., Cámara, M., and Williams, P. (2007) The *Pseudomonas aeruginosa* 4-quinolone signal molecules HHQ and PQS play multifunctional roles in quorum sensing and iron entrapment. *Chem. Biol.* 14, 87–96.
- (35) Bredenbruch, F., Geffers, R., Nimtz, M., Buer, J., and Häussler, S. (2006) The *Pseudomonas aeruginosa* quinolone signal (PQS) has an iron-chelating activity. *Environ. Microbiol.* 8, 1318–1329.
- (36) Jimenez, P. N., Koch, G., Thompson, J. A., Xavier, K. B., Cool, R. H., and Quax, W. J. (2012) The multiple signaling systems regulating virulence in *Pseudomonas aeruginosa*. *Microbiol. Mol. Biol. Rev.* 76, 46–65.
- (37) Drenkard, E. (2003) Antimicrobial resistance of *Pseudomonas aeruginosa* biofilms. *Microbes Infect.* 5, 1213–1219.
- (38) Alhede, M., Bjarnsholt, T., Givskov, M., and Alhede, M. (2014) *Pseudomonas aeruginosa* biofilms: mechanisms of immune evasion. *Adv. Appl. Microbiol.* 86, 1–40.
- (39) Lewenza, S. (2013) Extracellular DNA-induced antimicrobial peptide resistance mechanisms in *Pseudomonas aeruginosa*. *Front. Microbiol.* 4, 21.
- (40) Müsken, M., Di Fiore, S., Dötsch, A., Fischer, R., and Häussler, S. (2010) Genetic determinants of *Pseudomonas aeruginosa* biofilm establishment. *Microbiology* 156, 431–441.
- (41) Ilangovan, A., Fletcher, M., Rampioni, G., Pustelny, C., Rumbaugh, K., Heeb, S., Cámara, M., Truman, A., Chhabra, S. R., Emsley, J., and Williams, P. (2013) Structural basis for native agonist and synthetic inhibitor recognition by the *Pseudomonas aeruginosa* quorum sensing regulator PqsR (MvfR). *PLoS Pathog.* 9, e1003508.
- (42) Starkey, M., Lepine, F., Maura, D., Bandyopadhyaya, A., Lesic, B., He, J., Kitao, T., Righi, V., Milot, S., Tzika, A., and Rahme, L. (2014) Identification of anti-virulence compounds that disrupt quorum-

sensing regulated acute and persistent pathogenicity. *PLoS Pathog.* 10, e1004321.

(43) Wei, Q., and Ma, L. Z. (2013) Biofilm matrix and its regulation in *Pseudomonas aeruginosa*. *Int. J. Mol. Sci.* 14, 20983–21005.

(44) Chiang, W.-C., Nilsson, M., Jensen, P. Ø., Høiby, N., Nielsen, T. E., Givskov, M., and Tolker-Nielsen, T. (2013) Extracellular DNA shields against aminoglycosides in *Pseudomonas aeruginosa* biofilms. *Antimicrob. Agents Chemother.* 57, 2352–2361.

(45) Johnson, L., Horsman, S. R., Charron-Mazenod, L., Turnbull, A. L., Mulcahy, H., Surette, M. G., and Lewenza, S. (2013) Extracellular DNA-induced antimicrobial peptide resistance in *Salmonella enterica* serovar Typhimurium. *BMC Microbiol.* 13, 115.

(46) Jones, E. A., McGillivray, G., and Bakaletz, L. O. (2013) Extracellular DNA within a nontypeable *Haemophilus influenzae*-induced biofilm binds human beta defensin-3 and reduces its antimicrobial activity. *J. Innate Immun.* 5, 24–38.

(47) Das, T., and Manefield, M. (2012) Pyocyanin promotes extracellular DNA release in *Pseudomonas aeruginosa*. *PLoS One* 7, e46718.

(48) Häussler, S., and Becker, T. (2008) The pseudomonas quinolone signal (PQS) balances life and death in *Pseudomonas aeruginosa* populations. *PLoS Pathog.* 4, e1000166.

(49) Jander, G., Rahme, L. G., and Ausubel, F. M. (2000) Positive correlation between virulence of *Pseudomonas aeruginosa* mutants in mice and insects. *J. Bacteriol.* 182, 3843–3845.

(50) Essar, D. W., Eberly, L., Hadero, A., and Crawford, I. P. (1990) Identification and characterization of genes for a second anthranilate synthase in *Pseudomonas aeruginosa*: interchangeability of the two anthranilate synthases and evolutionary implications. *J. Bacteriol.* 172, 884–900.

(51) Christensen, G. D., Simpson, W. A., Younger, J. J., Baddour, L. M., Barrett, F. F., Melton, D. M., and Beachey, E. H. (1985) Adherence of coagulase-negative staphylococci to plastic tissue culture plates: a quantitative model for the adherence of staphylococci to medical devices. *J. Clin. Microbiol.* 22, 996–1006.

(52) O'Toole, G. A., Pratt, L. A., Watnick, P. I., Newman, D. K., Weaver, V. B., and Kolter, R. (1999) Genetic approaches to study of biofilms. *Methods Enzymol.* 310, 91–109.

(53) Frei, R., Breitbach, A. S., and Blackwell, H. E. (2012) 2-Aminobenzimidazole derivatives strongly inhibit and disperse *Pseudomonas aeruginosa* biofilms. *Angew. Chem., Int. Ed.* 51, 5226–5229.

(54) Elbing, K., and Brent, R. (2002) Media preparation and bacteriological tools, in *Curr. Protoc. Mol. Biol.* (Taylor, G. P., Ed.), pp 1.1.1–1.1.7, John Wiley & Sons, New York.

(55) Allesen-Holm, M., Barken, K. B., Yang, L., Klausen, M., Webb, J. S., Kjelleberg, S., Molin, S., Givskov, M., and Tolker-Nielsen, T. (2006) A characterization of DNA release in *Pseudomonas aeruginosa* cultures and biofilms. *Mol. Microbiol.* 59, 1114–1128.

(56) Ghafoor, A., Hay, I. D., and Rehm, B. H. A. (2011) Role of exopolysaccharides in *Pseudomonas aeruginosa* biofilm formation and architecture. *Appl. Environ. Microbiol.* 77, 5238–5246.

(57) Lembre, P., Lorentz, C., Di Martino, P. (2012) Exopolysaccharides of the Biofilm Matrix: A Complex Biophysical World, in *The Complex World of Polysaccharides* (Karunaratne, D. N., Ed.) 1st ed., pp 371–392, InTech, Rijeca.

(58) Sule, P., Wadhawan, T., Wolfe, A. J., Prüß, B. M. (2008) Promega Notes. *Promega Notes* 99. www.promega.de.

3 Results

3.5 Optimization of 2-sufonylpyrimidines to tackle biofilm formation and eDNA release of *Pseudomonas aeruginosa*

Andreas Thomann, Christian Brengel, Carsten Börger, Dagmar Kail, Anke Steinbach, Martin Empting and Rolf W. Hartmann,

Reproduced with permission from *ChemMedChem*; Published online: 12.10.2016, DOI: 10.1002/cmdc.201600419.

Copyright 2016 John Wiley and Sons 2016.

Publication V

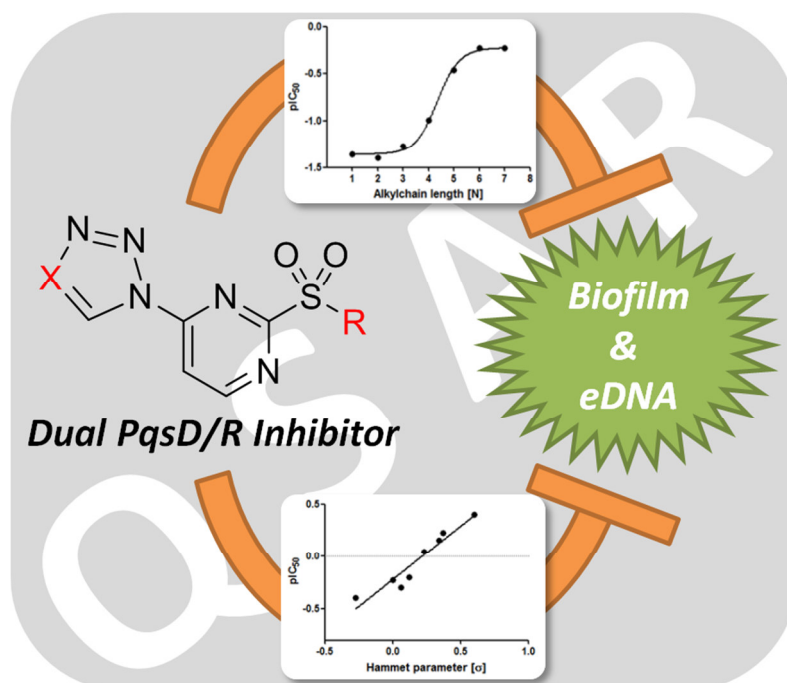


Figure 19. Graphical abstract of publication V.

Structure–Activity Relationships of 2-Sufonylpyrimidines as Quorum-Sensing Inhibitors to Tackle Biofilm Formation and eDNA Release of *Pseudomonas aeruginosa*

Andreas Thomann,^[a] Christian Brengel,^[a] Carsten Börger,^[b] Dagmar Kail,^[b] Anke Steinbach,^[a] Martin Empting,^{*,[a]} and Rolf W. Hartmann^{*,[a, c]}

Drug-resistant *Pseudomonas aeruginosa* (PA) strains are on the rise, making treatment with current antibiotics ineffective. Hence, circumventing resistance or restoring the activity of antibiotics by novel approaches is of high demand. Targeting the *Pseudomonas* quinolone signal quorum sensing (PQS-QS) system is an intriguing strategy to abolish PA pathogenicity without affecting the viability of the pathogen. Herein we report the structure–activity relationships of 2-sufonylpyrimidines, which were previously identified as dual-target inhibitors

of the PQS receptor PqsR and the PQS synthase PqsD. The SAR elucidation was guided by a combined approach using ligand efficiency and ligand lipophilicity efficiency to select the most promising compounds. In addition, the most effective inhibitors were rationally modified by the guidance of QSAR using Hansch analyses. Finally, these inhibitors showed the capacity to decrease biofilm mass and extracellular DNA, which are important determinants for antibiotic resistance.

Introduction

Bacterial resistance is one of the major challenges in drug discovery today, as increasingly more pathogens develop strategies to evade therapy and immune responses. Recently, the most challenging bacteria have been referred to as the ESKAPE pathogens: *Enterococcus faecium*, *Staphylococcus aureus*, *Klebsiella pneumoniae*, *Acinetobacter baumannii*, *Pseudomonas aeruginosa*, and *Enterobacter* spp.^[1] They can “escape” antibiotic treatment through intrinsic tolerance and/or acquired multi-drug resistance. Therefore, novel drug targets and new modes of action need to be discovered to provide a basis for the rational development of novel anti-infective agents.

Pseudomonas aeruginosa (PA) is a ubiquitously present Gram-negative opportunistic bacterium that predominantly infects immunocompromised patients suffering from cystic fibrosis,^[3] burn wounds^[4] or HIV.^[5] To establish an infection, PA has developed various virulence factors that damage epithelial cells^[6] and impair the immune system.^[7] In addition, the patho-

gen is able to embed itself into a heterogeneous hydrogel-like structure known as a biofilm.^[8] This matrix consists of various components such as extracellular DNA (eDNA), polysaccharides, and proteins which have been shown to be important concealing the pathogen from host defense mechanisms^[9] and antibiotics.^[10] In particular, eDNA has recently been discussed as one major factor that prevents the antibiotic activity of aminoglycosides^[11] and fluoroquinolones,^[12,13] which are the first choice to be combined with β -lactam antibiotics in the treatment of PA infections. Moreover, eDNA is heavily involved in resistance against antimicrobial peptides of the host's innate immune system.^[13,14]

Therefore, agents that decrease biofilm and eDNA hold great potential not only to restore antibiotic efficacy, but also to enable the human immune system to clear the infection. Biofilm formation and eDNA release are both controlled by cell-density-dependent communication systems in PA.^[17] This inter-bacterial signaling network uses small molecules to sense the presence of other bacteria and is referred to as quorum sensing (QS). Importantly, interference with QS does not affect the viability of PA.^[18] Hence, the disturbance of QS is a new approach, which has been shown to decrease pathogenicity in vivo with a lower potential for resistance development by circumventing selection pressure.^[19] One PA-specific QS signal is the *Pseudomonas* quinolone signal (PQS), which is a 2-alkyl-quinolone that regulates the production of virulence factors and biofilms.^[17,20] Addressing the PQS-QS system has the advantage of not interfering with the QS systems of other bacteria (e.g., targeting the widespread *las* and *rhl* systems)^[21] that are essential to human health (i.e., the gut microbiome); therefore, such a strategy should minimize potential side effects.

[a] A. Thomann, C. Brengel, Dr. A. Steinbach, Dr. M. Empting, Prof. Dr. R. W. Hartmann
Helmholtz Institute for Pharmaceutical Research Saarland,
Department of Drug Design and Optimization,
Campus E8.1, 66123 Saarbrücken (Germany)
E-mail: rolf.hartmann@helmholtz-hzi.de
martin.empting@helmholtz-hzi.de

[b] Dr. C. Börger, Dr. D. Kail
PharmBioTec GmbH, Science Park 1, 66123 Saarbrücken (Germany)

[c] Prof. Dr. R. W. Hartmann
Saarland University,
Department of Pharmacy, Pharmaceutical and Medicinal Chemistry
Campus C2.3, 66123 Saarbrücken (Germany)

Supporting information and the ORCID identification number(s) for the author(s) of this article can be found under <http://dx.doi.org/10.1002/cmdc.201600419>.

PQS is produced by the syntheses of the *pqsA–E* operon and PqsH.^[22] After the concentration of PQS reaches a certain threshold, the transcriptional regulator PqsR, also referred to as MvfR, is activated and induces the production of virulence factors like pyocyanin^[23] and biofilm^[24] formation, and drives forward the expression of the *pqsA–E* operon in a positive feedback auto-loop mechanism (Figure 1).^[23,25] Moreover, PQS-deficient mutants were shown to have strongly decreased pathogenicity in nematode models.^[26] These biological studies provided the basis for drug discovery campaigns targeting the syntheses of PQS^[27–29] and its receptor.^[18,30,31] The first discovered inhibitors showed anti-virulence as well as anti-biofilm activity and were effective in vivo.^[18,28,31]

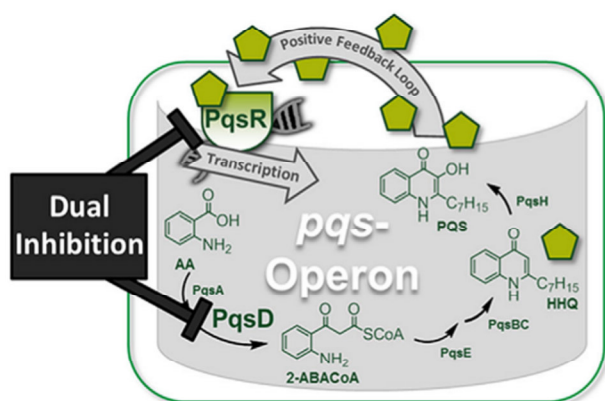


Figure 1. Schematic representation of the *Pseudomonas* quinolone signal quorum sensing system (PQS-QS). Interference with the PQS/HHQ receptor PqsR and a synthase (PqsD), critical for PQS and HHQ production, leads to more highly efficient attenuation of PA pathogenicity than single-target approaches.^[2] AA = anthranilic acid, 2-ABACoA = 2-aminobenzoyl acetate coenzyme A, HHQ = 2-heptyl-4-hydroxyquinoline, PQS = *Pseudomonas* quinolone signal.

We recently published a study on the rational discovery of the first dual-active compounds that simultaneously target PQS synthase (PqsD) and PqsR.^[2] The most effective compounds from this study, **1** and **2**, were found to be active against virulence factor production (pyocyanin, pyoverdine),

but also showed pronounced activity against biofilm formation and eDNA release in cellular assays using *Pseudomonas aeruginosa* PA14. Furthermore, we found that interference with PQS-QS and eDNA release increased the activity of ciprofloxacin under biofilm conditions. Additionally, we could decrease the pathogenicity of PA in an in vivo model by treating *Galleria mellonella* larvae with compound **1**. These promising results encouraged us to further modify the structure of **1** toward higher activity for its respective targets.

Herein we report the exploration of the chemical space of compounds **1** and **2**, as well as the quantitative structure–activity relationship (QSAR) through a Hansch analysis.^[32] Inspired by in silico flexible alignments with a substrate of PqsD (β -ketodecanoic acid)^[33] and the natural ligand of PqsR (HHQ)^[25] compounds were designed under the guidance of ligand efficiency (LE) and ligand lipophilicity efficiency Astex (LLE_{AT}) scores.^[34] The latter metric is exceptionally useful during the drug development process, as it not only evaluates compound activities based on molecular weight, but also on lipophilicity. Hence, this guidepost helps medicinal chemists circumvent the pitfall of an activity increase being based solely on a gain in hydrophobicity.^[35] A combination of both metrics and rational design strategies led to the discovery of potent, ligand-efficient and drug-like inhibitors of biofilm formation and eDNA release.

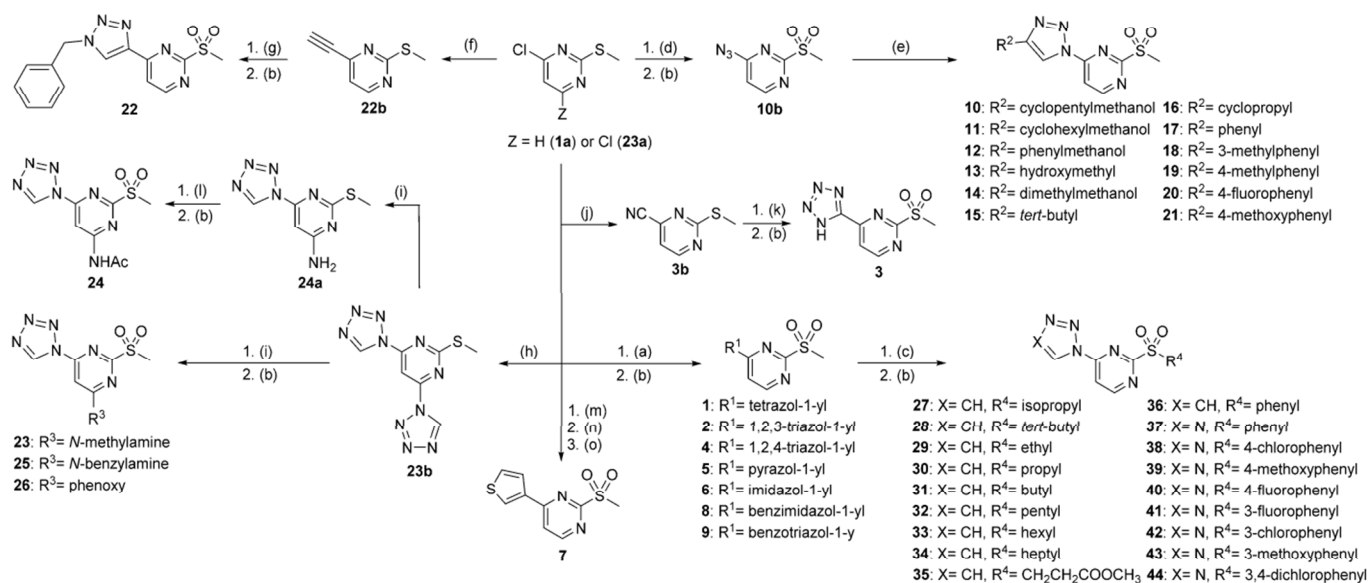
Results and Discussion

The synthesis of compounds listed in Table 1 was carried out by either S_NAr , cycloaddition of sodium azide, or Suzuki coupling and subsequent oxidation of the thioether. Triazole compounds listed in Table 2 were accessed by standard copper(I)-mediated azide–alkyne click reactions followed by oxidation. Tetrazole derivatives **23–26** could be obtained by a microwave-assisted S_NAr method coupled with an oxidation step. Dual inhibitors in Table 4 below were synthesized by replacing the sulfomethyl group of **1** or **2** by the corresponding thiol reactant and subsequent treatment with Oxone® (Scheme 1).

Using the initial hits **1** and **2** as starting points, we wanted to further improve the activity of the compounds by structural modifications. In a first step, we explored the chemical space

Table 1. Inhibition of PqsD and PqsR by compounds **1–9** and calculated LE and LLE_{AT} for the respective target.

Compd	R ¹	PqsD		PqsR	
		IC ₅₀ [μ M]	LE/LLE _{AT} [kcal/HA]	IC ₅₀ [μ M]	LE/LLE _{AT} [kcal/HA]
1 ^[2]	tetrazol-1-yl	21 \pm 2	0.44/0.66	15 \pm 3	0.45/0.67
2 ^[2]	1,2,3-triazol-1-yl	23 \pm 1	0.43/0.58	25 \pm 8	0.43/0.58
3	tetrazol-5-yl	>50; 35% \pm 15	–	>200; 11% \pm 9	–
4	1,2,4-triazol-1-yl	>25; 21% \pm 8	–	25 \pm 3	0.43/0.61
5	pyrazol-1-yl	>50; 41% \pm 3	–	175 \pm 39	0.35/0.45
6	imidazol-1-yl	50 \pm 7	0.40/0.54	75 \pm 26	0.38/0.52
7	thiophen-3-yl	>50; 3% \pm 1	–	>200; 33% \pm 0	–
8	benzimidazol-1-yl	33 \pm 6	0.33/0.39	146 \pm 34	0.28/0.34
9	benzotriazol-1-yl	17 \pm 4	0.35/0.41	107 \pm 25	0.29/0.35



Scheme 1. Synthesis of compounds 1–44: a) **1a**, *N*-heterocycle, TEA, DMF, microwave;^[15] b) thioether, Oxone[®] or *m*CPBA, EtOAc/H₂O or CH₂Cl₂; c) **1** or **2**, thiol, DMF, –20 °C; d) **1a**, NaN₃, DMF;^[15] e) **10b**, *t*BuOH/H₂O, CuSO₄, sodium ascorbate;^[2] f) **1a**, TMS-acetylene, TEA, CuI, (PPh₃)₂PdCl₂, 60 °C then TBAF/THF; g) **22b**, benzylazide, *t*BuOH/H₂O, CuSO₄, sodium ascorbate; h) **23a**, 1*H*-tetrazole, TEA, DMF, microwave;^[16] i) **23b**, TEA, DMF, microwave;^[16] j) **1a**, HI then CuCN, pyridine, reflux; k) **3b**, NaN₃, NH₄Cl, DMF, 80 °C; l) **24a**, (AcO)₂O, reflux; m) **1a**, TMS-Br, MeCN, 40 °C; n) **7a**, H₂O₂, ammonium molybdate tetrahydrate, EtOH, 0 °C; o) **7b**, Pd₂dba₃, PCy₃, K₃PO₄, 3-thiopheneboronic acid, dioxane/H₂O, 100 °C.

at the 4-position of pyrimidine and introduced several heterocycles (Scheme 1, Table 1). Regarding tetrazole substitution, compound **3**, a regioisomer of **1**, was only weakly active on PqsD and almost inactive on PqsR. This might arise either from the acidic character of the tetrazole, resulting in a negative charge (when deprotonated) or from the hydrogen bond donor properties (when protonated). These presumably uncompensated hydrogen bonds and/or ionic interactions might therefore be the root cause for the activity decrease due to desolvation penalties.^[36,37] With regard to other pentacycles (**4**–**6**) of the subset, azoles lacking a nitrogen atom at the 3-position (**4** and **5**) were less active on both targets than compounds **1** and **2**, while only **4** was equally active against PqsR. Interestingly, when switching from azoles to thiophene (**7**), activity was strongly impaired on both targets. In a next step, we enlarged the azole motif and introduced benzimidazole **8** and benzotriazole **9**. In comparison with **1**, we observed a loss of activity on PqsR for both compounds, whereas activity on PqsD could be maintained.

Analysis of ligand efficiency and ligand lipophilicity efficiency of this subset (LE and LLE_{AT}) still rendered compounds **1** and **2** to be the most promising scaffolds. Consequently, for all subsequent structure modifications, either triazole **2** or tetrazole **1** served as the core structure. Therefore, we introduced substituents at the 4-position of the triazolyl substituent of **2** (Table 2). Compound **10**, which we recently reported as a pure PqsR antagonist, is almost equally active on PqsR as **2**.^[2] Regarding its structure and activity, the hydroxy functionality of **10** does not seem to be beneficial for antagonism on PqsR, but is at least tolerated. This observation is quite unusual, as the introduction of non-interacting hydrophilic groups (e.g., hydroxy, amino) can lead to decreased activity due to desolva-

tion penalties.^[36,37] Thus, for physicochemical reasons we kept the hydroxy group and varied substituents at the methylene unit. Enlargement of cyclopentyl (**10**) to cyclohexyl (**11**) resulted in a decrease of activity on PqsR without any beneficial effect on PqsD. Introduction of phenyl (**12**) increased activity on PqsD but was not very well tolerated by PqsR. Thus, we decided to decrease the substituent size toward an unsubstituted hydroxy (**13**) and dimethyl-substituted derivative (**14**). Regarding PqsD, we could observe no restoration of activity upon decreasing size while keeping the hydroxy functionality in place (compare **2** with **10**–**14**). For PqsR we maintained activity relative to **2**. Next, the hydroxy group was exchanged for a methyl function (**15**), yielding a compound similar in size to **14** but lacking the issue of desolvation penalties (see above). The decreased activity of **15** on PqsR revealed the hydroxy group to be beneficial over methyl. For PqsD, a slight increase in activity (compare **14** and **15**) was observed, implying that the hydrophilicity might be more detrimental for activity than steric demand. From this series we concluded that the hydroxy function does not impair activity on PqsR, but improves LLE_{AT} due to its hydrophilicity (compare **2** and **13**). Although we could not increase activity on both targets relative to **2**, knowledge of the hydroxy group being in principal tolerated by PqsR could be valuable information for later-stage drug development if solubility or lipophilicity issues might arise. To further explore the applicability of a fragment-growing strategy starting at the 4-position of the triazole of **2**, we broadened the scope of substituents and introduced cyclopropyl (**16**) and phenyl groups (**17**). Although **16** did not show increased activity on both targets, **17** was about five times more active than its parent compound **2** regarding inhibition of PqsD. Hence, **17** was the most promising hit from this series, with ligand effi-

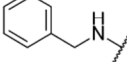
Table 2. Inhibition of PqsD and PqsR by compounds **10–22** and calculated LE and LLE_{AT} for the respective target.

Compd	R ²	PqsD		PqsR	
		IC ₅₀ [μM]	LE/ LLE_{AT} [kcal/HA]	IC ₅₀ [μM]	LE/ LLE_{AT} [kcal/HA]
10 ^[2]		> 50; 12% ± 2	–	26 ± 9	0.30/0.39
11		> 50; 14% ± 4	–	~ 50; 53% ± 12	0.27/0.34
12		~ 50; 52% ± 1	0.27/0.37	< 50; 74% ± 16	0.27/0.37
13		> 50; 24% ± 5	–	22 ± 4	0.38/0.62
14		> 50; 15% ± 3	–	27 ± 12	0.34/0.51
15		> 50; 44% ± 2	–	> 50; 40% ± 3	–
16		29 ± 5	0.35/0.44	25 ± 8	0.36/0.44
17		4 ± 0.3	0.36/0.41	< 200; 66% ± 8	–
18		> 10; 35% ± 8	–	> 10; 18% ± 10	–
19		> 10; 33% ± 3	–	> 10; 21% ± 6	–
20		> 10; 41% ± 1	–	> 10; 30% ± 13	–
21		> 25; 37% ± 0	–	> 50; 0% ± 0	–
22		> 50; 8% ± 7	–	> 50; 22% ± 3	–

ciencies in the preferable range of 0.3 kcal per heavy atom (HA) regarding activity on PqsD.^[34] Consequently, we substituted the phenyl ring with a methyl group at the 3- and 4-positions to further explore the size of the binding pocket. Besides the dramatic decrease in solubility (Supporting Information), from 200 μM determined for **17** to 10 μM for **18** and **19**, the potency was also decreased on PqsD. Additionally, only weak antagonism of PqsR was found for these compounds. Hence, we decided to introduce less hydrophobic substituents. The introduction of fluorine into the 4-position of phenyl (**20**) decreased solubility without increasing activity. For the methoxy substituent (**21**), we found a less dramatic loss in solubility

(50 μM) but lower potency than **17** on both targets. To investigate whether a more flexible moiety increases solubility and activity, we introduced a benzyl substituent. As copper(I)-mediated cycloaddition of benzylacetylene and **10b** (Scheme 1) was not successful, we decided to bioisosterically replace the 1,2,3-triazol-1-yl with 1,2,3-triazol-5-yl regarding the bonding to the 4-position of pyrimidine (**22**). Unfortunately, activity dropped toward PqsD and PqsR as well as solubility. Regarding activity and solubility, we conclude that an introduction of this subset of functional groups is not beneficial for the development of an efficient drug-like compound. Thus, further modifications of the structure of **1** were carried out at the 6-position

Table 3. Inhibition of PqsD and PqsR by compounds **23–26** and calculated LE and LLE_{AT} for the respective target.

Compd	R ³	PqsD		PqsR	
		IC ₅₀ [μM]	LE/LLE _{AT} [kcal/HA]	IC ₅₀ [μM]	LE/LLE _{AT} [kcal/HA]
23		>50; 0% ± 0	–	>50; 23% ± 6	–
24		–50; 50% ± 11	0.32/0.51	–50; 49% ± 4	0.32/0.51
25		>50; 36% ± 8	–	>50; 27% ± 4	–
26		3.2 ± 0.0	0.35/0.43	–50; 48% ± 0	0.27/0.36

of pyrimidine. We chose four substituents differing in size and functionality to be introduced (Table 3). For *N*-methylamine (**23**) we found an almost complete loss of activity on both targets. The same was true for acetamide (**24**). The enlarged flexible hydrophobic residue benzylamine (**25**) was also neither tolerated by PqsR nor PqsD. Introduction of phenoxy to the 6-position of pyrimidine (**26**) lead to an increase in potency on PqsD by about fourfold relative to **1** with an IC₅₀ value of 3.2 μM, but for PqsR a decrease was observed. Regarding ligand efficiencies, **26** is below the minimum LE score of 0.3 for PqsR, rendering this compound a suboptimal choice for further optimization. To derive a rational basis for further modifications to the structure of **2** we conducted flexible alignment experiments of **2** with the described substrate (β-ketodecanoic acid) of PqsD and the natural ligand (HHQ) of PqsR (Figure 2). In detail, the (1,2,3-triazol-1-yl)pyrimidine part of **2** matches the quinolone core of HHQ, and the pyrimidine N1 atom of **2** overlaps with N1 of PqsR's ligand HHQ. For β-ketodecanoic acid we observed a very good match of both hydrogen bond acceptor features of the carboxylic acid moiety with N1 and N2 of the pyrimidine of **2**. Furthermore, the ketone in the β-position of PqsD's substrate overlaps perfectly with an oxygen atom of the sulfone group of **2**. Thus, both alignments suggested the sulfomethyl group to be an ideal starting point for the introduction of an enlarged alkyl chain being potentially beneficial for activity on both targets. To investigate the steric dimensions of the pocket we synthesized compounds bearing isopropyl (**27**) and *tert*-butyl (**28**) at R⁴ (Table 4). For these compounds a loss in activity was observed on both targets. These results shed light on the architecture of the binding sites of PqsD and PqsR, as bulky substituents at R⁴ are not tolerated. Thus, we decided to synthesize unbranched derivatives with chain lengths ranging from 1 to 7 carbons (**2**, **29–34**). Notably, we achieved an increase in activity regarding PqsD inhibition when increasing chain length combined only slight losses in PqsR antagonism. Interestingly, a pronounced potency increase on PqsD was observed at a minimum chain length of 4 (com-

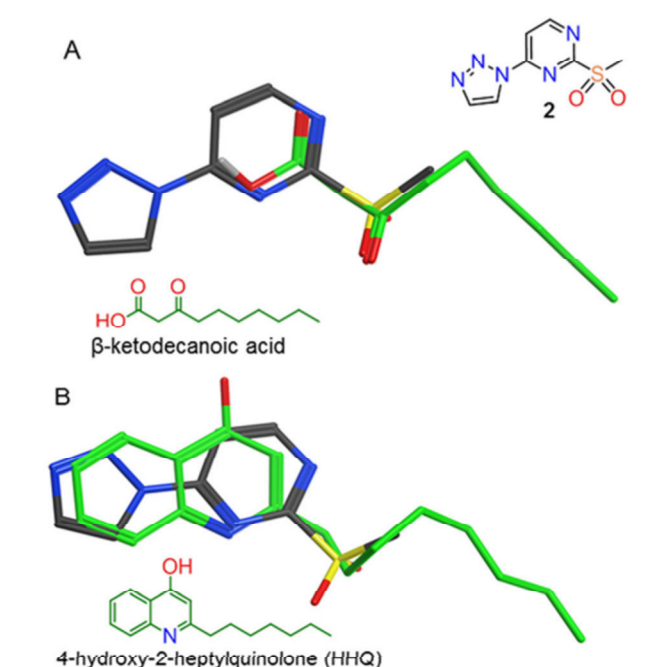
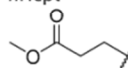


Figure 2. Best-scored flexible alignment (MOE 2014.09) of HHQ (green carbons, B) and **2** (grey carbons, B). Based on these results, an alignment of PqsD's artificial substrate β-ketodecanoic acid (green carbons, A) and **2** (grey carbons, A) was obtained, resulting in a related arrangement, providing a starting point for ligand-based optimization.

pare **29–31** with **2**), but activity leveled out at IC₅₀ = 1.7 μM regarding hexyl (**33**) and heptyl (**34**). To investigate the relationship of the length of the alkyl chain and activity on PqsD we correlated both parameters and retrieved a Hansch equation of sigmoidal shape (Figure 3B). The function showed a very high correlation of experimental versus calculated pIC₅₀ values ($r = 0.9984$, Figure 3C).

Regarding this correlation, the hexyl chain seems to be of ideal length to fill the hydrophobic channel possibly occupied by PqsD's substrate β-ketodecanoic acid being in good agree-

Table 4. Inhibition of PqsD and PqsR by compounds 27–44 and calculated LE and LLE_{AT} for the respective target.

Compd	R ⁴	X	PqsD		PqsR	
			IC ₅₀ [μM]	LE/LLE _{AT} [kcal/HA]	IC ₅₀ [μM]	LE/LLE _{AT} [kcal/HA]
27	<i>i</i> Pr	CH	> 50; 23% ± 7	–	~ 50; 49% ± 13	0.35/0.49
28	<i>t</i> Bu	CH	> 50; 27% ± 0	–	> 50; 24% ± 10	–
29	Et	CH	26 ± 1	0.40/0.52	14 ± 2	0.42/0.54
30	<i>n</i> Pr	CH	19 ± 3	0.39/0.47	19 ± 5	0.39/0.47
31	<i>n</i> Bu	CH	9.9 ± 1.5	0.39/0.43	30 ± 15	0.35/0.40
32	<i>n</i> Pent	CH	2.9 ± 0.5	0.41/0.41	> 50; 31% ± 0	–
33	<i>n</i> Hex	CH	1.7 ± 0.0	0.40/0.38	~ 50; 47% ± 22	0.30/0.28
34 ^[2]	<i>n</i> Hept	CH	1.7 ± 0.4	0.38/0.34	> 50; 17% ± 2	–
35		CH	14 ± 1	0.34/0.47	18 ± 7	0.33/0.46
36	Ph	CH	1.8 ± 0.1	0.40/0.44	30 ± 17	0.32/0.35
37	Ph	N	1.7 ± 0.2	0.40/0.49	16 ± 5	0.34/0.42
38	4-Cl-Ph	N	0.9 ± 0.1	0.40/0.44	< 50; 74% ± 3	0.29/0.36
39	4-OMe-Ph	N	2.5 ± 0.6	0.36/0.44	> 50; 42% ± 31	–
40	4-F-Ph	N	2.0 ± 0.3	0.38/0.47	21 ± 12	0.31/0.40
41	3-F-Ph	N	0.7 ± 0.1	0.41/0.49	26 ± 5	0.31/0.38
42	3-Cl-Ph	N	0.6 ± 0.1	0.41/0.45	17 ± 5	0.32/0.35
43	3-OMe-Ph	N	1.6 ± 0.0	0.37/0.44	> 50; 43% ± 27	–
44	3,4-di-Cl-Ph	N	0.4 ± 0.1	0.41/0.41	24 ± 5	0.29/0.30

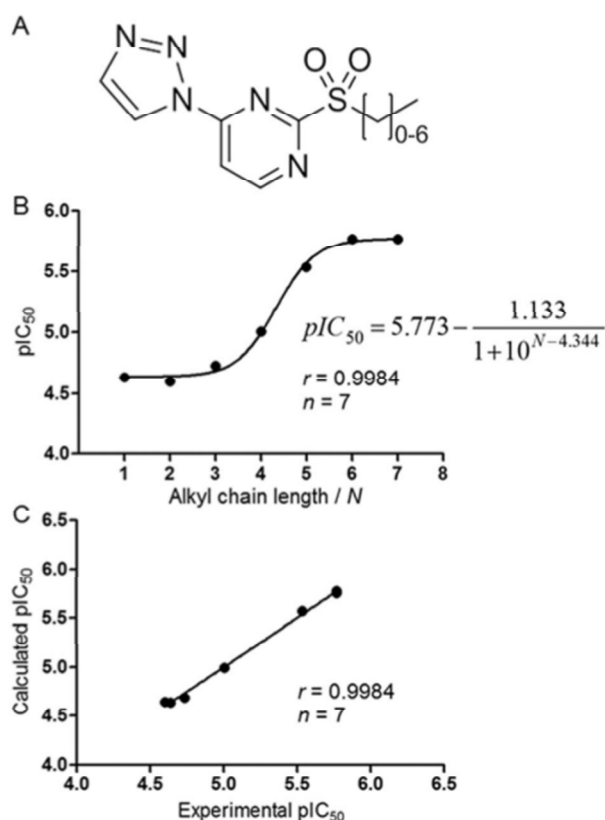


Figure 3. Hansch analysis of alkyl-substituted compounds 2 and 29–34 (A) covering chain lengths from 1 to 7 carbon atoms. Carbon atom count of the alkyl chain and the biological activity on PqsD showed a very high degree of correlation, resulting in a sigmoidal shape function (B), which was also true for the plot of calculated versus experimentally determined pIC₅₀ values (C).

ment with the flexible alignment (Figure 2 A). The IC₅₀ toward PqsR was ~50 μM for 33, but only residual activity was found when heptyl was introduced (34). Interestingly, relationships between alkyl chain length and activity were also observed for PQS and HHQ derivatives published by Hodgkinson, Lu, and Ilangovan corroborating our findings.^[31,38]

Regarding ligand efficiency metrics, compound 33 was still above the suggested score of 0.3 on both targets, with the LLE_{AT} value for PqsR being the exception (0.28). Thus, we introduced an ester functionality into the alkyl chain to achieve a more hydrophilic compound, thereby increasing LLE_{AT} (35). Interestingly, activity was restored on PqsR, but was impaired on PqsD. With regard to lipophilicity, represented by the LLE_{AT} score, we could improve the compound's properties, making it more efficient than its alkyl congener (compare 32 and 35).

In a next step, we investigated whether aromatic substituents are tolerated at R⁴. Thus, we introduced phenyl to 1 and 2 at R⁴. The resulting compounds (36 and 37) showed increased activity on PqsD and no loss of activity on PqsR. Interestingly, 37 had a better performance than 36 regarding activity on PqsR and LLE_{AT}. Hence, we chose 37 for further modifications at the phenyl ring. To rationalize the choice of substituents to be introduced, we followed the Topliss scheme and introduced methoxy and chlorine to the 4-position.^[39] Activity increased for the introduction of chlorine (38) and dropped for methoxy (39) regarding PqsD, highlighting the importance of electronic properties for potency. To investigate this relationship, we synthesized compounds 40–43. For these compounds a general trend could be observed: electron-withdrawing groups (EWGs) increase potency, while electron-donating groups (EDGs) result in decreased potency. Thus, we synthe-

sized **44** bearing two chlorine atoms at positions 2 and 4 of the sulfophenyl substituent. Corroborating our hypothesis, we achieved higher potency on PqsD with $IC_{50} = 0.4 \mu\text{M}$. To further rationalize our observation we set up a Hansch equation correlating σ Hammett parameters^[40] of the substituents (Figure 4B) with the corresponding biological activities (Figure 4C). The resulting equation showed very good correlation between the parameter and the biological activity; moreover, the predictability of the model could be verified by plotting calculated versus observed pIC_{50} values ($r = 0.9574$, Figure 4D). The plot of pIC_{50} versus lipophilic parameters π and $cLogP$ showed a lower degree of correlation ($r = 0.8416$ and 0.8348), rendering the electronic parameter to be the variable of choice for QSAR (Supporting Information).

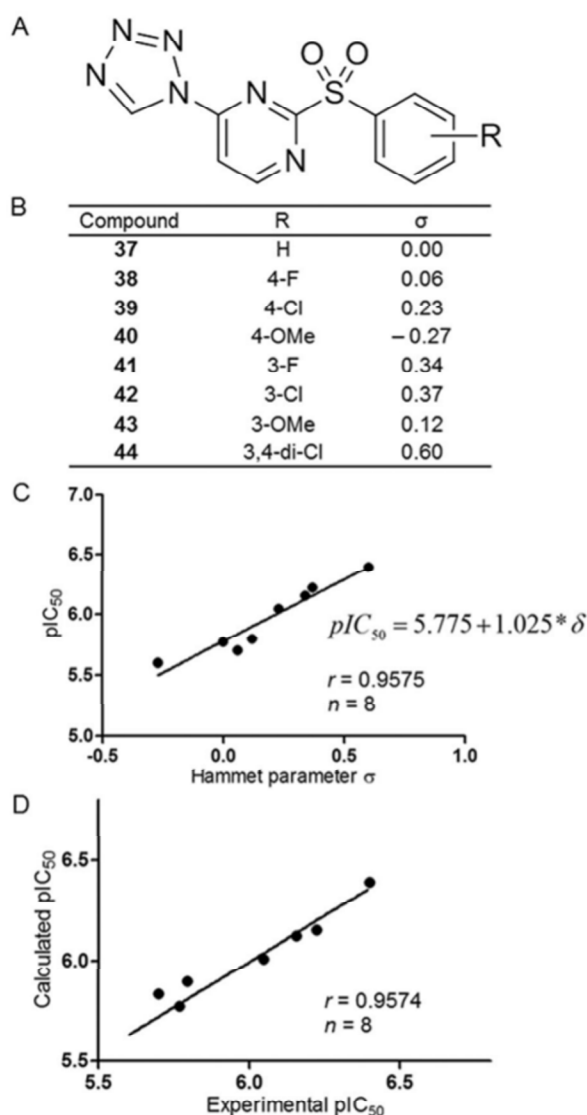


Figure 4. Hansch analysis of compounds **37–44** (A) substituted with a phenyl group functionalized with EWGs and EDGs (B). The Hammett parameter and biological activity versus PqsD showed a very high degree of correlation, resulting in a linear function (C). Very good predictivity of the model was found by correlating calculated versus experimentally determined pIC_{50} values (D).

Compound **44**, as well as most derivatives from this subset, are almost as active on PqsR as **1** (Table 3). Notably, LE/LLE_{AT} metrics calculated for compound **44** are in the desirable range for both targets. The PQS-QS is largely involved in the regulation of biofilm formation and eDNA release, which are two highly relevant biological determinants for PA resistance to antibiotics and immune response. To test whether our compounds are able to decrease the production of biofilm and eDNA, we conducted experiments using *Pseudomonas aeruginosa* PA14.^[41] Storz et al. have shown that the relationship between in vitro potency and in cellulo effectivity is highly dependent on structural modifications and cannot be easily explained by focusing only on physicochemical properties.^[27] Thus, we chose compounds **33** and **44**, both with promising activity in vitro, but reflecting a larger chemical space and tested them at a concentration of $100 \mu\text{M}$ for their ability to decrease biofilm formation and eDNA release by PA14. Indeed, both compounds significantly decreased biofilm volume and eDNA production (Figure 5) without impairing bacterial

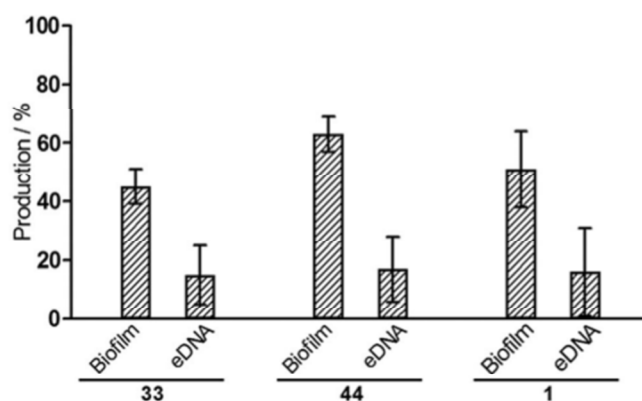


Figure 5. Effect of compounds **1**, **33**, and **44** at $100 \mu\text{M}$ on *Pseudomonas aeruginosa* PA14 biofilm formation (Biofilm) and release of extracellular DNA (eDNA) versus 1% DMSO solvent control, which was set to 100%.

growth. Although less potent at the targets, compound **33** was slightly more efficient in decreasing biofilm and eDNA than **44**. In addition, **33** showed similar inhibition of the two pathogenicity traits as compound **1**, suggesting that the improved PqsD efficacy compensates the losses of PqsR antagonism (Figure 5). One possible explanation might be differences in permeation through the Gram-negative cell envelope or interaction with the biofilm matrix. Therefore, the concentration of drug in the media might be higher than inside the cell, resulting in lower amounts of drug at the site of action. To corroborate these findings, we investigated whether **44** can inhibit pyocyanin production (see Supporting Information), a PQS-dependent virulence factor. Indeed, compound **44** showed lower efficacy (14% at $100 \mu\text{M}$) than compound **1** ($IC_{50} = 86 \mu\text{M}$) in a cellular assay which supports our latter hypothesis.

Conclusions

In this study, we report the ligand-based design and structural modification of dual-inhibitor compounds targeting two key players in the *Pseudomonas aeruginosa* virulence and biofilm machinery, namely PqsD and PqsR. Based on flexible alignment approaches and subsequent Hansch analyses we were able to discover potent and ligand-efficient PqsD inhibitors while keeping activity on the secondary target PqsR. The two investigated candidates from these approaches displayed a strong decrease in biofilm mass and eDNA release, two major causes of antibiotic treatment failure, as well as reduced host immune clearance. However, increasing activity on both targets at the same time is a difficult task. Nevertheless, we were successful in identifying hotspots at the ligands' structure, facilitating optimization toward one target (PqsD) while keeping activity on the second (PqsR). In general, polypharmacology is an intriguing approach to combat bacterial strains highly resistant to existing antibiotics, as multitarget drugs lower the potential of drug–drug interactions relative to combination strategies. Therefore, the compounds reported herein are promising candidates for further in vivo studies using, for example, an acute arthropod infection model.

Experimental Section

Determination of ligand efficiency (LE) and ligand lipophilicity efficiency Astex (LLE_{AT}) were carried out with Equations (1)–(11):

$$LE = \frac{\Delta G}{HAC} \quad (1)$$

$$LE \approx \frac{-R * T * \ln(IC_{50})}{HAC} \quad (2)$$

$$LE \approx \frac{R * T * \ln(10) * pIC_{50}}{HAC} \quad (3)$$

$$LE \approx \frac{1.4 * pIC_{50}}{HAC} \quad (4)$$

$$\Delta G^* = \Delta G - \Delta G_{lipo} \quad (5)$$

$$\Delta G^* \approx R * T * \ln(10) * (pIC_{50} - \text{Log}P) \quad (6)$$

$$LLE_{AT} = 0.11 - \frac{\Delta G^*}{HAC} \quad (7)$$

$$LLE_{AT} \approx 0.11 - \frac{R * T * \ln(10) * (pIC_{50} - \text{Log}P)}{HAC} \quad (8)$$

$$LLE_{AT} \approx 0.11 - \frac{-R * T * \ln(10) * (\text{Log}P - pIC_{50})}{HAC} \quad (9)$$

$$LLE_{AT} \approx 0.11 - \frac{-1.4 * (\text{Log}P - pIC_{50})}{HAC} \quad (10)$$

$$LLE_{AT} \approx 0.11 + 1.4 * \frac{\text{Log}P - pIC_{50}}{HAC} \quad (11)$$

in which HAC = heavy atom count.

The calculation of LE by Equations (1)–(4) was based on the findings of Shulz.^[42] The calculation of LLE_{AT} with Equations (5)–(8) was based on the work of Mortenson and Murray used for the calculation

of pIC₅₀-derived LLE_{AT} values by Equations (9)–(11), published by Thomann et al.^[35,43]

Synthesis and analytical characterization. NMR spectra were recorded on a Bruker Avance AV300 or a Bruker DRX500. The residual ¹H or ¹³C resonances of the > 99% deuterated solvents were used for internal reference of all spectra acquired (CDCl₃: ¹H 7.260 ppm, ¹³C 77.16 ppm; [D₆]DMSO: ¹H 2.500 ppm, ¹³C 39.52 ppm). Electrospray ionization (ESI) mass spectrometric data were recorded with either a Surveyor LC system MSQ electrospray mass spectrometer LC–MS couple (ThermoFisher, Dreieich, Germany) using an MeCN/H₂O gradient in positive mode (+), if not otherwise indicated 0.1% TFA was added if necessary, or by a Waters instrument containing a 2767 sample manager, a 2545 binary gradient pump, a 2998 PDA detector, and a 3100 electrospray mass spectrometer by use of an MeCN/H₂O gradient in positive mode (+); if not indicated otherwise 0.1% formic acid was added if necessary. Purity of final compounds was determined by the UV₂₅₄ trace of the LC chromatogram. Compounds **1**, **2**, **10**, **34**, **10a**, and **23a** were synthesized as previously described.^[2,16,43] Analytical and experimental details of intermediates can be found in the Supporting Information.

General procedure (b) for the oxidation of thioethers. Thioether (1 equiv) was dissolved in EtOAc and an aqueous solution of Oxone® (3 equiv) was added. The biphasic mixture was stirred vigorously at room temperature until TLC showed completion. The final products were purified as indicated.

2-(methylsulfonyl)-4-(1H-tetrazol-5-yl)pyrimidine (3). Compound **1a** (1 equiv) was suspended in 28% hydriodic acid and stirred at room temperature for 16 h. The suspension was extracted using CH₂Cl₂, washed with sat. NaHCO_{3(aq)} and dried over Na₂SO₄. Solvent was removed under reduced pressure to give **3a** as a yellow oil (yield 98%). The crude product was dissolved in pyridine and copper(I) cyanide was added (1.1 equiv). The mixture was held at reflux for 4 h and then acidified with 2 M HCl. The aqueous layer was extracted with EtOAc. The organic layer was dried over Na₂SO₄, filtered over a pad of silica and solvent was removed under reduced pressure to give **3b** as a brown oil (yield 99%). **3b** (1 equiv), NaN₃ (1.4 equiv), NH₄Cl (1.4 equiv) were dissolved in DMF and stirred at 80 °C under an inert atmosphere for 23 h. The reaction was acidified to pH 1 using 1 M HCl and the aqueous layer was extracted with EtOAc. The organic layer was dried over Na₂SO₄ and the solvent was removed under reduced pressure to give **3c** as a white solid (pure, 74%). **3** was synthesized according to general procedure b using **3c**. The mixture was extracted with EtOAc and solvent was removed under reduced pressure to give **3** as a white solid (28%). ¹H NMR ([D₆]DMSO, 300 MHz): δ = 3.5 (s, 3H), 8.5 (d, J = 5.1 Hz, 1H), 9.3 ppm (d, J = 5.1 Hz, 1H); ¹³C NMR ([D₆]DMSO, 126 MHz): δ = 39.1, 121.5, 153.5, 154.7, 161.1, 165.9 ppm; ESI-MS(+): m/z 226.7 [M + H]⁺; purity 99%.

General procedure for the synthesis of 4, 5, 6, 8 and 9. The compounds were synthesized as previously described for **1**.^[2] First the N-heterocycle (1 equiv) was quickly added to **1a** (1 equiv) followed by Et₃N (1 equiv). The mixture was stirred in a microwave for 10–20 min at 60–120 °C. Except if otherwise noted, thioethers (**4a–6a**, **8a** and **9a**) were oxidized according to procedure b.

2-(methylsulfonyl)-4-(1H-1,2,4-triazol-1-yl)pyrimidine (4). Compound **4a** (1 equiv) was oxidized using mCPBA (2.25 equiv) in CH₂Cl₂ at 0 °C. The crude product was purified by flash chromatography (EtOAc/hexane, 2:1) to give a white solid (39%). ¹H NMR (CDCl₃, 500 MHz): δ = 3.41 (s, 4H), 8.08 (d, J = 5.7 Hz, 1H), 8.19 (s, 1H), 9.02 (d, J = 5.4 Hz, 1H), 9.33 ppm (s, 1H); ¹³C NMR (CDCl₃,

126 MHz): δ = 39.2, 112.0, 143.1, 154.5, 156.3, 161.0, 165.8 ppm; ESI-MS(+): m/z 226.0 $[M+H]^+$; purity 96%.

2-(methylsulfonyl)-4-(1H-pyrazol-1-yl)pyrimidine (5). Compound **5a** (1 equiv) was oxidized using *m*CPBA (2.25 equiv) in CH_2Cl_2 at 0 °C. The crude product was purified by flash chromatography (EtOAc/hexane, 1:1) to give a white solid (65%). 1H NMR ($CDCl_3$, 500 MHz): δ = 3.40 ppm (s, 4H) 6.57 (dd, J = 2.8, 1.6 Hz, 1H) 7.85 (dd, J = 1.6, 0.6 Hz, 1H), 8.11 (d, J = 5.4 Hz, 1H); 8.66 (dd, J = 2.8, 0.6 Hz, 1H), 8.87 ppm (d, J = 5.4 Hz, 1H); ^{13}C NMR ($CDCl_3$, 126 MHz): δ = 39.1, 110.3, 111.3, 128.5, 145.2, 158.2, 159.6, 165.6 ppm; ESI-MS(+): m/z 225.0 $[M+H]^+$; purity 99%.

4-(1H-imidazol-1-yl)-2-(methylsulfonyl)pyrimidine (6). Compound **6a** (1 equiv) was oxidized using *m*CPBA (2.25 equiv) in CH_2Cl_2 at 0 °C. The crude product was purified by flash chromatography (EtOAc/MeOH, 9:1) to give a white solid (36%). 1H NMR (CD_3OD , 500 MHz): δ = 3.45 (s, 3H), 7.24 (s, 1H), 8.03 (d, J = 5.8 Hz, 1H), 8.08 (s, 1H), 8.80 (s, 1H), 9.05 ppm (d, J = 5.5 Hz, 1H); ^{13}C NMR (CD_3OD , 126 MHz): δ = 39.5, 113.1, 118.0, 132.0, 157.6, 162.4, 167.3 ppm; ESI-MS(+): m/z 225.0 $[M+H]^+$; purity 99%.

2-(methylsulfonyl)-4-(thiophen-3-yl)pyrimidine (7). To a mixture of **7b** (1 equiv) and PCy_3 (0.09 equiv) in dioxane was given Pd_2dba_3 (0.03 equiv), $K_3PO_4(aq)$ (2 equiv) and 3-thiopheneboronic acid (1.2 equiv). The reaction was stirred in a sealed tube for 1 h at 100 °C. The reaction was extracted three times with EtOAc and the solvent was removed under reduced pressure. The crude product was purified by preparative HPLC to give a white solid (22%). 1H NMR (CD_3OD , 300 MHz): δ = 3.43 (s, 3H), 7.61 (dd, J = 5.0, 3.0 Hz, 1H), 7.87 (d, J = 6.1 Hz, 1H), 8.04 (d, J = 5.4 Hz, 1H), 8.54 (d, J = 3.0 Hz, 1H), 8.90 ppm (d, J = 5.2 Hz, 1H); ^{13}C NMR (CD_3OD , 75 MHz): δ = 39.4, 120.5, 127.3, 128.9, 131.1, 139.6, 160.4, 162.9, 167.5 ppm; ESI-MS(+): m/z 241.0 $[M+H]^+$; purity 96%.

1-(2-(methylsulfonyl)pyrimidin-4-yl)-1H-benzo[d]imidazole (8). The crude product was purified by flash chromatography (EtOAc/MeOH, 98:2) to give a white solid (61%). 1H NMR ($[D_6]DMSO$, 300 MHz): δ = 3.52 (s, 3H), 7.35–7.57 (m, 2H), 7.82 (d, J = 7.9 Hz, 1H), 8.37 (d, J = 5.8 Hz, 1H), 8.57 (d, J = 8.2 Hz, 1H), 9.16 (d, J = 5.9 Hz, 1H), 9.27 ppm (s, 1H); ^{13}C NMR ($[D_6]DMSO$, 75 MHz): δ = 112.6, 115.7, 120.3, 124.6, 125.2, 131.2, 142.5, 144.4, 157.1, 160.3, 165.3 ppm; ESI-MS(+): m/z 274.8 $[M+H]^+$; purity 96%.

1-(2-(methylsulfonyl)pyrimidin-4-yl)-1H-benzo[d][1,2,3]triazole (9). Purified by flash chromatography (EtOAc/hexane, 9:1) to give a white solid (99%). 1H NMR ($CDCl_3$, 300 MHz): δ = 3.47 (s, 3H), 7.58 (t, J = 8.4 Hz, 1H), 7.77 (t, J = 8.4 Hz, 1H), 8.20 (d, J = 8.3 Hz, 1H), 8.50 (d, J = 5.7 Hz, 1H), 8.75 (d, J = 8.3 Hz, 1H), 9.04 ppm (d, J = 5.7 Hz, 1H); ^{13}C NMR ($CDCl_3$, 126 MHz): δ = 39.4, 112.4, 115.3, 120.5, 126.5, 130.9, 131.1, 147.0, 158.5, 159.7, 165.8 ppm; ESI-MS(+): m/z 338.8 $[M+MeCN+Na]^+$; purity 95%.

General procedure (d) for the synthesis of 11–21. The compounds were synthesized using the same procedure as reported for compound **10**.^[2] **10a** (1 equiv) was quickly dissolved in *t*BuOH/ H_2O (1:1) and the alkyne (1 equiv), $CuSO_4$ (0.02 equiv) and sodium ascorbate (0.1 equiv) was added and stirred at room temperature for 16 h.

cyclohexyl(1-(2-(methylsulfonyl)pyrimidin-4-yl)-1H-1,2,3-triazol-4-yl)methanol (11). The crude product was purified by flash chromatography (EtOAc/hexane, 7:3) to give a white solid (48%). 1H NMR ($[D_6]DMSO$, 300 MHz): δ = 1.21–2.10 (m, 11H), 3.47–3.67 (m, 3H), 5.17 (s, 1H), 8.42 (d, J = 5.5 Hz, 1H), 8.81 (s, 1H), 9.26 ppm (d, J = 5.5 Hz, 1H); ^{13}C NMR (75 MHz, $[D_6]DMSO$): δ = 22.0, 25.6, 37.9, 39.5, 68.5, 113.2, 119.2, 155.9, 158.3, 162.5, 165.9 ppm; purity 96%.

1-(2-(methylsulfonyl)pyrimidin-4-yl)-1H-1,2,3-triazol-4-yl)(phenyl)methanol (12). The crude product was purified by flash chromatography (EtOAc/hexane, 6:4) to give a white solid (54%). 1H NMR ($CDCl_3$, 300 MHz): δ = 3.11 (d, J = 3.6 Hz, 1H), 3.40 (s, 3H), 6.13 (d, J = 2.61 Hz, 1H), 7.30–7.44 (m, 3H), 7.45–7.54 (m, 2H), 8.36 (d, J = 5.6 Hz, 1H), 8.55 (s, 1H), 9.03 ppm (d, J = 5.5 Hz, 1H); ^{13}C NMR ($CDCl_3$, 75 MHz): δ = 39.2, 69.3, 112.5, 119.3, 126.4, 128.5, 128.9, 141.1, 152.9, 156.4, 160.7, 166.1 ppm; ESI-MS(+): m/z 332.1 $[M+H]^+$; purity 99%.

1-(2-(methylsulfonyl)pyrimidin-4-yl)-1H-1,2,3-triazol-4-yl)methanol (13). The crude product was purified by extraction with EtOAc to yield a white solid (74%). 1H NMR ($CDCl_3$, 300 MHz): δ = 2.40 (brs, 1H) 3.32–3.53 (s, 3H), 4.94 (s, 2H), 8.39 (d, J = 5.5 Hz, 1H), 8.73 (s, 1H), 9.08 ppm (d, J = 5.5 Hz, 1H); ^{13}C NMR ($[D_6]DMSO$, 75 MHz): δ = 39.7, 55.1, 113.2, 121.0, 150.5, 155.8, 162.6, 165.9 ppm; ESI-MS(+): m/z = 256.1 $[M+H]^+$; purity 99%.

2-(1-(2-(methylsulfonyl)pyrimidin-4-yl)-1H-1,2,3-triazol-4-yl)propan-2-ol (14). The crude product was purified by flash chromatography (EtOAc/hexane, 8:2) to yield a colorless oil (45%). 1H NMR ($CDCl_3$, 300 MHz): δ = 1.72 (s, 6H), 2.20–2.80 (brs, 1H), 3.44 (s, 3H), 8.38 (d, J = 5.49 Hz, 1H), 8.62 (s, 1H), 9.05 ppm (d, J = 5.49 Hz, 1H); ^{13}C NMR ($CDCl_3$, 75 MHz): δ = 30.3, 39.2, 68.6, 117.4, 112.5, 156.5, 157.3, 160.7, 166.2 ppm; ESI-MS(+): m/z 284.0 $[M+H]^+$; purity 99%.

4-(4-(tert-butyl)-1H-1,2,3-triazol-1-yl)-2-(methylsulfonyl)pyrimidine (15). The crude product was purified by flash chromatography (EtOAc/hexane, 7:3) to yield a white solid (22%). 1H NMR ($CDCl_3$, 300 MHz): δ = 1.44 (s, 9H), 3.44 (s, 3H), 8.37 (d, J = 5.6 Hz, 1H), 8.39 (s, 1H), 9.01 ppm (d, J = 5.5 Hz, 1H); ^{13}C NMR ($CDCl_3$, 75 MHz): δ = 30.0, 30.0, 31.0, 39.2, 112.4, 116.6, 156.6, 159.5, 160.3, 166.2 ppm; ESI-MS(+): m/z 282.0 $[M+H]^+$; purity 99%.

4-(4-cyclopropyl-1H-1,2,3-triazol-1-yl)-2-(methylsulfonyl)pyrimidine (16). The crude product was filtered over a pad of Celite®/silica to yield a white solid (83%). 1H NMR ($CDCl_3$, 300 MHz): δ = 0.81–1.01 (m, 2H), 1.02–1.16 (m, 2H), 1.96–2.21 (m, 1H), 3.42 (s, 3H), 8.34 (d, J = 5.5 Hz, 1H), 8.37 (s, 1H), 9.01 ppm (d, J = 5.49 Hz, 1H); ^{13}C NMR ($CDCl_3$, 75 MHz): δ = 6.6, 8.2, 39.2, 112.3, 117.3, 152.3, 156.3, 160.4, 166.1 ppm; ESI-MS(+): m/z 266.0 $[M+H]^+$; purity 99%.

2-(methylsulfonyl)-4-(4-phenyl-1H-1,2,3-triazol-1-yl)pyrimidine (17). The crude product was filtered over a pad of Celite®/silica to yield an off-white solid (87%). 1H NMR ($[D_6]DMSO$, 300 MHz): δ = 3.60 (s, 3H), 7.43 (t, J = 7.1 Hz, 1H), 7.52 (t, J = 7.0 Hz, 2H), 8.09 (d, J = 8.4 Hz, 2H), 8.47 (d, J = 5.6 Hz, 1H), 9.29 (d, J = 5.6 Hz, 1H), 9.60 ppm (s, 1H); ^{13}C NMR ($[D_6]DMSO$, 75 MHz): δ = 39.5, 113.4, 119.3, 126.3, 129.4, 129.5, 129.7, 148.4, 155.8, 162.6, 165.9 ppm; ESI-MS(+): m/z 302.0 $[M+H]^+$; purity 99%.

2-(methylsulfonyl)-4-(4-(*m*-tolyl)-1H-1,2,3-triazol-1-yl)pyrimidine (18). The crude product was filtered over a pad of Celite®/silica to yield a white solid (62%). 1H NMR ($CDCl_3$, 300 MHz): δ = 2.45 (s, 3H), 3.46 (s, 3H), 7.21 (d, J = 7.6 Hz, 1H), 7.39 (t, J = 7.6 Hz, 7H), 7.75 (d, J = 7.7 Hz, 1H), 7.80 (s, 1H), 8.43 (d, J = 5.5 Hz, 1H), 8.90 (s, 1H), 9.06 ppm (d, J = 5.5 Hz, 1H); ^{13}C NMR ($CDCl_3$, 75 MHz): δ = 21.4, 21.4, 39.3, 112.5, 116.9, 123.3, 126.8, 128.8, 129.0, 130.1, 138.9, 149.4, 156.4, 160.6, 166.2 ppm; ESI-MS(+): m/z 316.0 $[M+H]^+$; purity 99%.

2-(methylsulfonyl)-4-(4-(*p*-tolyl)-1H-1,2,3-triazol-1-yl)pyrimidine (19). The crude product was filtered over a pad of Celite®/silica to yield a white solid (61%). 1H NMR ($CDCl_3$, 300 MHz): δ = 2.43 (s, 3H), 3.46 (s, 3H), 7.32 (d, J = 8.01 Hz, 2H), 7.86 (d, J = 8.2 Hz, 2H),

8.43 (d, $J=5.5$ Hz, 1H), 8.87 (s, 1H), 9.06 ppm (d, $J=5.6$ Hz, 1H); ^{13}C NMR ($[\text{D}_6]\text{DMSO}$, 126 MHz): $\delta=21.4$, 39.2, 112.5, 116.5, 126.1, 129.8, 139.4, 149.3, 156.4, 160.5, 166.2 ppm; ESI-MS(+): m/z 316.0 $[M+H]^+$; purity 99%.

4-(4-(4-fluorophenyl)-1H-1,2,3-triazol-1-yl)-2-(methylsulfonyl)pyrimidine (20). The crude product was filtered over a pad of Celite®/silica to yield a white solid (40%). ^1H NMR (CDCl_3 , 300 MHz): $\delta=3.46$ (s, 3H), 7.20 (t, $J=8.6$ Hz, 2H), 7.93 (d, $J=5.3$ Hz, 1H), 7.96 (d, $J=5.4$ Hz, 1H), 8.43 (d, $J=5.5$ Hz, 1H), 8.88 (s, 1H), 9.07 ppm (d, $J=5.5$ Hz, 1H); ^{13}C NMR (CDCl_3 , 75 MHz): $\delta=39.2$, 112.5, 116.4, 116.8, 125.1, 128.0, 128.1, 148.4, 156.4, 160.6, 161.7, 164.9, 166.3 ppm; ESI-MS(+): m/z 319.8 $[M+H]^+$; purity 99%.

4-(4-(4-methoxyphenyl)-1H-1,2,3-triazol-1-yl)-2-(methylsulfonyl)pyrimidine (21). The crude product was filtered over a pad of Celite®/silica to yield a white solid (60%). ^1H NMR ($[\text{D}_6]\text{DMSO}$, 300 MHz): $\delta=3.59$ (s, 3H), 3.83 (s, 3H), 7.09 (d, $J=8.9$ Hz, 2H), 8.02 (d, $J=8.8$ Hz, 2H), 8.47 (d, $J=5.5$ Hz, 1H), 9.28 (d, $J=5.6$ Hz, 1H), 9.50 ppm (s, 1H); ^{13}C NMR ($[\text{D}_6]\text{DMSO}$, 126 MHz): $\delta=39.0$, 55.2, 112.8, 114.5, 117.7, 121.7, 127.2, 147.9, 155.4, 159.8, 162.0, 165.3 ppm; ESI-MS(+): m/z 331.8 $[M+H]^+$; purity 96%.

4-ethynyl-2-(methylthio)pyrimidine (22b). Compound **1a** (1 equiv) was dissolved in DMF and NEt_3 (3 equiv), TMS-acetylene (2 equiv), $(\text{PPh}_3)_2\text{PdCl}_2$ (0.03 equiv), and CuI (0.1 equiv) were added. The reaction was stirred under inert atmosphere for 2 h at 50 °C. Brine was added and the aqueous layer was extracted with EtOAc. The combined organic layers were dried over Na_2SO_4 and the solvent was removed under reduced pressure. The crude material was purified by flash chromatography (EtOAc/petroleum ether, 2:98) to yield **22a** as a colorless oil.^[44] The TMS-protected product was deprotected with 1.1 equiv of TBAF·3H₂O in THF for 2 h at room temperature. The reaction was filtered over a pad of silica and solvent was removed under reduced pressure to yield **22b** as a white solid in quantitative yield. ^1H NMR (CDCl_3 , 500 MHz): $\delta=2.57$ (s, 3H), 3.34 (s, 1H), 7.06 (d, $J=5.0$ Hz, 1H), 8.51 ppm (d, $J=4.7$ Hz, 1H); ^{13}C NMR (CDCl_3 , 126 MHz): $\delta=14.1$, 80.7, 81.4, 118.7, 149.8, 157.2, 173.4 ppm.

4-(1-benzyl-1H-1,2,3-triazol-4-yl)-2-(methylsulfonyl)pyrimidine (22). Compound **22b** (1 equiv) was dissolved in $t\text{BuOH}/\text{H}_2\text{O}$ (1:1) and benzylazide^[45] (1 equiv), sodium ascorbate (0.1 equiv), and CuSO_4 (0.02 equiv) were added. The mixture was stirred at room temperature for 16 h and then extracted with EtOAc. The combined organic layers were dried over Na_2SO_4 and purified by flash chromatography (EtOAc/hexane, 3:7) to yield **22c** as a white solid (60%). **22c** was oxidized using procedure b, and **22** was purified by flash chromatography (EtOAc/hexane, 1:1) to give a white solid (53%). ^1H NMR (CDCl_3 , 300 MHz): $\delta=3.36$ (s, 3H), 5.62 (s, 2H), 7.28–7.49 (m, 5H), 8.25–8.40 (m, 2H), 8.90 ppm (d, $J=5.2$ Hz, 1H); ^{13}C NMR (CDCl_3 , 75 MHz): $\delta=39.1$, 54.7, 118.7, 125.1, 128.3, 129.2, 129.3, 133.6, 145.1, 158.7, 159.3, 166.1 ppm; ESI-MS(+): m/z 268 $[M+H]^+$; purity 99%.

N-(2-(methylsulfonyl)-6-(1H-tetrazol-1-yl)pyrimidin-4-yl)acetamide (24). Compound **24a**^[16] was dissolved in acetic anhydride and stirred for 2 h at 140 °C. Solvent was removed under reduced pressure and the crude material was purified by flash chromatography (EtOAc/hexane, 7:3) to yield **24b** as a white solid (47%). **24b** was oxidized using procedure b. The crude material was purified by flash chromatography (EtOAc/hexane + formic acid, 7:3 + 0.1%) to give **24** as a white solid (70%). ^1H NMR ($[\text{D}_6]\text{DMSO}$, 300 MHz): $\delta=2.24$ (s, 3H), 3.54 (s, 3H), 8.80 (s, 1H), 10.46 (s, 1H), 11.98 ppm (s, 1H); ^{13}C NMR ($[\text{D}_6]\text{DMSO}$, 75 MHz): $\delta=24.2$, 24.4, 100.0, 142.2, 154.0, 161.4, 164.8, 171.6 ppm; purity 96%.

General procedure for the synthesis of 23, 25, 26. Synthesis of the thioethers was reported before.^[16] Oxidation was carried out following procedure b.

N-methyl-2-(methylsulfonyl)-6-(1H-tetrazol-1-yl)pyrimidin-4-amine (23). Purified by flash chromatography (EtOAc/hexane, 8:2) to yield a white solid (58%). ^1H NMR ($[\text{D}_6]\text{DMSO}$, 300 MHz): $\delta=2.78$ –3.16 (m, 3H), 3.41–3.54 (m, 3H), 6.97–7.32 (m, 1H), 8.55–9.06 (m, 1H), 10.06–10.45 ppm (m, 1H) (rotamers); ^{13}C NMR ($[\text{D}_6]\text{DMSO}$, 75 MHz): $\delta=28.1$, 96.3, 142.5, 151.2, 165.2, 165.8, 166.5 ppm; ESI-MS(+): m/z 227.8 $[M-\text{N}_2+H]^+$; purity 95%.

N-benzyl-2-(methylsulfonyl)-6-(1H-tetrazol-1-yl)pyrimidin-4-amine (25). The crude product was purified by flash chromatography (EtOAc/hexane, 1:1) to yield a white solid (37%). ^1H NMR ($[\text{D}_6]\text{DMSO}$, 300 MHz): $\delta=3.40$ (s, 3H), 4.69 (d, $J=5.7$ Hz, 2H), 7.27 (s, 1H), 7.33–7.45 (m, 5H), 9.22 (t, $J=5.7$ Hz, 1H), 10.23 ppm (s, 1H) (rotamers); ^{13}C NMR ($[\text{D}_6]\text{DMSO}$, 126 MHz): $\delta=44.2$, 95.7, 127.1, 127.3, 127.8, 128.5, 128.7, 137.9, 142.0, 151.1, 164.1, 165.9 ppm; ESI-MS(+): m/z 331.9 $[M+H]^+$, 303.9 $[M-\text{N}_2+H]^+$; purity 99%.

2-(methylsulfonyl)-4-phenoxy-6-(1H-tetrazol-1-yl)pyrimidine (26). The crude product was purified by flash chromatography (EtOAc/hexane, 1:1) to yield a white solid (38%). ^1H NMR (CDCl_3 , 300 MHz): $\delta=3.19$ (s, 3H), 7.22 (d, $J=8.1$ Hz, 2H), 7.38 (t, $J=7.5$ Hz, 1H), 7.51 (t, $J=7.5$ Hz, 2H), 7.71 (s, 1H), 9.65 ppm (s, 1H); ^{13}C NMR (CDCl_3 , 75 MHz): $\delta=38.7$, 99.1, 99.2, 120.9, 127.2, 130.3, 140.8, 151.4, 155.5, 166.2, 172.4 ppm; purity 95%.

General procedure for the synthesis of 27–44. The compounds were synthesized using the same route as reported for compound **34**,^[2] **1** (1 equiv for **37a–44a**), or **2** (1 equiv for compounds **27a–36a**) was quickly dissolved in DMF and K_2CO_3 (3 equiv) was added. The mixture was cooled to -20 °C and the thiol (1 equiv) was added at once. The reaction was allowed to continue until TLC showed full conversion. Resulting thioethers were oxidized using procedure b.

2-(isopropylsulfonyl)-4-(1H-1,2,3-triazol-1-yl)pyrimidine (27). The crude product was purified by flash chromatography (EtOAc/hexane, 1:1) to yield a white solid (63%). ^1H NMR (CDCl_3 , 300 MHz): $\delta=1.54$ (s, 9H), 7.92 (d, $J=1.3$ Hz, 1H), 8.41 (d, $J=5.4$ Hz, 1H), 8.73 (d, $J=1.3$ Hz, 1H), 9.16 ppm (d, $J=5.4$ Hz, 1H); ^{13}C NMR (CDCl_3 , 75 MHz): $\delta=23.9$, 61.2, 112.3, 121.8, 135.2, 156.1, 160.9, 164.6 ppm; ESI-MS(+): m/z 254.0 $[M+H]^+$; purity 95%.

2-(tert-butylsulfonyl)-4-(1H-1,2,3-triazol-1-yl)pyrimidine (28). The crude product was purified by flash chromatography (EtOAc/hexane, 1:1) to yield a white solid (54%). ^1H NMR (CDCl_3 , 300 MHz): $\delta=1.47$ (d, $J=6.9$ Hz, 6H), 4.01 (spt, $J=6.9$ Hz, 1H), 7.92 (d, $J=1.4$ Hz, 1H), 8.41 (d, $J=5.5$ Hz, 1H), 8.75 (d, $J=1.4$ Hz, 1H), 9.11 ppm (d, $J=5.5$ Hz, 1H); ^{13}C NMR (CDCl_3 , 75 MHz): $\delta=15.0$, 51.6, 112.5, 121.9, 135.2, 156.4, 160.9, 165.3 ppm; ESI-MS(+): m/z 268.0 $[M+H]^+$; purity 95%.

2-(ethylsulfonyl)-4-(1H-1,2,3-triazol-1-yl)pyrimidine (29). The crude product was purified by flash chromatography (EtOAc/hexane, 8:2) to yield a white solid (73%). ^1H NMR (CDCl_3 , 300 MHz): $\delta=1.49$ (t, $J=7.5$ Hz, 3H), 3.63 (q, $J=7.5$ Hz, 2H), 7.92 (d, $J=1.3$ Hz, 1H), 8.42 (d, $J=5.5$ Hz, 1H), 8.75 (d, $J=1.3$ Hz, 1H), 9.09 ppm (d, $J=5.5$ Hz, 1H); ^{13}C NMR (CDCl_3 , 75 MHz): $\delta=6.9$, 45.9, 112.6, 121.9, 135.2, 156.5, 160.9, 165.7 ppm; ESI-MS(+): m/z 240.0 $[M+H]^+$; purity 95%.

2-(propylsulfonyl)-4-(1H-1,2,3-triazol-1-yl)pyrimidine (30). The crude product was purified by flash chromatography (EtOAc/hexane, 3:7) to yield a white solid (88%). ^1H NMR (CDCl_3 , 300 MHz):

δ = 1.00–1.21 (m, 3H), 1.80–2.07 (m, 2H), 3.49–3.66 (m, 2H), 7.92 (d, J = 1.3 Hz, 1H), 8.41 (d, J = 5.5 Hz, 1H), 8.75 (d, J = 1.3 Hz, 1H), 9.09 ppm (d, J = 5.5 Hz, 1H); ^{13}C NMR (CDCl_3 , 75 MHz): δ = 13.2, 16.0, 53.0, 112.6, 121.9, 135.2, 156.4, 160.9, 166.0 ppm; ESI-MS(+): m/z 254.0 $[M+H]^+$; purity 97.0%.

2-(butylsulfonyl)-4-(1H-1,2,3-triazol-1-yl)pyrimidine (31). The crude product was purified by flash chromatography (EtOAc/hexane, 8:2) to yield a white solid (76%). ^1H NMR (CDCl_3 , 300 MHz): δ = 0.98 (t, J = 7.4 Hz, 3H), 1.54 (dq, J = 14.9, 7.4 Hz, 2H), 1.83–1.97 (m, 2H), 3.40–3.76 (m, 2H), 7.92 (d, J = 1.3 Hz, 1H), 8.41 (d, J = 5.5 Hz, 1H), 8.75 (d, J = 1.4 Hz, 1H), 9.09 ppm (d, J = 5.4 Hz, 1H); ^{13}C NMR (CDCl_3 , 75 MHz): δ = 13.5, 21.7, 24.0, 51.1, 112.6, 121.9, 135.2, 156.4, 160.9, 166.0 ppm; purity 99%.

2-(pentylsulfonyl)-4-(1H-1,2,3-triazol-1-yl)pyrimidine (32). The crude product was purified by flash chromatography (EtOAc/hexane, 4:6) to yield a white solid (79%). ^1H NMR (CDCl_3 , 300 MHz): δ = 0.78–1.04 (m, 3H), 1.25–1.57 (m, 4H), 1.92 (quin, J = 7.7 Hz, 2H), 3.51–3.72 (m, 2H), 7.92 (d, J = 0.8 Hz, 1H), 8.41 (d, J = 5.5 Hz, 1H), 8.65–8.83 (m, 1H), 9.09 ppm (d, J = 5.5 Hz, 1H); ^{13}C NMR (CDCl_3 , 75 MHz): δ = 13.6, 21.7, 22.1, 30.5, 51.3, 112.5, 121.9, 135.2, 156.4, 160.8, 165.9 ppm; ESI-MS(+): m/z 282.0 $[M+H]^+$; purity 96%.

2-(hexylsulfonyl)-4-(1H-1,2,3-triazol-1-yl)pyrimidine (33). Purified by flash chromatography (EtOAc/hexane, 1:9) to yield a white solid (71%). ^1H NMR (CDCl_3 , 300 MHz): δ = 0.89 (t, J = 7.2 Hz, 3H), 1.26–1.41 (m, 4H), 1.50 (quin, J = 7.8 Hz, 2H), 1.91 (quin, J = 7.5 Hz, 2H), 3.58 (t, J = 8.0 Hz, 2H), 7.92 (d, J = 1.0 Hz, 1H), 8.41 (d, J = 5.5 Hz, 1H), 8.75 (d, J = 1.3 Hz, 1H), 9.09 ppm (d, J = 5.5 Hz, 1H); ^{13}C NMR (CDCl_3 , 75 MHz): δ = 13.9, 22.0, 22.2, 28.1, 31.1, 51.3, 112.5, 121.9, 135.2, 156.4, 160.8, 166.0 ppm; ESI-MS(+): m/z 296.0 $[M+H]^+$; Purity 99%.

2-((4-(1H-1,2,3-triazol-1-yl)pyrimidin-2-yl)sulfonyl)ethyl acetate (35). The crude product was purified by flash chromatography (EtOAc/hexane, 1:1) to yield a white solid (42%). ^1H NMR (CDCl_3 , 300 MHz): δ = 3.00 (t, J = 7.5 Hz, 2H), 3.71 (s, 3H), 3.94 (t, J = 7.3 Hz, 2H), 7.92 (d, J = 1.3 Hz, 1H), 8.42 (d, J = 5.5 Hz, 1H), 8.75 (d, J = 1.3 Hz, 1H), 9.09 ppm (d, J = 5.5 Hz, 1H); ^{13}C NMR (CDCl_3 , 75 MHz): δ = 27.5, 46.9, 52.4, 112.8, 121.9, 135.3, 156.4, 160.9, 165.5, 170.4 ppm; ESI-MS(+): m/z 298.0 $[M+H]^+$; purity 95%.

2-(phenylsulfonyl)-4-(1H-1,2,3-triazol-1-yl)pyrimidine (36). The crude product was purified by flash chromatography (EtOAc/hexane, 6:4) to yield a white solid (23%). ^1H NMR (CDCl_3 , 300 MHz): δ = 7.59 (t, J = 7.2 Hz, 2H), 7.69 (t, J = 7.2 Hz, 1H), 8.01 (s, 2H), 8.13 (d, J = 5.5 Hz), 8.22 (d, J = 7.5 Hz, 2H), 8.97 ppm (d, J = 5.4 Hz, 1H); ^{13}C NMR (CDCl_3 , 75 MHz): δ = 111.8, 129.2, 129.9, 134.4, 137.3, 139.1, 157.4, 160.5, 167.0 ppm; ESI-MS(+): m/z 288.0 $[M+H]^+$; purity 99%.

2-(phenylsulfonyl)-4-(1H-tetrazol-1-yl)pyrimidine (37). The crude product was purified by flash chromatography (EtOAc/hexane, 1:1) to yield a white solid (91%). ^1H NMR (CDCl_3 , 300 MHz): δ = 7.64 (t, J = 8.1 Hz, 2H), 7.75 (t, J = 7.4 Hz, 1H), 8.15 (d, J = 8.5 Hz, 2H), 8.21 (d, J = 5.4 Hz, 1H), 9.15 (d, J = 5.4 Hz, 1H), 9.58 ppm (s, 1H); ^{13}C NMR (CDCl_3 , 75 MHz): δ = 112.5, 129.4, 129.9, 135.0, 136.4, 140.5, 154.0, 162.3, 167.2 ppm; ESI-MS(+): m/z 261 $[M-N_2+H]^+$; purity 99%.

2-((4-chlorophenyl)sulfonyl)-4-(1H-tetrazol-1-yl)pyrimidine (38). The crude product was purified by flash chromatography (EtOAc/hexane, 1:1) to yield a white solid (58%). ^1H NMR (CDCl_3 , 300 MHz): δ = 7.62 (dt, J = 8.8, 2.3 Hz, 2H), 8.09 (dt, J = 8.8, 2.3 Hz, 2H), 8.23 (d, J = 5.4 Hz, 1H), 9.13 (d, J = 5.4 Hz, 1H), 9.62 ppm (s, 1H);

^{13}C NMR (CDCl_3 , 126 MHz): δ = 166.9, 162.2, 154.1, 142.0, 140.5, 135.0, 131.3, 129.8, 112.7 ppm; purity 99%.

2-((4-methoxyphenyl)sulfonyl)-4-(1H-tetrazol-1-yl)pyrimidine (39). The crude product was purified by flash chromatography (EtOAc/hexane, 1:1) to yield a white solid (90%). ^1H NMR (CDCl_3 , 300 MHz): δ = 3.90 (s, 3H), 6.98–7.14 (m, 2H), 7.98–8.12 (m, 2H), 8.18 (d, J = 5.4 Hz, 1H), 9.14 (d, J = 5.4 Hz, 1H), 9.61 ppm (s, 1H); ^{13}C NMR (CDCl_3 , 126 MHz): δ = 55.8, 112.3, 114.8, 127.4, 132.2, 140.5, 154.0, 162.2, 164.9, 167.6 ppm; ESI-MS(+): m/z 285.2 $[M+H]^+$; purity 98%.

2-((4-fluorophenyl)sulfonyl)-4-(1H-tetrazol-1-yl)pyrimidine (40). The crude product was purified by flash chromatography (EtOAc/hexane, 1:1) to yield a white solid (74%). ^1H NMR (CDCl_3 , 300 MHz): δ = 7.27–7.40 (m, 2H), 8.04–8.28 (m, 3H), 9.14 (d, J = 5.4 Hz, 1H), 9.63 ppm (s, 1H); ^{13}C NMR (CDCl_3 , 75 MHz): δ = 112.7, 116.9, 132.3, 132.9, 140.5, 154.1, 162.2, 166.8, 167.1 ppm; ESI-MS(+): m/z 279.0 $[M-N_2+H]^+$; purity 99%.

2-((3-fluorophenyl)sulfonyl)-4-(1H-tetrazol-1-yl)pyrimidine (41). The crude product was purified by flash chromatography (EtOAc/hexane, 1:1) to yield a white solid (52%). ^1H NMR (CDCl_3 , 300 MHz): δ = 7.45 (tdd, J = 8.3, 8.3, 2.5, 1.0 Hz, 1H), 7.64 (td, J = 8.1, 5.2 Hz, 1H), 7.85 (ddd, J = 7.7, 1.9 Hz, 1H), 7.95 (ddd, J = 7.8, 1.0 Hz, 1H), 8.25 (d, J = 5.5 Hz, 1H), 9.16 (d, J = 5.4 Hz, 1H), 9.63 ppm (s, 1H); ^{13}C NMR (CDCl_3 , 75 MHz): δ = 166.7, 162.3, 162.5, 154.1, 140.5, 138.4, 131.2, 125.7, 122.3, 117.2, 112.8 ppm; ESI-MS(+): m/z 279.0 $[M-N_2+H]^+$; purity 99%.

2-((3-chlorophenyl)sulfonyl)-4-(1H-tetrazol-1-yl)pyrimidine (42). The crude product was purified by flash chromatography (EtOAc/hexane, 1:1) to yield a white solid (39%). ^1H NMR (CDCl_3 , 300 MHz): δ = 7.59 (t, J = 7.8 Hz, 1H), 7.71 (ddd, J = 1.0, 2.1, 8.0 Hz, 1H), 8.04 (ddd, J = 1.0, 1.8, 7.8 Hz, 1H), 8.13 (t, J = 1.9 Hz, 1H), 8.24 (d, J = 5.4 Hz, 1H), 9.15 (d, J = 5.4 Hz, 1H), 9.62 ppm (s, 1H); ^{13}C NMR (CDCl_3 , 126 MHz): δ = 113.5, 128.6, 130.5, 131.3, 135.8, 136.4, 180.7, 138.8, 141.2, 154.8, 163.0, 167.4 ppm; purity 99%.

2-((3-methoxyphenyl)sulfonyl)-4-(1H-tetrazol-1-yl)pyrimidine (43). The crude product was purified by flash chromatography (EtOAc/hexane, 1:1) to yield a white solid (75%). ^1H NMR (CDCl_3 , 300 MHz): δ = 3.89 (s, 3H), 7.19–7.27 (m, 1H), 7.53 (t, J = 8.1 Hz, 1H), 7.59–7.67 (m, 1H), 7.73 (dt, J = 7.7, 1.2 Hz, 1H), 8.21 (d, J = 5.4 Hz, 1H), 9.15 (d, J = 5.4 Hz, 1H), 9.60 ppm (s, 1H); ^{13}C NMR (CDCl_3 , 75 MHz): δ = 55.9, 112.6, 114.2, 121.5, 122.1, 130.5, 137.5, 140.6, 154.1, 160.2, 162.3, 167.2 ppm; ESI-MS(+): m/z 285.2 $[M+H]^+$; purity 99%.

2-((3,4-dichlorophenyl)sulfonyl)-4-(1H-tetrazol-1-yl)pyrimidine (44). The crude product was purified by flash chromatography (EtOAc/hexane, 1:1) to yield a white solid (36%). ^1H NMR ($[\text{D}_6]\text{DMSO}$, 300 MHz): δ = 7.94–8.04 (m, 1H), 8.06–8.17 (m, 1H), 8.28 (d, J = 2.0 Hz, 1H), 8.40 (d, J = 5.5 Hz, 1H), 9.31 (d, J = 5.5 Hz, 1H), 10.34 ppm (s, 1H); ^{13}C NMR ($[\text{D}_6]\text{DMSO}$, 75 MHz): δ = 130.1, 131.6, 132.5, 133.2, 137.2, 139.0, 143.0, 154.6, 163.0, 163.5, 165.5 ppm; ESI-MS(+): m/z 331.9 $[M-N_2+H]^+$, 303.9 $[M-2N_4+H]^+$; purity 99%.

Acknowledgements

We thank Carina Scheidt and Simone Amann (Helmholtz Institute for Pharmaceutical Research Saarland) for biological testing and Nadja Klippel (Saarland University) for supporting compound synthesis. C.B. and D.K. are grateful to the European Regional De-

velopment Fund and Saarland State Ministry for financial support (C/4-PBT-400-4/2010).

Keywords: biofilms · drug design · Hansch analysis · medicinal chemistry · nitrogen heterocycles · *P. aeruginosa*

- [1] H. W. Boucher, G. H. Talbot, J. S. Bradley, J. E. Edwards, D. Gilbert, L. B. Rice, M. Scheld, B. Spellberg, J. Bartlett, *Clin. Infect. Dis.* **2009**, *48*, 1–12.
- [2] A. Thomann, X. de Mello Martins, A. G. G. C. Brengel, M. Empting, R. W. Hartmann, *ACS Chem. Biol.* **2016**, *11*, 1279–1286.
- [3] J. C. Davies, *Paediatr. Respir. Rev.* **2002**, *3*, 128–134.
- [4] H. K. Estahbanati, P. P. Kashani, F. Ghanaatpisheh, *Burns* **2002**, *28*, 340–348.
- [5] J. L. Meynard, F. Barbut, M. Guiguet, D. Batisse, V. Lalande, D. Lesage, J. B. Guiard-Schmid, J. C. Petit, J. Frottier, M. C. Meyohas, *J. Infect.* **1999**, *38*, 176–181.
- [6] a) B. Rada, T. L. Leto, *Trends Microbiol.* **2013**, *21*, 73–81; b) Y.-M. Zhang, M. W. Frank, K. Zhu, A. Mayasundari, C. O. Rock, *J. Biol. Chem.* **2008**, *283*, 28788–28794.
- [7] a) M. E. Skindersoe, L. H. Zeuthen, S. Brix, L. N. Fink, J. Lazenby, C. Whittall, P. Williams, S. P. Diggle, H. Froekiaer, M. Cooley, M. Givskov, *FEMS Immunol. Med. Microbiol.* **2009**, *55*, 335–345; b) K. Kim, Y. U. Kim, B. H. Koh, S. S. Hwang, S.-H. Kim, F. Lépine, Y.-H. Cho, G. R. Lee, *Immunology* **2010**, *129*, 578–588; c) D. S. W. Hooi, B. W. Bycroft, S. R. Chhabra, P. Williams, D. I. Pritchard, *Infect. Immun.* **2004**, *72*, 6463–6470.
- [8] N. Høiby, O. Ciofu, T. Bjarnsholt, *Future Microbiol.* **2010**, *5*, 1663–1674.
- [9] M. Alhede, T. Bjarnsholt, M. Givskov, M. Alhede, *Adv. Appl. Microbiol.* **2014**, *86*, 1–40.
- [10] T.-F. Mah, B. Pitts, B. Pellock, G. C. Walker, P. S. Stewart, G. A. O'Toole, *Nature* **2003**, *426*, 306–310.
- [11] a) W.-C. Chiang, M. Nilsson, P. Ø. Jensen, N. Høiby, T. E. Nielsen, M. Givskov, T. Tolker-Nielsen, *Antimicrob. Agents Chemother.* **2013**, *57*, 2352–2361; b) H. Mulcahy, L. Charron-Mazenod, S. Lewenza, *PLoS Pathog.* **2008**, *4*, e1000213.
- [12] a) T. S. Walker, K. L. Tomlin, G. S. Worthen, K. R. Poch, J. G. Lieber, M. T. Saavedra, M. B. Fessler, K. C. Malcolm, M. L. Vasil, J. A. Nick, *Infect. Immun.* **2005**, *73*, 3693–3701; b) G. V. Tetz, N. K. Artemenko, V. V. Tetz, *Antimicrob. Agents Chemother.* **2009**, *53*, 1204–1209.
- [13] S. Lewenza, *Front. Microbiol.* **2013**, *4*, 21.
- [14] L. Johnson, S. R. Horsman, L. Charron-Mazenod, A. L. Turnbull, H. Mulcahy, M. G. Surette, S. Lewenza, *BMC Microbiol.* **2013**, *13*, 115.
- [15] A. Thomann, C. Börger, M. Empting, R. Hartmann, *Synlett* **2014**, *25*, 935–938.
- [16] A. Thomann, J. Eberhard, G. Allegretta, M. Empting, R. Hartmann, *Synlett* **2015**, *26*, 2606–2610.
- [17] J. Lee, L. Zhang, *Protein Cell* **2015**, *6*, 26–41.
- [18] C. Lu, C. K. Maurer, B. Kirsch, A. Steinbach, R. W. Hartmann, *Angew. Chem. Int. Ed.* **2014**, *53*, 1109–1112; *Angew. Chem.* **2014**, *126*, 1127–1130.
- [19] J. P. Gerdt, H. E. Blackwell, *ACS Chem. Biol.* **2014**, *9*, 2291–2299.
- [20] U. Komor, P. Bielecki, H. Loessner, M. Rohde, K. Wolf, K. Westphal, S. Weiss, S. Häussler, *Microbes Infect.* **2012**, *14*, 951–958.
- [21] a) C. T. O'Loughlin, L. C. Miller, A. Siryaporn, K. Drescher, M. F. Semmelhack, B. L. Bassler, *Proc. Natl. Acad. Sci. USA* **2013**, *110*, 17981–17986; b) T. Ishida, T. Ikeda, N. Takiguchi, A. Kuroda, H. Ohtake, J. Kato, *Appl. Environ. Microbiol.* **2007**, *73*, 3183–3188; c) J. D. Moore, F. M. Rossi, M. A. Welsh, K. E. Nyffeler, H. E. Blackwell, *J. Am. Chem. Soc.* **2015**, *137*, 14626–14639; d) M. A. Welsh, H. E. Blackwell, *Cell Chem. Biol.* **2016**, *23*, 361–369; e) O. Lidor, A. Al-Quntar, E. C. Pesci, D. Steinberg, *Sci. Rep.* **2015**, *5*, 16569; f) S. Y.-Y. Tan, S.-L. Chua, Y. Chen, S. A. Rice, S. Kjelleberg, T. E. Nielsen, L. Yang, M. Givskov, *Antimicrob. Agents Chemother.* **2013**, *57*, 5629–5641; g) K. T. O'Brien, J. G. Noto, L. Nichols-O'Neill, L. J. Perez, *ACS Med. Chem. Lett.* **2015**, *6*, 162–167.
- [22] a) C. E. Dulcey, V. Dekimpe, D.-A. Fauvel, S. Milot, M.-C. Groleau, N. Doucet, L. G. Rahme, F. Lépine, E. Déziel, *Chem. Biol.* **2013**, *20*, 1481–1491; b) S. L. Drees, S. Fetzner, *Chem. Biol.* **2015**, *22*, 611–618.
- [23] G. Xiao, J. He, L. G. Rahme, *Microbiology* **2006**, *152*, 1679–1686.
- [24] Q. Guo, W. Kong, S. Jin, L. Chen, Y. Xu, K. Duan, *J. Basic Microbiol.* **2014**, *54*, 633–643.
- [25] G. Xiao, E. Déziel, J. He, F. Lépine, B. Lesic, M.-H. Castonguay, S. Milot, A. P. Tampakaki, S. E. Stachel, L. G. Rahme, *Mol. Microbiol.* **2006**, *62*, 1689–1699.
- [26] L. A. Gallagher, S. L. McKnight, M. S. Kuznetsova, E. C. Pesci, C. Manoil, *J. Bacteriol.* **2002**, *184*, 6472–6480.
- [27] M. P. Storz, G. Allegretta, B. Kirsch, M. Empting, R. W. Hartmann, *Org. Biomol. Chem.* **2014**, *12*, 6094–6104.
- [28] M. P. Storz, C. K. Maurer, C. Zimmer, N. Wagner, C. Brengel, J. C. de Jong, S. Lucas, M. Müsken, S. Häussler, A. Steinbach, R. W. Hartmann, *J. Am. Chem. Soc.* **2012**, *134*, 16143–16146.
- [29] B. Lesic, F. Lépine, E. Déziel, J. Zhang, Q. Zhang, K. Padfield, M.-H. Castonguay, S. Milot, S. Stachel, A. A. Tzika, R. G. Tompkins, L. G. Rahme, *PLoS Pathog.* **2007**, *3*, 1229–1239.
- [30] a) T. Klein, C. Henn, J. C. de Jong, C. Zimmer, B. Kirsch, C. K. Maurer, D. Pistorius, R. Müller, A. Steinbach, R. W. Hartmann, *ACS Chem. Biol.* **2012**, *7*, 1496–1501; b) M. Zender, T. Klein, C. Henn, B. Kirsch, C. K. Maurer, D. Kail, C. Ritter, O. Dolezal, A. Steinbach, R. W. Hartmann, *J. Med. Chem.* **2013**, *56*, 6761–6774; c) M. Starkey et al., *PLoS Pathog.* **2014**, *10*, e1004321.
- [31] A. Ilangovan, M. Fletcher, G. Rampioni, C. Pustelny, K. Rumbaugh, S. Heeb, M. Cámara, A. Truman, S. R. Chhabra, J. Emsley, P. Williams, *PLoS Pathog.* **2013**, *9*, e1003508.
- [32] C. Hansch, P. P. Maloney, T. Fujita, R. M. Muir, *Nature* **1962**, *194*, 178–180.
- [33] D. Pistorius, A. Ullrich, S. Lucas, R. W. Hartmann, U. Kazmaier, R. Müller, *ChemBioChem* **2011**, *12*, 850–853.
- [34] A. L. Hopkins, G. M. Keserü, P. D. Leeson, D. C. Rees, C. H. Reynolds, *Nat. Rev. Drug Discovery* **2014**, *13*, 105–121.
- [35] P. N. Mortenson, C. W. Murray, *J. Comput.-Aided Mol. Des.* **2011**, *25*, 663–667.
- [36] S. Cabani, P. Gianni, V. Mollica, L. Lepori, *J. Solution Chem.* **1981**, *10*, 563–595.
- [37] E. Freire, *Drug Discovery Today* **2008**, *13*, 869–874.
- [38] a) C. Lu, B. Kirsch, C. Zimmer, J. C. de Jong, C. K. Maurer, M. Müsken, S. Häussler, A. Steinbach, R. W. Hartmann, *Chem. Biol.* **2012**, *19*, 381–390; b) J. Hodgkinson, S. D. Bowden, W. R. J. D. Galloway, D. R. Spring, M. Welch, *J. Bacteriol.* **2010**, *192*, 3833–3837.
- [39] J. G. Topliss, *J. Med. Chem.* **1972**, *15*, 1006–1011.
- [40] C. Hansch, A. Leo, R. W. Taft, *Chem. Rev.* **1991**, *91*, 165–195.
- [41] a) L. Friedman, R. Kolter, *Mol. Microbiol.* **2004**, *51*, 675–690; b) C. Coulon, E. Vinogradov, A. Filloux, I. Sadovskaya, *PLoS One* **2010**, *5*, e14220; c) V. Pawar, U. Komor, N. Kasnitz, P. Bielecki, M. C. Pils, B. Gocht, A. Moter, M. Rohde, S. Weiss, S. Häussler, *Antimicrob. Agents Chemother.* **2015**, *59*, 4974–4981.
- [42] M. D. Shultz, *Bioorg. Med. Chem. Lett.* **2013**, *23*, 5980–5991.
- [43] A. Thomann, J. Zapp, M. Hutter, M. Empting, R. W. Hartmann, *Org. Biomol. Chem.* **2015**, *13*, 10620–10630.
- [44] K. Gudmundsson, B. A. Johns (SmithKline Beecham Corp.), *Int. PCT Pub. No. WO2006055245 A2*, **2006**, 29.
- [45] K. Sander, T. Kottke, Y. Tanrikulu, E. Proschak, L. Weizel, E. H. Schneider, R. Seifert, G. Schneider, H. Stark, *Bioorg. Med. Chem.* **2009**, *17*, 7186–7196.

Received: August 19, 2016

Revised: September 27, 2016

Published online on ■■■■■, 0000

3.6 Biophysical Screening of a Focused Library for the Discovery of Novel Anti-mycobacterials Targeting CYP121

Chapter VI

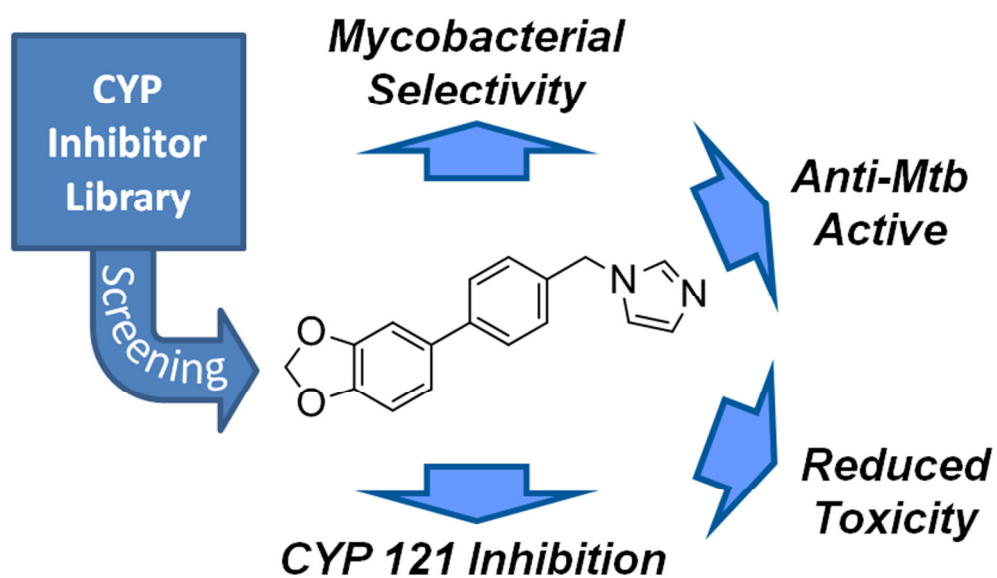


Figure 20. Graphical abstract of chapter VI.

3 Results

Abstract: The appearance of multi-drug resistance (MDR) combined with a generally complicated long-term treatment hamper the therapy of *Mycobacterium tuberculosis* (Mtb) infections. Therefore, the development of novel antimycobacterial agents with new modes of action is urgently required. CYP121 was shown to be a promising novel target for inhibition of mycobacterial growth. However, besides the identification of azole antifungals as molecules that interfere with this system, not many efforts have been made to develop new inhibitors. In this study, we describe the rational discovery of new CYP121 inhibitors by a systematic screening based on biophysical and microbiological methods. Best hits originating from only one structural class gave first information about molecular motifs required for binding and activity. The initial screening procedure was followed by mode of action studies and further biological characterizations. The results demonstrate a superior antimycobacterial efficacy and a reduced toxicity profile of our frontrunner compound compared to the reference econazole. Due to its low molecular weight, promising biological profile and advantageous physicochemical properties this compound displays an excellent starting point for further rational optimization.

INTRODUCTION

Tuberculosis belongs to the most lethal infectious diseases caused by bacteria. According to the WHO Global Tuberculosis Report,^[1] 1.5 million people died in 2013 due to infections caused by Mtb. This goes along with an estimated amount of 9 million new cases of Mtb infections arising each year. Despite a broad spectrum of first and second line antimycobacterial drugs, there is an antibiotic gap for the treatment of infections with multi-drug-resistant (MDR) and extensively-drug-resistant (XDR) Mtb.^[1] Additionally, alarming reports have been published describing totally-drug-resistant Mtb (TDR-TB).^[2] Moreover, tuberculosis still requires long-term treatment leading to an increased probability for non-compliance which impairs the therapeutic outcome.^[3] Hence, there is an urgent need for new antimycobacterial agents with novel modes of action which in best case could also lead to shorter treatment periods.

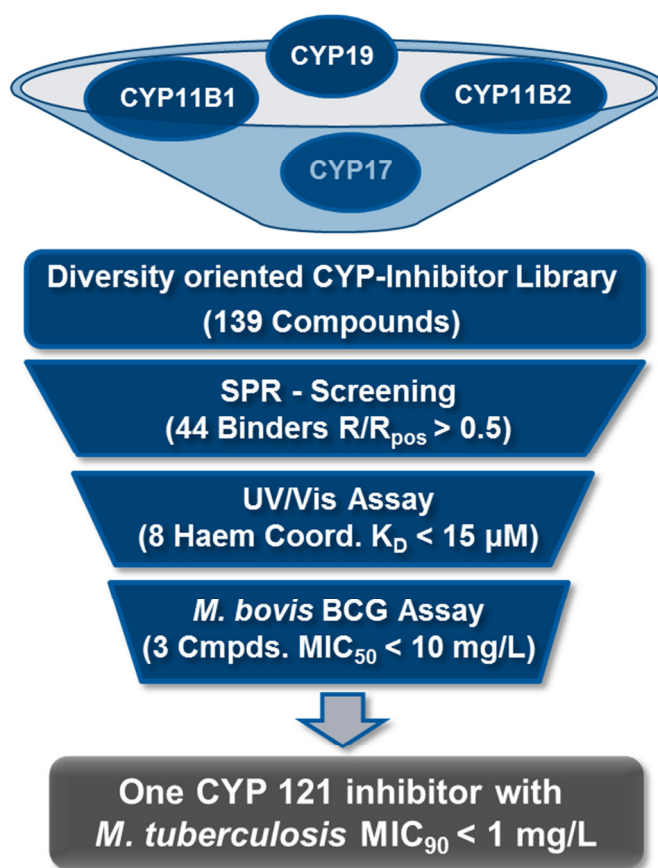
Driven by the elucidation of the Mtb genome in 1998^[4], new potential drug targets were identified.^[5] Interestingly, Mtb exhibits an unusual high number of twenty P450

enzymes in contrast to other bacteria. Further studies have revealed some of them to be essential for viability, survival and/or pathogenicity.^[6] Out of these, CYP121 was shown to be essential for bacterial growth by an *in vitro* knock out study.^[7] Moreover, the deficient strain could be revived by a complementary plasmid.^[7,8] The first evidence of CYP121 function in Mtb was derived from its gene position which is located in an operon harboring two enzymes involved in the formation of cyclo-di-l-tyrosine (cYY).^[9] *In vitro* studies provided proof, that CYP121 catalyzes the reaction of cYY to mycrocyclosin with high substrate specificity.^[9,10] The role of its substrate and product in the cellular setting remains to be elucidated. However, the variety of biological functions of diketopiperazines is well described e.g. as quorum sensing signals.^[11] Thus, besides development of antimycobacterials targeting CYP121, a small selective molecule with *in cellulo* efficiency may help to understand the precise function of CYP121.

Despite the fact that CYP121 is a potential target for Mtb treatment only little efforts have been undertaken to identify potent inhibitors. Hudson *et al.* published several compounds designed for selective CYP121 binding and inhibition. However, none of them were shown to be effective against Mtb.^[12] Fonveille *et al.* described a CYP121 inhibitory effect of cYY derivatives without data on bacterial growth.^[10,13] Regarding compounds with cellular activity, it was shown that azole antifungals bind tightly to CYP121 and exhibit an *in vitro* and *in vivo* activity against Mtb.^[14–19] Furthermore, the binding to the enzyme was in good correlation with the antimycobacterial effect.^[7,19] As the azole antifungals are active on Mtb cells and effective in mice infection models they display a valuable reference for antimycobacterial CYP inhibitors.^[14–19]

The essential role of CYP121 for Mtb survival and our expertise in developing potent and selective human steroidogenic CYP enzyme inhibitors, motivated us to identify novel CYP121 inhibitors with increased efficiency and improved properties compared to the azole antifungals.^[20] Potential antimycobacterial activity could provide further evidence of target validity, drugability and stimulate development of respective inhibitors towards new therapeutic agents bearing the potential to treat MDR and XDR Mtb infections. For these reasons, we established a screening strategy based on *in vitro* and cell-based assays (Scheme VI 1). By the use of a small highly diverse library composed of our CYP-inhibitors, we could identify a CYP121 inhibitor with increased antimycobacterial potency compared to positive control econazole. This

3 Results



Scheme VI 1. Hit finding progress. The initial library (139 compounds) was built of inhibitors designed for inhibition of human CYP11B1/2, CYP17 and CYP19 with regard to structural diversity. A positive SPR screening hit was defined by the coefficient of its response divided by the response of the positive control (econazole) which had to be above 0.5 ($R/R_{\text{pos}} > 0.5$). This resulted in 44 positives. From this preselection, eight compounds coordinated iron-heme with a $K_D < 15 \mu\text{M}$. These compounds were tested against BCGT and three showed a $\text{MIC}_{\text{BCGT}} < 10 \text{ mg/L}$. Finally, one compound was highly active on Mtb with a $\text{MIC}_{\text{Mtb}} < 1 \text{ mg/L}$.

compound possesses desirable physicochemical properties, low toxicity towards human cells and high antibacterial selectivity against Mtb, rendering it an appropriate candidate for further optimization.

RESULTS AND DISCUSSION

Library generation. For hit discovery we selected 139 compounds from our in-house CYP-inhibitor library designed for inhibition of CYP17, CYP19, CYP11B1 and B2 (Supporting Information). The screening library is composed of six different scaffolds to ensure a broad structural diversity (Figure VI 1). Additionally, known pharmacological profiles,

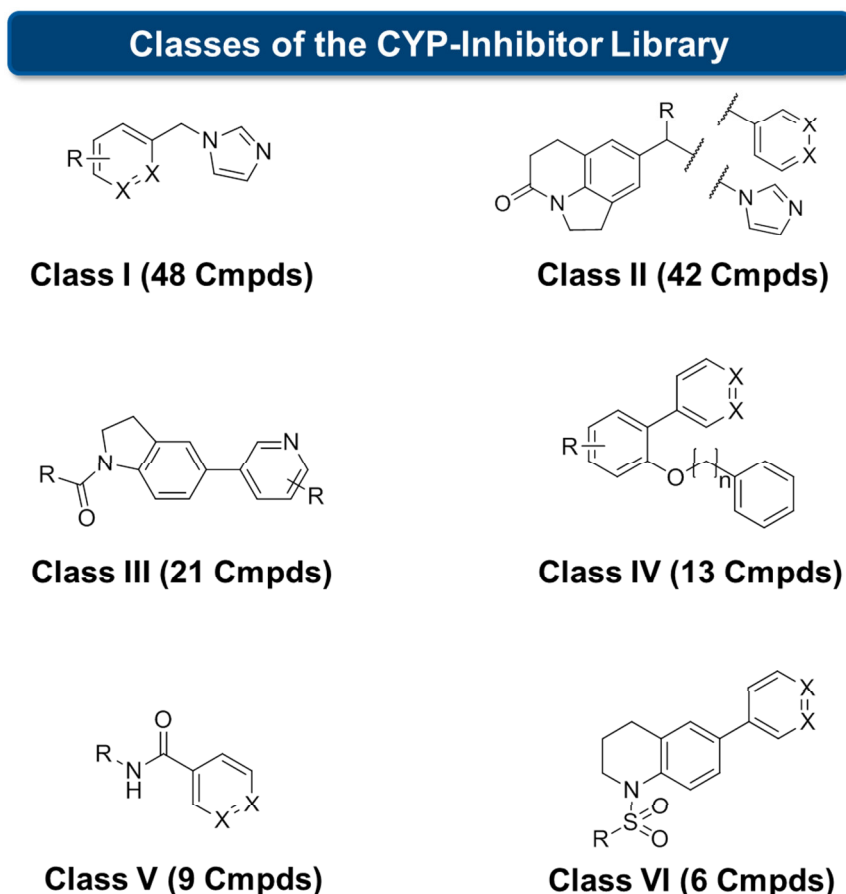


Figure VI 1. Classes of the library used for screening against CYP121 with their respective number of representatives stated in brackets. The structures represent the core scaffold of the compound where R is a substituent, X represent the position of either nitrogen or CH, and $[\]_n$ the alkyl chain length of n methylene units.

drug-likeness, and established synthetic routes of the compounds provide an ideal starting point for future optimization. As a reference compound we chose econazole which was shown to have the highest reported affinity to CYP121 (UV/Vis heme P450 binding assay) and the strongest inhibition of mycobacterial growth in the class of azole antifungals.^[16,19]

Enzyme expression, characterization and initial SPR Screening. As starting point for SPR screening we expressed CYP121 in a heterologous host (*E. coli* K12 BL21) and purified the protein by ion affinity chromatography (IMAC). Notably, addition of 1% Triton-X-100 into the lysis buffer during purification increased the protein yield by about 10-fold.^[21] The purity of the enzyme was determined by SDS-PAGE (Supp. Data, section 2, Figure S1). To ensure active protein conformation we conducted enzymatic *in vitro* activity tests. A first experiment to gain information about activity of P450 enzymes is the determination of CO-binding spectra.^[22] 50% of the expressed enzyme showed the typical P450 band of CO- bound heme after dithionate reduction

3 Results

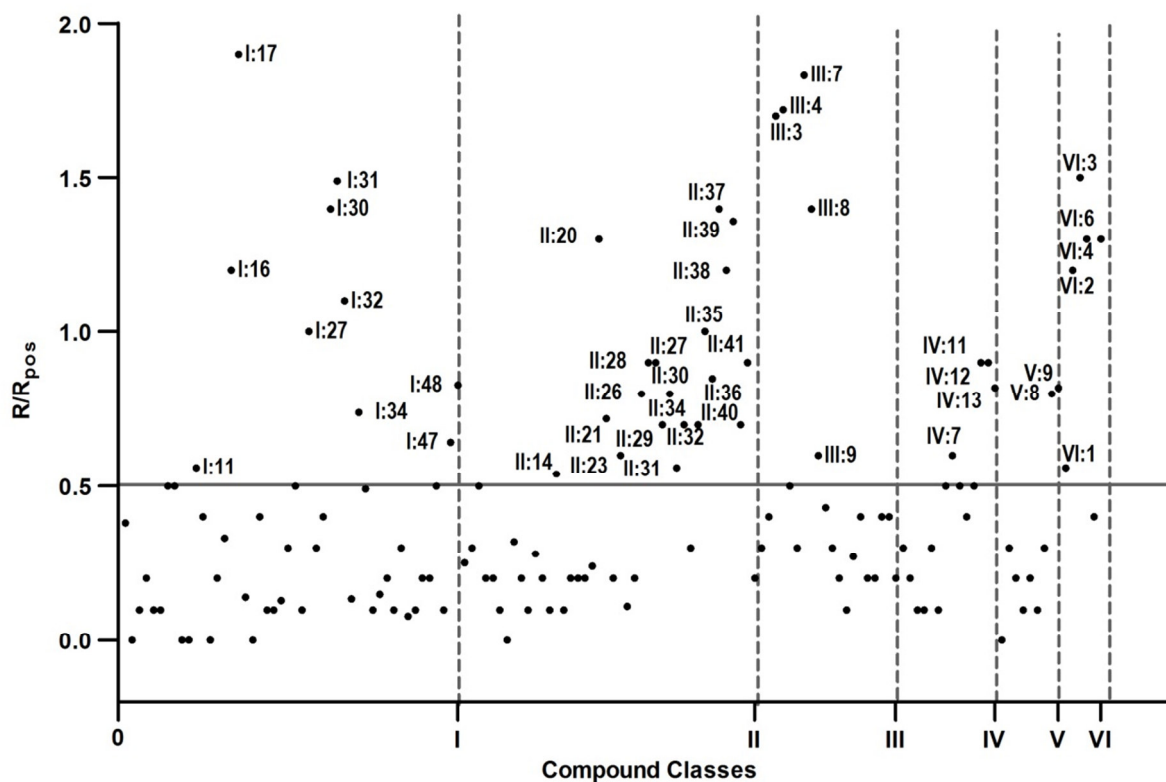


Figure VI 2. SPR screening results: compounds plotted *versus* their R/R_{pos} values. Econazole (100 μM) was used as a positive control and its SPR response was set to 1 (R_{pos}). The compounds were tested at a concentration of 100 μM and their response (R) was divided through the response of positive control (R/R_{pos}). Hit compounds possess R/R_{pos} values > 0.5 (horizontal solid grey line). Vertical dashed lines separate the six classes.

(Supp. Data, section 3, Figure S2 and S3). Using the same experimental conditions but replacing sodium dithionite, we were able to identify Etp1fd (516-618) as ferredoxin and Arh1_A18G as ferredoxin reductase, two proteins of the fungus/fission yeast *Schizosaccharomyces pombe*,^[23,24] as suitable heterologous electron transfer system for CYP121. Additionally, utilizing the latter system, we could show conversion of cYY to mycocyclusin proving enzymatic activity of CYP121 (Supp. Data, section 4, Figure S4 and S5).

For SPR immobilization of the protein we used the biotin-streptavidin interaction.^[25] Prior to immobilization we conjugated a biotin tag to CYP121. To confirm applicability of the SPR method, we determined a response curve of econazole to the target protein (Supp. Data, section 5, Figure S6).^[7] The SPR signal of econazole, measured in response units (RU), was set to one (R_{pos}). The binding event of library compounds (R) was referenced to the positive control and declared as R/R_{pos} . We defined $R/R_{\text{pos}} > 0.5$ as the threshold for hits from SPR screening procedure. Using this approach, we identified 44 binders out of 139 compounds with representatives from all of the six

classes (Figure VI 2). Notably, we found 17 compounds with higher responses than econazole (Supp. Data, section 6, Table S1).

Binding mode and affinity characterization via UV/Vis heme binding assay. The 44 SPR binders were investigated for their ability to interact with the iron(II)-heme by monitoring the shift of the characteristic absorbance band at 416 nm of CYP121 (Figure VI 3).^[7,12] In addition to the 44 SPR hits, we also took two weak SPR binders into consideration (**I:1** and **I:33**, $R/R_{\text{pos}} < 0.5$) to conduct a retrospective evaluation of the reliability of our SPR screening. McLean *et al.* reported that econazole has a tight-binding profile to CYP121 with a $K_D = 0.02 \mu\text{M}$.^[7] However, we observed a K_D of $3 \mu\text{M}$. This discrepancy could be due to a difference in UV/Vis spectrometric devices used and, thus, limited sensitivity. To provide a higher throughput employing 96-well plates, we were limited to a higher enzyme concentration which impairs measurement in lower nanomolar ranges. Compounds were initially tested at a concentration of $100 \mu\text{M}$ to identify iron-heme interactions and distinguish between type I (water bridged iron-interaction) and type II (direct iron-interaction) binding. 30 compounds showed a type II shift while none showed type I binding behavior. The latter compounds appear in class I, II, III and IV indicating that the catalytic center accepts imidazolyl- and pyridinyl-moieties for iron-heme coordination.

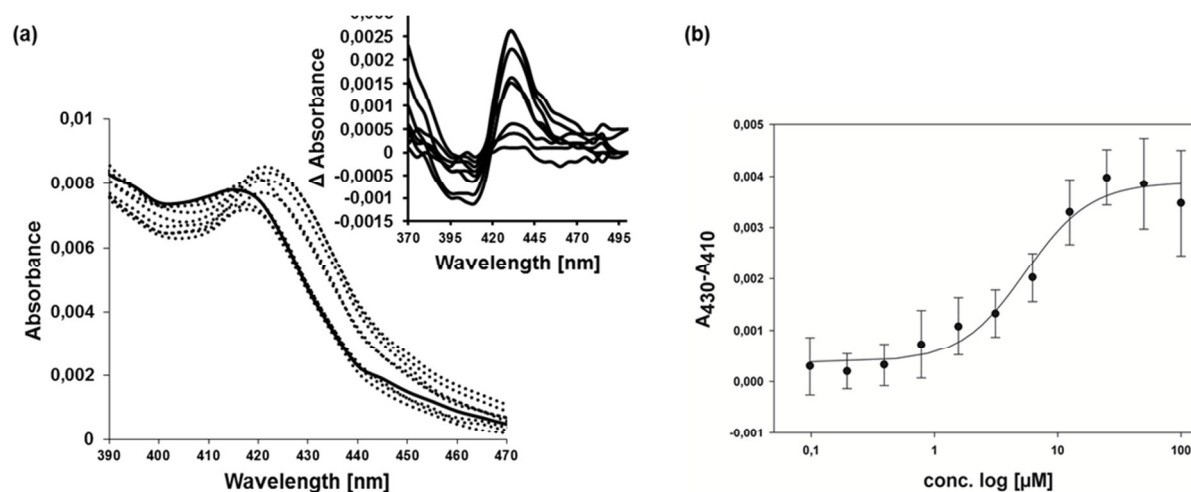


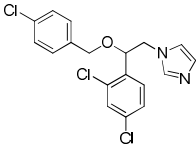
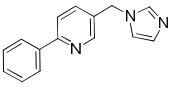
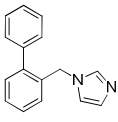
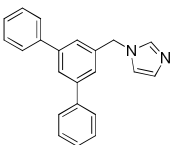
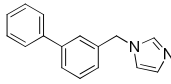
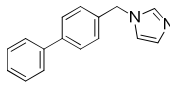
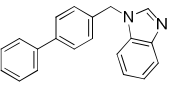
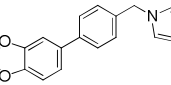
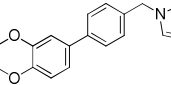
Figure 3. Binding of I:47 to CYP121 as determined from heme coordination assay. (a): UV/Vis spectrum (left inset) and difference spectra (upper right inset) were recorded of the enzyme in the presence of I:47 (100, 50, 25, 12.5, 6.25, 3.13, 1.56, 0.78, 0.39, 0.20, 0.10 μM ; dotted lines) and in the absence of I:47 (solid line). (b): The K_D value of I:47 was derived by non-linear fitting of the data using *Equations 1* and the difference in absorbation at 430 and 410 nm.

3 Results

I:1 and **I:33** (weak SPR binders) did not coordinate the heme-iron which emphasizes the suitability of our SPR screening procedure. The identified type II binders were further investigated regarding their K_D . For eight binders an affinity better than 15 μM was observed (Supp. Data, section 6, Table S1). Interestingly, this subset of compounds only arose from classes I and II. Pyridinyl (class II) as well as imidazolyl (class I) motifs were tolerated as heme coordinators while the imidazolyl ligands showed higher affinities (Supp. Data, section 6, Table S1). With regard to class I the highest affinity could be found for compounds decorated with hydrophobic and space-demanding moieties connected to the benzylimidazole substructure. This is also a structural trend in the class of antimycobacterial azoles (e.g. econazole, clotrimazole).^[7] The most affine binder **I:16** showed three-fold improved K_D compared to econazole ($K_D = 3 \mu\text{M}$) (Supp. Data, section 6, Table S1). Furthermore, two linearized, *para*-substituted biphenyl compounds of this class (**I:47** and **I:48**) possessed a CYP121 affinity comparable to econazole. As mentioned before, molecules with linear biphenyl units bearing an *N*-methylenbenzimidazolyl moiety instead of an unsubstituted benzylimidazolyl scaffold did not bind to the heme (**I:33**). Additionally, replacement of the interconnecting phenyl group within this class by pyridinyl resulted in inactive compounds (**I:1**). Moreover, the analysis of all regioisomers of benzylimidazol scaffolds substituted with phenyl revealed that the *para*- (**I:32**) and *meta*- (**I:30**) position lead to comparable affinities. A phenyl group at the *ortho*-position (**I:15**) impairs binding. The *para*-benzodioxine substituent of **I:48** and the *para*-benzodioxole substituent of **I:47** increase the affinity by about two- to threefold (Supp. Data, section 6 Table S1). However, compared to econazole our most active compounds showed similar (e.g.: **I:47**; 5 μM and **I:48**; 5 μM) or slightly better K_D (**I:16**; 1 μM) (Supp. Data, section 7, Figure S7). MIC determination in BCGT and Mtb. For investigating cellular activity we focused on those compounds with a K_D lower than 15 μM , but also added selected compounds showing low affinity to CYP121 as negative controls (Supp. Data, section 6, Table S1). In this setting, econazole was used as described antimycobacterial reference compound.^[26] For initial screening on mycobacterial growth inhibition we used the bovine strain BCGT. The strain serves as a suitable substitute for Mtb as it carries a copy of CYP121 in its genome with an overall amino acid identity of 100% in comparison to its Mtb congener (Supp. Data, section 8, Figure S8).^[27] Regarding the more complex situation in the cellular context, the six identified classes have to be discussed

separately. In case of subset III to VI, we could only detect weak growth inhibition ($MIC_{BCGT} > 10$ mg/L; Supp. Data, section 6, Table S1). In class II three compounds were found to have a K_D value below $15 \mu M$ but none of them had MIC_{BCGT} below 10 mg/L (**I:20**, see Supp. Data, section 6, Table S1). For econazole, we observed a $MIC_{BCGT} = 5.4$ mg/L which is in good correlation to previous findings.^[26] Most active compounds were observed in class I (Supp. Data, section 9, Figure S9 and S10). The best heme-binder to CYP121 (**I:16**) with a three-fold increased affinity compared to econazole showed a MIC_{BCGT} of 1.6 mg/L. For **I:47** and **I:48** we could determine MIC_{BCGT} s = 0.3 mg/L and 2 mg/L which renders **I:47** to be the most potent antimycobacterial compound in this subset. The MIC tests of negative controls out of class I (**I:1** and **I:33**) showed no significant growth inhibition. Within class I results of the MIC assay are in good correlation to the K_D values on the target enzyme CYP121 (Table VI 1). To test the potency of the most effective antimycobacterial compounds against the human pathogen Mtb, we used the MABA assay system.

Table VI 1. Structures, relative SPR responses (R/R_{pos}), binding affinities (K_D) and antimycobacterial activities of econazole, most active hits (**I:16**, **I:47**, **I:48**), examples for negatives (**I:1**, **I:33**) and for moderately active hits (**I:15**, **I:30**, **I:32**).

Cmpd.	SPR [R/R_{pos}]	Haem K_D [μM]	MIC_{BCGT} [mg/L]	MIC_{BCGT} [μM]	MIC_{Mtb} [mg/L]	MIC_{Mtb} [μM]
 econazole	1	3	5.4	14	4.2 ^b	11 ^b
 I:1	0.4	>100	>25	>100	-	-
 I:15	0.3	34	9.6	41	-	-
 I:16	1.2	1	1.6	5	1.9	6
 I:30	1.4	11	2.6	11	11.2	48
 I:32	1.1	14	7.0	30	9.6	41
 I:33	0.1	>100	>25	>100	-	-
 I:47	0.6	5	0.3	1	0.3	1
 I:48	0.6	5	2.0	7	3.5	12

^a Eco = econazole, ^b MIC_{Mtb} determined previously.^[26]

3 Results

For MIC_{Mtb} determination we chose the common laboratory strain H₃₇Rv. In several studies the MIC_{Mtb} value of econazole was determined ranging from 0.12 mg/L to 8 mg/L.^[7,17] To facilitate comparability of the MIC_{Mtb} values, we referenced them to results made in our assay system where a MIC_{Mtb} for econazole of 4.2 mg/L was determined previously.^[26] The most effective compounds were **I:47** with MIC_{Mtb} = 0.3 mg/L followed by **I:16** (MIC_{Mtb} = 1.9 mg/L) and **I:48** (MIC_{Mtb} = 3.5 mg/L, see Table VI 1). Notably, in terms of cellular efficiency metrics, **I:47** has an AE = 0.39 and hence, a higher AE than econazole (0.24) and rifampicin (0.16) (Supp. Data, section 10, Table S2).

Toxicity on human cell lines. The azole antifungals are known to attenuate growth of several human cell lines.^[28,29] To compare cellular toxicity of econazole with our three most promising hits we used HEK293 cells in a MTT-based assay.^[30] 6.0 mg/L of econazole killed 50% of HEK 293 cell population after 48 h. Notably, the toxicity of our most active antimycobacterial compounds was lower compared to the azole antifungal drug (**I:16** LD₅₀ = 6.1 mg/L; **I:47** LD₅₀ = 18.6 mg/L; **I:48** 22.3 mg/L). For comparability reasons, we calculated the toxicity factor for **I:47** (MIC_{Mtb}/LD₅₀), which revealed a 44-fold improvement compared to econazole (Table VI 2). One of the most prominent undesirable effects of azole antifungals is their hepatotoxicity observed in mice.^[29,31] For this reason, we also conducted toxicity experiments employing HepG2 cells. We could observe an approximately 2-fold increased toxicity for econazole (3.1 mg/L) and **I:16** (3.9 mg/L) compared to HEK293 cells. The LD₅₀ of **I:47** was 17.1 mg/L which is close to the toxicity seen in HEK cells. (*vide supra*, Supp. Data, section 11, Table S3).

Table VI 2. Comparison of human cellular toxicity and anti-Mtb effect.

Compound	MIC _{Mtb} [mg/L]	LD ₅₀ HEK 293 cells [mg/L]	Toxicity factor MIC _{Mtb} /LD ₅₀ ^a
Eco	4.2	6.0	1.4
I:16	1.9	6.1	3.2
I:47	0.3	18.6	62.0
I:48	3.5	22.3	6.4

^a Toxicity factor (MIC_{Mtb} (Mtb) divided by LD₅₀ (HEK293)) was used to enhance comparability of compounds with regard to their antimycobacterial effect.

In vitro and in cellulo mode of action studies. In addition to the binding constant, we determined inhibition of CYP121 enzymatic reaction by **I:47**. The enzyme catalyzes the formation of an intramolecular C-C bond between the carbon atoms in *ortho*-position to the hydroxyl-group of the phenol-moiety of cYY resulting in the production of mycocyclosin.^[9] For assessing CYP121 activity we used an artificial redox-system from *Schizosaccharomyces pombe* (ferredoxin Etp1fd (516-618) and ferredoxin reductase Arh1_A18G).^[24] This redox-system is known for its broad applicability as electron-donor for CYP enzymatic reactions but firstly described for CYP121 herein. Indeed, we could observe an inhibition of product formation confirming **I:47** to be a potent inhibitor of mycocyclosin production by interference with CYP121 *in vitro* (Supp. Data, SI section 1).

To gather further evidence for target-based mycobacterial selectivity towards other bacteria, we assessed the activity of our compounds on growth of *E. coli* TolC as a representative for Gram-negative bacteria and *S. aureus* Newmann strain for Gram-positive. The results show no significant growth inhibition of **I:47** and **I:48** against the latter bacteria ($MIC_{Mtb} > 100\mu\text{M}$ or $> 25\text{ mg/L}$). In contrast to econazole and **I:16** that showed certain inhibitory effects for *E. coli* and *S. aureus* in higher concentrations (Supp. Data, section 12, Figure S11).

Physicochemical and selectivity profile of I:47. The aforementioned compounds were originally designed as inhibitors of human CYP17, CYP19 and CYP11B1/2 known to be involved in steroid biosynthesis. I:47 was initially synthesized as an inhibitor of CYP17. The compound showed only a low activity on CYP17 compared to other inhibitors with an $IC_{50} = 3.1\ \mu\text{M}$. Additionally, only a 48 % inhibition of aromatase at a concentration of $25\ \mu\text{M}$ was observed.^[32]

Regarding physicochemical properties suitable for permeation through the cellular membranes, one has to differentiate between biological barriers of human and mycobacterial origin. For humans, a guidepost for appropriate physicochemical properties is the Lipinski's rule of five for oral bioavailability of drugs (< 5 hydrogen bond donors, ≤ 10 hydrogen bond acceptors, $MW < 500\ \text{Da}$, $\log P \leq 5$).^[33] Our frontrunner compound **I:47** fulfils all four criteria (0 hydrogen bond donors, 3 hydrogen bond acceptors, $MW = 278\ \text{Da}$, $\log P = 3.1$) (Supp. Data, section 13). To the best of our knowledge, akin correlations for physicochemical properties with

3 Results

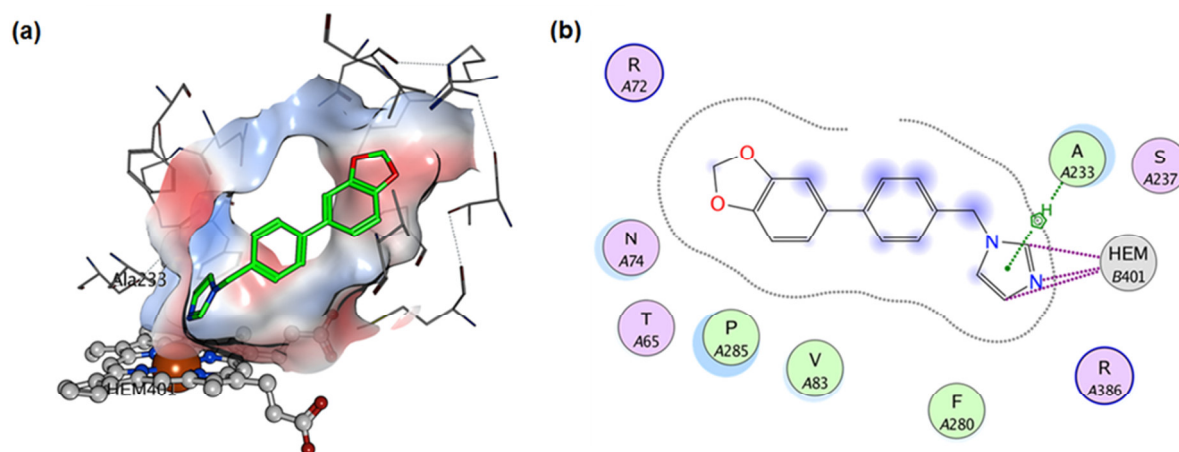


Figure VI 4. Molecular docking of **I:47** against the prepared co-crystal structure of CYP121. Heme coordination was a prerequisite for the docking process which was achieved by placing a pharmacophore feature on the interacting metal and ligand position. Resulting docking poses were sorted by score (E_{refine}) and the highest scored pose is depicted as 3D model (a) and 2D-interaction chart (b). **I:47** shows close van der Waals contacts to surrounding amino acids but also possibilities for compound enlargement (b). The grey surface in panel (a) represents the van der Waals surface of the protein, which is also shown as dotted lines in panel (b).

mycobacterial membrane passage were not set up, yet. Thus, a respective guide for compound development is still missing.^[34]

Molecular modelling studies on the binding mode of I:47. As a type II binding profile was observed for **I:47**, we set up a constrained docking protocol to predict its binding mode to the heme center of CYP121. Docking to the active site of CYP121 was restricted by two essential pharmacophore features reflecting the direct interaction between the coordinated iron and **I:47** (type II binding). The resulting docking poses were sorted by their predicted binding energies and the best scored docking pose was chosen for further studies (Figure VI 4). This modelling approach revealed new possibilities for further derivatization or rigidification. For instance, intramolecular linking of the methylene bridge at the imidazolyl unit with the *ortho*-position of phenyl using e.g. a five-membered ring should be tolerated by CYP121 and increase affinity through reduction of entropic penalties upon binding. Furthermore, the central hydrophobic aromatic moiety shows Van-der-Waals contacts to flanking hydrophobic amino acids Phe-168 and Met-62. Regarding steric factors, the ring could easily rotate in this position. This degree of rotatable freedom might be necessary to place the aforementioned phenyl in a suitable position to grant access to a large flat subpocket (composed of Met-61, Asn-84 and the backbone of Asn-83) which could then be reached by substituents at its 2-position. The 1,3-

benzodioxole moiety was placed in a hydrophilic subpocket, formed by Arg-72, Asn-74 and Thr-65, which is in good accordance with the low lipophilicity of this motif (cLogP = 0.27). Moreover, the 5-position of 1,3-benzodioxole holds great potential for further enlargement of the molecule, as it directly points to another subpocket which is decorated with several hydrophobic amino acids, namely Leu-73, Phe-280, Leu-284 and the sidechain of Gln-385.

CONCLUSION

Despite the fact that CYP121 had been reported to be a potential target for the treatment of Mtb infections, not many inhibitors with cellular activity had been discovered. Herein we have presented a rational screening approach to address CYP121 by a small library focused on privileged scaffolds for CYP enzyme inhibition. The identified compounds could help to clarify the hitherto unknown role of CYP121 in Mtb metabolism and provide a good starting point for a drug optimization program.

Our search for new inhibitors of CYP121 started with an initial SPR screen of the aforementioned focused library. As the compounds were designed for P450 inhibition we observed a high number of binders (32%). The identified compound classes differed highly with regard to their structures. Obviously, the large pocket of CYP121 (1350 Å³) which is necessary for the sterically demanding enzyme reaction can accept a large variety of differently shaped molecules.^[7,9,35,36] However, it has to be noted that the SPR method does not exclude compound attachment outside the enzymes active site.

For rational design approaches it is of high interest to clarify the binding mode and affinity of our hit compounds. A common method for P450 enzymes to address this issue is the heme coordination assay.^[7] All SPR-binders from classes III, IV, V and VI had only weak affinity to the heme-iron ($K_D > 100\mu\text{M}$). **IV:13** is the only compound from this subset that could be titrated and gave a K_D of 62 μM (Supp. Data, section 6, Table S1). Therefore, we conclude that most of the compounds from these classes do not bind directly to heme but address another unknown site. This information could, however, be valuable for fragment-linking approaches at a later stage of drug development. For classes I and II we identified eight compounds with K_D values below 15 μM . Notably, the best compounds of class II (**II:20** and **II:34**) contained a

3 Results

space-demanding trityl-moiety. It was discussed for a crystal structure of CYP121 (PDB-ID: 1N40) that Arg-386 may restrict access of voluminous moieties to the iron-heme.^[35] Nevertheless, we observed that the enzyme can accommodate space-demanding molecules at the heme-site as shown by our UV/Vis experiments. Binders with the best affinity were found in class I. A comparison of compound structures and binding efficiencies within this class gave first evidence for properties needed to gain affinity towards CYP121. Imidazolyl head group linked by an methylene bridge to a hydrophobic core can be considered as an important basic structure for a good binding efficiency (**I:16**, **I:47** and **I:48**). In case of the linearized compounds, an *N*-methylenbenzimidazolyl head group (**I:33**), *ortho*-substituted biphenyl system (**I:15**), and an interconnecting pyridinyl (**I:1**) ring had unfavorable binding properties. In a hit optimization process these structural characteristics should be avoided. In contrast to this observation, a *para*-benzodioxine substituent (**I:48**) and a *para*-benzodioxole substituent (**I:47**) linked to the biphenyl system increases affinity. This might provide a possible position for further derivatization. Our docking study supports this result as this motif was predicted to be placed in a subpocket having a great potential for new interactions.

A straightforward approach for target validation is to correlate on-target potency and cellular activity. Although it has to be noted, that such a correlation can be flawed by the fact that compounds might also be inefficient due to e.g. poor membrane penetration. We hypothesized that class II might be a prime example for compounds that poorly permeate the membrane of mycobacteria and, thus, cannot reach their intracellular target. This could be an explanation for the lack of *in cellulo* activity although a moderate affinity to the target was measured.

Class I is the most remarkable of the six classes showing reasonable affinity towards CYP121 and, more importantly, also high activity *in cellulo* against Mtb and BCGT. Furthermore, the on-target affinity of class I compounds directly correlates with their activity on mycobacteria which provides further evidence of a CYP121-dependent effect. In detail, on-target inactive compounds like **I:1** and **I:33** had no activity against BCGT, while moderate binders e.g. **I:15**, **I:30** and **I:32** had low antimycobacterial effects. Finally, compounds with highest affinity (**I:16**, **I:47**, **I:48**) were the most potent in the cellular setting. Especially, compounds **I:16**, **I:47**, and **I:48** are even more effective on mycobacteria than the positive control, econazole, although no

optimization has been undertaken, yet (Table VI 1). In terms of antibacterial efficiency (AE), **I:47** is superior to econazole and the first-line drug rifampicin indicating an excellent optimization potential of this novel inhibitor class. Moreover, we could provide data that **I:47** does not only bind to CYP121 but does also inhibit the enzyme reaction (Supp. Data, section 4). The correlation between MIC and K_D bares minor inconsistencies, which might be due to poor penetration through the mycobacterial cell wall of some compounds (see e.g. **I:47** and econazole). A highly lipophilic molecule (e.g. econazole cLogP = 5.3 vs. **I:47** cLogP = 3.1) might be trapped in this lipophilic barrier containing mycolic acids and slowly or only partially released into the mycobacterial cytoplasm. This results in lower cellular activity than expected from on-target affinities. A second explanation for the differences in MIC and K_D , at least for econazole, is its promiscuous behavior in different growth inhibition assays. This suggests that there are additional targets for econazole. An explanation for the antibacterial activity of econazole against *E. coli* and *S. aureus* was already provided before. In these studies econazole was described as an inhibitor of Flavohemoglobin.^[37] Further possible target systems of azole antifungals within Mtb metabolism have also been described.^[38] However, evaluation of **I:47** and **I:48** leads to the conclusion that these novel structures are of improved selectivity towards Mtb with a good correlation of CYP121 affinity and antimycobacterial activity. Furthermore, the two compounds possess lower toxicity against human cells than determined for econazole. Although toxicity to hepatocytes was low, it is of high interest to clarify potential inhibition of metabolizing CYP enzymes (e.g. CYP3A4). These results further underline the target-based mycobacterial specificity of our compounds, at least in the subset of bacterial and human cells tested. Taken together the *in vitro* and cell-based studies conducted herein, CYP121 is most certainly the major target of **I:47** and **I:48**.

In summary, we have reported a biophysical screening procedure employing a focused library of privileged scaffolds, which ultimately lead to the discovery of novel CYP121 inhibitors. From this process, **I:47** turned out to be the most promising hit compound pairing convincing antimycobacterial activity and bacterial selectivity with a good toxicity profile. Furthermore, this compound exhibits a fragment-like molecular weight and preferable physiochemical properties that fulfil the Lipinski rules for oral bioavailability (Supp. Data, section 13). Thus, **I:47** is an excellent starting point for rational structure-based drug discovery. Our *in silico* studies revealed several

3 Results

possible modifications to be investigated in future optimization steps. Additionally, the inhibitor might be a suitable candidate for an *in vivo* proof-of-concept study towards validation of CYP121 as a drug target.

ACKNOWLEDGEMENT

The author wishes to thank the following scientists for their experimental contributions:

Christian Brengel (HIPS): He performed the UV/VIS and *in vitro* enzyme assay and the SPR Screening and determined K_D 's. He transformed the CYP121, Arh and Etp harboring plasmids into heterologous host. He assisted and performed the MIC assays (*M. bovis BCG*) and Proteinexpressions/purifications. He synthesized mycrocyclosine. He performed the LC-MS quantification of the *in vitro* enzyme reaction.

Dr. Sang-Hyun Cho (Institute for Tuberculosis Research, Chicago): He performed the Mtb assay.

Dr. Jörg Haupenthal (HIPS): He performed the LD_{50} experiments with human cell lines.

Alexander Schifrin (Saarland University): He determined the COD spectra for CYP121 and identified the redox electron-transfer system (Arh and Etp).

Ahmed Kamal (HIPS): He synthesized cYY.

Guiseppe Allegretta (HIPS): He developed the HPLC-MS/MS method for the CYP121 *in vitro* assay

EXPERIMENTAL SECTION

SPR-Screening: SPR binding studies were performed using a Reichert SR7500DC instrument optical biosensor (Reichert Technologies, Munich, DE) and SAD500m sensor chips obtained from XanTec Bioanalytics. CYP121 was immobilized on a SAD500m sensor chip at 12 °C using standard biotin-streptavidin complexation. The surface of both channels was quenched by a 3 min injection of 0.003 mg/mL biotin.

CYP121 was immobilized at densities between 5000 and 6000 RU for binding studies.

UV/Vis heme P450 binding assay. Optical titration experiments were performed in 96 well plates (Greiner, Kremsmünster, AT; transparent round bottom). The data were recorded using Tecan infinite M200Pro Nano Quant (Tecan Groupe Ltd., Männedorf, DE). Absorbance of enzyme and enzyme-inhibitor complex was measured between 350 and 500 nm in 1 nm steps with 10 flashes. Compounds were titrated from DMSO stock solutions maintaining a final DMSO concentration of 1%. CYP121 was used in a concentration of 0.25 μM . Data were plotted as optical shift *versus* ligand concentration. **Equation VI 1 (Eq. VI 1)** was used for non-linear regression of the resulting dose–response curves employing the Levenberg–Marquardt algorithm of Sigma Plot 12 (Systat Software GmbH, Erkrath, DE).

$$f = y_{min} + \frac{y_{max} - y_{min}}{1 + \left(\frac{x}{K_D}\right)^{-slope}}$$

Equation VI 1. f is the observed difference in absorbance at wavelengths 410 nm and 430 nm within the difference spectrum (see Figure VI 3) at ligand concentration x . This difference spectrum is obtained by subtracting the pure heme absorption spectrum from those with ligand present. y_{max} refers to the absorbance change at ligand saturation, y_{min} is the extrapolated minimal difference in absorbance; K_D refers to the dissociation constant of the CYP121 ligand complex.^[19]

Determination of BCGT MIC_{BCGT} by OD₆₀₀ assay. A pre-culture of BCGT was grown in 7H9 medium supplemented with ADC Enrichment for 10 days. The assay was performed in 48 well plates (Greiner, Kremsmünster, AT). Prior to culture addition, compounds were serially diluted in DMSO to fit a final DMSO concentration of 1%. For compound susceptibility the pre-culture was diluted 1:100 with fresh medium (7H9 + ADC enrichment). After 168 h of incubation at 37 °C and 80% air moisture, bacterial growth was measured by determination of OD₆₀₀. Absorption data was recorded on a Polarstar Omega Multidetector Plate Reader (BMG LABTECH, Ortenberg, DE). Graphs were plotted with GraphPad Prism using OneSite Log IC₅₀ model provided by the software. MIC_{BCGT} was defined as the concentration at which 50 percent of growth was detected in accordance with previous methods used.^[26] In analogy to ligand efficiency, which relates activity of compounds to their number of heavy atoms, a new metric has been introduced: antibacterial efficiency (AE).^[39] This coefficient was developed for better comparability of antimicrobial compounds differing in molecular weight (**Eq. VI 2**).

3 Results

$$AE = -\ln\left(\frac{MIC}{NHA}\right)$$

Equation VI 2. *AE* refers to the antibacterial efficiency, *MIC* is the minimal inhibitory concentration, and *NHA* equals the number of heavy atoms in a given compound.

Human cytotoxicity assay. HEK 293 cells (2×10^5 cells per well) were seeded in 24-well, flat-bottomed plates (Greiner Bioscience, Kremsmünster, AT). Culturing of cells, incubations and OD measurements were performed as described previously^[30] with minor modifications. 24 h after seeding of the cells the incubation was started by the addition of the compounds from DMSO stock solutions to a final DMSO concentration of 1%. The living cell mass was determined 48 h after addition of the compounds and was followed by the calculation of LD₅₀ values. The calculation of the LC₅₀ values was performed by plotting the percent inhibition vs. the concentration of inhibitor on a semi-logarithmic plot. From this, the molar concentration causing 50% reduction of the living cell mass was calculated. At least three independent experiments were performed for each compound.

Supporting Information. Chemical synthesis of cYY and Mycocyclusin, SDS-PAGE of His-tagged CYP121, Activity of CYP121/ CO Spectra, LC-MS analysis of in vitro CYP121 enzyme reaction and effect of I:47, Surface Plasmon Resonance Sensorgram of econazole, Screening overview, K_D determination by UV-VIS Heme coordination assay, Protein Blast of Mtb H₃₇R_V CYP121 (Rv2276) and *M. bovis* BCG Pasteur CYP121 (BCG_2293), MIC_{BCGT} determination against *Mycobacterium bovis*, Calculation of antimicrobial efficiency, Toxicity assessment against human cancer cell lines HEK293 and HepG2, MIC against *Escherichia coli* and *Staphylococcus aureus* in comparison to growth inhibition against *Mycobacterium bovis* BCG, Physicochemical data.

REFERENCES FOR CHAPTER VI

- [1] World Health Organization, Available at: http://www.who.int/tb/publications/global_report/en/2015.
- [2] a) Z. F. Udwadia, R. A. Amale, K. K. Ajbani, C. Rodrigues, *Clin. Infect. Dis.* **2012**, *54*, 579–581; b) A. A. Velayati, M. R. Masjedi, P. Farnia, P. Tabarsi, J. Ghanavi, A. H. Ziazarifi, S. E. Hoffner, *Chest* **2009**, *136*, 420–425;
- [3] L. E. Connolly, P. H. Edelstein, L. Ramakrishnan, *PLoS Med.* **2007**, *4*, e120.
- [4] S. T. Cole et al., *Nature* **1998**, *393*, 537–544.

- [5] K. Duncan, *Curr. Pharm. Des.* **2004**, *10*, 3185–3194.
- [6] K. J. McLean, D. Clift, D. G. Lewis, M. Sabri, P. R. Balding, M. J. Sutcliffe, D. Leys, A. W. Munro, *Trends Microbiol.* **2006**, *14*, 220–228.
- [7] K. J. McLean et al., *J. Biol. Chem.* **2008**, *283*, 33406–33416.
- [8] A. G. Tsolaki, A. E. Hirsh, K. DeRiemer, J. A. Enciso, M. Z. Wong, M. Hannan, Goguet de la Salmoniere, Yves-Olivier L, K. Aman, M. Kato-Maeda, P. M. Small, *Proc. Natl. Acad. Sci. U. S. A.* **2004**, *101*, 4865–4870.
- [9] P. Belin et al., *Proc. Natl. Acad. Sci. U. S. A.* **2009**, *106*, 7426–7431.
- [10] M. Fonvielle, M.-H. Le Du, O. Lequin, A. Lecoq, M. Jacquet, R. Thai, S. Dubois, G. Grach, M. Gondry, P. Belin, *J. Biol. Chem.* **2013**, *288*, 17347–17359.
- [11] M. B. Martins, I. Carvalho, *Tetrahedron* **2007**, *63*, 9923–9932.
- [12] S. A. Hudson, K. J. McLean, S. Surade, Y.-Q. Yang, D. Leys, A. Ciulli, A. W. Munro, C. Abell, *Angew. Chem., Int. Ed.* **2012**, *51*, 9311–9316.
- [13] P. Belin, A. Lecoq, M.-H. Beaurepaire Ledu, M. Gondry, J.-L. Pernodet, *Patent EP2088143A1* **2009**.
- [14] Z. Ahmad, S. Sharma, G. K. Khuller, P. Singh, J. Faujdar, V. M. Katoch, *International journal of antimicrobial agents* **2006**, *28*, 543–544.
- [15] Z. Ahmad, S. Sharma, G. K. Khuller, *FEMS Microbiol. Lett.* **2006**, *261*, 181–186.
- [16] Z. Ahmad, S. Sharma, G. K. Khuller, *FEMS microbiology letters* **2006**, *258*, 200–203.
- [17] Z. Ahmad, S. Sharma, G. K. Khuller, *FEMS microbiology letters* **2005**, *251*, 19–22.
- [18] S. T. Byrne, S. M. Denkin, P. Gu, E. Nuermberger, Y. Zhang, *J. Med. Microbiol.* **2007**, *56*, 1047–1051.
- [19] K. J. McLean, K. R. Marshall, A. Richmond, I. S. Hunter, K. Fowler, T. Kieser, S. S. Gurcha, G. S. Besra, A. W. Munro, *Microbiology* **2002**, *148*, 2937–2949.
- [20] a) M.-P. Lézé, M. Le Borgne, P. Pinson, A. Paluszczak, M. Duflos, G. Le Baut, R. W. Hartmann, *Bioorganic & medicinal chemistry letters* **2006**, *16*, 1134–1137; b) H. Bayer, C. Batzl, R. W. Hartman, A. Mannschreck, *Journal of medicinal chemistry* **1991**, *34*, 2685–2691; c) F. Leroux, T. U. Hutschenreuter, C. Charrière, R. Scopelliti, R. W. Hartmann, *HCA* **2003**, *86*, 2671–2686; d) M. Voets, I. Antes, C. Scherer, U. Müller-Vieira, K. Biemel, S. Marchais-Oberwinkler, R. W. Hartmann, *Journal of medicinal chemistry* **2006**, *49*, 2222–2231; e) S. Lucas, R. Heim, C. Ries, K. E. Schewe, B. Birk, R. W. Hartmann, *Journal of medicinal chemistry* **2008**, *51*, 8077–8087;
- [21] K. J. McLean et al., *J. Inorg. Biochem.* **2002**, *91*, 527–541.
- [22] T. Omura, R. Sato, *J. Biol. Chem.* **1964**, *239*, 2379–2385.
- [23] K. M. Ewen, B. Schiffler, H. Uhlmann-Schiffler, R. Bernhardt, F. Hannemann, *FEMS Yeast Res.* **2008**, *8*, 432–441.
- [24] J. J. Müller, F. Hannemann, B. Schiffler, K. M. Ewen, R. Kappl, U. Heinemann, R. Bernhardt, *J. Inorg. Biochem.* **2011**, *105*, 957–965.
- [25] H. Morgan, D. M. Taylor, *Biosens. Bioelectron.* **1992**, *7*, 405–410.
- [26] S. G. Franzblau et al., *Tuberculosis* **2012**, *92*, 453–488.
- [27] M. Altaf, C. H. Miller, D. S. Bellows, R. O'Toole, *Tuberculosis* **2010**, *90*, 333–337.

3 Results

- [28] I. Benko, F. Hernádi, A. Megyeri, A. Kiss, G. Somogyi, Z. Tegye, F. Kraicsovits, P. Kovács, *J. Antimicrob. Chemother.* **1999**, *43*, 675–681.
- [29] H. M. Korashy, A. Shayeganpour, D. R. Brocks, El-Kadi, Ayman O S, *Toxicol. Sci.* **2007**, *97*, 32–43.
- [30] J. Hauptenthal, C. Baehr, S. Zeuzem, A. Piiper, *Int. J. Cancer* **2007**, *121*, 206–210.
- [31] C.-F. Liu, C.-H. Lin, C.-C. Lin, Y.-H. Lin, C.-F. Chen, C.-K. Lin, S.-C. Lin, *Toxicology* **2004**, *196*, 87–93.
- [32] B. G. Wachall, M. Hector, Y. Zhuang, R. W. Hartmann, *Bioorg. Med. Chem.* **1999**, *7*, 1913–1924.
- [33] C. A. Lipinski, F. Lombardo, B. W. Dominy, P. J. Feeney, *Adv. Drug Deliver. Rev.* **2001**, *46*, 3–26.
- [34] A. Koul, E. Arnoult, N. Lounis, J. Guillemont, K. Andries, *Nature* **2011**, *469*, 483–490.
- [35] D. Leys, C. G. Mowat, K. J. McLean, A. Richmond, S. K. Chapman, M. D. Walkinshaw, A. W. Munro, *J. Biol. Chem.* **2003**, *278*, 5141–5147.
- [36] C. Tanford, *Science* **1978**, *200*, 1012–1018.
- [37] a) L. S. Nobre, S. Todorovic, Tavares, Ana Filipa N, E. Oldfield, P. Hildebrandt, M. Teixeira, L. M. Saraiva, *J. Bacteriol.* **2010**, *192*, 1527–1533; b) R. A. Helmick, A. E. Fletcher, A. M. Gardner, C. R. Gessner, A. N. Hvitved, M. C. Gustin, P. R. Gardner, *Antimicrob. Agents Chemother.* **2005**, *49*, 1837–1843;
- [38] a) H. M. Guardiola-Diaz, L.-A. Foster, D. Mushrush, A. D. Vaz, *Biochem. Pharmacol.* **2001**, *61*, 1463–1470; b) Boshoff, Helena I M, T. G. Myers, B. R. Copp, M. R. McNeil, M. A. Wilson, C. E. Barry, *J. Biol. Chem.* **2004**, *279*, 40174–40184; c) A. Milano, M. R. Pasca, R. Provvedi, A. P. Lucarelli, G. Manina, Ribeiro, Ana Luisa de Jesus Lopes, R. Manganelli, G. Riccardi, *Tuberculosis* **2009**, *89*, 84–90;
- [39] a) A. L. Hopkins, C. R. Groom, A. Alex, *Drug discovery today* **2004**, *9*, 430–431; b) L. G. Czaplowski et al., *Bioorganic & medicinal chemistry letters* **2009**, *19*, 524–527;

3.7 Discovery and Biophysical Evaluation of First Low Nanomolar Hits Targeting CYP125 of *M. tuberculosis*

Andreas Thomann,⁺ Christian Brengel,⁺ Alexander Schifrin, Jens Eberhard, and Rolf W. Hartmann

⁺ both authors contributed equally to this work

Reproduced with permission from *ChemMedChem*; Published online: 28.09.2016, DOI: 10.1002/cmdc.201600361

Copyright 2016 John Wiley and Sons.

Publication VII

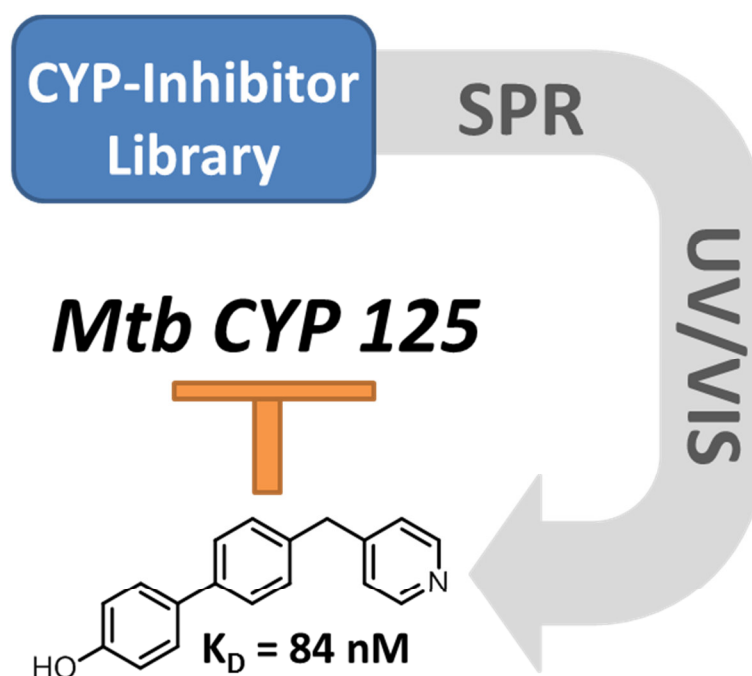


Figure 21. Graphical abstract of publication VII.

Discovery and Biophysical Evaluation of First Low Nanomolar Hits Targeting CYP125 of *M. tuberculosis*

Christian Brengel^{†, [a]}, Andreas Thomann^{†, [a]}, Alexander Schifrin,^[b] Jens Eberhard,^[a] and Rolf W. Hartmann^{*[a, c]}

Tuberculosis, which is predominantly caused by *Mycobacterium tuberculosis* (Mtb), is still the most lethal bacterial infection with 1.5 million casualties in 2014. Moreover, the fact that the appearance of resistant mutants and long-term treatment are coupled with economic problems in developing countries hampers an efficient therapy. Interference with the essential cholesterol metabolism of Mtb could be a promising novel strategy to fight Mtb infections. CYP125, a P450 enzyme in Mtb, has been shown to play an important role in this meta-

bolic pathway. For this reason, we used a combined screening approach involving surface plasmon resonance spectroscopy and a heme coordination assay to identify new CYP125 binders by employing a focused P450-inhibitor library. We identified the first hits with high affinity and favorable ligand efficiencies. Furthermore, frontrunner compounds also showed selectivity toward CYP121 specific to Mtb and required for its survival. To date, these are the first compounds targeting CYP125 with low nanomolar affinity.

Introduction

Since the discovery of the first drugs for the therapy of tuberculosis (TB) in the 1940s, many new compounds and therapeutic regimes have been developed to improve treatment of TB.^[1,2] Despite the great success, the World Health Organization (WHO) registered 9 million new infections and 1.5 million cases of death caused by the disease in 2014.^[3] Key problems are the long-term treatment of at least 6 months, the development of resistance against anti-TB drugs, and co-infections with human immunodeficiency virus (HIV). In this respect, new anti-TB drugs should address these points and most preferably decrease hospitalization and increase therapeutic success of treatment-resistant TB.^[2,4] For these reasons, there is an urgent need for new drug targets with novel modes of action to improve the portfolio of anti-TB drugs.

In 2007, Chang et al. identified an interesting sequence in the genome of *Mycobacterium tuberculosis* (Mtb) that was found to be required for mycobacterial growth in macrophages. The so-called "igr" operon (derived from "intracellular growth") was also confirmed to be essential for the full virulence of Mtb in an in vivo scenario.^[5] In subsequent studies, it

was shown that the respective operon was involved in the cholesterol metabolism of Mtb. Therein, a Δ igr mutant was not able to grow on cholesterol, and supplementation of an additional source of nutrition demonstrated only insufficient recovery of growth. These findings suggested an intoxicating effect caused by the sterol.^[6] In the same year, CYP125, a P450 enzyme encoded in the igr operon, was reported to efficiently metabolize cholesterol.^[7] Capyk et al. generated a Δ cyp125 knock-out strain of *M. bovis* BCG that was unable to survive on cholesterol-supplemented medium, which indicated that the cytochrome P450 (CYP) enzyme was a key player in cholesterol detoxification. However, this finding was not confirmed by a Δ cyp125 mutant of *M. tuberculosis* H₃₇R_v.^[8] Further investigations explained this observation with the presence of a compensatory enzyme, namely, CYP142, in the laboratory H₃₇R_v strain. However, the latter enzyme was not present in the clinical isolate CDC1551, which brought into question the clinical relevance of this bypass.^[9,10] Moreover, in this study the previous results found for BCG were corroborated, which still render CYP125 as a key enzyme for cholesterol metabolism.^[9]

As metabolism of cholesterol plays an essential role in the persistence and virulence of Mtb, interference with the key player CYP125 could be a new promising strategy for TB treatment.^[6,9,11] Until today, besides azole antifungals, there is only one inhibitor of CYP125 described: LP10.^[7,12] Interestingly, LP10 was not designed for inhibition of CYP125 but was discovered as an inhibitor of CYP51 from *Trypanosoma cruzi*.^[13] CYP125 inhibition was only moderate, which was explained by the fact that its affinity is lower than that of the substrate cholesterol-4-en-3-one (CHN).^[12]

Herein, we employed a combined biophysical screening approach for the discovery of new CYP125 binders with increased affinity and favorable ligand efficiency.^[14] The compounds dis-

[a] C. Brengel,[†] A. Thomann,[†] Dr. J. Eberhard, Prof. Dr. R. W. Hartmann
Helmholtz Institute for Pharmaceutical Research Saarland,
Department of Drug Design and Optimization,
Campus E8.1, 66123 Saarbrücken (Germany)
E-mail: rolf.hartmann@helmholtz-hzi.de

[b] A. Schifrin
Department of Biochemistry, Saarland University,
Campus B2.2, 66123 Saarbrücken (Germany)

[c] Prof. Dr. R. W. Hartmann
Department of Pharmacy, Pharmaceutical and Medicinal Chemistry,
Saarland University, Campus C2.3, 66123 Saarbrücken (Germany)

[[†]] These authors contributed equally to this work.

Supporting Information for this article can be found under <http://dx.doi.org/10.1002/cmdc.201600361>.

covered showed affinity for CYP125 that was 7 to 70 times higher than that of its substrate **CHN**, and thus, they are promising starting points for future drug-optimization campaigns.

Results and Discussion

Library generation

For surface plasmon resonance (SPR) spectroscopy guided identification of CYP125 binders, we started with a hand-picked selection of 132 compounds from our in-house CYP inhibitor library focusing on structural diversity. The library contained compounds designed for inhibition of human steroidal P450 enzymes, especially CYP17, CYP11B1/2, and CYP19.^[15–36] These inhibitors are privileged to interact with P450 enzymes because of their nitrogen-containing heterocycles, which enable coordination to the iron(II) center of heme.^[15] In general, huge benefits arise from the use of focused libraries: the hit rates are usually much higher, the biological activities are already known for the compounds, and derivatization is often easy, as synthetic routes are already established. Thus, for our compounds inhibition data for steroidogenic and hepatic CYP enzymes as well as cytotoxicity data were available. For the evaluation of our library compounds, two described inhibitors of CYP125, namely, econazole (**Eco**) and **LP10**, served as reference compounds.^[7,12]

SPR spectroscopy screening

CYP125 used for in vitro experiments was expressed in the heterologous host *E. coli* BL21 DE3 and was purified by affinity chromatography. The correct folding and function of the enzyme were confirmed with carbon monoxide binding spectra.^[37] In these studies, we were also able to identify a new heterologous electron-transfer system composed of Etp1fd (516–618) as ferredoxin and Arh1A18G as reductase.^[38,39] Biotinylated CYP125 was bound to the streptavidin-labeled SPR spectroscopy sensor chip.^[40]

The reference compound **Eco** was reported to form a type II complex with the heme iron of CYP125.^[7] For initial validation of our SPR spectroscopy technique, we confirmed **Eco** binding at a concentration of 100 μM to immobilized CYP125 (Figure S1 in the Supporting Information). For all library compounds, the binding response of **Eco** (R_{pos}) was set to 1. The compounds were tested at the same concentration (100 μM) and their binding response (R) was referenced to the response of the positive control (R/R_{pos}). All compounds with an R/R_{pos} value ≥ 1 were regarded as hits in the following experiments and were defined as SPR binders. The screening of the in-house library consisting of 132 compounds resulted in 22 binders that showed broad structural variety. The observed hit rate ($\approx 17\%$) was high, which confirmed our initial hypothesis that choosing privileged structures would result in lower attrition rates (Figure 1).

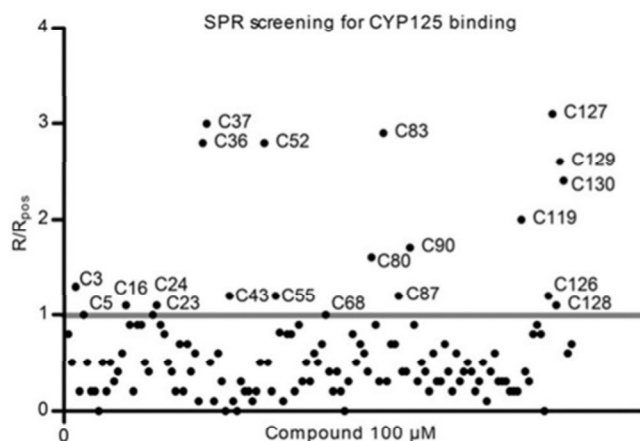


Figure 1. Result of the SPR spectroscopy screening. Of the 132 compounds, 22 were hits with $R/R_{\text{pos}} \geq 1$ with R = response of econazole (**Eco**), R_{pos} = response of library compound.

UV/Vis heme P450 binding assay

To derive detailed information of compound binding behavior, we chose the UV/Vis spectroscopy heme coordination assay for P450 enzyme interaction.^[41] The assay was used to determine the binding affinity and the putative binding mode of our hits determined by SPR spectroscopy. Such experiments, employing CYP125, were already described for **Eco**, the substrate **CHN**, and **LP10**.^[7,9,12] In our study, we selected these three compounds as positive controls and three weak SPR binders (i.e., **C25**, **C53**, and **C59**) as negative controls ($R/R_{\text{pos}} < 1$, see Table S1 and Figure 2).^[7] **LP10** and **CHN** bound as previously reported to CYP125 with slight differences in the K_{D} values [$K_{\text{D}}(\text{CHN}) = 6.1 \mu\text{M}$, $K_{\text{D}}(\text{LP10}) = 4.6 \mu\text{M}$; $K_{\text{D}}(\text{CHN}_{\text{hit}}) = 1.2 \mu\text{M}$, $K_{\text{D}}(\text{LP10}_{\text{hit}}) = 1.7 \mu\text{M}$].^[9,12] For **LP10**, an increase in the absorbance of the low-spin band at $\lambda = 420 \text{ nm}$ was previously described (such compounds are defined as reverse type I binders), which we confirmed in our experiments.^[12] Interestingly, for econazole we observed type I binding behavior with $K_{\text{D}} = 0.94 \mu\text{M}$, which differs from the type II profile with $K_{\text{D}} = 11 \mu\text{M}$ described by McLean et al.^[7] Notably, the co-crystal structure of econazole bound to CYP125 (PDB ID: 3IW2) shows a water bridge interaction with the iron heme, which supports our finding.^[7] From the initial 22 binders obtained from the SPR spectroscopy hits, we identified 14 compounds that showed binding to the CYP125 heme with $K_{\text{D}} < 30 \mu\text{M}$ (Table S1). It was previously described that the iron of the native enzyme is in equilibrium between low spin and high spin.^[7] Thus, a reverse type I binding as observed for **LP10** might also be possible for some of our compounds.^[12] Out of the 14 heme coordinators, nine showed a characteristic type II or reverse type I profile. Their binding resulted in an absorbance maximum at a wavelength higher than that of **LP10** (Table S2), and hence, a type II interaction might be more plausible than a reverse type I. Nevertheless, determination of a precise binding mode might require analysis of the co-crystal structure of our hits and CYP125. For convenience, in the following we use the term type II shift profile. With regard to type I binding behavior, we identified another seven compounds fulfilling this profile. In

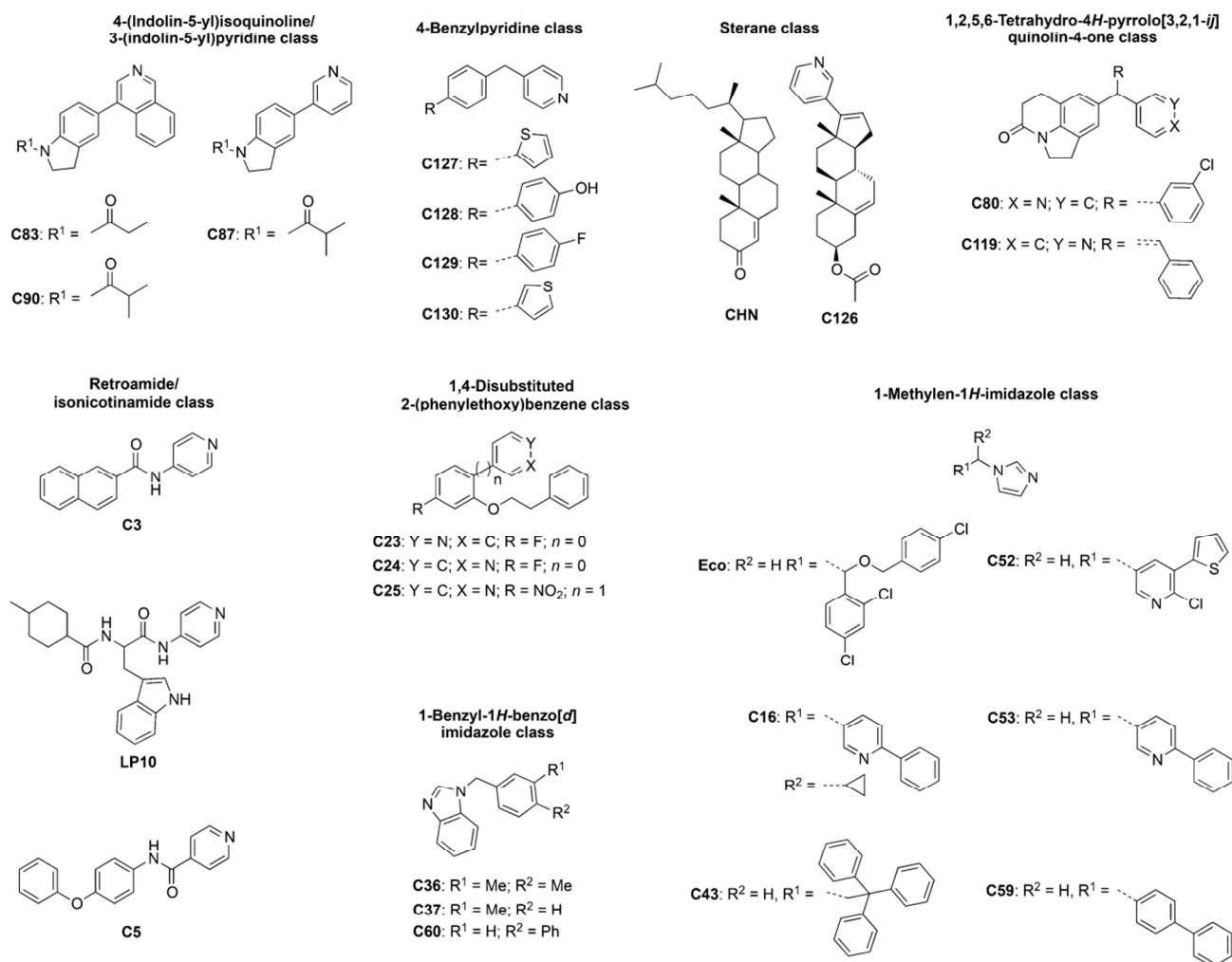


Figure 2. Chemical structures of the 22 hits as obtained by SPR spectroscopy.

terms of structural requirements necessary for type II versus type I binding, we identified a common motif. For type II binders, a flexible alkylene unit (e.g., as in **C43** and **C127–C130**) or an amide bond (e.g., as in **C3** and **C5**) together with a linear structure and unsubstituted coordinating head group were found to be beneficial. Notably, the crystal structure of CYP125 with its substrate **CHN** (PDB ID: 2X5W) shows a narrow channel occupied by the alkyl side chain of the substrate. This channel might be preferably accessible by linear, less bulky molecules, which in turn could then directly interact with the iron(II) center. For type I binders, we found different structural features. Either the compounds had bulky coordinating head groups (e.g., as in **C36**, **C37**, and **C60**) or bulky substituents in close proximity to the coordinating head group (e.g., as in **C16**, **C23**, and **C24**). In addition, none of the type I binders had a linear structure similar to that observed for the type II binding compounds. These structural characteristics might prevent the type I compounds from entering the abovementioned narrow channel, and hence, those molecules can only interact with the iron(II) center through a water bridge.

Five hits as obtained by SPR spectroscopy did not seem to exhibit a heme coordination behavior (Table S1). The binders with highest affinity, that is, **C24** (type I: 0.26 μM) as well as **C127**, **C128**, and **C130** (type II: **C127** = 0.85 μM ; **C128** = 0.084 μM ; **C130** = 0.17 μM), displayed K_D values in the nanomolar range, which, to the best of our knowledge, renders them the most affine compounds to CYP125 described to date (Table S1). The weak binders ($R/R_{\text{pos}} < 1$), as determined by SPR spectroscopy, with a high structural relationship to strong binders were chosen for SPR spectroscopy screening procedure validation (Table S1; compounds **C25**, **C59**, and **C53**): **C25** is an example of a weak binder that is structurally strongly related to the strong SPR spectroscopy and heme binders **C23** and **C24** (Figure 2). As expected, **C25** did not interact with the heme iron (Table S1). Furthermore, **C53** and **C59**, showing distinct structural analogy to **Eco**, exhibited low affinity in the SPR spectroscopy experiment. Thus, we were interested in determining whether these compounds were false positives and, therefore, tested them for heme coordination. Again, none of these compounds showed binding to CYP125 in the UV/Vis assay, which validated our initial screen. Notably, we obtained

several compounds (Table S1; compounds **C45**, **C52**, **C83**, **C87**, **C90**, and **C119**) with a stronger SPR spectroscopy response than that shown by **Eco** ($R/R_{\text{pos}} \geq 1$) that did not interact with the heme iron. Such compounds are expected to bind to other binding sites of the protein without interacting with the iron in the catalytic center. They were excluded from the screening procedure but are still interesting, as they might function as fragments in merging or linking strategies with type I or type II binders. However, with the information of the respective binding modes, one can more quickly and more rationally decide how to modify the binders or even how to combine given structures to generate inhibitors with higher activities.

Structure–binding relationships and ligand efficiencies

The gathered data from the two binding assays provide fundamental information for preliminary structure–binding relationships (Table 1 and Table S1). The ligand efficiency (LE) as a classification index is not only indicative of the affinity of a compound but it also takes its molecular weight into consideration: the LE is the free-energy contribution for binding (expressed in kcal) per heavy atom (HA) of the molecule.^[14] These data were calculated to estimate if a compound would be suitable for efficient drug discovery with regard to its size and affinity ($LE > 0.3$). Having a look at the head groups needed for interaction with the heme iron, a first structure–activity relationship (SAR) observation could be made. In the case of the methylene-bridged imidazole residues, only **Eco** was found to bind in the nanomolar range (Table S1). All other compounds containing such a structure were only weak binders or did not show any heme iron coordination (i.e., compounds **C16**, **C43**, and **C52**). In contrast to this, most pyridinyl and benzimidazolyl head groups linked to different core structures were tolerated by the enzyme. In these subgroups, we identified type I as well as type II binders depending on the core structure. Notably, all benzimidazolyl-substituted compounds showed binding to

CYP125 in both test systems (Figure 2), especially **C60** with a K_D value of 0.28 μM and a LE of 0.42 kcal HA^{-1} . The two derivatives of this subset having the phenyl residue replaced by a methyl group showed even higher LE scores (**C36**: 0.46 kcal HA^{-1} , **C37**: 0.49 kcal HA^{-1}) (Table S1). This underlines the potential of the 1-benzyl-1*H*-benzo[d]imidazole class as a promising starting point for hit optimization, as these compounds are still in the molecular weight range of fragments (< 300 Da). The SPR spectroscopy screening yielded various compounds bearing a pyridinyl head group linked to different core structures (Figure 2). In general, compounds with a 4-(indolin-5-yl)isoquinoline or 3-(indolin-5-yl)pyridine scaffold did not show heme interaction at the tested concentrations and were therefore excluded from further investigations. The isonicotinamide and corresponding retroamide compounds (i.e., **C3** and **C5**) share some degree of structural similarity to literature-described CYP125 inhibitor **LP10**. Both compounds generated a type II shift. The K_D values and LE (**LP10**: 6.1 μM and 0.24 kcal HA^{-1} ; **C5**: 28 μM and 0.29 kcal HA^{-1}) are in an acceptable range for CYP125 inhibition but are lower than those seen for other high-affinity ligands from the focused library. These structures should be regarded as second choices if the more affine were to compounds fail in a subsequent optimization process. The binders found in the 1,2,5,6-tetrahydro-4*H*-pyrrolo[3,2,1-*ij*]quinolin-4-one class were of moderate affinity with a type II binding profile (Table 1). Because of their low affinities combined with their high molecular weights, **C80** and **C119** were deemed unsuitable for structural optimization regarding CYP125 inhibition. High-affinity binders were identified in the 1,4-disubstituted 2-(phenylethoxy)benzene-substituted and 4-benzylpyridine-substituted subset (Figure 2). The latter derivatives were found to bind in a type I mode to the enzyme. Interestingly, repositioning of the coordinating nitrogen atom from the *para* position to the *meta* position in the heteroaromatic ring of this compound class resulted in a sixfold increase in the binding affinity for **C24** ($K_D = 0.26 \mu\text{M}$) relative to that of

Table 1. Heme binding affinity data, binding profiles, and selectivity factors of CYP125 binders against Mtb CYP121 and the bypass enzyme CYP142.

Compd	CYP125 ^[a]			CYP142 ^[a]			CYP121 ^[a]		SF ^[b]	
	Type	K_D [μM]	LE [kcal mol^{-1}]	Type	K_D [μM]	LE [kcal mol^{-1}]	Type	K_D [μM]	142 vs. 125	121 vs. 125
C3 ^[19]	II	19 ± 0.7	0.35	II	0.89 ± 1.05	0.45	weak	> 100	0.047	> 5.26
C5 ^[18]	II	28 ± 1.4	0.29	II	6.2 ± 0.6	0.14	weak	> 100	0.224	> 3.57
C16 ^[17]	I	16 ± 6.9	0.32	I	19.7 ± 2.6	0.31	II	> 100	1.232	> 6.25
C23 ^[21]	I	1.5 ± 0.6	0.37	I	1.8 ± 1.0	0.17	II	7.2 ± 0.5	1.193	4.80
C24 ^[21]	I	0.26 ± 0.38	0.42	I	1.5 ± 0.4	0.18	II	11.7 ± 4.3	5.896	45.00
C36 ^[27,28]	I	1.3 ± 0.7	0.46	I	3.4 ± 0.7	0.19	no	> 100	2.637	> 76.92
C37 ^[27,28]	I	1.1 ± 0.7	0.49	no	> 100	0.33	no	> 100	90.909	> 90.91
C43 ^[27,28]	II	13.1 ± 0.9	0.26	II	0.14 ± 0.35	0.37	II	8.8 ± 3.0	0.011	0.67
C60 ^[27,28]	I	0.28 ± 0.50	0.42	I	0.18 ± 0.002	0.43	no	> 100	0.654	> 357.14
C126 ^[20]	II	2.1 ± 0.3	0.27	no	> 100	–	no	> 100	> 47.619	> 47.62
C127 ^[20]	II	0.85 ± 0.25	0.47	II	0.096 ± 0.012	0.55	II	2.6 ± 0.2	0.113	3.06
C128 ^[20]	II	0.084 ± 0.014	0.50	II	0.008 ± 0.014	0.57	II	1.33 ± 0.9	0.095	15.83
C129 ^[20]	II	1.34 ± 0.35	0.41	II	0.062 ± 0.023	0.50	II	2.5 ± 0.3	0.046	1.87
C130 ^[20]	II	0.17 ± 0.05	0.53	II	0.252 ± 0.041	0.51	II	1.8 ± 0.1	1.448	10.34
LP10 ^[12]	II	6.1 ± 1.5	0.24	II	5.02 ± 1.75	0.25	II	34.3 ± 5.5	0.823	5.62
Eco ^[c]	I	0.941 ± 0.060	0.35	II	0.77 ± 0.15	0.36	II	2.8 ± 0.2	0.815	2.98
CHN ^[d]	I	4.6 ± 1.5	0.27	I	0.94 ± 0.20	0.30	no	> 100	1.896	> 200.00

[a] Mean value of at least three experiments and the standard deviation. [b] SF = selectivity factor. [c] **Eco** = econazole. [d] **CHN** = cholest-4-en-3-one.

C23 ($K_D = 1.5 \mu\text{M}$) (Table 1). A reason for this increase could be a privileged angle for interaction of the nitrogen atom with the coordinating water molecule linked to the heme iron or a more favorable interaction with other residues of the protein. With a LE score of $0.42 \text{ kcal HA}^{-1}$, **C24** has considerable potential for further optimization. Most interestingly, highly active compounds were also observed in the group of 4-benzylpyridines. Three of the four compounds were found to bind with low micromolar to nanomolar affinity to CYP125 (**C127**: $0.85 \mu\text{M}$; **C128**: $0.085 \mu\text{M}$; **C129**: $1.34 \mu\text{M}$; **C130**: $0.17 \mu\text{M}$). Moreover, the low molecular weights of these compounds resulted in remarkable LE scores (**C127**: $0.47 \text{ kcal HA}^{-1}$; **C128**: $0.50 \text{ kcal HA}^{-1}$; **C129**: $0.41 \text{ kcal HA}^{-1}$; **C130**: $0.53 \text{ kcal HA}^{-1}$). The *p*-hydroxyphenyl residue increased the affinity relative to that of the *p*-fluorophenyl group. Presumably, an electron-rich aromatic system is preferred or the hydroxy group has additional interactions with the target. Regarding five-membered heterocycles, the electron-rich thiophene compounds (i.e., **C127** and **C130**) also showed high affinity. In particular, we observed a difference between the thiophene regional isomers in the class of the aforementioned derivatives, whereby the 2-substituted **C127** compound was superior in terms of affinity over the 3-substituted **C130** congener (Table 2). From the 132 initially tested compounds, **C128** was the one with the highest affinity to CYP125 and is the most affine compound described in the literature to date. With a K_D value that is 55-fold lower than that of the substrate **CHN** ($K_D = 4.6 \mu\text{M}$), **C128** should be a highly efficient inhibitor of the enzyme reaction.

Selectivity among P450 enzymes

As the library compounds were originally designed for the inhibition of human steroidogenic enzymes, it was important to compare their activities toward human steroidogenic and hepatic enzymes as well as bacterial CYP enzymes (Table 2). Most compounds from our library were active in the nanomolar range against their respective target.^[15–36] From our 14 heme binders, we selected five on the basis of their LE scores to be the most promising hits (i.e., compounds **C24**, **C60**, **C127**, **C128**, and **C130**) for further selectivity evaluation. Compounds out of the 2-(phenylethoxy)benzene class were found to be potent inhibitors of CYP11B1 and CYP11B2. Although **C24** showed good binding affinity to CYP125 ($K_D = 0.26 \mu\text{M}$), an improvement in selectivity toward the CYP11B1 and CYP11B2 enzymes is necessary [$\text{IC}_{50}(\text{CYP11B1})$: $51 \mu\text{M}$, $\text{IC}_{50}(\text{CYP11B2})$:

$84 \mu\text{M}$]. The frontrunner compound of the 1-benzyl-1*H*-benzo-[*d*]imidazole class, that is, **C60** ($K_D = 0.28 \mu\text{M}$), was not active against CYP17 (6% inhibition at $2 \mu\text{M}$) or CYP19 (2% inhibition at $0.5 \mu\text{M}$) and showed only weak inhibition of CYP11B2. The IC_{50} value against CYP11B1 ($\text{IC}_{50} = 0.197 \mu\text{M}$) was found to lie in a similar range as the K_D value against CYP125. However, it should be noted that K_D values are typically lower than IC_{50} values.^[42] Looking at the activity of the 4-substituted 4-benzylpyridines, we observed similar values for **C127** and **C130** on CYP125, CYP17, CYP11B1, and CYP11B2, but **C128** was an exception, as it showed moderate selectivity over CYP17, CYP19, CYP11B1, CYP11B2, and CYP3A4 (Table 2).

As the basis of our strategy was to interfere with a crucial function during host adaptation of Mtb, we were interested to study whether the herein-found inhibitors might also bind to an essential consistently expressed CYP enzyme of Mtb. We chose CYP121, an enzyme essential for Mtb *in vitro*, for the latter-mentioned counter screen. In addition, we incorporated CYP142, the bypass enzyme of the CYP125 enzyme reaction in Mtb H₃₇Rv, to study the possibility of a dual target strategy.^[10,43] Here, we determined selectivity factors (SFs) to enhance comparability. Upon looking at the compounds with nanomolar binding affinity to CYP125, we obtained different profiles depending on the compound class (Table 1). Compound **C24** was found to be a selective binder of CYP125, with regard to CYP142, but it showed less selectivity to CYP121 (SF_{CYP142}: 6; SF_{CYP121}: 45). This is in contrast to **C60**, which was also found to bind tightly to the bypass CYP142 enzyme and was a much weaker inhibitor of CYP121 (SF_{CYP142}: 0.6; SF_{CYP121} > 350). With regard to CYP142, selectivity might not be desirable, as blockage of the bypass could increase the effectivity of the cholesterol metabolism targeted approach, at least in the laboratory H₃₇Rv strain. In general, the 4-benzylpyridines **C127**, **C128**, and **C130** possess a tight binding profile and convincing LE scores on CYP142 and selectivity toward CYP121, and **C128** is the most promising compound overall (**C128**: SF_{CYP142}: 1; SF_{CYP121}: 16, Table 1).

Conclusions

In this study, 132 compounds of a focused cytochrome P450 inhibitor library were screened by using two biophysical assays to identify nanomolar binders to CYP125. This procedure led to the identification of 22 hit compounds with high structural diversity. Further investigations employing a UV/Vis heme coor-

Table 2. Selectivity profile of most affine CYP125 heme ligands ($K_D < 1 \mu\text{M}$) versus human CYP enzymes.

Compd	K_D [nM]			IC_{50} ^[a] [nM]		
	CYP125	CYP17	CYP11B1	CYP11B2	CYP19	CYP3A4
C24	260	–	51	84	–	–
C60	280	6 at 2000	197	1903	2 at 500	–
C127	850	577	422	331	–	–
C128	84	248	251	341	3070	3210
C130	174	647	415	796	–	–

[a] Mean value of at least three experiments, standard deviation less than 25%.

dination assay characterized five compounds as type I binders and nine compounds as type II binders with K_D values below 30 μM . Five of these compounds (type II: **C127** = 0.85 μM , **C128** = 0.085 μM , and **C130** = 0.174 μM ; type I: **C24** = 0.26 μM , **C60** = 0.28 μM) were found to bind to the heme site of CYP125 in the nanomolar range. Thereby, their affinities were higher than that of the substrate cholest-4-en-3-one (**CHN**), which makes them interesting candidates with a possibly high inhibitory potential. Furthermore, these compounds showed affinity to CYP125 that was 7- to 70-fold higher than that of the reported inhibitor **LP10**. Frontrunner compound **C128** is, to the best of our knowledge, the first-described low-nanomolar CYP125 binder. In addition, this compound was found to bind tightly to the bypass enzyme of CYP125 (i.e., CYP142), which provides a good starting point for in cellulo proof of principle studies in *M. tuberculosis* laboratory strain H₃₇R_v. The selectivity among human (e.g., CYP11B1/B2, CYP19, CYP17, and CYP3A4) and another essential Mtb P450 enzyme (e.g., CYP121) was given for some inhibitors investigated in this study. However, an improvement in selectivity is important to circumvent potential later-stage side effects originating from occlusion of steroid and/or xenobiotic metabolism by CYP enzymes in humans. Moreover, compounds identified in this study might also be useful as scientific tools to further support the investigation of the intensively discussed cholesterol metabolism in Mtb, as some of them block both enzymes known for **CHN** transformation (i.e., CYP125 and CYP142). Furthermore, owing to their low molecular weights, excellent water solubilities, and high ligand efficiencies, the herein reported compounds are promising first hits for the development of novel antimycobacterial drugs targeting an essential metabolic pathway in Mtb.

Experimental Section

Bacterial strains and growth conditions

The bacterial strain used in this study was *E. coli* K12 BL21 DE3 for protein expression.

Chemical synthesis and analytical characterization

Compounds for testing [i.e., **LP10**, econazole (**Eco**), and cholest-3-en-4-one (**CHN**)] were purchased from commercial suppliers and were used without further purification. Procedures for the synthesis of library compounds were previously reported.^[15–36] Detailed information can be found in Section S6 of the Supporting Information.

Biological methods

Protein expression, purification, and biotinylation: *E. coli* K12 BL21 DE3 cells were transformed with plasmid harboring *cyp125* gene (CYP125A1/pCWori).^[9] The previously described enzyme expression and purification method was slightly modified and was used for the CYP125, CYP142, and CYP121 constructs.^[7,44] His₆-tagged protein was expressed in *E. coli* K12 BL21 DE3 and was purified by using a single affinity chromatography step. Briefly, *E. coli* K12 BL21 DE3 cells containing the plasmid were grown in terrific broth medium containing 100 $\mu\text{g mL}^{-1}$ ampicillin at 37 °C until an optical

density at $\lambda = 600$ nm of ~ 0.8 MAU was reached. Protein expression was then induced by the addition of 0.5 mM isopropyl β -D-thiogalactopyranoside (IPTG) and 0.5 mM δ -aminolevulinic acid, and the bacteria were grown for an additional 36 h at 25 °C and 200 rpm. The cells were harvested by centrifugation (5000 rpm, 10 min, 4 °C), and the cell pellet was resuspended in 100 mL of binding buffer containing 1% Triton-X-100 (50 mM Tris-HCl, 300 mM NaCl, 20 mM imidazole, 10% glycerol, pH 7.2) and were lysed by sonication for a total process time of 2.5 min. Cellular debris was removed by centrifugation (18500 rpm, 40 min, 4 °C), and the supernatant was filtered through a syringe filter (0.2 μm). The clear lysate was immediately applied to a Ni-NTA affinity column, washed with binding buffer, and eluted with a one-step gradient of 500 mM imidazole. The protein-containing fractions were buffer exchanged to storage buffer (140 mM NaCl, 10 mM Na₂HPO₄, 2.7 mM KCl, 1.8 mM KH₂PO₄, and 10% glycerol (v/v), pH 7.2) by using a PD10 column (GE Healthcare) and were judged pure by SDS-PAGE analysis. Protein was stored in aliquots at -80 °C at a final concentration of 50 μM . Before SPR spectroscopy, streptavidin immobilization CYP125 was biotinylated. For biotinylation, EZ-linked Sulfo-NHS-LC-LC-Biotin (Thermo Science) was dissolved in storage buffer (140 mM NaCl, 10 mM Na₂HPO₄, 2.7 mM KCl, 1.8 mM KH₂PO₄, and 10% glycerol (v/v)) with CYP125 in 1:1 molar ratio. The solution was incubated on ice for 2 h and was mixed carefully every 30 min. Biotinylated CYP121 was purified by a size-exclusion column by using storage buffer and stored at -80 °C at a final concentration of 10 μM .^[40]

Spectroscopic characterization of enzyme activity: Ferredoxin Etp1fd (516–618) and ferredoxin reductase Arh1A18G from the fission yeast *Schizosaccharomyces pombe* were expressed and purified as previously described.^[38,39] Functionality of CYP125 and electron transfer was assayed by the occurrence of the characteristic peak at approximately $\lambda = 450$ nm, related to the reduced, CO-bound heme complex. The assay was conducted as described with slight modifications.^[37] CYP125 (2 μM) was reduced through the addition of a few grains of sodium dithionite or incubation with NADPH (100 μM), Etp1fd (516618) (40 μM), and Arh1A18G (2 μM) and was divided into two cuvettes to record a baseline. One of the samples was saturated with carbon monoxide for 60 s and difference spectra were recorded until the peak at approximately $\lambda = 450$ nm reached saturation.

SPR spectroscopy screening: SPR spectroscopy binding studies were performed by using a Reichert SR7500DC instrument optical biosensor (Reichert Technologies) and SAD500m sensor chips obtained from XanTec Bioanalytics. CYP125 was immobilized on a SAD500m sensor chip at 12 °C by using standard biotin-streptavidin complexation. The surface of both channels was quenched by a 3 min injection of 3 $\mu\text{g mL}^{-1}$ biotin. CYP125 was immobilized at densities between 5000 and 6000 RU for binding studies.

UV/Vis heme P450 binding assay: Optical titration experiments were performed in 96-well plates (Greiner; transparent round-bottom). The data were recorded by using a Tecan infinite M200Pro (Nano Quant). Absorbance of enzyme and enzyme–inhibitor complex was measured between $\lambda = 350$ and 500 nm in 1 nm steps with 10 flashes. Compounds were titrated from DMSO stock solutions to a final DMSO concentration of 1%. CYP125, CYP121, and CYP142 were used at a concentration of 0.25 μM . Data were plotted by optical shift versus ligand concentration. Variable slope model was used for nonlinear regression of resulting dose–response curves by employing GraphPad Prism 5.

Acknowledgements

We thank Prof. Ortiz de Montellano for kindly providing plasmids pCWori/cyp125 and pCWori/cyp142A1^[9] and Prof. Munro for kindly providing pHAT2/cyp121 harboring plasmid. We thank Prof. Bernhard for fruitful discussions, for providing plasmids harboring Arh1A18G and Etp1fd, and for the possibility to characterize the enzymes by UV/Vis spectroscopy in her laboratory.

Keywords: anti-infectives · biophysics · inhibitors · *Mycobacterium tuberculosis* · screening

- [1] M. D. Iseman, *Eur. Respir. J.* **2002**, *20*, 875.
 [2] A. Zumla, P. Nahid, S. T. Cole, *Nat. Rev. Drug Discovery* **2013**, *12*, 388–404.
 [3] World Health Organization, **2014**.
 [4] A. Koul, E. Arnout, N. Lounis, J. Guillemont, K. Andries, *Nature* **2011**, *469*, 483–490.
 [5] J. C. Chang, N. S. Harik, R. P. Liao, D. R. Sherman, *J. Infect. Dis.* **2007**, *196*, 788–795.
 [6] J. C. Chang, M. D. Miner, A. K. Pandey, W. P. Gill, N. S. Harik, C. M. Sassetti, D. R. Sherman, *J. Bacteriol.* **2009**, *191*, 5232–5239.
 [7] K. J. McLean, P. Lafite, C. Levy, M. R. Cheesman, N. Mast, I. A. Pikuleva, D. Leys, A. W. Munro, *J. Biol. Chem.* **2009**, *284*, 35524–35533.
 [8] J. K. Capyk, R. Kalscheuer, G. R. Stewart, J. Liu, H. Kwon, R. Zhao, S. Okamoto, W. R. Jacobs, L. D. Eltis, W. W. Mohn, *J. Biol. Chem.* **2009**, *284*, 35534–35542.
 [9] H. Ouellet, S. Guan, J. B. Johnston, E. D. Chow, P. M. Kells, A. L. Burlingame, J. S. Cox, L. M. Podust, P. R. Ortiz de Montellano, *Mol. Microbiol.* **2010**, *77*, 730–742.
 [10] J. B. Johnston, H. Ouellet, P. R. Ortiz de Montellano, *J. Biol. Chem.* **2010**, *285*, 36352–36360.
 [11] A. K. Pandey, C. M. Sassetti, *Proc. Natl. Acad. Sci. USA* **2008**, *105*, 4376–4380.
 [12] H. Ouellet, P. M. Kells, P. R. Ortiz de Montellano, L. M. Podust, *Bioorg. Med. Chem. Lett.* **2011**, *21*, 332–337.
 [13] C.-K. Chen, P. S. Doyle, L. V. Yermalitskaya, Z. B. Mackey, K. K. H. Ang, J. H. McKerrow, L. M. Podust, *PLoS Neglected Trop. Dis.* **2009**, *3*, e372.
 [14] C. Abad-Zapatero, J. T. Metz, *Drug Discovery Today* **2005**, *10*, 464–469.
 [15] L. Yin, S. Lucas, F. Maurer, U. Kazmaier, Q. Hu, R. W. Hartmann, *J. Med. Chem.* **2012**, *55*, 6629–6633.
 [16] B. G. Wachall, M. Hector, Y. Zhuang, R. W. Hartmann, *Bioorg. Med. Chem.* **1999**, *7*, 1913–1924.
 [17] J. Emmerich, Q. Hu, N. Hanke, R. W. Hartmann, *J. Med. Chem.* **2013**, *56*, 6022–6032.
 [18] M. Balcells, J. Avilla, J. Profitos, R. Canela, *J. Agric. Food Chem.* **2000**, *48*, 83–87.
 [19] S. S. Gunatilleke, C. M. Calvet, J. B. Johnston, C.-K. Chen, G. Erenburg, J. Gut, J. C. Engel, K. K. H. Ang, J. Mulvaney, S. Chen, M. R. Arkin, J. H. McKerrow, L. M. Podust, *PLoS Neglected Trop. Dis.* **2012**, *6*, e1736.
 [20] Q. Hu, C. Jagusch, U. E. Hille, J. Hauptenthal, R. W. Hartmann, *J. Med. Chem.* **2010**, *53*, 5749–5758.
 [21] Q. Hu, J. Kunde, N. Hanke, R. W. Hartmann, *Eur. J. Med. Chem.* **2015**, *96*, 139–150.
 [22] Q. Hu, M. Negri, K. Jahn-Hoffmann, Y. Zhuang, S. Olgen, M. Bartels, U. Müller-Vieira, T. Lauterbach, R. W. Hartmann, *Bioorg. Med. Chem.* **2008**, *16*, 7715–7727.
 [23] Q. Hu, L. Yin, C. Jagusch, U. E. Hille, R. W. Hartmann, *J. Med. Chem.* **2010**, *53*, 5049–5053.
 [24] M. Pinto-Bazurco Mendieta, A. E. Mariano, M. Negri, Q. Hu, U. E. Hille, C. Jagusch, K. Jahn-Hoffmann, U. Müller-Vieira, D. Schmidt, T. Lauterbach, R. W. Hartmann, *Arch. Pharm.* **2008**, *341*, 597–609.
 [25] C. Jagusch, M. Negri, U. E. Hille, Q. Hu, M. Bartels, K. Jahn-Hoffmann, M. Pinto-Bazurco Mendieta, A. E. Mariano, B. Rodenwaldt, U. Müller-Vieira, D. Schmidt, T. Lauterbach, M. Recanatini, A. Cavallid, R. W. Hartmann, *Bioorg. Med. Chem.* **2008**, *16*, 1992–2010.
 [26] U. E. Hille, Q. Hu, C. Vock, M. Negri, M. Bartels, U. Müller-Vieira, T. Lauterbach, R. W. Hartmann, *Eur. J. Med. Chem.* **2009**, *44*, 2765–2775.
 [27] U. E. Hille, C. Zimmer, C. A. Vock, R. W. Hartmann, *ACS Med. Chem. Lett.* **2011**, *2*, 2–6.
 [28] U. E. Hille, C. Zimmer, J. Hauptenthal, R. W. Hartmann, *ACS Med. Chem. Lett.* **2011**, *2*, 559–564.
 [29] C. Zimmer, M. Hafner, M. Zender, D. Ammann, R. W. Hartmann, C. A. Vock, *Bioorg. Med. Chem. Lett.* **2011**, *21*, 186–190.
 [30] L. Yin, Q. Hu, R. W. Hartmann, *J. Med. Chem.* **2013**, *56*, 460–470.
 [31] L. Yin, Q. Hu, J. Emmerich, M. M.-C. Lo, F. Metzger, A. Ali, R. W. Hartmann, *J. Med. Chem.* **2014**, *57*, 5179–5189.
 [32] M. Voets, I. Antes, C. Scherer, U. Müller-Vieira, K. Biemel, S. Marchais-Oberwinkler, R. W. Hartmann, *J. Med. Chem.* **2006**, *49*, 2222–2231.
 [33] M.-P. Lézé, M. Le Borgne, P. Pinson, A. Paluszczak, M. Duflos, G. Le Baut, R. W. Hartmann, *Bioorg. Med. Chem. Lett.* **2006**, *16*, 1134–1137.
 [34] H. Bayer, C. Batzl, R. W. Hartman, A. Mannschreck, *J. Med. Chem.* **1991**, *34*, 2685–2691.
 [35] F. Leroux, T. U. Hutschenreuter, C. Charrière, R. Scopelliti, R. W. Hartmann, *Helv. Chim. Acta* **2003**, *86*, 2671–2686.
 [36] W. Zhu, Q. Hu, N. Hanke, C. J. van Koppen, R. W. Hartmann, *J. Med. Chem.* **2014**, *57*, 7811–7817.
 [37] T. Omura, R. Sato, *J. Biol. Chem.* **1964**, *239*, 2379–2385.
 [38] K. M. Ewen, B. Schiffler, H. Uhlmann-Schiffler, R. Bernhardt, F. Hanneemann, *FEMS yeast Res.* **2008**, *8*, 432–441.
 [39] J. J. Müller, F. Hannemann, B. Schiffler, K. M. Ewen, R. Kappl, U. Heineemann, R. Bernhardt, *J. Inorg. Biochem.* **2011**, *105*, 957–965.
 [40] K. Hüsecken, S. Hinsberger, W. A. M. Elgaher, J. Hauptenthal, R. W. Hartmann, *Future Med. Chem.* **2014**, *6*, 1551–1565.
 [41] a) B. J. Wilson, S. Orrenius, *Biochim. Biophys. Acta, Gen. Subj.* **1972**, *261*, 94–101; b) J. B. Schenkman, H. Remmer, R. W. Estabrook, *Mol. Pharmacol.* **1967**, *3*, 113–123.
 [42] B. T. Burlingham, T. S. Widlanski, *J. Chem. Educ.* **2003**, *80*, 214.
 [43] K. J. McLean, P. Carroll, D. G. Lewis, A. J. Dunford, H. E. Seward, R. Neeli, M. R. Cheesman, L. Marsollier, P. Douglas, W. E. Smith, I. Rosenkrands, S. T. Cole, D. Leys, T. Parish, A. W. Munro, *J. Biol. Chem.* **2008**, *283*, 33406–33416.
 [44] a) H. Ouellet, L. M. Podust, P. R. Ortiz de Montellano, *J. Biol. Chem.* **2008**, *283*, 5069–5080; b) H. Ouellet, J. Lang, M. Couture, P. R. Ortiz de Montellano, *Biochemistry* **2009**, *48*, 863–872.

Received: July 18, 2016

Revised: September 1, 2016

Published online on ■■■■■, 0000

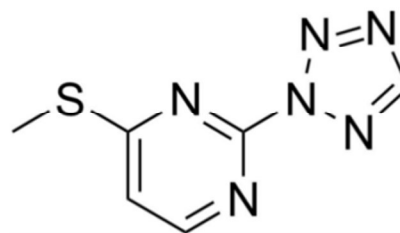
3.8 Crystal structure of 4-methylsulfanyl-2-(2*H*-tetrazol-2-yl)pyrimidine

Andreas Thomann, Volker Huch and Rolf W. Hartmann

Reproduced with the permission from *Acta Cryst.*; **2015**; E71, o1051-o1052; DOI:
10.1107/S2056989015023634

Copyright 2015 International Union of Crystallography.

Publication VIII



Crystal structure of 4-methylsulfanyl-2-(2H-tetrazol-2-yl)pyrimidine

Andreas Thomann,^a Volker Huch^b and Rolf W. Hartmann^{a,c*}

^aHelmholtz-Institute for Pharmaceutical Research Saarland (HIPS), Department for Drug Design and Optimization (DDOP), Saarland University, Campus E8.1, D-66123 Saarbruecken, Germany, ^bDepartment of Inorganic Chemistry, Saarland University, Campus B2.2, D-66123 Saarbruecken, Germany, and ^cDepartment of Pharmacy, Pharmaceutical and Medicinal Chemistry, Saarland University, Campus C2.3, D-66123 Saarbruecken, Germany. *Correspondence e-mail: rolf.hartmann@helmholtz-hzi.de

Received 1 December 2015; accepted 9 December 2015

Edited by H. Stoeckli-Evans, University of Neuchâtel, Switzerland

The title compound, C₆H₆N₆S, crystallized with two independent molecules (*A* and *B*) in the asymmetric unit. The conformation of the two molecules differs slightly. While the tetrazole ring is inclined to the pyrimidine ring by 5.48 (7) and 4.24 (7)° in molecules *A* and *B*, respectively, the N—C—S—C torsion angles of the thiomethyl groups differ by *ca* 180°. In the crystal, the *A* and *B* molecules are linked *via* a C—H···N hydrogen bond. They stack along the *b*-axis direction forming columns within which there are weak π – π interactions present [shortest inter-centroid distance = 3.6933 (13) Å].

Keywords: crystal structure; tetrazole; pyrimidine; thio; heterocycles; S_NAr reactions; π – π interactions.

CCDC reference: 1441424

1. Related literature

For applications of tetrazolyl-substituted aromatic systems in metal–ligand research, see: Kim *et al.* (2008); Stoessel *et al.* (2010); in drug development, see: Pasternak *et al.* (2012); Biswas *et al.* (2015); in polymer synthesis, see: Yu *et al.* (2008); Sengupta *et al.* (2010). For the synthesis of 4-methylsulfanyl-2-(1H-tetrazol-1-yl)pyrimidine and the title compound, see: Thomann *et al.* (2014).

2. Experimental

2.1. Crystal data

C ₆ H ₆ N ₆ S	$\gamma = 102.695 (8)^\circ$
$M_r = 194.23$	$V = 819.9 (4) \text{ \AA}^3$
Triclinic, <i>P</i> $\bar{1}$	$Z = 4$
$a = 6.3001 (17) \text{ \AA}$	Mo $K\alpha$ radiation
$b = 7.393 (2) \text{ \AA}$	$\mu = 0.35 \text{ mm}^{-1}$
$c = 18.159 (5) \text{ \AA}$	$T = 143 \text{ K}$
$\alpha = 91.407 (7)^\circ$	$0.22 \times 0.22 \times 0.01 \text{ mm}$
$\beta = 95.864 (7)^\circ$	

2.2. Data collection

Bruker APEXII CCD diffractometer	15501 measured reflections
Absorption correction: multi-scan (SADABS; Bruker, 2010)	4581 independent reflections
$T_{\min} = 0.716$, $T_{\max} = 0.746$	3596 reflections with $I > 2\sigma(I)$
	$R_{\text{int}} = 0.028$

2.3. Refinement

$R[F^2 > 2\sigma(F^2)] = 0.034$	283 parameters
$wR(F^2) = 0.086$	All H-atom parameters refined
$S = 1.01$	$\Delta\rho_{\text{max}} = 0.35 \text{ e \AA}^{-3}$
4581 reflections	$\Delta\rho_{\text{min}} = -0.30 \text{ e \AA}^{-3}$

Table 1
Hydrogen-bond geometry (Å, °).

<i>D</i> –H··· <i>A</i>	<i>D</i> –H	H··· <i>A</i>	<i>D</i> ··· <i>A</i>	<i>D</i> –H··· <i>A</i>
C2–H1···N9 ⁱ	0.89 (2)	2.58 (2)	3.203 (2)	129 (2)

Symmetry code: (i) $x - 1, y, z$.

Data collection: APEX2 (Bruker, 2010); cell refinement: SAINT (Bruker, 2010); data reduction: SAINT; program(s) used to solve structure: SHELXS97 (Sheldrick 2008); program(s) used to refine structure: SHELXL2014 (Sheldrick, 2015); molecular graphics: PLATON (Spek, 2009); software used to prepare material for publication: SHELXL2014 and PLATON.

Acknowledgements

We thank Nadja Klippel for the synthesis of the title compound.

Supporting information for this paper is available from the IUCr electronic archives (Reference: SU5253).

References

- Biswas, D., Ding, F.-X., Dong, S., Gu, X., Jiang, J., Pasternak, A., Suzuki, T., Vacca, J. & Xu, S. (2015). PCT Int. Appl. WO2015103756 A1.
- Bruker (2010). *APEX2*, *SAINTE* and *SADABS*. Bruker AXS Inc., Madison, Wisconsin, USA.
- Kim, Y.-J., Lee, K.-E., Jeon, H.-T., Huh, H. S. & Lee, S. W. (2008). *Inorg. Chim. Acta*, **361**, 2159–2165.
- Pasternak, A., Dejesus, R. K., Zhu, Y., Yang, L., Walsh, S., Pio, B., Shahripour, A., Tang, H., Belyk, K. & Kim, D. (2012). PCT Int. Appl. WO 2012058134 A1.
- Sengupta, O. & Mukherjee, P. S. (2010). *Inorg. Chem.* **49**, 8583–8590.
- Sheldrick, G. M. (2008). *Acta Cryst.* **A64**, 112–122.
- Sheldrick, G. M. (2015). *Acta Cryst.* **C71**, 3–8.
- Spek, A. L. (2009). *Acta Cryst.* **D65**, 148–155.
- Stoessel, P., Heil, H., Jooseten, D., Pflumm, C., Gerhard, A. & Breuning, E. (2010). PCT Int. Appl. WO 2010086089 A1.
- Thomann, A., Börger, C., Empting, M. & Hartmann, R. W. (2014). *Synlett*, **25**, 935–938.
- Yu, L., Zhang, Z., Chen, X., Zhang, W., Wu, J., Cheng, Z., Zhu, J. & Zhu, X. (2008). *J. Polym. Sci. A Polym. Chem.* **46**, 682–691.

4 Concluding discussion and perspectives

4.1 Novel synthetic methods to access substituted pyrimidines

Pyrimidines are highly valuable heterocycles in medicinal chemistry as they frequently appear in FDA-approved drugs. Pyrimidines are hydrophilic but not protonated under physiological conditions, which makes them an ideal choice as a core scaffold for orally bioavailable drugs. Synthetic chemists in general, but medicinal chemists in particular, are usually interested to simplify synthetic methods, increase yield, and save time and money on the route to the final compound. However, in the field of pyrimidine chemistry, to the best of our knowledge, only traditional approaches towards introduction of substituents have been reported. These require disadvantageous prerequisites as discussed in chapter 1.6. Thus, one aim of the thesis was to develop a novel strategy to gain fast access towards substituted pyrimidines while circumventing the flaws of traditional pyrimidine chemistry. Inspired by the work on pyridine chemistry by Vera-Luc *et al.*,^[80] we tested whether a similar procedure (neat conditions, microwave) might be suitable for our pyrimidine scaffold (see Paper I and VIII). Indeed, as for pyridine, 1*H*-benzotriazole could be attached within minutes in quantitative yield without the need of solvent, catalyst, inert atmosphere conditions or strong bases. Motivated by these results, we tested the scope of these reaction conditions and, interestingly, substituted benzimidazoles and benzotriazoles could also be successfully linked to the pyrimidine core. By broadening the scope towards five-membered heterocycles we saw that almost all unsubstituted *N*-pentacycles could be attached by this methodology to pyrimidine as well. Regarding limitations, only pyrrol and indole fall out of the scope, as they do not react. To the best of our knowledge this is the only method to synthesize 4-tetrazolyl-2-(methylthio)pyrimidines directly (**1/20**^{*}), since several trials using the traditional approach which employs sodium azide, trimethyl orthoformate and an amino-substituted pyrimidine in acetic acid failed in our hands. This pentacycle is of high interest in medicinal chemistry, due to its metabolic stability, suitability as bioisoster for carboxylic acid, amides or esters (when substituted at N1 or N2) and of high hydrophilicity making compounds more soluble. In addition, as we were the first to synthesize 4-tetrazolyl-2-(thiomethyl)pyrimidines as precursor for dual inhibitor compounds, we were also interested in the chemistry

^{*}In the following chapters the compounds are numbered with two identifiers, separated by a slash: a roman number referring to the publication or chapter they were described in, followed by their identifier within the respective publication or chapter.

of tetrazoles to generate a compound library. Gaining synthetic access to the 6-position of pyrimidine, while keeping the tetrazole in 4-position was the major goal to be accomplished for rapid library generation. As we were the first to discover this particular scaffold as a bioactive entity, the challenge was to develop a new chemistry with the requirements of a medicinal chemistry environment (see chapter 2, paragraph II). Inspired by an unexpected quantitative conversion that occurred during the deprotection of a TMS-protected triazole (Figure 22), we hypothesized that we could use this information to generate a novel reactive intermediate granting access to the aforementioned class. This intermediate should be substituted with the azole of choice at the 4- and 6-position of 2-thiomethylpyrimidine and one of the pentacycle is then to be the leaving group for a nucleophile of interest. 2-(methylthio)-4,6-di(1*H*-tetrazol-1-yl)pyrimidine (**III/1**) is the mentioned intermediate which can be achieved in high yields in minutes under microwave irradiation (Paper III). To clarify the regiochemistry of the attached tetrazole moieties, which cannot be univocally elucidated by NMR, we crystallized the compound and derived an X-ray crystal structure. As for the unexpected conversion mentioned above, the tetrazole substituent can be replaced in a microwave reaction by a broad scope of substrates covering thio-, amino- and hydroxyl nucleophiles as well as *N*-pentacycles. To investigate the robustness of the approach and with regard to the fact that **III/1** can be obtained in high yield, we investigated if the reaction is applicable for a one-pot setup as well. Indeed, all tested substrates reacted smoothly in a one-pot reaction *via in situ* generated **III/1** within 20 minutes.

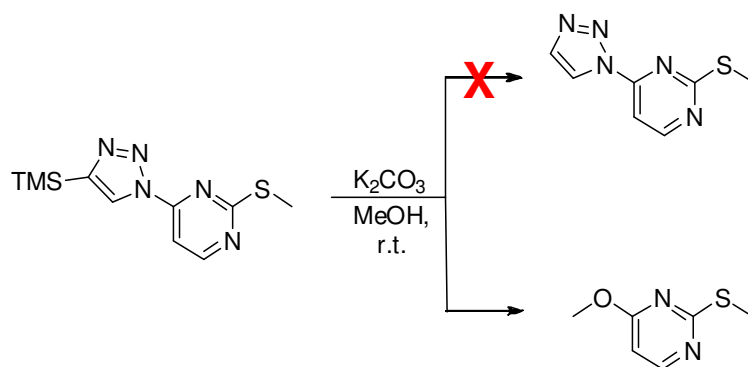


Figure 22. Deprotection of the TMS-protected triazole moiety in 4-position of 2-thiomethylpyrimidine did not yield the unprotected compound but yielded 4-methoxy-2-thiomethylpyrimidine in quantitative yield.

4 Concluding discussion and perspectives

In summary, two novel approaches were developed enabling fast and efficient synthesis of substituted pyrimidines. Furthermore, the methodology seems to be suitable for combinatorial chemistry approaches. In the future, this novel synthetic route might speed up drug discovery efforts focused on pyrimidine scaffolds but could also inspire synthetic chemists to transfer these findings to other heterocycles.

4.2 Two approaches - one goal: fighting treatment-resistant bacterial infections of the respiratory tract

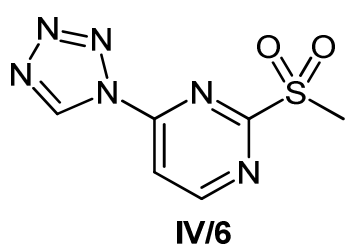
The respiratory tract diseases cystic fibrosis and tuberculosis have many things in common: both illnesses are caused by bacteria, long term hospitalization is often required, resistance development hinders or makes treatment ineffective and dormant or persisting pathogens are hard to eradicate with common antibiotics. Thus, in this thesis two different approaches were pursued to address the latter mentioned problems. For PA, the pathogen involved in cystic fibrosis-associated pulmonary infection, a novel strategy was investigated trying to circumvent resistance development by interference with the non-vital QS machinery to lower pathogenicity (see chapter 4.2.1). Such agents may help to establish a new paradigm in anti-infective treatment of cystic fibrosis patients and could lead to first “pathogenicity-blockers” with lowered resistance development. In case of Mtb, the major pathogen causing tuberculosis, a classical antibiotic drug discovery campaign was initiated by addressing two novel potential drug targets. Ideally, the developed compounds should not show any cross resistance to any other anti-mycobacterial drug. Thus, the identified compounds could serve as starting point for the development of new anti-mycobacterial drug candidates to broaden the portfolio of anti-tuberculosis treatment options (see chapter 4.2.2).

4.2.1 Addressing PqsD and PqsR to reduce pathogenicity of *Pseudomonas aeruginosa*

Disruption of virulence-associated targets has proven to be a valuable approach towards the reduction of pathogenicity of PA. Pioneering work in this field which was conducted in previous studies on PqsD and PqsR, dealt with compounds that were either of limited drug-likeness due to high lipophilicity resulting in low solubility or of

4 Concluding discussion and perspectives

limited cellular efficiency.^[46,50,52] Thus, the development of hydrophilic, drug-like compounds with the capability to pass the Gram-negative cell envelope to effect virulence factors without impairing growth is a formidable challenge. Nevertheless, the use of aforementioned inhibitors of PqsD and antagonists of PqsR led us to a novel polypharmacological concept. By a combination of both compounds we could increase the beneficial outcome regarding virulence factor production with respect to the effect of the single agent alone. These conceptual studies on dual inhibition of auto-loop regulated systems paved the way for the development of dual active inhibitors. In the compound class of 2-sulfonylpyrimidines, we identified a common scaffold for the inhibition of PqsD and antagonism on PqsR. Reduction to the essential common structural features necessary for activity, lead to the discovery of the first reported dual PqsD/PqsR inhibitor **IV/5**. The discovered hit compound was then further modified with a strong focus on hydrophilicity. The latter was exclusively addressed by the use of a Ligand Lipophilicity Efficiency score as a guidepost for drug design. This led us to the design of **IV/6** (Figure 23) which was also active on both targets but of higher lipophilic efficiency and solubility than its parent compound **IV/5**. As it is of tremendous importance in drug discovery to validate a compound as early as possible in the optimization process, we challenged the inhibitor against cultures of PA in planktonic and biofilm state. As the compound showed promising activity against two major virulence factors, pyocyanin and pyoverdine, without impairing PA growth, we extended our studies on biofilm formation. The positive outcome on biofilm formation aroused our interest to investigate in depth how **IV/6** interferes with the biofilm architecture. In these studies, besides reduction of polysaccharide and protein content of the biofilm, we observed a prominent decrease of extracellular DNA (eDNA) release. The eDNA of PA is one of the major determinants for antibiotic tolerance as well as resistance to host defensive peptides like LL-37 in the biofilm.^[27] Thus, we were motivated to see if the reduction of eDNA might partly or fully restore the efficacy of an antibiotic against biofilm-encapsulated



IC_{50} PqsD = 21 μ M (LLE = 0.67)
 IC_{50} PqsR = 15 μ M (LLE = 0.66)
 $cLogD_{7.4}$ = -1.16
MW = 226.21 g/mol
Solubility = 1000 μ M

Figure 23. Physicochemically improved hit **IV/6** with dual activity on PqsD and PqsR

4 Concluding discussion and perspectives

PA. Indeed, compound **IV/6** reduced PA's ability to tolerate Ciprofloxacin treatment and could restore its antibacterial activity in a combination experiment. As *in vitro* results were promising we wanted to validate the compound in an *in vivo* model to have the most promising starting point for drug optimization. Thus, we decided to challenge the compound in our established infection model employing *Galleria mellonella* larvae. In these trials, administration of 1.25 nmol (= 0.63 mg/kg) of **IV/6** granted the survival of larvae and protected about 60% of the population against PA infection. In summary, the *in vivo* validation, the compounds low molecular weight and convincing physicochemical properties rendered this inhibitor an ideal hit for optimization. To improve target affinities, we identified three positions for possible prolongation of the molecule, which were easily accessible *via* our novel synthetic methodology (see Paper I and III, Figure 24). Exchanging the tetrazole substituent at position R² by different six-membered, five-membered or bicyclic aromatic systems led to an impairment of activity on both targets, rendering 1*N*-tetrazole and 1*N*-1,2,3-triazole the group of choice from the investigated subset. Next, we explored whether we could gain higher activity by growing from the 4-position of the 1,2,3-triazolyl moiety at R². The enlargement of the western part (R²) of the molecule resulted in higher activity on PqsD and elevated antagonism on PqsR. However, a major drawback was the strongly reduced solubility of such compounds and the strong drop of the LLE score. As physicochemical properties and a rational metrical guidance is of great importance to keep focus on developing drug-like molecules, we defined this particular position as unsuitable for further optimizations. Introduction of different substituents at R³ (e.g., *N*-aminomethyl, *N*-acetamide, phenoxy) yielded only compounds of either reduced activity or undesirable ligand efficiency. Thus, by probing R³, we recognized that the common pharmacophore for dual inhibition is much narrower than we initially thought. Hence, we used computational methods in a

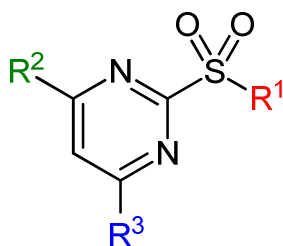
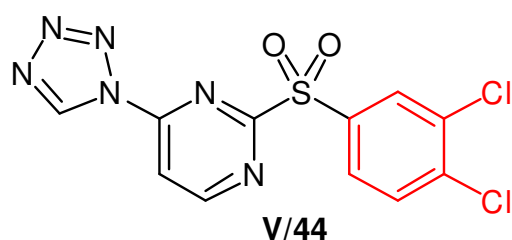


Figure 24. The development of novel synthetic methods enabled the generation of substituted pyrimidines at R¹, R² and R³ by a robust route to generate a library of dual active inhibitors for deriving SAR information.

4 Concluding discussion and perspectives

ligand-based approach and conducted a flexible alignment of our initial hit **IV/5** and the natural ligand of PqsR (HHQ) as well as a described substrate of PqsD (β -decanoic acid, see Paper V). These studies drew our attention to R¹ which might be suitable for the introduction of alkyl chains. The alkyl substituted compounds were of increased activity on PqsD which could be correlated with the chain length introduced using a Hansch approach. However, the most effective compound **V/34** (hexyl chain) was of slightly reduced activity on PqsR ($IC_{50} \sim 50\mu M$). In light of these new results, we tested whether PqsR and PqsD could accommodate other substituents at R¹. A phenyl substituent increased activity on PqsD and was tolerated by PqsR. Hence, we conducted a Topliss derivatization of the phenyl ring.^[81] It turned out, that the Hammett constant of introduced groups at the phenyl ring strongly correlated with the biological activity on PqsD. A Hansch analysis, suggesting the introduction of stronger electron-withdrawing groups, led to the discovery of an improved hit with higher potency on PqsD (**V/44**). This compound possesses very good ligand efficiency indices and, additionally, its activity on PqsR was not impaired compared to the initial hit **IV/6** (see chapter V and Figure 25). As one of the desired features of the inhibitor class within this work was increased susceptibility against Ciprofloxacin and reduced biofilm volume we tested if dual active compounds **V/44** and **V/34** were able to interfere with these resistance determinants. Indeed, both compounds reduced biofilm formation and, in good accordance with the initial hit **IV/6**, also inhibited eDNA release into the biofilm matrix.

As PqsD is a validated anti-biofilm target, we were interested if we could generate new starting points for fragment-based inhibitor design with desirable properties (low molecular weight, high solubility, high Ligand Efficiencies). From our studies on the tetrazole-azido equilibrium at 4-azidopyrimidines (Paper II), we gained access to stabilized tetrazolo[1,5-*c*]pyrimidines that share a high degree of similarity towards adenine (Figure 26). This moiety is a reappearing motif in many natural compounds



IC_{50} PqsD = 0.4 μM (LLE = 0.41)
 IC_{50} PqsR = 24 μM (LLE = 0.30)
 $cLogD_{7.4}$ = 1.67
MW = 357.2 g/mol
Solubility = 100-200 μM

Figure 25. Ligand-based design guided by LLE & QSAR led to the discovery of a dual inhibitor compound (**V/44**) with increased activity on PqsD.

4 Concluding discussion and perspectives

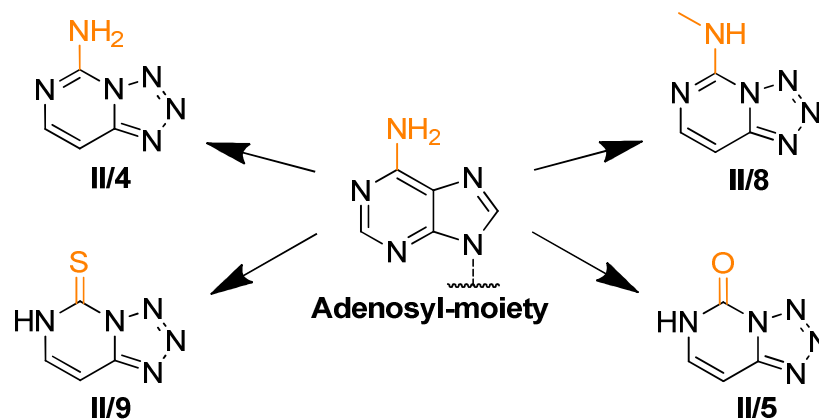


Figure 26. Comparison of stabilized tetrazolo[1,5-*c*]pyrimidines with the naturally occurring adenosyl motif.

also being part of PqsD's substrates (malonyl and anthraniloyl-coenzyme A). Thus, by simple comparison of adenine with tetrazolo[1,5-*c*]pyrimidines, we hypothesized that these compounds might inhibit the enzyme reaction. Interestingly, thionyl derivative **II/9** and carbonyl derivative **II/5** showed prominent inhibition of PqsD in the low micromolar range. In terms of efficiency these compounds represent excellent starting points for future fragment-linking or -growing approaches. These improved hits could then pave the way towards our long term goal: developing novel drug-like anti-virulence agents with the perspective to improve treatment of PA infections.

In summary, we could successfully apply a concept study towards the design of dual target inhibitors, which were further improved regarding activity on PqsD leading to biofilm-active agents with preferable physicochemical properties. In depth analysis of the azido-tetrazole equilibrium was used to identify fragments suitable for FBDD in the future.

4.2.2 The cytochrome P450 enzymes 121 and 125 as novel drug targets for the treatment of mycobacterial infections

Identification of a suitable and validated drug target is the primary goal before any drug discovery can be conducted. For an antibiotic drug target a few hallmarks need to be fulfilled. For example, the function needs to be essential for bacterial growth and the target must not have an identical copy in mammals. For CYP121 and CYP125 the first aspect was shown in *in vitro* and *in vivo* experiments.^[71,76] The second requirement can be checked by a protein blast search of the mycobacterial protein sequences *versus* the human proteome. For CYP121, the most homologous

4 Concluding discussion and perspectives

protein was CYP17 with an overall amino acid identity of 29% and a homology of 44%. Regarding CYP125, the blast search delivered CYP2R1 to be the most identical protein found in humans with an amino acid identity of 24% and an overall homology of 41%. These pre-conditions render CYP121 and CYP125 ideal target candidates for anti-mycobacterial drug discovery regarding selectivity towards human CYP enzymes, which is important for circumventing potential toxic side effects.

Finding a hit structure for a drug target can be achieved by different approaches: randomly, by screening a library of millions of lead-like compounds, hundreds of fragments or by more rational approaches. As shown by our group for PqsD, a general trend regarding the screening method used is: the more information about a target is available (e.g., X-ray structures, substrates, known inhibitors) the higher the chances are to increase hit rates.^[53] Driven by this rationale, we made use of inhibitors especially designed to interfere with the function of CYP P450 enzymes to build a privileged library for the discovery of drug-like compounds targeting CYP121 and CYP125. This library was of small size (< 150 compounds) but covered a chemical space of six different scaffolds. In detail, these compounds were developed to target human CYP enzymes from the human steroidogenic pathway, namely CYP11B1/B2 (11 β -hydroxylases),^[82] CYP17 (steroid-17 α -hydroxylase) and CYP19 (aromatase).^[83] As the primary screening technology we used surface plasmon resonance spectroscopy (SPR) which allowed us to identify first binders in an automated medium throughput fashion. Fortunately, a common binder, the antifungal drug Econazole, was already known to bind to the hemes of CYP121 and CYP125 and was able to inhibit growth of mycobacteria.^[69,79] Thus, the compound served as positive control in all subsequent assays. In the SPR screening, Econazole's response (R_{pos}) was chosen as reference to evaluate the hits. Therefore, we introduced a metric which is the quotient of the response of the hit (R) divided by the response of Econazole (R_{pos}). Every compound which had at least a $R/R_{\text{pos}} \geq 0.5$ was regarded as a hit and hence subject to further investigation in the UV-VIS heme binding assay. For CYP121 we had a hit rate of 33% while for CYP125 17% of the library compounds were binders regarding the aforementioned score. The compounds were further evaluated by their ability to bind to the iron(II) center of the heme of respective enzymes. For this reason, we chose photometric UV-VIS analysis as an assay to address this question. The basis for this experiment is the fact that upon binding to the heme – either by direct coordination to iron center or indirectly by

4 Concluding discussion and perspectives

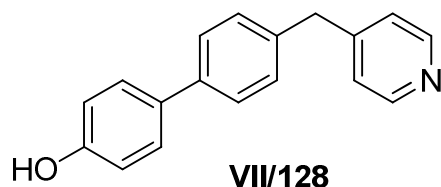


Figure 27. Chemical structure of CYP125/142 dual inhibitor **VII/128** which was the most promising hit derived from the screening campaign against CYP125 as potential anti-mycobacterial agent.

forming an H-bond to the labile aqua-ligand, a test compound changes the UV-VIS spectrum of the CYP enzyme (Chapter 1.8). This phenomenon was used to derive dissociation constant of binders (K_D) and to differ between the two possible heme binding types (Chapter 1.8). For CYP121 we found eleven compounds with a K_D below 10 μM all of which showed a type II binding profile. 14 compounds had an affinity to CYP125 below 30 μM including six type I and eight type II binders. The most potent compound, **VII/128**, had already an affinity in the low nanomolar range ($K_D = 0.085 \mu\text{M}$, Figure 27). Notably, this compound was also active on CYP142, a bypass enzyme for the CYP125 reaction reported in the laboratory strain Mtb H37Rv,^[84] with a K_D of 0.008 μM . Although this enzyme was only found in the laboratory strain Mtb H₃₇Rv to date, this finding might give a hint how future resistance could develop. In this respect, a dual inhibitor of CYP125 and CYP142 might be superior over single target compounds. These compounds are somehow also related to quorum sensing inhibitors, as they are not lethal for the bacterium *per se*, but become active as soon as the bacterium enters the host.

Regarding CYP121, the best binders were further evaluated for their potential to inhibit mycobacterial cell growth. Three of the eleven compounds showed an anti-mycobacterial activity against a bovine strain which was below 10 $\mu\text{g/mL}$. To validate the compound for the human pathogen Mtb, we conducted an additional growth inhibition assay employing this pathogen. From the three compounds, one compound (**VI/I:47**, Figure 28) inhibited bacterial growth with a MIC_{90} of 0.3 $\mu\text{g/mL}$ which is in

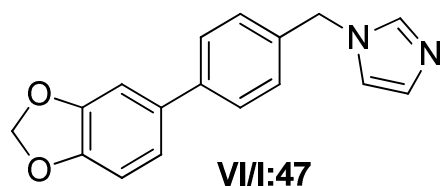


Figure 28. Chemical structure of CYP121 inhibitor **VI/I:47** which was the most promising hit regarding its anti-mycobacterial effect ($\text{MIC}_{90} = 0.3 \mu\text{g/mL}$) against the human pathogen Mtb.

the same range as the first line drug ethambutol (0.4 $\mu\text{g}/\text{mL}$).^[85] Interestingly, **VI/I:47** was almost inactive on CYP17, the human enzyme for which it was originally synthesized.^[86] However, for further biological profiling, we tested the compound in a HEK cell assay to evaluate its toxicity on human cells. **VI/I:47** was almost 20 times less toxic to human than to mycobacterial cells underlining the great potential for drug development. Thus, we conducted docking experiments to the crystal structure of CYP121 and retrieved a binding pose suggesting hot spots for further structure modifications (Paper VI). In the future, for the identified CYP121 inhibitor **VI/I:47**, evaluation of the compound in macrophage infection models and *in vivo* profiling in a mouse model are planned. Furthermore, as the crystallization conditions for CYP121 are reported, a prospective co-crystal structure of the enzyme and **VI/I:47** is plausible which could serve as the basis for the structure-guided design towards a more potent anti-mycobacterial compound. Regarding the potential of the identified CYP125 inhibitors, a cellular proof of their efficacy has to be provided. Therefore, regarding the mode of action and the mechanism of CYP125, a macrophage infection model needs to be established to reliably simulate the *in vivo* scenario. However, although the identified compounds show already lead-like activities on the target, further structure modifications need to be carried out to circumvent selectivity issues with their originally intended human targets but which is highly probable based on our initial *in silico* selectivity screen using a protein blast search (*vide supra*).

5 References

- [1] M. Leewenhoek, R. de Graaf, *Philos. Trans. R. Soc. London* **1673**, *8*, 6037–6038.
- [2] R. Koch, *Beiträge zur Biologie der Pflanzen* **1876**, *2*, 277–310.
- [3] a) J. F. Acar, S. Francoual, *J. Antimicrob. Chemother.* **1990**, *26 Suppl B*, 207–213; b) K. Julian, K. Kosowska-Shick, C. Whitener, M. Roos, H. Labischinski, A. Rubio, L. Parent, L. Ednie, L. Koeth, T. Bogdanovich et al., *Antimicrob. Agents Chemother.* **2007**, *51*, 3445–3448; c) B. Li, S. Wendlandt, J. Yao, Y. Liu, Q. Zhang, Z. Shi, J. Wei, D. Shao, S. Schwarz, S. Wang et al., *J. Antimicrob. Chemother.* **2013**, *68*, 1251–1255; d) A. E. Clatworthy, E. Pierson, D. T. Hung, *Nat. Chem. Biol.* **2007**, *3*, 541–548.
- [4] G. Klebe, *Wirkstoffdesign. Entwurf und Wirkung von Arzneistoffen*, Spektrum Akademischer Verlag, Heidelberg, **2009**.
- [5] C. G. Wermuth, C. R. Ganellin, P. Lindberg, L. A. Mitscher, *Pure Appl. Chem.* **1998**, *70*.
- [6] *Molecular Operating Environment (Version 2013.08)*, Chemical Computing Group Inc., 1010 Sherbooke St. West, Suite #910, Montreal, QC, Canada, H3A 2R7, **2015**.
- [7] E. Mutschler, *Arzneimittelwirkungen. Lehrbuch der Pharmakologie und Toxikologie : mit einführenden Kapiteln in die Anatomie, Physiologie und Pathophysiologie*, Wiss. Verl.-Ges., Stuttgart, **2008**.
- [8] M. J. Nieto, F. L. Alovero, R. H. Manzo, M. R. Mazzieri, *Eur. J. Med. Chem.* **2005**, *40*, 361–369.
- [9] C. Hansch, P. P. Maloney, T. Fujita, R. M. Muir, *Nature* **1962**, *194*, 178–180.
- [10] a) R. D. Cramer, D. E. Patterson, J. D. Bunce, *J. Am. Chem. Soc.* **1988**, *110*, 5959–5967; b) H. Kubinyi, *Handbook of Chemoinformatics: From Data to Knowledge in 4 Volumes* **2008**, 1555–1574.
- [11] a) N. Roberts, J. Martin, D. Kinchington, A. Broadhurst, J. Craig, I. Duncan, S. Galpin, B. Handa, J. Kay, A. Krohn et al., *Science* **1990**, *248*, 358–361; b) J. Erickson, D. Neidhart, J. VanDrie, D. Kempf, X. Wang, D. Norbeck, J. Plattner, J. Rittenhouse, M. Turon, N. Wideburg et al., *Science* **1990**, *249*, 527–533.
- [12] a) K. Wüthrich, *J. Biol. Chem.* **1990**, *265*, 22059–22062; b) W. Kühlbrandt, *Methods Mol. Biol.* **2013**, *955*, 1–16.
- [13] V. K. Vyas, R. D. Ukawala, M. Ghate, C. Chinthra, *Indian J. Pharm. Sci.* **2012**, *74*, 1–17.
- [14] D. B. Kitchen, H. Decornez, J. R. Furr, J. Bajorath, *Nat. Rev. Drug Discov.* **2004**, *3*, 935–949.
- [15] S. J. Teague, *Nat. Rev. Drug Discov.* **2003**, *2*, 527–541.
- [16] J. D. Durrant, J. A. McCammon, *BMC biology* **2011**, *9*, 71.
- [17] P. J. Hajduk, J. Greer, *Nat. Rev. Drug Discov.* **2007**, *6*, 211–219.
- [18] S. A. Hudson, K. J. McLean, S. Surade, Y.-Q. Yang, D. Leys, A. Ciulli, A. W. Munro, C. Abell, *Angew. Chem. Int. Ed.* **2012**, *51*, 9311–9316.
- [19] S. A. Hudson, S. Surade, A. G. Coyne, K. J. McLean, D. Leys, A. W. Munro, C. Abell, *ChemMedChem* **2013**, *8*, 1451–1456.
- [20] C. W. Murray, M. L. Verdonk, *J. Comput. Aided Mol. Des.* **2002**, *16*, 741–753.
- [21] D. C. Rees, M. Congreve, C. W. Murray, R. Carr, *Nat. Rev. Drug Discov.* **2004**, *3*, 660–672.
- [22] S. L. Gellatly, Hancock, Robert E W, *Pathog. Dis.* **2013**, *67*, 159–173.

- [23] D. Asboe, V. Gant, H. M. Aucken, D. A. Moore, S. Umasankar, J. S. Bingham, M. E. Kaufmann, T. L. Pitt, *AIDS* **1998**, *12*, 1771–1775.
- [24] A. D. Valderrey, M. J. Pozuelo, P. A. Jiménez, M. D. Maciá, A. Oliver, R. Rotger, *Diagn. Microbiol. Infect. Dis.* **2010**, *68*, 20–27.
- [25] M. Bard, L.-J. Couderc, A. G. Saimot, A. Scherrer, I. Frachon, F. Seigneur, I. Caubarrere, *Eur. Respir. J.* **1998**, *11*, 771–775.
- [26] M. C. Bruce, L. Poncz, J. D. Klinger, R. C. Stern, J. F. Tomashefski, D. G. Dearborn, *Am. Rev. Respir. Dis.* **1985**, *132*, 529–535.
- [27] S. Lewenza, *Front. Microbiol.* **2013**, *4*, 21.
- [28] B. Rada, T. L. Leto, *Immunol. Res.* **2009**, *43*, 198–209.
- [29] B. Rada, P. Gardina, T. G. Myers, T. L. Leto, *Mucosal Immunol.* **2011**, *4*, 158–171.
- [30] Y.-A. Que, R. Hazan, B. Strobel, D. Maura, J. He, M. Kesarwani, P. Panopoulos, A. Tsurumi, M. Giddey, J. Wilhelmy et al., *PloS one* **2013**, *8*, e80140.
- [31] J. Lee, L. Zhang, *Protein Cell* **2015**, *6*, 26–41.
- [32] J. E. González, N. D. Keshavan, *Microbiol. Mol. Biol. Rev.* **2006**, *70*, 859–875.
- [33] T. Bjarnsholt, M. Givskov, *Curr. Infect. Dis. Rep.* **2008**, *10*, 22–28.
- [34] S. B. Tay, W. S. Yew, *Int. J. Mol. Sci.* **2013**, *14*, 16570–16599.
- [35] S. P. Diggle, P. Lumjiaktase, F. Dipilato, K. Winzer, M. Kunakorn, D. A. Barrett, S. R. Chhabra, M. Cámara, P. Williams, *Chem. Biol.* **2006**, *13*, 701–710.
- [36] a) J. P. Gerdt, H. E. Blackwell, *ACS Chem. Biol.* **2014**, *9*, 2291–2299; b) L. A. Gallagher, S. L. McKnight, M. S. Kuznetsova, E. C. Pesci, C. Manoil, *J. Bacteriol.* **2002**, *184*, 6472–6480.
- [37] C. E. Dulcey, V. Dekimpe, D.-A. Fauvelle, S. Milot, M.-C. Groleau, N. Doucet, L. G. Rahme, F. Lépine, E. Déziel, *Chem. Biol.* **2013**, *20*, 1481–1491.
- [38] S. L. Drees, S. Fetzner, *Chem. Biol.* **2015**, *22*, 611–618.
- [39] a) Hooi, Doreen S W, B. W. Bycroft, S. R. Chhabra, P. Williams, D. I. Pritchard, *Infect. Immun.* **2004**, *72*, 6463–6470; b) M. E. Skindersoe, L. H. Zeuthen, S. Brix, L. N. Fink, J. Lazenby, C. Whittall, P. Williams, S. P. Diggle, H. Froekiaer, M. Cooley et al., *FEMS Immunol. Med. Microbiol.* **2009**, *55*, 335–345; c) K. Kim, Y. U. Kim, B. H. Koh, S. S. Hwang, S.-H. Kim, F. Lépine, Y.-H. Cho, G. R. Lee, *Immunology* **2010**, *129*, 578–588; d) C. Legendre, F. J. Reen, M. J. Mooij, G. P. McGlacken, C. Adams, F. O'Gara, *Infect. Immun.* **2012**, *80*, 3985–3992; e) S. P. Diggle, K. Winzer, S. R. Chhabra, K. E. Worrall, M. Cámara, P. Williams, *Mol. Microbiol.* **2003**, *50*, 29–43.
- [40] Y.-M. Zhang, M. W. Frank, K. Zhu, A. Mayasundari, C. O. Rock, *J. Biol. Chem.* **2008**, *283*, 28788–28794.
- [41] M. P. Storz, C. K. Maurer, C. Zimmer, N. Wagner, C. Brengel, de Jong, Johannes C, S. Lucas, M. Müsken, S. Häussler, A. Steinbach et al., *J. Am. Chem. Soc.* **2012**, *134*, 16143–16146.
- [42] M. P. Storz, G. Allegretta, B. Kirsch, M. Empting, R. W. Hartmann, *Org. Biomol. Chem.* **2014**, *12*, 6094–6104.
- [43] G. Allegretta, E. Weidel, M. Empting, R. W. Hartmann, *Eur. J. Med. Chem.* **2015**, *90*, 351–359.
- [44] a) C. A. Lipinski, F. Lombardo, B. W. Dominy, P. J. Feeney, *Adv. Drug Deliv. Rev.* **2001**, *46*, 3–26; b) R. O'Shea, H. E. Moser, *J. Med. Chem.* **2008**, *51*, 2871–2878.

5 References

- [45] E. Déziel, S. Gopalan, A. P. Tampakaki, F. Lépine, K. E. Padfield, M. Saucier, G. Xiao, L. G. Rahme, *Mol. Microbiol.* **2005**, *55*, 998–1014.
- [46] C. Lu, B. Kirsch, C. Zimmer, de Jong, Johannes C, C. Henn, C. K. Maurer, M. Müsken, S. Häussler, A. Steinbach, R. W. Hartmann, *Chem. Biol.* **2012**, *19*, 381–390.
- [47] A. Ilangovan, M. Fletcher, G. Rampioni, C. Pustelny, K. Rumbaugh, S. Heeb, M. Cámara, A. Truman, S. R. Chhabra, J. Emsley et al., *PLoS pathog.* **2013**, *9*, e1003508.
- [48] a) M. Starkey, F. Lepine, D. Maura, A. Bandyopadhaya, B. Lesic, J. He, T. Kitao, V. Righi, S. Milot, A. Tzika et al., *PLoS pathog.* **2014**, *10*, e1004321; b) T. Klein, C. Henn, de Jong, Johannes C, C. Zimmer, B. Kirsch, C. K. Maurer, D. Pistorius, R. Müller, A. Steinbach, R. W. Hartmann, *ACS Chem. Biol.* **2012**, *7*, 1496–1501; c) J. H. Sahner, C. Brengel, M. P. Storz, M. Groh, A. Plaza, R. Müller, R. W. Hartmann, *J. Med. Chem.* **2013**, *56*, 8656–8664; d) E. Weidel, de Jong, Johannes C, C. Brengel, M. P. Storz, A. Braunshausen, M. Negri, A. Plaza, A. Steinbach, R. Müller, R. W. Hartmann, *J. Med. Chem.* **2013**, *56*, 6146–6155.
- [49] M. Zender, T. Klein, C. Henn, B. Kirsch, C. K. Maurer, D. Kail, C. Ritter, O. Dolezal, A. Steinbach, R. W. Hartmann, *J. Med. Chem.* **2013**, *56*, 6761–6774.
- [50] J. H. Sahner, M. Empting, A. Kamal, E. Weidel, M. Groh, C. Börger, R. W. Hartmann, *Eur. J. Med. Chem.* **2015**, *96*, 14–21.
- [51] C. Lu, C. K. Maurer, B. Kirsch, A. Steinbach, R. W. Hartmann, *Angew. Chem. Int. Ed.* **2014**, *126*, 1127–1130.
- [52] S. Hinsberger, de Jong, Johannes C, M. Groh, J. Haupenthal, R. W. Hartmann, *Eur. J. Med. Chem.* **2014**, *76*, 343–351.
- [53] E. Weidel, M. Negri, M. Empting, S. Hinsberger, R. W. Hartmann, *Future Med. Chem.* **2014**, *6*, 2057–2072.
- [54] a) R. C. Hunter, V. Klepac-Ceraj, M. M. Lorenzi, H. Grotzinger, T. R. Martin, D. K. Newman, *Am. J. Resp. Cell Mol. Biol.* **2012**, *47*, 738–745; b) C. C. Caldwell, Y. Chen, H. S. Goetzmann, Y. Hao, M. T. Borchers, D. J. Hassett, L. R. Young, D. Mavrodi, L. Thomashow, G. W. Lau, *Am. J. Pathol.* **2009**, *175*, 2473–2488; c) E. Mowat, S. Paterson, J. L. Fothergill, E. A. Wright, M. J. Ledson, M. J. Walshaw, M. A. Brockhurst, C. Winstanley, *Am. J. Respir. Crit. Care Med.* **2011**, *183*, 1674–1679; d) B. Rada, T. L. Leto, *Trends Microbiol.* **2013**, *21*, 73–81.
- [55] World Health Organization, *Global tuberculosis report 2015*, World Health Organization, [S.I.], **2015**.
- [56] M. Gengenbacher, Kaufmann, Stefan H E, *FEMS Microbiol. Rev.* **2012**, *36*, 514–532.
- [57] J. D. Ernst, *Nat. Rev. Immunol.* **2012**, *12*, 581–591.
- [58] van den Boogaard, Jossy, G. S. Kibiki, E. R. Kisanga, M. J. Boeree, R. E. Aarnoutse, *Antimicrob. Agents Chemother.* **2009**, *53*, 849–862.
- [59] N. Kapoor, S. Pawar, T. D. Sirakova, C. Deb, W. L. Warren, P. E. Kolattukudy, *PloS one* **2013**, *8*, e53657.
- [60] WHO, *Multidrug-resistant tuberculosis (MDR-TB) 2013 Update* **2013**.
- [61] P.B. Danielson, Bentham Science Publisher, *Curr. Drug Metab.* **2002**, *3*, 561–597.
- [62] J. H. Dawson, M. Sono, *Chem. Rev.* **1987**, *87*, 1255–1276.

- [63] a) A. Haddad, M. Davis, R. Lagman, *Support. Care Cancer* **2007**, *15*, 251–257; b) M. Bureik, M. Lisurek, R. Bernhardt, *Biol. Chem.* **2002**, *383*, 1537–1551.
- [64] M. J. Coon, *Annu. Rev. Pharmacool. Toxicol.* **2005**, *45*, 1–25.
- [65] D. Werck-Reichhart, R. Feyereisen, *Genome Biol.* **2000**, *1*, REVIEWS3003.
- [66] S. A. Hudson, K. J. McLean, A. W. Munro, C. Abell, *Biochem. Soc. T.* **2012**, *40*, 573–579.
- [67] A. Luthra, I. G. Denisov, S. G. Sligar, *Arch. Biochem. Biophys.* **2011**, *507*, 26–35.
- [68] P. Belin, Le Du, Marie H el ene, A. Fielding, O. Lequin, M. Jacquet, J.-B. Charbonnier, A. Lecoq, R. Thai, M. Cour on, C. Masson et al., *Proc. Natl. Acad. Sci. U. S. A.* **2009**, *106*, 7426–7431.
- [69] K. J. McLean, K. R. Marshall, A. Richmond, I. S. Hunter, K. Fowler, T. Kieser, S. S. Gurcha, G. S. Besra, A. W. Munro, *Microbiol.* **2002**, *148*, 2937–2949.
- [70] L. M. Podust, T. L. Poulos, M. R. Waterman, *Proc. Natl. Acad. Sci. U. S. A.* **2001**, *98*, 3068–3073.
- [71] K. J. McLean, P. Carroll, D. G. Lewis, A. J. Dunford, H. E. Seward, R. Neeli, M. R. Cheesman, L. Marsollier, P. Douglas, W. E. Smith et al., *J. Biol. Chem.* **2008**, *283*, 33406–33416.
- [72] C. M. Sasseti, D. H. Boyd, E. J. Rubin, *Mol. Microbiol.* **2003**, *48*, 77–84.
- [73] J. K. Capyk, R. Kalscheuer, G. R. Stewart, J. Liu, H. Kwon, R. Zhao, S. Okamoto, W. R. Jacobs, L. D. Eltis, W. W. Mohn, *J. Biol. Chem.* **2009**, *284*, 35534–35542.
- [74] X. Yang, J. Gao, I. Smith, E. Dubnau, N. S. Sampson, *J. Bacteriol.* **2011**, *193*, 1473–1476.
- [75] H. Ouellet, J. B. Johnston, de Montellano, Paul R Ortiz, *Trends Microbiol.* **2011**, *19*, 530–539.
- [76] S. L. Kendall, Rison, Stuart C G, F. Movahedzadeh, R. Frita, N. G. Stoker, *Trends Microbiol.* **2004**, *12*, 537–544.
- [77] P. Belin, A. Lecoq, M.-H. Beaurepaire Ledu, M. Gondry, J.-L. Pernodet, *Patent EP2088143A1* **2009**.
- [78] H. Ouellet, P. M. Kells, Ortiz de Montellano, Paul R, L. M. Podust, *Bioorg. Med. Chem. Lett.* **2011**, *21*, 332–337.
- [79] K. J. McLean, P. Lafite, C. Levy, M. R. Cheesman, N. Mast, I. A. Pikuleva, D. Leys, A. W. Munro, *J. Biol. Chem.* **2009**, *284*, 35524–35533.
- [80] P. Vera-Luque, R. Alajar n, J. Alvarez-Builla, J. J. Vaquero, *Org. Lett.* **2006**, *8*, 415–418.
- [81] J. G. Topliss, *J. Med. Chem.* **1972**, *15*, 1006–1011.
- [82] L. Schiffer, S. Anderko, F. Hannemann, A. Eiden-Plach, R. Bernhardt, *J. Steroid Biochem. Mol. Biol.* **2015**, *151*, 38–51.
- [83] M. Akhtar, J. N. Wright, P. Lee-Robichaud, *J. Steroid Biochem. Mol. Biol.* **2011**, *125*, 2–12.
- [84] M. D. Driscoll, K. J. McLean, C. Levy, N. Mast, I. A. Pikuleva, P. Lafite, Rigby, Stephen E J, D. Leys, A. W. Munro, *J. Biol. Chem.* **2010**, *285*, 38270–38282.
- [85] L. B. Heifets, M. D. Iseman, P. J. Lindholm-Levy, *Antimicrob. Agents Chemother.* **1986**, *30*, 927–932.
- [86] B. G. Wachall, M. Hector, Y. Zhuang, R. W. Hartmann, *Bioorg. Med. Chem.* **1999**, *7*, 1913–1924.

6 Supporting information

6.1 Supporting information for Publication I

Supporting Information

Microwave assisted synthesis of 4-substituted 2-methylthiopyrimidines

Andreas Thomann^a, Carsten Börger^b, Martin Empting^a and Rolf W. Hartmann^{a,c,*}

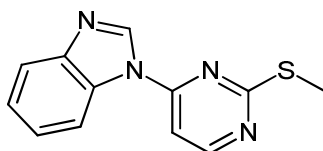
^aHelmholtz-Institute for Pharmaceutical Research Saarland, Saarland University, Campus C2.3, D-66123 Saarbrücken, Germany

^bPharmBioTec GmbH, Saarland University, Science Park 1, D-66123 Saarbrücken, Germany

^cPharmaceutical and Medicinal Chemistry, Saarland University, Campus C2.3, D-66123 Saarbrücken, Germany

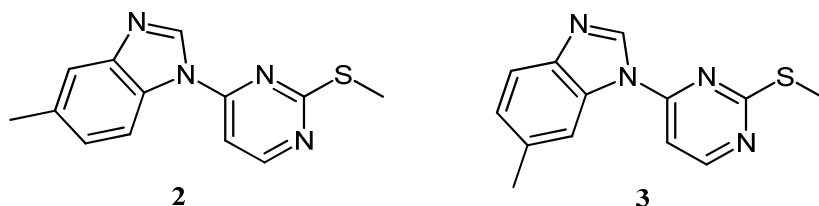
Analytical Data

Compound 1:



¹H NMR (300MHz, CHLOROFORM-*d*): δ = 8.68 (s, 1 H), 8.63 (d, *J*=5.6 Hz, 1 H), 8.21 (d, *J*=7.6 Hz, 1 H), 7.88 (d, *J*=7.3 Hz, 1 H), 7.35 - 7.50 (m, 2 H), 7.22 (d, *J*=5.6 Hz, 1 H), 2.68 ppm (s, 3 H); ¹³C NMR (75MHz, CHLOROFORM-*d*): δ = 174.1, 159.0, 155.8, 145.0, 140.6, 131.7, 125.0, 124.3, 121.1, 114.0, 104.1, 14.4 ppm; ESI-MS: 243.1 [M+H]⁺.

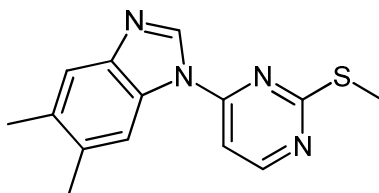
Compound 2+3:



¹H NMR (300MHz, CHLOROFORM-*d*): δ = 8.53 - 8.67 (m, 4 H), 8.05 (d, *J*=8.4 Hz, 1 H), 7.98 (s, 1 H), 7.73 (d, *J*=8.2 Hz, 1 H), 7.65 (s, 1 H), 7.10 - 7.34 (m, 4 H), 2.68 (s, 3 H), 2.67 (s, 3 H), 2.54 (s, 3 H), 2.51 ppm (s, 3 H); ¹³C NMR (75MHz, CHLOROFORM-*d*): δ = 159.0, 158.9, 155.8, 155.8, 145.3, 143.1, 140.5, 140.1, 135.1, 134.2, 131.7, 129.5, 126.4, 125.7, 120.9, 120.5, 113.9, 113.5, 104.1, 103.9, 22.1, 21.5, 14.3 ppm; ESI-MS: 257.1 [M+H]⁺.

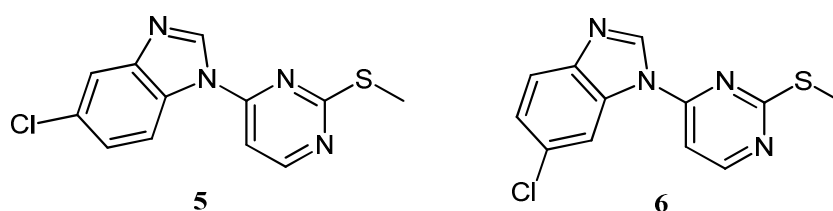
Compound 4:

6 Supporting information



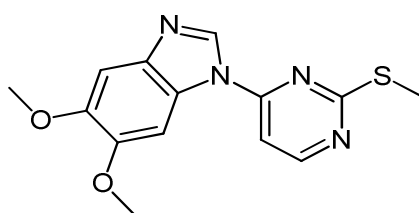
^1H NMR (300MHz, CHLOROFORM-*d*): δ = 8.55 - 8.61 (m, 2 H), 7.93 (s, 1 H), 7.59 (s, 1 H), 7.17 (d, J = 5.6 Hz, 1 H), 2.67 (s, 3 H), 2.42 (s, 3 H), 2.39 ppm; ^{13}C NMR (75MHz, CHLOROFORM-*d*): δ = 174.0, 158.9, 155.8, 143.5, 139.8, 134.2, 133.3, 129.8, 121.0, 114.2, 103.9, 20.8, 20.2, 14.3 ppm (s, 3 H); ESI-MS: 271.1 $[\text{M}+\text{H}]^+$.

Compound 5+6:

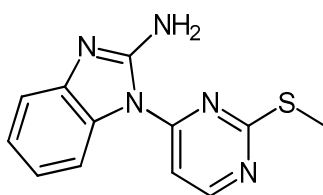


^1H NMR (300 MHz, CHLOROFORM-*d*) δ = 8.57 - 8.68 (m, 4H), 8.30 (s, 1H), 8.19 (d, J = 8.75 Hz, 1H), 7.85 (s, 1H), 7.77 (d, J = 8.57 Hz, 1H), 7.32 - 7.45 (m, 2H), 7.17 (d, J = 5.77 Hz, 2H), 2.69 (s, 3H), 2.67 (s, 3H); ^{13}C NMR (75MHz, CHLOROFORM-*d*): δ = 159.1, 155.6, 141.5, 140.9, 125.5, 124.9, 121.7, 120.8, 115.1, 114.7, 104.0, 14.4 ppm; ESI-MS: 277.1 $[\text{M}+\text{H}]^+$.

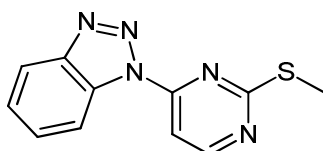
Compound 7:



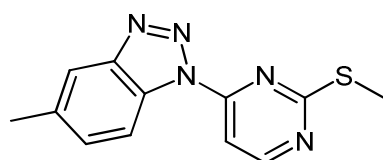
^1H NMR (300MHz, CHLOROFORM-*d*): δ = 8.58 (d, J =5.7 Hz, 1 H), 8.43 (s, 1 H), 7.90 (s, 1 H), 7.29 (s, 1 H), 7.13 (d, J =5.7 Hz, 1 H), 3.98 (s, 3 H), 3.96 (s, 3 H), 2.67 ppm (s, 3 H); ^{13}C NMR (75MHz, CHLOROFORM-*d*): δ = 174.0, 158.7, 156.0, 148.2, 147.7, 138.6, 138.3, 125.2, 103.6, 102.3, 97.9, 56.4, 56.2, 14.3 ppm; ESI-MS: 303.1 $[\text{M}+\text{H}]^+$.

Compound 8:

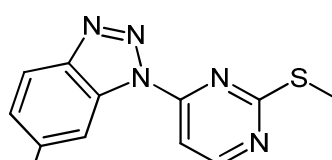
^1H NMR (300MHz, CHLOROFORM-*d*): δ = 8.66 (d, $J=5.7$ Hz, 1 H), 7.42 - 7.57 (m, 2 H), 7.37 (d, $J=5.6$ Hz, 1 H), 7.23 (d, $J=7.6$ Hz, 1 H), 7.11 (t, $J=8.2$ Hz, 1 H), 6.56 (br. s., 2 H), 2.63 ppm (s, 3 H); ^{13}C NMR (75MHz, CHLOROFORM-*d*): δ = 173.2, 159.1, 156.8, 153.4, 143.2, 131.0, 124.1, 120.6, 117.2, 110.6, 106.4, 14.2 ppm; ESI-MS: 258.1 $[\text{M}+\text{H}]^+$.

Compound 9:

mp: 178 °C; UV-VIS (MeOH) (nm): 203, 242, 263, 311(sh), 320; FT-IR (cm⁻¹): 3097, 2156, 2017, 1893, 1596, 1564, 1552, 1506, 1486, 1463, 1428, 1347, 1324, 1306, 1288, 1242, 1205, 1144, 1121, 1090, 1065, 1039, 1009, 976, 917, 864, 841, 826, 801; ^1H NMR (300 MHz, CHLOROFORM-*d*) δ = 2.82 (s, 3 H), 7.55 (t, $J = 8.3$ Hz, 1 H), 7.70 (t, $J = 8.9$ Hz, 1 H), 8.06 (d, $J = 5.9$ Hz, 1 H), 8.18 (d, $J = 8.3$ Hz, 1 H), 8.57 (d, $J = 8.3$ Hz, 1 H), 8.72 (d, $J = 5.9$ Hz, 1 H), 9.19 ppm (br. s, 1 H); ^{13}C NMR (75 MHz, CHLOROFORM-*d*) δ = 14.3, 103.2, 115.6, 116.4, 122.0, 131.6, 135.1, 157.9, 159.3, 161.0, 174.1 ppm; ESI-MS: 244.1 $[\text{M}+\text{H}]^+$; HRMS: $[\text{M}+\text{H}]^+$ calc 244.06514, found 244.06501.

Compound 10+11:

10

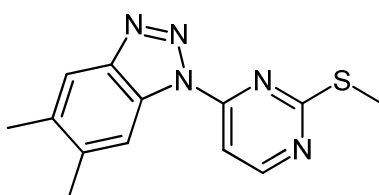


11

^1H NMR (300MHz, CHLOROFORM-*d*): δ = 8.66 (d, $J=5.5$ Hz, 2 H), 8.46 (d, $J=8.5$ Hz, 1 H), 8.39 (s, 1 H), 8.00 (d, $J=8.5$ Hz, 1 H), 7.91 (s, 1 H), 7.90 (s, 2 H), 7.47 (d, $J=8.6$ Hz, 1 H), 7.32 (d, $J=8.5$ Hz, 1 H), 2.72 (s, 3 H), 2.71 (s, 3 H), 2.60 (s, 3 H), 2.56 ppm (s, 3 H) ^{13}C NMR (75MHz, CHLOROFORM-*d*): δ = 173.4, 158.8, 157.5, 157.3, 147.5, 145.5, 140.6, 135.8, 131.6, 131.6, 129.5, 127.6, 119.6, 119.3, 114.4, 105.1, 105.0, 22.3, 21.5, 14.5, 14.4 ppm; ESI-MS: 258.1 $[\text{M}+\text{H}]^+$.

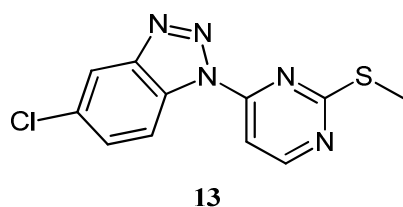
6 Supporting information

Compound 12:

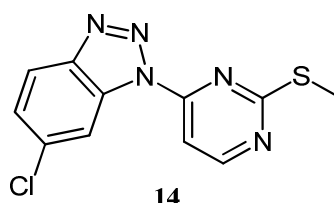


^1H NMR (300MHz, CHLOROFORM-*d*): δ = 8.64 (dd, $J=5.5, 1.1$ Hz, 1 H), 8.34 (s, 1 H), 7.89 (dd, $J=5.6, 1.0$ Hz, 1 H), 7.85 (s, 1 H), 2.72 (s, 3 H), 2.48 (s, 3 H), 2.44 ppm (s, 3 H); ^{13}C NMR (75MHz, CHLOROFORM-*d*): δ = 173.3, 158.7, 157.4, 146.0, 140.1, 135.4, 130.0, 119.4, 114.5, 105.0, 21.2, 20.4, 14.4 ppm; ESI-MS: 272.1 $[\text{M}+\text{H}]^+$.

Compound 13+14:



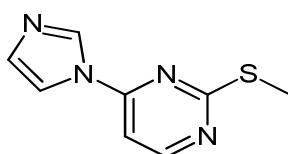
13



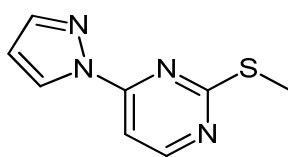
14

^1H NMR (300MHz, CHLOROFORM-*d*): δ = 8.70 (d, $J=5.5$ Hz, 2 H), 8.66 (s, 1 H), 8.57 (d, $J=8.8$ Hz, 1 H), 8.14 (s, 1 H), 8.07 (d, $J=8.8$ Hz, 1 H), 7.87 - 7.95 (m, 2 H), 7.63 (d, $J=8.8$ Hz, 1 H), 7.49 (d, $J=8.8$ Hz, 1 H), 2.73 (s, 3 H), 2.71 ppm (s, 3 H); ^{13}C NMR (75MHz, CHLOROFORM-*d*): δ = 159.1, 147.5, 145.4, 136.2, 130.5, 126.7, 121.1, 119.7, 115.8, 115.0, 105.0, 105.0, 14.5 ppm; ESI-MS: 278.1 $[\text{M}+\text{H}]^+$.

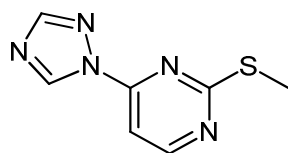
Compound 15:



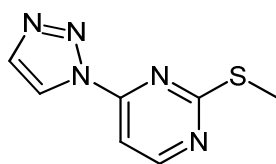
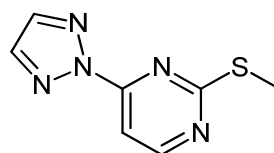
^1H NMR (300MHz, CHLOROFORM-*d*): δ = 8.58 (d, $J=5.5$ Hz, 1 H), 8.44 (s, 1 H), 7.66 (s, 1 H), 7.23 (s, 1 H), 6.96 (d, $J=5.5$ Hz, 1 H), 2.62 ppm (s, 3 H); ^{13}C NMR (126MHz, CHLOROFORM-*d*): δ = 174.0, 159.3, 154.5, 135.1, 131.5, 115.6, 103.2, 14.2 ppm; ESI-MS: 193.1 $[\text{M}+\text{H}]^+$.

Compound 16:

^1H NMR (300MHz, CHLOROFORM-*d*): δ = 8.51 (dd, $J=2.7, 0.6$ Hz, 1 H), 8.48 (d, $J=5.5$ Hz, 1 H), 7.71 (d, $J=1.0$ Hz, 1 H), 7.50 (d, $J=5.5$ Hz, 1 H), 6.43 (dd, $J=2.7, 1.6$ Hz, 1 H), 2.54 ppm (s, 3 H) ^{13}C NMR (75MHz, CHLOROFORM-*d*): δ = 172.6, 158.9, 143.8, 127.6, 109.0, 103.8, 14.2 ppm; ESI-MS: 193.1 $[\text{M}+\text{H}]^+$.

Compound 17:

^1H NMR (300MHz, CHLOROFORM-*d*): δ = 9.22 (s, 1 H), 8.66 (d, $J=5.4$ Hz, 1 H), 8.14 (s, 1 H), 7.51 (d, $J=5.4$ Hz, 1 H), 2.63 ppm (s, 3 H); ^{13}C NMR (75MHz, CHLOROFORM-*d*): δ = 173.4, 159.9, 155.0, 153.7, 142.2, 104.1, 14.2 ppm; ESI-MS: 194.1 $[\text{M}+\text{H}]^+$.

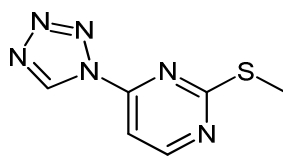
Compound 18+19:**18****19**

^1H NMR (300MHz, CHLOROFORM-*d*): δ = 8.70 (d, $J=5.4$ Hz, 1 H), 8.66 (d, $J=5.5$ Hz, 0.3 H), 8.61 (d, $J=0.8$ Hz, 1 H), 7.96 (s, 0.6 H), 7.86 (d, $J=0.8$ Hz, 1 H), 7.83 (d, $J=5.4$ Hz, 1 H), 7.67 (d, $J=5.5$ Hz, 0.3 H), 2.66 (s, 1 H), 2.63 ppm (s, 3 H); ^{13}C NMR (75MHz, CHLOROFORM-*d*): δ = 173.7, 159.8, 159.2, 154.9, 138.0, 134.5, 121.1, 104.9, 14.3, 14.2 ppm; ESI-MS: 194.1 $[\text{M}+\text{H}]^+$.

No change in the ratio of regioisomers was observed when applying different temperatures (60°C, 20 min, 50 Watt, yield 22%; 100°C, 10 min, 50 Watt, yield: 73%).

6 Supporting information

Compound 20:



^1H NMR (300MHz, CHLOROFORM-*d*): δ = 9.56 (s, 1 H), 8.79 (d, $J=5.2$ Hz, 1 H), 7.71 (d, $J=5.3$ Hz, 1 H), 2.65 ppm (s, 3 H); ^{13}C NMR (126MHz, CHLOROFORM-*d*): δ = 174.5, 160.6, 152.8, 140.1, 105.2, 14.3 ppm; ESI-MS: 195.1 $[\text{M}+\text{H}]^+$.

6.2 Supporting information for Publication II

Supporting Information

Steering the Azido-Tetrazole Equilibrium of 4-Azidopyrimidines *via* substituent variation – Implications for Drug Design and Azide Alkyne Cycloadditions

Andreas Thomann^[a], Josef Zapp^[b], Michael Hutter^[c], Martin Empting^{*[a]} and Rolf W. Hartmann^{*[a,d]}

[a] Helmholtz Institute for Pharmaceutical Research; Department for Drug Design and Optimization; Campus C 2.3, 66123 Saarbrücken (Germany)

E-mail: Rolf.Hartmann@helmholtz-hzi.de

[b] Saarland University; Department of Pharmaceutical Biology; Campus C2.2, 66123 Saarbrücken (Germany)

[c] Saarland University; Center for Bioinformatics; Campus E2.1, 66123 Saarbrücken (Germany)

[d] Saarland University; Department for Pharmaceutical and Medicinal Chemistry; Campus C2.3, 66123 Saarbrücken (Germany)

Content

I. Experimental

- a) Chemical Synthesis
- b) X-ray crystallography
- c) Determination of pK_a
- d) Molecular Modelling and Density Functional Calculations
- e) Calculated physicochemical properties of compounds **1-9**
- f) Calculation of Ligand Efficiency (LE) and Ligand Lipophilicity Efficiency_{Astex} (LLE_{Astex})
- g) *In vitro* PqsD inhibition assay
- h) SPAAC of **3**, **4** and **5** under neutral, basic and acidic pH
- i) SPAAC reactionkinetics of **4** at pH 1.5, 2.5, 4.1 and **15** at pH 1.4 and pH 7.0

II. Spectral data

- a) ^1H -NMR spectra
- b) DMSO- d_6 titration of **4** in CDCl_3 monitored by ^1H -NMR
- c) Acidic, basic and neutral ^1H -NMR of **4** and **5**
- d) ^{13}C -NMR spectra
- e) ^{15}N -NMR spectra
- f) Temperature gradient ^1H -NMR of **3**
- g) IR-spectra

III. References

I. Experimental

All reagents used were of reagent grade or higher. ^1H and ^{13}C -NMR spectra were recorded on Bruker Fourier spectrometers (500/300 or 176/126/75 MHz) at ambient temperature with the chemical shifts recorded as δ values in ppm units by reference to the hydrogenated residues of deuteriated solvent as internal standard. Coupling constants (J) are given in Hz, and signal patterns are indicated as follows: s, singlet; d, doublet; dd, doublet of doublets; t, triplet; m, multiplet, br, broad signal. The Surveyor LC system consisted of a pump, an autosampler, and a PDA detector. Mass spectrometry was performed on a MSQ electrospray mass spectrometer (ThermoFisher, Dreieich, Germany). The system was operated by the standard software Xcalibur. A RP C18 NUCLEODUR 100-5 (125 mm \times 3 mm) column (Macherey-Nagel GmbH, Dühren, Germany) was used as the stationary phase. All solvents were HPLC grade. In a gradient run, the percentage of acetonitrile (containing 0.1% trifluoroacetic acid) was increased from an initial concentration of 0% at 0 min to 100% at 15 min and kept at 100% for 5 min. The injection volume was 10 μl , and flow rate was set to 800 $\mu\text{L}/\text{min}$. MS analysis was carried out at a spray voltage of 3800 V and a capillary temperature of 350 $^{\circ}\text{C}$ and a source CID of 10 V. Spectra were acquired in positive mode from 100 to 1000 m/z at 254 nm for the UV trace. IR Spectra were recorded on a Perkin Elmer FT-IR Spectrum 100 spectrometer equipped with an UATR accessory. High Resolution mass Spectrometry for compounds **5** and **9** were performed on a Dionex Ultimate 3000 RSLC system using a Waters BEH C18, 50 \times 2.1 mm, 1.7 μm dp column by injection of two μl methanolic sample. Separation was achieved by a linear gradient with (A) H₂O + 0.1 % FA to (B) ACN + 0.1 % FA at a flow rate of 600 $\mu\text{l}/\text{min}$ and 45 $^{\circ}\text{C}$. The gradient was initiated by a 0.33 min isocratic step at 5 % B, followed by an increase to 95 % B in 9 min to end up with a 1 min flush step at 95 % B before reequilibration under the initial conditions. UV and MS detection were performed simultaneously. Coupling the HPLC to the MS was supported by an Advion Triversa Nanomate nano-ESI system attached to a Thermo Scientific Orbitrap. Mass spectra were acquired in centroid mode ranging from 200 – 2000 m/z at a resolution of R = 30000. High Resolution Mass Spectrometry for compounds **1-4**, **6-8** and **10-12** was performed on a Dionex Ultimate 3000 RSLC system using a Waters BEH C18, 50 \times 2.1 mm, 1.7 μm dp column. Separation of 1 μL sample was achieved by a linear gradient with (A) H₂O + 0.1 % FA to (B) ACN + 0.1 % FA at a flow rate of 600 $\mu\text{l}/\text{min}$ and 45 $^{\circ}\text{C}$. The

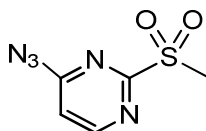
gradient was initiated by a 1 min isocratic step at 5 % B, followed by an increase to 95 % B in 6 min to end up with a 1.5 min step at 95 % B before reequilibration under the initial conditions. UV spectra were recorded by a DAD in the range from 200 to 600 nm. The LC flow was split to 75 μ l/min before entering the maXis 4G hr-ToF mass spectrometer (Bruker Daltonics, Bremen, Germany) using the standard ESI source. Mass spectra were acquired in centroid negative mode ranging from 150 – 2000 m/z at a 2 Hz scan speed.

Caution: *High nitrogen-content compounds are known to be instable. Although we experienced no difficulties in handling these compounds, all experiments were performed in small scale and with best safety precautions (e.g. gloves, protective eyewear, labcoat, shield)!*

6 Supporting information

a) Chemical synthesis

1: 4-azido-2-(methylsulfonyl)pyrimidine



2.0 g (12 mmol) of **3** was dissolved in EtOAc (30 ml) and 22.2g Oxone (36 mmol) dissolved in 50 ml water was added. The mixture was stirred for 3 hrs at ambient temperature. The aqueous layer was extracted 3 times with 60 ml EtOAc. The combined organic layers were dried over Na₂SO₄ and the solvent was removed *in vacuo* to yield **1** as a pale yellow solid (2.2 g, 92%).

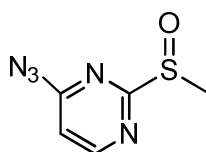
¹H-NMR (300 MHz, DMSO-*d*₆): δ = 8.90 (d, *J*=5.5 Hz, 1 H), 7.40 (d, *J*=5.5 Hz, 1 H), 3.41 ppm (s, 3 H) ppm

¹³C-NMR (75 MHz, DMSO-*d*₆): δ = 165.2, 163.4, 160.0, 113.8 ppm

ESI-MS(+): *m/z* 200.0 [M+H]⁺

HRMS: *m/z* calcd. for C₅H₆N₅O₂S⁺: 200.02367 found: 200.02353 [M+H]⁺

2: 4-azido-2-(methylsulfinyl)pyrimidine



70mg (0.4 mmol) of **3** was dissolved in EtOAc (5 ml) and 60mg oxone (0.2 mmol) dissolved in 5 ml water was added. The mixture was stirred for 3 hours at ambient temperature. The aqueous layer was extracted 3 times with 30 ml EtOAc. The combined organic layers were dried over NaSO₄ and the solvent was removed *in vacuo*. The residue was purified by flashchromatography (ethylacetate:methanol, 97.5:2.5) to yield **2** as a white solid (15 mg, 17%).

Tetrazole: $^1\text{H-NMR}$ (300 MHz, $\text{DMSO-}d_6$) $\delta = 8.82$ (d, $J = 5.49$ Hz, 1H), 7.22 (d, $J = 5.49$ Hz, 1H), 2.90 (s, 3H) ppm

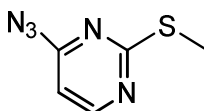
Azide: $^1\text{H-NMR}$ (300 MHz, $\text{DMSO-}d_6$) $\delta = 8.58 - 8.68$ (m, 1H), $8.37 - 8.49$ (m, 1H), 3.16 (s, 3H) ppm

$^{13}\text{C-NMR}$ (75 MHz, $\text{DMSO-}d_6$): $\delta = 174.1, 163.4, 160.3, 112.1, 40.1$ ppm

ESI-MS(+): m/z 184.1 $[\text{M}+\text{H}]^+$

HRMS: m/z calcd. for $\text{C}_5\text{H}_6\text{N}_5\text{OS}^+$: 184.02876 found: 184.02844 $[\text{M}+\text{H}]^+$

3: 4-azido-2-(methylthio)pyrimidine



3.2 g of 4-chloro-2-(methylthio)pyrimidine (20 mmol) was dissolved in DMF (60 ml) and 4.0 g NaN_3 (60 mmol) was added. The suspension was stirred at ambient temperature for 72 hours. To the mixture was added 200 ml water and the aqueous layer was extracted 3 times with 300ml EtOAc. The combined organic layers were dried over NaSO_4 , filtered and the solvent was removed *in vacuo* to obtain a brownish oil. Residual DMF was removed by azeotropic distillation with heptane to yield **3** as a pale yellow solid (3.3 g, 98%).

Tetrazole: $^1\text{H-NMR}$ (300 MHz, $\text{DMSO-}d_6$) $\delta = 8.37$ (d, $J = 6.33$ Hz, 1H), 7.99 (d, $J = 6.33$ Hz, 1H), 2.80 (s, 3H) ppm

Azide: $^1\text{H-NMR}$ (300 MHz, $\text{DMSO-}d_6$) $\delta = 8.49$ (d, $J = 5.40$ Hz, 1H), 6.78 (d, $J = 5.59$ Hz, 1H), 2.52 (s, 3H) ppm

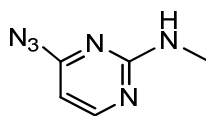
$^{13}\text{C-NMR}$ (75 MHz, CDCl_3) $\delta = 173.0, 161.9, 158.1, 152.9, 149.1, 145.5, 105.8, 105.0, 14.0, 13.5$ ppm

ESI-MS(+): m/z 168.1 $[\text{M}+\text{H}]^+$

HRMS: m/z calcd. for $\text{C}_5\text{H}_6\text{N}_5\text{S}^+$: 169.03384 found: 168.03362 $[\text{M}+\text{H}]^+$

6 Supporting information

4: 4-azido-N-methylpyrimidin-2-amine



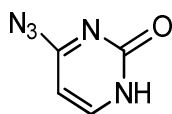
100 mg of **1** (0.5 mmol) was dissolved in EtOH, 203 μ l TEA (1.5 mmol) and 130 μ l 40% aminomethyl in water (3 mmol) was added in a krimp vial. The mixture was heated to 60°C for 3 hrs. Solvent was removed *in vacuo* and the residue was purified by flashchromatography (Ethylacetate:Hexane, 1:1) to yield **4** as white needles (60 mg, 80%).

¹H-NMR (300 MHz, DMSO-*d*₆) δ = 8.90 (br. s., 1H), 8.01 (d, J = 6.24 Hz, 1H), 7.23 (d, J = 6.24 Hz, 1H), 3.06 (d, J = 3.26 Hz, 3H) ppm

¹³C-NMR (75 MHz, DMSO-*d*₆) δ = 150.3, 148.0, 145.2, 96.3, 27.8 ppm

ESI-MS(+): m/z 151.0 [M+H]⁺

HRMS: m/z calcd. for C₅H₇N₆⁺: 151.07267 found: 151.07249 [M+H]⁺

5: 4-azidopyrimidin-2(1H)-one

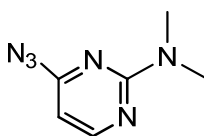
100 mg (0.5 mmol) of **1** was dissolved in Dioxane (2 ml) and 20 mg NaOH (0.5 mmol) in 3 ml Water was added. The mixture was heated to 100°C in a krimp vial for 3 hours. Solvent was removed *in vacuo* and the residue was purified by flashchromatography (ethylacetate:hexane, 7:3) yielding **5** as a white solid (30 mg, 43%).

¹H-NMR (300 MHz, DMSO-*d*₆) δ = 12.44 (br. s., 1H), 7.68 (d, J = 7.36 Hz, 1H), 6.99 (d, J = 7.36 Hz, 1H) ppm

¹³C-NMR (75 MHz, DMSO-*d*₆) δ = 152.0, 143.3, 136.9, 92.7 ppm

ESI-MS(+): m/z 138.0 [M+H]⁺

HRMS: m/z calcd for C₄H₂N₅O⁻:136.0265 found: 136.0266 [M-H]⁻

6: 4-azido-N,N-dimethylpyrimidin-2-amine

100 mg (0.5 mmol) of **1** was dissolved in THF, 203μl TEA (1.5 mmol) and 750 μl of dimethylamine in THF (1.5mmol) was added. The mixture was heated to 60°C in a krimp vial. Solvent was removed *in vacuo* and the residue was purified by flashchromatography (ethylacetate:hexane, 2:8) to yield **6** as a colorless oil (50mg, 61%).

Tetrazole: 7.97 (d, J = 6.15 Hz, 1H), 7.29 (d, J = 6.05 Hz, 1H), 3.50 (s, 6H) ppm

Azide: ¹H-NMR (300 MHz, DMSO-*d*₆) δ = 8.23 (d, J = 5.22 Hz, 1H), 6.15 (d, J = 5.22 Hz, 1H), 3.11 (s, 6H) ppm

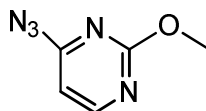
¹³C-NMR (75 MHz, DMSO-*d*₆) δ = 161.5, 161.3, 159.7, 98.2, 36.3 ppm

6 Supporting information

ESI-MS(+): m/z 165.0 [M+H]⁺

HRMS: m/z calcd. for C₆H₉N₆⁺: 165.08832 found: 165.08836 [M+H]⁺

7: 4-azido-2-methoxypyrimidine



100 mg (0.5 mmol) of **1** was dissolved in dry MeOH and 105 mg sodium methanolate 40% in methanol (0.75 mmol) was added. The mixture was stirred at room temperature in a krimp vial. Solvent was removed *in vacuo* and the residue was purified by flashchromatography (ethylacetate:hexane, 1:9) to yield **7** as a white solid (15 mg, 20%).

Tetrazole: ¹H-NMR (300 MHz, DMSO-*d*₆) δ = 8.48 (d, J = 5.40 Hz, 1H), 6.72 (d, J = 5.40 Hz, 1H), 3.92 (s, 3H) ppm

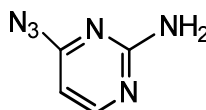
Azide: ¹H-NMR (300 MHz, DMSO-*d*₆) δ = 8.16 (d, J = 6.43 Hz, 1H), 7.80 (d, J = 6.43 Hz, 1H), 4.29 (s, 3H) ppm

¹³C-NMR (126 MHz, DMSO-*d*₆): δ = 164.9, 163.3, 161.0, 151.7, 148.0, 146.2, 104.7, 103.4, 57.0, 54.7 ppm

ESI-MS(+): m/z 152.0 [M+H]⁺

HRMS: m/z calcd. for C₅H₆N₅O⁺: 152.05669 found: 152.05643 [M+H]⁺

8: 4-azidopyrimidin-2-amine



100 mg (0.5 mmol) of **1** was dissolved in 2 ml MeOH, 1.3 ml of 7 N Ammonia in MeOH (1.7 mmol) and 203 μl TEA (1.5 mmol) was added. The mixture was heated to 60°C in a Krimp vial. Solvent was removed *in vacuo* and the residue was purified by

flashchromatography (Ethylacetate:Hexane, 6:4) to yield **8** as a brownish solid (30 mg, 44%).

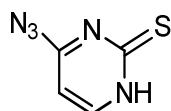
$^1\text{H-NMR}$ (300 MHz, $\text{DMSO-}d_6$) δ = 8.54 (br. s., 2H), 7.95 (d, J = 6.24 Hz, 1H), 7.23 (d, J = 6.33 Hz, 1H) ppm

$^{13}\text{C-NMR}$ (75 MHz, $\text{DMSO-}d_6$) δ = 150.6, 148.3, 146.2, 96.6 ppm

ESI-MS(+): m/z 137.0 $[\text{M}+\text{H}]^+$

HRMS: m/z calcd. for $\text{C}_4\text{H}_5\text{N}_6^+$: 137.05702 found: 137.05644 $[\text{M}+\text{H}]^+$

9: 4-azidopyrimidine-2(1H)-thione



100 mg (0.5 mmol) of **1** was given to a mixture of EtOH (2.5 ml) and 0.025M HCl_{aq} (2.5 ml). 158 mg of NaS_2O_3 (1 mmol) was added and the suspension was refluxed for 16 hours. A white precipitate formed which was filtered, washed 3 times with water and dried *in vacuo* to give **9** as a white solid (35 mg, 45%).

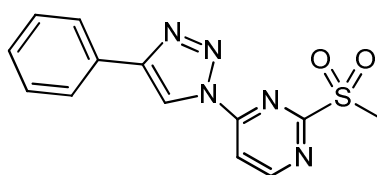
$^1\text{H-NMR}$ (300 MHz, $\text{DMSO-}d_6$) δ = 14.15 (br. s., 1H), 7.77 (d, J = 7.26 Hz, 1H), 7.43 (d, J = 7.26 Hz, 1H) ppm

$^{13}\text{C-NMR}$ (75 MHz, $\text{DMSO-}d_6$) δ = 165.8, 148.1, 136.7, 97.9 ppm

ESI-MS(+): m/z 154.0 $[\text{M}+\text{H}]^+$

HRMS: m/z calcd. for $\text{C}_4\text{H}_2\text{N}_5\text{S}^-$: 152.0036 found: 152.0009 $[\text{M}-\text{H}]^-$

10: 2-(methylsulfonyl)-4-(4-phenyl-1H-1,2,3-triazol-1-yl)pyrimidine



6 Supporting information

100 mg of **1** (0.5 mmol) and 51 mg phenylacetylene (0.5 mmol) was dissolved in 5ml *tert*BuOH:H₂O (1:1), 10 mg sodium ascorbate (0.1 mmol) and 2.5 mg CuSO₄·5H₂O (0.02 mmol) was added argon atmosphere. The mixture was stirred at ambient temperature for 24 hours. The reaction mixture was extracted 3 times with EtOAc and the solvent was removed *in vacuo*. The residue was purified by flash chromatography (Ethylacetate:Hexane, 1:1) to yield **10** as a white solid (82 mg, 55%).

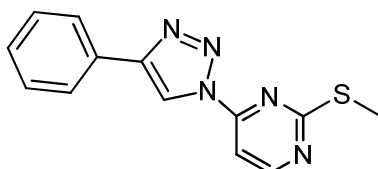
¹H-NMR (300 MHz, DMSO-*d*₆) δ = 9.60 (s, 1H), 9.29 (d, J = 5.59 Hz, 1H), 8.47 (d, J = 5.59 Hz, 1H), 7.99 - 8.19 (m, 2H), 7.48 - 7.58 (m, 2H), 7.24 - 7.48 (m, 1H), 3.60 (s, 3H) ppm

¹³C-NMR (75 MHz, DMSO-*d*₆) δ = 165.9, 162.6, 155.8, 148.4, 129.7, 129.5, 129.4, 126.3, 119.3, 113.4, 39.5 ppm

ESI-MS(+): m/z 302 [M+H]⁺

HRMS: m/z calcd. for C₁₃H₁₂N₅O₂S⁺: 302.07062 found: 302.07065 [M+H]⁺

11: 2-(methylthio)-4-(4-phenyl-1H-1,2,3-triazol-1-yl)pyrimidine



83 mg of **3** (0.5 mmol) and 51 mg phenylacetylene (0.5 mmol) was dissolved in 5ml *tert*BuOH:H₂O (1:1), 10 mg sodium ascorbate (0.1 mmol) and 2.5mg CuSO₄·5H₂O (0.02 mmol) was added under inert atmosphere. The mixture was stirred at ambient temperature for 24 hours. The reaction mixture was extracted 3 times with EtOAc and the solvent was removed *in vacuo*. The residue was purified by flash chromatography (ethylacetate:hexane, 3:7) to yield **11** as a brownish solid (108 mg, 81%).

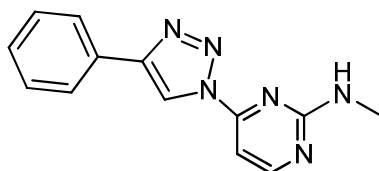
¹H-NMR (300 MHz, CDCl₃) δ = 8.78 (s, 1H), 8.71 (d, J = 5.40 Hz, 1H), 7.91 - 8.04 (m, 2H), 7.85 (d, J = 5.40 Hz, 1H), 7.44 - 7.58 (m, 2H), 7.35 - 7.44 (m, 1H), 2.66 (s, 3H) ppm

¹³C-NMR (75 MHz, CDCl₃) δ = 173.7, 159.6, 154.9, 148.5, 129.6, 129.0, 128.9, 126.0, 116.5, 104.8, 14.3 ppm

ESI-MS(+): m/z 270.0 [M+H]⁺

HRMS: m/z calcd. for C₁₃H₁₂N₅S⁺: 270.08079 found: 270.08099 [M+H]⁺

12: N-methyl-4-(4-phenyl-1H-1,2,3-triazol-1-yl)pyrimidin-2-amine



75 mg of **1** (0.5 mmol) and 51 mg phenylacetylene (0.5 mmol) was dissolved in 5 ml *tert*BuOH:H₂O (1:1), 100 mg sodium ascorbate (0.5 mmol) and 25 mg CuSO₄·5H₂O (0.1 mmol) was added. The mixture was stirred at ambient temperature for 24 hrs. The reaction mixture was extracted 3 times with EtOAc and the solvent was removed *in vacuo*. The residue was purified by flash chromatography (ethylacetate:hexane, 1:1) to yield **12** as a brownish solid (64 mg, 51 %).

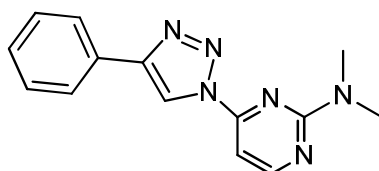
¹H-NMR (300 MHz, CDCl₃) δ = 8.73 (s, 1H), 8.47 (d, J = 5.12 Hz, 1H), 7.88 - 8.02 (m, 2H), 7.35 - 7.57 (m, 4H), 5.36 (br. s., 1H), 3.11 (d, J = 5.12 Hz, 3H) ppm

¹³C-NMR (75 MHz, CDCl₃) δ = 162.8, 160.8, 155.8, 148.0, 129.9, 128.9, 128.6, 126.0, 116.4, 98.7, 28.5 ppm

ESI-MS(+): m/z 253.3 [M+H]⁺

HRMS: m/z calcd. for C₁₃H₁₃N₆⁺: 253.11962 found: 253.11971 [M+H]⁺

14: N,N-dimethyl-4-(4-phenyl-1H-1,2,3-triazol-1-yl)pyrimidin-2-amine



54 mg of **6** (0.3 mmol) and 34 mg phenylacetylene (0.3 mmol) was dissolved in 3 ml *t*BuOH:H₂O (1:1), 7.5 mg sodium ascorbate (0.0375 mmol) and 2 mg CuSO₄·5H₂O (0.0075 mmol) was added under inert atmosphere. The mixture was stirred at

6 Supporting information

ambient temperature for 24 hrs. The reaction mixture was extracted 3 times with EtOAc and the solvent was removed *in vacuo*. The residue was purified by flash chromatography (ethylacetate:hexane 3:7,) to yield **14** as a colorless solid (64 mg, 68 %).

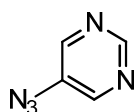
^1H NMR (500 MHz, CDCl_3) δ 8.72 (s, 1H), 8.50 (d, $J = 5.36$ Hz, 1H), 7.91 - 8.01 (m, 2H), 7.45 - 7.52 (m, 2H), 7.40 (tt, $J = 1.30, 7.60$ Hz, 1H), 7.34 (d, $J = 5.04$ Hz, 1H), 3.28 (s, 6H)

^{13}C NMR (126 MHz, CDCl_3) $\delta = 161.9, 160.4, 155.4, 147.9, 130.0, 128.9, 128.6, 126.0, 116.3, 97.0, 37.1$

ESI-MS(+): m/z 267.0 $[\text{M}+\text{H}]^+$

HRMS: m/z calcd. for $\text{C}_{14}\text{H}_{15}\text{N}_6^+$: 267.13527 found: 267.13506 $[\text{M}+\text{H}]^+$

15: 5-azidopyrimidine



15 was synthesized as reported before with minor modifications.¹ Briefly, to a solution of 50 mg of pyrimidine-5-boronic acid (0.4 mmol) in MeOH (5 ml) was added 60 mg sodium azide (1.0 mmol) and CuSO_4 (0.04 mmol). The suspension was stirred vigorously at room temperature until TLC showed complete conversion of starting material. 50 ml water was added and the aqueous layer was extracted three times with EtOAc. The combined organic layers were dried over sodium sulfate and filtered over a double layer pad of Celite[®] and silica. Solvent was removed under reduced pressure to obtain the title compound as an off white solid (30 mg, 63 %). Analytical data is in good accordance with the published spectral data of Grimes et al.¹

FT-IR (cm^{-1}): 3205, 3022, 2925, 2393, 2258, 2191, **2108**, 1727, 1574, 1557, 1437, 1415, 1354, 1296, 1191, 1167, 1097, 1036, 905, 884, 715, 693

^1H -NMR (500 MHz, MeOD) $\delta = 8.61$ (s, 2H), 8.93 (s, 1H) ppm

^{13}C -NMR (126 MHz, MeOD) $\delta = 138.5, 149.2, 155.3$ ppm

ESI-MS(+): m/z 122.0 [M+H]⁺

b) X-Ray Crystallography

Crystallization of **3**:

100 mg of **3** was dissolved in hot chloroform. Crystals formed after 2 days at ambient temperature.

CCDC-Number: 1045217

Crystallization of **4**:

20 mg of **4** was dissolved in hot chloroform. Crystals formed after 4 days at ambient temperature.

CCDC-Number: 1045218

Crystallization of **5**:

20 mg of **5** was dissolved in hot MeOH. Crystals formed after 3 days at ambient temperature.

CCDC-Number: 1045219

X-ray structure determination of **3-5**

Crystals suitable for single-crystal x-ray analysis were obtained as described above. The data were collected at 133 K on a BrukerAXS X8Apex CCD diffractometer operating with graphite-monochromatized Mo K α radiation. Frames of 0.5° oscillation were exposed; deriving data in the θ range of 2 to 30° with a completeness of ~99%. Structure solution and full least-squares refinement with anisotropic thermal parameters of all non-hydrogen atoms and rigid group refinement of the hydrogen were performed using SHELX² (The final refinement result in: [1] R1= 0.026; [2] R1= 0.036; [3] R1= 0.043. Crystallographic data for the structures have been deposited

6 Supporting information

with the Cambridge Crystallographic Data Centre, CCDC, 12 Union Road, Cambridge CB21EZ, UK. Copies of the data can be obtained free of charge on quoting the depository numbers CCDC (www.ccdc.cam.ac.uk/data_request/cif).

c) Determination of pK_a

The pK_a 's of **5** and **9** were measured using the SiriusT3 automatic titration system (Sirius Analytical Ltd, Forest Row, UK) and the software supplied with the machine for the refinement of the experimental data. Standard solutions of hydrochloric acid 0.5 M and potassium hydroxide 0.5 M in Millipore water were used as acid and base titrant, respectively. The ionic strength of the water used for dissolving the samples was adjusted adding potassium chloride obtaining a 0.15 M solution. A solution of 50 % acetonitrile - 50 % Millipore water was prepared and potassium chloride was added in it for obtaining a final mixture 50 % acetonitrile with 0.15 M KCl. In each experiment, **5** was titrated three times in water media from high to low pH, while **9** was titrated three times in acetonitrile – water solution (first titration in 42 %, second titration in 38 % and third titration in 32 % of acetonitrile) from basic to acidic pH. Three independent experiments were performed per each compound at room temperature.

d) Molecular Modelling and Density Functional Calculations

Modelling of steric clash of the aminodimethyl group and N2 of tetrazol of compound **6**:



Based on the crystalstructure of **4** (CCDC-Number: 1045218) an additional methylgroup was introduced to the methylamine, resulting in the tetrazole tautomer of compound **6** (left figure). Steric clashes, indicated in orange, occur between methyl C and N2 of tetrazole, resulting in an energy demand of 4.6 kcal to accommodate this

structure. Energy minimization *in vacuo* with AMBER 10:EHT solvation model R-field (MOE) of this structure (right figure, pink structure) yielded a conformation where the methyl group and the tetrazole evade this clash which is accompanied by a deformation of the tetrazolo[1,5-*c*]pyrimidine ring (right figure, grey structure=before energy minimization, pink structure=after energy minimization)

Modelling of compound **5** and **9** into the adenosyl bindingsite of PqsD:

To predict the binding mode of compound **5** and **9** the cocrystal structure of PqsD with anthranoyl-CoA (PDB code: 3H77) was used. The anthranoyl-CoA chain was deleted and only the adenosine moiety was kept for further experiments. The adenosine was modified using Molecular Operating Environment, Chemical Computing Group to compound **5** and **9** and the resulting structures, and the residues in 3.5Å proximity were energy minimized inside the binding site of adenosine. For energy minimization MMFF94x (Merck Forcefield) of MOE software package was used with the preset standard parameters.

Energy optimization of compounds **1-9** and solvation contributions:

Structures were energetically optimized at B3LYP/aug-cc-pVDZ level of theory using default parameters. Single point energies were obtained applying the COSMO solvent model³ as implemented in NWChem (Version 6.1)⁴. The dielectric constants and solvent radii used were for water (78.0, 1.37), for DMSO (47.24, 2.455), and for CHCl₃ (4.8069, 2.715), respectively.

6 Supporting information

e) Calculated physicochemical properties of compounds 1-9

Physicochemical properties were calculated using ACD/Percepta version 2012 (Build 2203, 29 jan. 2013), ACD/Labs. Calculation of LogP values was done using consensus LogP model and for pKa calculation the pKa classic module was used.

Cmpd	cLogD _{7,4}		cLogP		cpK _a		Exp
	T	A	T	A	T	A	
1	-1.16	0.37	-1.16	0.37			
2	-1.34	0.05	-1.34	0.05			
3	-0.06	1.96	-0.06	1.96			
4	-0.79	1.49	-0.79	1.49			
5	-2.63	-0.74	-1.21	-0.72	5.9	8.7	6.8
6	-0.59	1.72	-0.59	1.72			
7	-0.22	1.21	-0.22	1.21			
8	-1.05	0.88	-1.05	0.88			
9	-0.64	-1.35	-0.15	-0.35	7.1	6.4	4.6

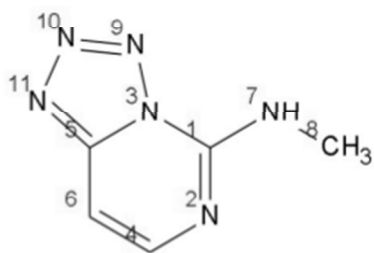
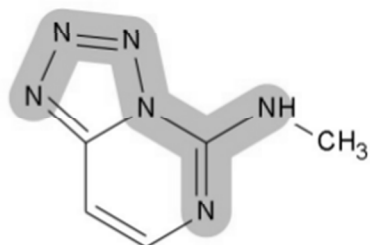
T=Tetrazol, A=Azide, Exp= experimentally determined.

**ACD/Labs****ACD/Labs***ACD/pKa GALAS Module Report***Date:** July 23, 2015 4:20 PM**Software name and version:** ACD/Percepta 14.0.0 (Build 2726)**Compound name:****Structure:**

No acid pKa

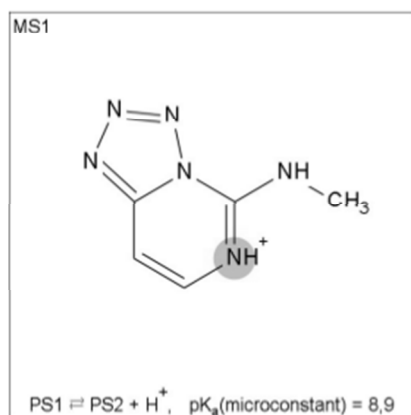
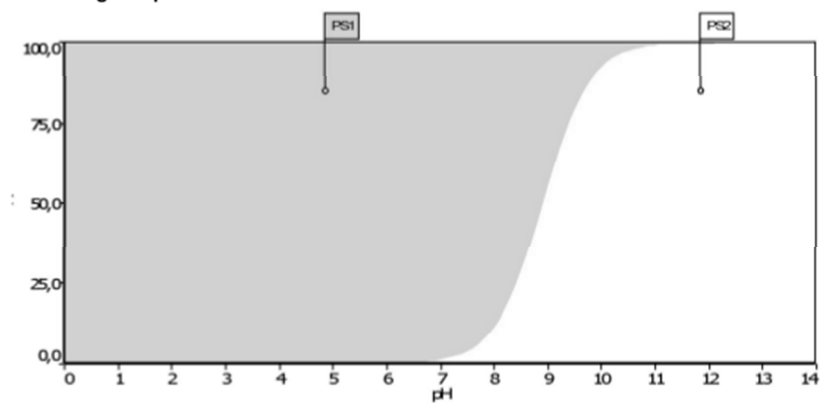
Strongest pKa(Base): 8,9 +- 2,3

8,9 +- 2,3 (Atom number: 2), 100% MS1



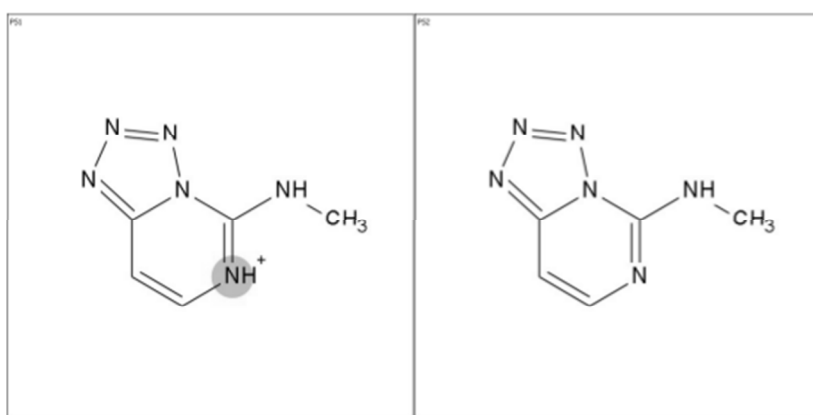
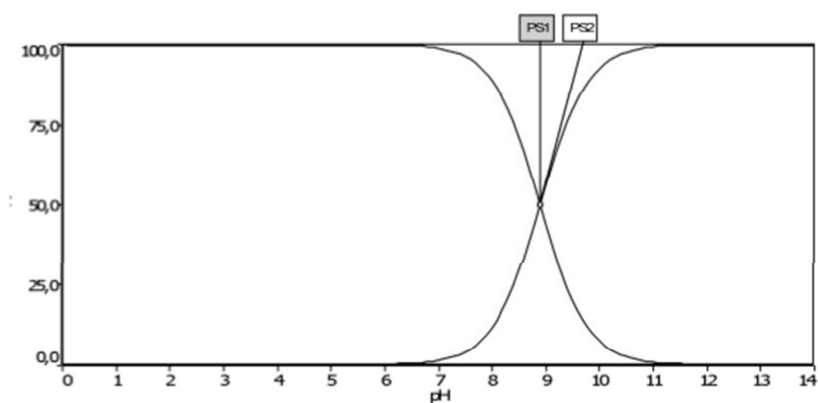
6 Supporting information

Net Charge vs pH



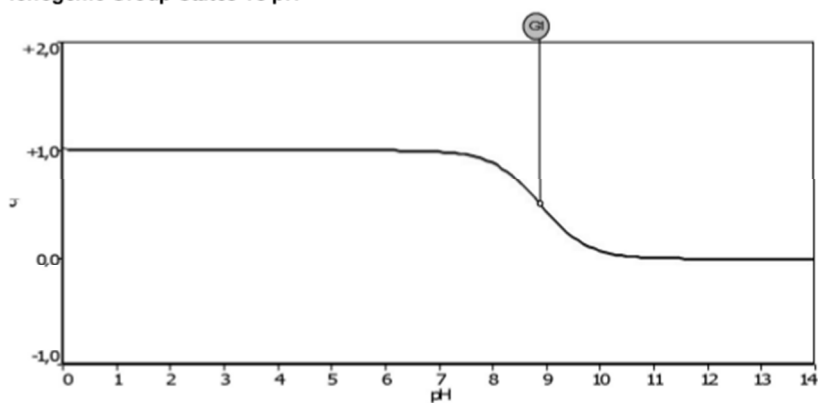
	1,7	2	3	4	4,6	5	6	6,5	7	7,4	8	9	10	11
q = 0	0,00	0,00	0,00	0,00	0,00	0,00	0,00	0,00	0,01	0,03	0,11	0,56	0,93	0,99
q = +1	1,00	1,00	1,00	1,00	1,00	1,00	1,00	1,00	0,99	0,97	0,89	0,44	0,07	0,01

Protonation State vs pH

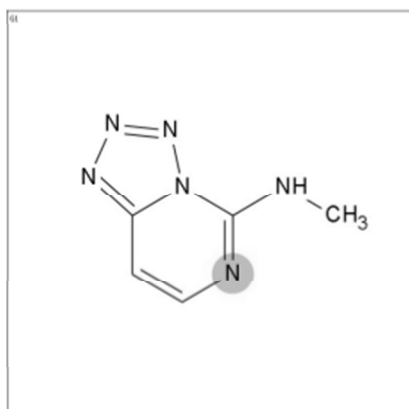


	1,7	2	3	4	4,6	5	6	6,5	7	7,4	8	9	10	11
PS1	1,00	1,00	1,00	1,00	1,00	1,00	1,00	1,00	0,99	0,97	0,89	0,44	0,07	0,01
PS2	0,00	0,00	0,00	0,00	0,00	0,00	0,00	0,00	0,01	0,03	0,11	0,56	0,93	0,99

Ionogenic Group States vs pH



6 Supporting information



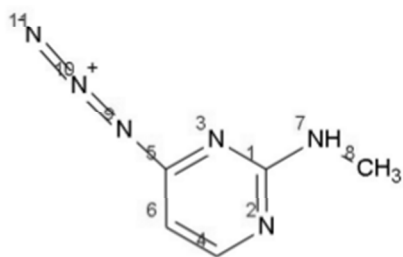
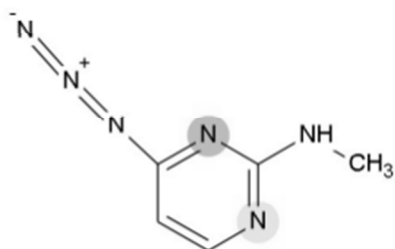
	1,7	2	3	4	4,6	5	6	6,5	7	7,4	8	9	10	11
G1	1,00	1,00	1,00	1,00	1,00	1,00	1,00	1,00	0,99	0,97	0,89	0,44	0,07	0,01
TC	1,00	1,00	1,00	1,00	1,00	1,00	1,00	1,00	0,99	0,97	0,89	0,44	0,07	0,01

**ACD/Labs****ACD/Labs***ACD/pKa GALAS Module Report***Date:** July 23, 2015 4:22 PM**Software name and version:** ACD/Percepta 14.0.0 (Build 2726)**Compound name:****Structure:**

No acid pKa

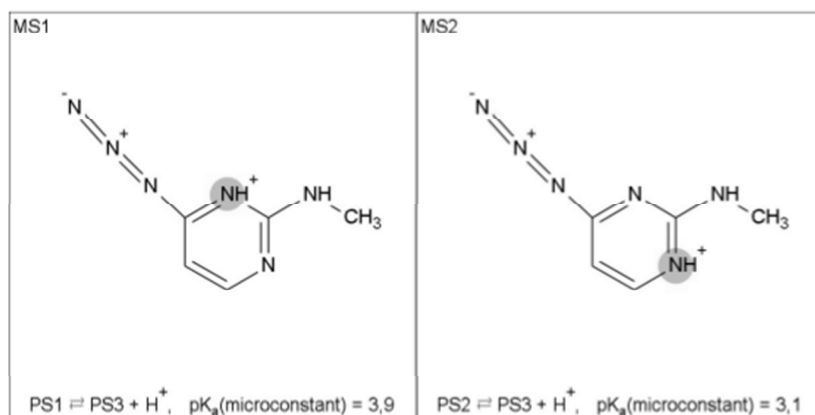
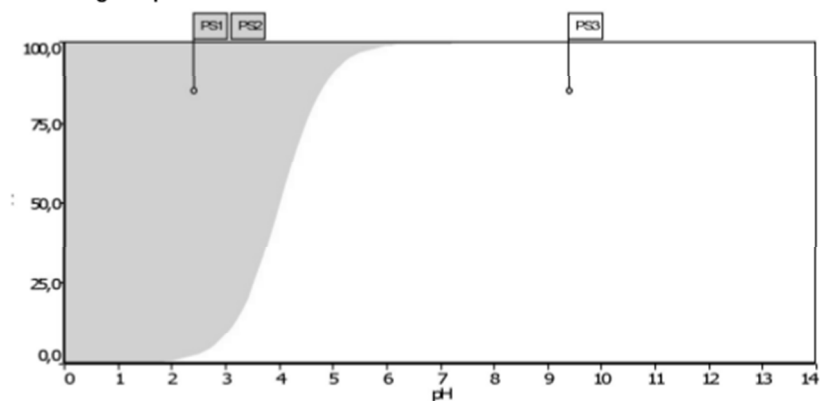
Strongest pKa(Base): 4,0 +/- 0,8

4,0 +/- 0,8 (Atom number: 3,2), 88% MS1, 12% MS2



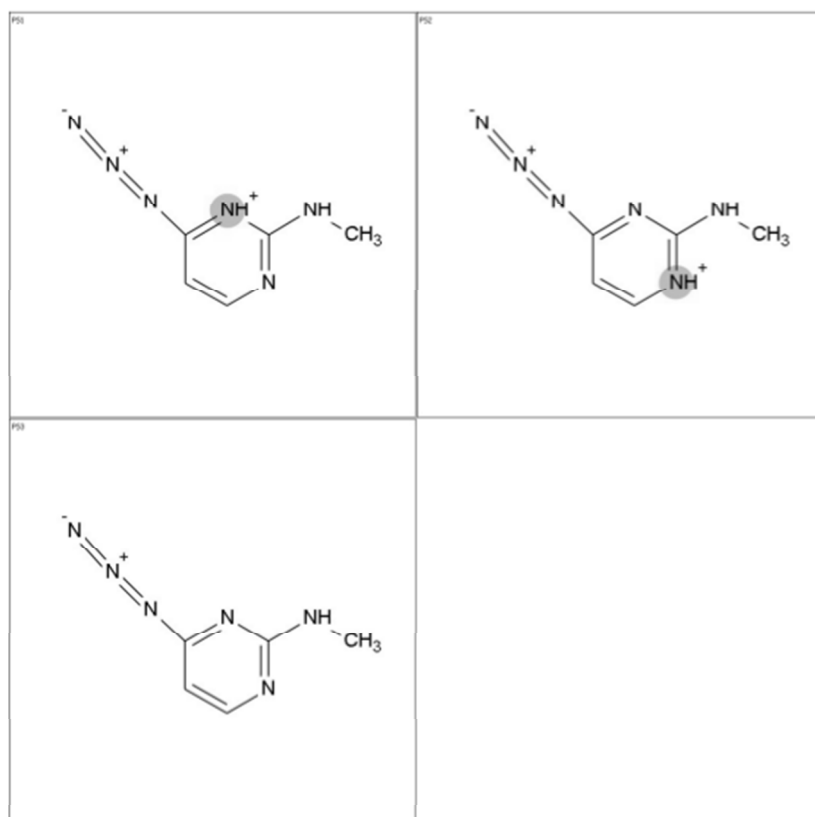
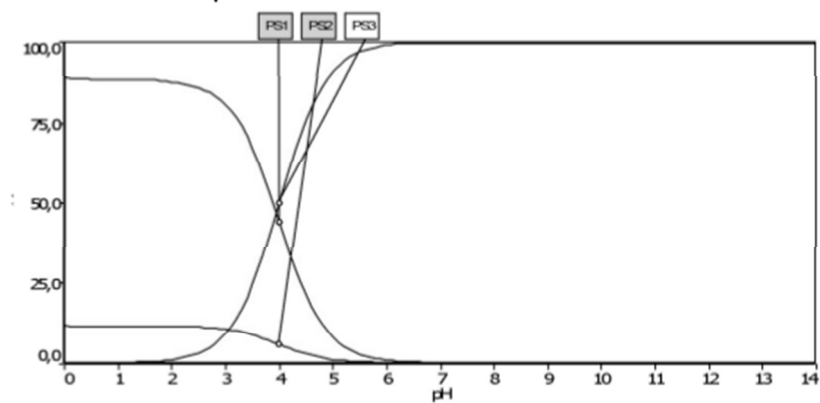
6 Supporting information

Net Charge vs pH



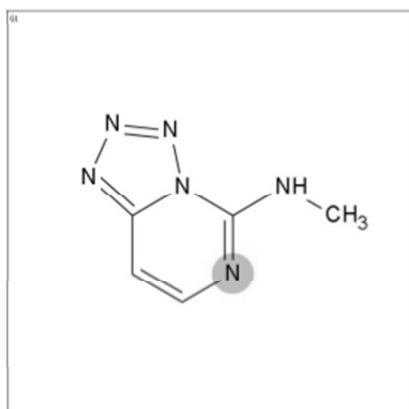
	1,7	2	3	4	4,6	5	6	6,5	7	7,4	8	9	10	11
q = 0	0,00	0,01	0,09	0,50	0,80	0,91	0,99	1,00	1,00	1,00	1,00	1,00	1,00	1,00
q = +1	1,00	0,99	0,91	0,50	0,20	0,09	0,01	0,00	0,00	0,00	0,00	0,00	0,00	0,00
q = +2	0,00	0,00	0,00	0,00	0,00	0,00	0,00	0,00	0,00	0,00	0,00	0,00	0,00	0,00

Protonation State vs pH



	1,7	2	3	4	4,6	5	6	6,5	7	7,4	8	9	10	11
PS1	0,88	0,88	0,80	0,44	0,18	0,08	0,01	0,00	0,00	0,00	0,00	0,00	0,00	0,00
PS2	0,11	0,11	0,10	0,06	0,02	0,01	0,00	0,00	0,00	0,00	0,00	0,00	0,00	0,00

6 Supporting information



	1,7	2	3	4	4,6	5	6	6,5	7	7,4	8	9	10	11
G1	1,00	1,00	1,00	1,00	1,00	1,00	1,00	1,00	0,99	0,97	0,89	0,44	0,07	0,01
TC	1,00	1,00	1,00	1,00	1,00	1,00	1,00	1,00	0,99	0,97	0,89	0,44	0,07	0,01

f) Calculation of Ligand Efficiency (LE) and Ligand Lipophilicity Efficiency (LLE_{Astex})

LE of compounds **5** and **9** was calculated based on their IC₅₀:⁵

$$LE = 1.4 * \frac{pIC_{50}}{NHA} \quad (NHA = \text{Number of heavy atoms})$$

LLE_{Astex} was calculated using IC₅₀'s with minor changes to the formula, based on the findings of Shultz^{5,6}:

$$LLE_{Astex} = 0.11 + 1.4 * \frac{pIC_{50} - cLogP}{NHA}$$

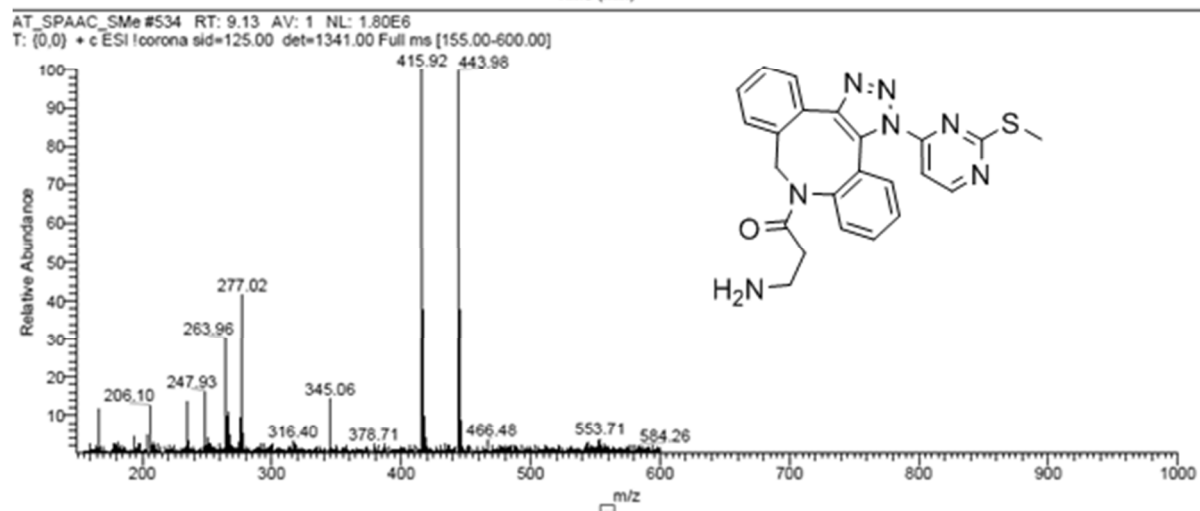
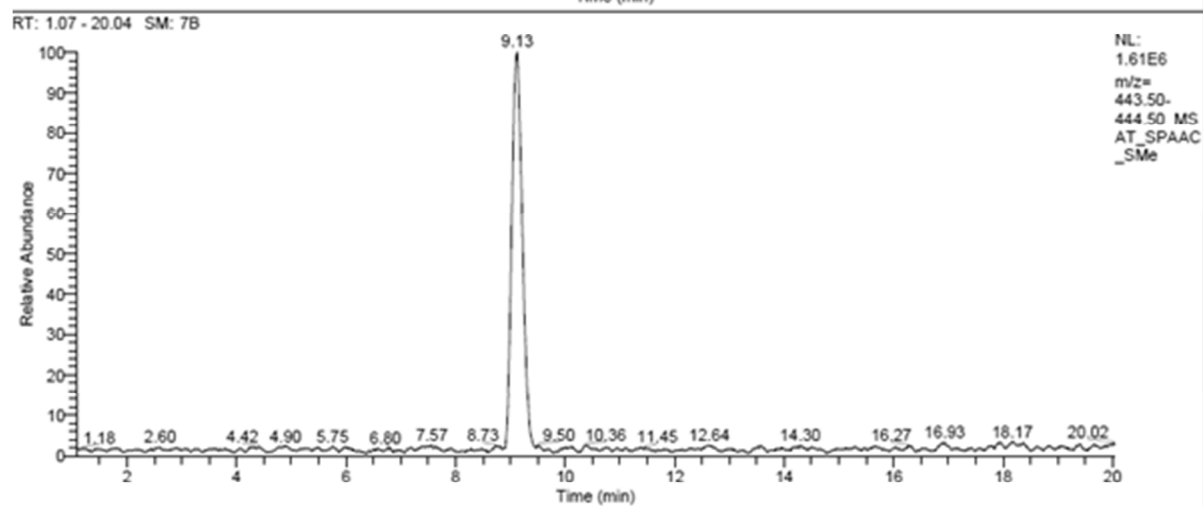
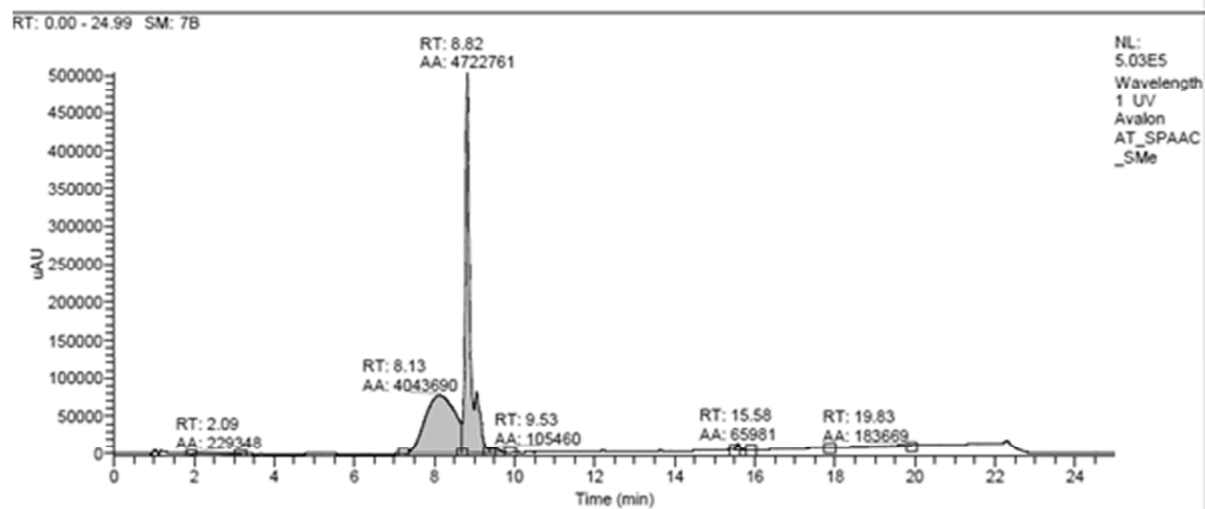
g) In vitro PqsD Inhibition Assay

PqsD In vitro Inhibition Assay: The assay was performed monitoring enzyme activity by measuring HHQ formed by condensation of anthraniloyl-CoA and β-ketodecanoic acid. The reaction mixture contained MOPS buffer (0.05 M, pH 7.0) with 0.005 % (w/v) Triton X-100, 0.1 μM of the purified enzyme, and inhibitor. The test compounds were dissolved in DMSO and diluted with buffer. The final DMSO concentration was 0.5%. After 10 min preincubation at 37 °C, the reaction was started by the addition anthraniloyl-CoA to a final concentration of 5 μM and β-ketodecanoic acid to a final concentration of 70 μM. Reactions were stopped by addition of MeOH containing 1 μM amitriptyline as internal standard for LC/MS-MS analysis. HHQ was quantified using a HPLC-MS/MS mass spectrometer (Thermo Fisher, Dreieich, Germany) in ESI mode. Ionization of HHQ and the internal standard amitriptyline was optimized in each case. The solvent system consisted of 10 mM ammonium acetate (A) and acetonitrile (B), both containing 0.1 % trifluoroacetic acid. The initial concentration of B in A was 45%, increasing the percentage of B to 100 % in 2.8 min and keeping it at 98% for 0.7 min with a flow of 500 μl/min. The column used was a NUCLEODUR-C18, 100-3/125-3 (Macherey & Nagel, Dueren, Germany). Control reactions without the inhibitor, but including identical amounts of DMSO, were performed in parallel, and the amount of HHQ produced was set to 100 %. All reactions were performed in triplicate except for adenine and hypoxanthine which were performed as single point measurements at 50 μM. Hypoxanthine inhibited 9% HHQ formation whereas adenine inhibited 0% HHQ formation.

6 Supporting information

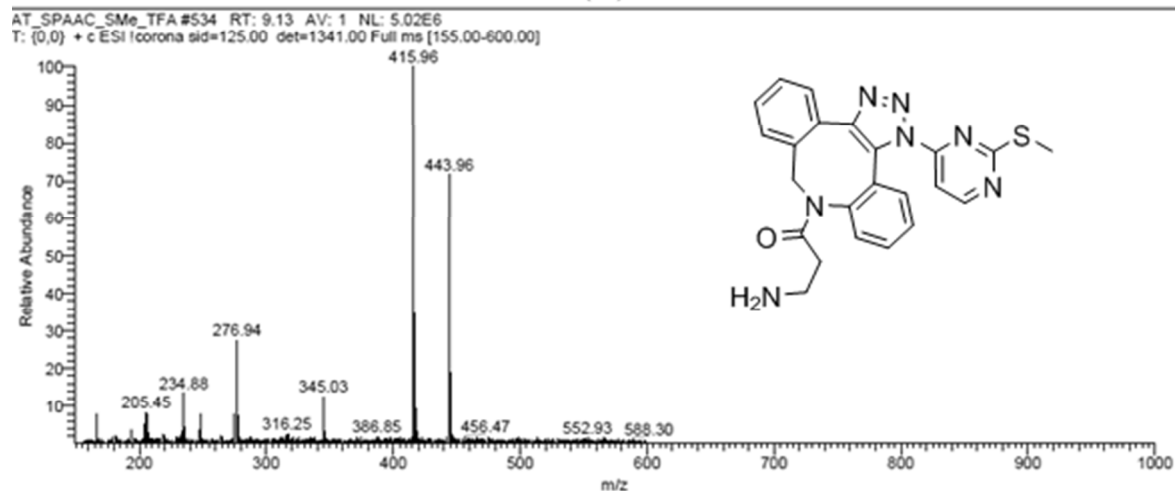
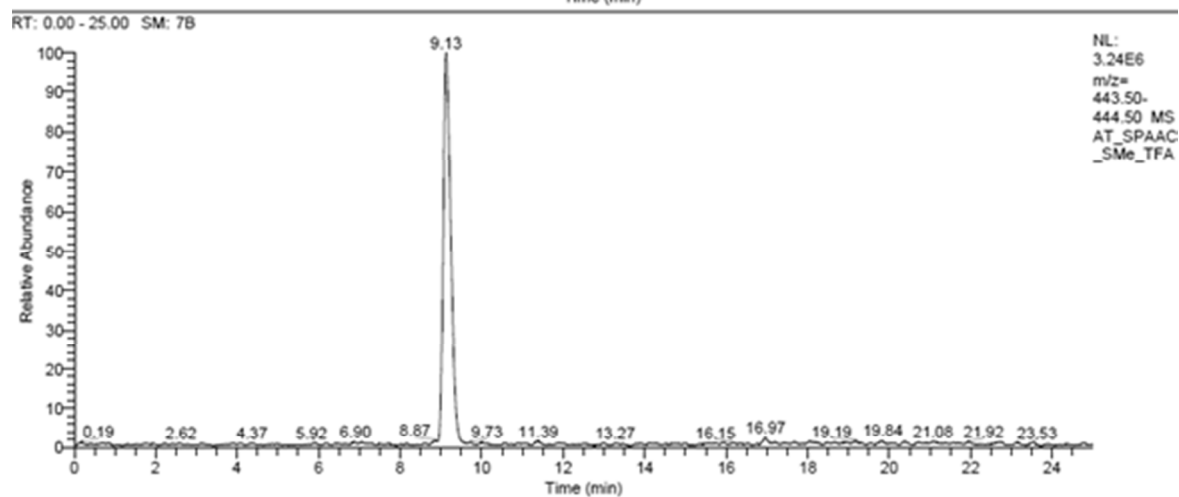
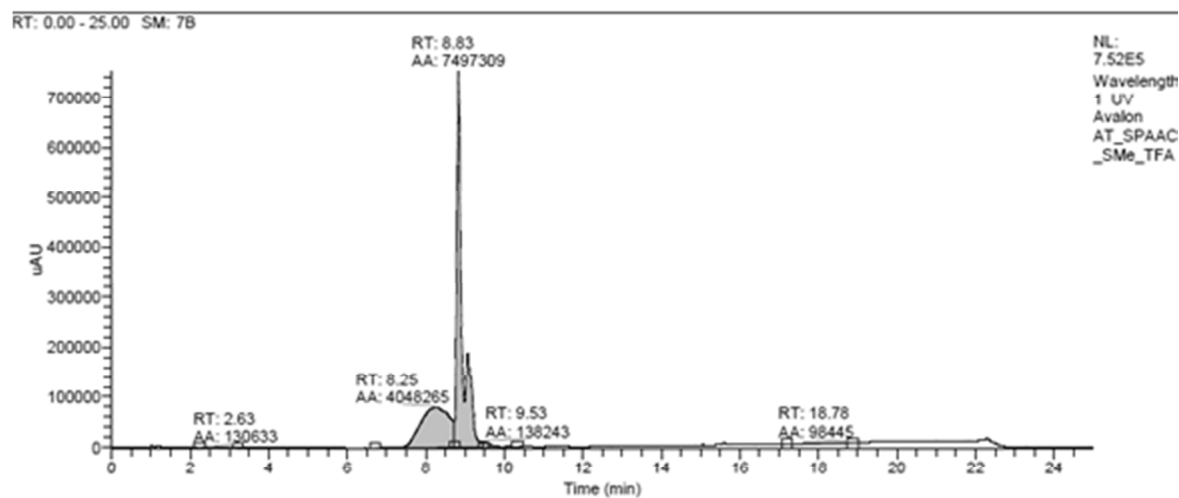
h) SPAAC reactionkinetics of 3, 4 and 5 under neutral, basic and acidic pH

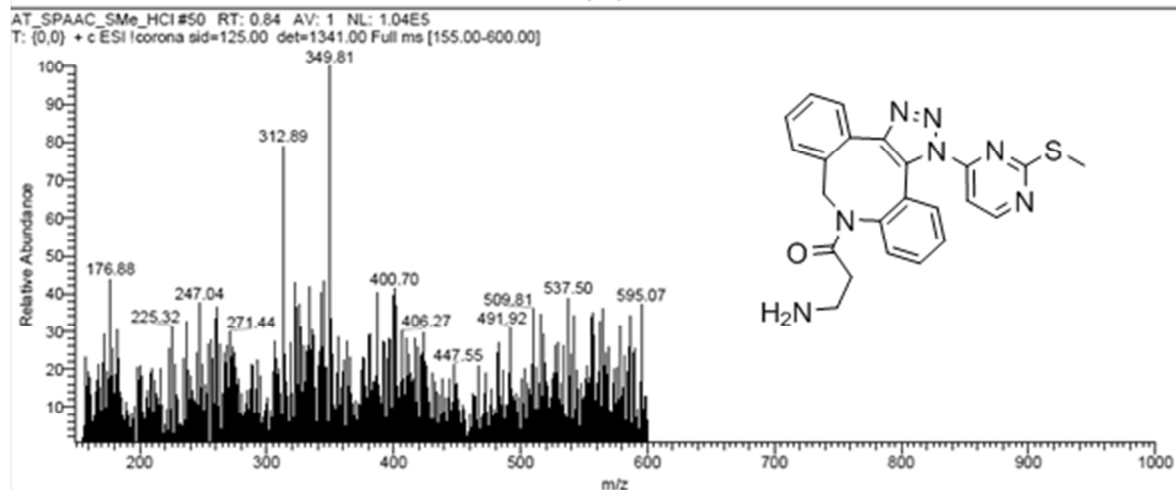
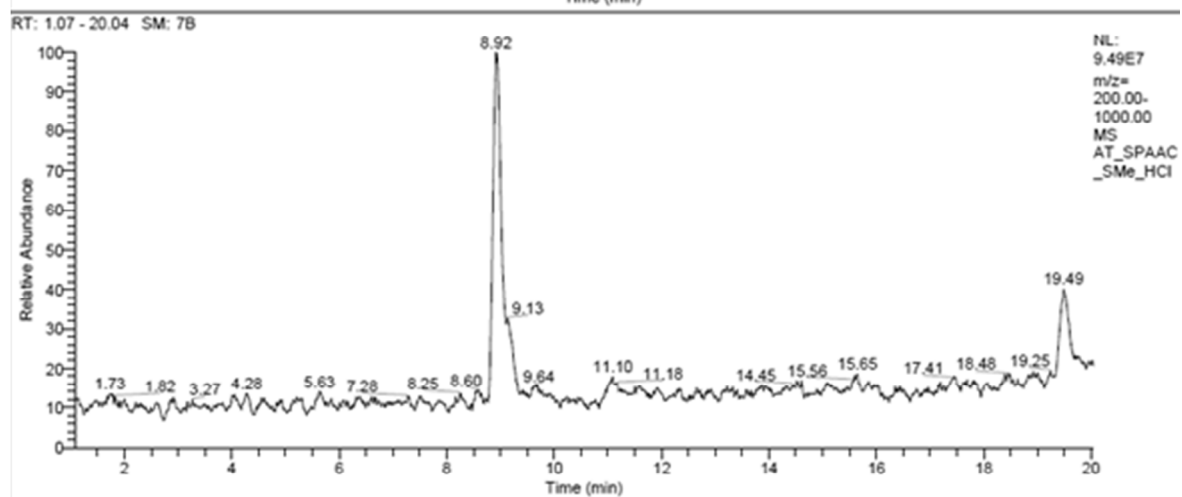
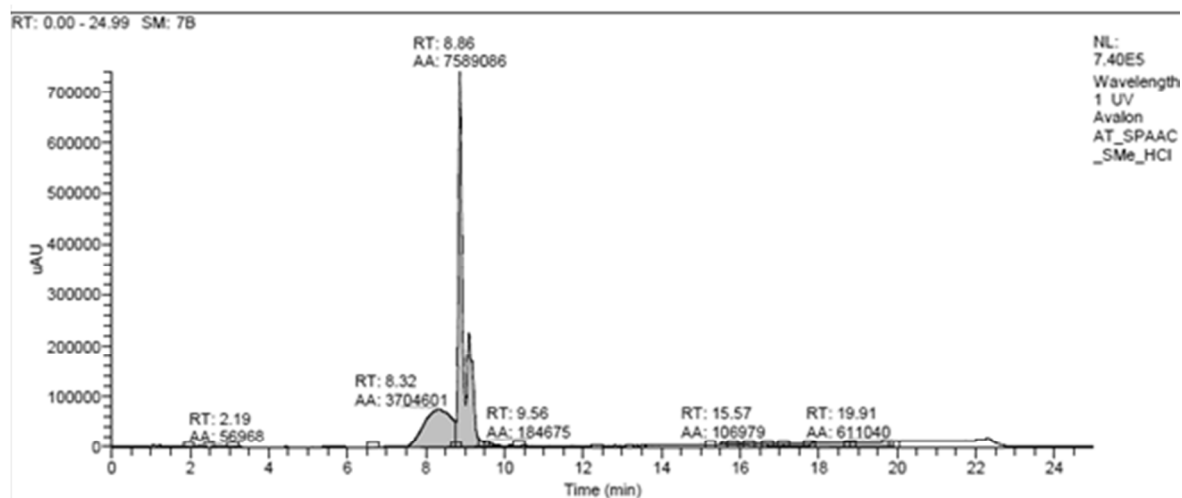
10 μl of Dibenzocyclooctyne-amine (100 mM DMSO Stock) and 20 μl of the corresponding azide-compound (50 mM in *tert*BuOH:Water [1:1]) was added to 1000 μl of *tert*BuOH:Water (1:1) and shaken at room temperature for 1 hr for neutral conditions. For acidic conditions 0.2 % TFA or 0.1 M HCl was and for basic conditions 0.1 M NaOH was used in 1000 μl *tert*BuOH:Water (1:1) final. 10 μl of the reaction mixture was injected into the LC-MS System.

LC-MS Run of **3** under neutral conditions

6 Supporting information

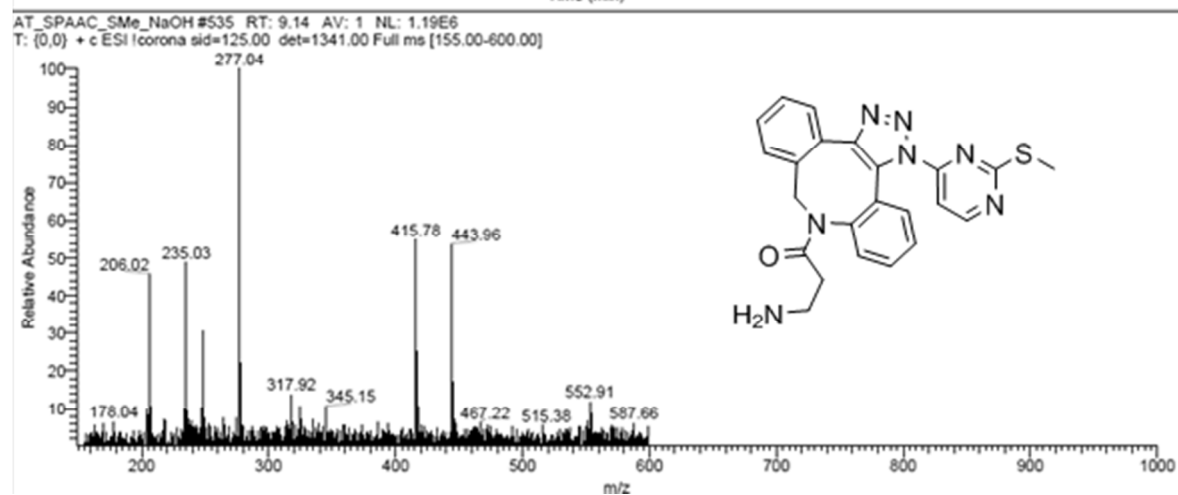
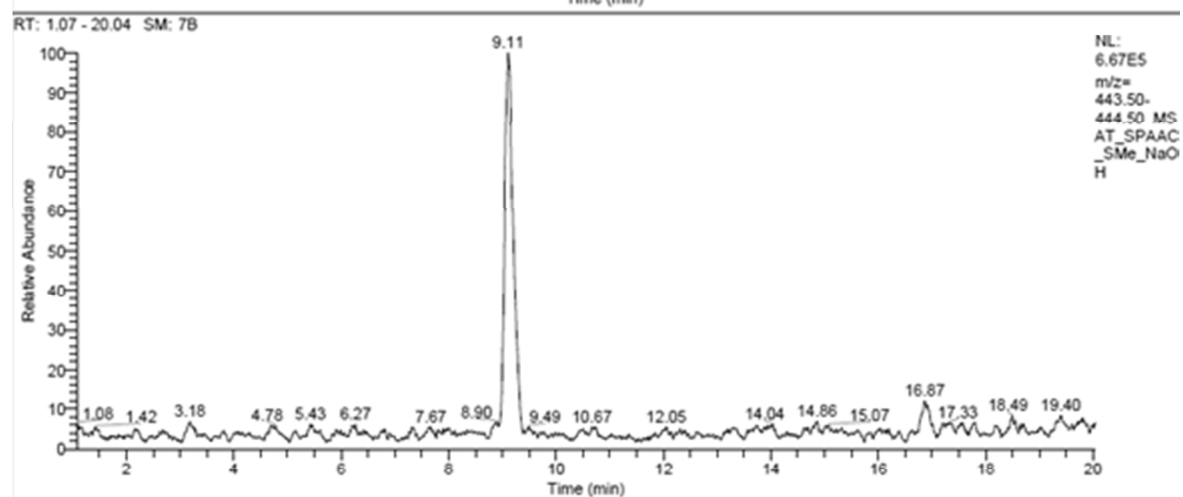
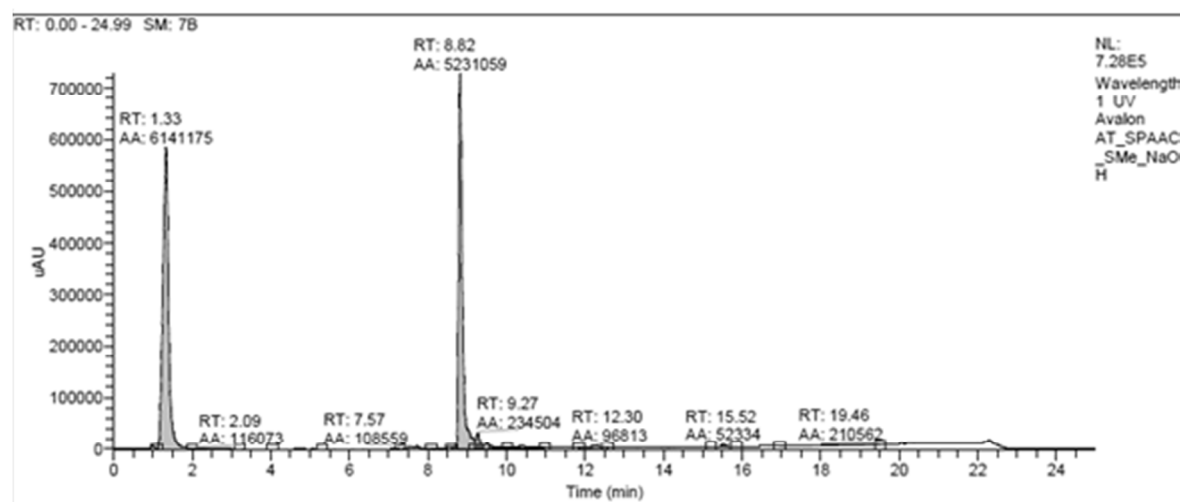
LC-MS Run of **3** under acid conditions (0.2% TFA)

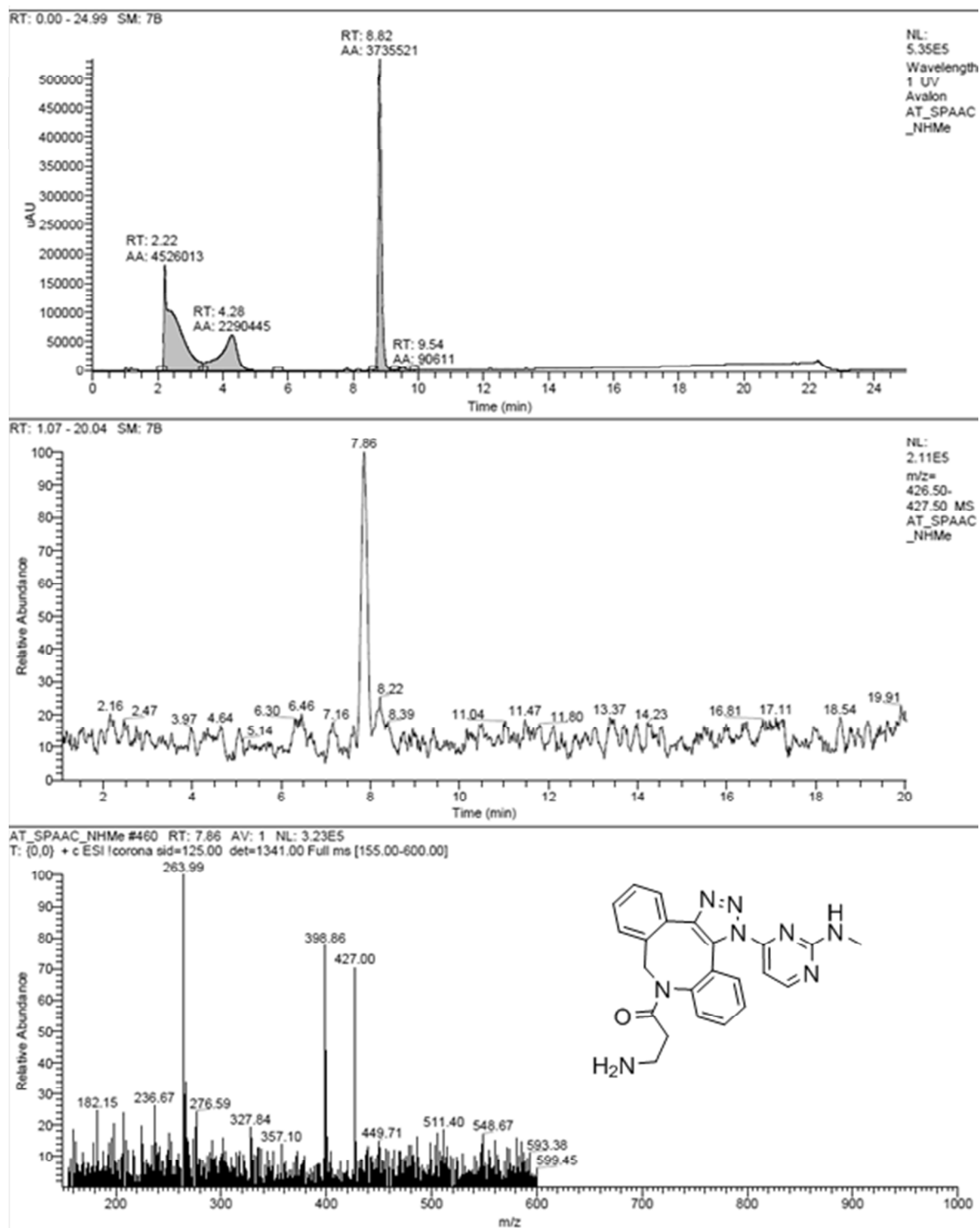


LC-MS Run of **3** under acid conditions (0.1 M HCl)

6 Supporting information

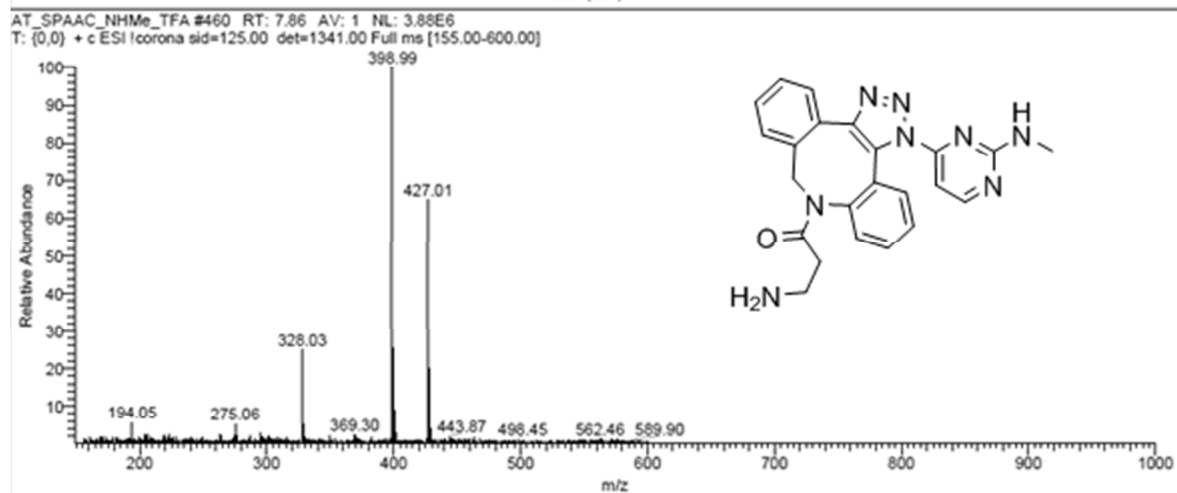
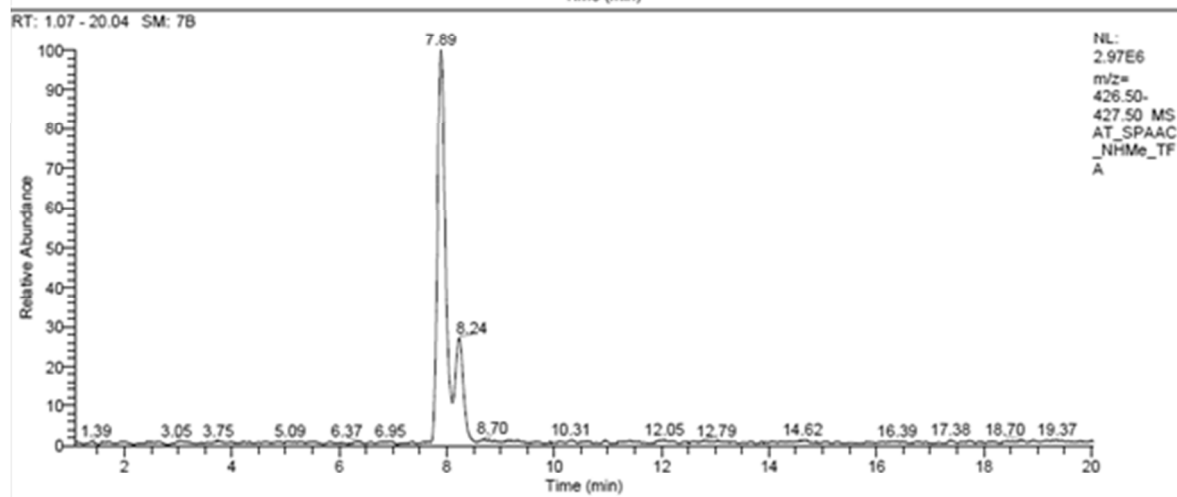
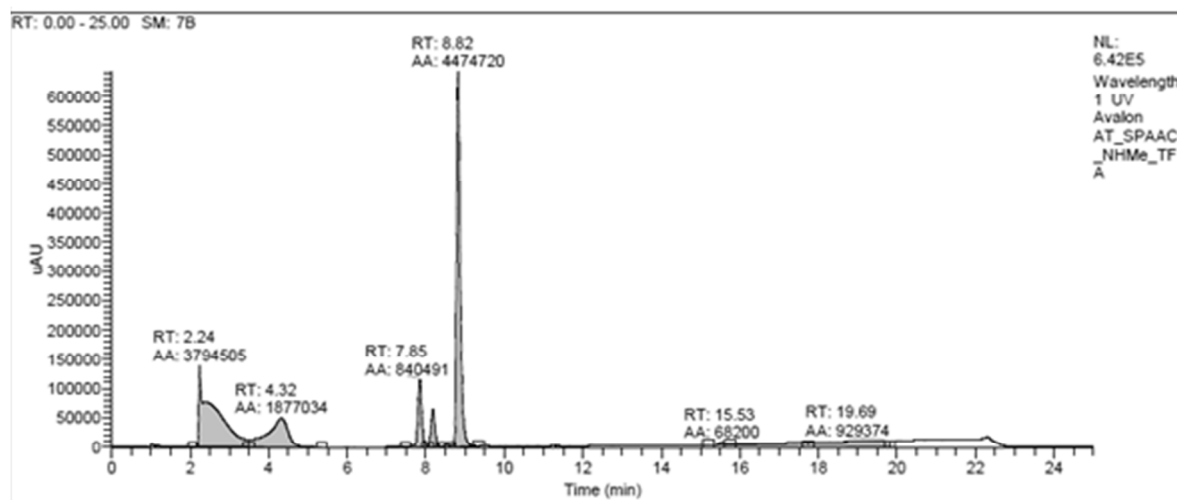
LC-MS Run of **3** under basic conditions (0.1 M NaOH)

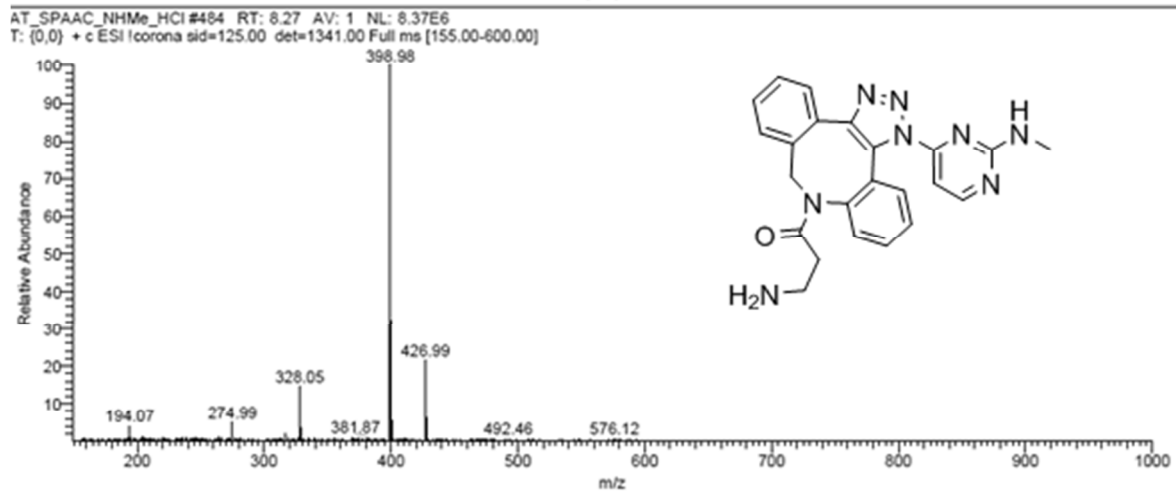
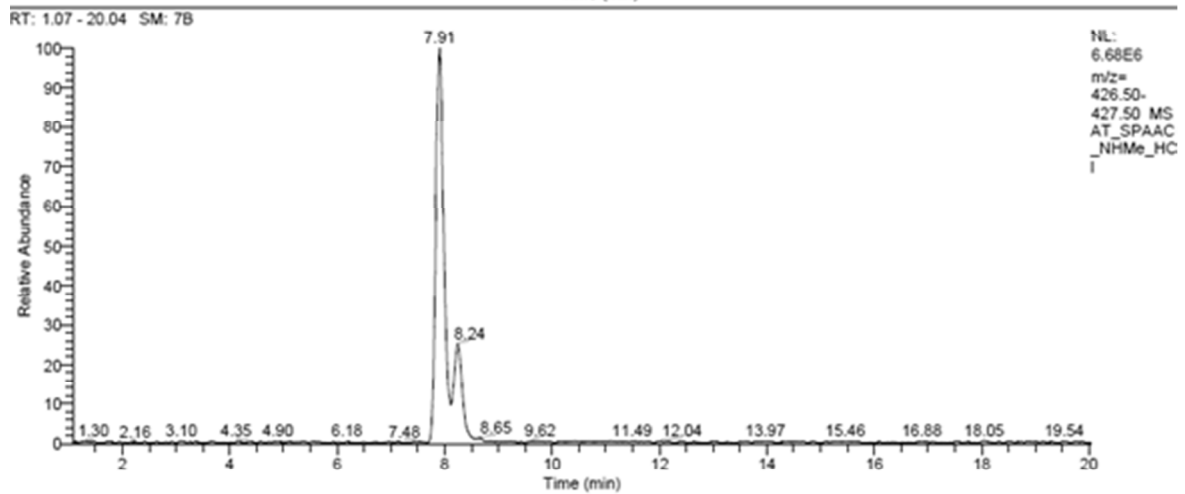
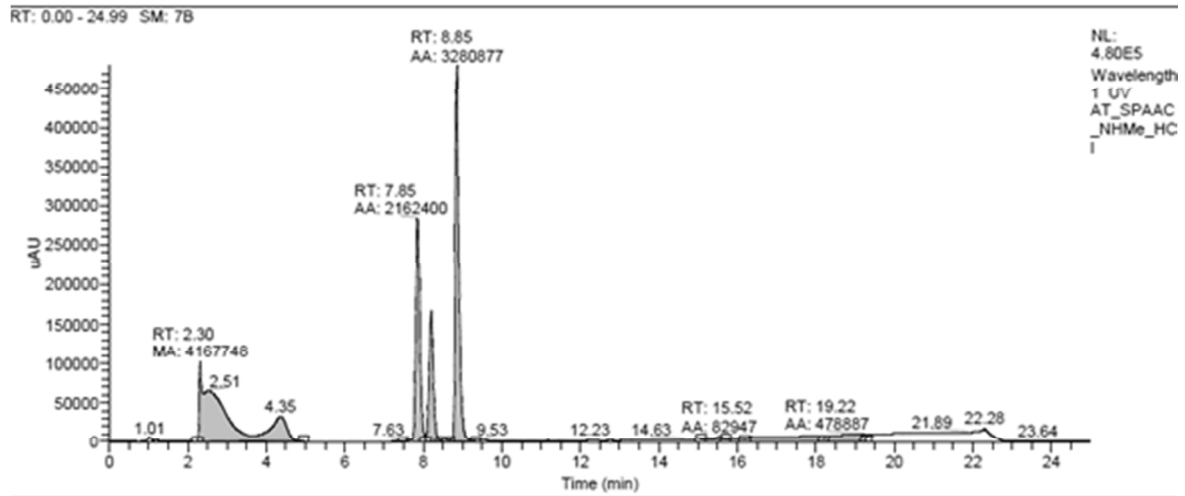


LC-MS Run of **4** under neutral conditions:

6 Supporting information

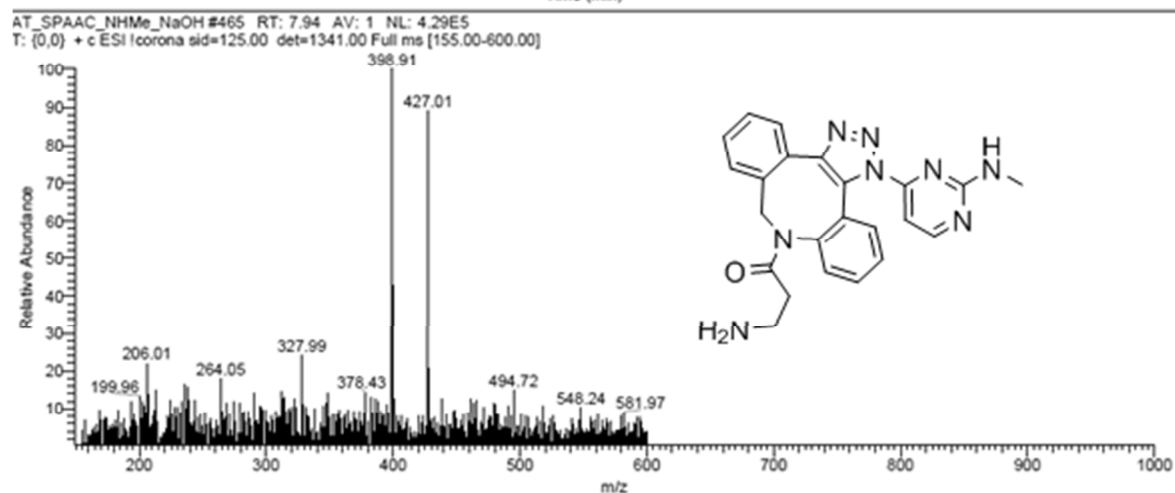
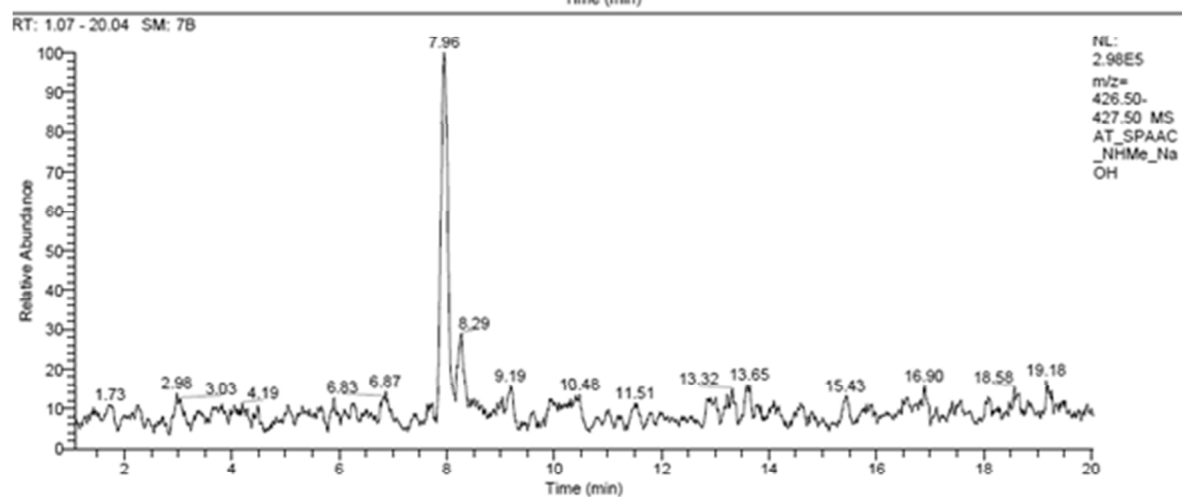
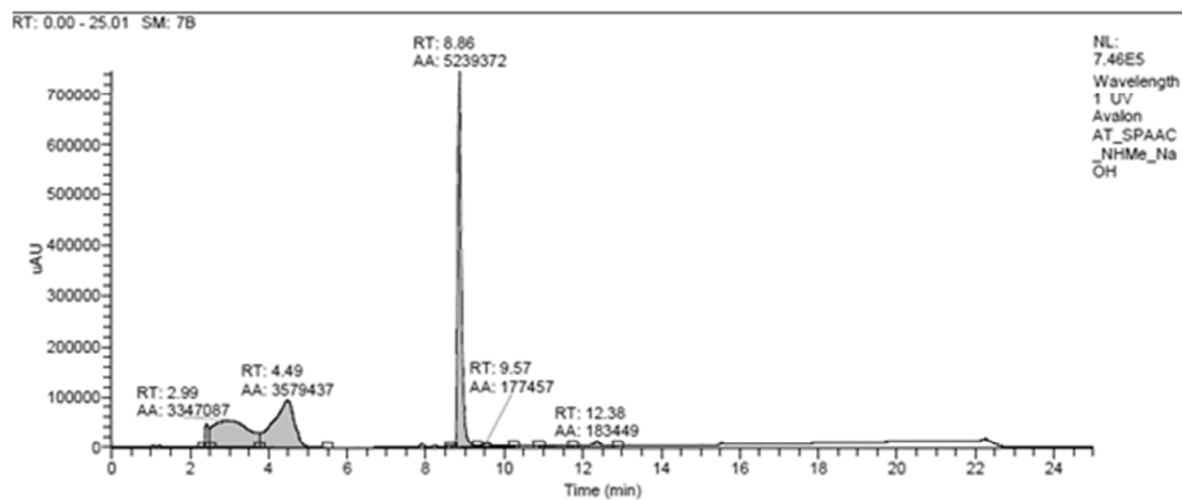
LC-MS Run of **4** under acid conditions (0.2% TFA):

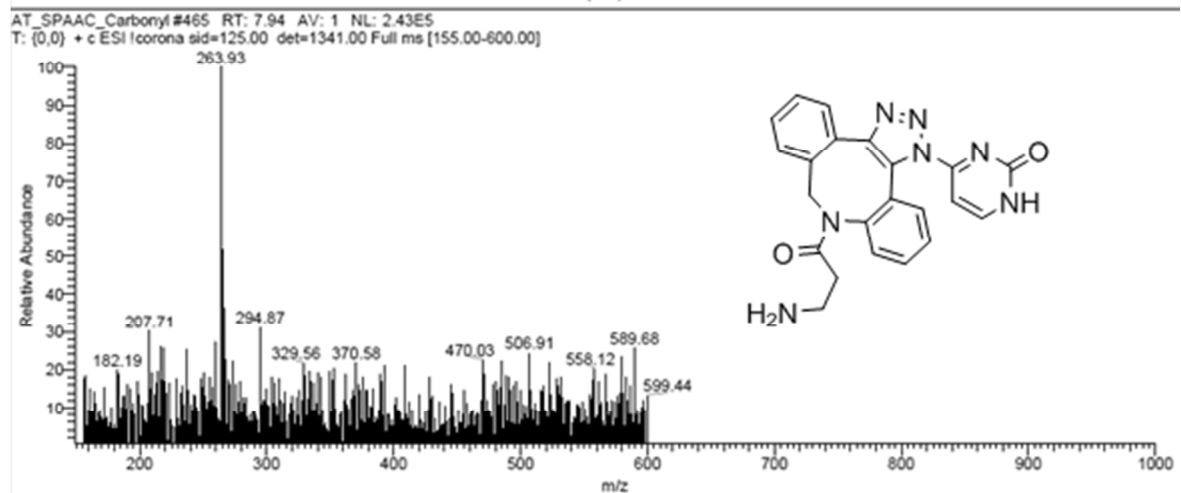
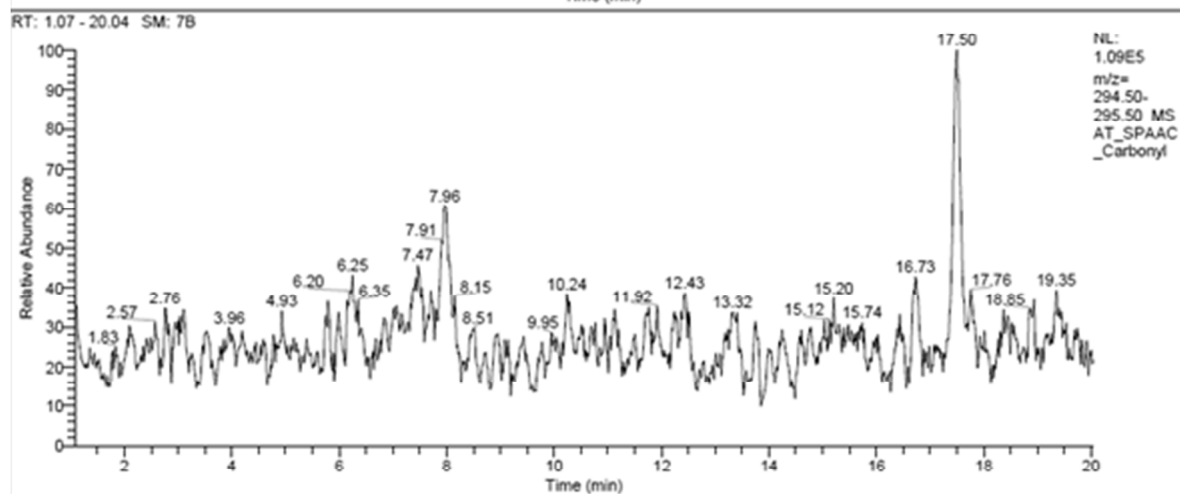
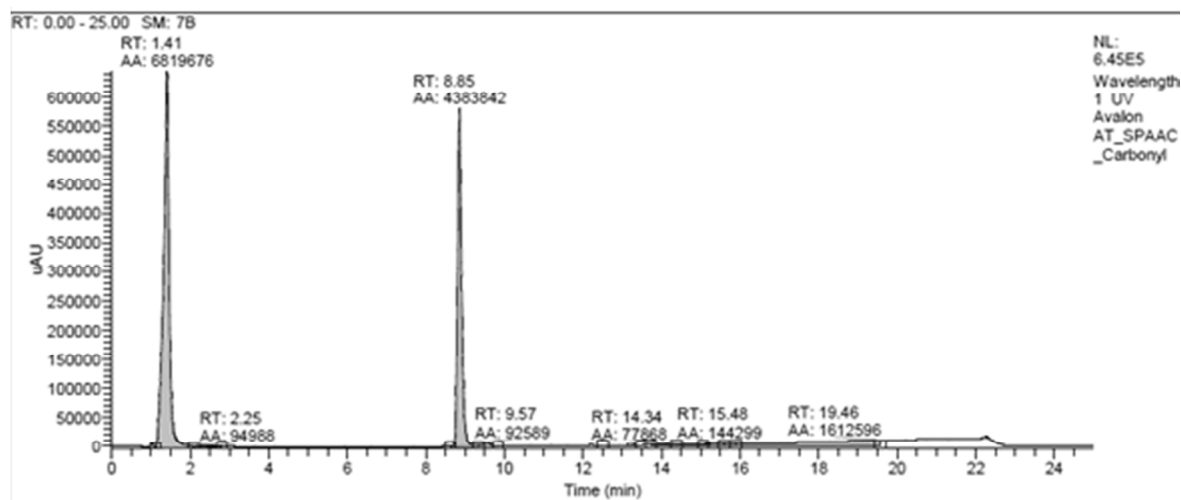


LC-MS Run of **4** under acid conditions (0.1 M HCl):

6 Supporting information

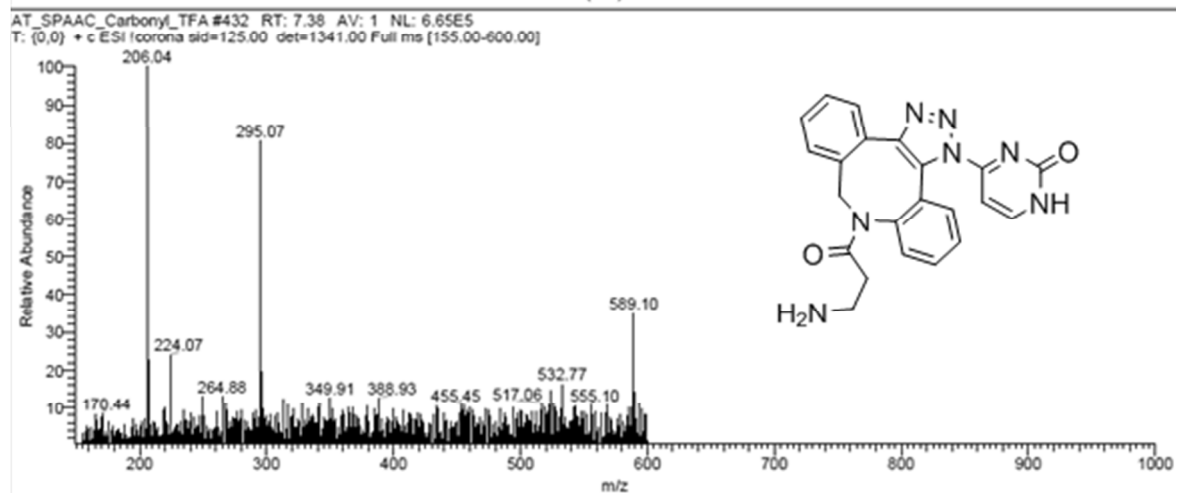
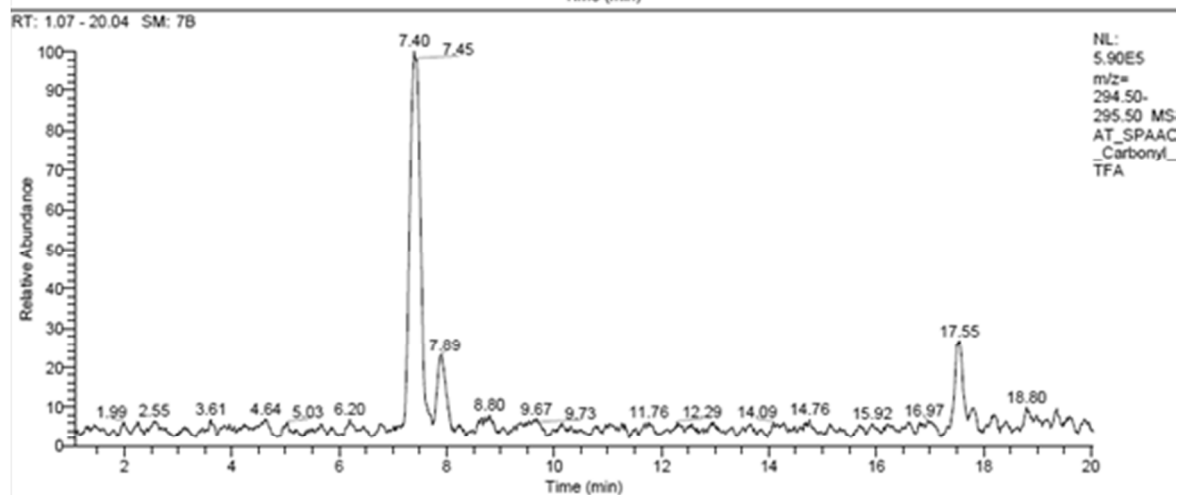
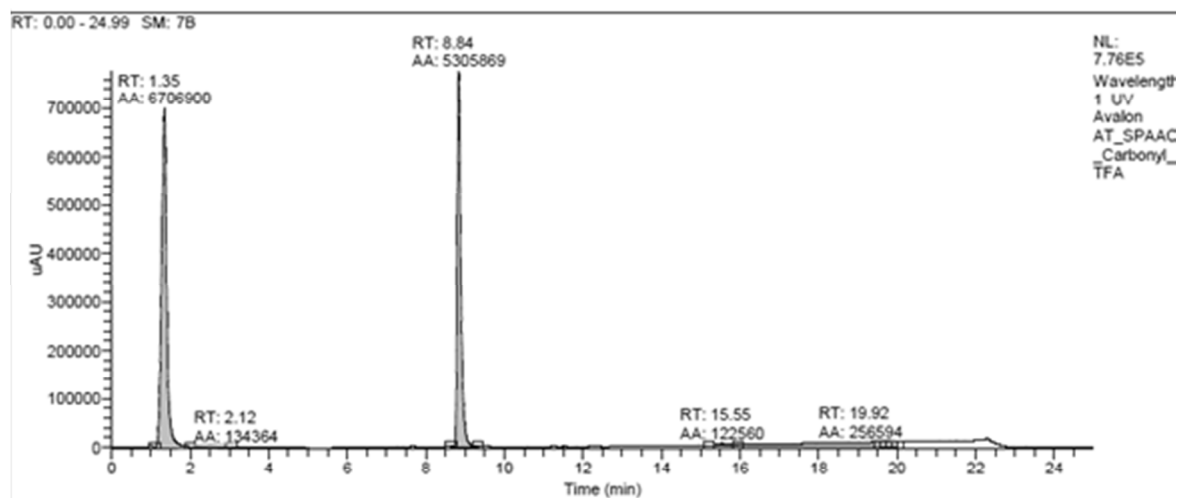
LC-MS Run of **4** under basic conditions (0.1 M NaOH):

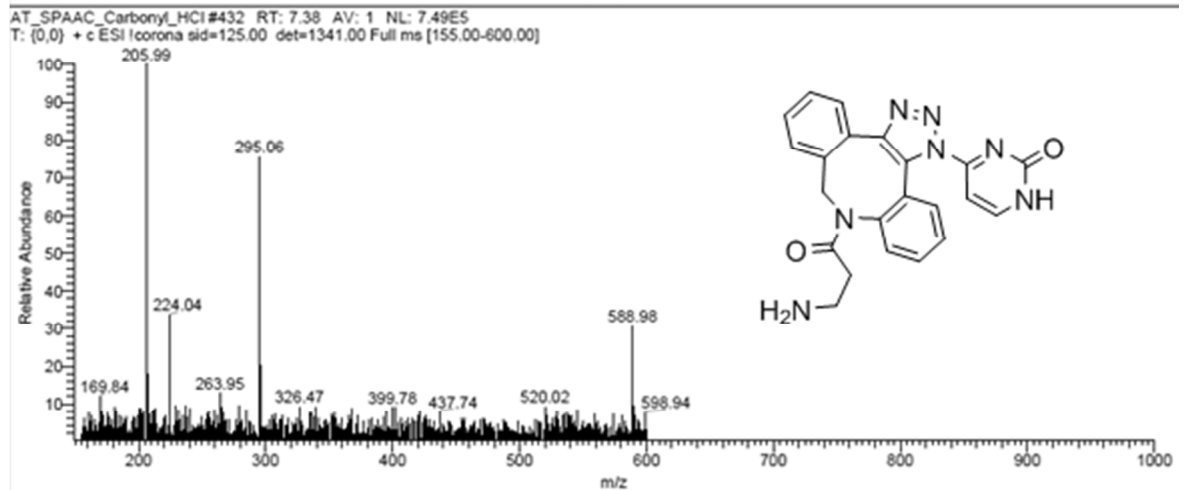
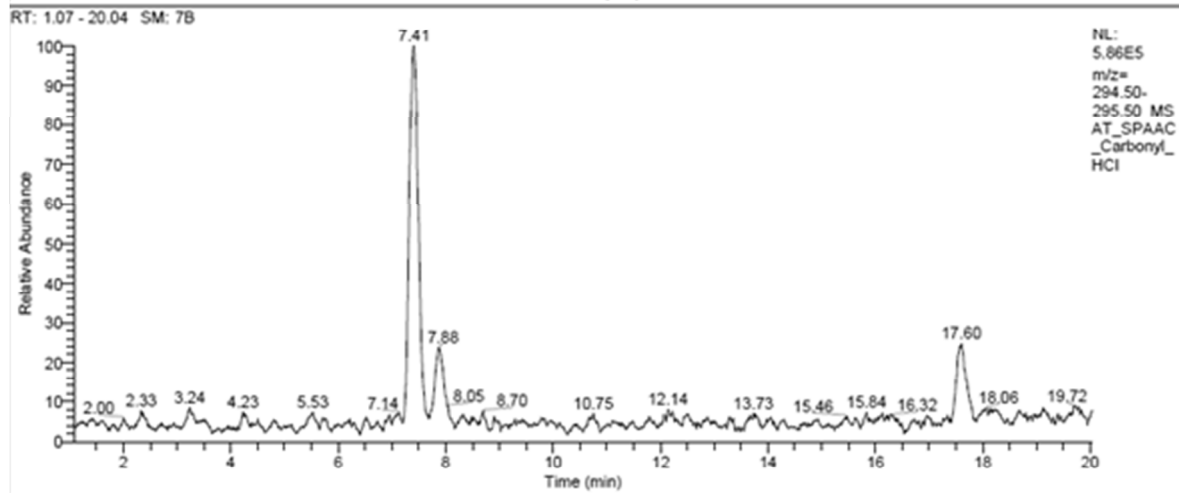
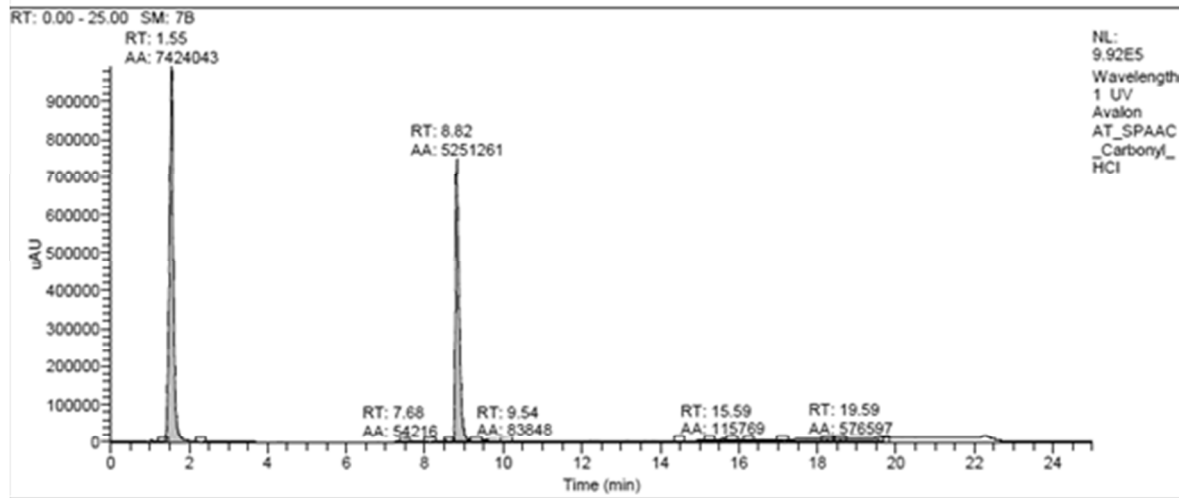


LC-MS Run of **5** under neutral conditions

6 Supporting information

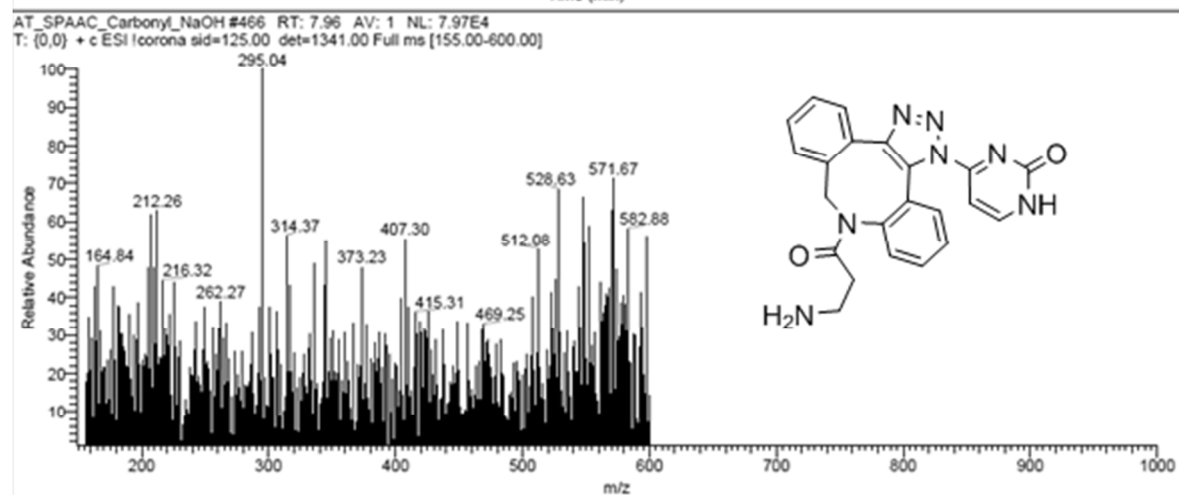
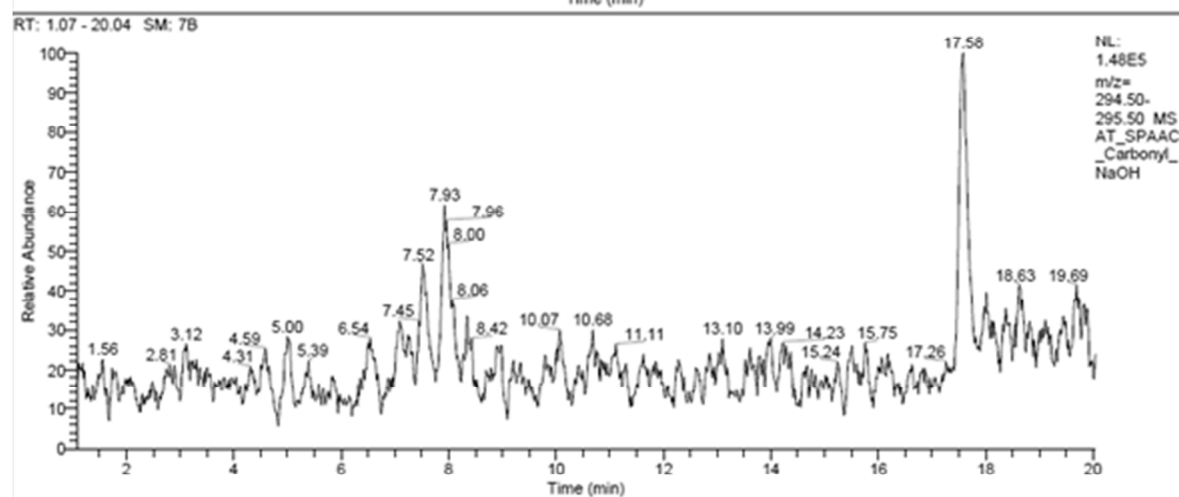
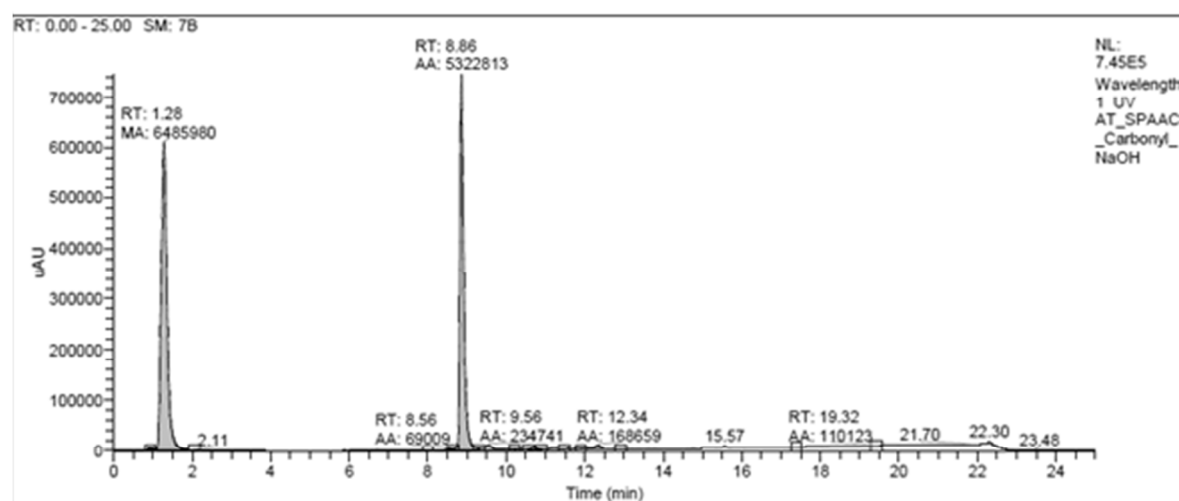
LC-MS Run of **5** under acid conditions (0.2%TFA)



LC-MS Run of **5** under acid conditions (0.1 M HCl)

6 Supporting information

LC-MS Run of **5** under basic conditions (0.1 M NaOH)



i) SPAAC reactionkinetic of 4 at pH 1.5, 2.5 and 4.1 and 15 at pH 1.4 and pH 7.0**Compound 4:*****pH 1.5***

Time [min]	AUC of 4 [mAU]	4 [%]	AUC of product [mAU]	Product [%]
30	5734933	91.7	518946	8.3
60	5602499	83.6	1101498	16.4
90	5268856	77.8	1499674	22.2
120	5003182	72.2	1924425	27.8
150	4871904	67.8	2311144	32.2
180	1370705	63.7	779760	36.3

pH 2.5

Time [min]	AUC of 4 [mAU]	4 [%]	AUC of product [mAU]	Product [%]
30	5695140	97.6	138559	2.4
60	5178777	96.1	210430	3.9
90	5230687	95.5	244025	4.5
120	5262583	94.1	329738	5.9
150	5207051	92.8	403243	7.2
180	5176146	91.9	455522	8.1

6 Supporting information

pH 4.1

Time [min]	AUC of 4 [mAU]	4 [%]	AUC of product [mAU]	Product [%]
30	4860187	99.3	31833	0.7
60	4855123	98.5	74656	1.5
90	5065370	98.1	99397	1.9
120	5005964	97.8	114435	2.2
150	5102021	97.5	132920	2.5
180	5058522	97.5	129192	2.5

Compound 15:

pH 1.4

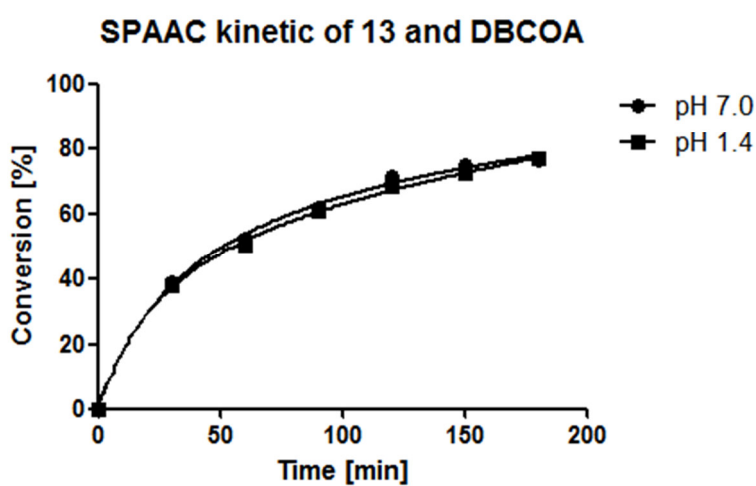
Time [min]	AUC of DBCOA ^a [mAU]	DBCOA ^a [%]	AUC of product [mAU]	Product [%]
30	3749764	62.2	2281874	37.8
60	3128959	49.9	3138413	50.1
90	2705288	39.2	4199670	60.8
120	2153357	31.7	4642839	68.3
150	2053435	27.9	5296846	72.1
180	1702508	23.4	5561344	76.6

^aDBCOA = Dibenzocyclooctyne-amine

pH 7.0

Time [min]	AUC of DBCOA ^a [mAU]	DBCOA ^a [%]	AUC of product [mAU]	Product [%]
30	2912988	61.2	1850148	38.8
60	2577175	47.8	2812106	52.2
90	1980938	38.1	3220216	61.9
120	1698357	28.9	4181186	71.1
150	1483145	25.2	4412387	74.8
180	1387631	23.5	4528455	76.5

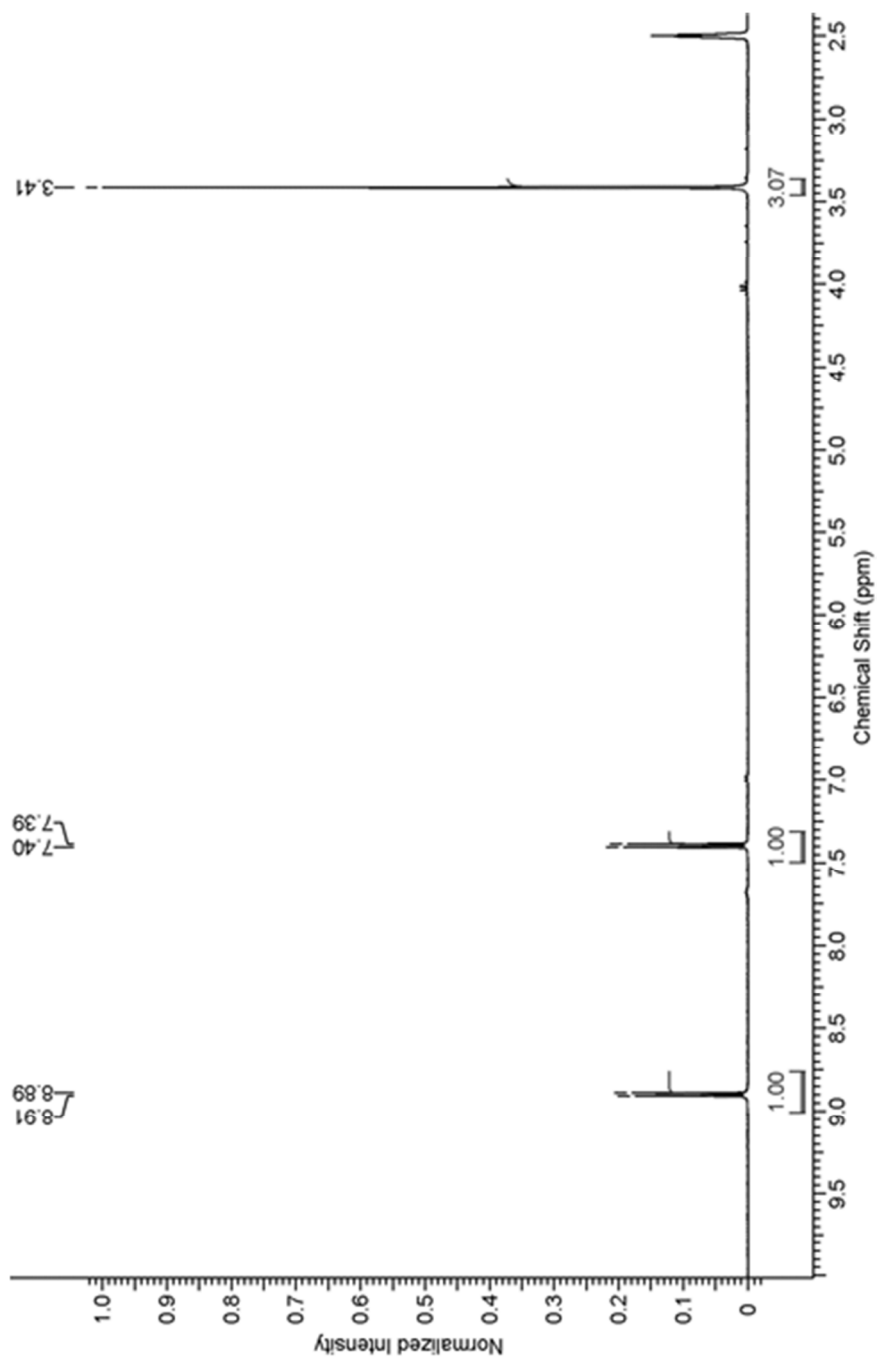
^aDBCOA = Dibenzocyclooctyne-amine

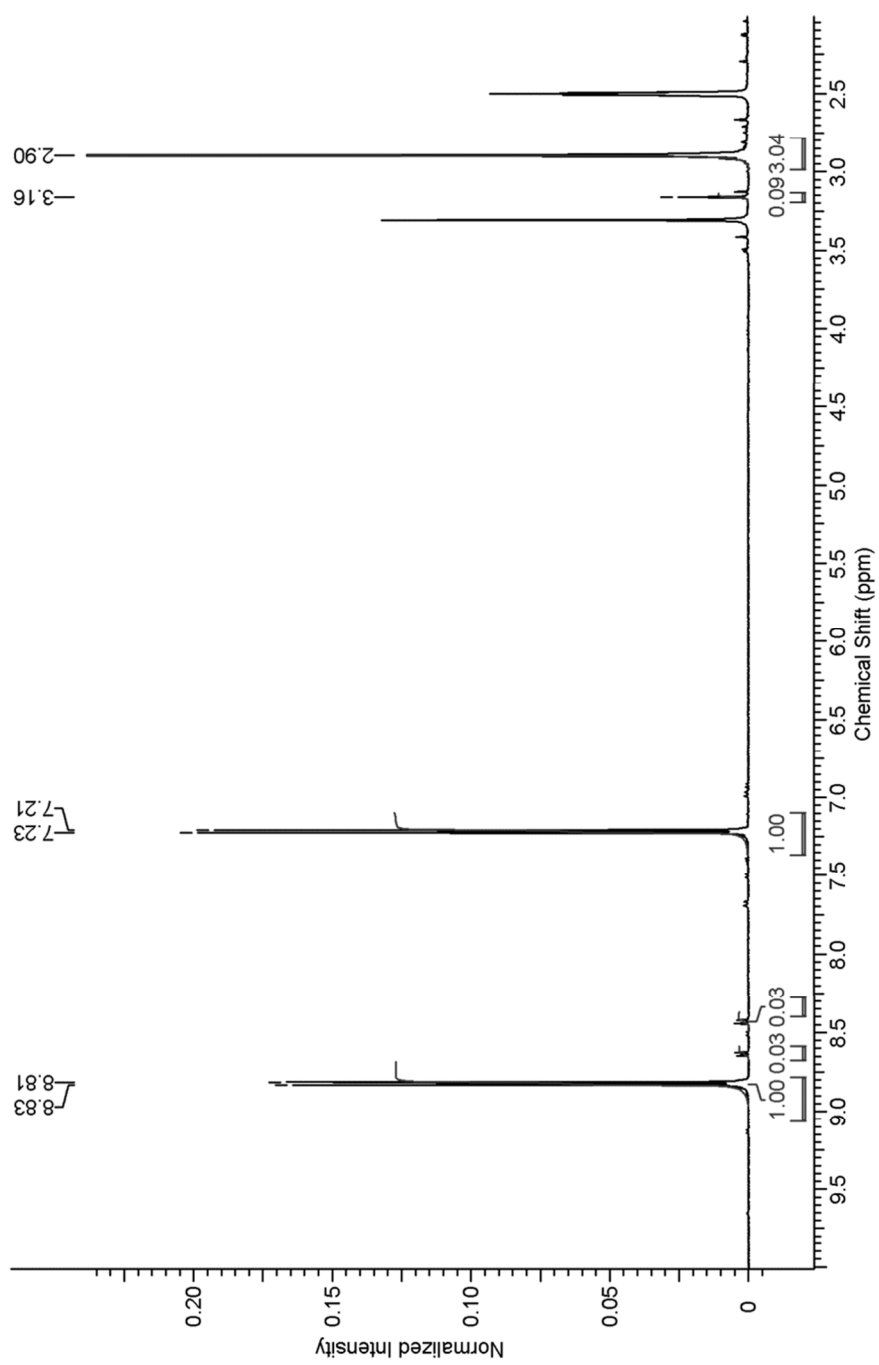


II. Spectral Data

a) $^1\text{H-NMR}$ Spectra

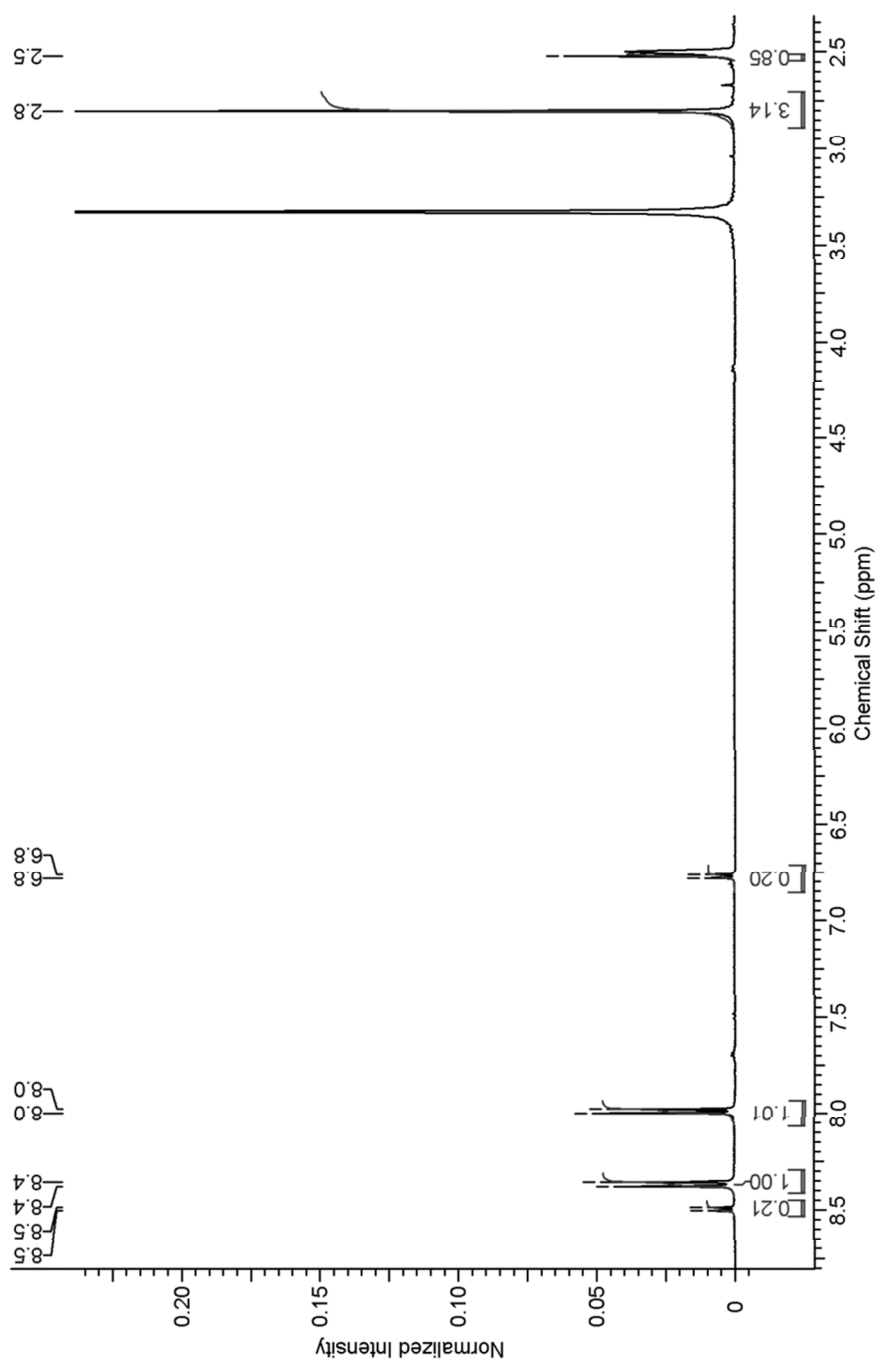
$^1\text{H-NMR}$ of 1

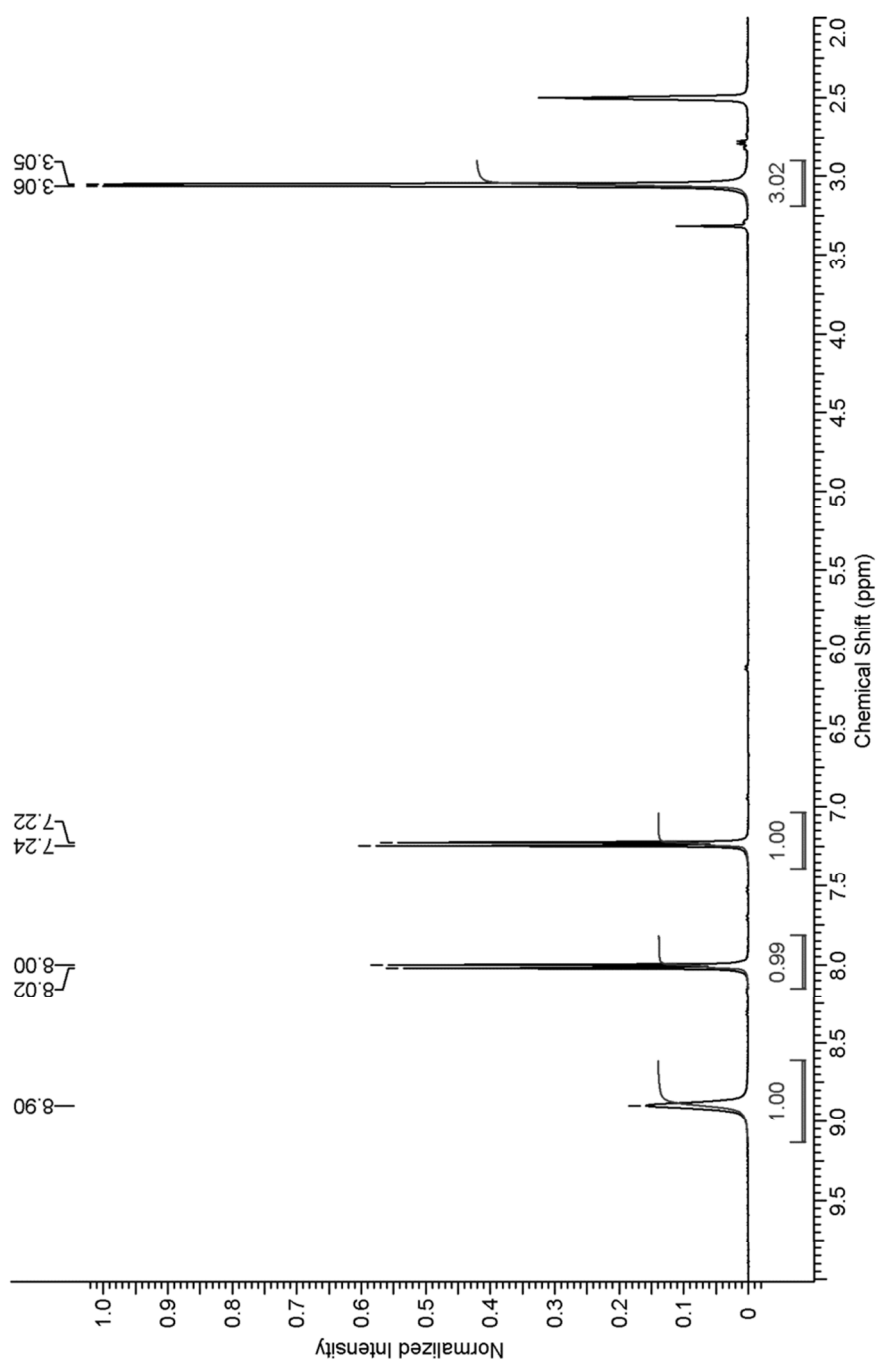


$^1\text{H-NMR}$ of **2**

6 Supporting information

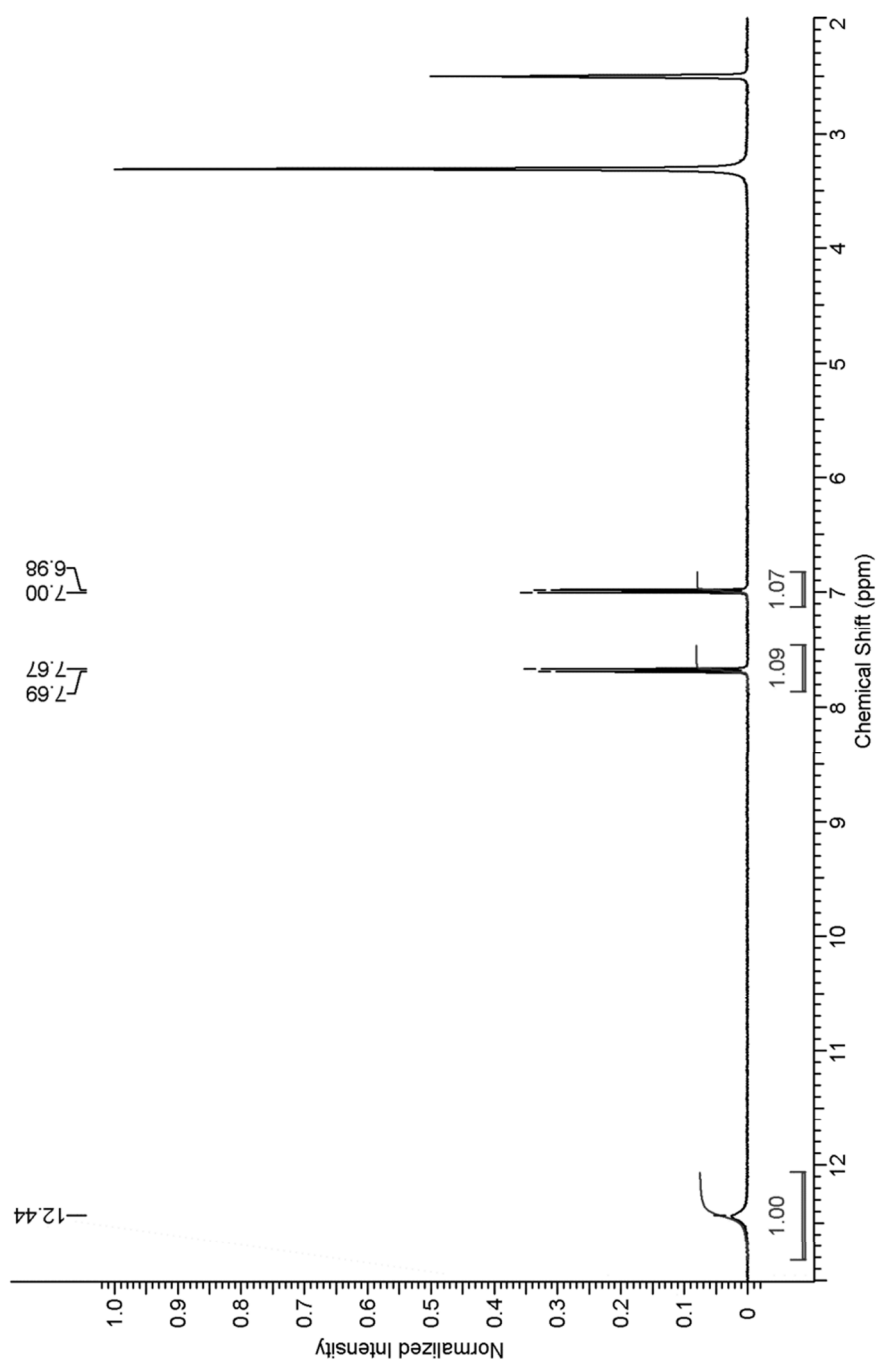
$^1\text{H-NMR}$ of **3**

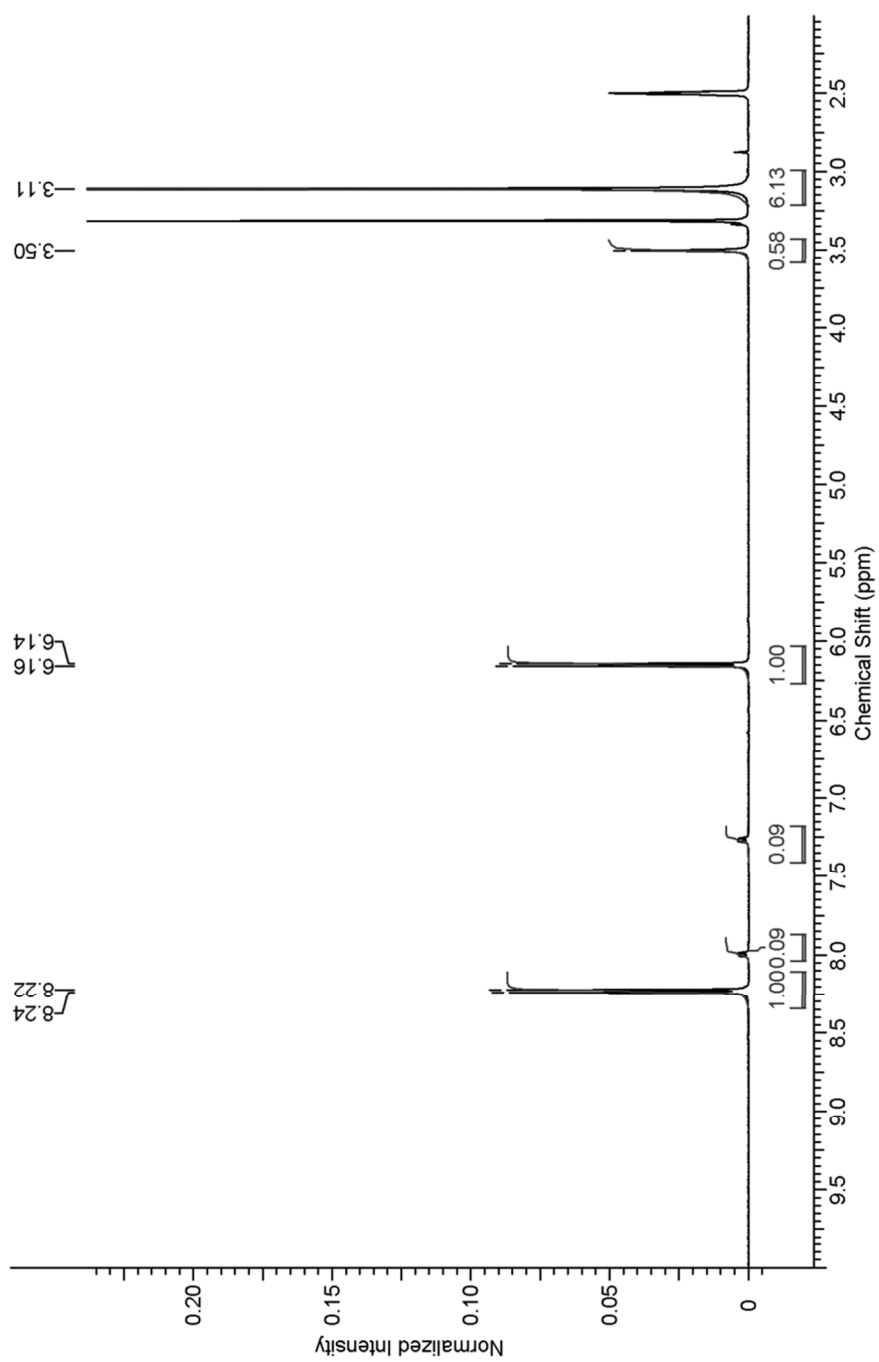


$^1\text{H-NMR}$ of **4**

6 Supporting information

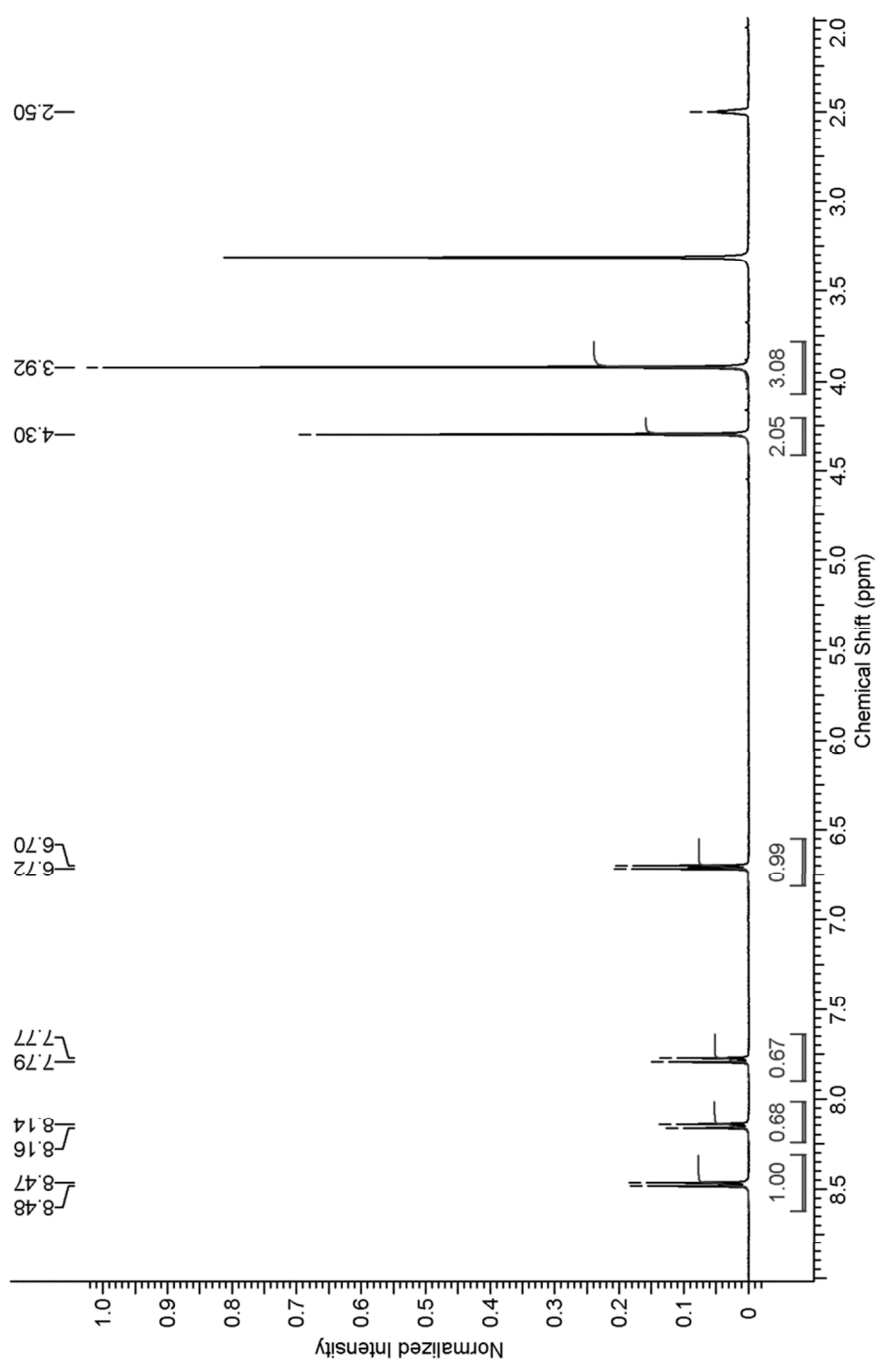
$^1\text{H-NMR}$ of **5**

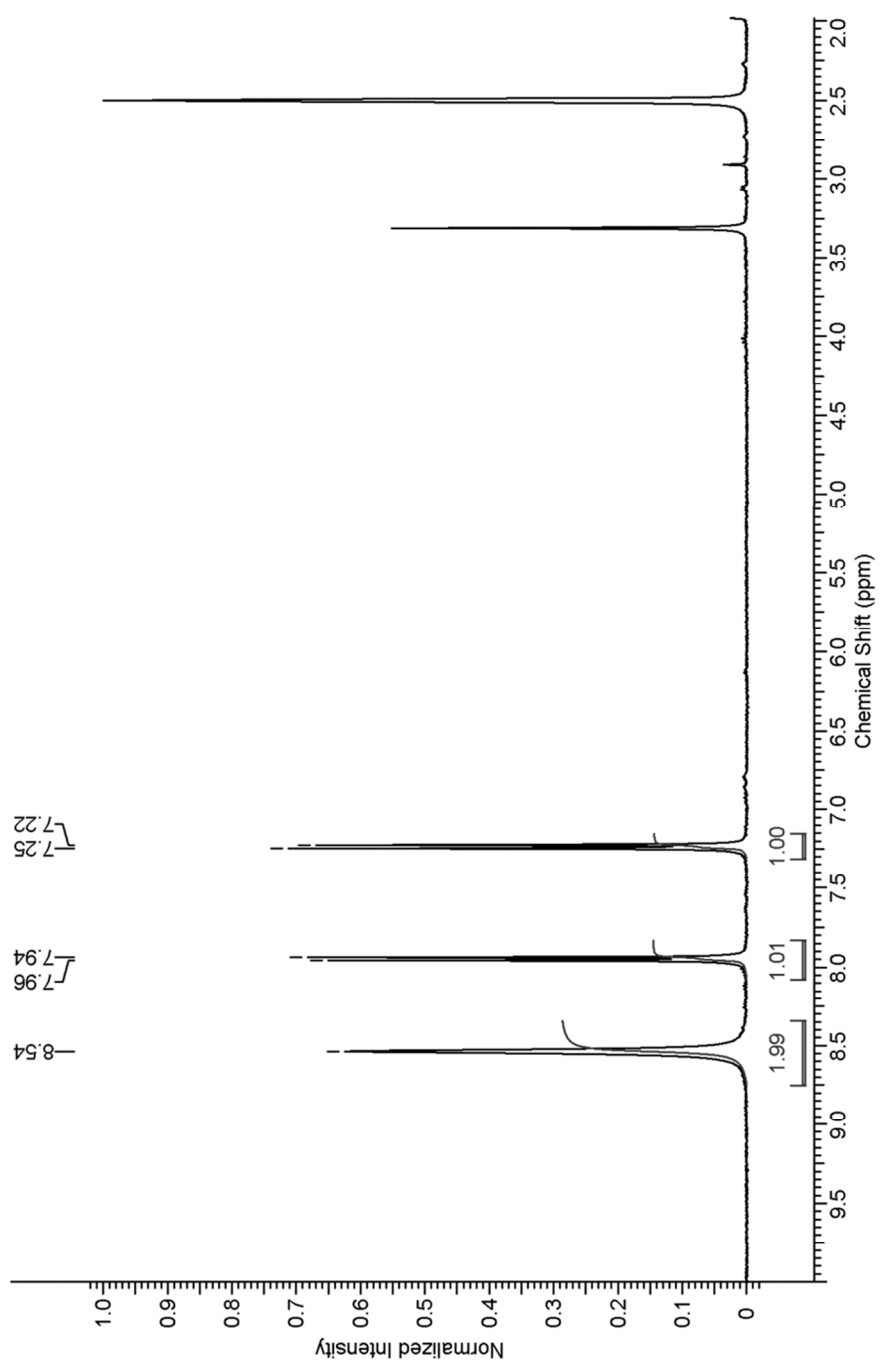


$^1\text{H-NMR}$ of **6**

6 Supporting information

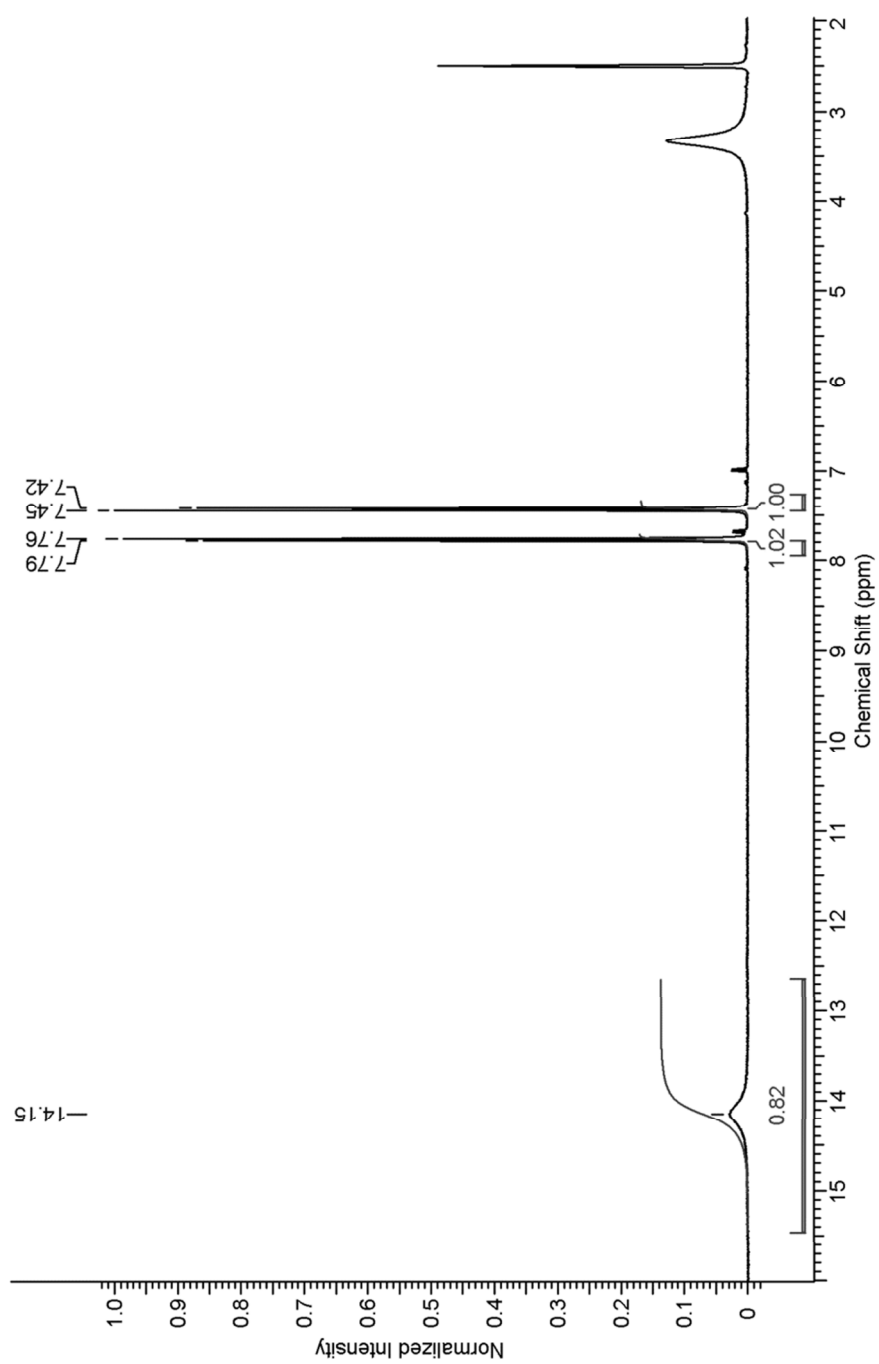
$^1\text{H-NMR}$ of **7**



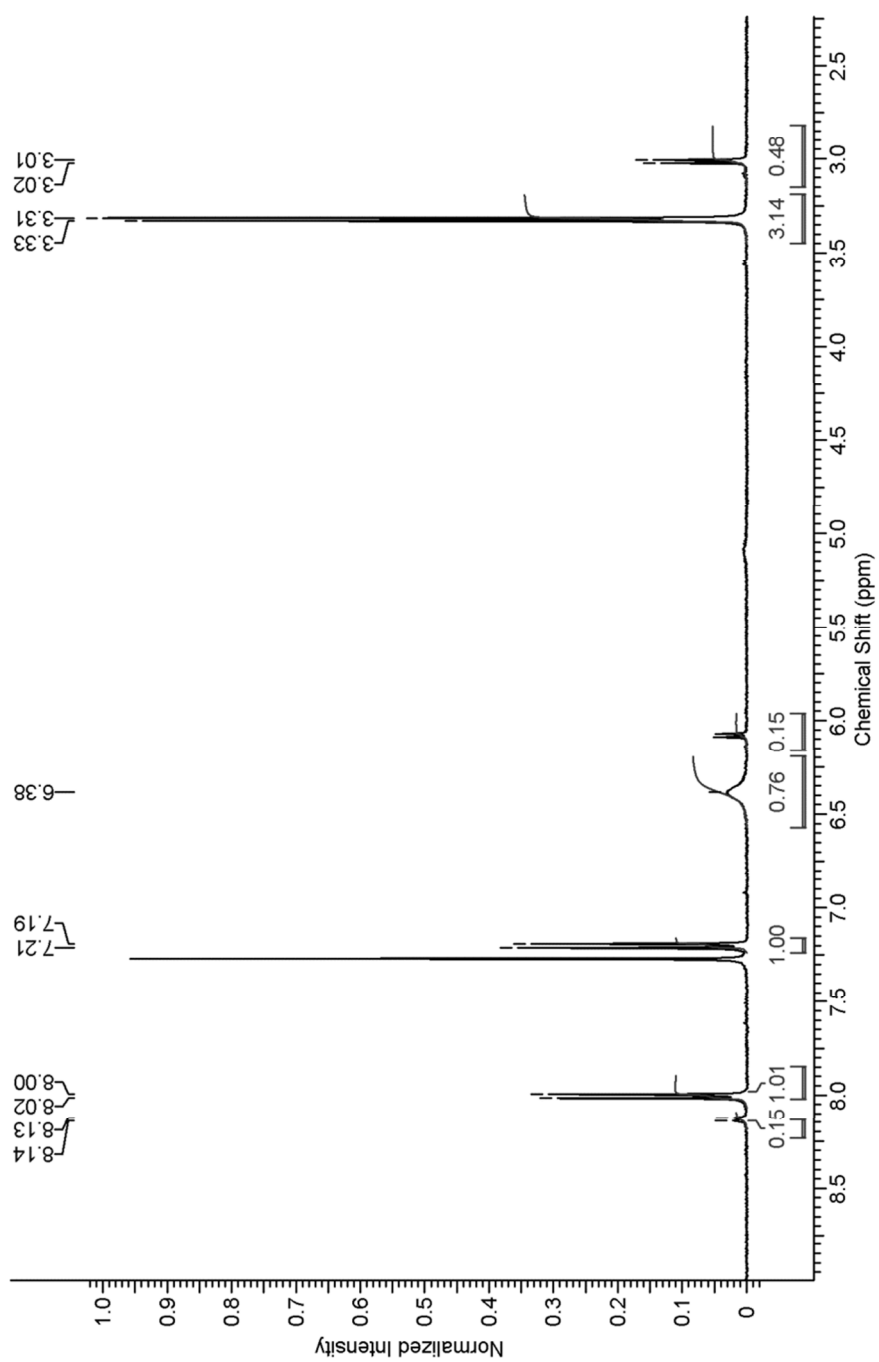
$^1\text{H-NMR}$ of **8**

6 Supporting information

$^1\text{H-NMR}$ of **9**

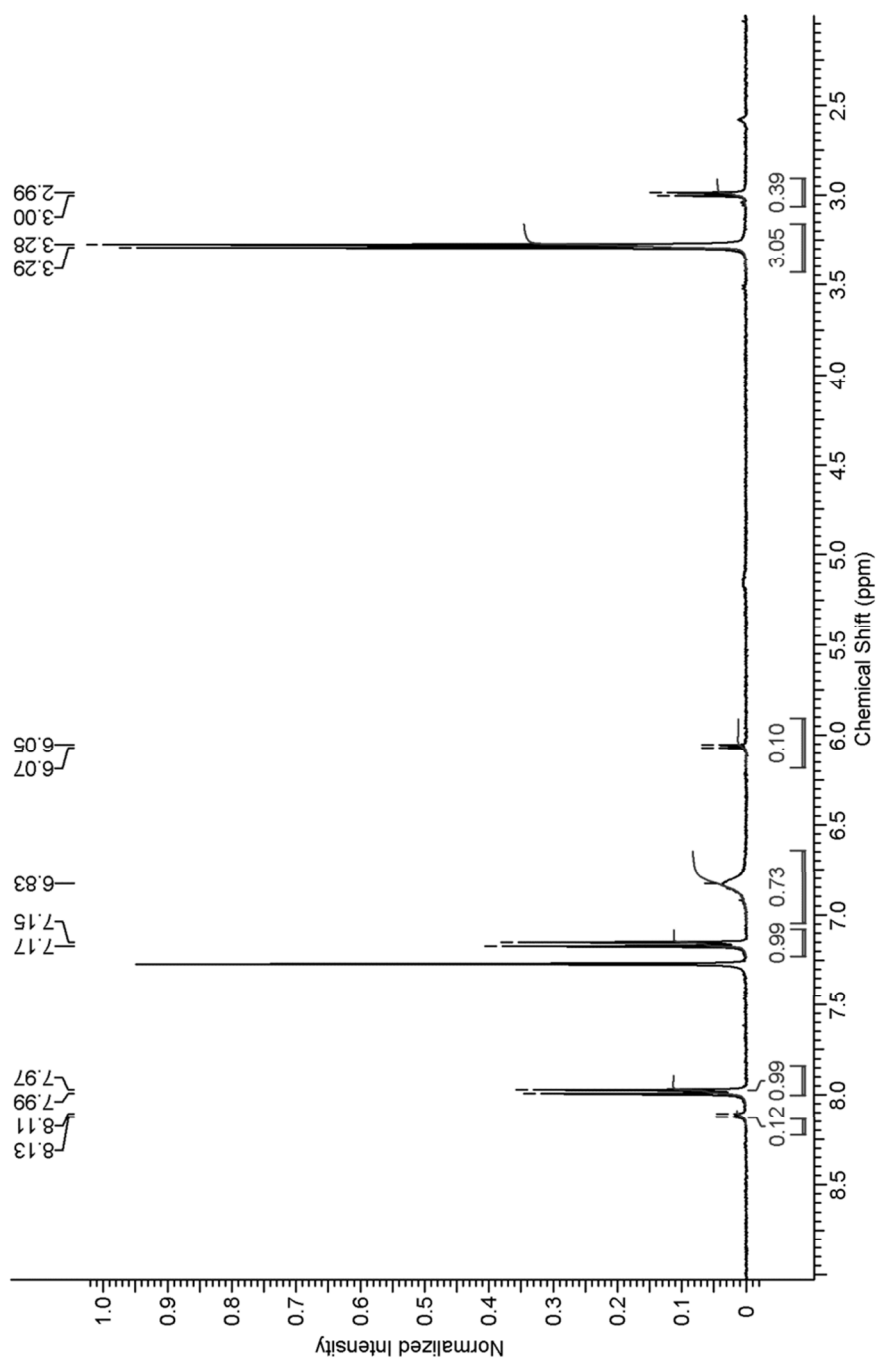


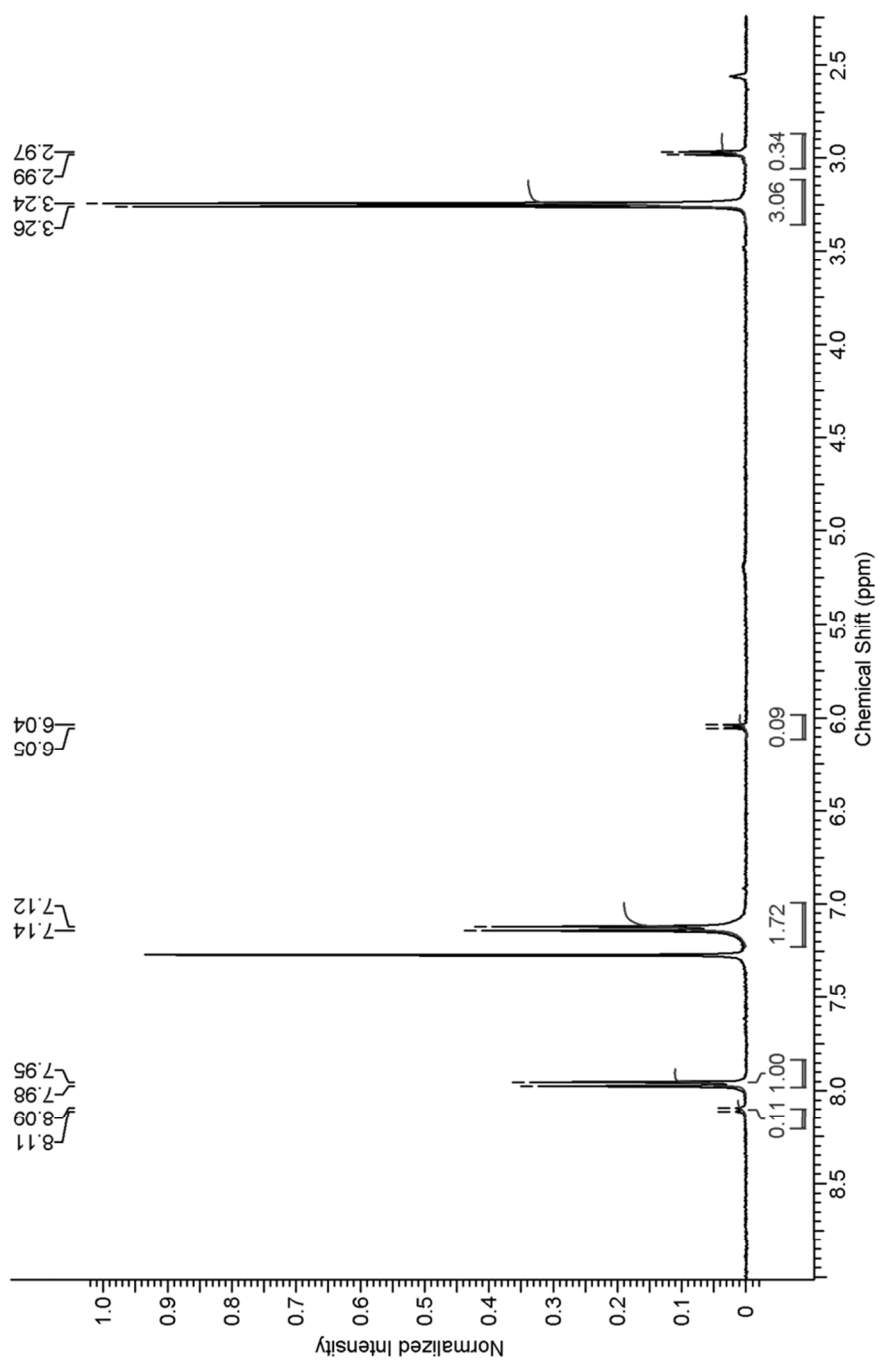
The small peaks close to the dublets at 7.77 and 7.43 are possibly due to thionyl-thiol tautomerization

b) DMSO- d_6 titration of 4 in $CDCl_3$ monitored by 1H -NMR0% DMSO – 1H -NMR of 4 in $CDCl_3$ 

6 Supporting information

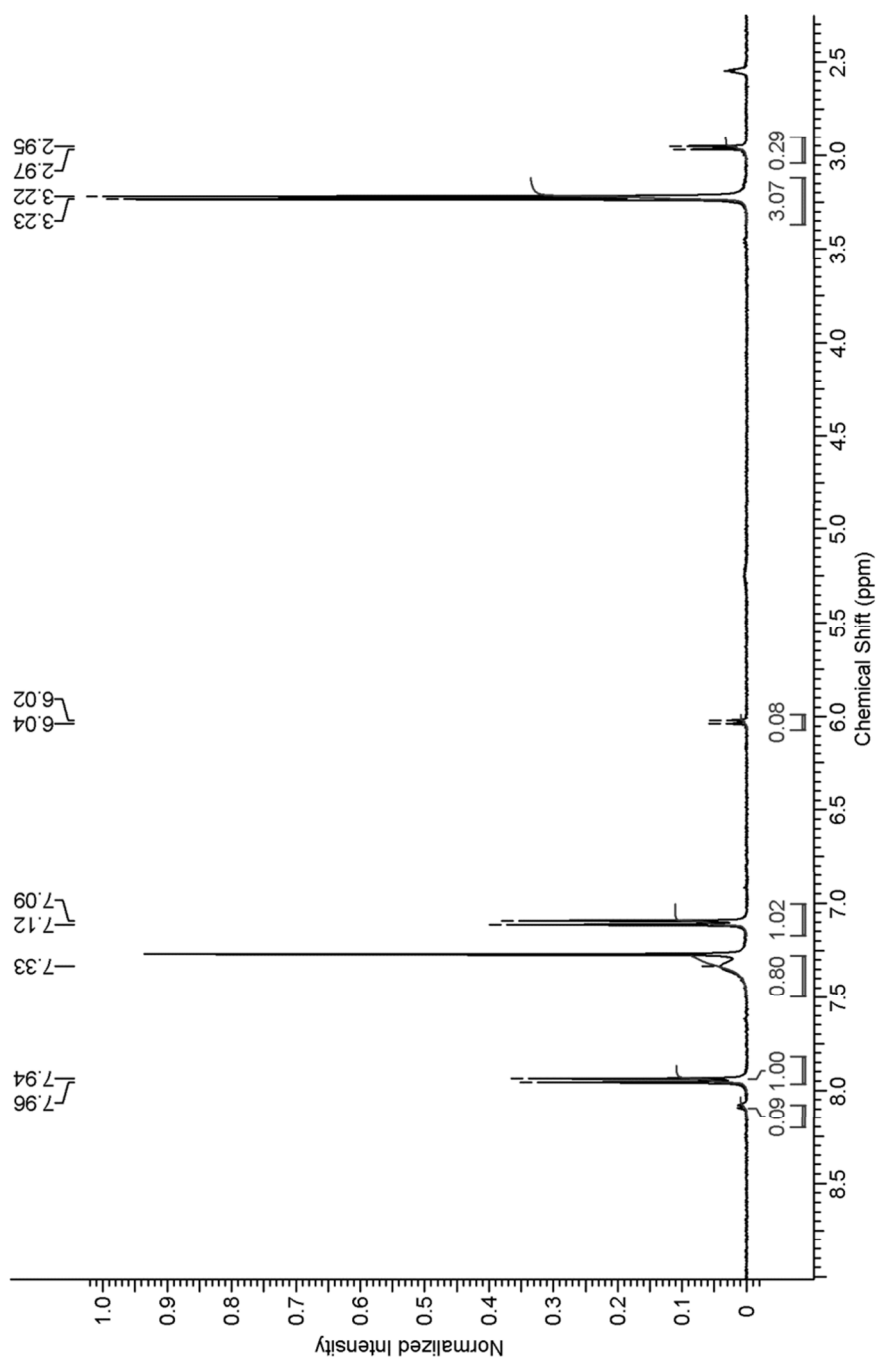
1% DMSO – $^1\text{H-NMR}$ of **4** in CDCl_3

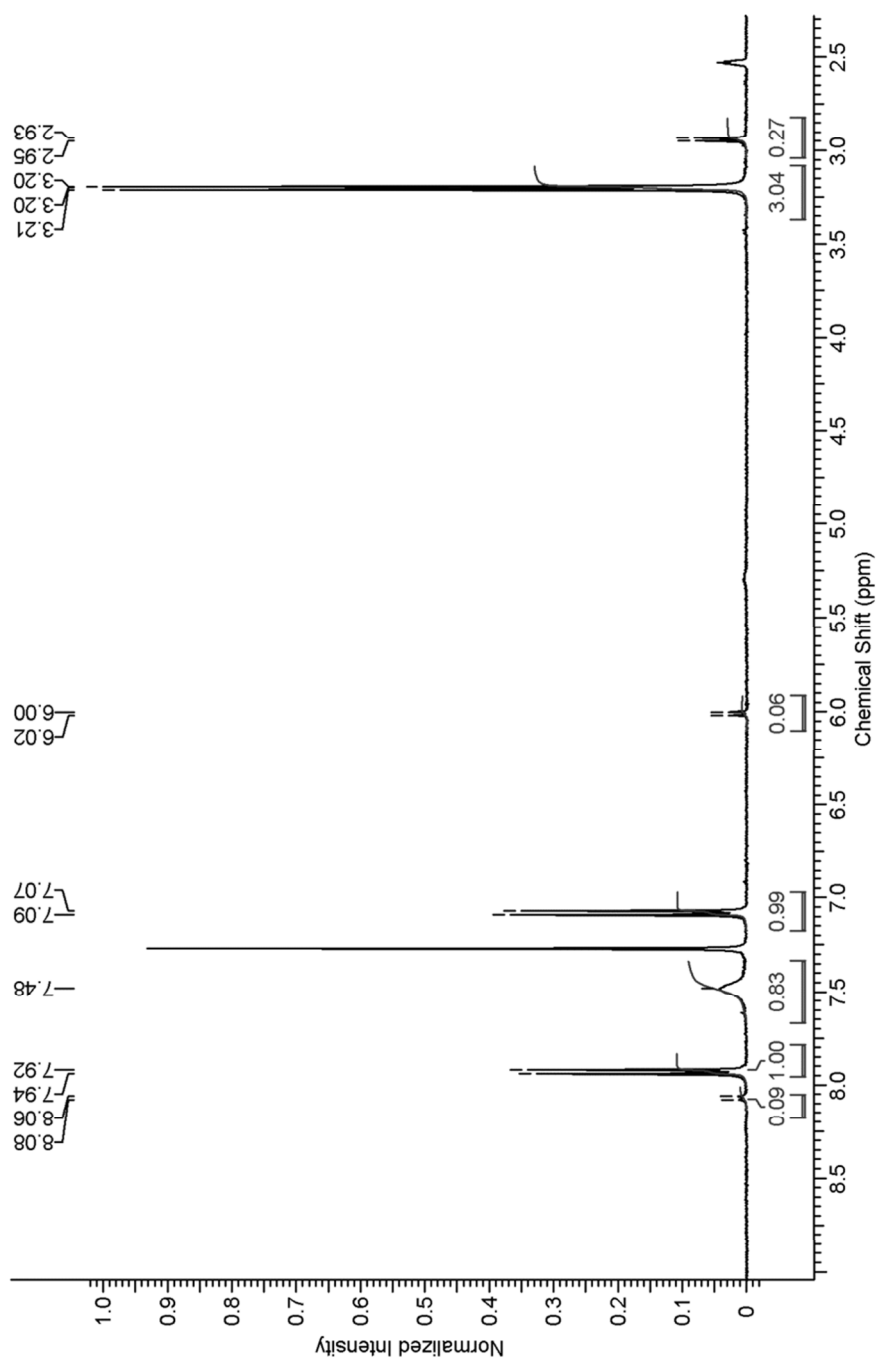


2% DMSO – ^1H -NMR of **4** in CDCl_3 

6 Supporting information

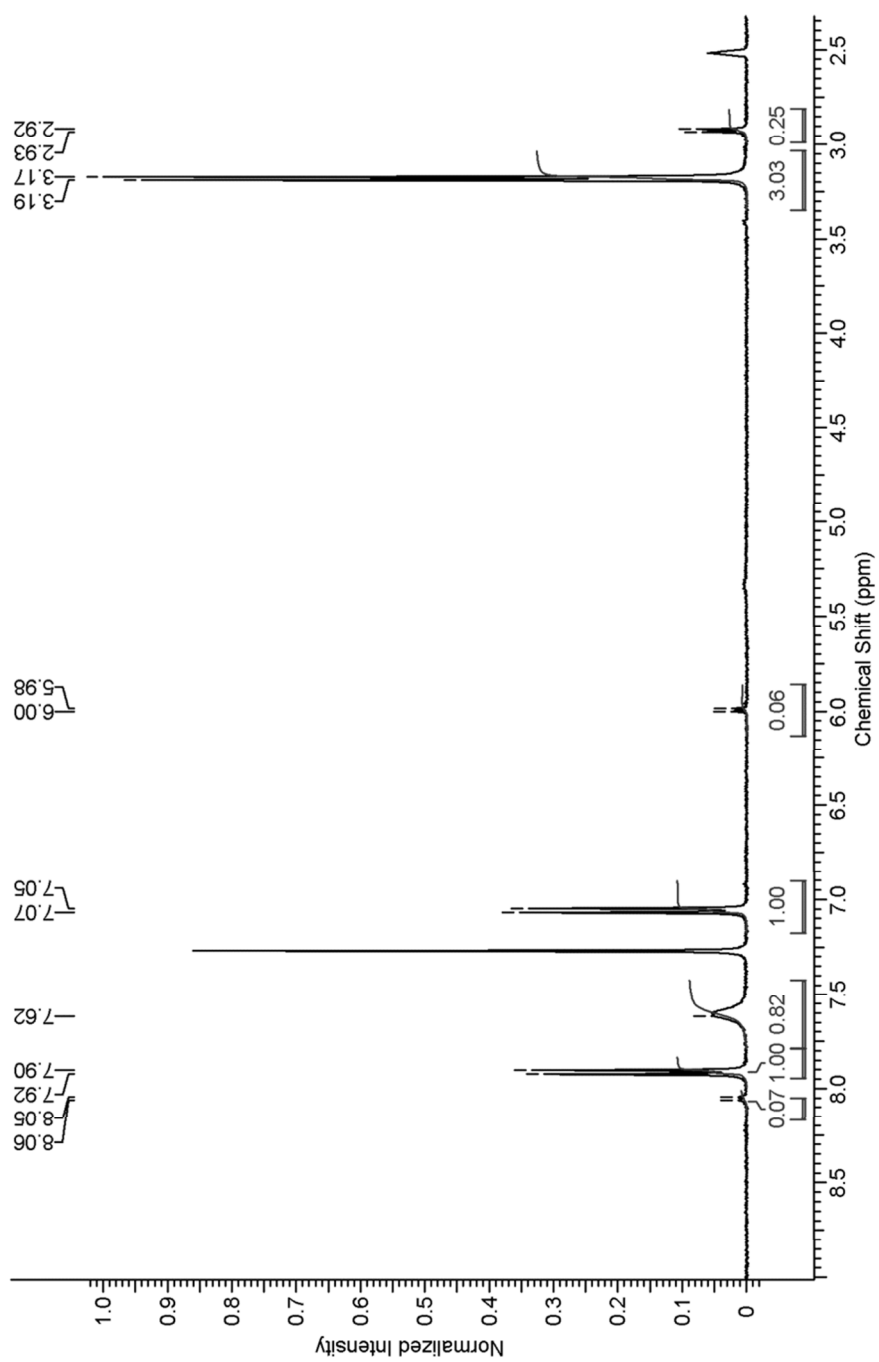
2.9% DMSO – $^1\text{H-NMR}$ of **4** in CDCl_3

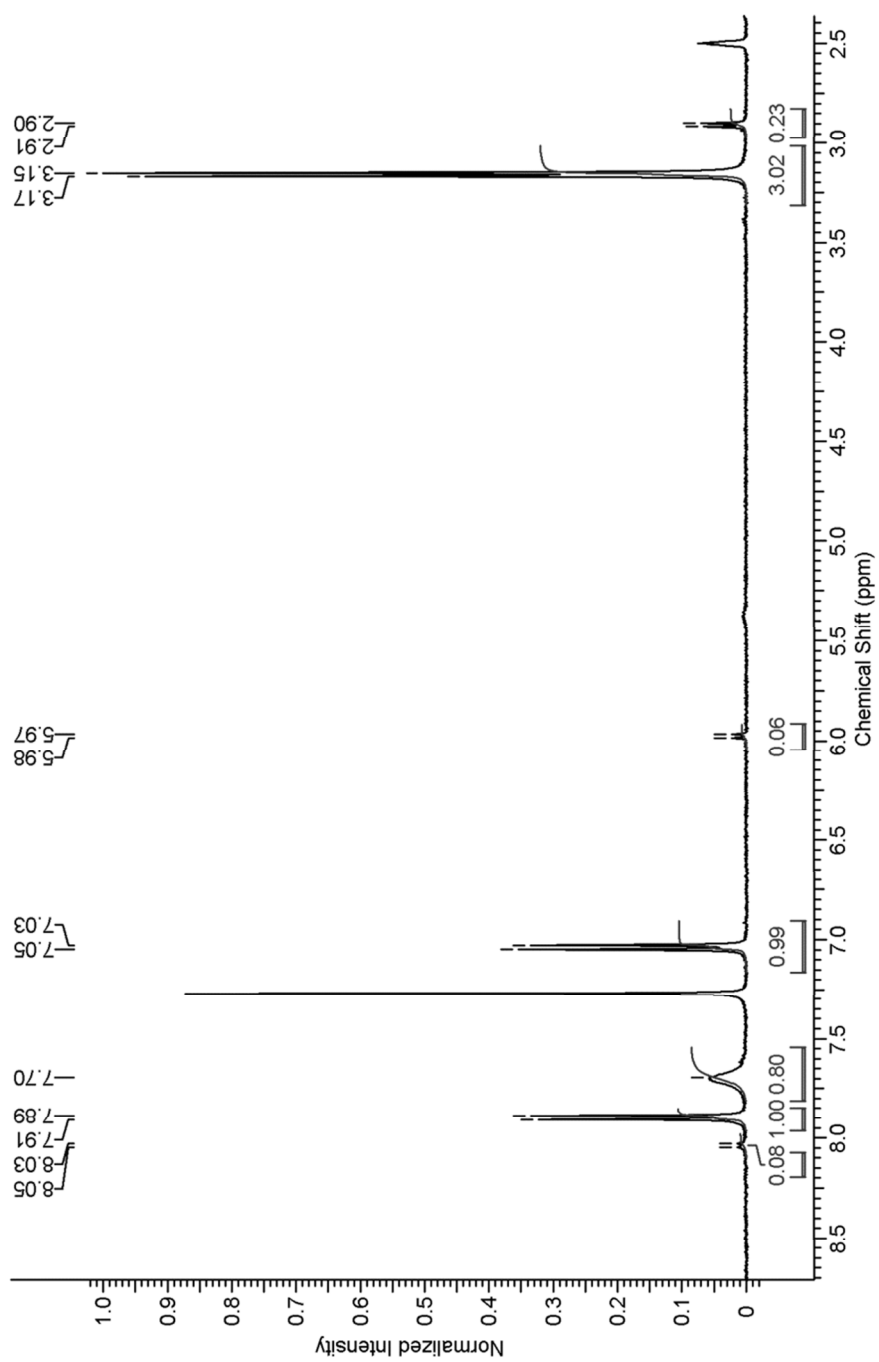


3.8% DMSO – $^1\text{H-NMR}$ of **4** in CDCl_3 

6 Supporting information

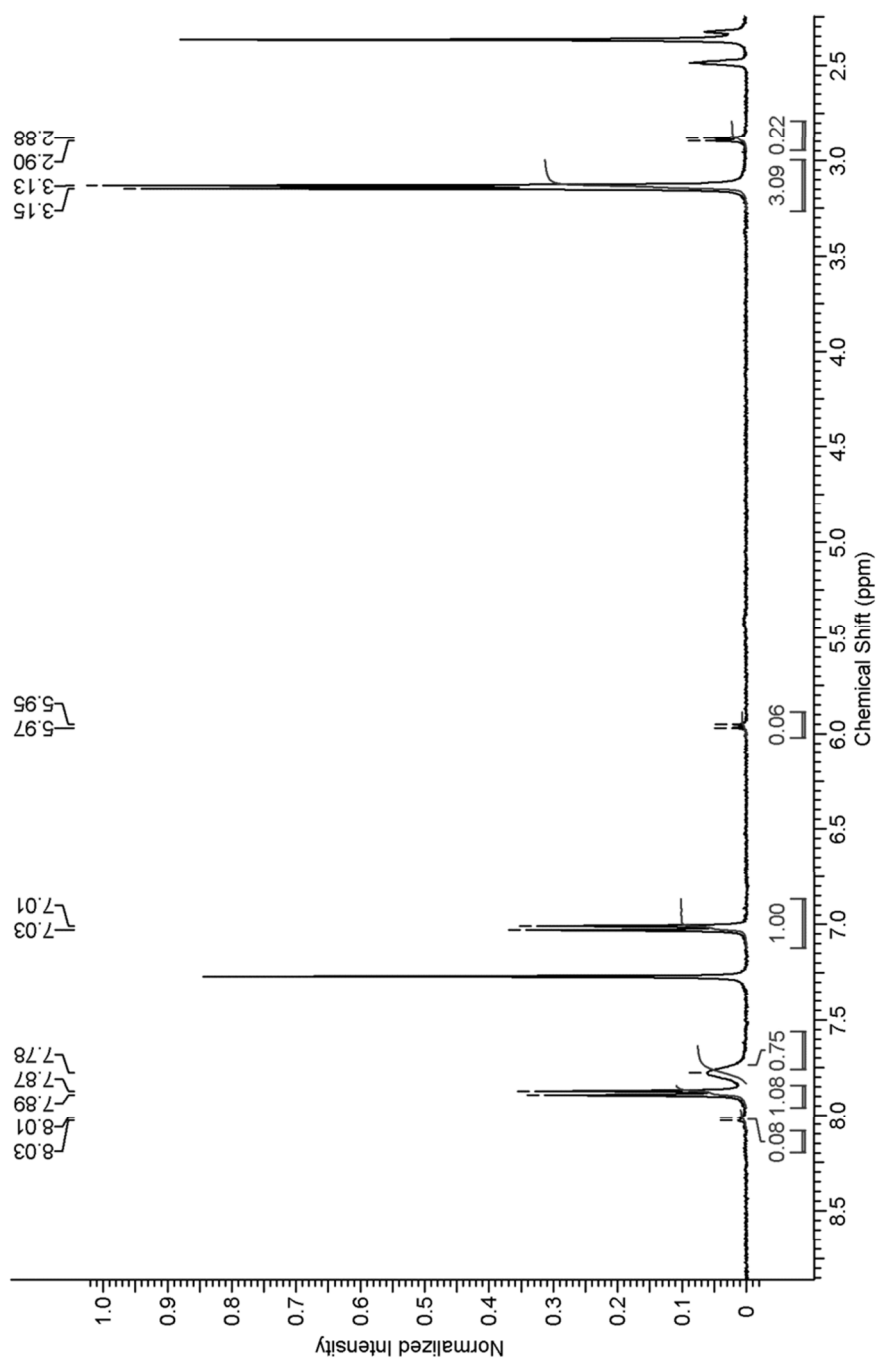
4.8% DMSO – $^1\text{H-NMR}$ of **4** in CDCl_3

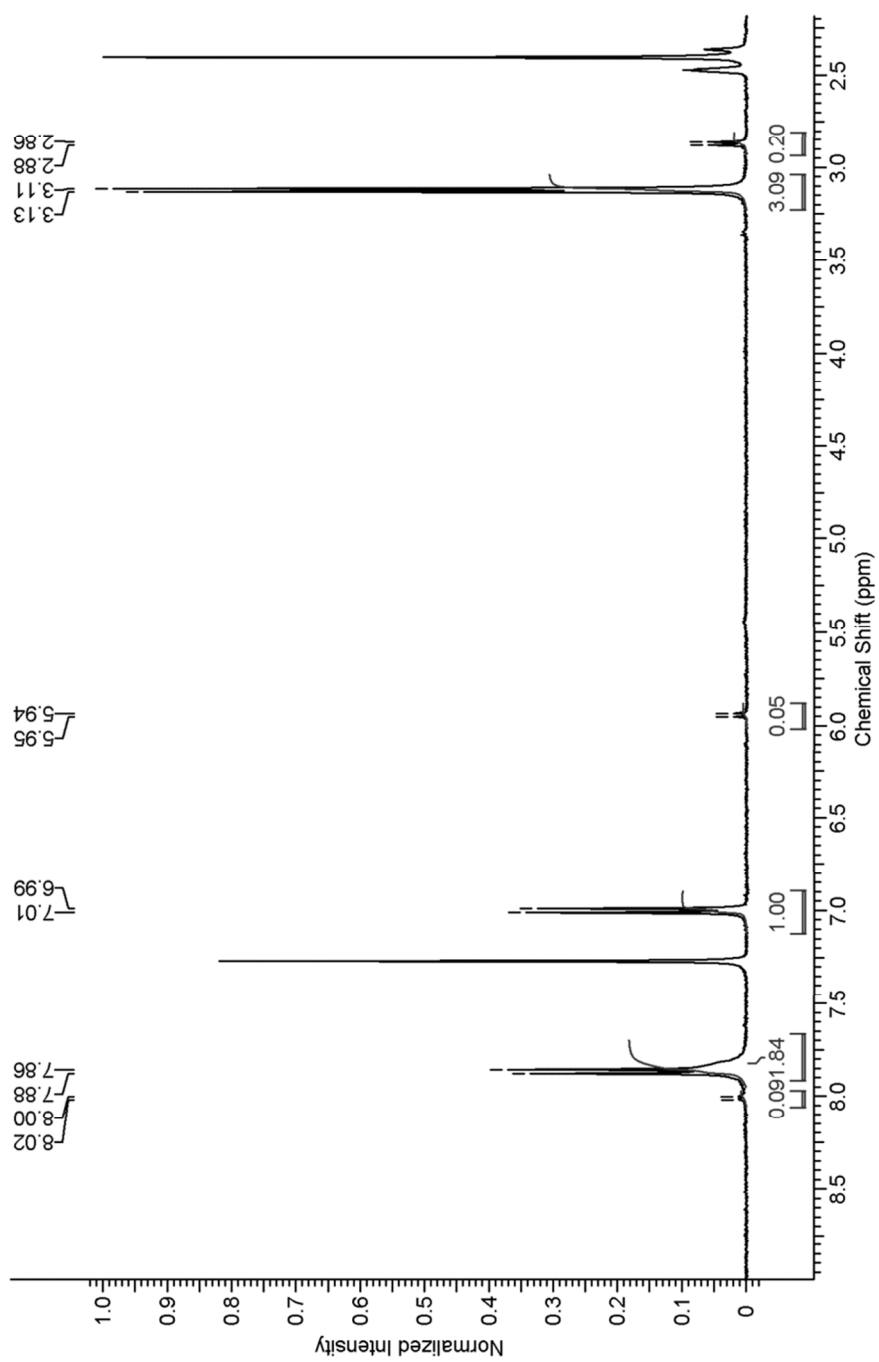


5.7% DMSO – $^1\text{H-NMR}$ of **4** in CDCl_3 

6 Supporting information

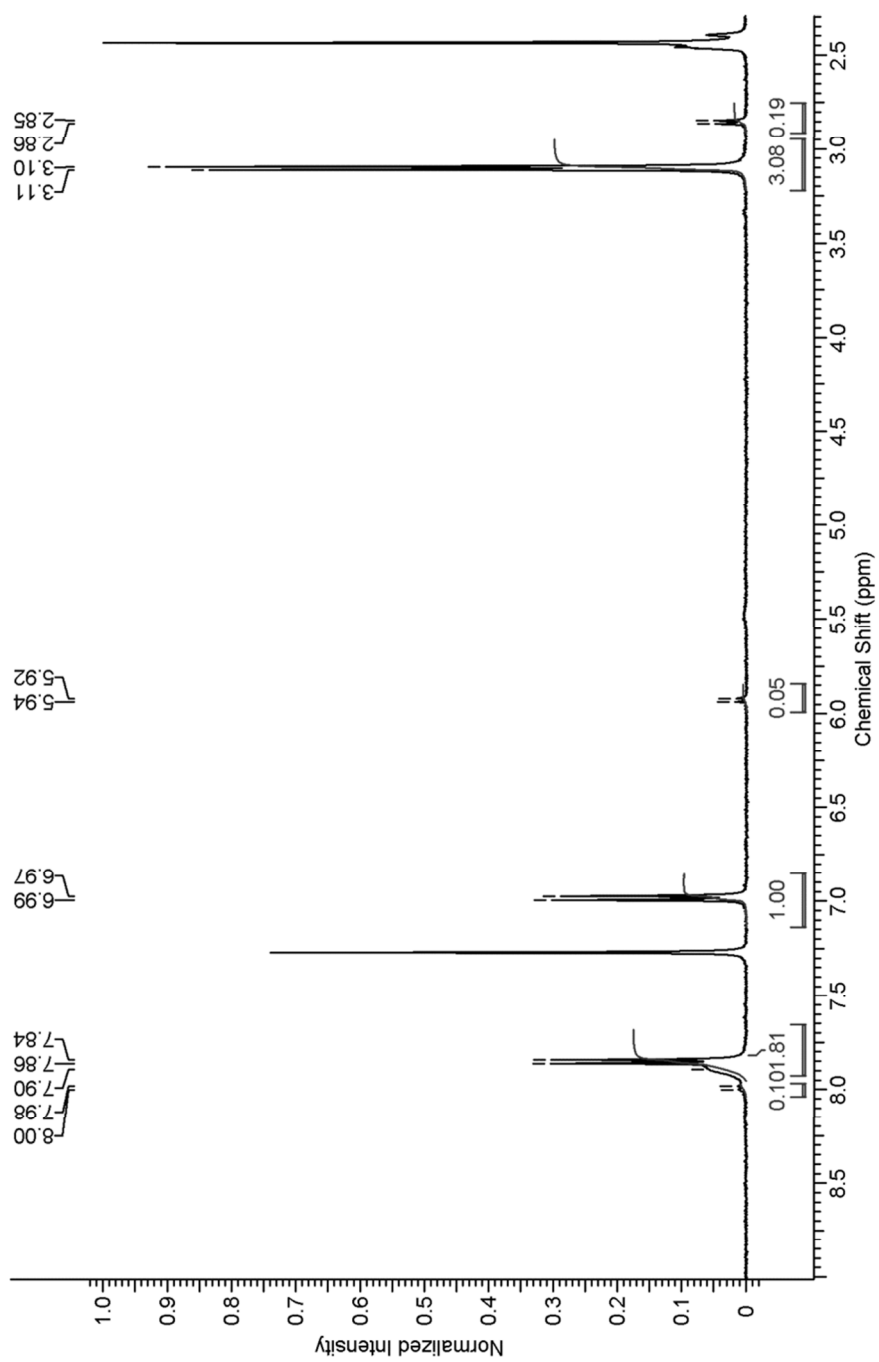
6.4% DMSO – $^1\text{H-NMR}$ of **4** in CDCl_3

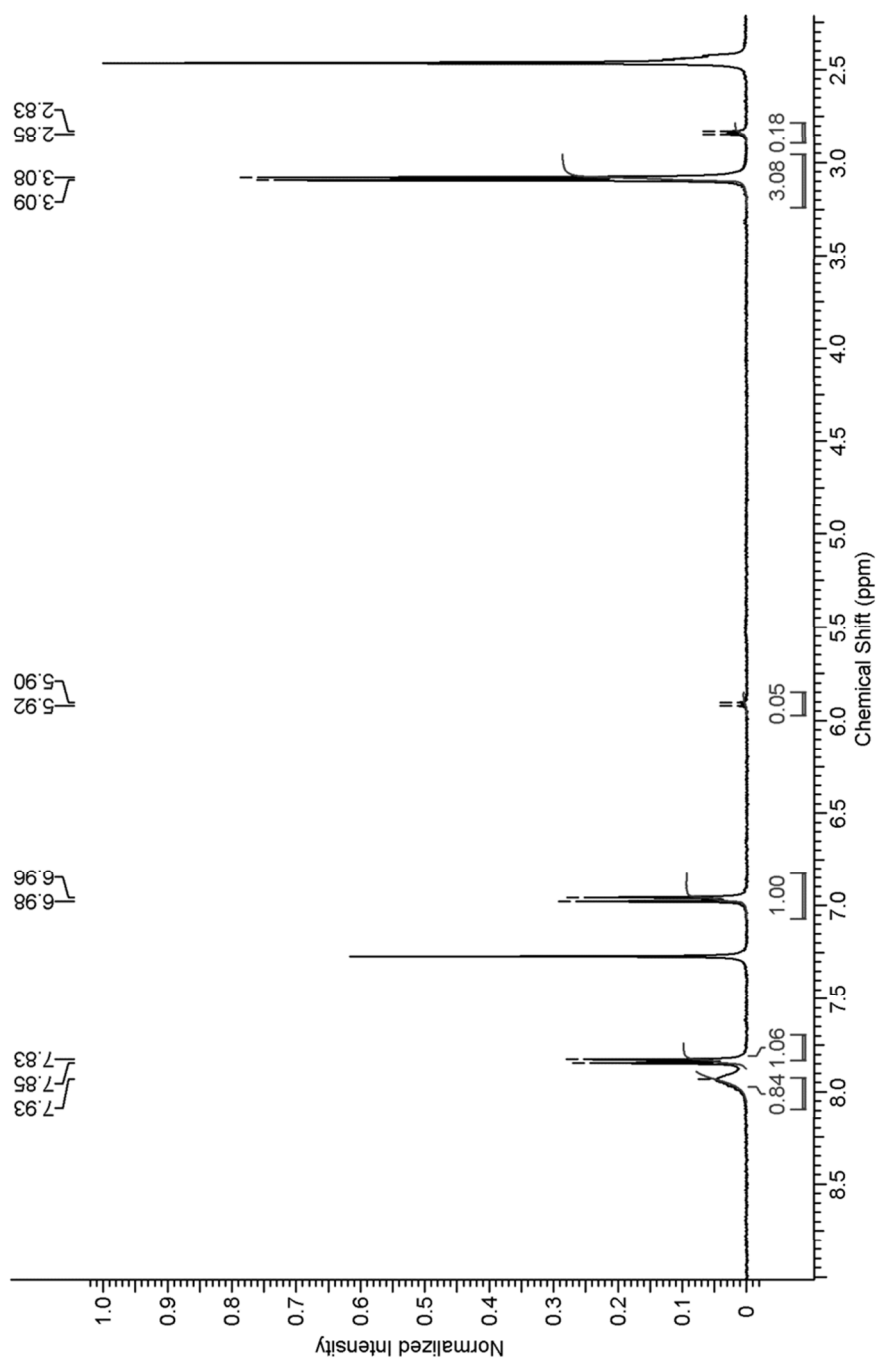


7.4DMSO – $^1\text{H-NMR}$ of **4** in CDCl_3 

6 Supporting information

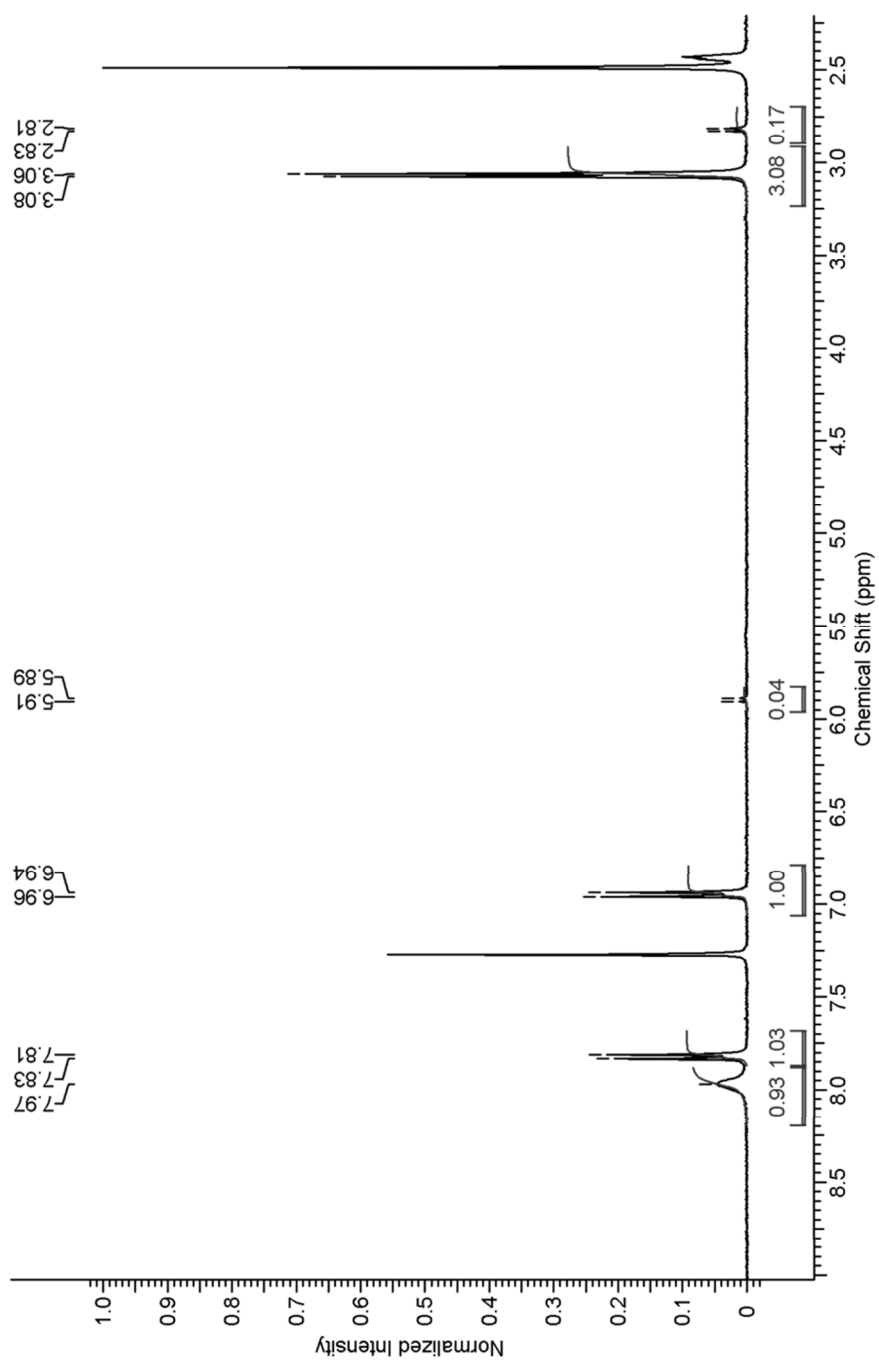
8.3% DMSO – $^1\text{H-NMR}$ of **4** in CDCl_3

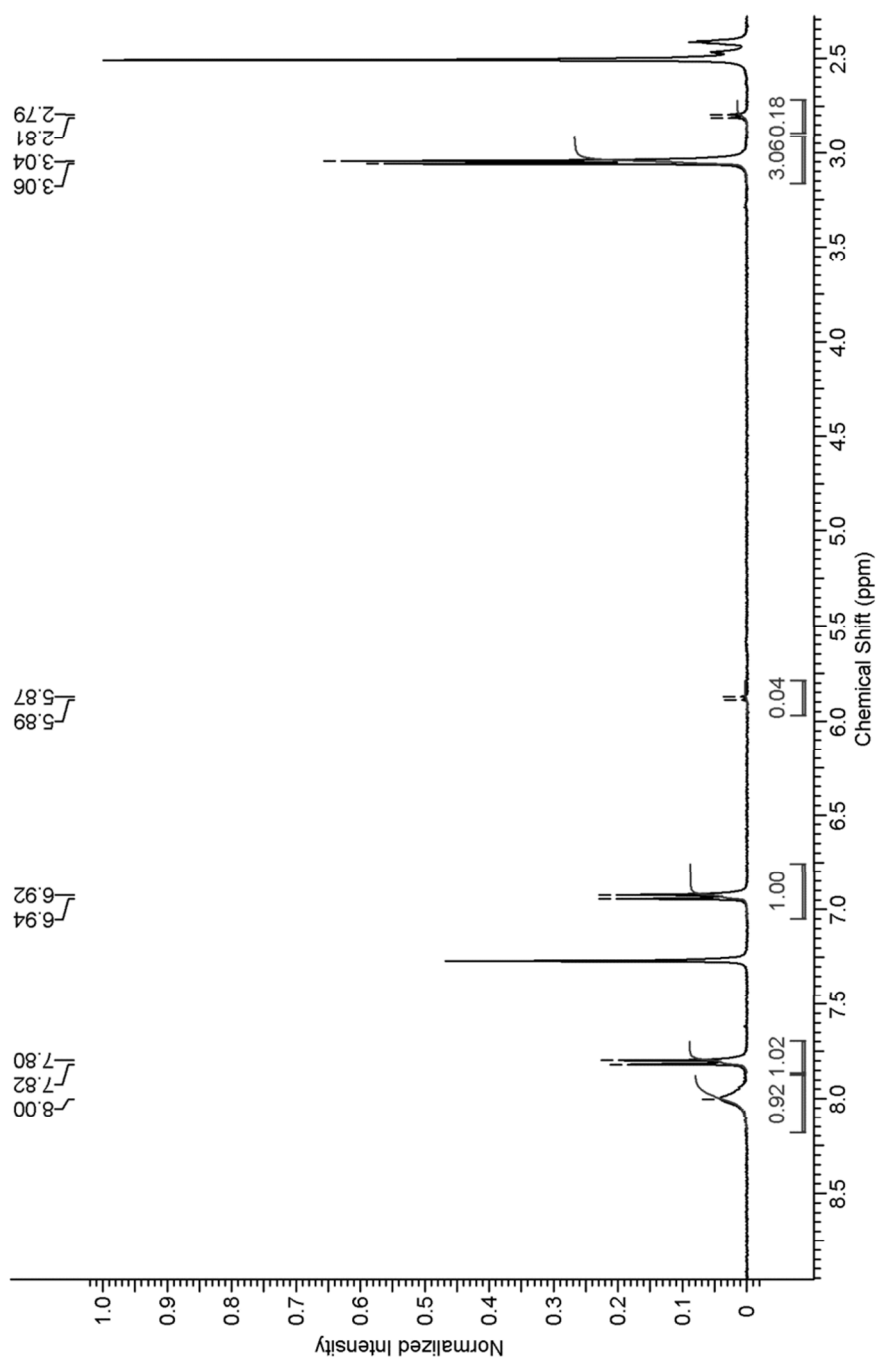


9.1% DMSO – $^1\text{H-NMR}$ of **4** in CDCl_3 

6 Supporting information

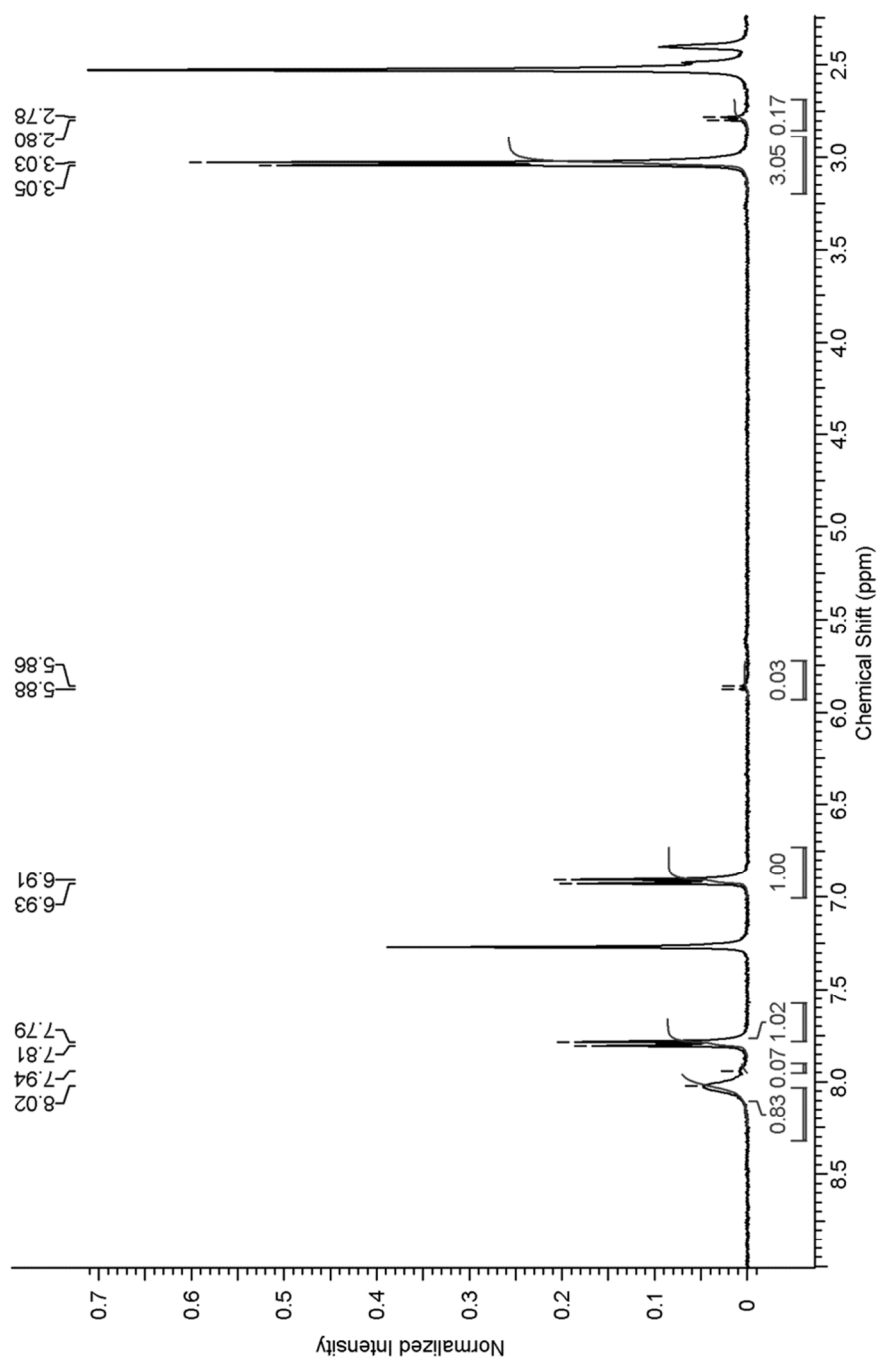
9.9% DMSO – $^1\text{H-NMR}$ of **4** in CDCl_3

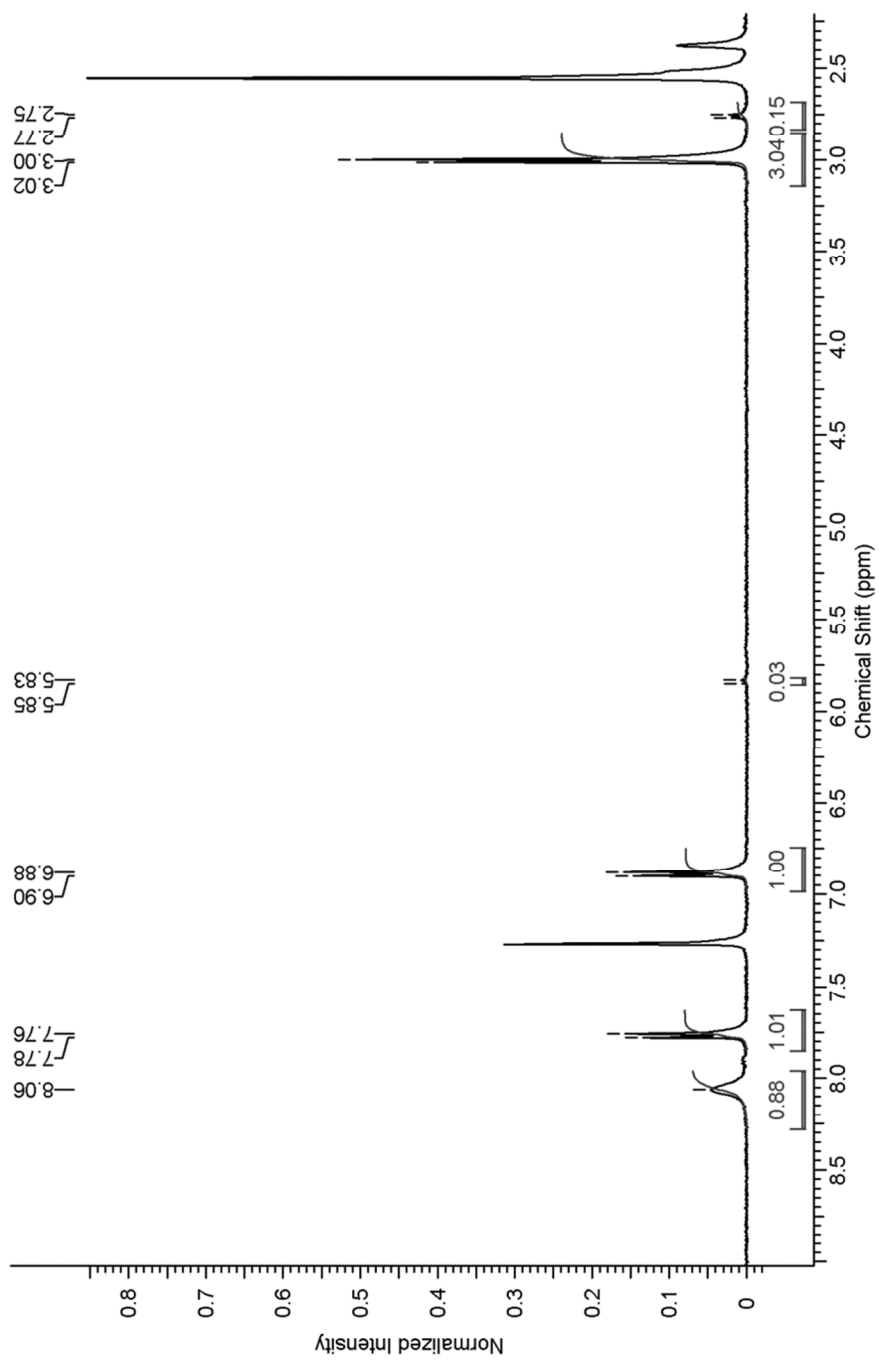


10.7% DMSO – $^1\text{H-NMR}$ of **4** in CDCl_3 

6 Supporting information

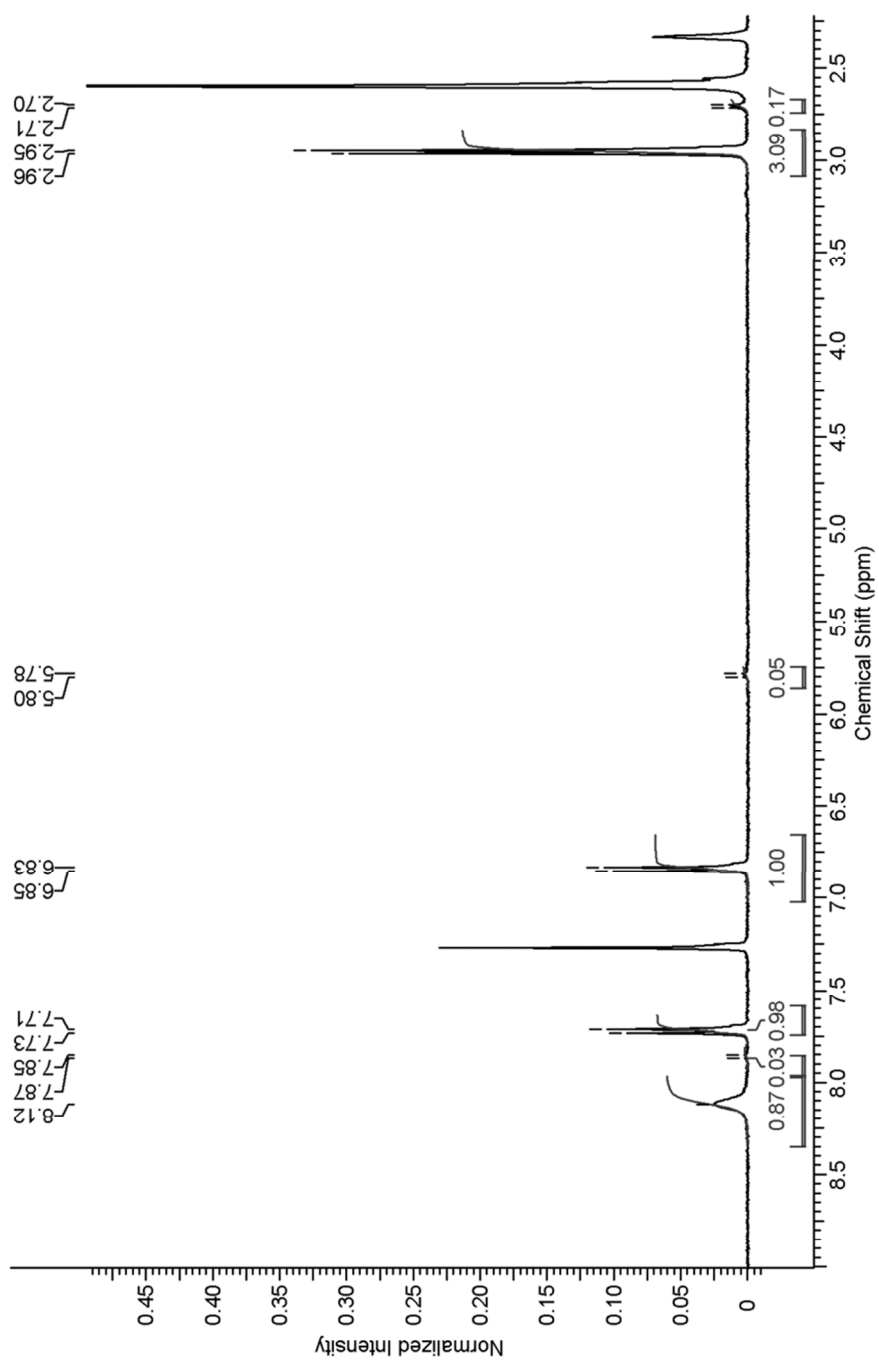
11.5% DMSO – $^1\text{H-NMR}$ of **4** in CDCl_3

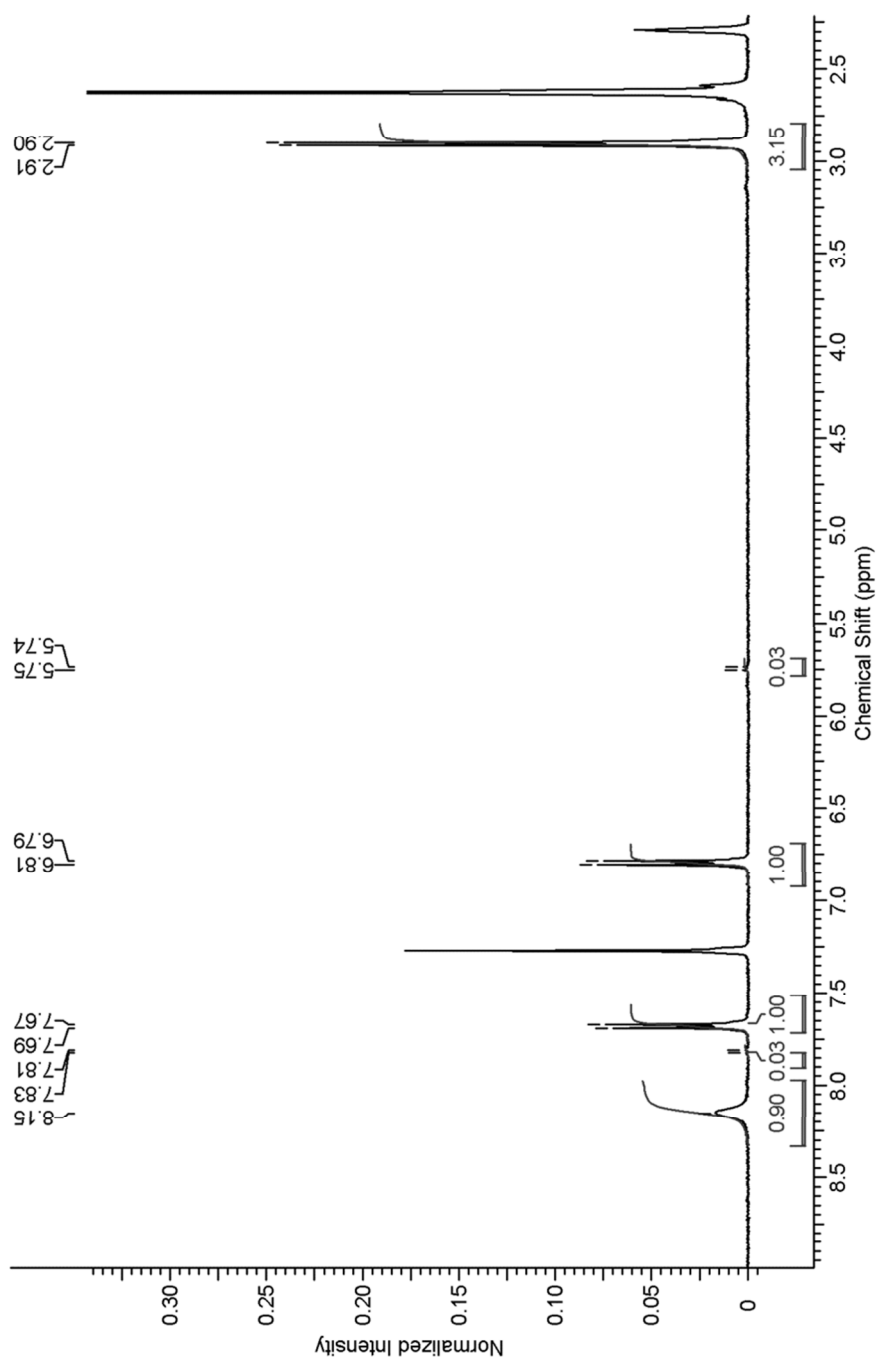


12.9% DMSO – $^1\text{H-NMR}$ of **4** in CDCl_3 

6 Supporting information

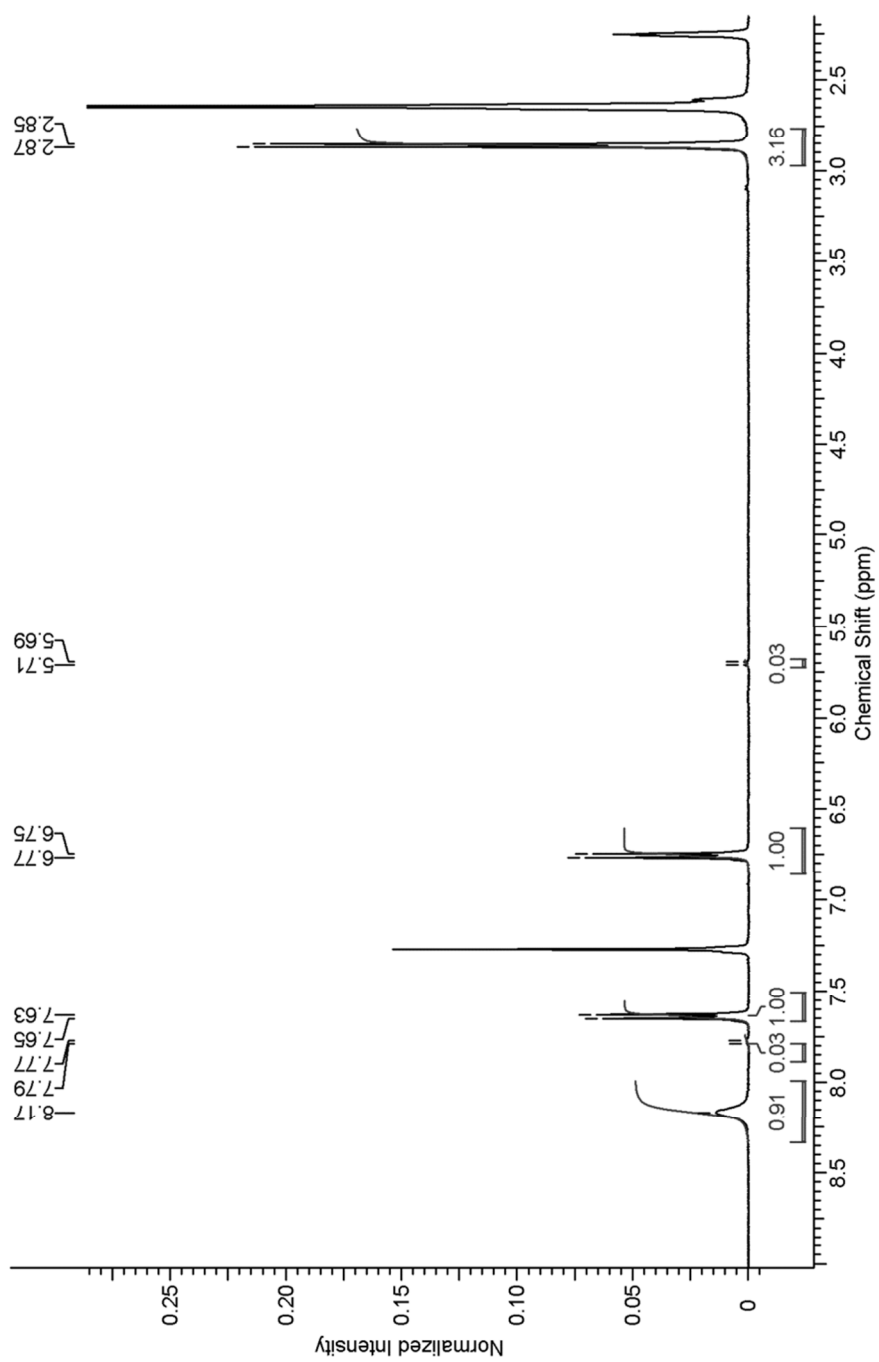
15.6% DMSO – $^1\text{H-NMR}$ of **4** in CDCl_3

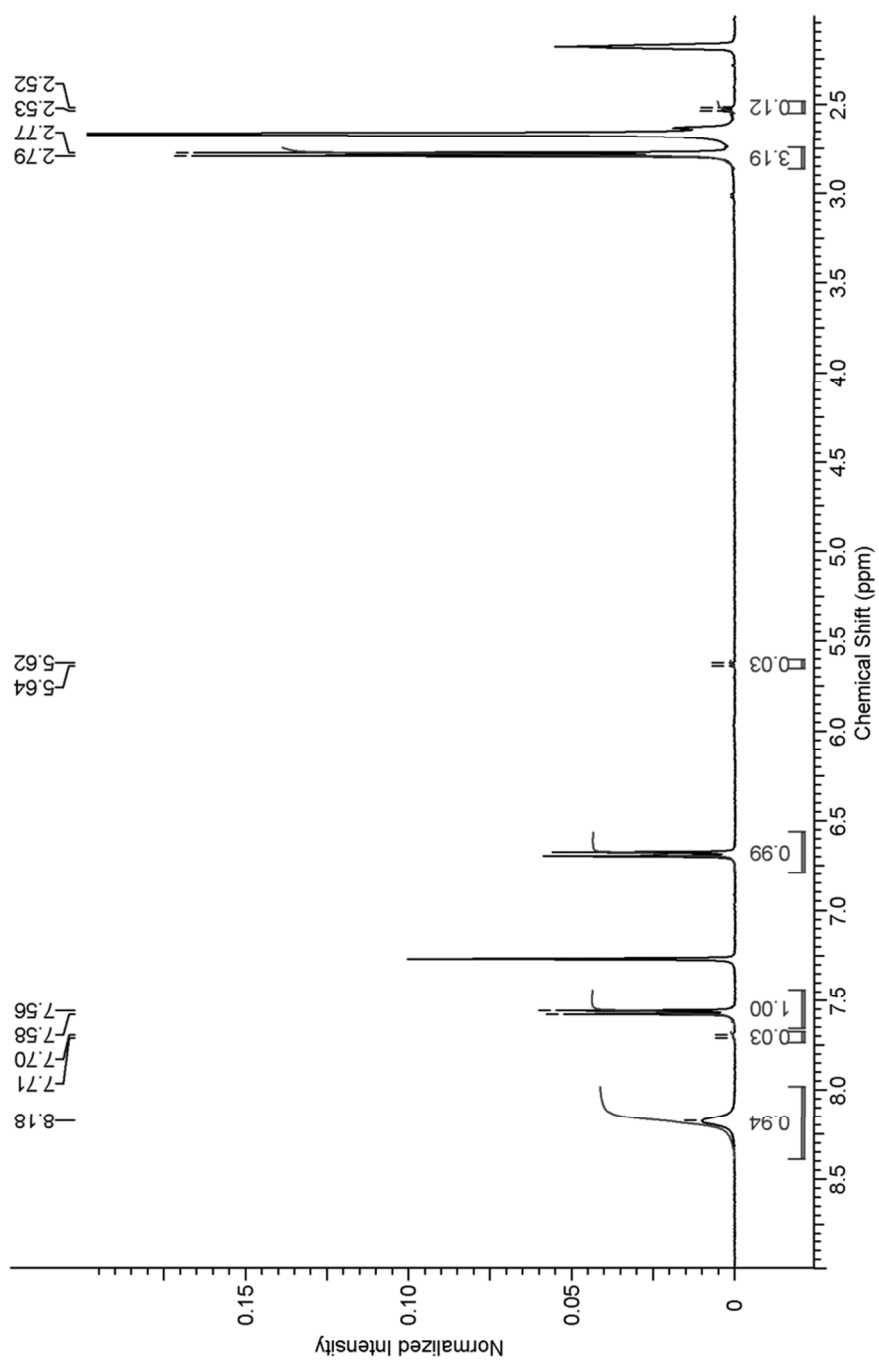


18.1% DMSO – $^1\text{H-NMR}$ of **4** in CDCl_3 

6 Supporting information

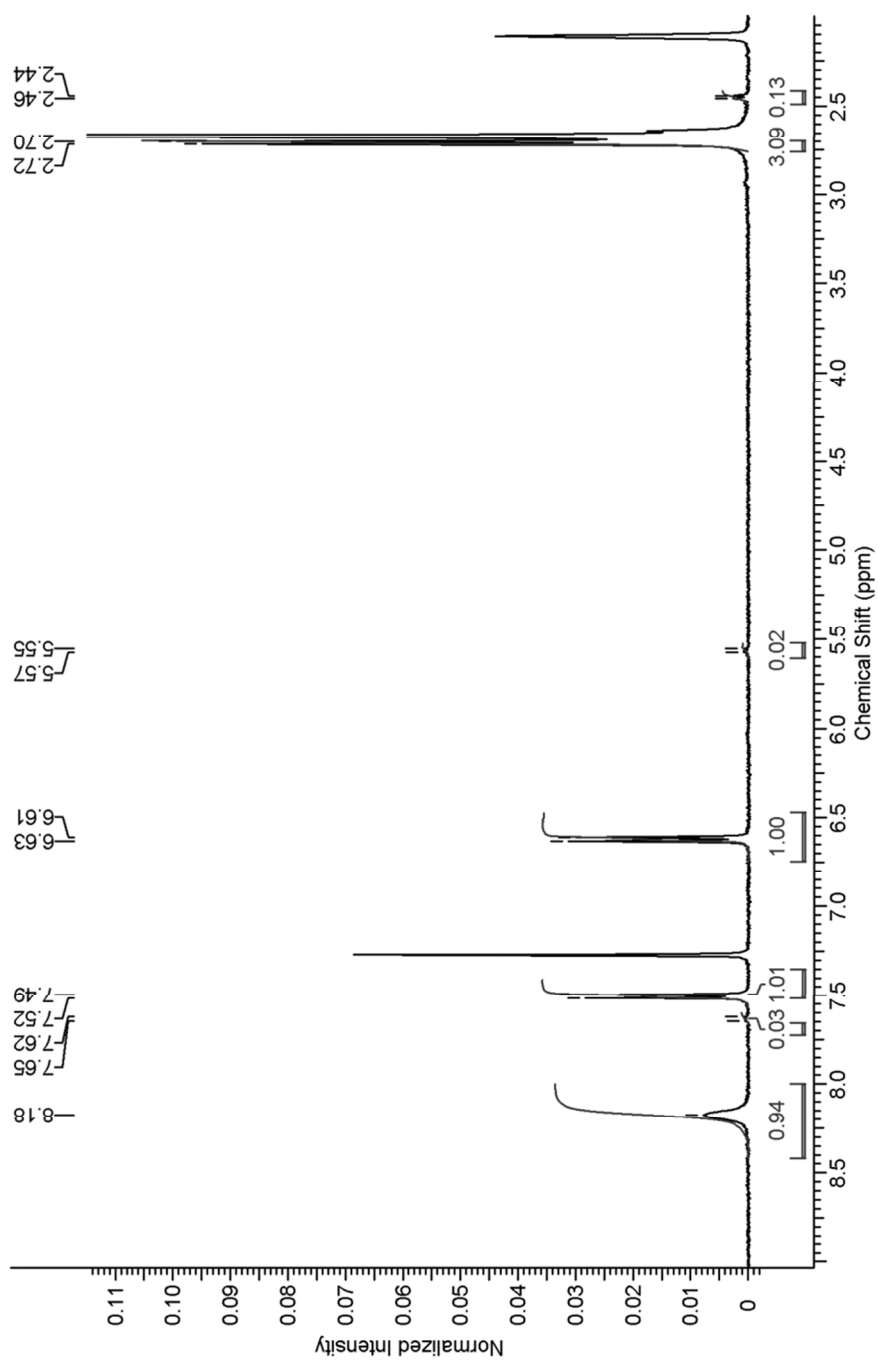
20.5% DMSO – $^1\text{H-NMR}$ of **4** in CDCl_3



24.8 DMSO – $^1\text{H-NMR}$ of **4** in CDCl_3 

6 Supporting information

28.7%DMSO – $^1\text{H-NMR}$ of **4** in CDCl_3



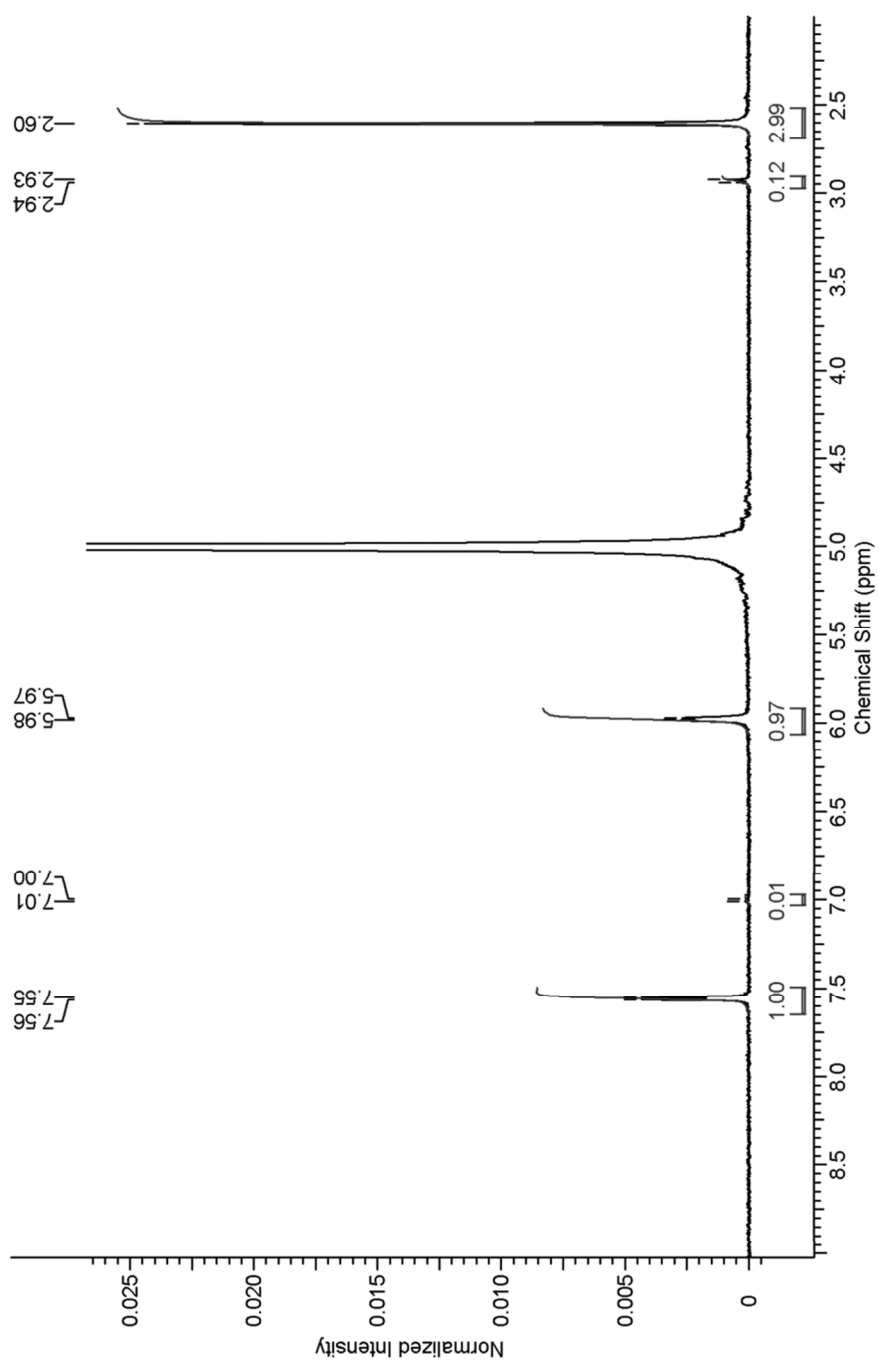
¹H-NMR shift of the NH-signal and percentage of azide-integrals to tetrazole-integrals of 4 under DMSO titration in CDCl₃

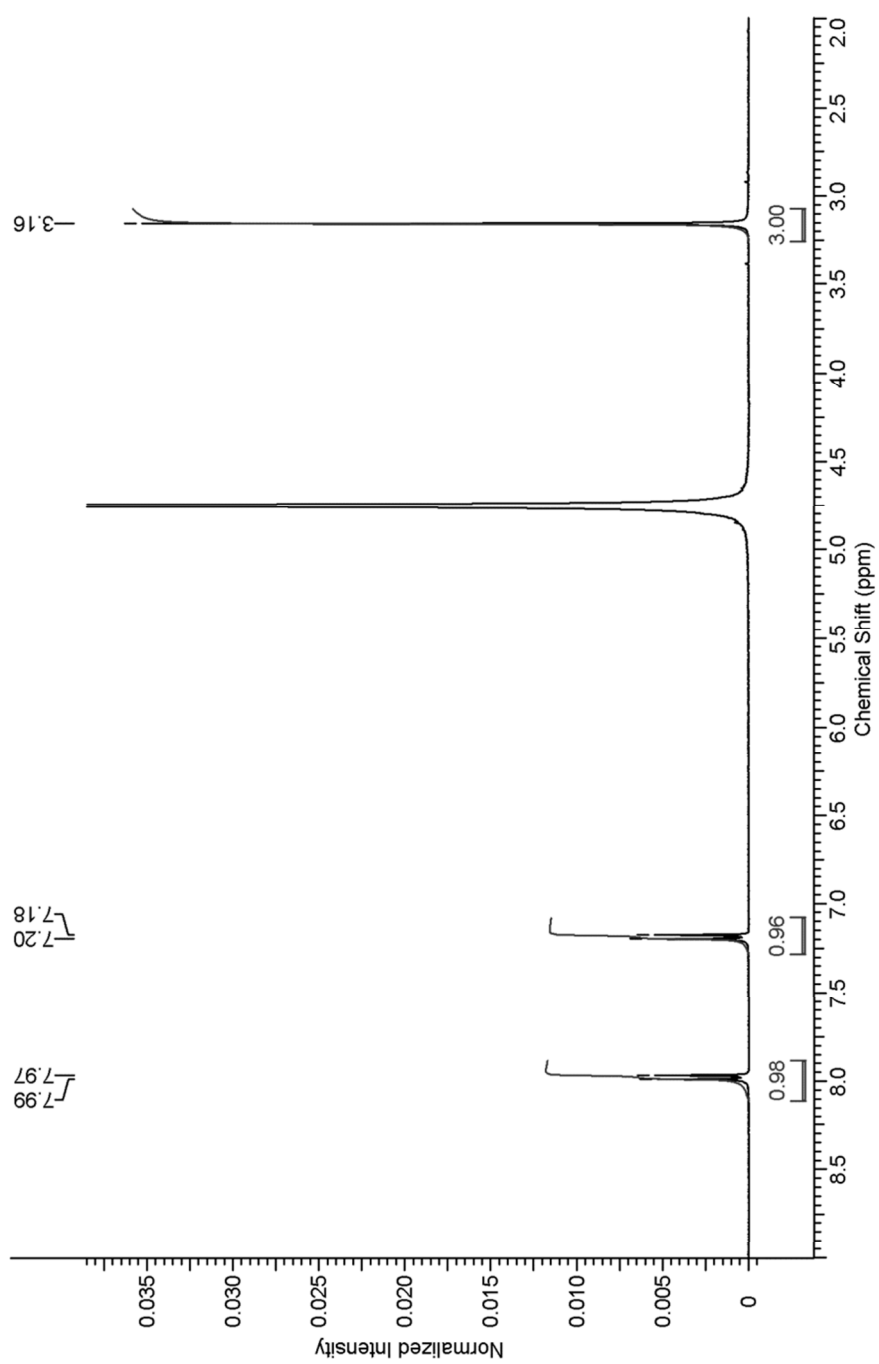
DMSO [%]	NH-shift [ppm]	Azide [%]	Tetrazole [%]
0.0	6.38	15.0	85.0
1.0	6.83	11.0	89.0
2.0	7.13	9.0	91.0
2.9	7.33	8.0	92.0
3.8	7.48	7.0	93.0
4.8	7.61	6.0	94.0
5.7	7.70	5.7	94.3
6.5	7.78	5.7	94.4
7.4	7.83	5.0	95.1
8.3	7.89	4.8	95.3
9.1	7.94	4.8	95.2
9.9	7.97	4.1	95.9
10.7	8.00	3.7	96.3
11.5	8.02	3.7	96.3
12.9	8.06	3.0	97.0
15.6	8.11	4.0	96.1
18.1	8.15	2.8	97.2
20.5	8.17	2.9	97.1
24.8	8.18	2.7	97.3
28.7	8.18	2.6	97.4

6 Supporting information

c) Acidic, basic and neutral $^1\text{H-NMR}$ of 4 and 5

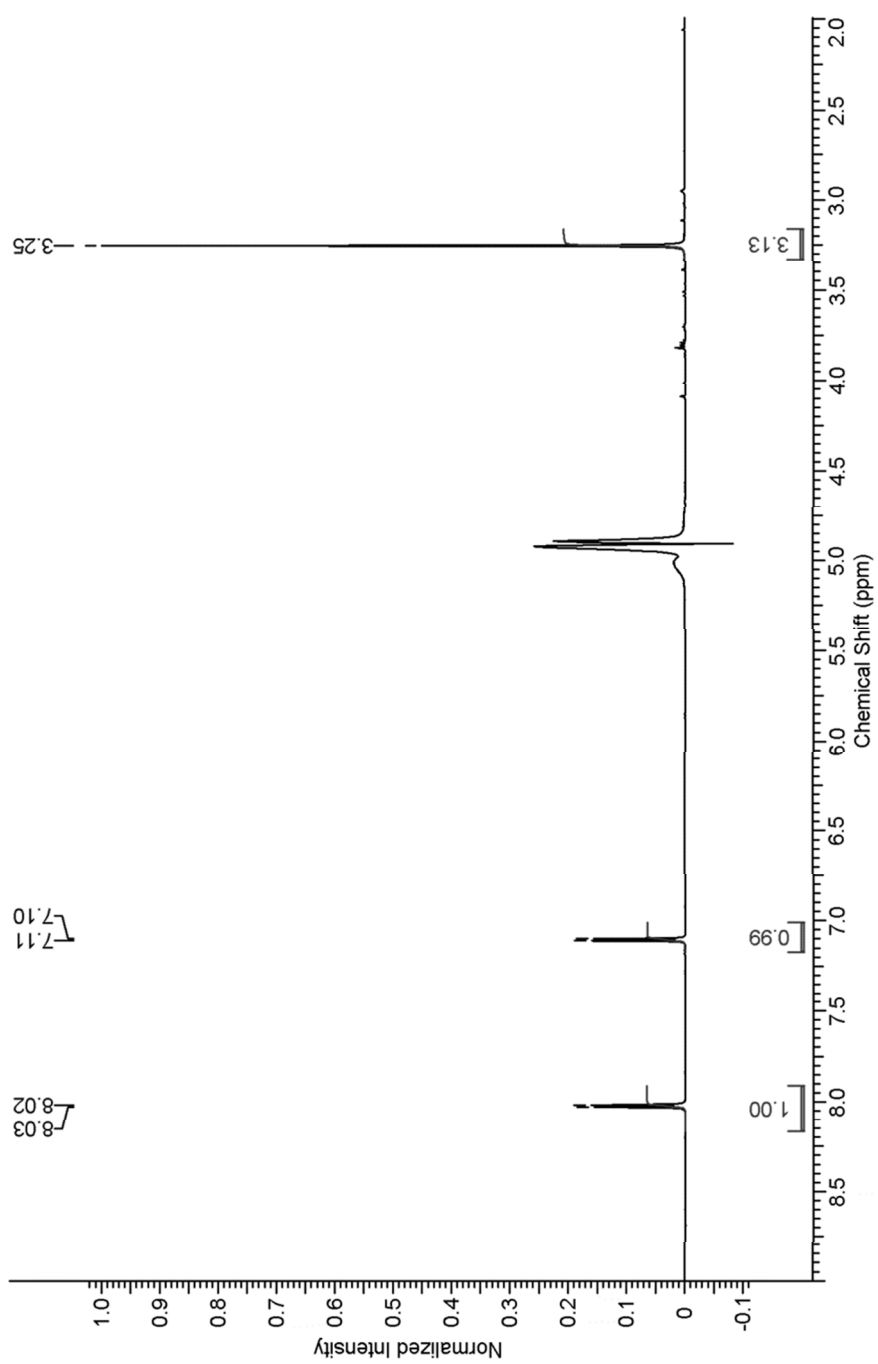
$^1\text{H-NMR}$ of 4 in D_2O (acidic + TFA)



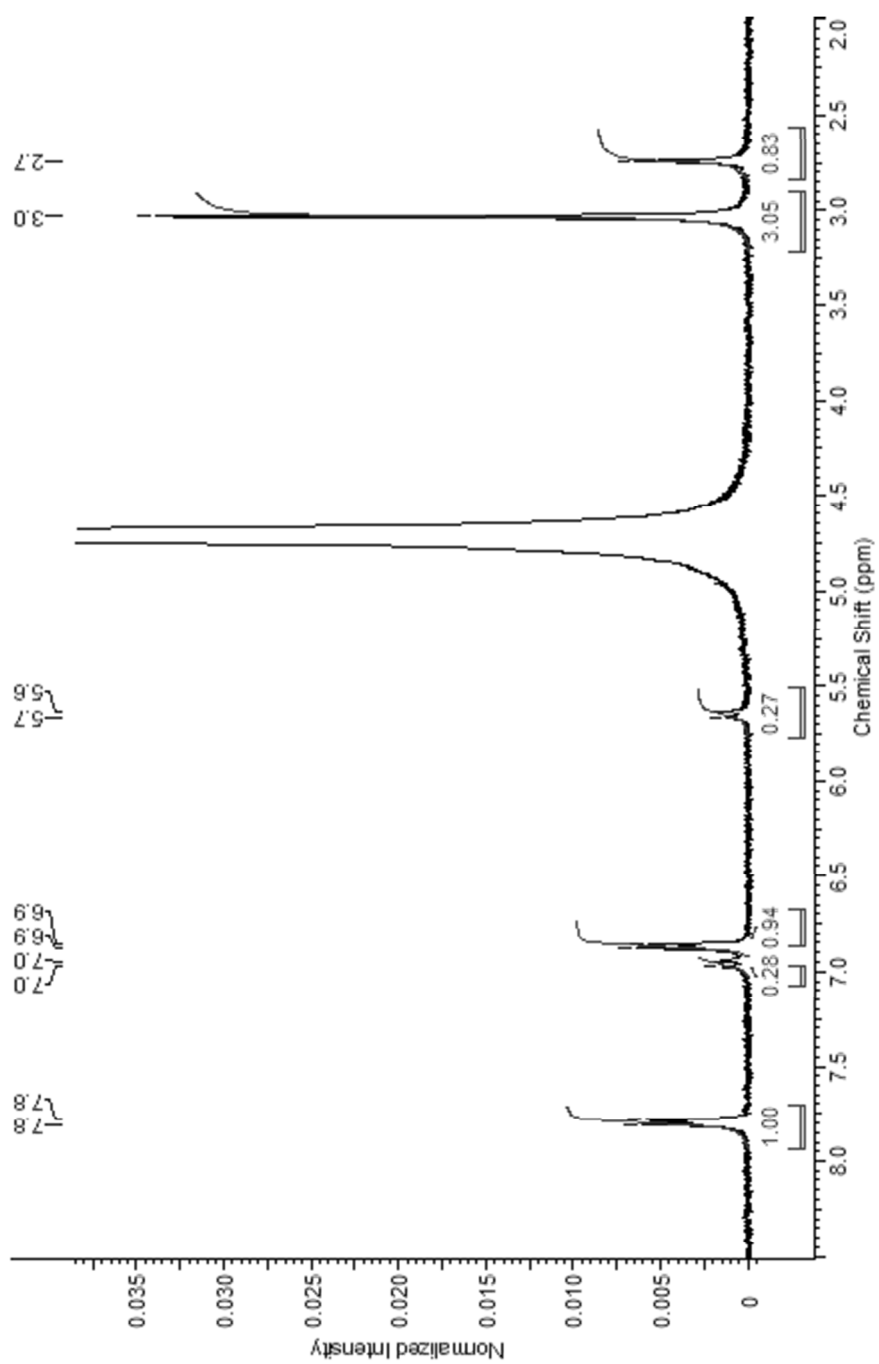
$^1\text{H-NMR}$ of **4** in D_2O (neutral)

6 Supporting information

$^1\text{H-NMR}$ of **4** in D_2O (basic + 0.1M NaOH)

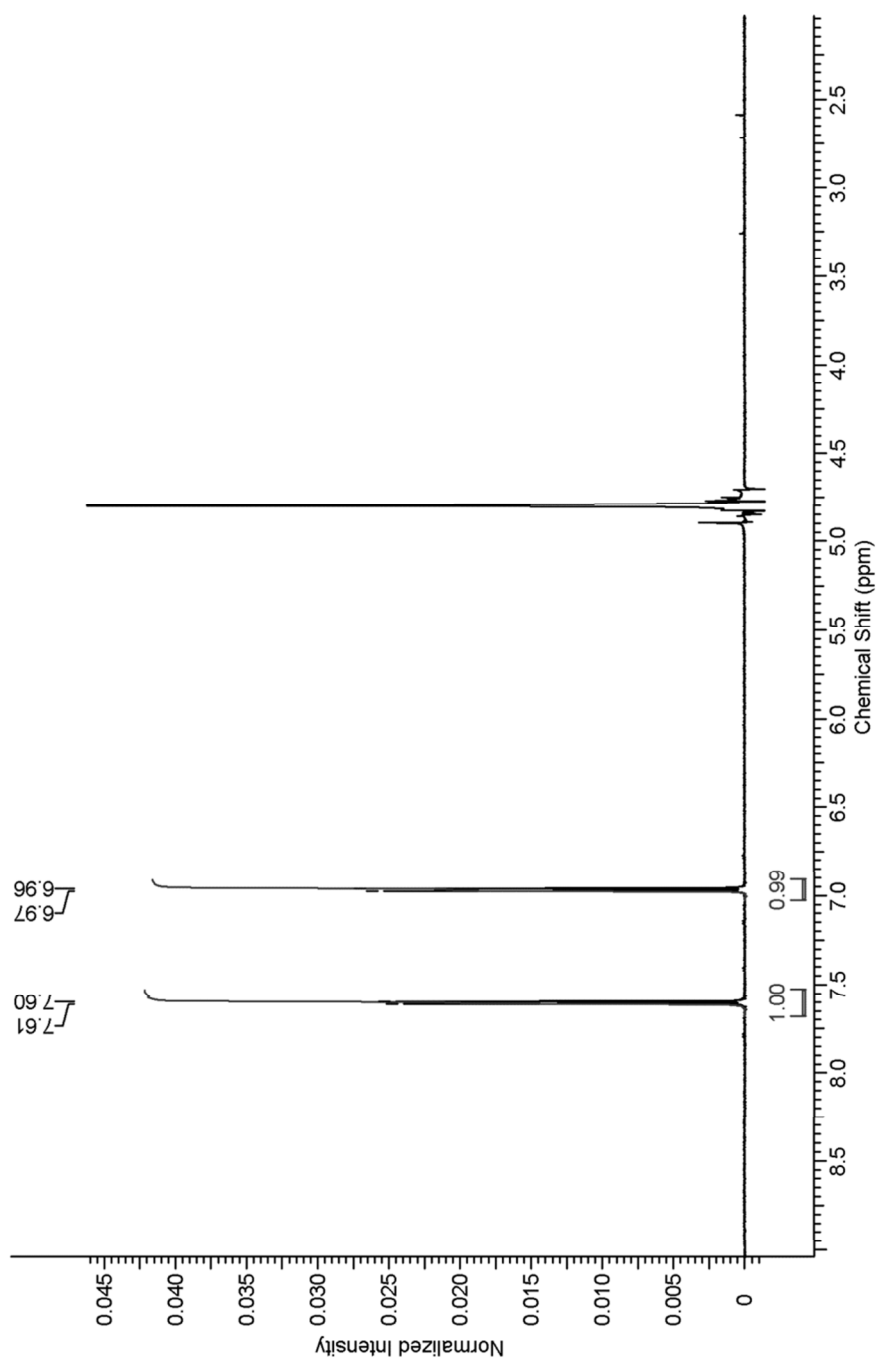


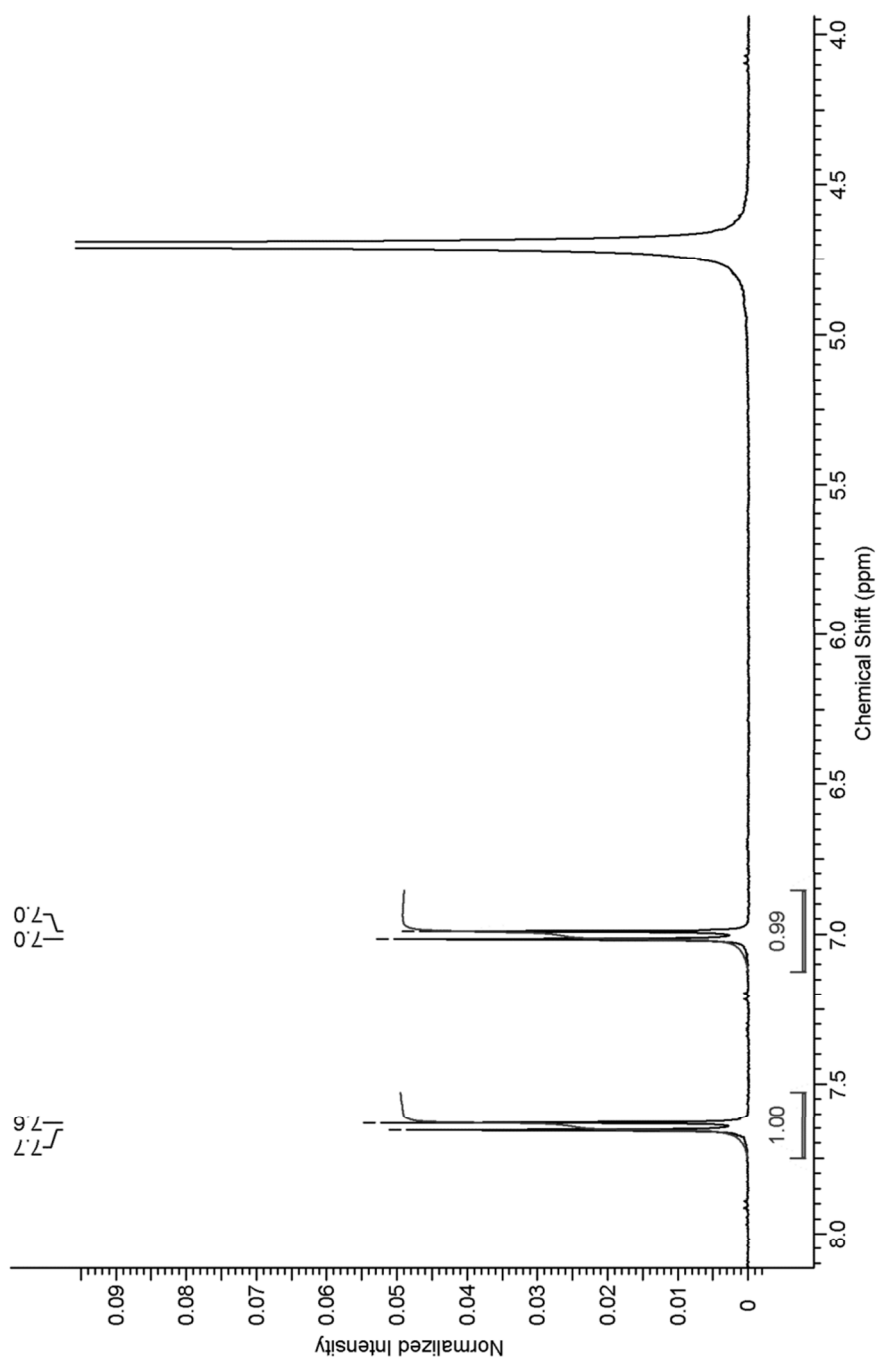
$^1\text{H-NMR}$ of **4** in D_2O (basic + 1M NaOH)



6 Supporting information

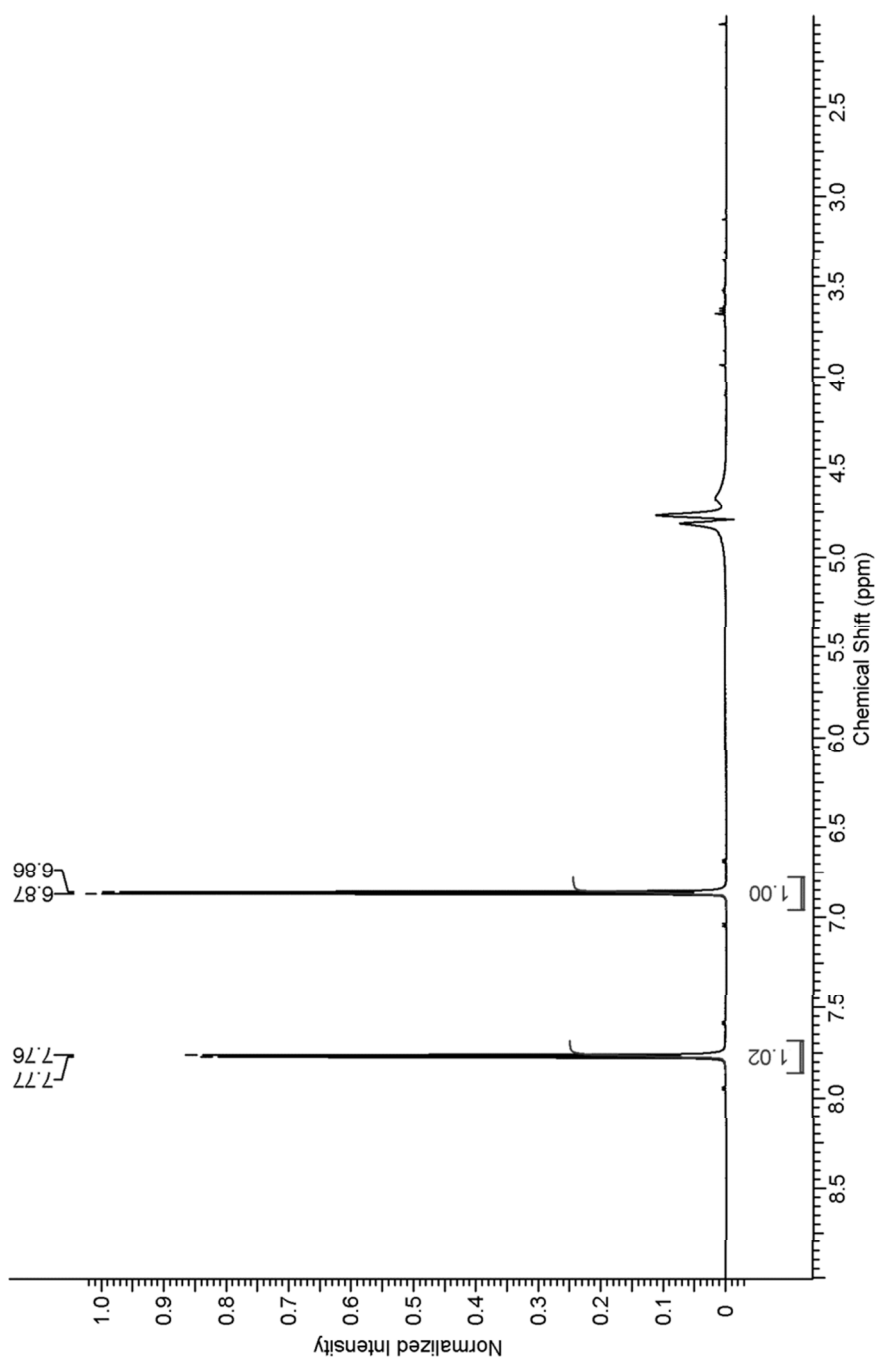
$^1\text{H-NMR}$ of **5** in D_2O (acidic + TFA)

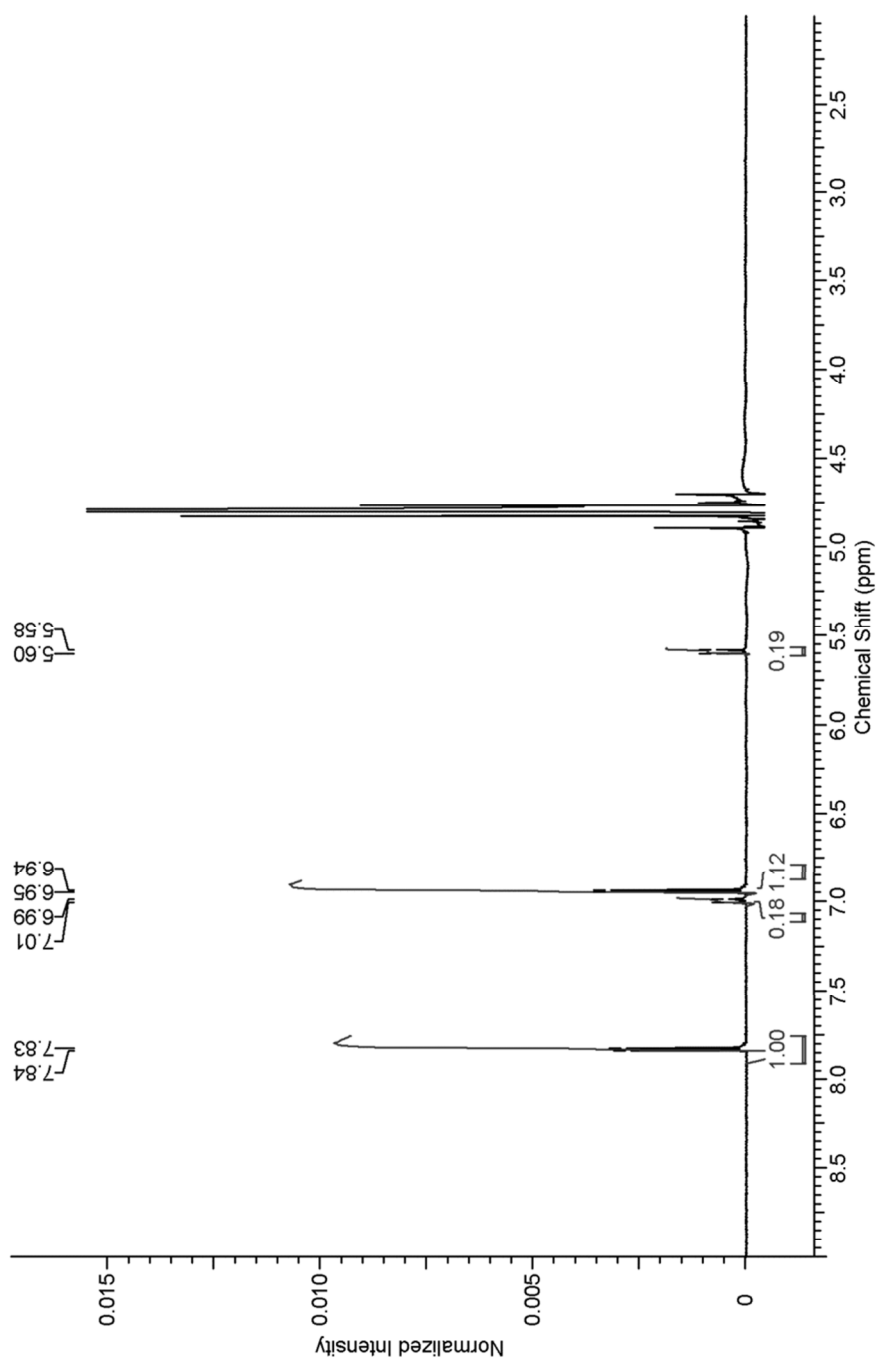


$^1\text{H-NMR}$ of **5** in D_2O (neutral)

6 Supporting information

$^1\text{H-NMR}$ of **5** in D_2O (basic + 0.1M NaOH)

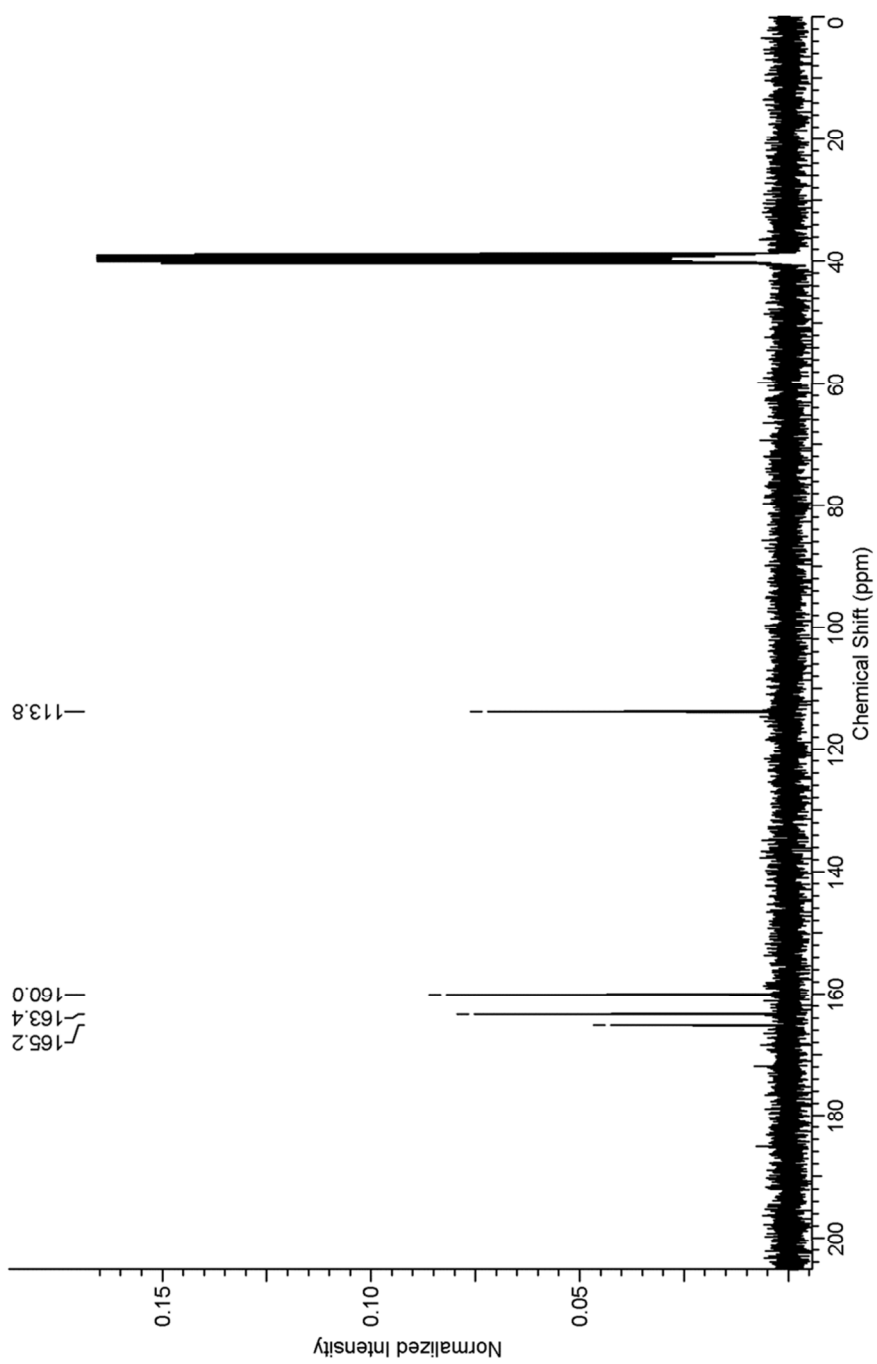


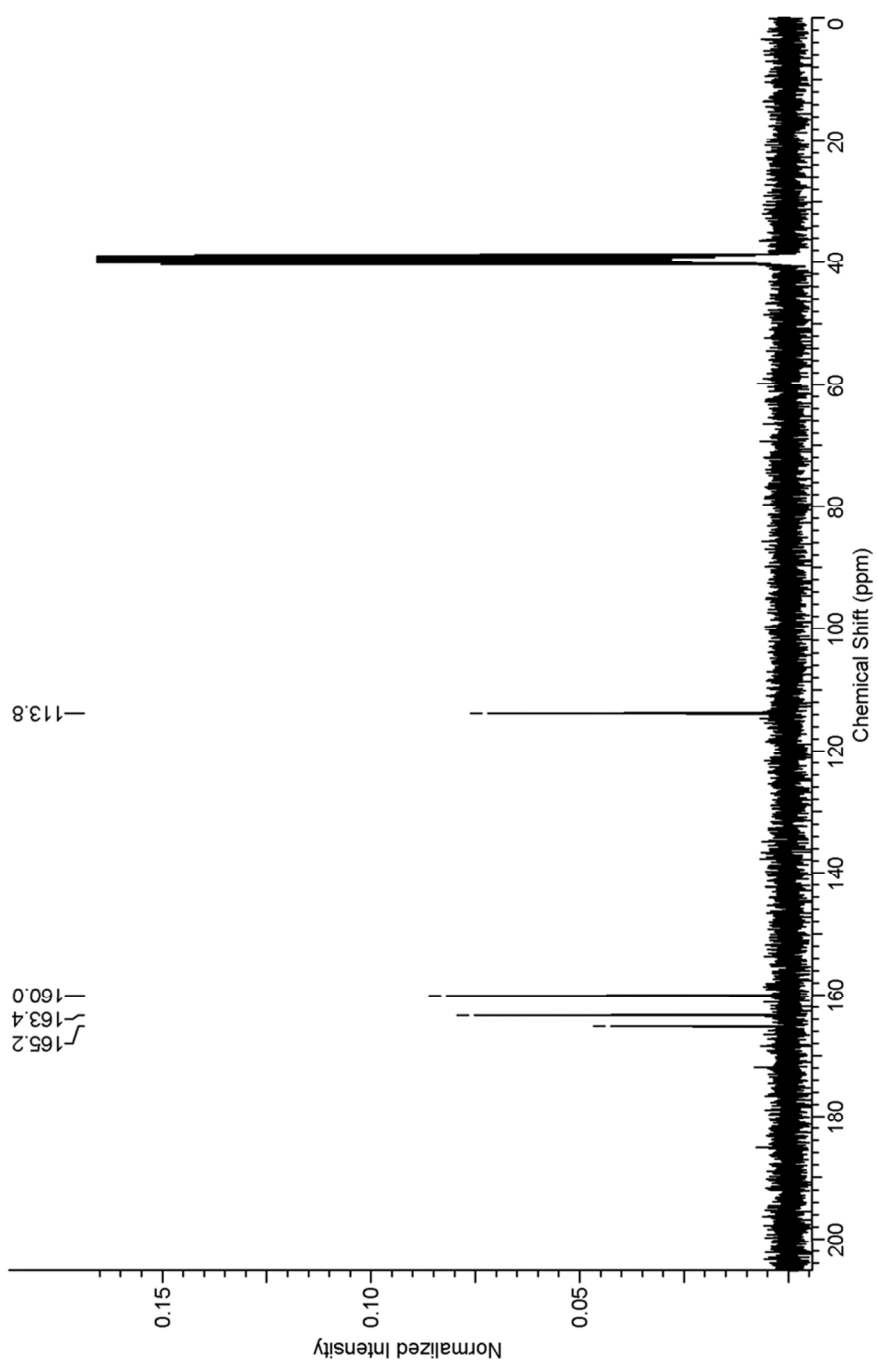
$^1\text{H-NMR}$ of **5** in D_2O (basic + 1M NaOH)

6 Supporting information

d) $^{13}\text{C-NMR}$ Spectra

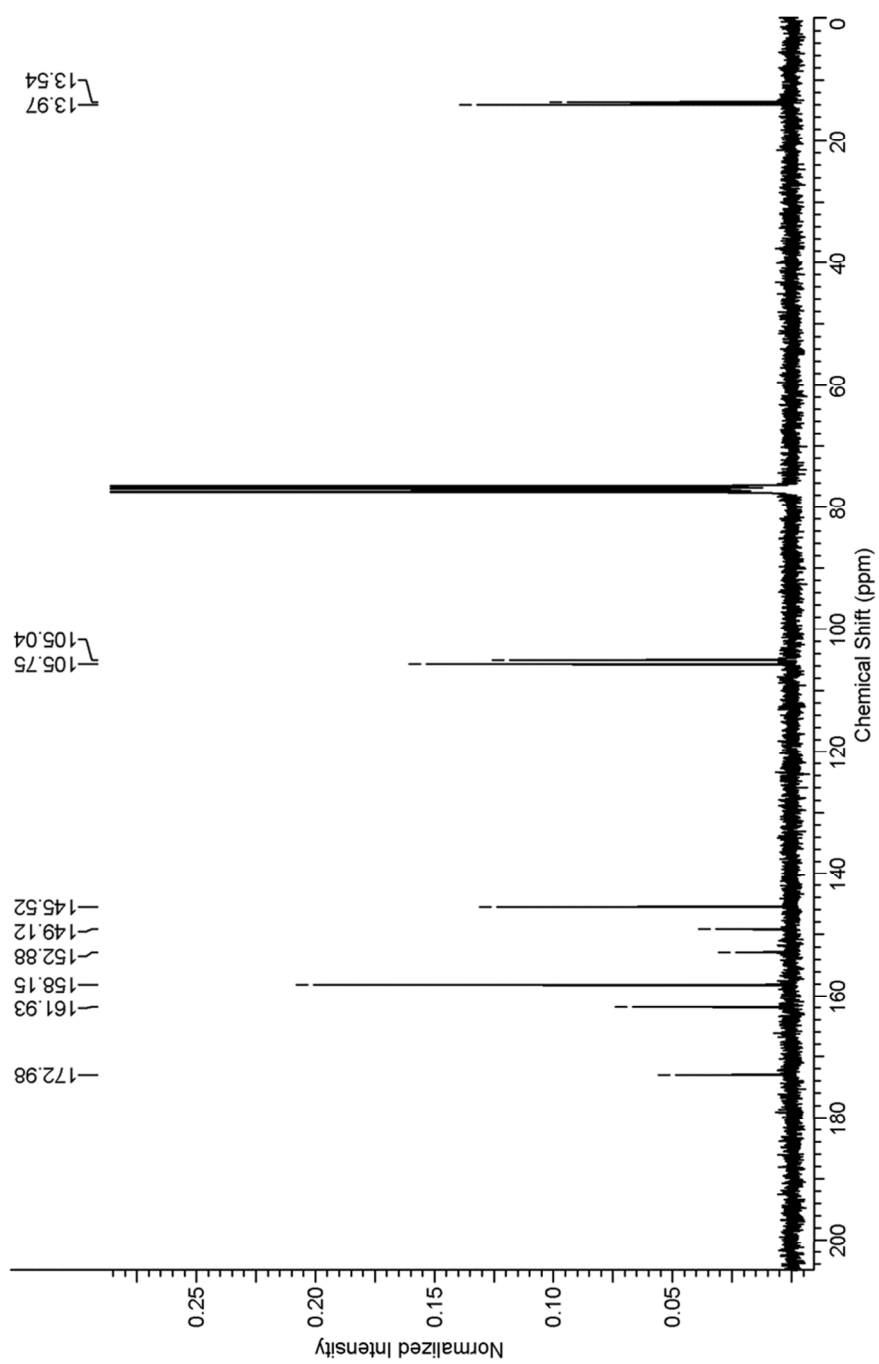
$^{13}\text{C-NMR}$ of **1**

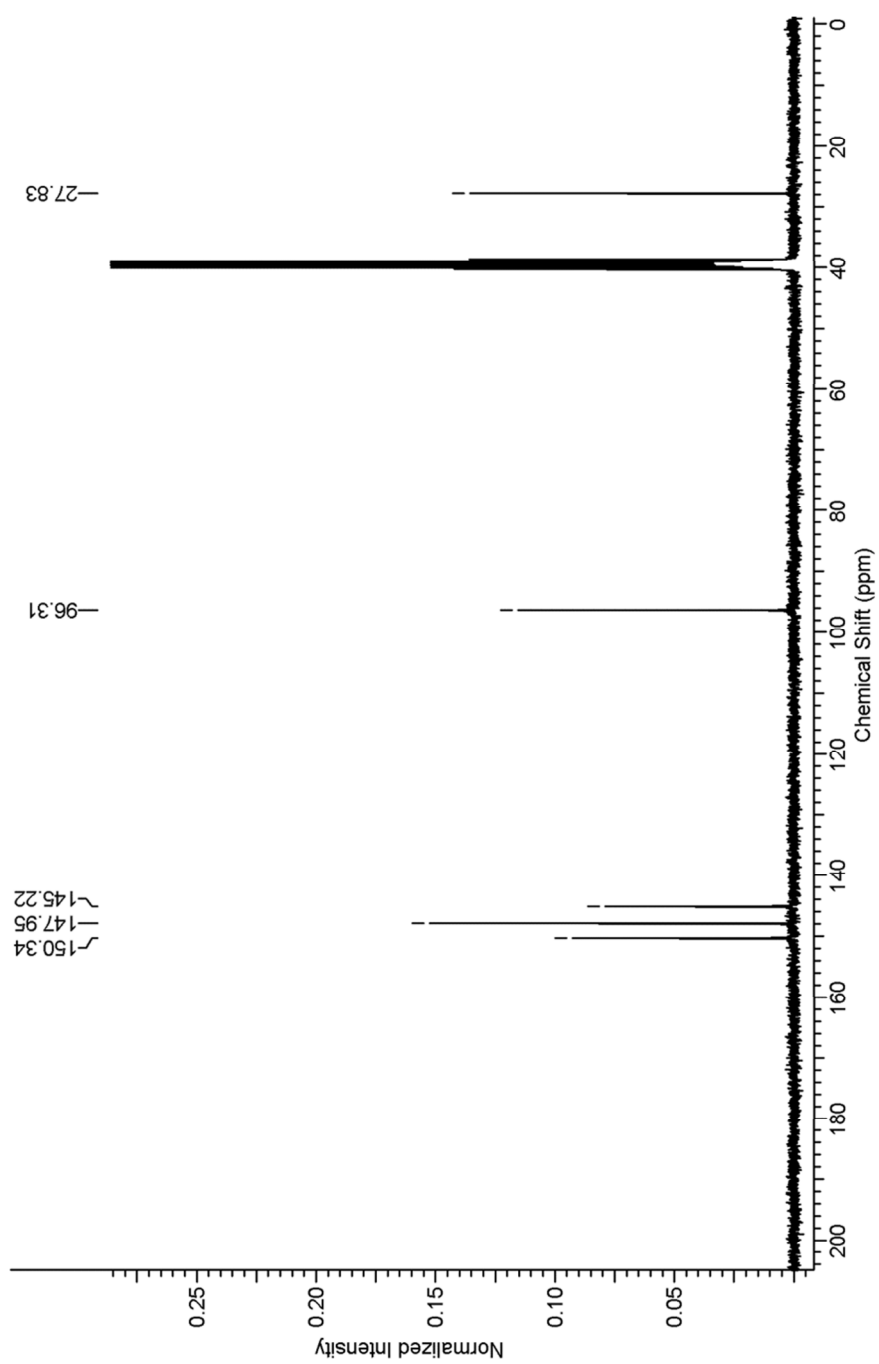


^{13}C -NMR of **2**

6 Supporting information

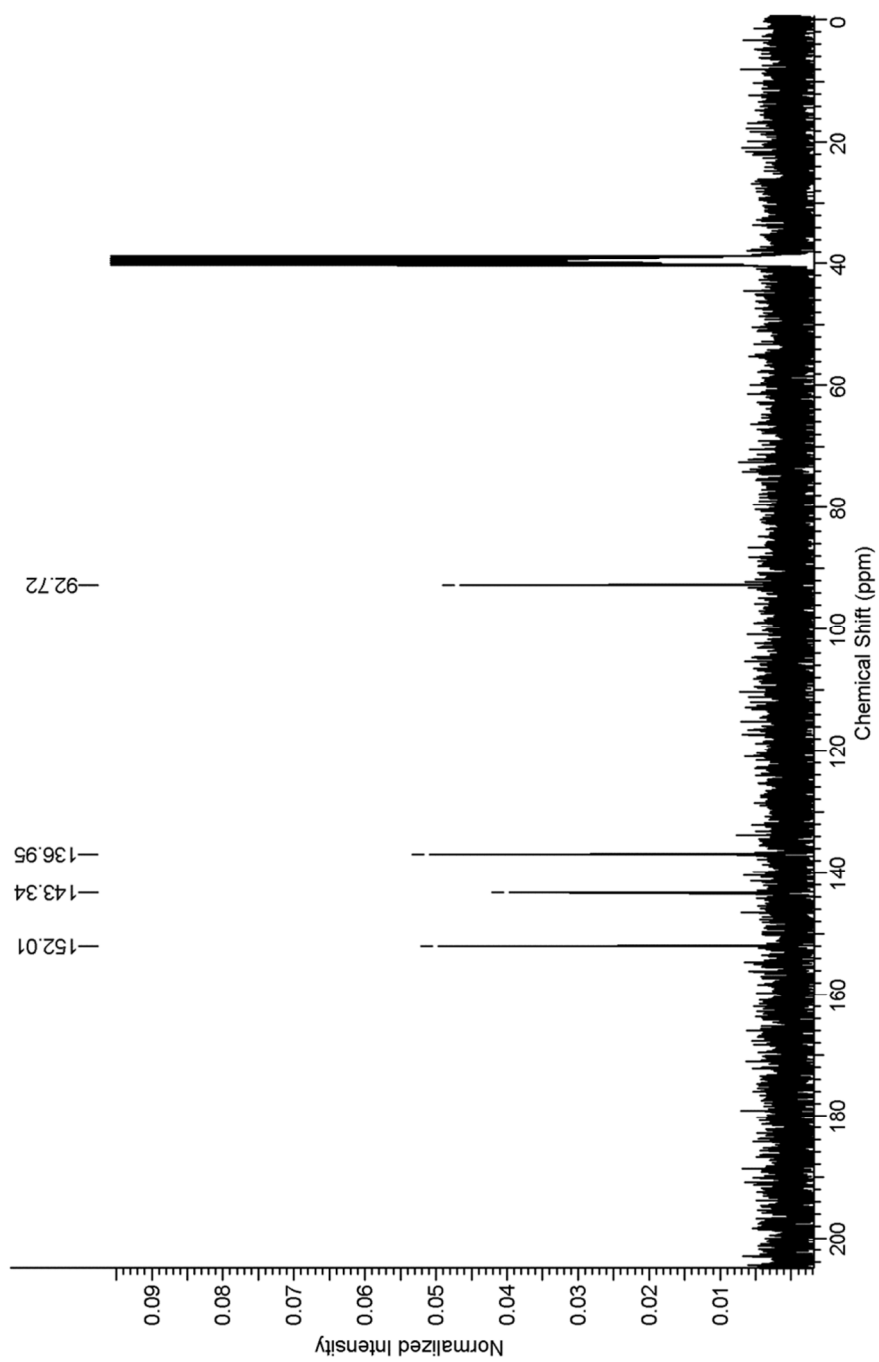
^{13}C -NMR of **3**

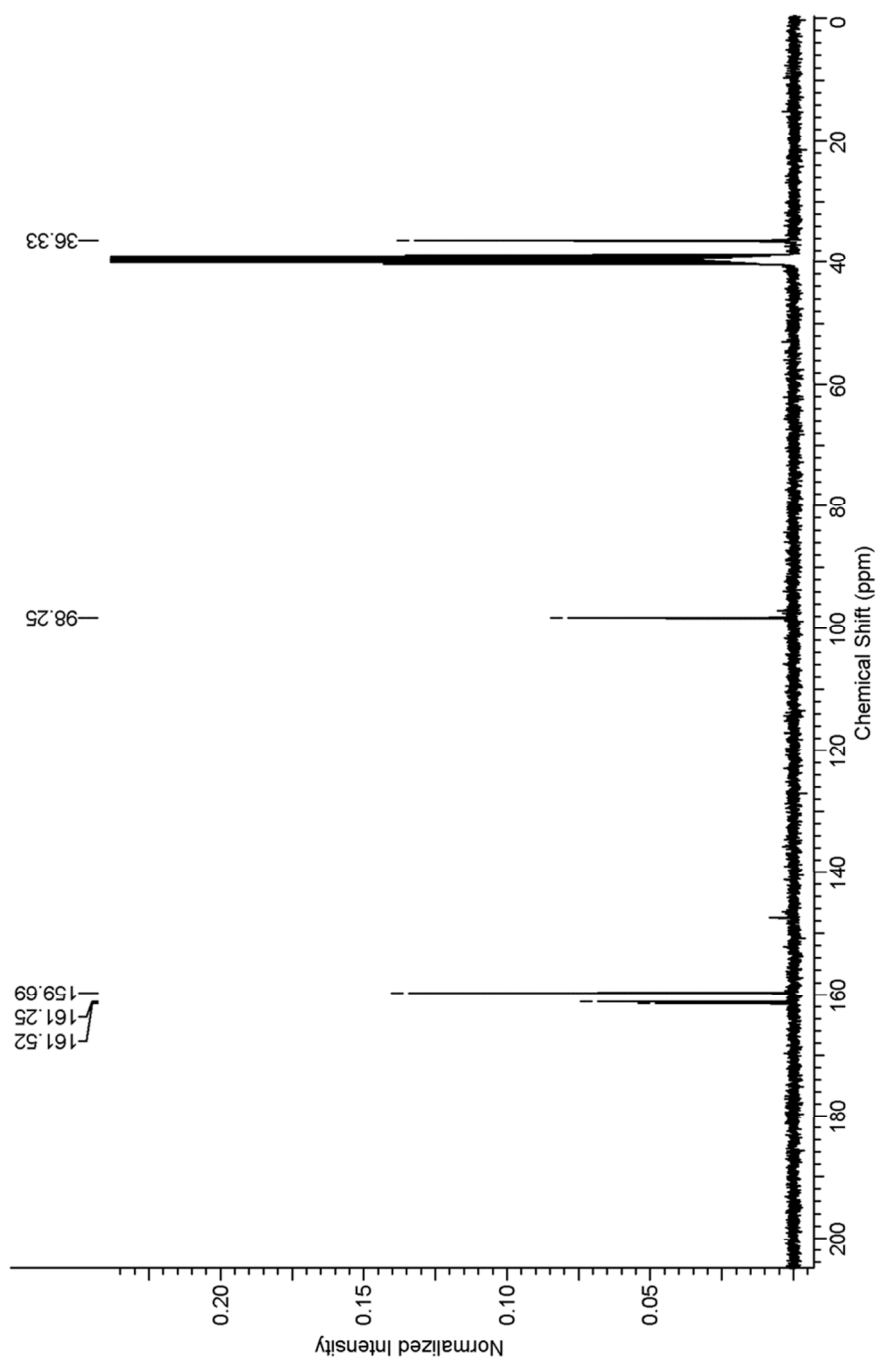


^{13}C -NMR of **4**

6 Supporting information

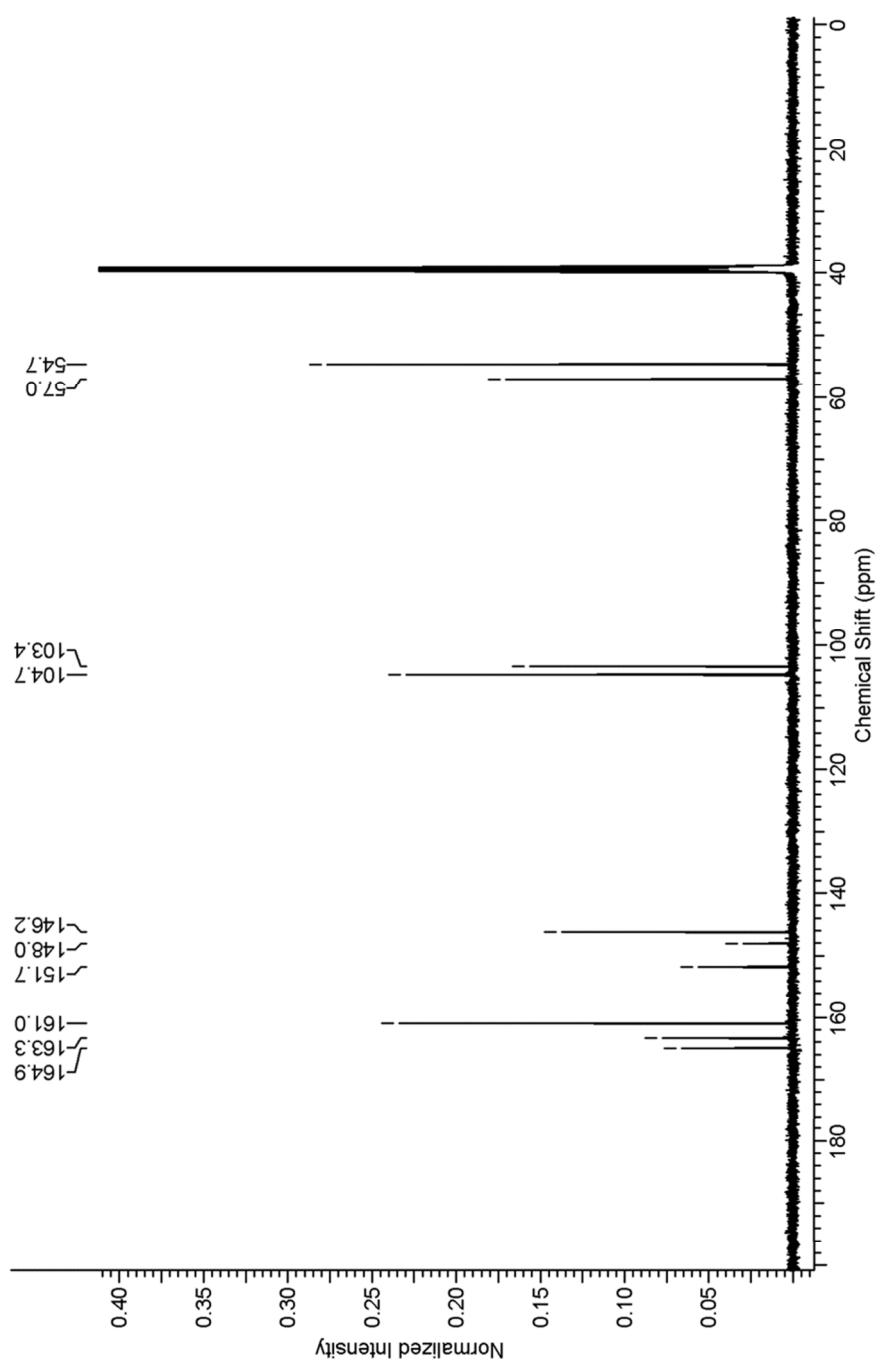
^{13}C -NMR of **5**

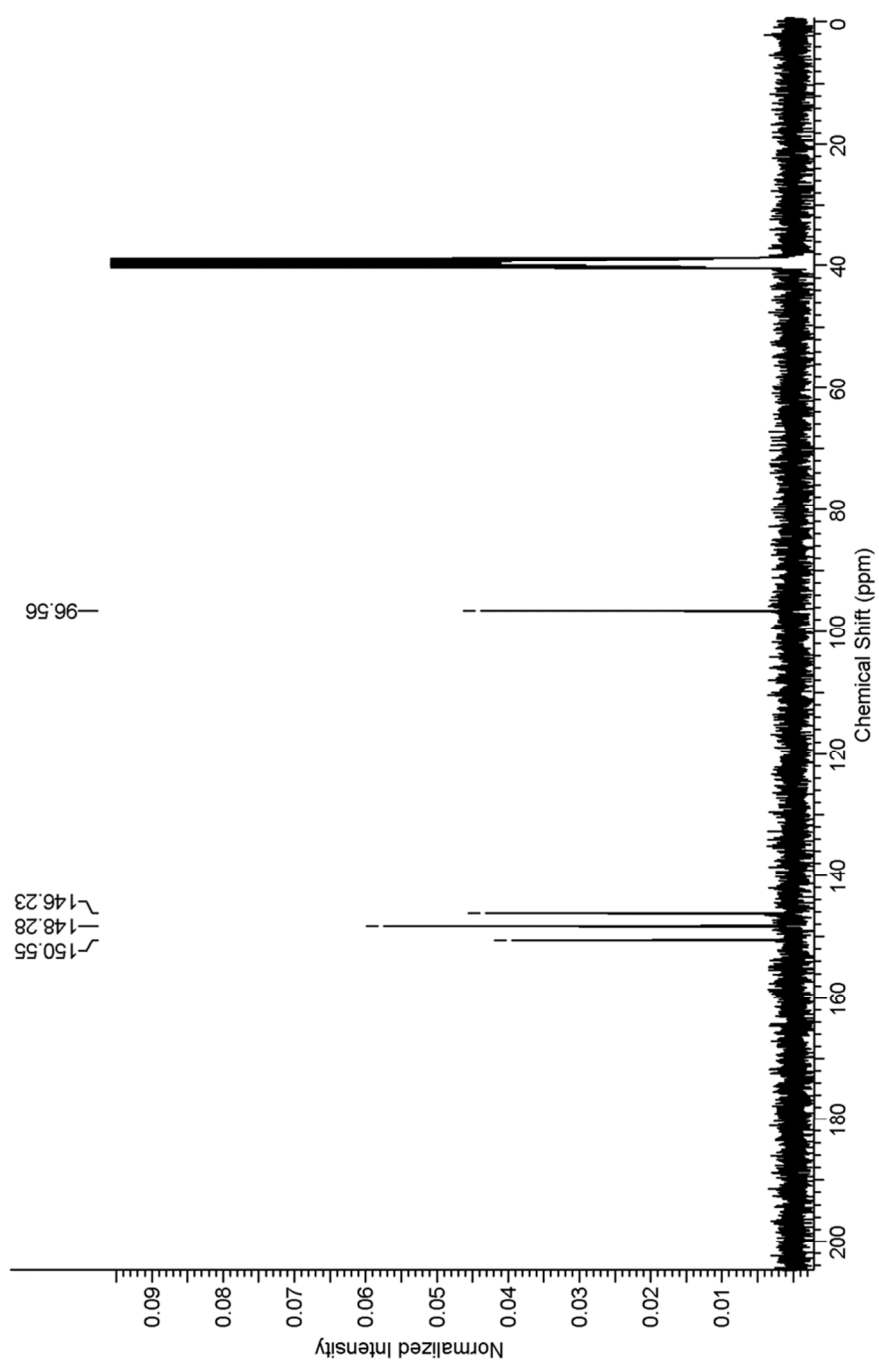


^{13}C -NMR of **6**

6 Supporting information

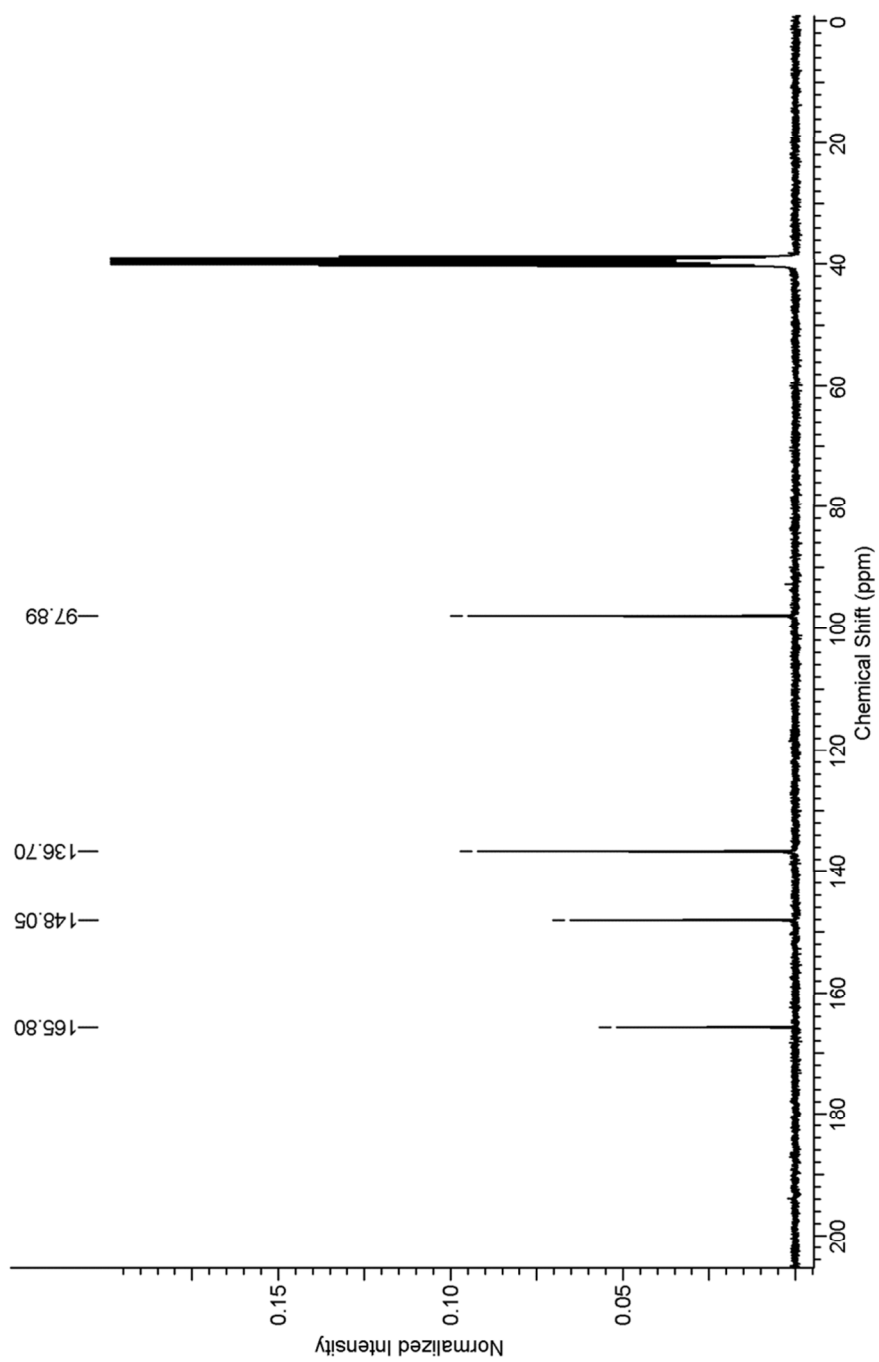
^{13}C -NMR of 7

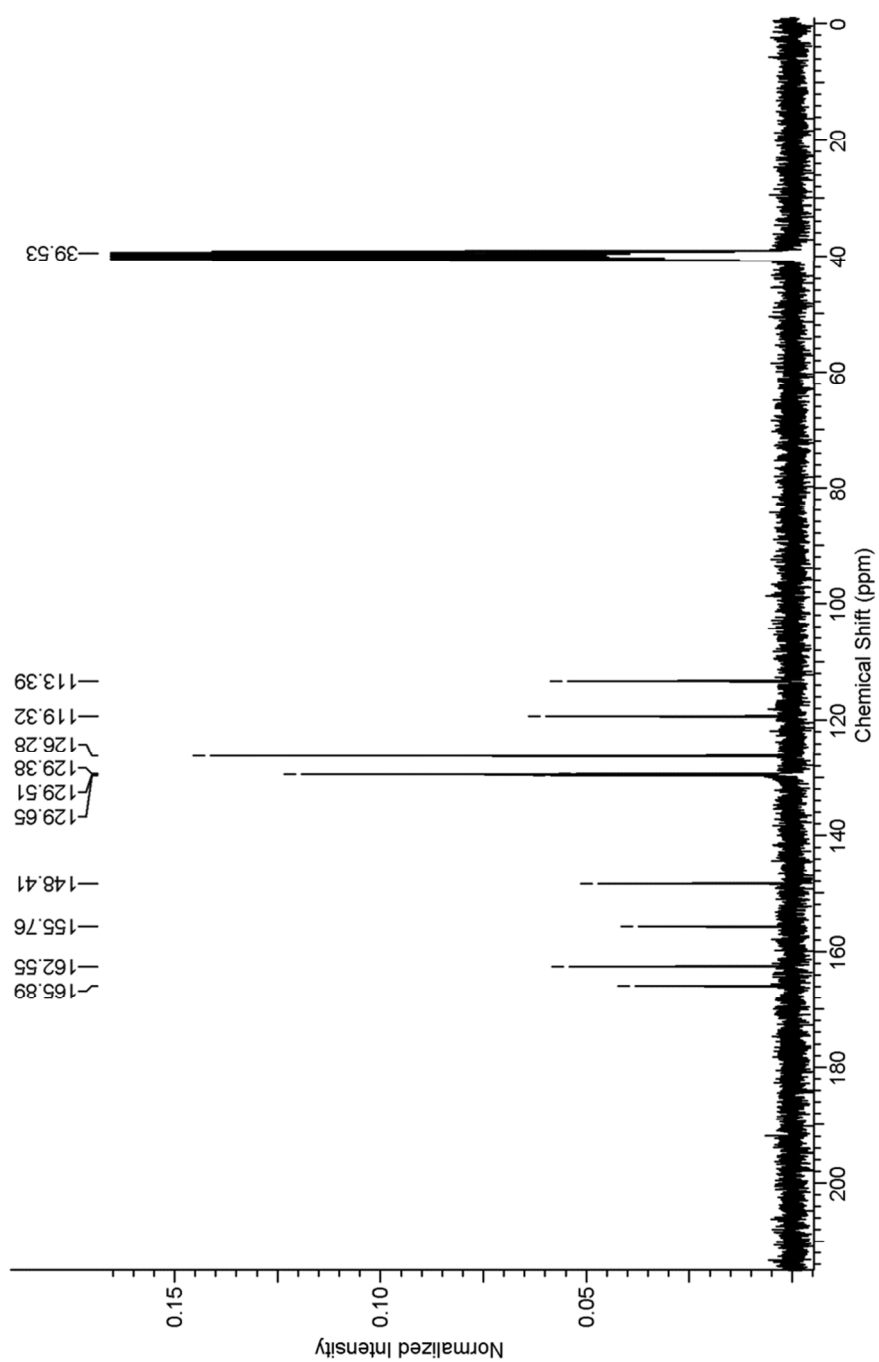


^{13}C -NMR of **8**

6 Supporting information

^{13}C -NMR of **9**

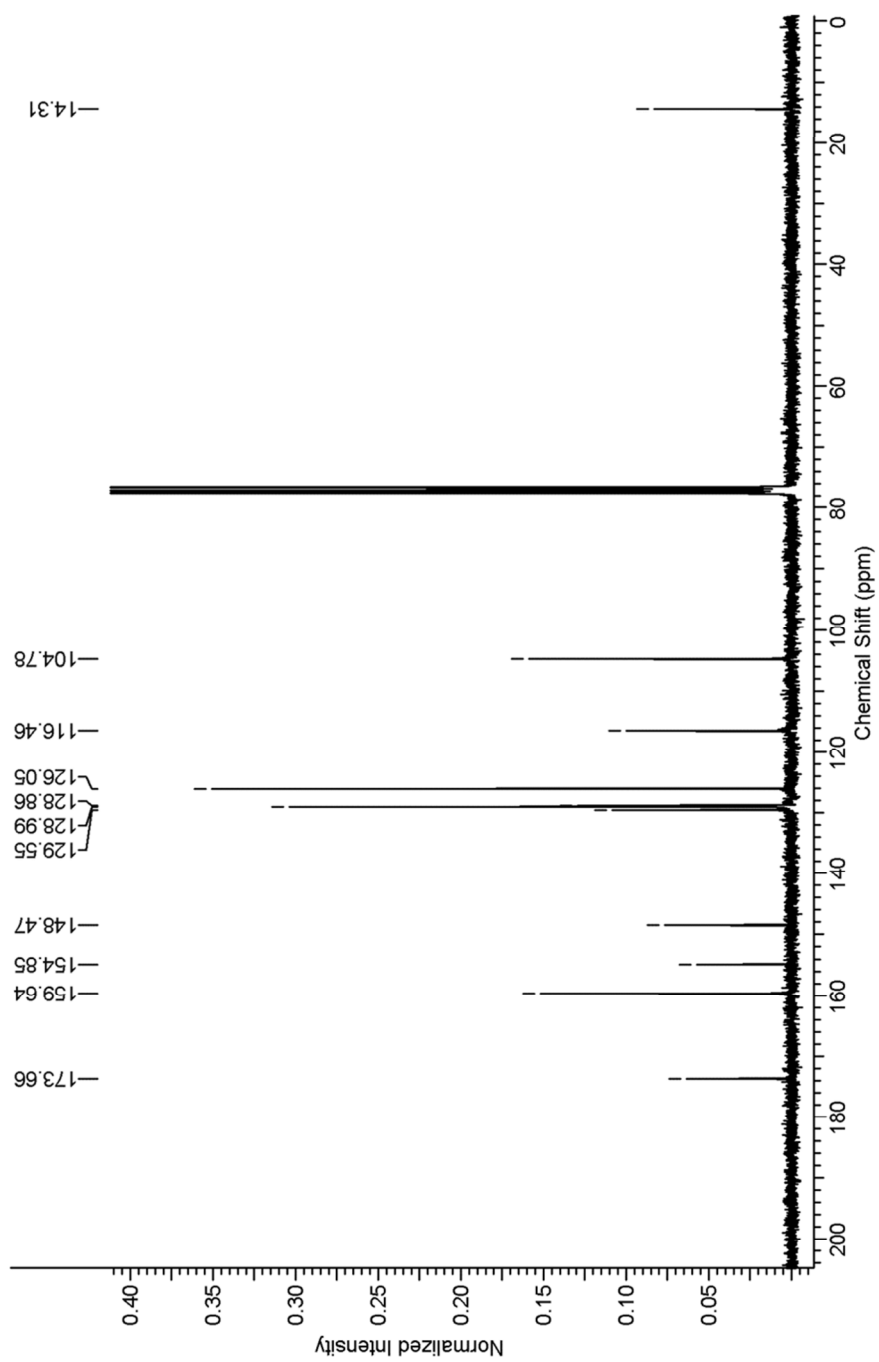


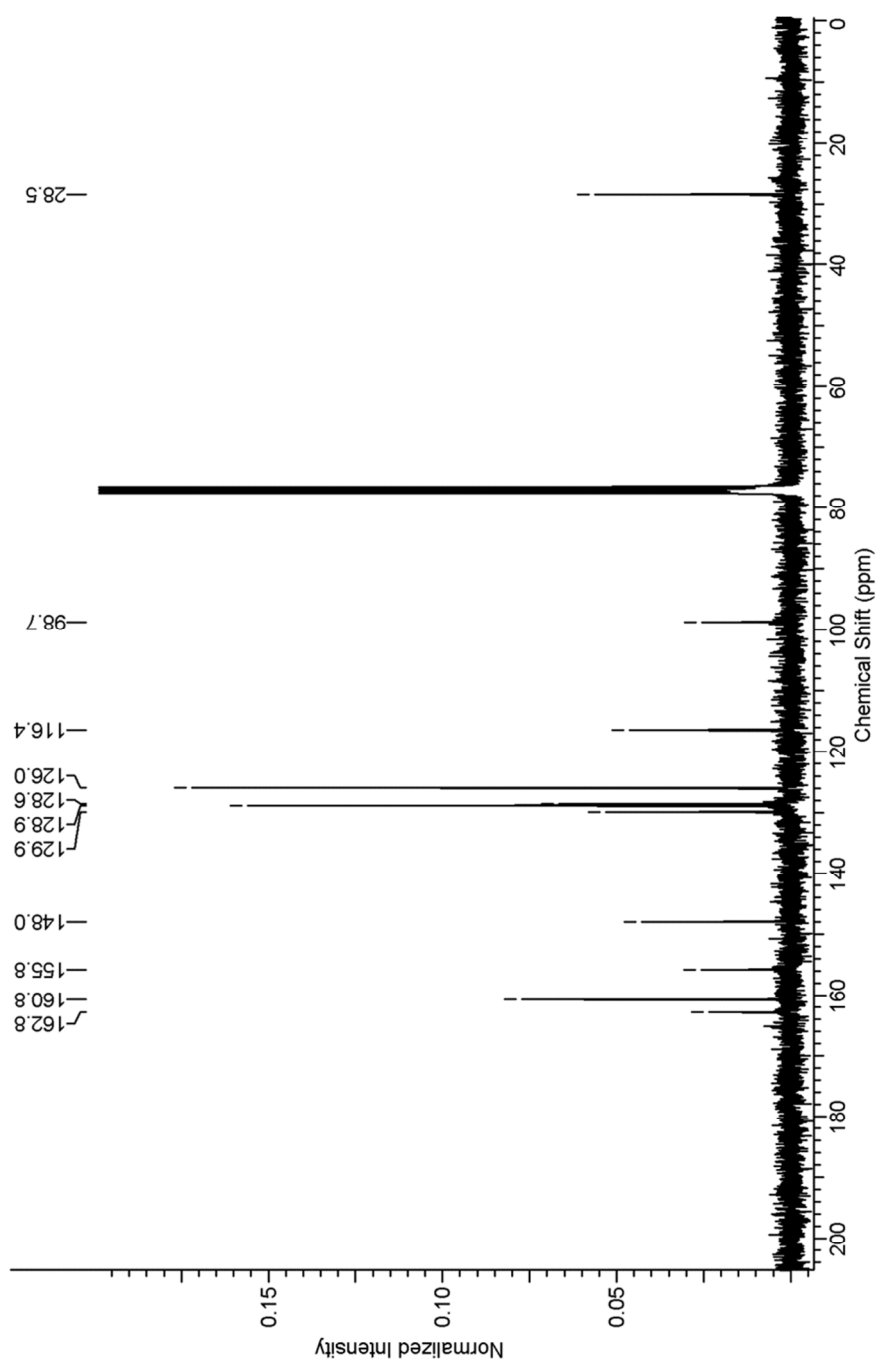
^{13}C -NMR of **10**

^{13}C -Signal of the methyl group at 39.53 was also detected by ^1H -HMQC

6 Supporting information

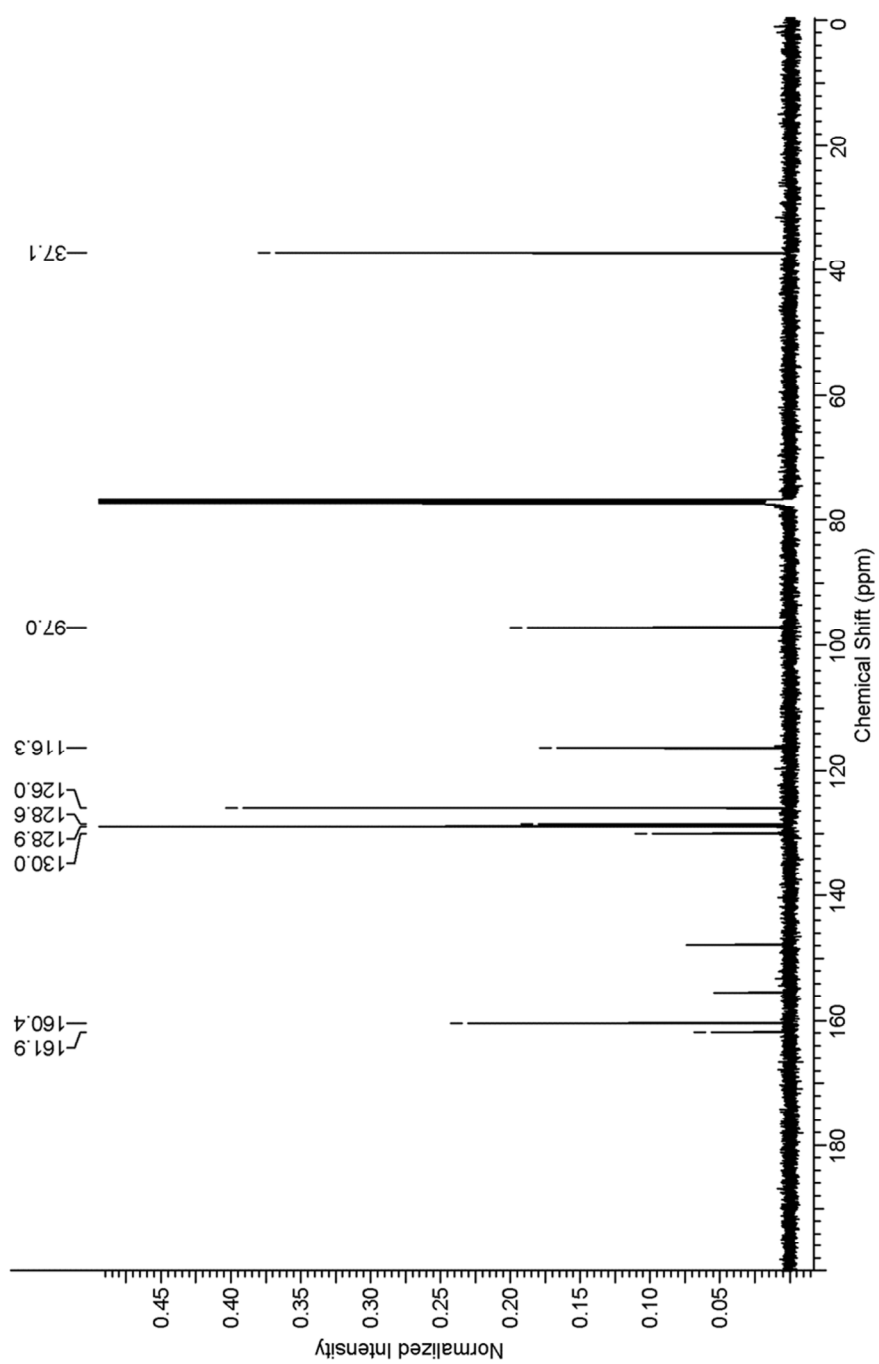
^{13}C -NMR of 11

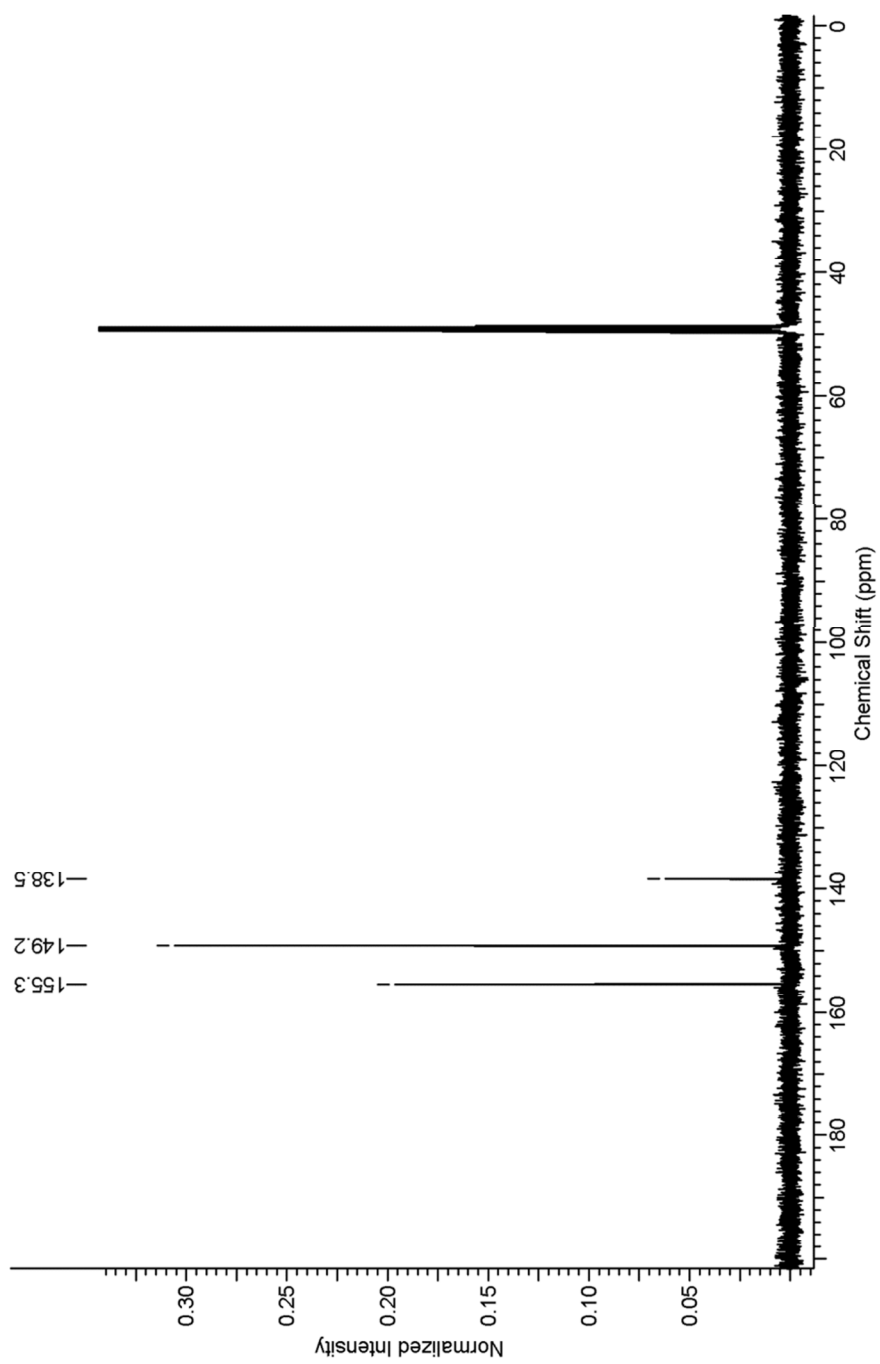


^{13}C -NMR of **12**

6 Supporting information

^{13}C -NMR of **14**

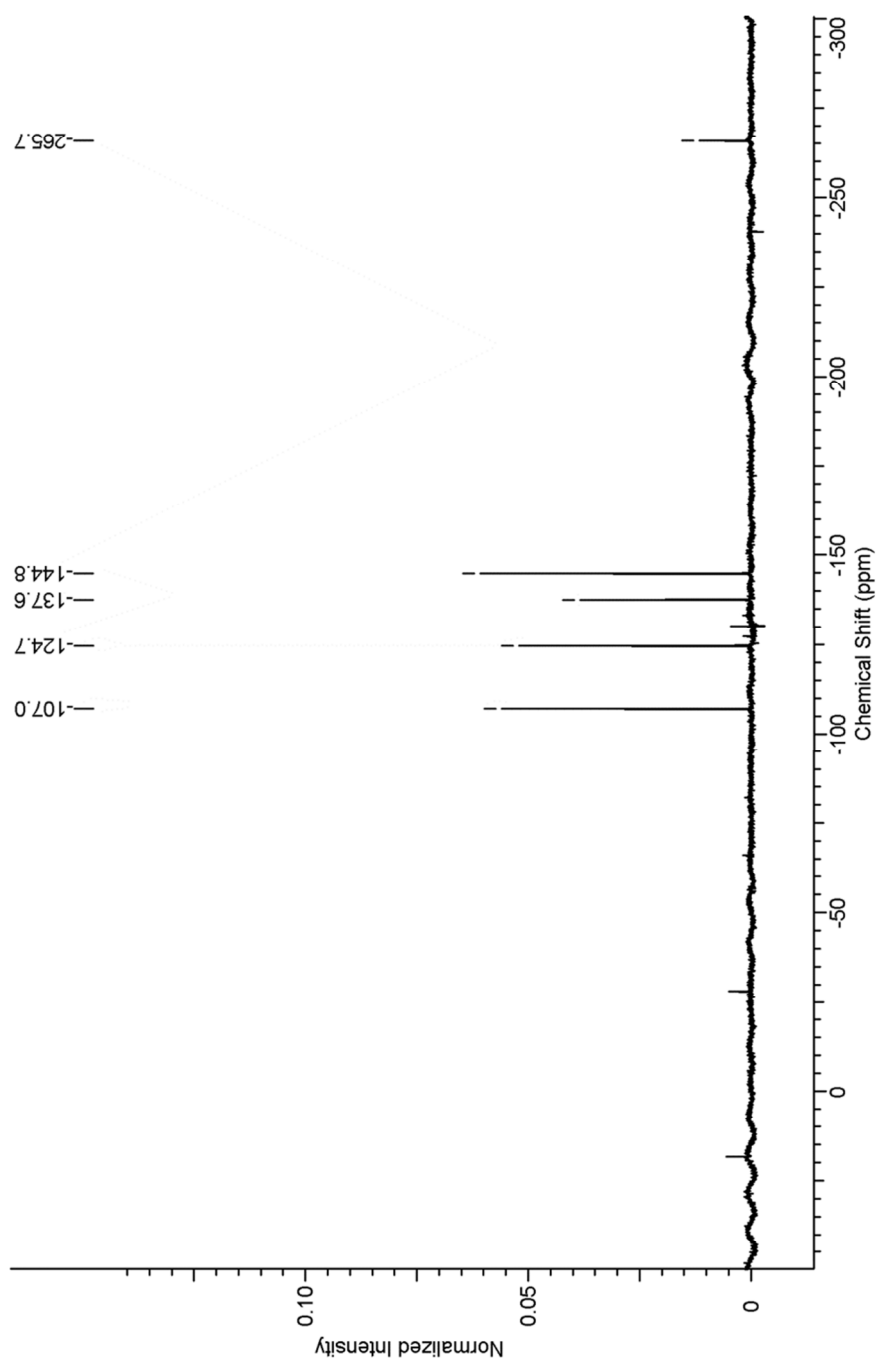


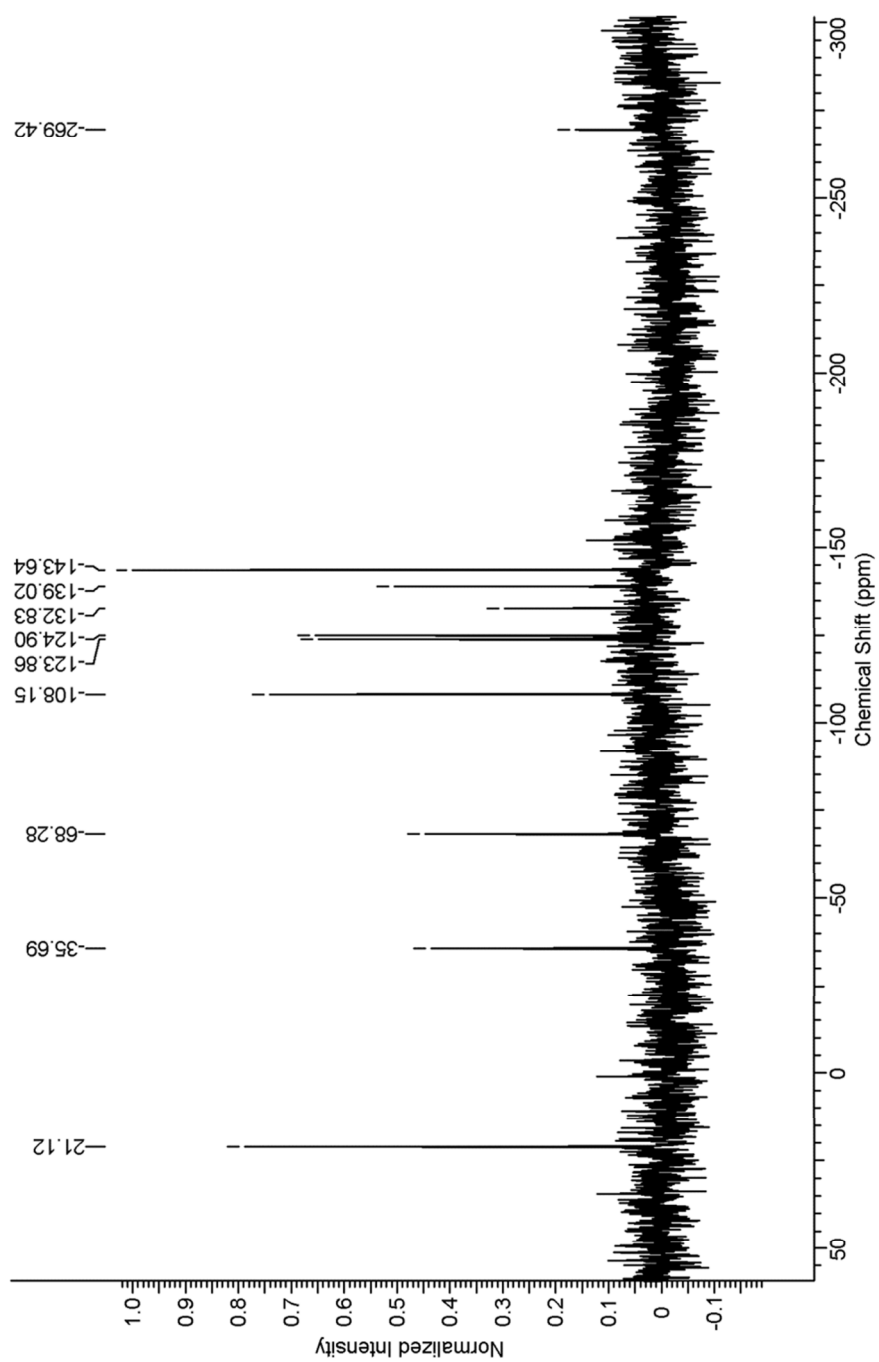
^{13}C -NMR of **15**

6 Supporting information

e) ^{15}N -NMR Spectra

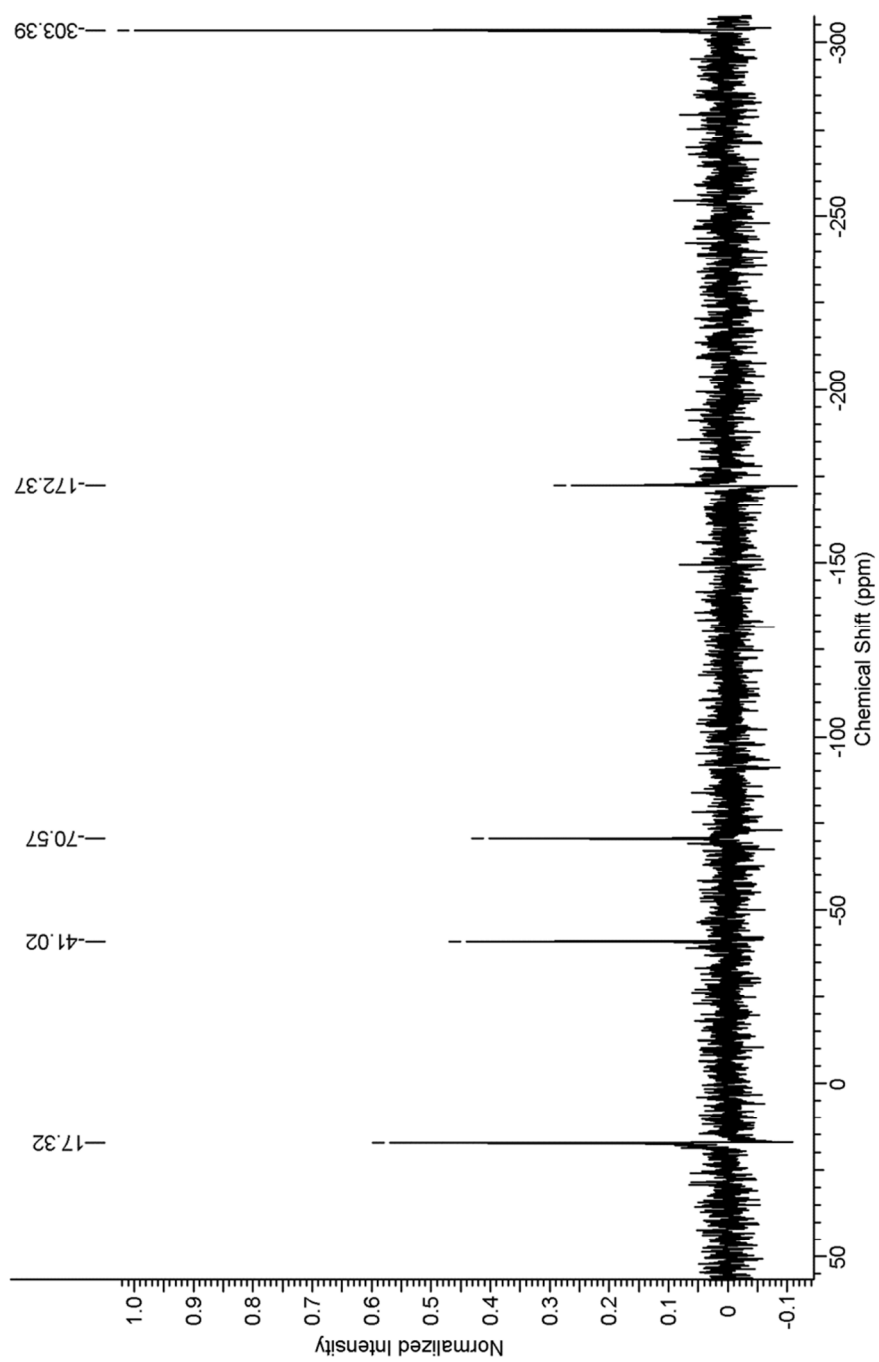
^{15}N -NMR of 1

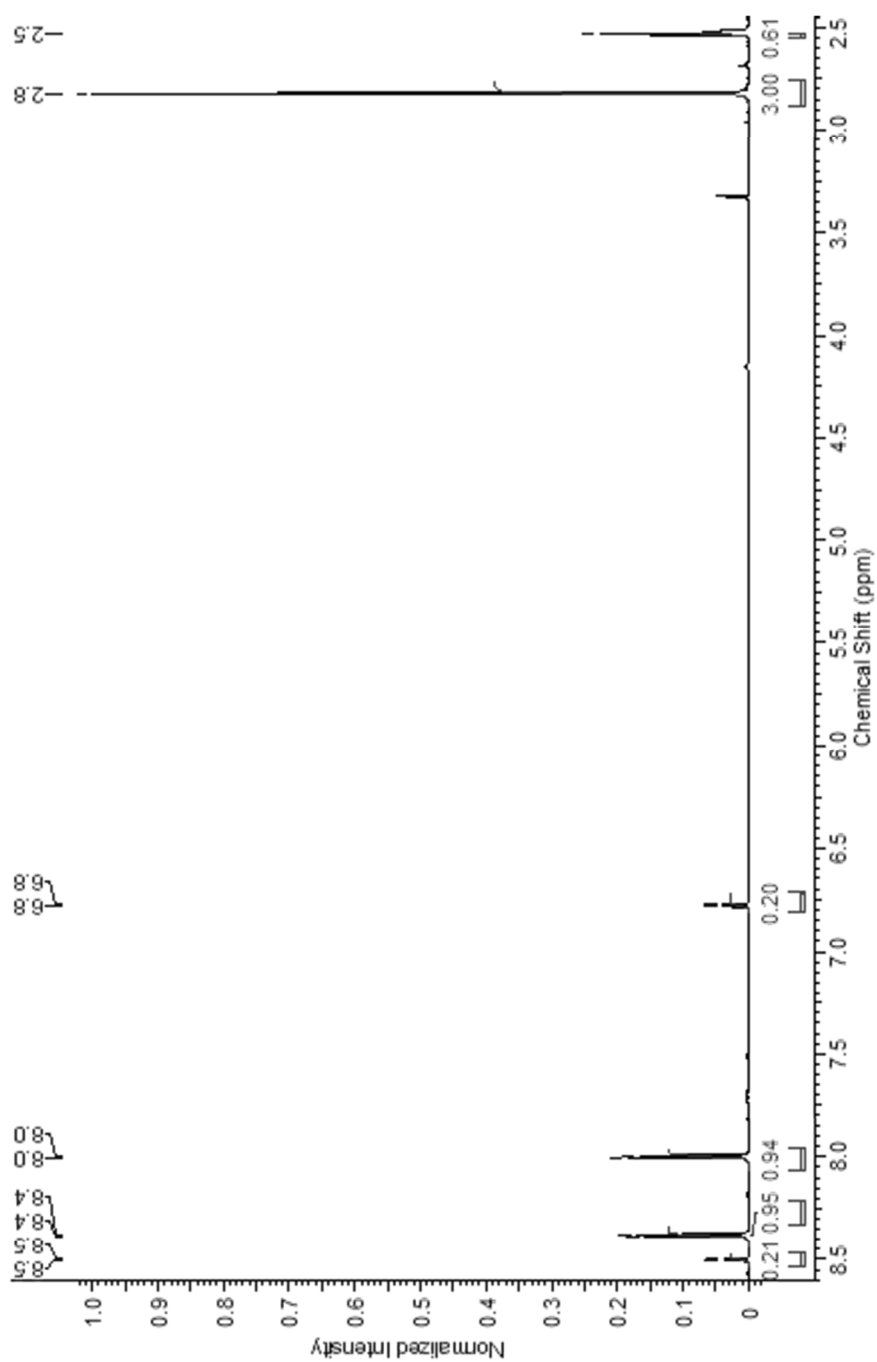


^{15}N -NMR of **3**

6 Supporting information

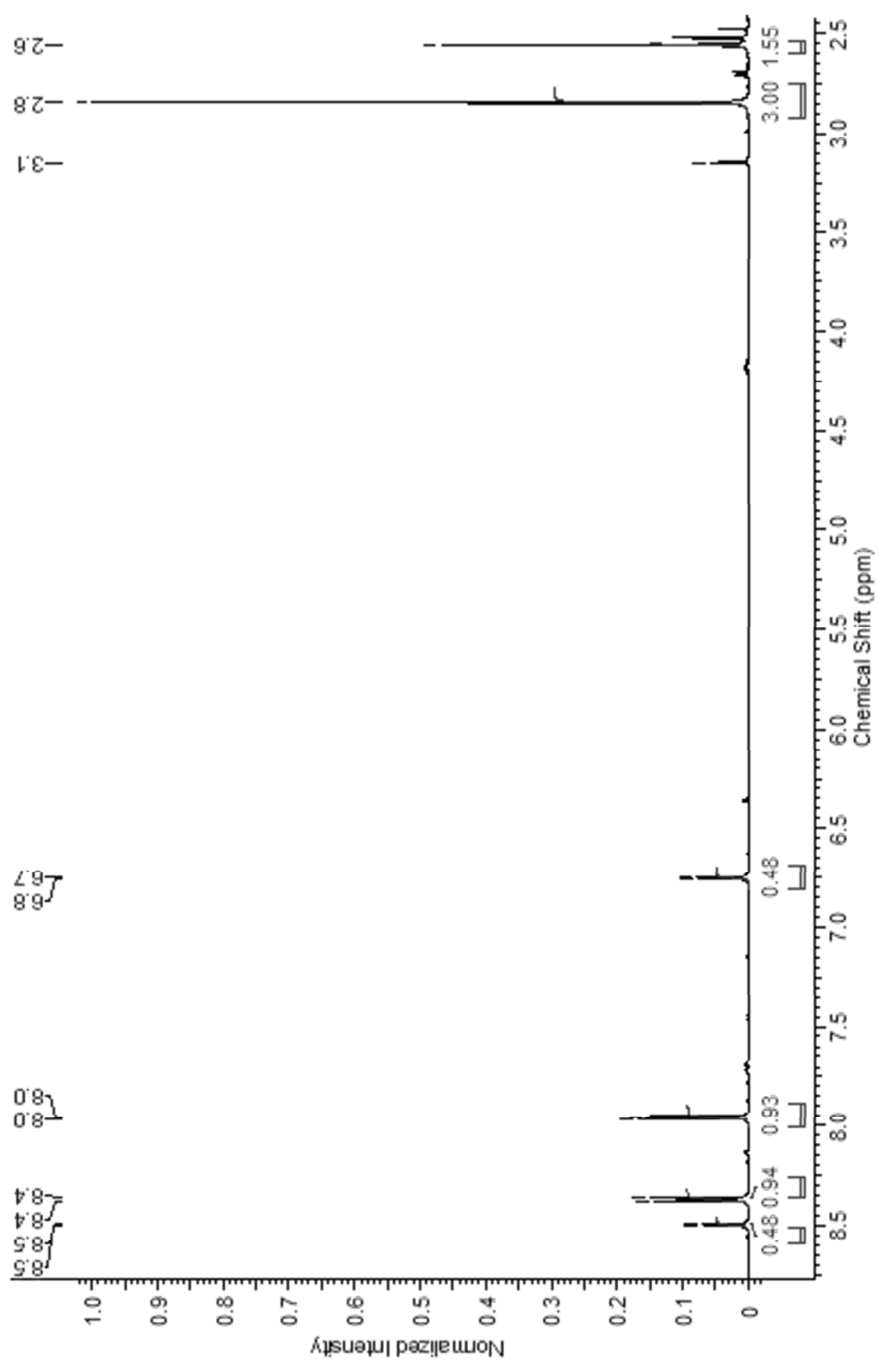
^{15}N -NMR of **4**

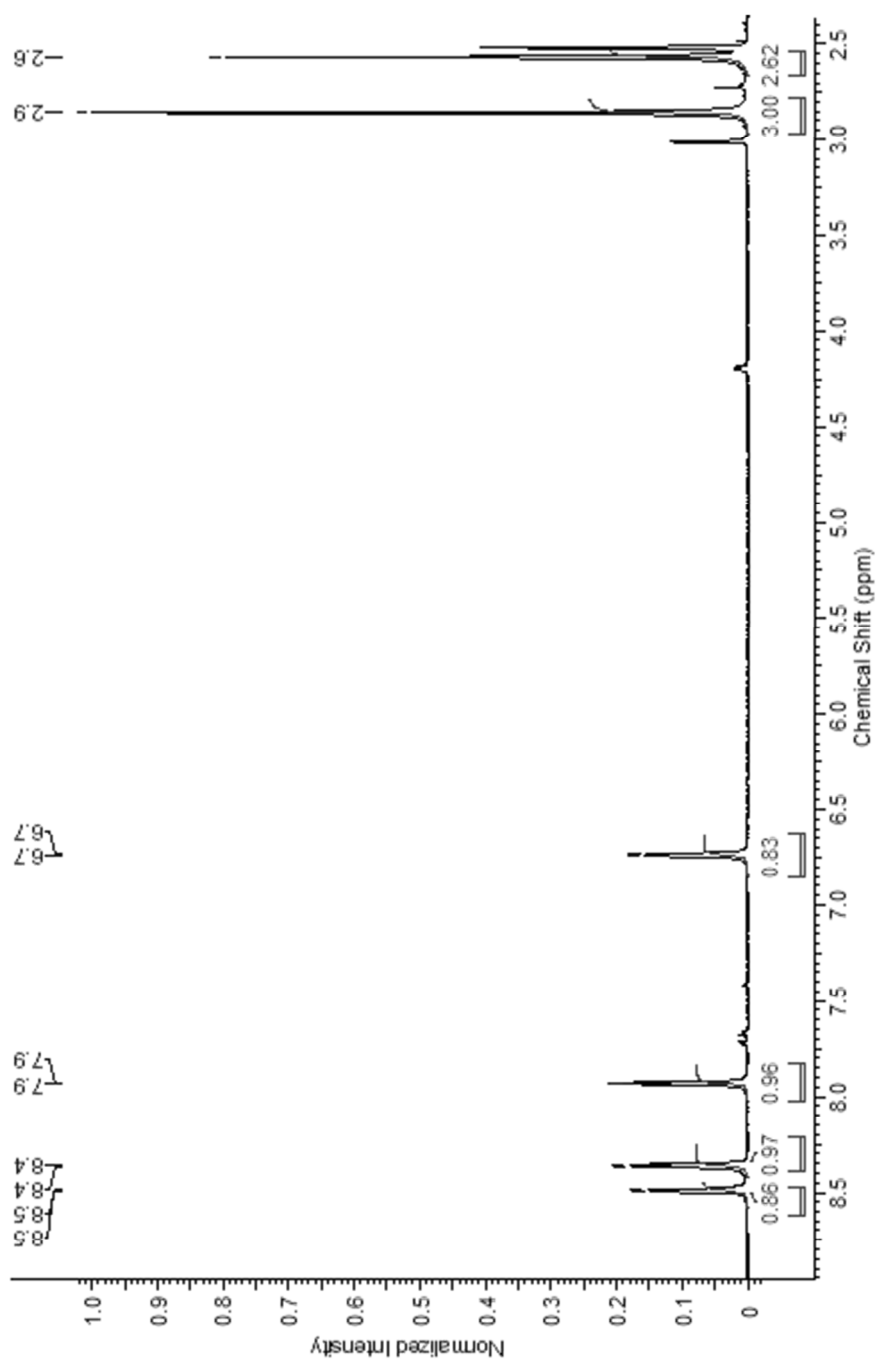


f) *Temperature gradient* $^1\text{H-NMR}$ of **3****3** in DMSO at 300K

6 Supporting information

3 in DMSO at 333K

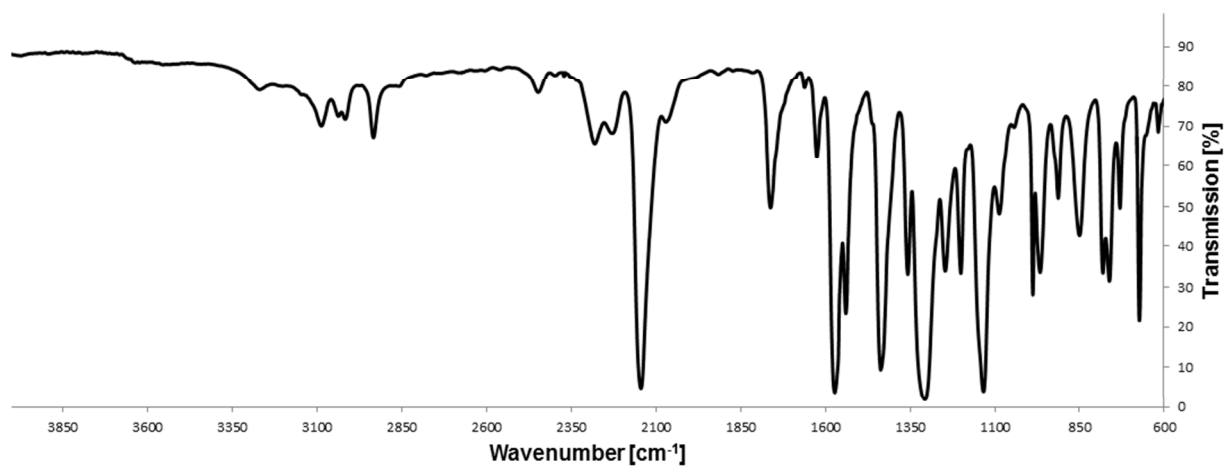


3 in DMSO at 353K

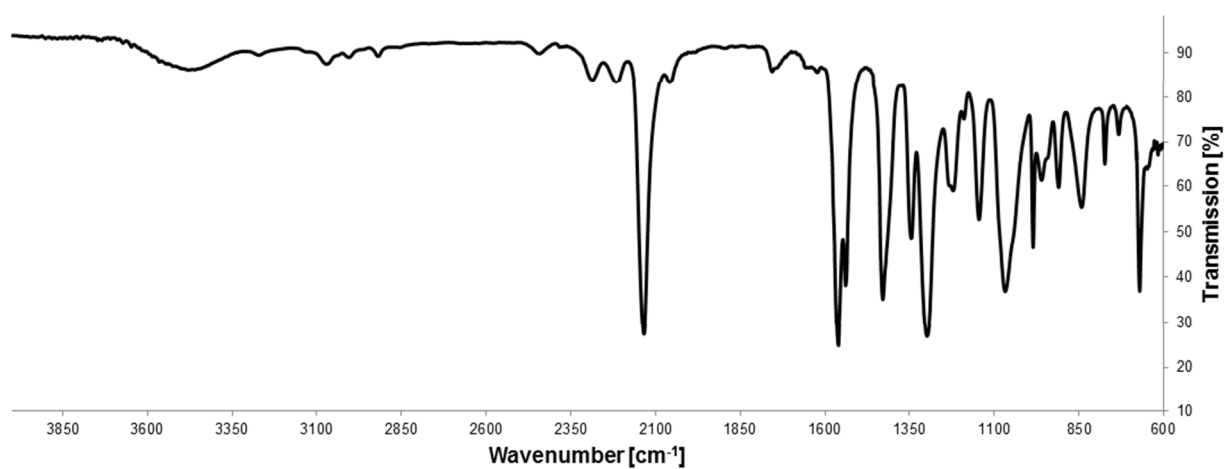
6 Supporting information

g) IR-Spectra

IR Spectrum of **1**



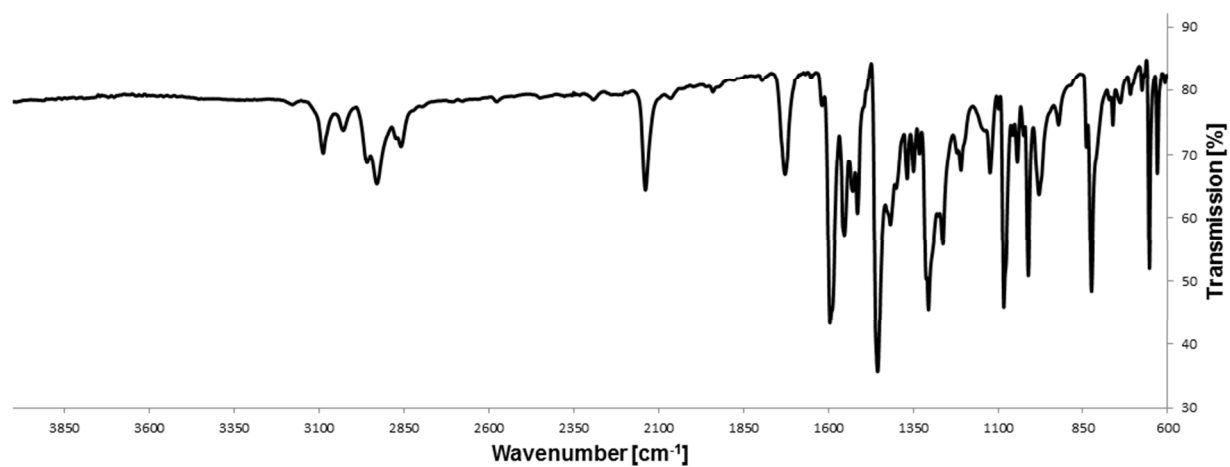
FT-IR (cm⁻¹): 3086, 3015, 2932, 2446, 2279, 2228, **2143**, 1761, 1661, 1624, 1571, 1539, 1435, 1356, 1306, 1246, 1200, 1133, 1086, 987, 966, 912, 850, 781, 761, 730, 673, 617

IR Spectrum of **2**

FT-IR (cm⁻¹): 3480, 3072, 2919, 2443, 2287, 2216, **2134**, 2058, 1756, 1560, 1539, 1428, 1345, 1299, 1221, 1189, 1144, 1068, 985, 960, 909, 842, 773, 732, 670, 622, 616, 585, 578, 572, 564, 553

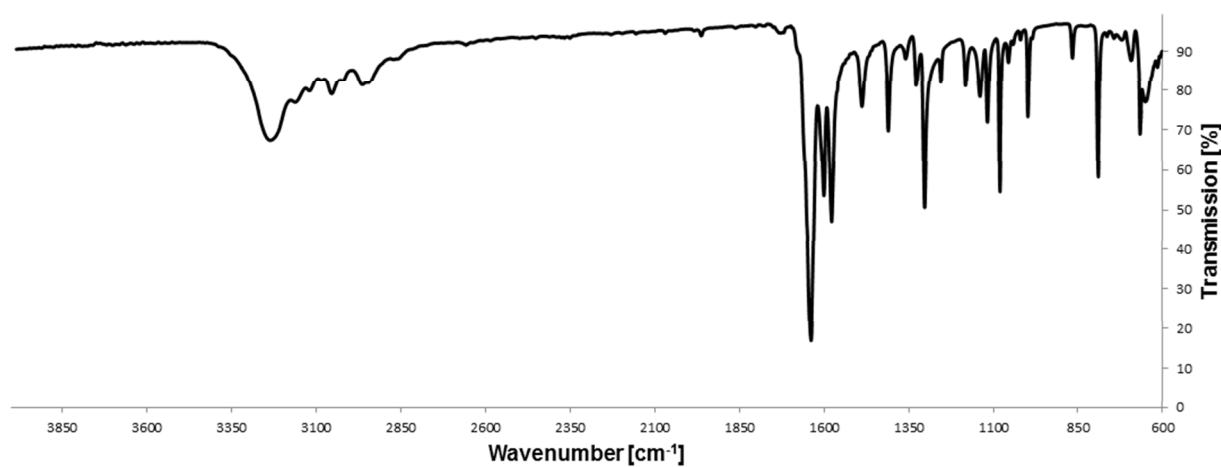
6 Supporting information

IR Spectrum of **3**



FT-IR (cm^{-1}): 3087, 3028, 2929, 2858, **2138**, 1727, 1595, 1553, 1528, 1514, 1455, 1417, 1368, 1349, 1332, 1306, 1263, 1210, 1124, 1084, 1057, 1044, 1025, 1012, 980, 922, 840, 826, 762, 740, 710, 676, 655, 631

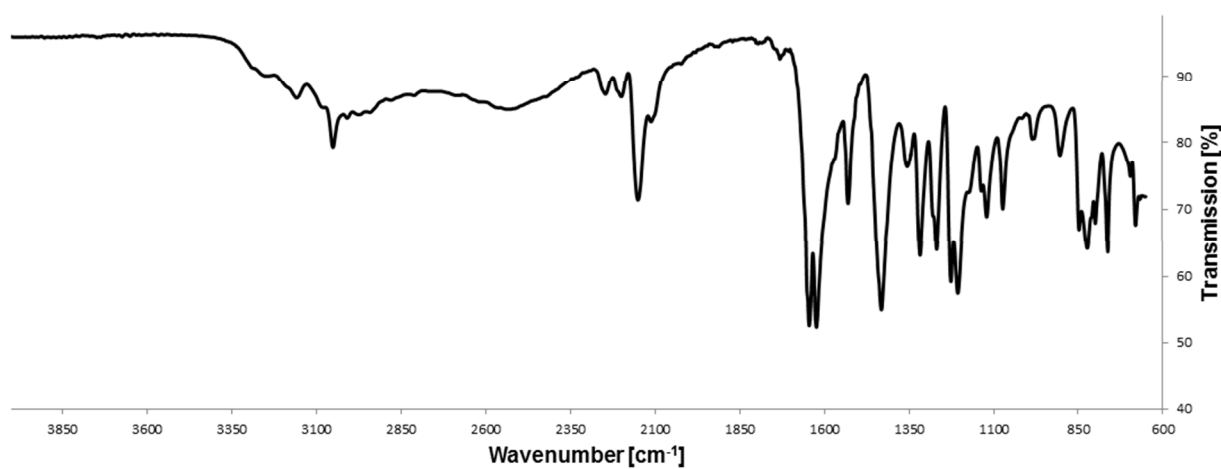
IR Spectrum of 4



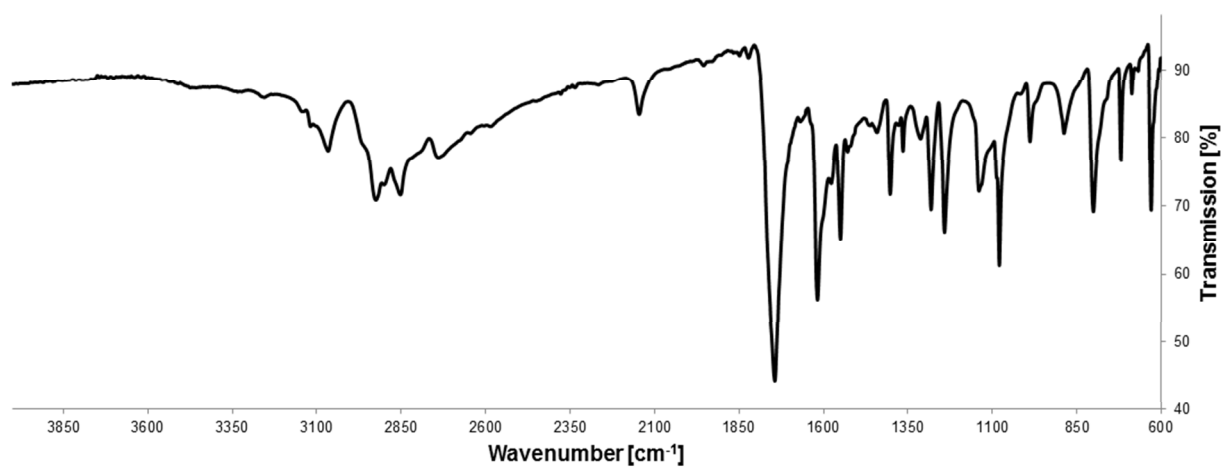
FT-IR (cm^{-1}): 3234, 3053, 2956, 1963, 1728, 1639, 1601, 1579, 1488, 1410, 1360, 1328, 1304, 1256, 1182, 1140, 1117, 1081, 1057, 1021, 998, 868, 791, 722, 694, 667, 651

6 Supporting information

IR Spectrum of **4** hydrochloric salt (lyophilized)



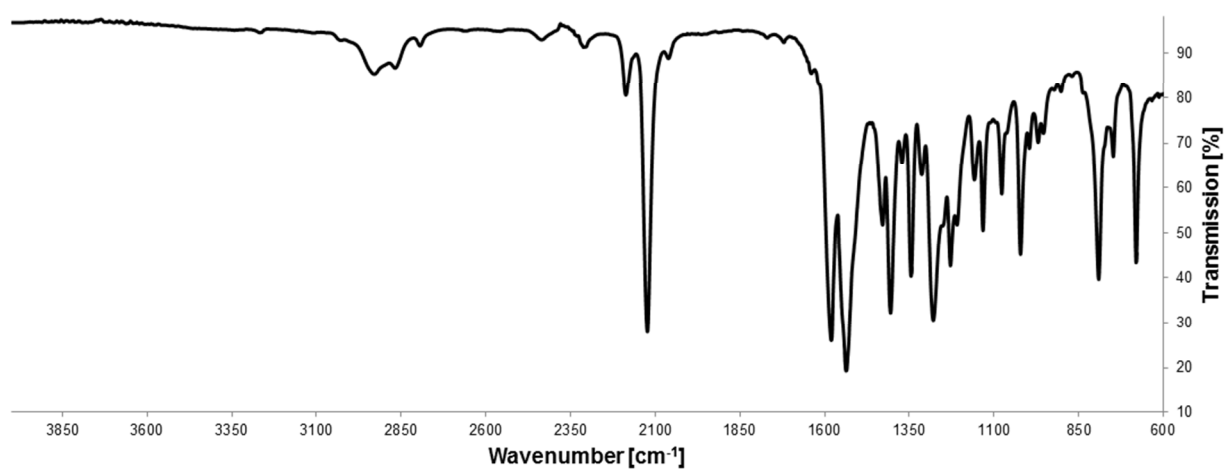
FT-IR (cm⁻¹): 3157, 3050, 2528, 2245, 2198, **2149**, 1645, 1623, 1529, 1431, 1354, 1317, 1268, 1226, 1205, 1120, 1072, 985, 903, 847, 824, 799, 763, 695, 680

IR-Spectrum of **5**

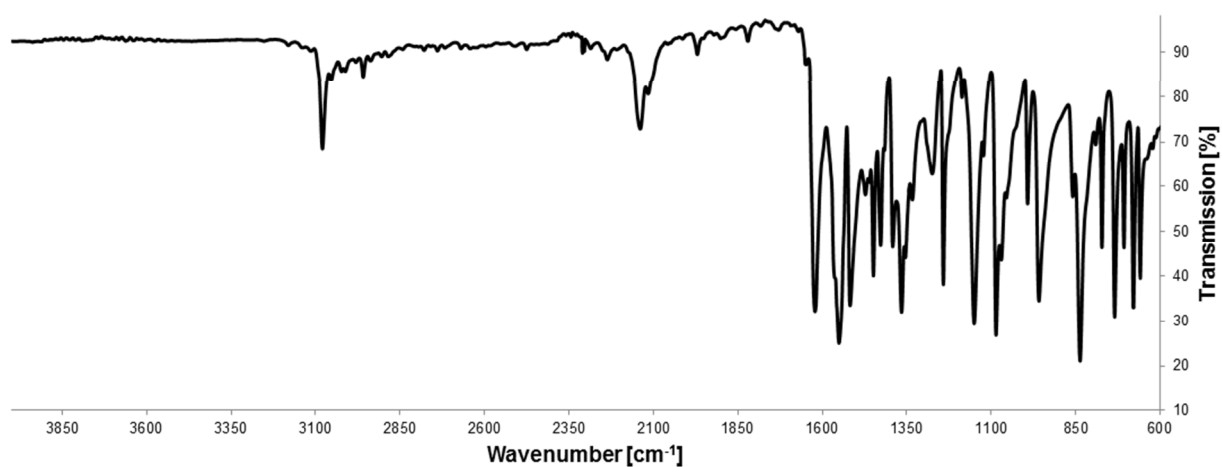
FT-IR (cm⁻¹): 3068, 2925, 2854, 2733, **2145**, 1822, 1744, 1618, 1550, 1528, 1441, 1403, 1364, 1312, 1282, 1242, 1138, 1080, 988, 888, 802, 719, 687, 631

6 Supporting information

IR-Spectrum of **6**



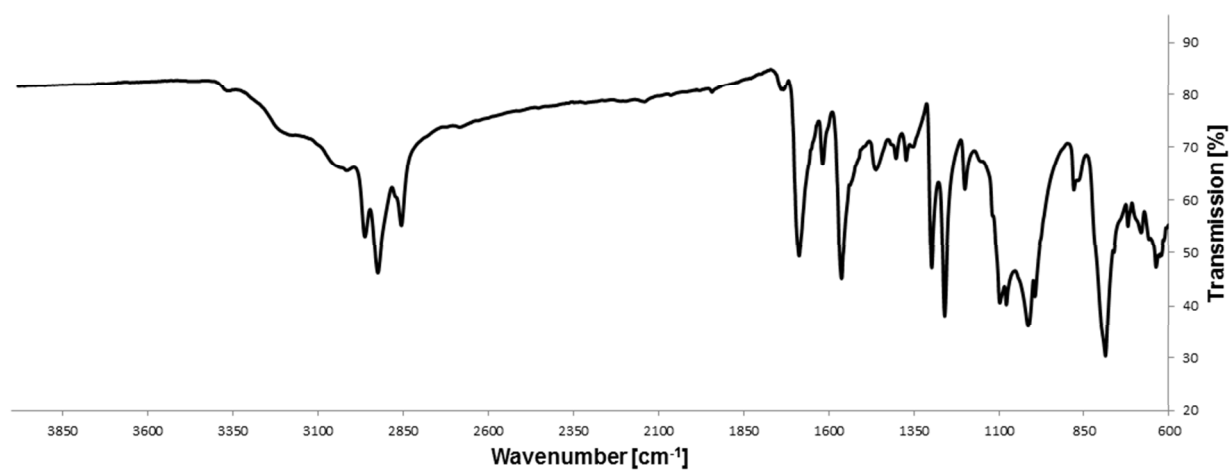
FT-IR (cm⁻¹): 2930, 2436, 2313, 2187, **2123**, 1581, 1536, 1429, 1406, 1372, 1345, 1314, 1279, 1229, 1209, 1158, 1133, 1077, 1022, 996, 970, 954, 791, 748, 681

IR-Spectrum of **7**

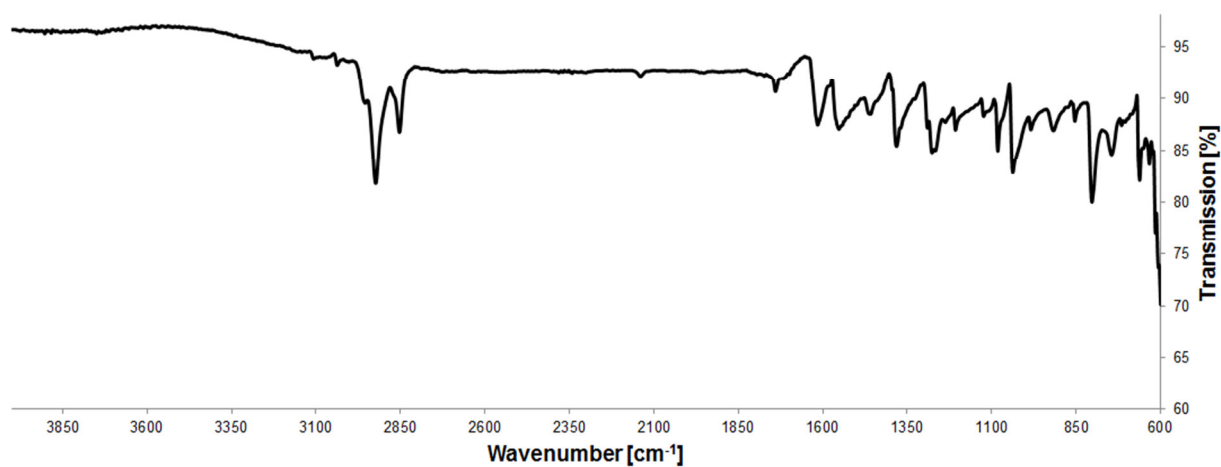
FT-IR (cm⁻¹): 3080, 3013, 2960, 2311, 2238, **2139**, 1971, 1822, 1622, 1551, 1518, 1473, 1449, 1428, 1392, 1366, 1354, 1334, 1275, 1242, 1187, 1151, 1123, 1086, 1070, 993, 959, 859, 837, 791, 773, 735, 707, 679, 659

6 Supporting information

IR-Spectrum of **8**



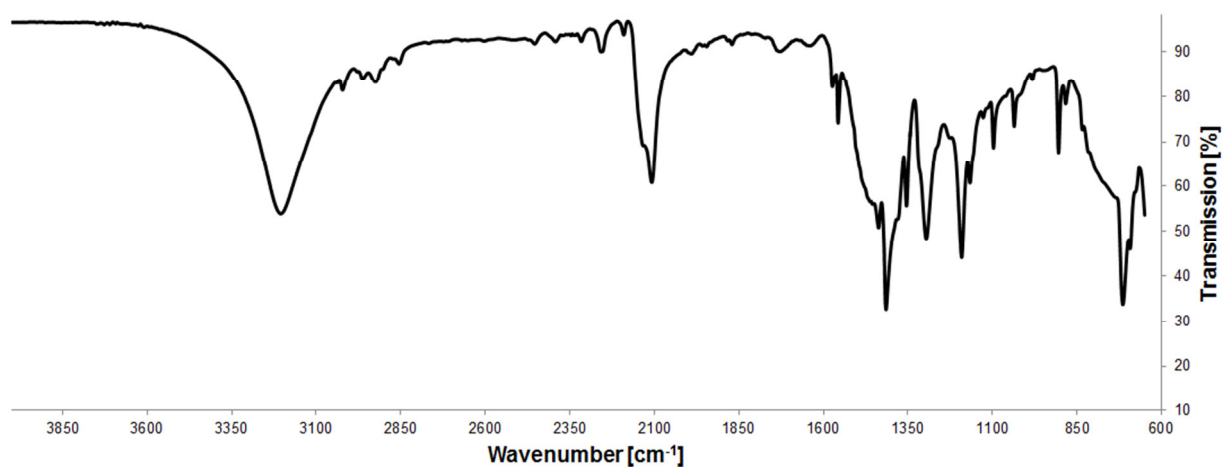
FT-IR (cm^{-1}): 2960, 2924, 2854, 1735, 1687, 1617, 1562, 1460, 1401, 1371, 1297, 1259, 1199, 1097, 1078, 1014, 994, 879, 786, 720, 682, 638

IR-Spectrum of **9**

FT-IR (cm⁻¹): 2924, 2854, 1740, 1614, 1547, 1461, 1382, 1276, 1207, 1082, 1038, 984, 918, 854, 803, 745, 663, 633

6 Supporting information

IR-Spectrum of **15**



FT-IR (cm⁻¹): 3205, 3022, 2925, 2393, 2258, 2191, **2108**, 1727, 1574, 1557, 1437, 1415, 1354, 1296, 1191, 1167, 1097, 1036, 905, 884, 715, 693

III. References

- 1 K. D. Grimes, A. Gupte and C. C. Aldrich, *Synthesis*, **2010**, 2010, 1441–1448.
- 2 G. M. Sheldrick, *Acta Crystallogr., Sect. A: Found. Crystallogr.*, **2008**, 64, 112–122.
- 3 A. Klamt and G. Schüürmann, *J. Chem. Soc., Perkin Trans. 2*, **1993**, 799.
- 4 M. Valiev, E. J. Bylaska, N. Govind, K. Kowalski, T. P. Straatsma, H. van Dam, D. Wang, J. Nieplocha, E. Apra, T. L. Windus and W. A. de Jong, *Comput. Phys. Commun.*, 2010, 181, 1477–1489.
- 5 M. D. Shultz, *Bioorg. Med. Chem. Lett.*, **2013**, 23, 5980–5991.
- 6 P. N. Mortenson and C. W. Murray, *J. Comput. Aided. Mol. Des.*, **2011**, 25, 663–667.

6 Supporting information

6.3 Supporting information for Publication III

Supporting Information

Mild and Catalyst-free Microwave-assisted Synthesis of 4,6-Disubstituted 2-Methylthiopyrimidines – Exploiting Tetrazole as an Efficient Leaving Group

Andreas Thomann^a, Jens Eberhard^a, Giuseppe Allegretta^a, Martin Empting^a and Rolf W. Hartmann^{a,b*}

^aHelmholtz-Institute for Pharmaceutical Research Saarland, Saarland University, Campus C 2.3, D-66123 Saarbrücken, Germany

^bPharmaceutical and Medicinal Chemistry, Saarland University, Campus C 2.3, D-66123 Saarbrücken, Germany
Fax: +49-681-302-70308
E-mail: rolf.hartmann@helmholtz-hzi.de

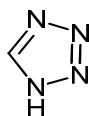
Instrumentation for routine analysis

NMR spectra were recorded on a Bruker Avance AV 300 or a Bruker DRX 500. The residual proton, ¹H, or carbon ¹³C resonances of the >99 % deuterated solvents were used for internal reference of all spectra acquired. (CDCl₃ ¹H 7.260 ppm, ¹³C 77.16 ppm; DMSO-d₆, ¹H 2.500 ppm, ¹³C 39.52 ppm).

Electrospray ionization (ESI) mass spectrometry were recorded with a Surveyor LC system MSQ electrospray mass spectrometer LC-MS couple (ThermoFisher, Dreieich, Germany) by use of an acetonitrile/water gradient in positive mode (+), if not indicated otherwise. 0.1% TFA was added if necessary.

Analytical and Experimental Data

1H-Tetrazole:



Sodium azide (0.2 mol, 13 g), ammonium chloride (0.2 mol, 10.7 g) and ethyl orthoformate (0.6 mol, 89 g) were charged in a round bottom flask. Glacial acid (0.8 mol, 46 ml) was added slowly at room temperature. After addition, the mixture was stirred at 80°C for 16 hrs. The reaction mixture was evaporated to dryness in dynamic vacuum (at 40°C) and the resulting colorless residue was resuspended in boiling acetone and filtered hot (G4 glass frit). The acetone was removed *in vacuo* and the colorless residue was recrystallized from ethyl acetate to yield 1H-tetrazole as colorless needles (7.1 g, 51%).

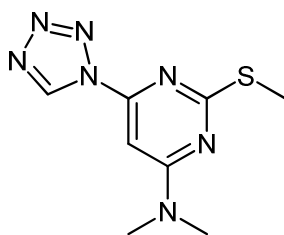
ESI-MS(-): m/z 68.9 [M-H]⁻

¹H NMR (300 MHz, DMSO-*d*₆): δ = 9.38 ppm (s, 1 H)

¹³C NMR (75 MHz, DMSO-*d*₆): δ = 143.2 ppm

General Procedure for the synthesis of compounds 2-24:

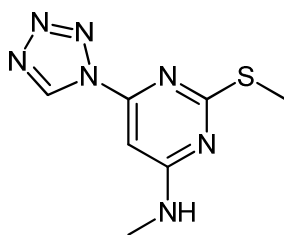
1 equivalent of starting material (either compound **1** (for cmpds **2-24**) or 4,6-dichloro-2-thiomethylpyrimidine (for cmpds **1**, **17op**)) was dissolved in the solvent indicated in Table 3 or 4. The reactant (for equivalents see Table 3 or 4) and 1 equivalent of base was added at once and the mixture was stirred in a capped vial in a CEM Discover SP microwave oven connected to a CEM Explorer SP 12S autosampler for the indicated time and temperature (see Table 3 and 4). Isolation and purification of the desired compounds was achieved either by addition of water and subsequent filtration (**2**, **3**, **5-8**, **13-20**, **22**) or by column chromatography (**4**, **9-12**, **21**, **23**, **24**).

Compound 2:

ESI-MS(+): m/z 210.0 [M-N₂+H]⁺

¹H NMR (300 MHz, DMSO-*d*₆): δ = 10.12 (s, 1 H), 6.88 (s, 1 H), 3.20 (br. s, 6 H), 2.54 ppm (s, 3 H)

¹³C NMR (75 MHz, DMSO-*d*₆): δ = 171.1, 162.4, 151.9, 141.8, 86.9, 86.6, 13.0 ppm

Compound 3:

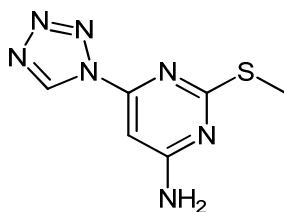
ESI-MS(+): m/z 196.0 [M-N₂+H]⁺

¹H NMR (300 MHz, DMSO-*d*₆): δ = 10.10 (s, 1 H), 8.07 (d, *J*=4.1 Hz, 1 H), 6.73 (s, 1 H), 2.91 (d, *J*=4.6 Hz, 3 H), 2.54 ppm (s, 3 H)

¹³C NMR (75 MHz, DMSO-*d*₆): δ = 172.5, 163.8, 151.0, 142.1, 90.0, 27.5, 14.1 ppm

6 Supporting information

Compound 4:

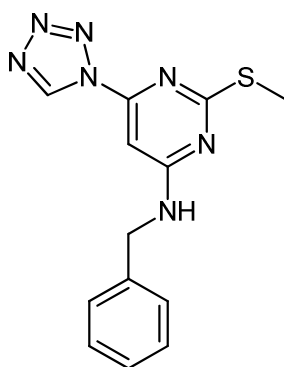


ESI-MS(+): m/z 182.0 $[M-N_2+H]^+$

1H NMR (300 MHz, DMSO- d_6) δ = 10.10 (s, 1H), 7.59 (br. s., 2H), 6.73 (s, 1H), 2.52 (s, 3H)

^{13}C NMR (75 MHz, DMSO- d_6): δ = 171.8, 164.9, 151.7, 141.6, 141.4, 13.4 ppm

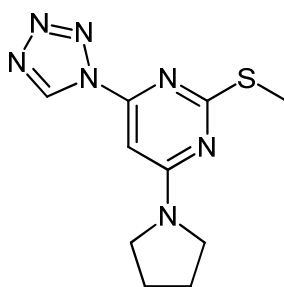
Compound 5:



ESI-MS(+): m/z 299.9 $[M+H]^+$, 271.9 $[M-N_2+H]^+$

1H NMR (300 MHz, DMSO- d_6): δ = 10.09 (s, 1 H), 8.62 (t, $J=5.3$ Hz, 1 H), 7.16-7.50 (m, 5 H), 6.86 (s, 1 H), 4.64 (d, $J=5.5$ Hz, 2 H), 2.41 - 2.51 ppm (m, 3 H)

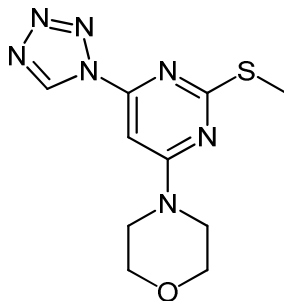
^{13}C NMR (300 MHz, DMSO- d_6): δ = 172.4, 163.3, 152.0, 143.4, 139.2, 129.6, 128.3, 127.1, 90.6, 44.4, 14.0 ppm

Compound 6:

ESI-MS(+): m/z 236.0 $[M-N_2+H]^+$

^1H NMR (300 MHz, CHLOROFORM-*d*): δ = 9.45 (s, 1 H), 6.65 (s, 1 H), 3.71 (t, $J=6.6$ Hz, 2 H), 3.46 (t, $J=6.6$ Hz, 2 H), 2.55 (s, 3 H), 1.85-2.24 ppm (m, 4 H)

^{13}C NMR (75 MHz, CHLOROFORM-*d*): δ = 116.1, 111.8, 108.0, 102.9, 80.8, 64.2, 55.9, 55.5, 51.3 ppm

Compound 7:

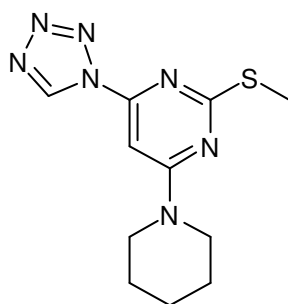
ESI-MS(+): m/z 251.8 $[M-N_2+H]^+$

^1H NMR (300 MHz, CHLOROFORM-*d*): δ = 9.39 (s, 1 H), 6.81 (s, 1 H), 3.42-4.07 (m, 8 H), 2.48 ppm (s, 3 H)

^{13}C NMR (75 MHz, CHLOROFORM-*d*): δ = 172.8, 162.6, 152.9, 140.3, 86.3, 66.3, 44.5, 14.2 ppm

6 Supporting information

Compound 8:

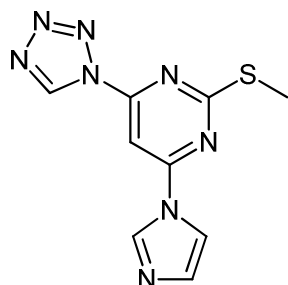


ESI-MS(+): m/z 278.2 $[M+H]^+$, 251.2 $[M-N_2+H]^+$

1H NMR (300 MHz, CHLOROFORM-*d*): δ = 9.45 (s, 1 H), 6.88 (s, 1 H), 3.73 (br. s, 4 H), 2.54 (s, 3 H), 1.62-1.79 ppm (m, 6 H)

^{13}C NMR (75 MHz, CHLOROFORM-*d*): δ = 172.5, 162.0, 152.8, 140.4, 140.2, 45.7, 25.6, 24.4, 14.2 ppm

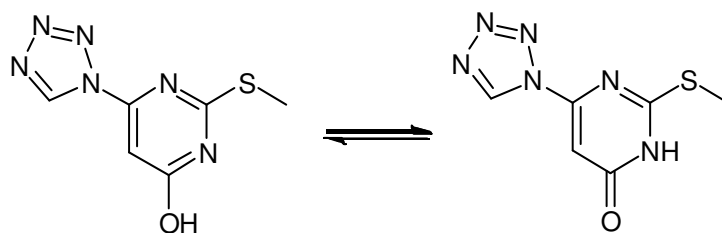
Compound 9:



ESI-MS(+): m/z 232.9 $[M-N_2+H]^+$

1H NMR (300 MHz, DMSO-*d*₆): δ = 10.35 (s, 1 H), 8.87 (s, 1 H), 8.22 (s, 2 H), 7.22 (s, 1 H), 2.71 ppm (s, 3 H)

^{13}C NMR (75 MHz, DMSO-*d*₆): δ = 173.3, 156.8, 154.1, 142.3, 136.2, 131.2, 116.8, 93.8, 14.0 ppm

Compound 10:

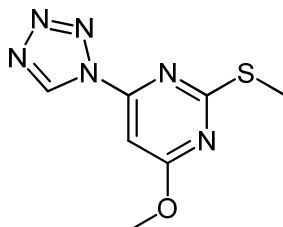
ESI-MS: a signal for the molecular ion was not found

^1H NMR (300 MHz, $\text{DMSO}-d_6$): δ = 10.28 (s, 1 H), 7.04 (s, 1 H), 2.62 ppm (s, 3 H)

^{13}C NMR (75 MHz, $\text{DMSO}-d_6$): δ = 173.0, 162.4, 153.3, 142.5, 90.8, 14.2 ppm

FT-IR (cm^{-1}): 3107, 2936, 2732, 2288, 2235, 2185, 1626, 1588, 1523, 1474, 1439, 1391, 1347, 1332, 1294, 1238, 1186, 1139, 1100, 1081, 1013, 980, 966, 936, 822, 793, 763, 723, 773

$\text{pK}_a = 3.17 \pm 0.05$

Compound 11:

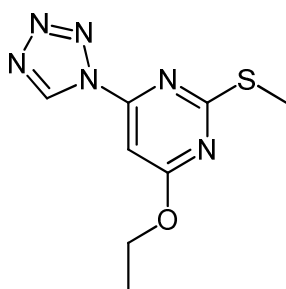
ESI-MS(+): m/z 197.0 $[\text{M}-\text{N}_2+\text{H}]^+$

^1H NMR (300 MHz, $\text{CHLOROFORM}-d$): δ = 9.48 (s, 1 H), 7.08 (s, 1 H), 4.09 (s, 3 H), 2.64 ppm (s, 3 H)

^{13}C NMR (75 MHz, $\text{CHLOROFORM}-d$): δ = 173.9, 171.0, 153.4, 140.3, 92.6, 91.2, 14.2 ppm

6 Supporting information

Compound 12:

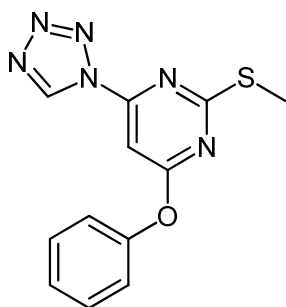


ESI-MS(+): m/z 239.1 $[M+H]^+$, 211.1 $[M-N_2+H]^+$

1H NMR (500 MHz, CHLOROFORM-*d*): δ = 9.48 (s, 1 H), 7.04 (s, 1 H), 4.53 (q, $J=7.1$ Hz, 2 H), 2.57 (s, 3 H), 1.44 ppm (t, $J=7.1$ Hz, 3 H)

^{13}C NMR (126 MHz, CHLOROFORM-*d*): δ = 173.7, 170.6, 153.4, 140.2, 92.0, 64.0, 14.2, 14.2 ppm

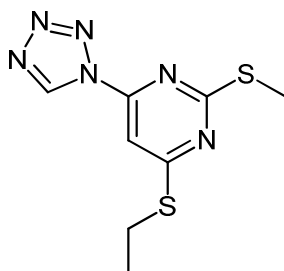
Compound 13:



ESI-MS(+): m/z 258.9 $[M-N_2+H]^+$

1H NMR (300 MHz, CHLOROFORM-*d*) δ = 9.43 (s, 1 H), 7.40 (d, $J=7.7$ Hz, 2H), 6.97-7.31 (m, 4H), 2.42 (s, 3H)

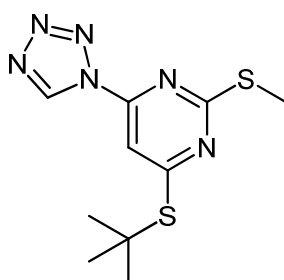
^{13}C NMR (75 MHz, CHLOROFORM-*d*) δ = 174.4, 170.9, 154.3, 151.9, 140.3, 129.8, 126.4, 121.4, 91.5, 14.2

Compound 14:

ESI-MS(+): m/z 227.1 $[M+H]^+$, 255.1 $[M-N_2+H]^+$

^1H NMR (300 MHz, CHLOROFORM-*d*): δ = 9.42 (s, 1 H), 7.43 (s, 1 H), 3.20 (q, $J=7.4$ Hz, 2 H), 2.55 (s, 3 H), 1.36 ppm (t, $J=7.4$ Hz, 3 H)

^{13}C NMR (75 MHz, CHLOROFORM-*d*): δ = 174.5, 173.2, 151.0, 140.3, 102.2, 102.1, 24.5, 14.2 ppm

Compound 15:

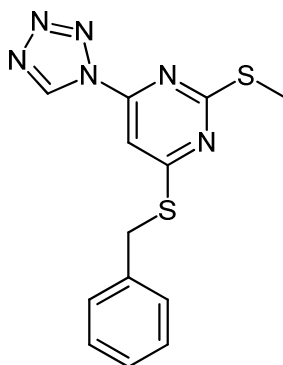
ESI-MS(+): m/z 283.2 $[M+H]^+$, 255.1 $[M-N_2+H]^+$

^1H NMR (300 MHz, CHLOROFORM-*d*): δ = 9.41 (s, 1 H), 7.38 (s, 1 H), 2.55 (s, 3 H), 1.60 ppm (s, 9 H)

^{13}C NMR (75 MHz, CHLOROFORM-*d*): δ = 175.6, 173.0, 150.8, 140.2, 103.0, 49.8, 30.3, 14.5 ppm

6 Supporting information

Compound 16:

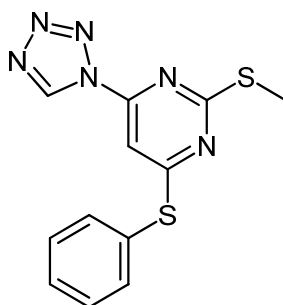


ESI-MS(+): m/z 317.2 $[M+H]^+$, 289.1 $[M-N_2+H]^+$

1H NMR (300 MHz, CHLOROFORM-*d*): δ = 9.40 (s, 1 H), 7.44 (s, 1 H), 6.99-7.39 (m, 5 H), 4.44 (s, 2 H), 2.53 ppm (s, 3 H)

^{13}C NMR (75 MHz, CHLOROFORM-*d*) δ = 173.7, 173.4, 151.1, 140.4, 140.2, 136.0, 128.9, 128.8, 127.7, 102.1, 102.0, 34.2, 14.3

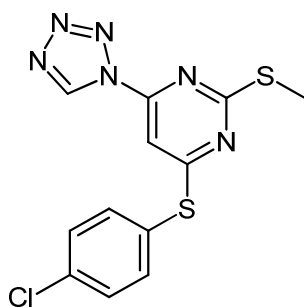
Compound 17/17op:



ESI-MS(+): m/z 303.1 $[M+H]^+$, 275.1 $[M-N_2+H]^+$

1H NMR (300 MHz, CHLOROFORM-*d*): δ = 9.38 (s, 1 H), 7.32-7.73 (m, 5 H), 7.07 (s, 1 H), 2.38 ppm (s, 3 H)

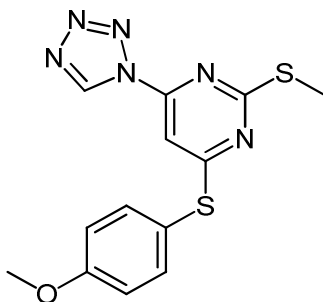
^{13}C NMR (75 MHz, CHLOROFORM-*d*): δ = 176.9, 173.3, 152.1, 140.4, 140.2, 135.9, 130.9, 130.2, 126.6, 14.2 ppm

Compound 18:

ESI-MS(+): m/z 337.3 $[M+H]^+$, 309.1 $[M-N_2+H]^+$

^1H NMR (300 MHz, CHLOROFORM-*d*): δ = 9.36 (s, 1 H), 7.29-7.60 (m, 4 H), 7.12 (s, 1 H), 2.33 ppm (s, 3 H)

^{13}C NMR (75 MHz, CHLOROFORM-*d*): δ = 175.7, 173.5, 152.0, 140.4, 140.1, 137.4, 137.1, 130.3, 125.0, 14.2 ppm

Compound 19:

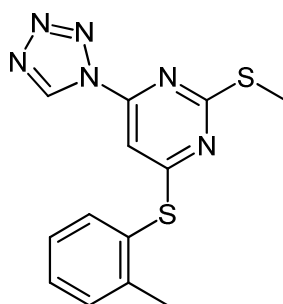
ESI-MS(+): m/z 305.0 $[M-N_2+H]^+$

^1H NMR (300 MHz, CHLOROFORM-*d*): δ = 9.46 (s, 1 H), 7.54 (d, $J=8.1$ Hz, 2 H), 6.87-7.18 (m, 3 H), 3.82-4.00 (m, 3 H), 2.51 ppm (s, 3 H)

^{13}C NMR (75 MHz, CHLOROFORM-*d*): δ = 178.1, 173.1, 161.7, 152.1, 140.3, 137.4, 116.9, 115.8, 100.3, 55.5, 14.2 ppm

6 Supporting information

Compound 20:

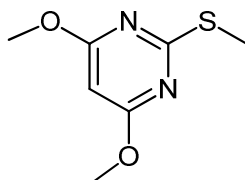


ESI-MS(+): m/z 289.0 $[M+H]^+$

^1H NMR (300 MHz, $\text{DMSO-}d_6$): δ = 10.22 (s, 1 H), 7.66 (d, $J=7.5$ Hz, 1 H), 7.48-7.59 (m, 2 H), 7.34 - 7.45 (m, 1 H), 7.05 (s, 1 H), 2.44 (s, 3 H), 2.37 ppm (s, 3 H)

^{13}C NMR (75 MHz, $\text{DMSO-}d_6$): δ = 174.5, 172.2, 152.1, 142.8, 142.0, 136.8, 131.4, 131.3, 127.6, 125.6, 100.7, 20.3, 13.6 ppm

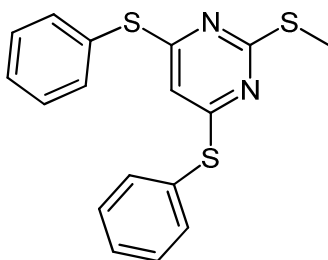
Compound 21:



ESI-MS(+): m/z 187.0 $[M+H]^+$

^1H NMR (300 MHz, $\text{CHLOROFORM-}d$): δ = 5.73 (s, 1 H), 3.92 (s, 6 H), 2.56 ppm (s, 3 H)

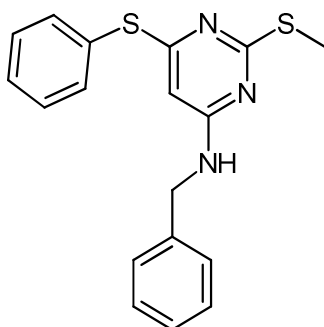
^{13}C NMR (75 MHz, $\text{CHLOROFORM-}d$): δ = 171.1, 170.9, 85.3, 54.0, 14.0 ppm

Compound 22:

ESI-MS(+): m/z 343.0 [M+H]⁺

¹H NMR (300 MHz, DMSO-*d*₆) δ = 7.33-7.46 (m, 10H), 5.72 (s, 1H), 2.32 (s, 3H)

¹³C NMR (75 MHz, DMSO-*d*₆): δ = 172.0, 170.8, 136.3, 135.8, 130.9, 130.5, 126.8, 107.2, 13.9 ppm

Compound 23:

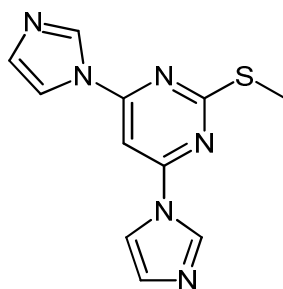
ESI-MS(+): m/z 340.0 [M+H]⁺

¹H NMR (300 MHz, CHLOROFORM-*d*): δ = 7.46 (d, J=7.2 Hz, 2 H), 7.28-7.39 (m, 3 H), 7.15-7.26 (m, 3 H), 7.09 (d, J=7.3 Hz, 2 H), 5.33 (s, 1 H), 5.00 (s, 1 H), 4.28 (br. s., 2 H), 2.34 ppm (s, 3 H)

¹³C NMR (126 MHz, CHLOROFORM-*d*): δ = 170.8, 161.4, 135.8, 129.6, 129.5, 128.7, 128.6, 127.4, 127.3, 45.2, 13.9 ppm

6 Supporting information

Compound 24:



ESI-MS(+): m/z 258.8 $[M+H]^+$

^1H NMR (300 MHz, $\text{DMSO-}d_6$): δ = 8.71 (t, $J=1.0$ Hz, 2 H), 8.07 (t, $J=1.4$ Hz, 2 H), 7.90 (s, 1 H), 7.22 (dd, $J=1.6, 0.8$ Hz, 2 H), 2.64 ppm (s, 3 H)

^{13}C NMR (75 MHz, $\text{DMSO-}d_6$): δ = 172.8, 156.3, 135.8, 131.0, 130.8, 116.6, 90.3, 13.6 ppm

Crystallization of compound 1:

10 mg of **1** was dissolved in a minimum amount of hot methanol (~800 μl). The clear solution was allowed to cool down to room temperature and left standing open to atmosphere for slow evaporation. Colorless, needle shaped crystals formed after 2 days.

CCDC Number 1052351 contains the supplementary crystallographic data for this paper. These data can be obtained free of charge from the Cambridge Crystallographic Data Centre *via* www.ccdc.cam.ac.uk/data_request/cif.

SI Table 1. Conditions tried to obtain N,N-dimethyl-2-(methylthio)-6-(1*H*-tetrazol-1-yl)pyrimidin-4-amine starting from 6-chloro-N,N-dimethyl-2-(methylthio)pyrimidin-4-amine

Method	Conditions
Heating	DMF, TEA, 60-140°C, 1-2 eq tetrazole, 24 hrs ^[a]
Microwave	DMF, TEA, 60-140°C, 1-2 eq tetrazole, 1 hr ^[a]
Heating	Neat, 2 eq tetrazole, 130°C, 24 hrs ^[a]

[a] TLC showed no conversion of starting material

Determination of the pK_a of compound 10:

The pK_a of **10** was measured using the SiriusT3 automatic titration system (Sirius Analytical Ltd, Forest Row, UK) and the software supplied with the machine for the refinement of the experimental data. Standard solutions of hydrochloric acid 0.5 M and potassium hydroxide 0.5 M in Millipore water were used as acid and base titrant, respectively. The ionic strength of the water used for dissolving the samples was adjusted adding potassium chloride obtaining a 0.15 M solution. A solution of 50 % acetonitrile – 50 % Millipore water was prepared and potassium chloride was added in it for obtaining a final mixture 50 % acetonitrile with 0.15 M KCl. In each experiment **10** was titrated three times in acetonitrile – water solution (first titration in 42 %, second titration in 35 % and third titration in 27 % of acetonitrile) from basic to acidic pH. Three independent experiments were performed per each compound at room temperature. The pK_a was obtained by linear extrapolation of the pK_a of each experiment resulting in a pK_a = 3.17 ± 0.05 and in a acceptable coefficient of determination (R² = 0.8927).

6 Supporting information

6.4 Supporting information for Publication IV

Supporting Information

Application of dual inhibition concept within looped autoregulatory systems towards anti-virulence agents against *Pseudomonas aeruginosa* infections

Andreas Thomann^{‡,†}, Antonio G. de Mello Martins^{‡,†}, Christian Brengel[†], Martin Empting^{†,*}, Rolf W. Hartmann^{†,§,*}

† Helmholtz Institute for Pharmaceutical Research Saarland (HIPS), Department for Drug Design and Optimization, Campus E 8.1, 66123 Saarbrücken, Germany;

§ Department of Pharmacy, Pharmaceutical and Medicinal Chemistry, Saarland University, Campus C 2.3, 66123 Saarbrücken, Germany;

‡ These authors contributed equally to this work.

E-mail: rolf.hartmann@helmholtz-hzi.de and martin.empting@helmholtz-hzi.de

Content

I. General experimental information - Chemistry

- a. Chemical synthesis of compounds **3-6**
- b. Crystallization of **6a** and X-ray crystallography
- c. ¹³C-NMR and HSQC spectra of compounds **3-6**
- d. LC purity of compounds **3-6**

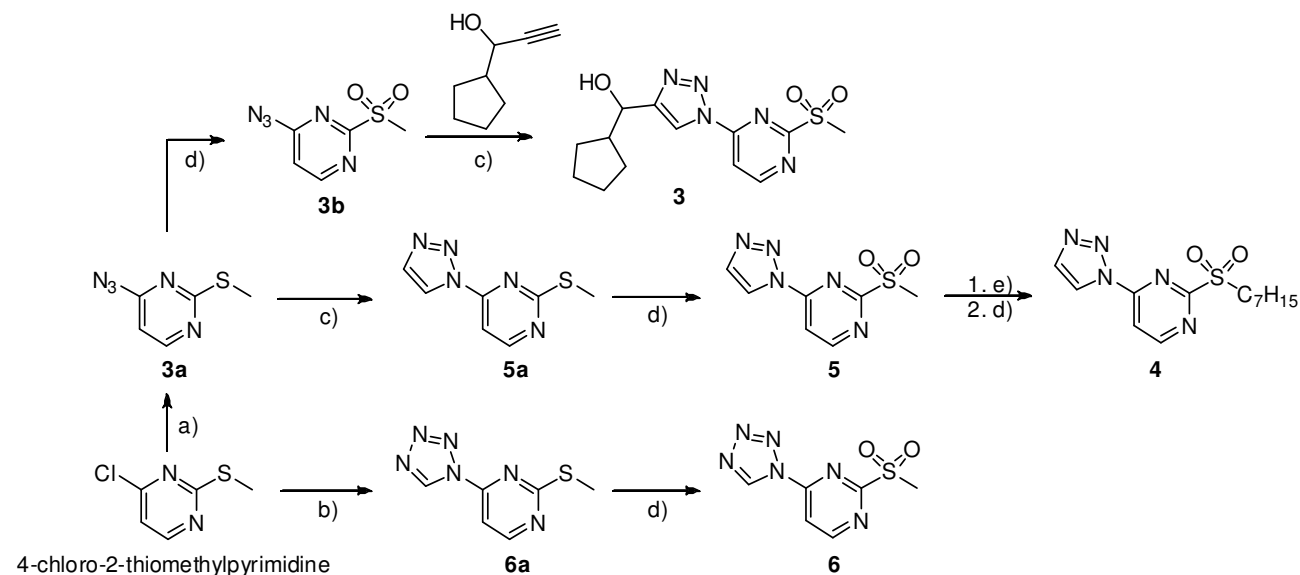
II. General experimental information - Biology

- a. Chemicals, bacterial strains, and media
- b. Pyocyanin assay
- c. Prolonged Pyocyanin Assay
- d. Antibiofilm effects of compound **2**
- e. Growth curves of *P. aeruginosa* PA14
- f. PqsD *in vitro* assay
- g. PqsR *in vitro* assay

III. References

I. General experimental information - Chemistry

a. Chemical Synthesis of compounds 3-6



Compounds **3a**, **3b** and **6a** were synthesized as reported before.^{1,2}

b. Crystallization of **6a** for X-ray crystallography

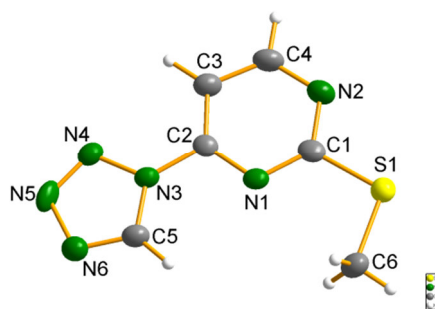


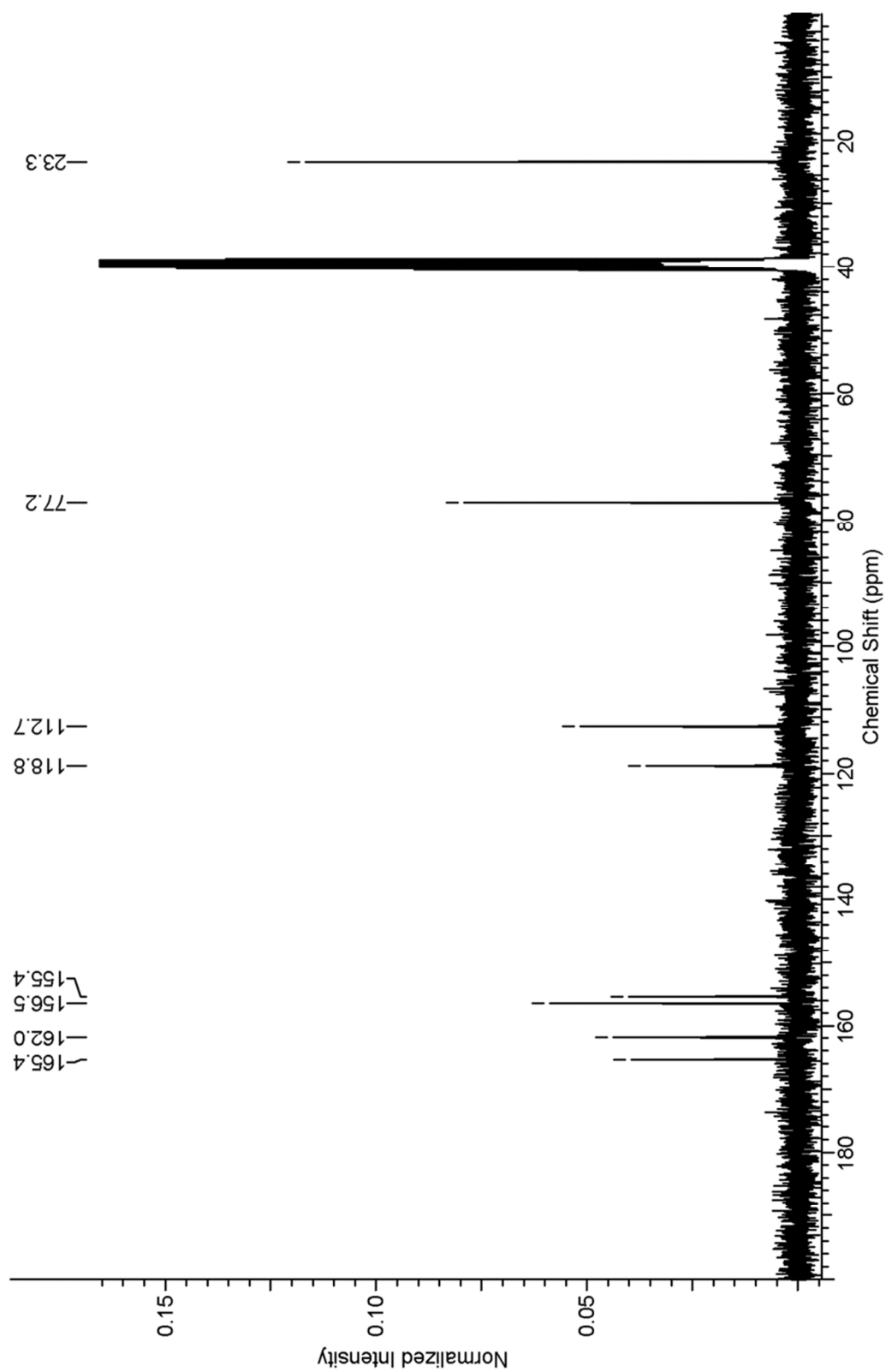
Figure S1. X-ray crystal structure of compound **6a** (green = nitrogen, grey = carbon, yellow = sulfur, white = hydrogen).

6a was dissolved in hot chloroform and left standing open to atmosphere to allow evaporation. Colorless needles formed after 3 weeks. CCDC 1432241 contains the supplementary crystallographic data for this paper. These data can be obtained free of charge from The Cambridge Crystallographic Data Centre via www.ccdc.cam.ac.uk/getstructures.

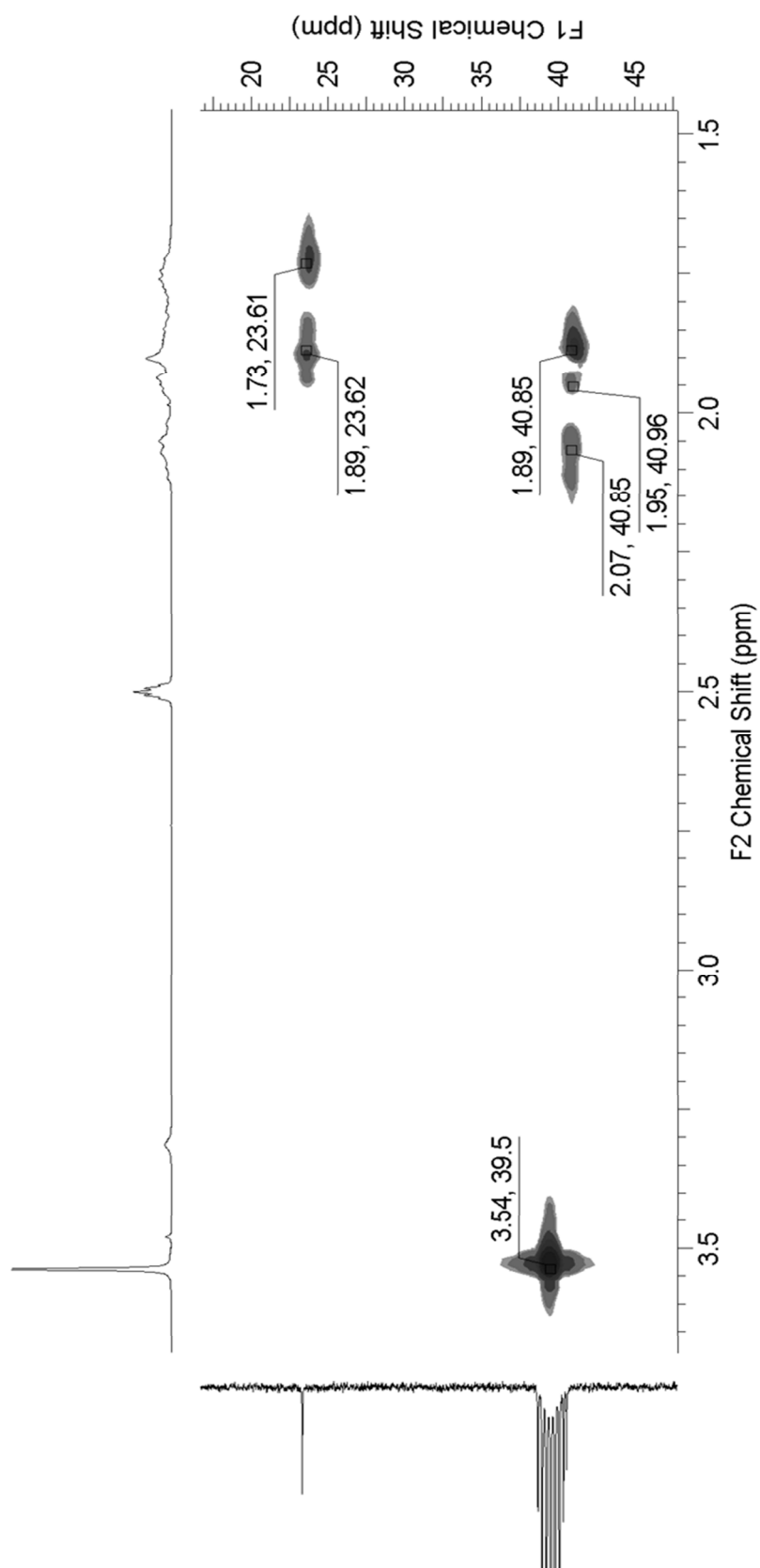
6 Supporting information

c. ^{13}C -NMR spectra

^{13}C NMR of compound 3

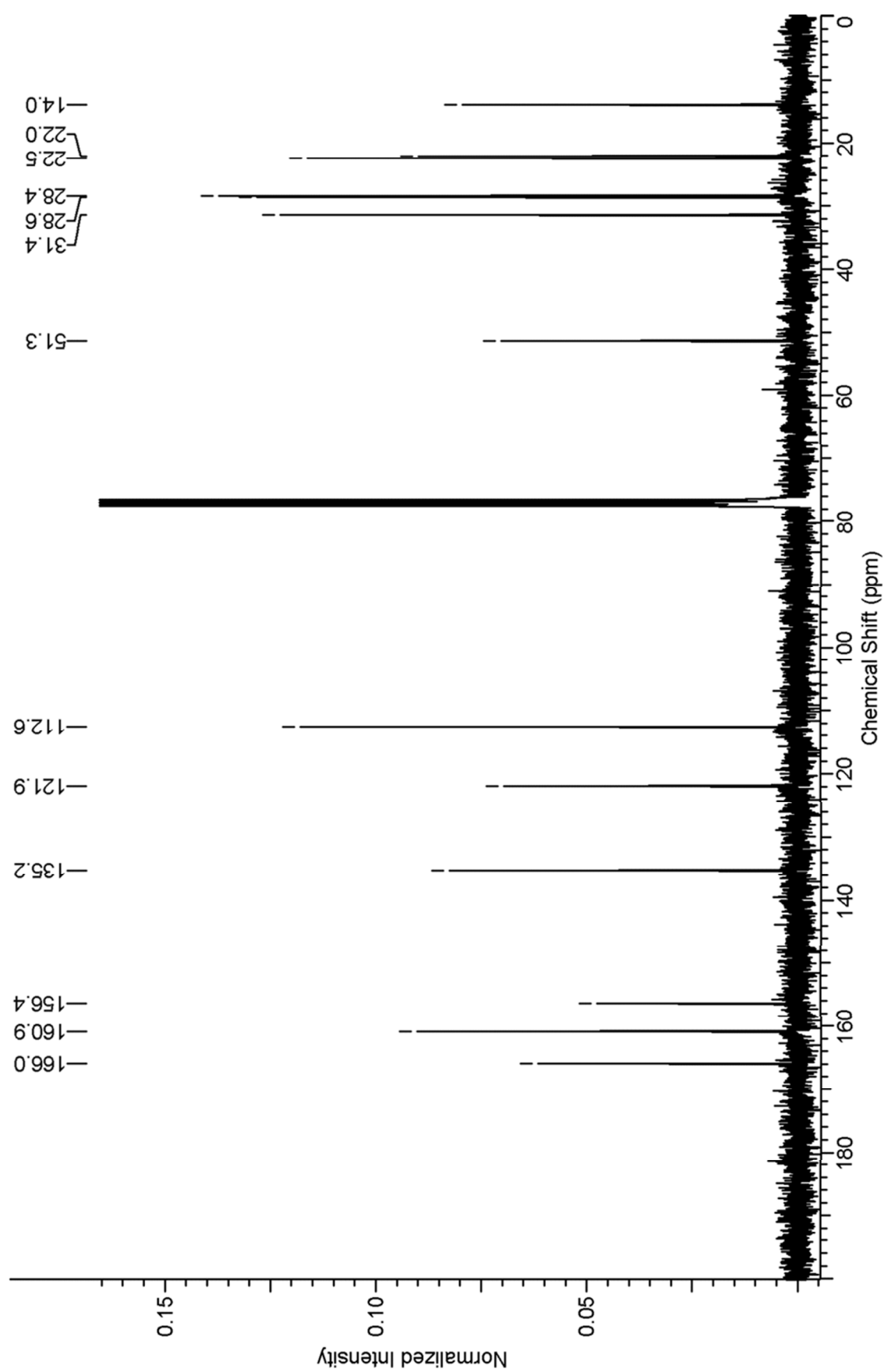


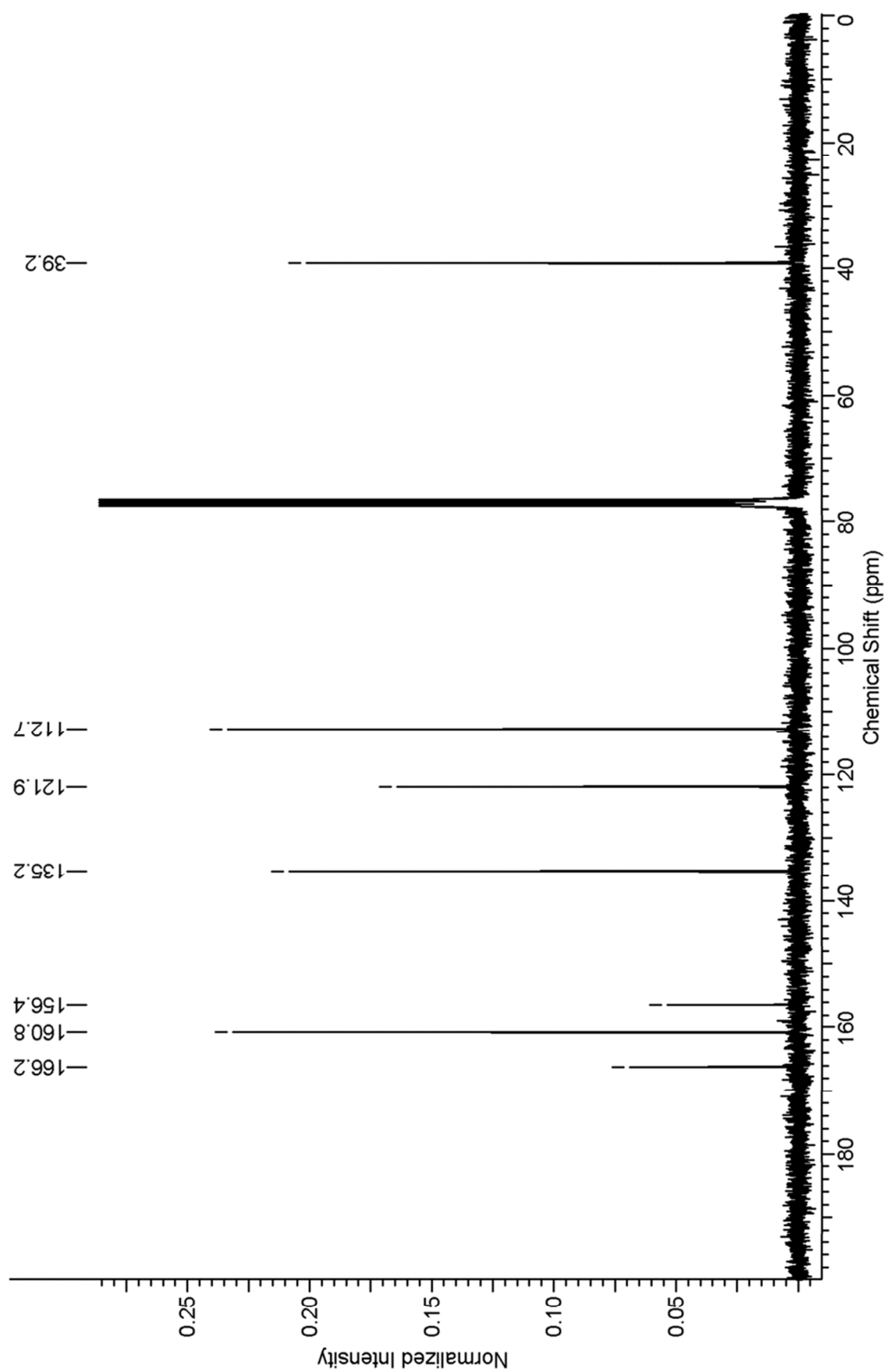
HSQC NMR of compound 3



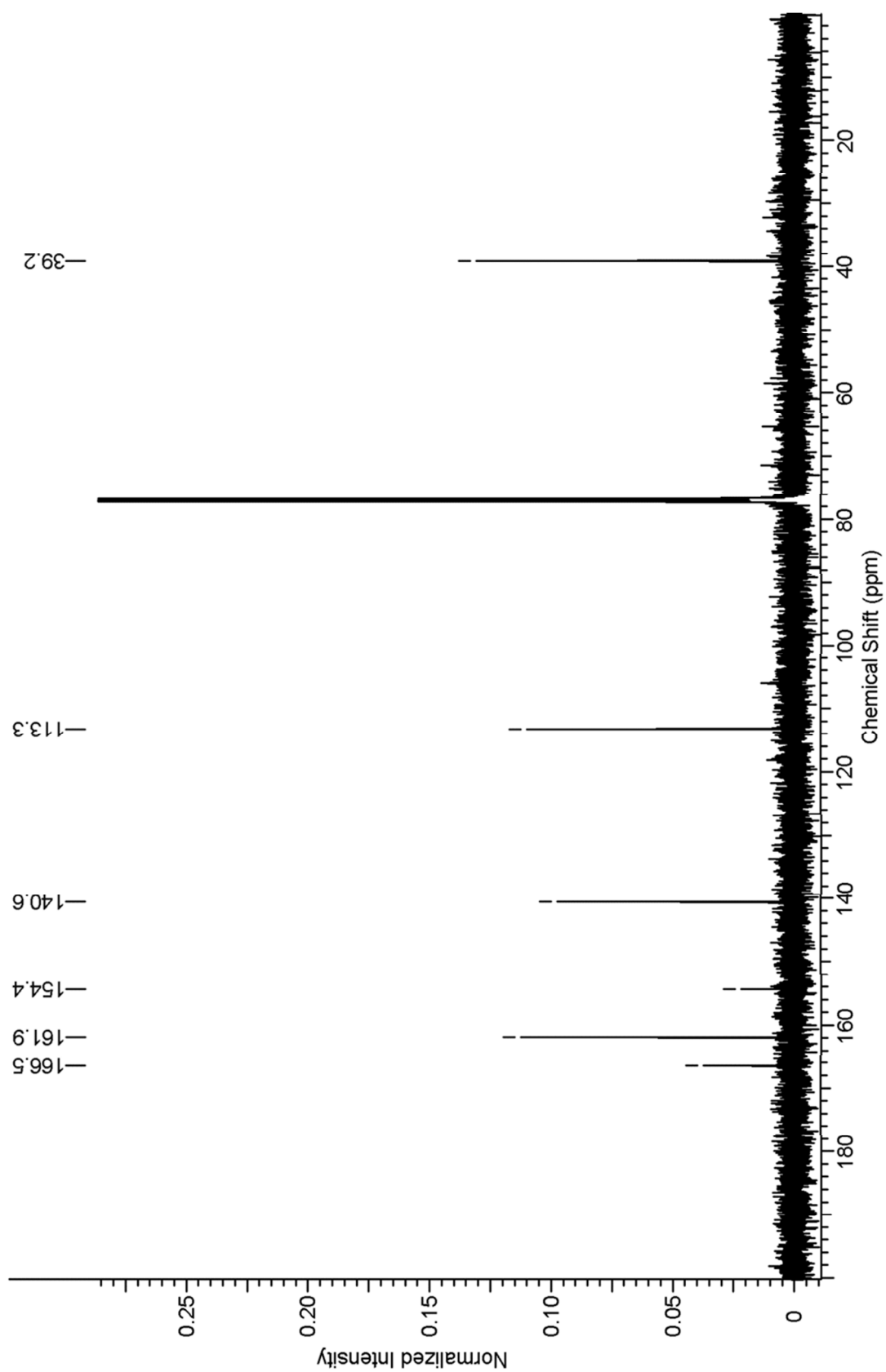
6 Supporting information

^{13}C NMR of compound 4



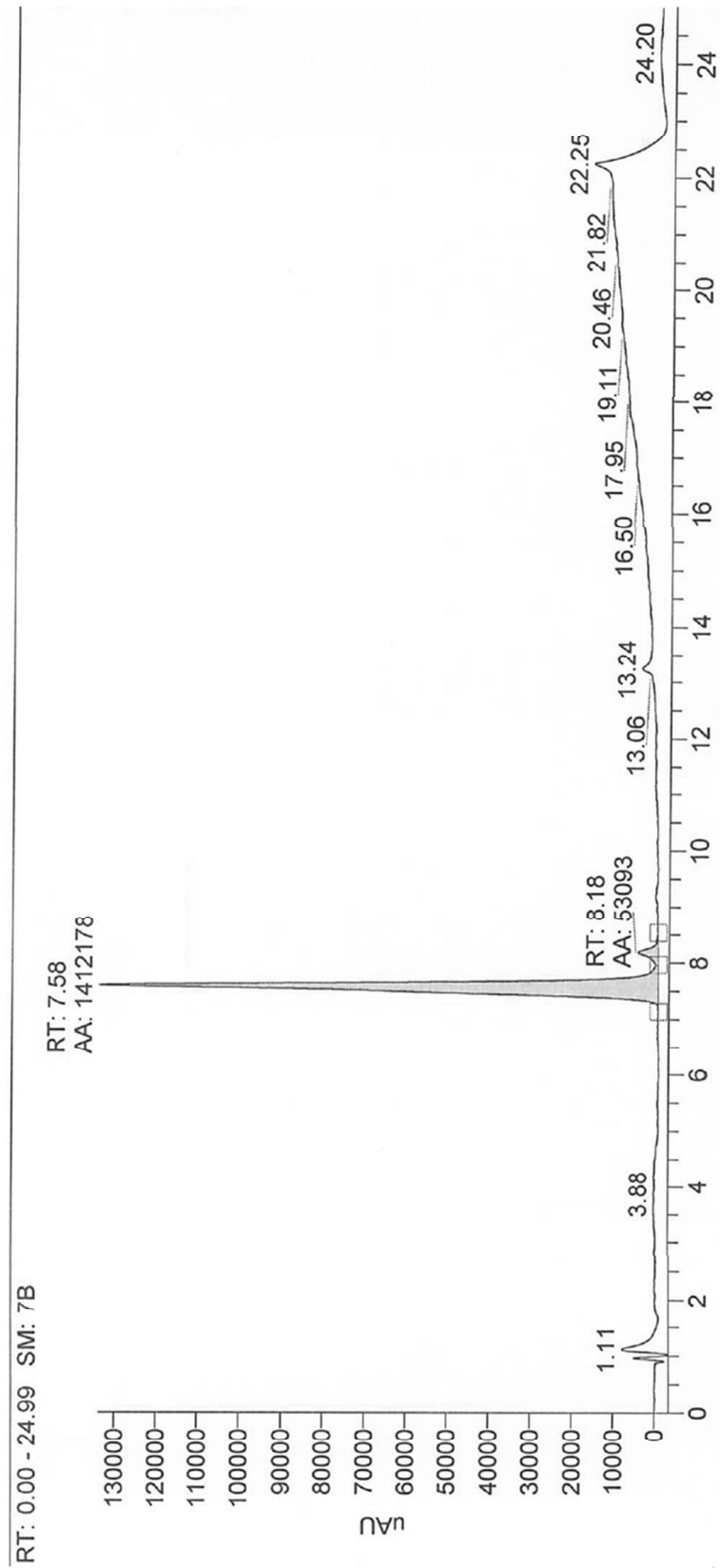
^{13}C NMR of compound 5

^{13}C NMR compound 6

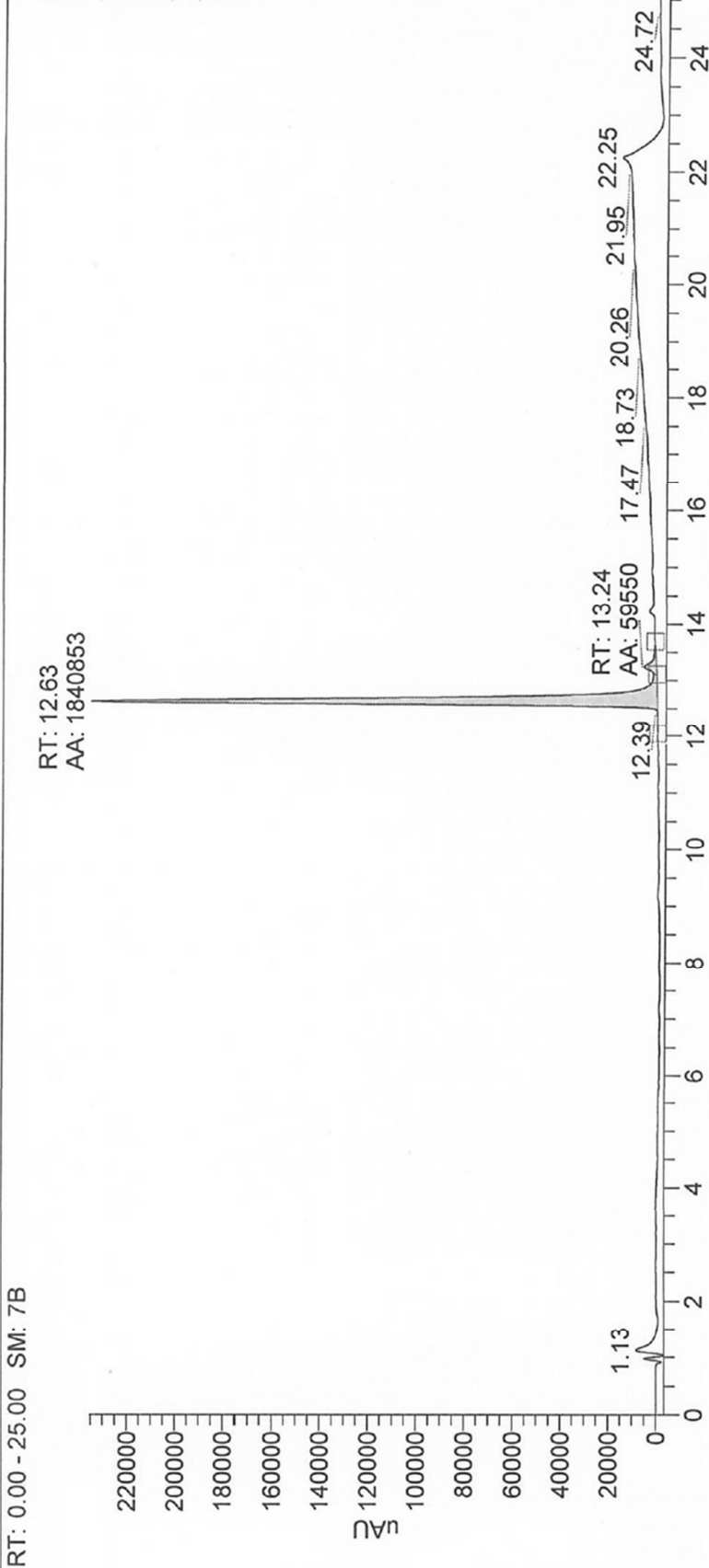


d. LC purity of compounds 3-6

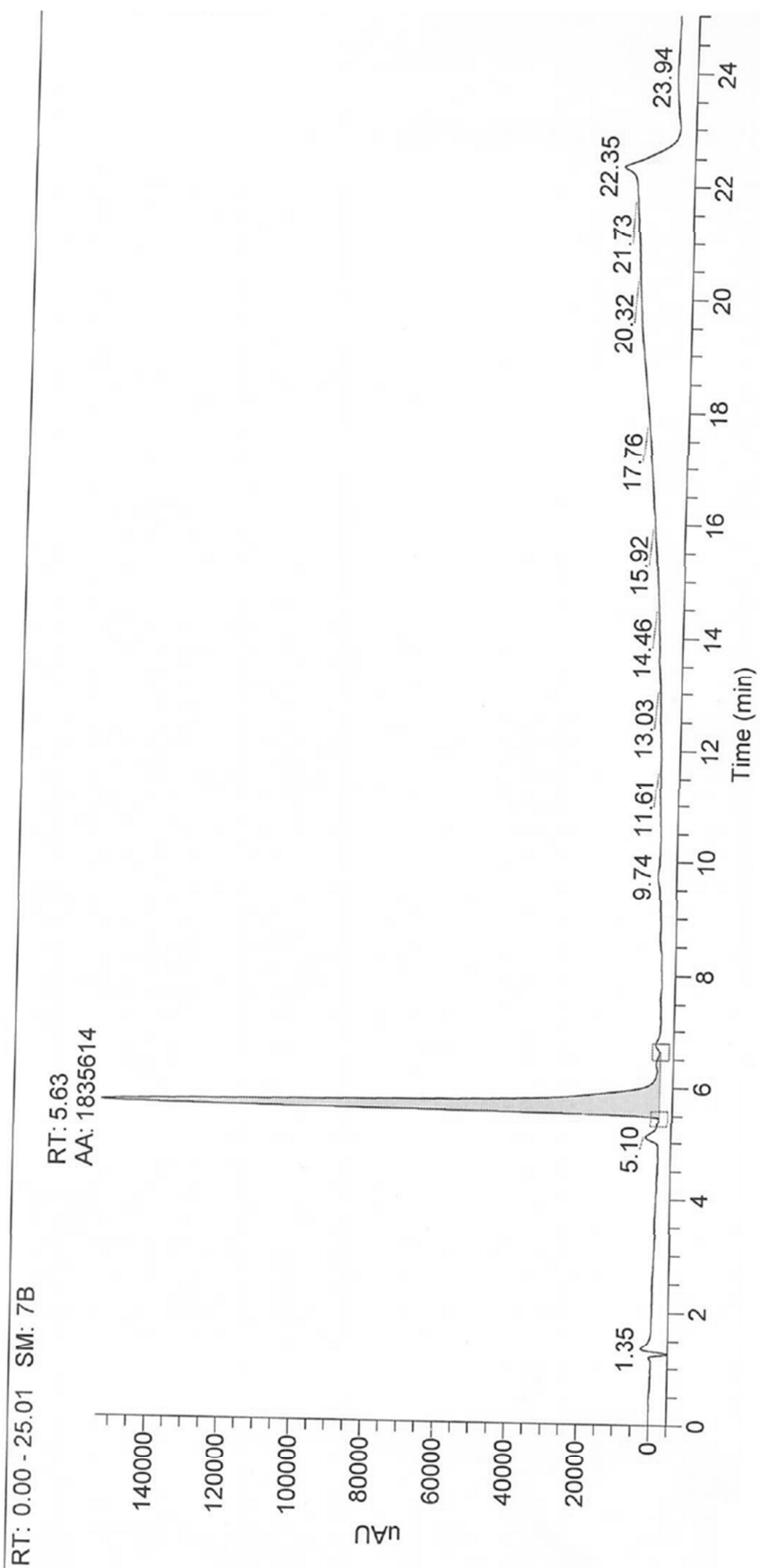
Compound 3



Compound 4



Compound 5



Compound 6



II. General experimental information – Biology

a. Chemicals, bacterial strains, and media

Yeast extract was obtained from Fluka (Neu-Ulm, Germany), peptone and casein from Merck (Darmstadt, Germany), Bacto™ Tryptone from BD Biosciences (Heidelberg, Germany), and Gibco® PBS from Life Technologies (Darmstadt, Germany). Salts and organic solvents of analytical grade were obtained from VWR (Darmstadt, Germany).

P. aeruginosa PA14 strain, and isogenic *pqsR* knockout mutant were stored in glycerol stocks at -80 °C.

Minimal medium PPGAS³ and Luria Bertani (LB) were used.

b. Pyocyanin assay

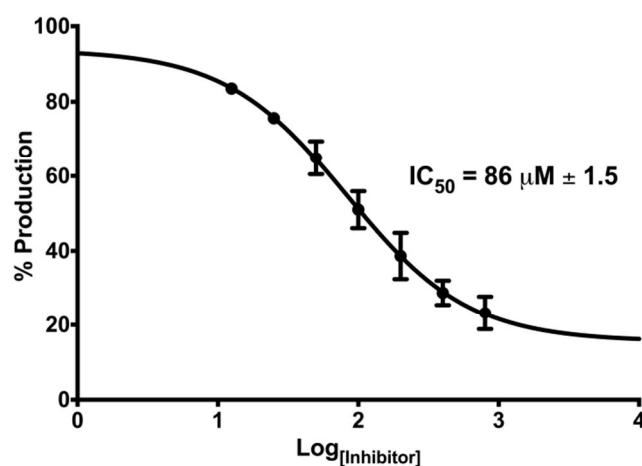


Figure S2. IC₅₀ curve of the improved inhibitory effect of **6** on pyocyanin production, an indicative of PqsR antagonism. Error bars represent standard error of three independent experiments ($n = 3$).

6 Supporting information

c. Prolonged Pyocyanin Assay.

Effect of long-term PqsD inhibition on pyocyanin formation was assessed as previously described (pyocyanin assay) with slight modifications. Initially, treated (compound **1**) and untreated cultures were incubated for 24 h under aerobic conditions. pyocyanin levels and bacterial density were determined from extracted culture aliquots. Obtained OD₆₀₀ values were used to re-calculate the necessary dilution factors of each replicate for a final density of 0.02, transferred into a new plate with fresh PPGAS medium and DMSO or compound **1** for additional 24 h, accordingly. Pyocyanin formation and cell growth were again assessed as previously described, making up for a total of 48 h of incubation with treated samples under constant, long-term PqsD inhibition.

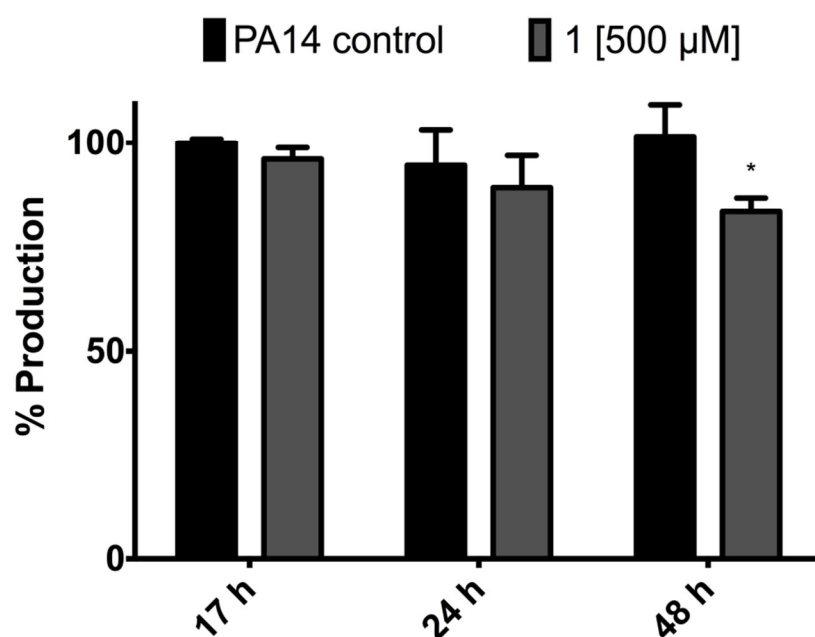


Figure S3. Long-term effect of PqsD inhibitor **1** on pyocyanin production in PA14 wild type. Treatment with 500 μM of **1** led to a reduction of pyocyanin levels to 83.5 ± 3.2 % after 48 h of incubation. The differences in values (compared to control) determined for 17 h and 24 h were not significant. All values are relative to a DMSO control without addition of inhibitors. Error bars represent the standard deviation of three independent experiments ($n = 3$). * = $p < 0.05$.

d. Growth curves of *P. aeruginosa* PA14

Cultures of PA14 were diluted in PPGAS medium, adjusted to an initial OD₆₀₀ of 0.02, and 1.5 mL added in triplicates into 24-well plates (Greiner Bio-One, Kremsmünster, Austria). Cultivation conditions as described above (SI, section II-a). Stock solutions of compound **6** in DMSO were diluted 1:100 to a final DMSO concentration of 1% (v/v), DMSO alone was used as control. Bacterial growth was measured over 48 h as a function of OD₆₀₀ using FLUOstar Omega (BMG LabTech, Ortenberg, Germany).

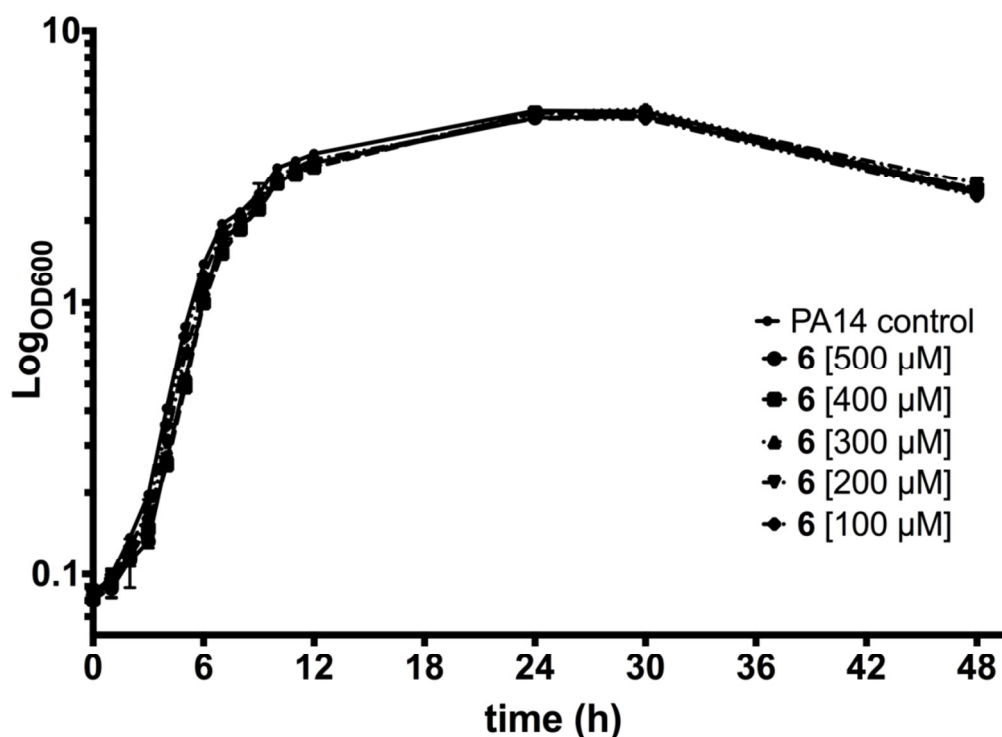


Figure S3. Growth curves of PA14 in PPGAS minimal medium in the absence (control) and presence of varying concentrations (100 μM to 500 μM) of compound **6**.

6 Supporting information

e. Antibiofilm effects of compound 2

Effects of compound 2 on Biofilm

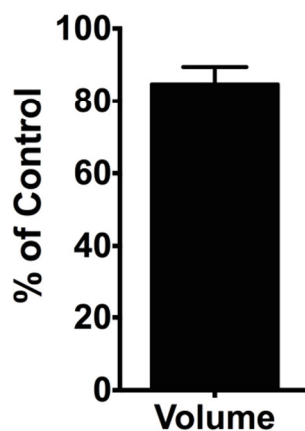


Figure S5. Effects of compound 2 (15 μ M; solubility maximum) on volume of *P. aeruginosa* strain PA14 biofilm. Experiment was performed as described in the experimental section of the main text. Error bars represent standard error of at least two independent experiments.

f. PqsD *in vitro* assay

The assay was performed as reported before.⁴

g. PqsR *in vitro* assay

The assay was performed in *E. Coli* DH5 α as reported before.⁵

III. References

- (1) Thomann, A., Börger, C., Empting, M., and Hartmann, R. (2014) Microwave-Assisted Synthesis of 4-Substituted 2-Methylthiopyrimidines. *Synlett* 25, 935–938. DOI: 10.1055/s-0033-1340860.
- (2) Thomann, A., Zapp, J., Hutter, M., Empting, M., and Hartmann, R. W. (2015) Steering the azido-tetrazole equilibrium of 4-azidopyrimidines via substituent variation - implications for drug design and azide-alkyne cycloadditions. *Org. Biomol. Chem.* 13, 10620–10630. DOI: 10.1039/C5OB01006C.
- (3) Zhang, Y., and Miller, R. M. (1992) Enhanced octadecane dispersion and biodegradation by a *Pseudomonas* rhamnolipid surfactant (biosurfactant). *Appl. Environ. Microbiol.* 58, 3276–3282.
- (4) Storz, M. P., Maurer, C. K., Zimmer, C., Wagner, N., Brengel, C., de Jong, Johannes C, Lucas, S., Müsken, M., Häussler, S., Steinbach, A., and Hartmann, R. W. (2012) Validation of PqsD as an anti-biofilm target in *Pseudomonas aeruginosa* by development of small-molecule inhibitors. *J. Am. Chem. Soc.* 134, 16143–16146. DOI: 10.1021/ja3072397.
- (5) Lu, C., Maurer, C. K., Kirsch, B., Steinbach, A., and Hartmann, R. W. (2014) Overcoming the unexpected functional inversion of a PqsR antagonist in *Pseudomonas aeruginosa*: an in vivo potent antivirulence agent targeting pqs quorum sensing: An In Vivo Potent Antivirulence Agent Targeting pqs Quorum Sensing. *Angew. Chem. Int. Ed. Engl.* 53, 1109–1112. DOI: 10.1002/anie.201307547.

6 Supporting information

6.5 Supporting information for Publication V

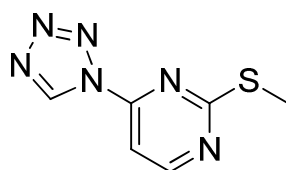
Content

- I. Purification, yield and compound characterization
- II. Biological assays
- III. Solubility of compounds 1 – 44
- IV. Correlation of π and cLogP with pIC₅₀ of compounds 37 – 44
- V. Molecular modeling and Hansch analysis
- VI. References

6 Supporting information

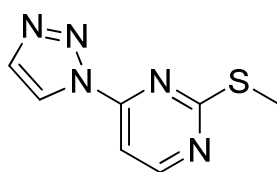
I. Purification, yield and compound characterization

2-(methylthio)-4-(1H-tetrazol-1-yl)pyrimidine (1b):



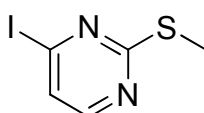
As previously described.^[1]

2-(methylthio)-4-(1H-1,2,3-triazol-1-yl)pyrimidine (2a):



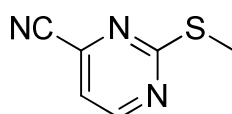
As previously described.^[2]

4-iodo-2-(methylthio)pyrimidine (3a):

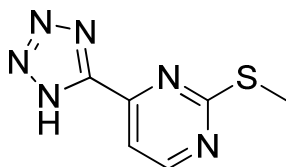


Purification and yield see experimental section in the manuscript. ¹H NMR (CDCl₃, 300 MHz): δ = 7.98 (d, *J* = 5.1 Hz, 1H), 7.38 (d, *J* = 5.1 Hz, 1H), 2.53 ppm (s, 3 H); ¹³C NMR (CDCl₃, 75 MHz): δ = 173.2, 155.7, 129.3, 127.2, 14.3 ppm.

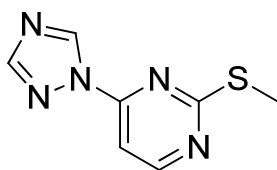
2-(methylthio)pyrimidine-4-carbonitrile (3b):



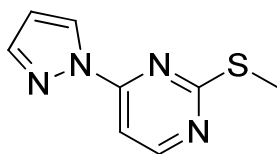
Purification and yield see experimental section in the manuscript. ¹H NMR (CDCl₃, 300 MHz): δ = 8.71 (d, *J* = 4.8 Hz, 1H), 7.26 (d, *J* = 4.8 Hz, 1H), 2.58 ppm (s, 3 H); ¹³C NMR (CDCl₃, 75 MHz): δ = 175.2, 158.6, 141.3, 118.7, 115.2, 14.2 ppm.

2-(methylthio)-4-(1H-tetrazol-5-yl)pyrimidine (3c):

Purification and yield see experimental section in the manuscript. ^1H NMR (CDCl_3 , 300 MHz): δ = 8.77 (d, J = 5.0 Hz, 1 H), 7.91 (d, J = 5.0 Hz, 1 H), 6.09 (br. s, 1 H), 2.62 ppm (s, 3 H); ^{13}C NMR (CDCl_3 , 75 MHz): δ = 173.8, 159.0, 151.4, 113.8, 14.2 ppm.

2-(methylthio)-4-(1H-1,2,4-triazol-1-yl)pyrimidine (4a):

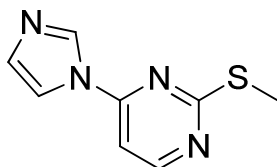
As previously described.^[1]

2-(methylthio)-4-(1H-pyrazol-1-yl)pyrimidine (5a):

As previously described.^[1]

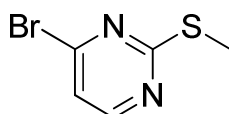
4-(1H-imidazol-1-yl)-2-(methylthio)pyrimidine (6a):

6 Supporting information



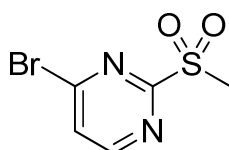
As previously described.^[1]

4-bromo-2-(methylthio)pyrimidine (7a):



To a solution of 4-chloro-2-(methylthio)pyrimidine in ACN was added TMSBr and the mixture was stirred for 24 h at 40 °C under argon (pink color). Afterwards, the reaction was quenched by the addition of a sat. solution of NaHCO₃ (45 mL). The aqueous phase was extracted twice with EtOAc (40 mL) and the combined organic layers were washed with water and brine (each 30 mL), dried (Na₂SO₄) and concentrated under reduced pressure. The crude product was purified by flash chromatography (cyclohexane:ethyl acetate, 9:1) to yield an off white solid (96%). ¹H NMR (CDCl₃, 300 MHz): δ = 8.25 (d, *J* = 5.2 Hz, 1 H), 7.15 (d, *J* = 5.2 Hz, 1 H), 2.56 ppm (s, 4 H). ¹³C NMR (CDCl₃, 75 MHz): δ = 173.9, 157.2, 152.5, 120.3, 14.3 ppm.

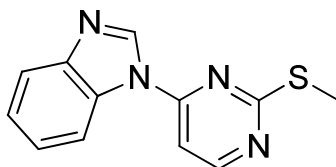
4-bromo-2-(methylsulfonyl)pyrimidine (7b):



To a solution of **7a** in EtOH was added a mixture of H₂O₂ and ammonium molybdate tetrahydrate at 0 °C and stirring continued overnight in an ice bath. Afterwards, the crude mixture was concentrated under reduced pressure and the residue taken up in water/EtOAc 1:1 (50 mL). The organic phase was separated and the aqueous one extracted twice with EtOAc. The combined organic phases were dried over MgSO₄ and concentrated under reduced pressure. The crude product was purified by flash chromatography (cyclohexane:ethyl acetate = 1:1) to give a white solid (94%). ¹H

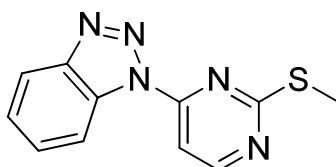
NMR (CDCl₃, 300 MHz): δ = 8.69 (d, J = 5.2 Hz, 1 H), 7.76 (d, J = 5.2 Hz, 1 H), 3.38 ppm (s, 4 H); ¹³C NMR (CDCl₃, 75 MHz): δ = 166.1, 158.5, 154.7, 128.6, 39.1 ppm.

1-(2-(methylthio)pyrimidin-4-yl)-1H-benzo[d]imidazole (8a):



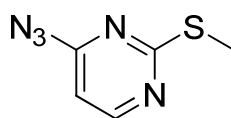
As previously described.^[1]

1-(2-(methylthio)pyrimidin-4-yl)-1H-benzo[d][1,2,3]triazole (9a):



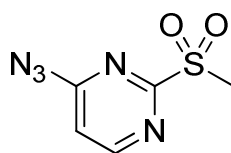
As previously described.^[1]

4-azido-2-(methylthio)pyrimidine (10a):



As described previously.^[3]

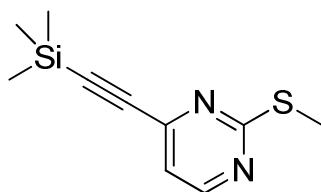
4-azido-2-(methylsulfonyl)pyrimidine (10b):



As described previously.^[3]

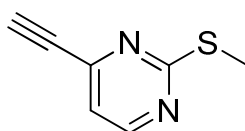
6 Supporting information

4-ethynyl-2-(methylthio)pyrimidine (22a):



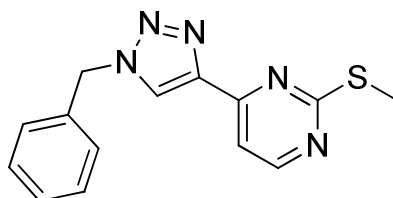
22a was prepared as previously described. Analytical data is in good accordance with the literature.^[4] ¹H NMR (CDCl₃, 300MHz): δ = 8.47 (d, J = 5.0 Hz, 1 H), 7.02 (d, J = 5.0 Hz, 1 H), 2.57 (s, 3 H), 0.28 ppm (s, 9 H).

4-ethynyl-2-(methylthio)pyrimidine (22b):

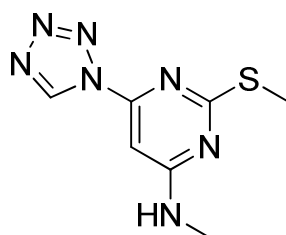


Purification and yield see experimental section in the manuscript. Analytical data is in good accordance with the literature.^[4] ¹H NMR (CDCl₃, 500 MHz): δ = 8.51 (d, J = 4.7 Hz, 1 H), 7.06 (d, J = 5.0 Hz, 1 H), 3.34 (s, 1 H), 2.57 ppm (s, 3 H); ¹³C NMR (CDCl₃, 126 MHz): δ = 173.4, 157.2, 149.8, 118.7, 81.4, 80.7, 14.1 ppm.

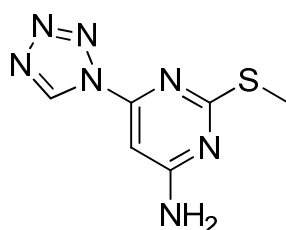
4-(1-benzyl-1H-1,2,3-triazol-4-yl)-2-(methylthio)pyrimidine (22c):



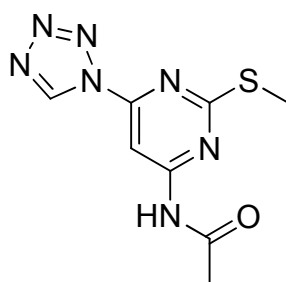
Flash chromatography (ethyl acetate:hexane, 2:8); white solid (60%). ¹H NMR (CDCl₃, 300 MHz): δ = 8.58 (d, J = 5.1 Hz, 1 H), 8.15 (s, 1 H), 7.77 (d, J = 5.2 Hz, 1 H), 7.36 - 7.47 (m, 3 H), 7.28 - 7.36 (m, 2 H), 5.60 (s, 2 H), 2.57 ppm (s, 3 H); ¹³C NMR (CDCl₃, 75 MHz): δ = 172.6, 157.9, 157.2, 146.6, 134.1, 129.3, 129.0, 128.2, 123.7, 111.7, 54.5, 14.1 ppm.

***N*-methyl-2-(methylthio)-6-(1*H*-tetrazol-1-yl)pyrimidin-4-amine (23b):**

As previously described.^[5]

2-(methylthio)-6-(1*H*-tetrazol-1-yl)pyrimidin-4-amine (24a):

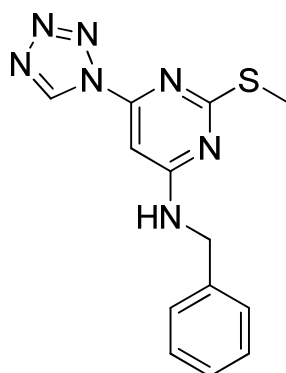
As previously described.^[5]

***N*-(2-(methylthio)-6-(1*H*-tetrazol-1-yl)pyrimidin-4-yl)acetamide (24b):**

Flash chromatography (ethyl acetate:hexane, 7:3); white solid (47%). ¹H NMR (DMSO-*d*₆, 300 MHz): δ = 11.33 (s, 1 H), 10.28 (s, 1 H), 8.35 (s, 1 H), 2.63 (s, 3 H), 2.19 ppm (s, 3 H); ¹³C NMR (DMSO-*d*₆, 75 MHz): δ = 172.8, 171.7, 160.5, 154.0, 142.1, 93.8, 24.8, 14.3 ppm.

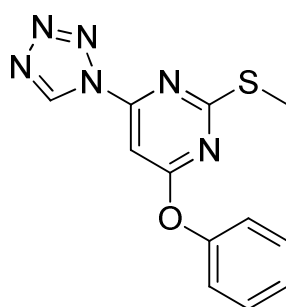
6 Supporting information

***N*-benzyl-2-(methylthio)-6-(1*H*-tetrazol-1-yl)pyrimidin-4-amine (25a)**



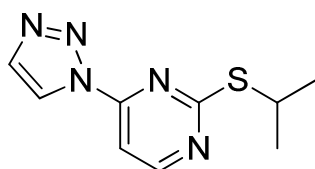
As previously described.^[5]

2-(methylthio)-4-phenoxy-6-(1*H*-tetrazol-1-yl)pyrimidine (26a):

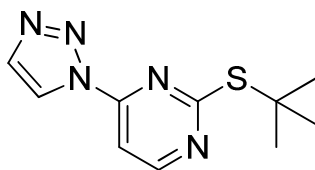


As previously described.^[5]

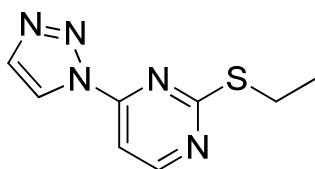
2-(isopropylthio)-4-(1*H*-1,2,3-triazol-1-yl)pyrimidine (27a):



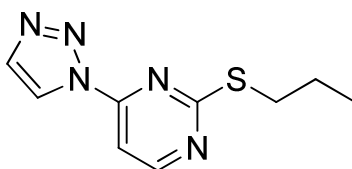
The crude product was directly taken to the next step without further purification.

2-(*tert*-butylthio)-4-(1*H*-1,2,3-triazol-1-yl)pyrimidine (28a):

Flash chromatography (ethyl acetate:hexane, 3:7); white solid (62%). ^1H NMR (CDCl_3 , 500 MHz): δ = 8.69 (d, J = 5.4 Hz, 1 H), 8.56 (d, J = 1.3 Hz, 1 H), 7.86 (d, J = 1.3 Hz, 1 H), 1.68 ppm (s, 9 H); ^{13}C NMR (CDCl_3 , 126 MHz): δ = 174.0, 159.6, 154.6, 134.6, 121.1, 104.8, 47.9, 29.9 ppm.

2-(ethylthio)-4-(1*H*-1,2,3-triazol-1-yl)pyrimidine (29a):

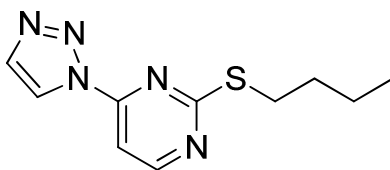
Flash chromatography (ethyl acetate:hexane, 2:8); white solid (36%). ^1H NMR (CDCl_3 , 300 MHz): δ = 8.69 (d, J = 5.4 Hz, 1 H), 8.59 (d, J = 1.3 Hz, 1 H), 7.85 (d, J = 1.3 Hz, 1 H), 7.81 (d, J = 5.4 Hz, 1 H), 3.21 (q, J = 7.4 Hz, 2 H), 1.44 ppm (t, J = 7.4 Hz, 3 H); ^{13}C NMR (CDCl_3 , 75 MHz): δ = 173.4, 159.8, 154.9, 134.5, 121.1, 104.9, 25.5, 14.2 ppm.

2-(propylthio)-4-(1*H*-1,2,3-triazol-1-yl)pyrimidine (30a):

Flash chromatography (ethyl acetate:hexane, 2:8); white solid (57%). ^1H NMR (CDCl_3 , 300 MHz): δ = 8.69 (dd, J = 5.4, 0.8 Hz, 1 H), 8.53 - 8.63 (m, 1 H), 7.84 - 7.89 (m, 1 H), 7.81 (dd, J = 5.4, 0.9 Hz, 1 H), 3.19 (td, J = 7.3, 0.8 Hz, 2 H), 1.82 (sxt, J = 7.3 Hz, 2 H), 1.00 - 1.17 ppm (m, 3 H); ^{13}C NMR (CDCl_3 , 75 MHz): δ = 173.5, 159.8, 154.9, 134.5, 121.1, 104.9, 33.1, 22.4, 13.5 ppm.

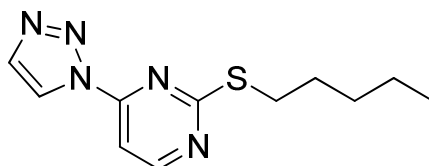
6 Supporting information

2-(butylthio)-4-(1H-1,2,3-triazol-1-yl)pyrimidine (31a):



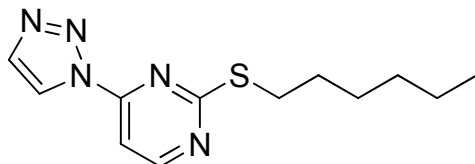
Flash chromatography (ethyl acetate:hexane, 2:8); white solid (72%). ^1H NMR CDCl_3 , 300 MHz): δ = 8.69 (d, J = 5.4 Hz, 1 H), 8.58 (d, J = 1.2 Hz, 1 H), 7.86 (d, J = 1.2 Hz, 1 H), 7.81 (d, J = 5.4 Hz, 1 H), 3.21 (t, J = 7.4 Hz, 2 H), 1.69 - 1.85 (m, 2 H), 1.52 (dq, J = 14.9, 7.4 Hz, 2 H), 0.88 - 1.08 ppm (m, 3 H); ^{13}C NMR (CDCl_3 , 75 MHz): δ = 173.5, 159.8, 154.9, 134.5, 121.1, 104.8, 31.0, 30.9, 22.0, 13.6 ppm.

2-(pentylthio)-4-(1H-1,2,3-triazol-1-yl)pyrimidine (32a):



Flash chromatography (ethyl acetate:hexane, 2:8); white solid (62%). ^1H NMR (CDCl_3 , 300 MHz): δ = 8.68 (d, J = 5.4 Hz, 1 H), 8.58 (d, J = 1.2 Hz, 1 H), 7.86 (d, J = 1.2 Hz, 1 H), 7.81 (d, J = 5.4 Hz, 1 H), 3.14 - 3.25 (m, 2 H), 1.79 (quin, J = 7.4 Hz, 2 H), 1.29 - 1.55 (m, 4 H), 0.85 - 0.99 ppm (m, 3 H); ^{13}C NMR (CDCl_3 , 75 MHz): δ = 173.6, 159.8, 154.9, 134.5, 121.1, 104.8, 31.1, 31.1, 28.6, 22.2, 13.9 ppm.

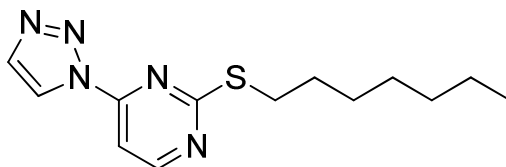
2-(hexylthio)-4-(1H-1,2,3-triazol-1-yl)pyrimidine (33a):



Flash chromatography (ethyl acetate:hexane, 1:9); white solid (48%). ^1H NMR (CDCl_3 , 300 MHz): δ = 8.69 (d, J = 5.4 Hz, 1 H), 8.59 (d, J = 1.3 Hz, 1 H), 7.86 (d, J = 1.3 Hz, 1 H), 7.81 (d, J = 5.4 Hz, 1 H), 3.13 - 3.27 (m, 2 H), 1.79 (quin, J = 7.4 Hz, 2 H), 1.43 - 1.55 (m, 2 H), 1.34 (dq, J = 7.3, 3.6 Hz, 4 H), 0.84 - 0.93 ppm (m, 3 H); ^{13}C

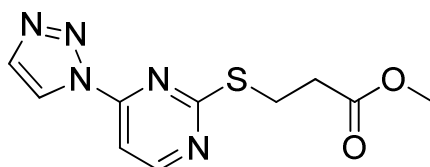
NMR (CDCl₃, 75 MHz): δ = 173.6, 159.8, 154.9, 134.5, 121.1, 104.9, 31.4, 31.2, 28.9, 28.6, 22.5, 14.0 ppm.

2-(heptylthio)-4-(1H-1,2,3-triazol-1-yl)pyrimidine (34a):



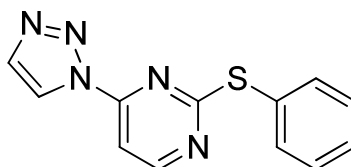
As previously described.^[2]

methyl 3-((4-(1H-1,2,3-triazol-1-yl)pyrimidin-2-yl)thio)propanoate (35a):



Flash chromatography (ethyl acetate:hexane, 3:7); white solid (59%). ¹H NMR (CDCl₃, 500 MHz): δ = 8.70 (d, J = 5.4 Hz, 1 H), 8.63 (d, J = 1.6 Hz, 1 H), 7.86 (d, J = 5.4, 1 H), 7.85 (d, J = 5.4, 1 H), 3.73 (s, 3 H), 3.46 (t, J = 6.9 Hz, 2 H), 2.86 ppm (t, J = 7.3 Hz, 2 H); ¹³C NMR (CDCl₃, 126 MHz): 172.5, 172.2, 160.0, 155.0, 134.6, 121.2, 105.2, 51.9, 34.0, 26.2 ppm.

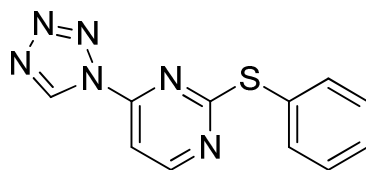
2-(phenylthio)-4-(1H-1,2,3-triazol-1-yl)pyrimidine (36a):



The crude product was directly used for the next step without further purification.

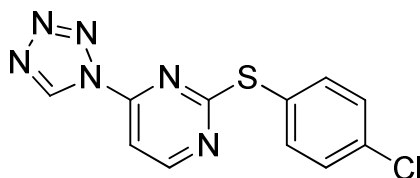
6 Supporting information

2-(phenylthio)-4-(1*H*-tetrazol-1-yl)pyrimidine (37a):



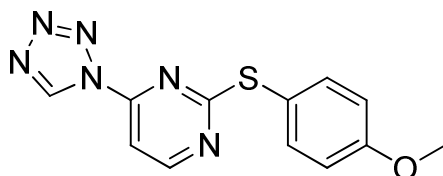
Flash chromatography (ethyl acetate:hexane, 2:8); white solid (57%). ¹H NMR (CDCl₃, 300 MHz): δ = 9.06 (s, 1 H), 8.76 (d, *J* = 5.2 Hz, 1 H), 7.59 - 7.71 (m, 3 H), 7.45 - 7.58 ppm (m, 3 H); ¹³C NMR (CDCl₃, 75 MHz): δ = 174.4, 161.0, 152.9, 140.1, 135.6, 130.1, 129.5, 128.1, 105.5 ppm.

2-((4-chlorophenyl)thio)-4-(1*H*-tetrazol-1-yl)pyrimidine (38a):

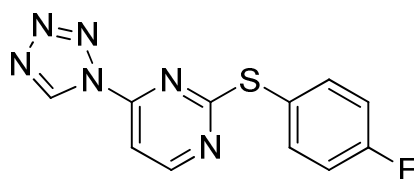


Flash chromatography (ethyl acetate:hexane, 3:7), white solid (63%). ¹H NMR (CDCl₃, 300 MHz): δ = 9.18 (s, 1 H), 8.76 (d, *J* = 5.3 Hz, 1 H), 7.72 (d, *J* = 5.3 Hz, 1 H), 7.58 (dt, *J* = 8.6, 2.4 Hz, 2 H), 7.48 ppm (dt, *J* = 8.7, 2.3 Hz, 2 H); ¹³C NMR (CDCl₃, 126 MHz): δ = 173.8, 161.1, 153.0, 140.0, 136.8, 136.6, 129.7, 126.5, 105.9 ppm.

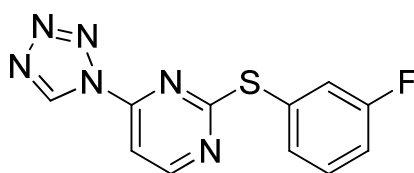
2-((4-methoxyphenyl)thio)-4-(1*H*-tetrazol-1-yl)pyrimidine (39a):



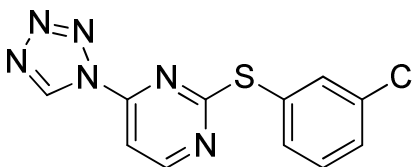
Flash chromatography (ethyl acetate:hexane, 2:8); white solid (64%). ¹H NMR (CDCl₃, 500 MHz): δ = 9.14 (s, 1 H), 8.76 (d, *J* = 5.4 Hz, 1 H), 7.67 (d, *J* = 5.4 Hz, 1 H), 7.48 - 7.61 (m, 2 H), 6.93 - 7.08 (m, 2 H), 3.89 ppm (s, 3 H); ¹³C NMR (CDCl₃, 126 MHz): δ = 175.1, 161.2, 161.0, 152.9, 140.1, 137.3, 118.6, 115.0, 105.3, 55.4 ppm.

2-((4-fluorophenyl)thio)-4-(1*H*-tetrazol-1-yl)pyrimidine (40a):

Flash chromatography (ethyl acetate:hexane, 2:8); white solid (64%). ¹H NMR (CDCl₃, 500 MHz): δ 9.15 (s, 1 H), 8.76 (d, *J* = 5.4 Hz, 1 H), 7.71 (d, *J* = 5.4 Hz, 1 H), 7.57 - 7.66 (m, 2 H), 7.13 - 7.24 ppm (m, 2 H); ¹³C NMR (CDCl₃, 126 MHz): δ = 174.4, 164.2, 161.3, 153.2, 140.3, 138.1, 123.6, 117.0, 106.0 ppm.

2-((3-fluorophenyl)thio)-4-(1*H*-tetrazol-1-yl)pyrimidine (41a):

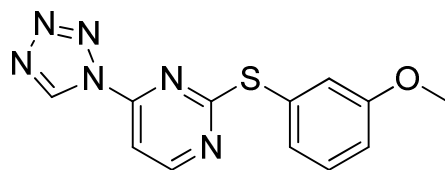
Flash chromatography (ethyl acetate:hexane, 15:85); white solid (77%). ¹H NMR (CDCl₃, 500 MHz) δ 9.15 (s, 1H), 8.78 (d, *J* = 5.4 Hz, 1H), 7.72 ppm (d, *J* = 5.4 Hz, 1H), 7.35 - 7.53 (m, 3H), 7.20 - 7.27 (m, 1H); ¹³C NMR (CDCl₃, 126 MHz) δ 173.6, 162.7, 161.1, 153.0, 140.0, 131.2, 130.7, 129.9, 122.4, 117.3, 105.9 ppm.

2-((3-chlorophenyl)thio)-4-(1*H*-tetrazol-1-yl)pyrimidine (42a):

Flash chromatography (ethyl acetate:hexane, 3:7), white solid (63%). ¹H NMR (CDCl₃, 300 MHz): δ = 9.07 (s, 1 H), 8.70 (d, *J* = 5.3 Hz, 1 H), 7.65 (d, *J* = 5.3 Hz, 1 H), 7.60 (t, *J* = 1.8 Hz, 1 H), 7.45 (tt, *J* = 7.5, 1.5 Hz, 2 H), 7.36 ppm (t, *J* = 7.6 Hz, 1 H); ¹³C NMR (CDCl₃, 126 MHz): δ = 173.5, 161.2, 153.0, 140.0, 135.3, 134.9, 133.6, 130.4, 130.3, 129.8, 105.9 ppm.

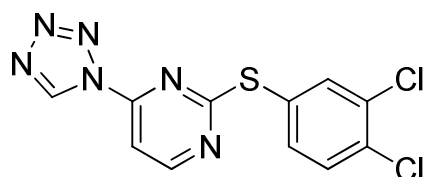
6 Supporting information

2-((3-methoxyphenyl)thio)-4-(1*H*-tetrazol-1-yl)pyrimidine (43a):



Flash chromatography (ethyl acetate:hexane, 2:8); white solid (74%). ¹H NMR (CDCl₃, 500 MHz): δ = 9.13 (s, 1 H), 8.77 (d, *J* = 5.0 Hz, 1 H), 7.69 (d, *J* = 5.4 Hz, 1 H), 7.37 - 7.46 (m, 1 H), 7.23 (dt, *J* = 7.6, 1.3 Hz, 1 H), 7.18 - 7.21 (m, 1 H), 7.07 (ddd, *J* = 8.3, 2.6, 0.8 Hz, 1 H), 3.85 ppm (s, 3 H); ¹³C NMR (CDCl₃, 126 MHz): δ = 174.4, 161.1, 160.2, 152.9, 140.1, 130.2, 129.0, 127.7, 120.9, 115.8, 105.5, 55.5 ppm

2-((3,4-dichlorophenyl)thio)-4-(1*H*-tetrazol-1-yl)pyrimidine (44a):



Flash chromatography (ethyl acetate:hexane, 3:7), white solid (79%). ¹H NMR (CDCl₃, 300 MHz): δ = 9.24 (s, 1 H), 8.77 (d, *J* = 5.3 Hz, 1 H), 7.77 (d, *J* = 2.0 Hz, 1 H), 7.75 (d, *J* = 5.4 Hz, 1 H), 7.54 - 7.62 (m, 1 H), 7.44 - 7.52 ppm (m, 1 H); ¹³C NMR (CDCl₃, 75 MHz): δ = 173.0, 161.2, 153.1, 140.0, 136.9, 134.8, 134.5, 133.4, 131.2, 127.9, 106.2 ppm.

II. Biological assays

PqsD in vitro enzyme inhibition assay

The assay was performed as previously described.^[6] Briefly, the assay was performed monitoring enzyme activity by measuring HHQ formed by condensation of anthraniloyl-CoA and β -ketodecanoic acid. The reaction mixture contained MOPS buffer (0.05 M, pH 7.0) with 0.005% (w/v) Triton X-100, 0.1 μ M of the purified enzyme and inhibitor. The test compounds were dissolved in DMSO and diluted with buffer. The final DMSO concentration was 0.5%. After 10 min preincubation at 37 °C, the reaction was started by the addition anthraniloyl-CoA to a final concentration of 5 μ M and β -ketodecanoic acid to a final concentration of 70 μ M. Reactions were stopped by addition of MeOH containing 1 μ M amitriptyline as internal standard for LC/MS–MS analysis. HHQ was quantified using a HPLC-MS/MS mass spectrometer (ThermoFisher, Dreieich, Germany) in ESI mode. Ionization of HHQ and the internal standard amitriptyline was optimized in each case. The solvent system consisted of 10 mM ammonium acetate (A) and acetonitrile (B), both containing 0.1% trifluoroacetic acid. The initial concentration of B in A was 45%, increasing the percentage of B to 100% in 2.8 min and keeping it at 98% for 0.7 min with a flow of 500 μ L/min. The column used was a NUCLEODUR-C18, 100–3/125–3 (Macherey Nagel, Dühren, Germany). Control reactions without the inhibitor, but including identical amounts of DMSO, were performed in parallel and the amount of HHQ produced was set to 100%. All experiments were performed in at least duplicates except compound 26 which was determined once.

PqsR reporter gene assay in E. coli

The assay was performed as previously described.^[7] The ability of the compounds to either stimulate or antagonize the PqsR-dependent transcription was analysed using a β -galactosidase reporter gene assay in *E. coli* expressing PqsR. A culture of *E. coli* DH5 α cells containing the plasmid pEAL08-2, which encodes PqsR under the control of the tac promoter and the β -galactosidase reporter gene lacZ controlled by the pqsA promoter, were co incubated with test compound. Antagonistic effects of compounds were assayed in the presence of 50 nM PQS. After incubation, β -galactosidase activity was measured spectrophotometrically at OD_{420nm} using

6 Supporting information

POLARstar Omega (BMG Labtech, Ortenberg, Germany) and expressed as percent stimulation of controls. All experiments were at least performed in duplicates.

P. aeruginosa PA14 biofilm assay and detection of extracellular DNA

The assays were performed as previously described.^[2] For the determination of biofilm mass, *P. aeruginosa* PA14 strain was cultivated in 96 well plates using M63 medium. CV staining was used to detect compound effects on the overall biofilm biomass. Impact on eDNA was assessed by incubation of biofilm with propidium iodine solution (0,05 mg ml⁻¹) for 3 h and detection of specific fluorescence at 620 nm after a thorough washing step with 18MΩ H₂O.

Levels of pyocyanin have been determined as published previously.^[2]

III. Solubility of compounds 1 – 44

SI Table 2. Solubility of compounds 1 – 44 as 2% DMSO in water mixtures determined by visual inspection.

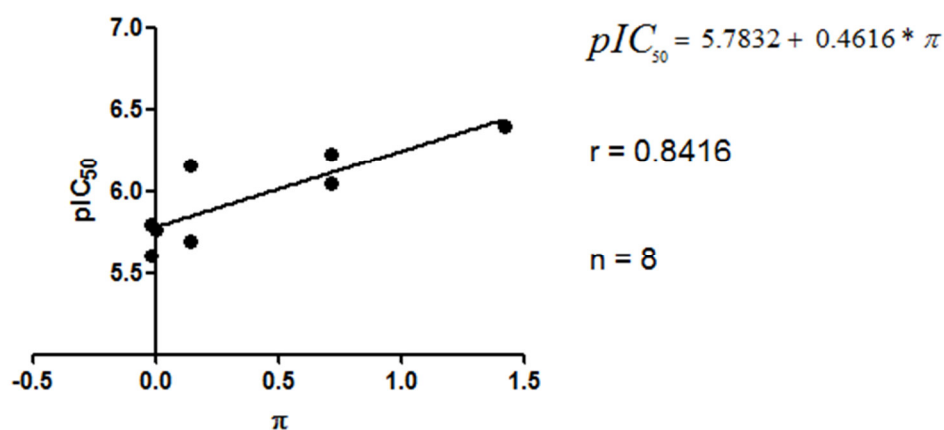
Compound	Solubility [μM]	Compound	Solubility [μM]
1	≥ 1000	23	≥ 200
2	≥ 200	24	≥ 200
3	≥ 200	25	≥ 200
4	≥ 200	26	≥ 200
5	≥ 200	27	≥ 200
6	≥ 200	28	≥ 200
7	≥ 200	29	≥ 200
8	≥ 200	30	≥ 200
9	≥ 200	31	≥ 200
10	≥ 200	32	≥ 200
11	≥ 200	33	≥ 200
12	≥ 200	34	100
13	≥ 200	35	≥ 200
14	≥ 200	36	≥ 200
15	≥ 200	37	≥ 200
16	≥ 200	38	≥ 200
17	≥ 200	39	≥ 200
18	10	40	≥ 200
19	10	41	≥ 200
20	50	42	≥ 200
21	50	43	≥ 200
22	≥ 200	44	100

6 Supporting information

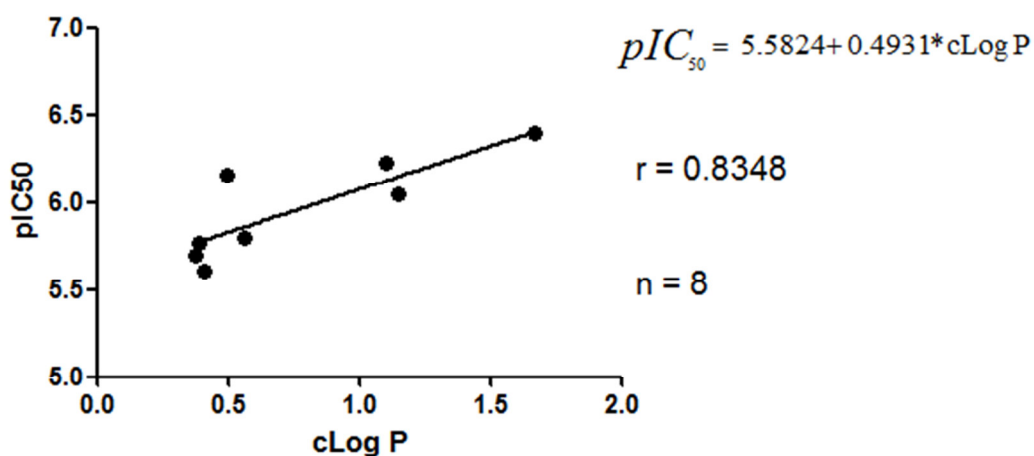
IV. Correlation of π and cLogP with pIC_{50} of compounds 37 – 44

SI Table 2. Summary of pIC_{50} , cLogP and π values for compounds 37 – 44 with corresponding groups attached to the sulfophenyl residue.

Compound	Group	pIC_{50}	cLogP	π
37	H	4.638	0.39	0.00
38	4-F	4.602	0.37	0.14
39	4-Cl	4.732	1.15	0.71
40	4-OMe	5.004	0.41	-0.02
41	3-F	5.537	0.49	0.14
42	3-Cl	5.769	1.10	0.71
43	3-OMe	5.769	0.56	-0.02
44	3,4-di-Cl	4.638	1.67	1.42



SI Figure 1. Correlation of pIC_{50} of compounds 37 – 44 and π



SI Figure 2. Correlation of pIC_{50} of compounds 37 – 44 and cLogP

V. Molecular modeling and Hansch analysis

Molecular Modeling (Flexible alignment)

For the flexible alignment of HHQ/ β -decanoic acid and compound **2** Molecular Operating Environment (Chemical Computing Group) was used with the following general parameters: Forcefield = MMF94x; Alignment Mode = Flexible; Iteration Limit = 200; Failure Limit = 20; Energy Cutoff = 15. Settings used for HHQ alignment: Volume = 1; Aromaticity = 1; LogP (o/w) = 1; H-Bond Acceptor = 3; Hydrophobe = 1; Hydrophobe –Don/Acc = -1; H-Bond Acc projection = 1; Aromatic Center = 1. CO₂-type Centroid = 1. Settings used for β -decanoic acid: H-Bond Donor = 3; LogP (o/w) = 1; H-Bond Acc Projection = 1; CO₂-type Centroid = 1. The resulting alignment was then sorted by score and the best rated was refined using all Atom Based Similarity and Projected Pharmacophore Similarity Terms.

Physicochemical Properties

Physicochemical properties calculation was performed as reported before.^[3]

Hansch Analysis

pIC₅₀ values were plotted against either the Hammett parameter of substituent or the alkyl chain length. Graphs were fitted using Graph Pad Prism 5 (GraphPad Software Inc.). To derive the Hansch equations for the Hammett parameter versus pIC₅₀ the “linear regression model” and for alkyl chain length versus pIC₅₀ the “One site – Fit logIC₅₀” model was used.

VI. References

- [1] A. Thomann, C. Börger, M. Empting, R. Hartmann, *Synlett* **2014**, *25*, 935–938.
- [2] A. Thomann, de Mello Martins, Antonio G G, C. Brengel, M. Empting, R. W. Hartmann, *ACS Chem. Biol.* **2016**, *11*, 1279–1286.
- [3] A. Thomann, J. Zapp, M. Hutter, M. Empting, R. W. Hartmann, *Org. Biomol. Chem.* **2015**, *13*, 10620–10630.
- [4] K. Gudmundsson, B. A. Johns, *Patent WO 2006/055245 A2* **2006**, 29.
- [5] A. Thomann, J. Eberhard, G. Allegretta, M. Empting, R. Hartmann, *Synlett* **2015**, *26*, 2606–2610.
- [6] M. P. Storz et al., *J. Am. Chem. Soc* **2012**, *134*, 16143–16146.
- [7] C. Lu, C. K. Maurer, B. Kirsch, A. Steinbach, R. W. Hartmann, *Angew. Chem.* **2014**, *126*, 1127–1130.

6.6 Supporting information for Chapter VI

Supporting Information

Biophysical Screening of a Focused Library for the Discovery of CYP121 Inhibitors as Novel Antimycobacterials

Content

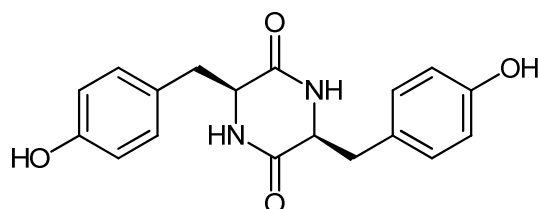
1. Chemical synthesis cYY and Mycocyclosin
 - 1.1 Synthesis of cyclo-di-L-tyrosine (cYY)
 - 1.2 Synthesis of mycocyclosine
2. SDS-PAGE of His-tagged CYP121
3. Activity of CYP121/ CO Spectra
4. LC-MS analysis of *in vitro* CYP121 enzyme reaction and effect of I:47
5. Surface Plasmon Resonance Sensorgram of econazole
6. Screening overview
7. K_D determination by UV-VIS Heme coordination assay
8. Protein Blast of Mtb H₃₇R_V CYP121 (Rv2276) and M. bovis BCG Pasteur CYP121 (BCG_2293)
9. MIC_{BCGT} determination against *Mycobacterium bovis*
10. Calculation of antimicrobial efficiency
11. Toxicity assessment against human cancer cell lines HEK293 and HepG2
12. MIC against *Escherichia coli* and *Staphylococcus aureus* in comparison to growth inhibition against *Mycobacterium bovis* BCG
13. Physicochemical data
14. Bacterial strains and growth conditions
15. Chemical synthesis and analytical characterization. Chemicals were purchased from commercial suppliers and used without further purification
16. Protein expression, purification and biotinylation
17. In silico binding mode
18. Physicochemical properties
19. Cyp121 *in vitro* enzyme inhibition assay
20. Determination MIC_{Mtb} using MABA
21. MIC_{Eco} E. coli ToIC and MIC_{Sa} S.aureus Newman
22. Spectroscopic characterization of enzyme activity
23. References

6 Supporting information

1. Chemical synthesis cYY and Mycocyclosin:

1.1 Synthesis of cyclo-di-*L*-tyrosine (cYY)

cyclo-di-*L*-tyrosine (cYY):

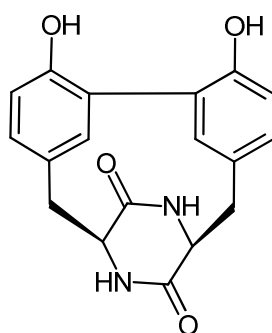


cYY was synthesized as previously described.¹ Spectral data is in accordance with the previously published results:¹

¹H NMR (300 MHz, DMSO-*d*₆) δ 9.19 (s, 1H), 7.75 (d, *J* = 2.6 Hz, 1H), 7.05 – 6.78 (m, 2H), 6.78 – 6.55 (m, 2H), 3.85 (s, 1H), 2.54 (dd, *J* = 4.6 Hz, 1H), 2.11 (dd, *J* = 13.7, 6.5 Hz, 1H); ¹³C NMR (75 MHz, DMSO) δ 166.7, 156.5, 131.2, 127.0, 115.5, 56.2, 39.3; ESI-MS(+) = *m/z* 327.1 [M+H]⁺.

1.2 Synthesis of mycocyclosine

Mycocyclosine:



Mycocyclosine was synthesized as previously described.^{1,2} Spectral data is in accordance with the previously published results:¹

¹H NMR (300 MHz, DMSO-*d*₆) δ 7.98 (s, 1H), 6.84 (dd, *J* = 2.51, 7.9 Hz, 1H), 6.62 (d, *J* = 8.1 Hz, 1H), 6.58 (d, *J* = 2.4 Hz, 1H), 4.32 (d, *J* = 4.8 Hz, 1H), 3.46 (d, *J* = 15.7 Hz, 1H), 2.64 (dd, *J* = 5.73, 15.6 Hz, 1H).

2. SDS-PAGE of His-tagged CYP121

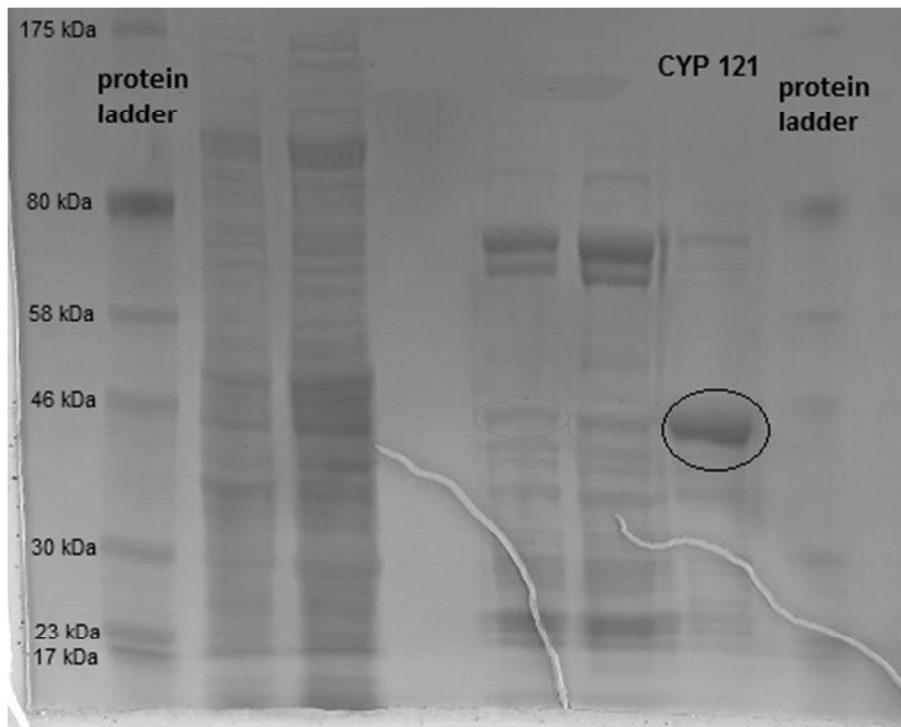


Figure S1. SDS-PAGE of Ni-NTA purified heterologous expressed CYP121. The band corresponds to a molecular mass of > 46000 Da which is in good accordance with the calculated protein mass of 43256 Da.

3. Activity of CYP121/ CO Spectra

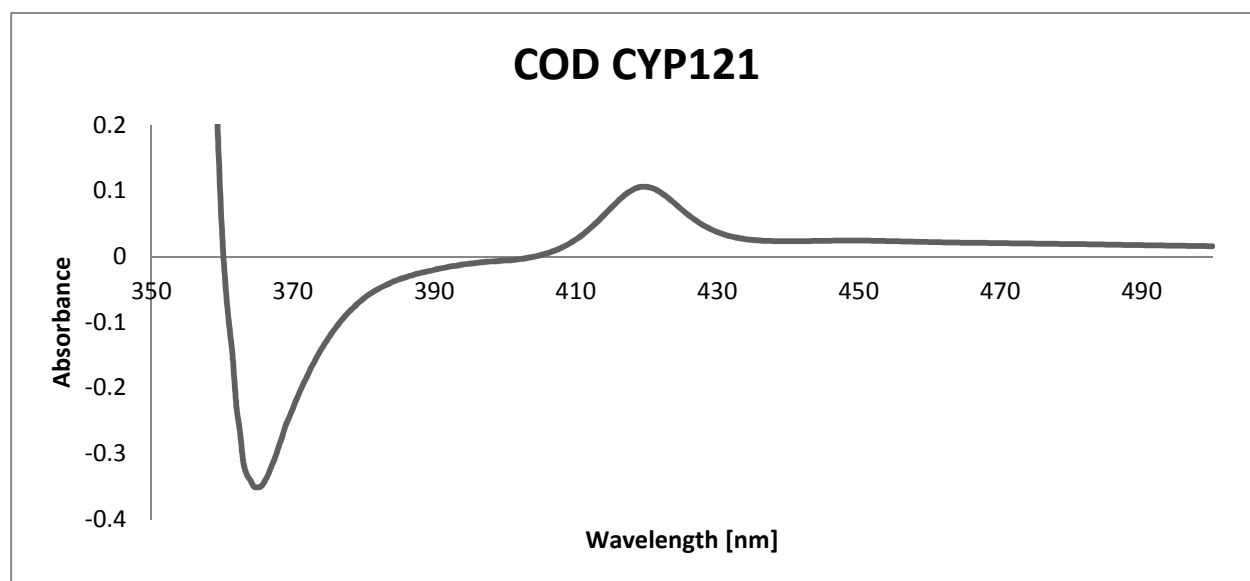


Figure S2. UV-VIS carbonmonoxide difference spectra (COD) of CYP121 after treatment with sodium sulfide and carbonmonoxide. The characteristic band at ~420 nm shows CO coordination to the reduced iron-heme.

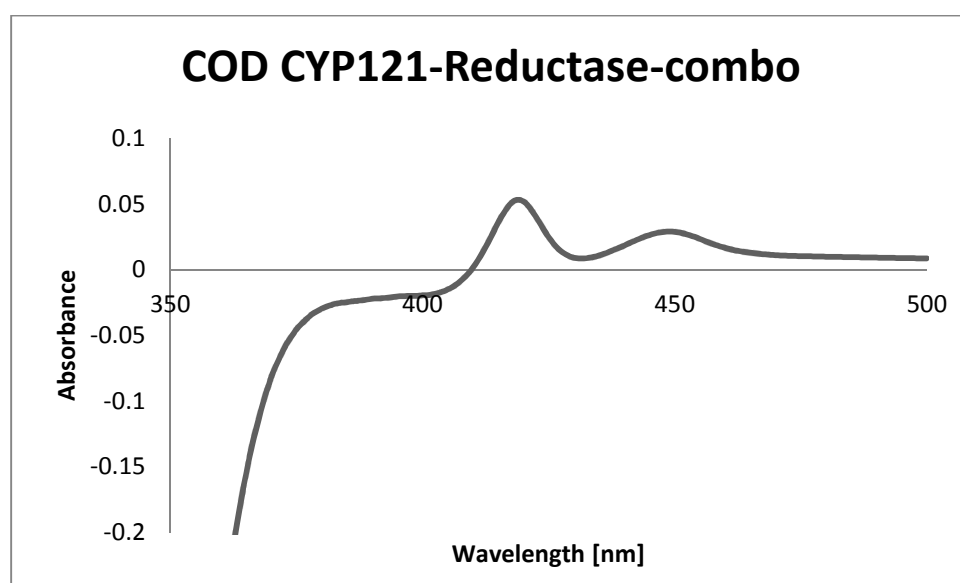


Figure S3. UV-VIS carbonmonoxide difference spectra (COD) of CYP121 after incubation with reductase Arh1_A18G and ferredoxin Etp1fd (516-618) followed by carbonmonoxide treatment. The characteristic band at ~420 nm shows CO coordination to the reduced iron-heme

4. LC-MS analysis of *in vitro* CYP121 enzyme reaction and effect of I:47

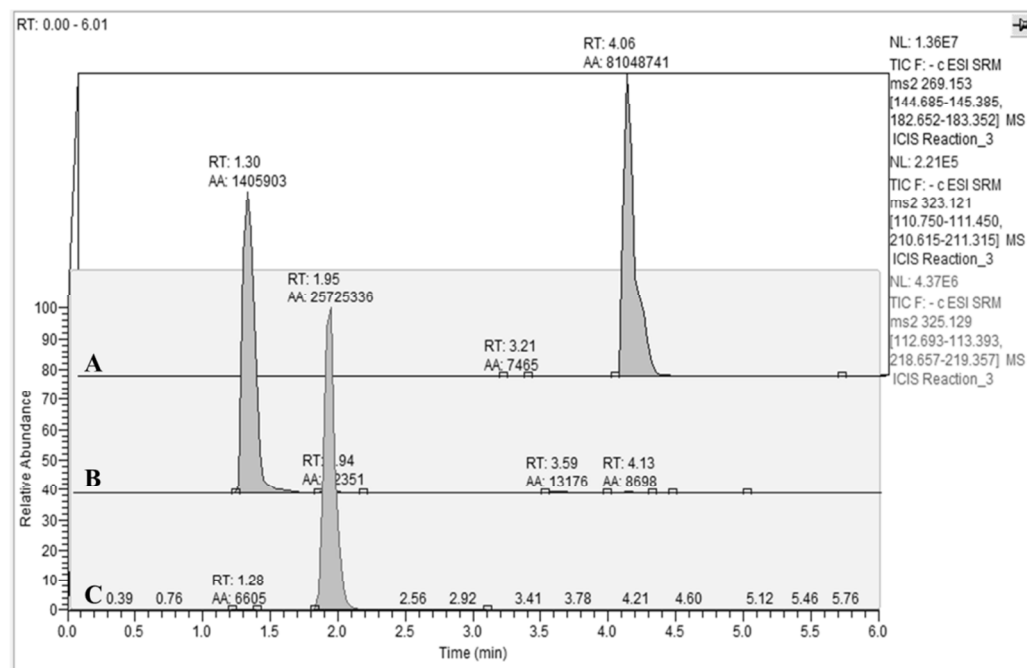


Figure S4. LC-MS/MS quantification of CYP121 enzyme reaction: internal standard estrone $t_R = 4.05$ min (A); mycocyclusin $t_R = 1.30$ min (B); cYY $t_R = 1.95$ min (C).

6 Supporting information

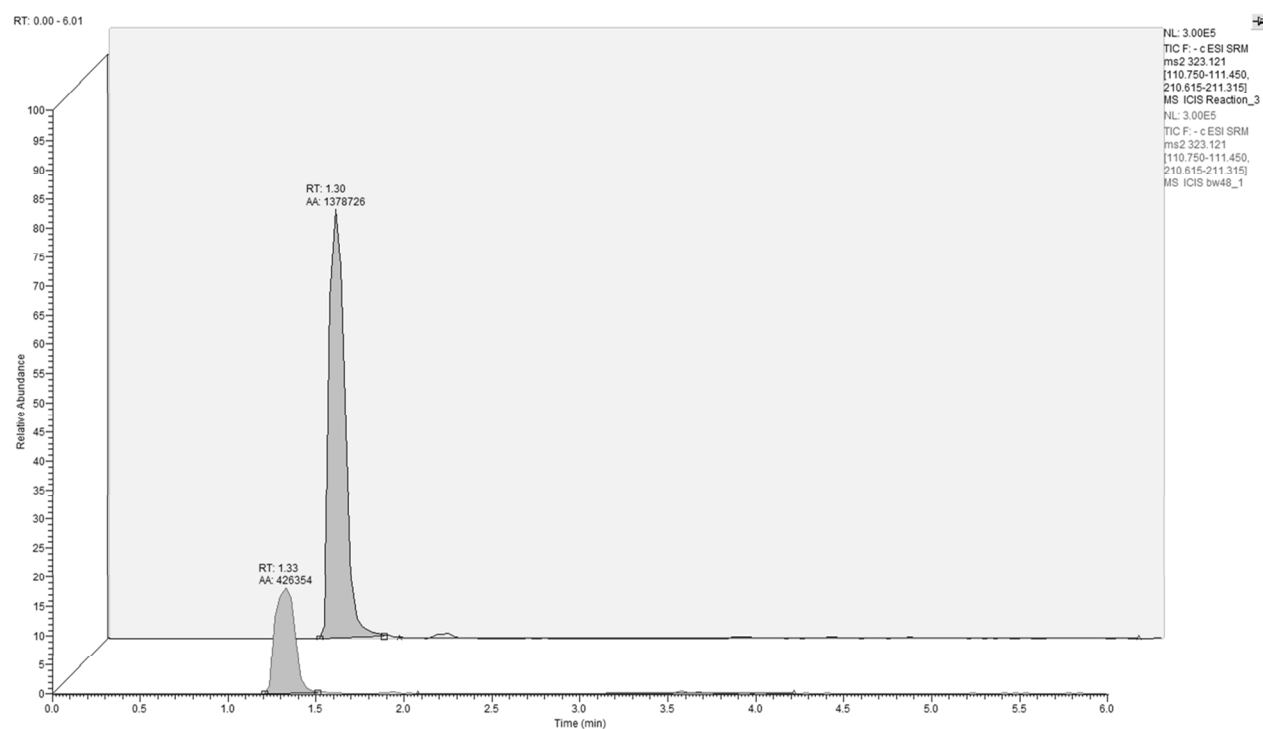


Figure S5. LC-MS/MS based quantification of CYP121 *in vitro* enzyme reaction product mycocyclusin with addition of **I:47** (100 μ M, lower chromatogram) and without the presence of the inhibitor (upper chromatogram).

5. Surface Plasmon Resonance Sensorgram of Econazole

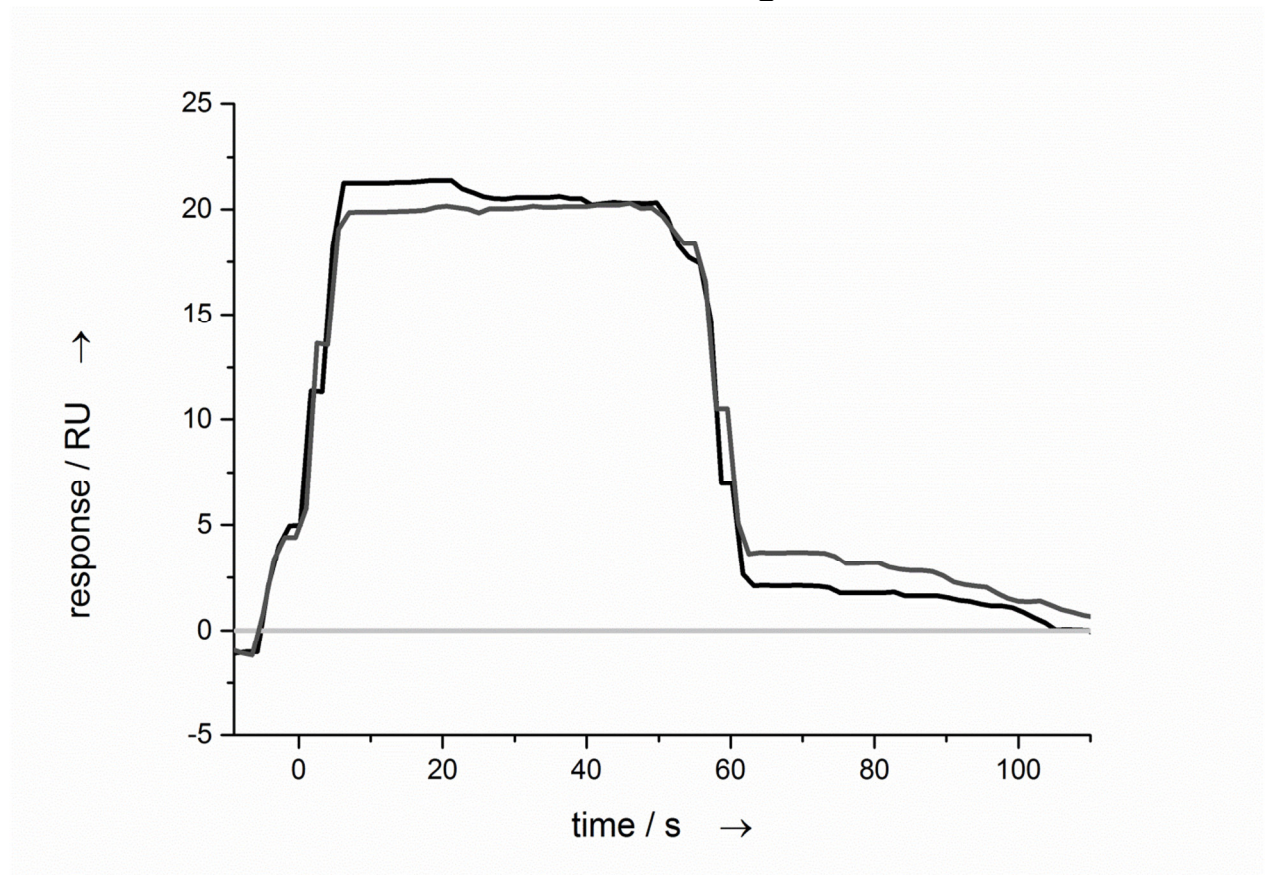


Figure S6. Representative example for SPR binding curve of econazole to CYP121 injected from 100 μ M sample.

6. Screening overview

Table S1. Overview of the results of SPR screening, Heme binding assay, BCG and Mtb growth inhibition and MIC determination

Cmpd	SPR [R/Rpos]	Heme coord. ^a	Heme- K _D [μM]	BCGT Inhibition @ 100 μM [%]	MIC _{BCGT} [μM]	MIC _{Mtb} [μM]
I:1	0.4	N		10		
I:2	0					
I:3	0.1					
I:4	0.2					
I:5	0.1					
I:6	0.1					
I:7	0.5					
I:8	0.5					
I:9	0					
I:10	0					
I:11	0.6	N				
I:12	0.4					
I:13	0					
I:14	0.2					
I:15	0.3	Y (T-II)	34	87	41	
I:16	1.2	Y (T-II)	1	78	5	6
I:17	1.9	Y (T-II)	3	65	38	
I:18	0.1					
I:19	0					
I:20	0.4					
I:21	0.1					
I:22	0.1					
I:23	0.1					
I:24	0.3					
I:25	0.5					
I:26	0.1					
I:27	1.0	Y (T-II)	weak			
I:28	0.3					
I:29	0.4					
I:30	1.4	Y (T-II)	11	94	11	48
I:31	1.5	N				
I:32	1.1	Y (T-II)	14	85	30	41
I:33	0.1	N		0		
I:34	0.7	Y (T-II)	29	25		
I:35	0.5					
I:36	0.1					
I:37	0.2					
I:38	0.2					

I:39	0.1					
I:40	0.3					
I:41	0.1					
I:42	0.1					
I:43	0.2					
I:44	0.2					
I:45	0.5					
I:46	0.1					
I:47	0.6	Y (T-II)	5	87	1	1
I:48	0.8	Y (T-II)	5	88	7	12
<hr/>						
II:1	0.3					
II:2	0.3					
II:3	0.5					
II:4	0.2					
II:5	0.2					
II:6	0.1					
II:7	0.0					
II:8	0.3					
II:9	0.2					
II:10	0.1					
II:11	0.3					
II:12	0.2					
II:13	0.1					
II:14	0.5	N				
II:15	0.1					
II:16	0.2					
II:17	0.2					
II:18	0.2					
II:19	0.2					
II:20	1.3	Y (T-II)	9	48		
II:21	0.7	Y (T-II)	31			
II:22	0.2					
II:23	0.6	N				
II:24	0.1					
II:25	0.2					
II:26	0.8	Y (T-II)	16			
II:27	0.9	Y (T-II)	20			
II:28	0.9	Y (T-II)	19			
II:29	0.7	Y (T-II)	62			
II:30	0.8	Y (T-II)	weak			
II:31	0.6	Y (T-II)	weak			
II:32	0.7	Y (T-II)	weak			
II:33	0.3					
II:34	0.7	Y (T-II)	12	0		
II:35	1.0	Y (T-II)	weak			
II:36	0.9	Y (T-II)	16			
II:37	1.4	Y (T-II)	50			
II:38	1.2	Y (T-II)	weak			
II:39	1.4	N				

6 Supporting information

II:40	0.7	Y (T-II)	27	
II:41	0.9	Y (T-II)	13	7
II:42	0.2			
<hr/>				
III:1	0.3			
III:2	0.4			
III:3	1.7	Y (T-II)	weak	20
III:4	1.7	N		20
III:5	0.5			
III:6	0.3			
III:7	1.8	N		18
III:8	1.4	Y (T-II)	weak	5
III:9	0.6	Y (T-II)	weak	
III:10	0.4			
III:11	0.3			
III:12	0.2			
III:13	0.1			
III:14	0.3			
III:15	0.4			
III:16	0.2			
III:17	0.2			
III:18	0.4			
III:19	0.4			
III:20	0.2			
III:21	0.3			
<hr/>				
IV:1	0.2			
IV:2	0.1			
IV:3	0.1			
IV:4	0.3			
IV:5	0.1	N		
IV:6	0.5			
IV:7	0.6	N		
IV:8	0.5			
IV:9	0.4			
IV:10	0.5			60
IV:11	0.9	Y (T-II)	weak	
IV:12	0.9	N		
IV:13	0.8	Y (T-II)	62	
<hr/>				
V:1	0.0			
V:2	0.3			
V:3	0.2			
V:4	0.1			
V:5	0.2			
V:6	0.1			
V:7	0.3			
V:8	0.8	N		
V:9	0.8	N		
<hr/>				
VI:1	0.6	N		50
VI:2	1.2	N		
VI:3	1.5	N		
VI:4	1.3	N		
VI:5	0.4			

VI:6	1.3	N				
Eco^b	1.0	Y (T-II)	3	71	14	11 ³
cYY^c		Y (T-I)	12			

^an= no, y= yes, T-I = type I binding profile, T-II = type II binding profile, ^b Eco = econazole, cYY = cyclo-di-*L*-tyrosine

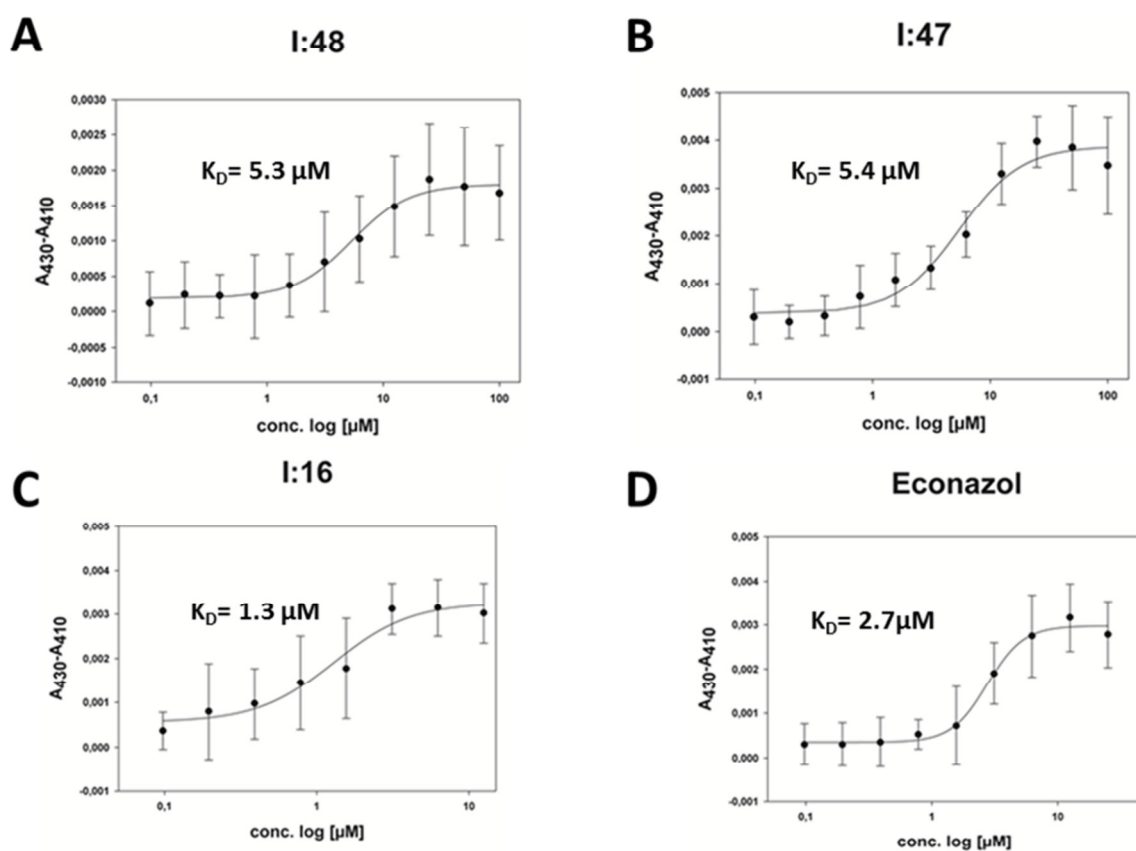
7. K_D determination by UV-VIS Heme coordination assay

Figure S7. Determination of K_D 's by titration of **I:48** (A), **I:47** (B), **I:16** (C) and **econazole** (D) and monitoring the difference between the absorption at 430 nm minus absorption at 410 nm in the presence of CYP121. Graphs were plotted with SigmaPlot using Marquardt - Levenberg algorithm.

8. Protein Blast of Mtb H₃₇R_v CYP121 (Rv2276) and M. bovis BCG Pasteur CYP121 (BCG_2293)

Range 1: 1 to 396 [Graphics](#) ▼ Next Match ▲ Previous Match

Score	Expect	Method	Identities	Positives	Gaps
800 bits(2066)	0.0	Compositional matrix adjust.	396/396(100%)	396/396(100%)	0/396(0%)
Query 1		MTATVLLLEVPFSARGDRIPDAVAELRTRPIRKVRTITGAEAWLVSSYALCTQVLEDRRF			60
Sbjct 1		MTATVLLLEVPFSARGDRIPDAVAELRTRPIRKVRTITGAEAWLVSSYALCTQVLEDRRF			60
Query 61		SMKETAAAGAPRLNALTVPPEVVNMGNIADAGLRKAVMKAITPKAPGLEQFLRDTANSL			120
Sbjct 61		SMKETAAAGAPRLNALTVPPEVVNMGNIADAGLRKAVMKAITPKAPGLEQFLRDTANSL			120
Query 121		LDNLITEGAPADLRNDFADPLATALHCKVLGIPQEDGPKLFRSLSIAFMSSADPIPAAKI			180
Sbjct 121		LDNLITEGAPADLRNDFADPLATALHCKVLGIPQEDGPKLFRSLSIAFMSSADPIPAAKI			180
Query 181		NWDRDIEYMAGILENPNITTTGLMGELSRLRKDPAYSHVSDLEFATIGVTFFGAGVISTGS			240
Sbjct 181		NWDRDIEYMAGILENPNITTTGLMGELSRLRKDPAYSHVSDLEFATIGVTFFGAGVISTGS			240
Query 241		FLTTALISLIQRPQLRNLLHEKPELIPAGVEELLRINLSFADGLPRLATADIQVGDVLR			300
Sbjct 241		FLTTALISLIQRPQLRNLLHEKPELIPAGVEELLRINLSFADGLPRLATADIQVGDVLR			300
Query 301		KGELVLVLLLEGANFDPEHFPNPGSIELDRPNPTSHLAFGRGQHFCPGSALGRRHAQIGIE			360
Sbjct 301		KGELVLVLLLEGANFDPEHFPNPGSIELDRPNPTSHLAFGRGQHFCPGSALGRRHAQIGIE			360
Query 361		ALLKKMPGVDLAVPIDQLVWRTRFQRRIPERLPVLW	396		
Sbjct 361		ALLKKMPGVDLAVPIDQLVWRTRFQRRIPERLPVLW	396		

Figure S8. Results of the Protein Blast of Mtb CYP121 (upper sequence) and BCGT CYP121 (lower sequence) showing 100% amino acid identity between both proteins.

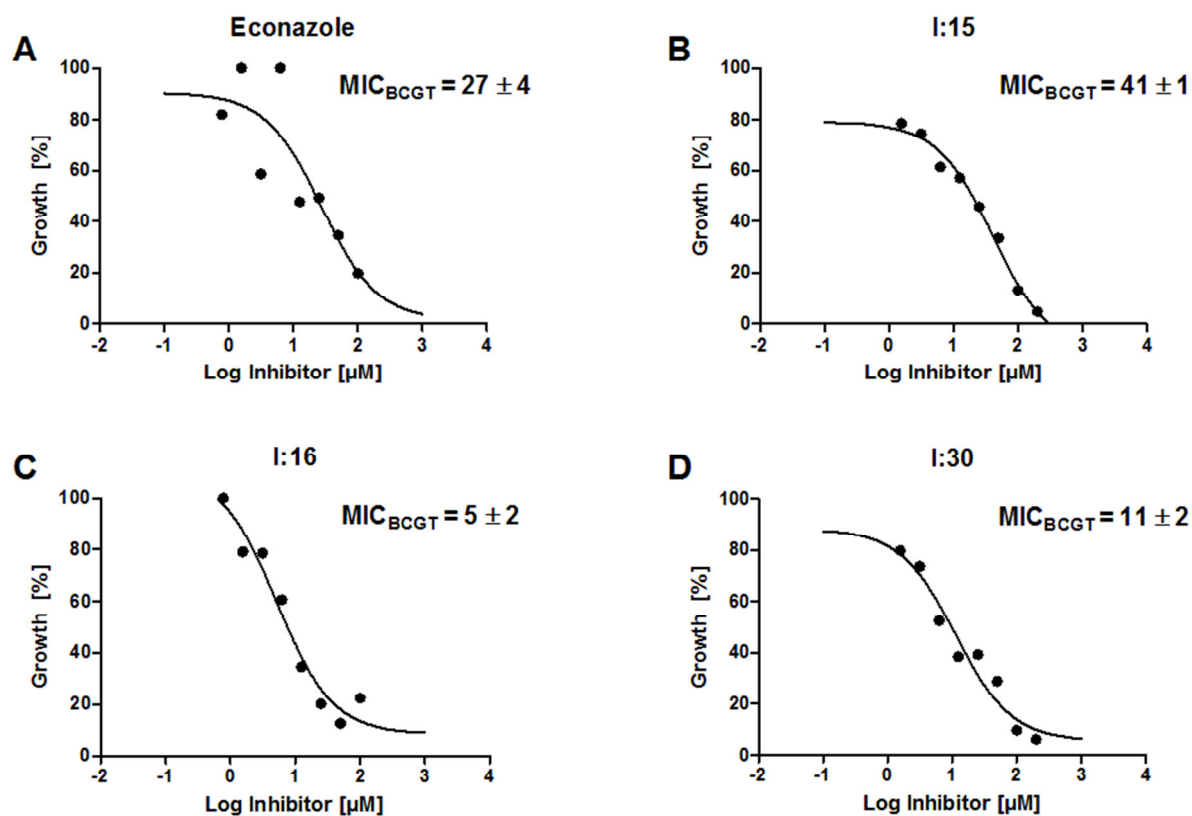
9. MIC_{BCGT} determination against *Mycobacterium bovis*

Figure S9. Growth inhibition of BCG *versus* control (%) of **econazole** (A), **I:15** (B), **I:16** (C), **I:30** (D) of concentrations ranging from 100-1.56 µM of the respective compounds. Endpoint optical density was measured at 600 nm. MIC_{BCGT} were determined by GraphPad Prism using OneSite Log IC₅₀ model provided by the software.

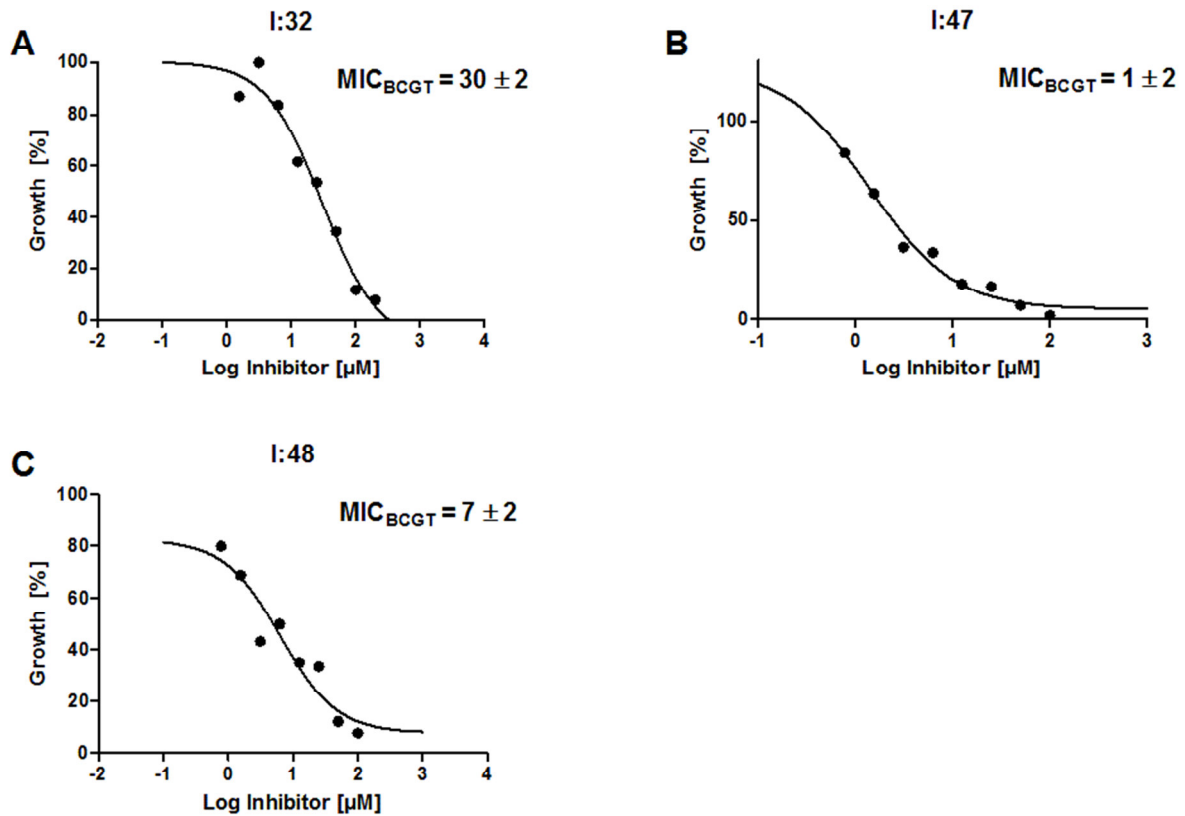


Figure S10. Growth inhibition of BCG *versus* control (%) of **I:32** (A), **I:47** (B), **I:48** (C) of concentrations ranging from 100-1.56 μM of the respective compounds. Endpoint optical density was measured at 600 nm. MIC_{BCGT} were determined by GraphPad Prism using OneSite Log IC₅₀ model provided by the software.

10. Calculation of antimicrobial efficiency

$$\text{Antibacterial Efficiency} = -\ln\left(\frac{\text{MIC}}{\text{NHA}}\right)$$

Table S2. Antimicrobial efficiency ⁴ of **I:16**, **I:30**, **I:32**, **I:47**, **I:48**, **econazole**, **isoniazide** and **rifampicine** calculated for effects on *Mycobacterium tuberculosis*.

Cmp d.	MIC [mg/L]	MW	NHA^a	Antibacterial Efficiency
I:16	1.90	310	24	0.26
I:30	11.20	234	18	0.25
I:32	9.60	234	18	0.26
I:47	0.30	278	21	0.39
I:48	3.50	292	22	0.26
Eco	4.20	382	23	0.24
INH^b	0.05	137	10	0.99
Rif^c	0.11	823	57	0.16

^aNHA = number of heavy atoms, INH = isoniazide ³, Rif = rifampicine ³.

11. Toxicity assessment against human cancer cell lines HEK293 and HepG2

SI Table 3. Toxicity data against human cancer cell lines HEK293 and HepG2 of **I:47**, **I:16** and **econazole** (Eco).

Compounds	LD ₅₀	SD	LD ₅₀	LD ₅₀	SD	LD ₅₀
	HEK293 [μM]		HEK293 [mg/L]	HepG2 [μM]		HepG2 [mg/L]
I:47	66.9	5.3	18.6	47.5	8.1	17.1
I:16	19.6	3.8	6.1	12.1	2.8	3.9
Eco	15.6	3.8	6.0	11.8	4.3	3.1

12. MIC against *Escherichia coli* and *Staphylococcus aureus* in comparison to growth inhibition against *Mycobacterium bovis* BCG

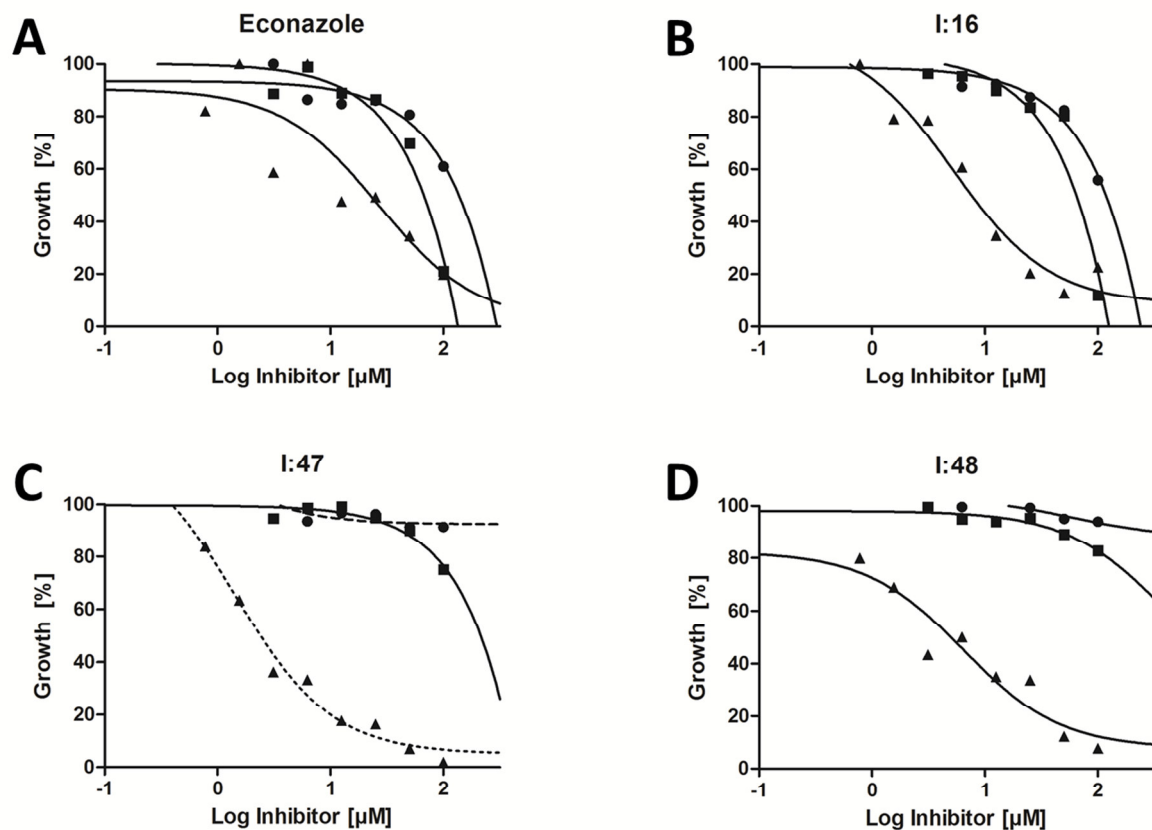


Figure S11. Comparison of growth inhibition of **econazole** (A), **I:16** (B), **I:47** (C) and **I:48** (D) against *M. bovis* (▲, $c = 1.56 - 100 \mu\text{M}$), *E. coli* (■, $c = 3.125 - 100 \mu\text{M}$), *S. aureus* (●, $c = 3.125 - 100 \mu\text{M}$) of concentrations ranging from 100-0.725 μM of the respective compounds. Endpoint optical density was measured at 600 nm. Graphs were plotted with GraphPad Prism using OneSite Log IC_{50} model provided by the software.

13. Physicochemical data:

I:16



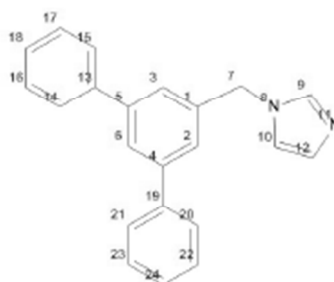
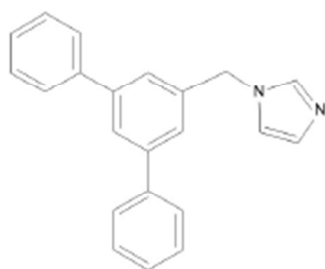
ACD/Labs
ACD/LogP Classic Module Report

Date: February 17, 2015 9:47 AM

Software name and version: ACD/Percepta 14.0.0 (Build 2203)

Compound name:

Structure:



Calculated LogP: 5.26 ± 0.35

6 Supporting information

LogP Calculation Protocol:

Increments of the functional groups:

1. -1,86 (experimental value), atom(s) number: 9, 11, 8

Increments of the Carbon atoms:

2. +0,53 (experimental value), atom(s) number: 7
3. +0,37 (experimental value), atom(s) number: 10
4. +0,37 (experimental value), atom(s) number: 12
5. -0,08 (experimental value), atom(s) number: 1
6. -0,08 (experimental value), atom(s) number: 5
7. -0,08 (experimental value), atom(s) number: 4
8. -0,08 (experimental value), atom(s) number: 19
9. -0,08 (experimental value), atom(s) number: 13
10. +0,37 (experimental value), atom(s) number: 3
11. +0,37 (experimental value), atom(s) number: 2
12. +0,37 (experimental value), atom(s) number: 6
13. +0,37 (experimental value), atom(s) number: 21
14. +0,37 (experimental value), atom(s) number: 20
15. +0,37 (experimental value), atom(s) number: 15
16. +0,37 (experimental value), atom(s) number: 14
17. +0,37 (experimental value), atom(s) number: 23
18. +0,37 (experimental value), atom(s) number: 22
19. +0,37 (experimental value), atom(s) number: 17
20. +0,37 (experimental value), atom(s) number: 16
21. +0,37 (experimental value), atom(s) number: 24
22. +0,37 (experimental value), atom(s) number: 18

Interactions through aromatic system:

- 8-9 +0,29 (experimental value), atom(s) number: 19, 4, 6, 5, 13

Interactions through aliphatic system:

- 1-5 +0,28 (experimental value), atom(s) number: 1, 7, 8

Increments of the ring interactions

Increments of the ring interactions

Increments of the ring interactions

I:47



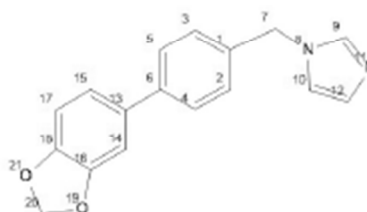
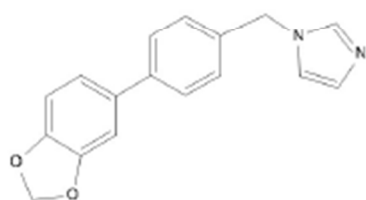
ACD/Labs
ACD/LogP Classic Module Report

Date: February 17, 2015 9:59 AM

Software name and version: ACD/Percepta 14.0.0 (Build 2203)

Compound name:

Structure:



Calculated LogP: 3,08 +- 0,37

6 Supporting information

LogP Calculation Protocol:

Increments of the functional groups:

1. +0.43 (experimental value), atom(s) number: 20, 21, 19
2. -1.86 (experimental value), atom(s) number: 9, 11, 8

Increments of the Carbon atoms:

3. +0.53 (experimental value), atom(s) number: 7
4. +0.37 (experimental value), atom(s) number: 10
5. +0.37 (experimental value), atom(s) number: 12
6. +0.08 (experimental value), atom(s) number: 16
7. +0.08 (experimental value), atom(s) number: 18
8. -0.08 (experimental value), atom(s) number: 1
9. -0.08 (experimental value), atom(s) number: 13
10. -0.08 (experimental value), atom(s) number: 6
11. +0.37 (experimental value), atom(s) number: 14
12. +0.37 (experimental value), atom(s) number: 17
13. +0.37 (experimental value), atom(s) number: 3
14. +0.37 (experimental value), atom(s) number: 2
15. +0.37 (experimental value), atom(s) number: 15
16. +0.37 (experimental value), atom(s) number: 5
17. +0.37 (experimental value), atom(s) number: 4

Interactions through aromatic system:

- 1-10 0.00 (approximated value), atom(s) number: 19, 16, 14, 13, 6

Interactions through aliphatic system:

- 2-8 +0.28 (experimental value), atom(s) number: 1, 7, 8

Increments of the ring interactions

Increments of the ring interactions

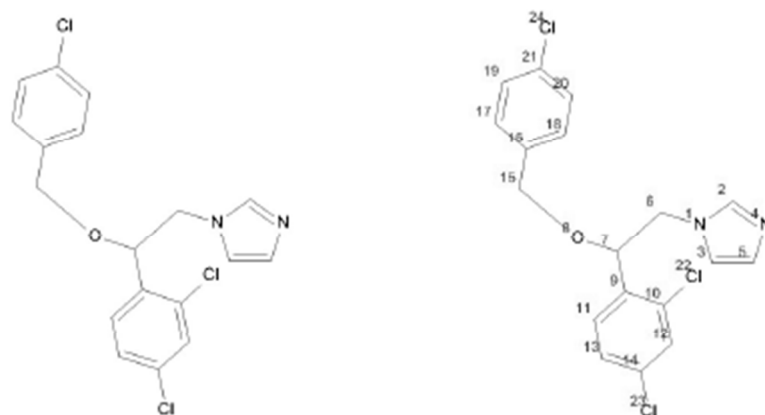
Econazole**ACD/Labs**
ACD/LogP Classic Module Report

Date: February 17, 2015 10:16 AM

Software name and version: ACD/Percepta 14.0.0 (Build 2203)

Compound name: Econazole

Structure:



Calculated LogP: 5.32 +- 0.55

6 Supporting information

LogP Calculation Protocol:

Increments of the functional groups:

1. -1,86 (experimental value), atom(s) number: 2, 4, 1
2. +1,04 (experimental value), atom(s) number: 22
3. +1,04 (experimental value), atom(s) number: 23
4. +1,04 (experimental value), atom(s) number: 24
5. -1,90 (experimental value), atom(s) number: 8

Increments of the Carbon atoms:

6. +0,53 (experimental value), atom(s) number: 15
7. +0,53 (experimental value), atom(s) number: 6
8. -0,03 (experimental value), atom(s) number: 7
9. +0,37 (experimental value), atom(s) number: 3
10. +0,37 (experimental value), atom(s) number: 5
11. -0,08 (experimental value), atom(s) number: 10
12. -0,08 (experimental value), atom(s) number: 14
13. -0,08 (experimental value), atom(s) number: 21
14. -0,08 (experimental value), atom(s) number: 9
15. -0,08 (experimental value), atom(s) number: 16
16. +0,37 (experimental value), atom(s) number: 12
17. +0,37 (experimental value), atom(s) number: 13
18. +0,37 (experimental value), atom(s) number: 20
19. +0,37 (experimental value), atom(s) number: 19
20. +0,37 (experimental value), atom(s) number: 11
21. +0,37 (experimental value), atom(s) number: 18
22. +0,37 (experimental value), atom(s) number: 17

Interactions through aromatic system:

- 2-3 +0,01 (experimental value), atom(s) number: 22, 10, 12, 14, 23

Interactions through aliphatic system:

- 14-15 -0,05 (experimental value), atom(s) number: 16, 15, 8, 7, 9
- 1-14 -0,01 (experimental value), atom(s) number: 9, 7, 6, 1
- 1-5 +0,64 (experimental value), atom(s) number: 1, 8, 7, 8
- 5-14 +0,65 (experimental value), atom(s) number: 9, 7, 8
- 5-15 +0,65 (experimental value), atom(s) number: 16, 15, 8
- 1-15 +0,10 (approximated value), atom(s) number: 16, 15, 8, 7, 6, 1

Referenced data:

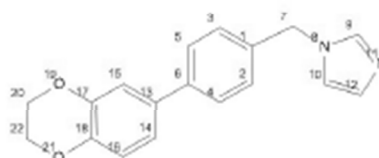
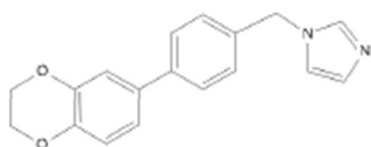
**ACD/Labs****ACD/Labs***ACD/LogP Classic Module Report*

Date: February 17, 2015 10:03 AM

Software name and version: ACD/Percepta 14.0.0 (Build 2203)

Compound name:

Structure:



Calculated LogP: 2,63 +- 0,39

6 Supporting information

LogP Calculation Protocol:

Increments of the functional groups:

1. -1,86 (experimental value), atom(s) number: 9, 11, 8
2. -0,55 (experimental value), atom(s) number: 19
3. -0,55 (experimental value), atom(s) number: 21

Increments of the Carbon atoms:

4. +0,56 (experimental value), atom(s) number: 20
5. +0,56 (experimental value), atom(s) number: 22
6. +0,53 (experimental value), atom(s) number: 7
7. +0,37 (experimental value), atom(s) number: 10
8. +0,37 (experimental value), atom(s) number: 12
9. +0,08 (experimental value), atom(s) number: 17
10. +0,08 (experimental value), atom(s) number: 18
11. -0,08 (experimental value), atom(s) number: 1
12. -0,08 (experimental value), atom(s) number: 13
13. -0,08 (experimental value), atom(s) number: 6
14. +0,37 (experimental value), atom(s) number: 15
15. +0,37 (experimental value), atom(s) number: 16
16. +0,37 (experimental value), atom(s) number: 3
17. +0,37 (experimental value), atom(s) number: 2
18. +0,37 (experimental value), atom(s) number: 14
19. +0,37 (experimental value), atom(s) number: 5
20. +0,37 (experimental value), atom(s) number: 4

Interactions through aromatic system:

- 3-13 -0,10 (experimental value), atom(s) number: 6, 13, 14, 16, 18, 21
- 2-13 -0,15 (experimental value), atom(s) number: 6, 13, 15, 17, 19
- 2-3 -0,09 (experimental value), atom(s) number: 19, 17, 18, 21

Interactions through aliphatic system:

- 2-3 +0,29 (experimental value), atom(s) number: 21, 22, 20, 19
- 1-11 +0,28 (experimental value), atom(s) number: 1, 7, 8

Increments of the ring interactions

Increments of the ring interactions

14. Bacterial strains and growth conditions.

Bacterial strains used in this study were *Mycobacterium bovis* DSM-43990 (BCGT), *Mycobacterium tuberculosis* H₃₇Rv (Mtb), *Escherichia coli* TolC acr A/B deficient, *Staphylococcus aureus* (Newman strain) and *E. coli* K12 BL21. Mammalian cell lines for cytotoxicity evaluation were HEK293 (human embryonic kidney) and Hep2G (human liver carcinoma cells) cells. Mycobacteria were cultured in 7H9GC-Tween⁵ or Middlebrook 7H9 broth complemented with ADC Enrichment (Middlebrook). *E. coli* TolC and *S. aureus* tests were performed in lysogenic broth (LB) and LB plus ADC Enrichment.

15. Chemical synthesis and analytical characterization.

Chemicals were purchased from commercial suppliers and used without further purification. Column flash chromatography was performed on silica gel (40–63 μm), and reaction progress was monitored by TLC on TLC Silica Gel 60 F₂₅₄ plates (Merck, Darmstadt, Germany). All moisture-sensitive reactions were performed under nitrogen atmosphere using anhydrous solvents. ¹H and ¹³C NMR spectra were recorded on Bruker Fourier spectrometers (300 MHz) at ambient temperature with the chemical shifts recorded as δ values in ppm units by reference to the hydrogenated residues of deuterated solvent as internal standard. Coupling constants (J) are given in Hertz (Hz), and signal patterns are indicated as follows: s, singlet; d, doublet; dd, doublet of doublets; t, triplet; m, multiplet, br, broad signal. The purity of the final compounds was >95% measured by HPLC with UV detection at 254 nm. The SpectraSystem LC system consisted of a pump, an autosampler, and a UV/Vis detector (ThermoFisher, Dreieich, Germany). Mass spectrometry was performed on an LC-coupled Surveyor MSQ electrospray mass spectrometer (ThermoFisher, Dreieich, Germany). The system was operated by the Xcalibur software. An RP C18 NUCLEODUR ec 100-5 125 \times 3 mm 5 μm column (Macherey-Nagel GmbH, Düren, Germany) was used as the stationary phase. All solvents were HPLC grade. In a gradient run, the percentage of acetonitrile (containing 0.1 % trifluoroacetic acid) was increased from an initial concentration of 0 % at 0 min to 100 % at 15 min and kept at 100 % for 5 min. The injection volume was 10 μL , and flow rate was set to 800 $\mu\text{L}/\text{min}$. MS analysis was carried out at a spray voltage of 3800 V, a source CID of 10 V and a capillary temperature of 350 $^{\circ}\text{C}$. Spectra were acquired in positive mode from 100 to 1000 m/z.

6 Supporting information

cYY and mycocyclosin were synthesized as described.^{6–8} Experimental details on modification of cYY and mycocyclosin synthesis and analytical data can be found in the Supplementary Data (Supp. Data, section 1).

The synthesis of library compounds has been described previously: class I^{9–14}, class II^{15,16}, class III¹⁷, class IV¹⁸, class V¹⁹, and class VI²⁰.

16. Protein expression, purification and biotinylation.

E. coli K12 BL21 (DE3) cells were transformed with plasmid harboring *cyp121* gene (pHAT2/*cyp121*).²¹

The previously described²² enzyme expression and purification method was slightly modified: His₆-tagged CYP121 (H₆-CYP121) was expressed in *E. coli* K12 BL21 and purified using a single affinity chromatography step. Briefly, *E. coli* K12 BL21 cells containing the pHAT2/*cyp121* were grown in terrific broth medium containing 100 µg/mL ampicillin at 37 °C until an OD₆₀₀ of approximately 0.8 units was reached, followed by induction with 0.5 mM IPTG and 0.5 mM δ-aminolevulinic acid for 36 h at 25 °C and 200 rpm. The cells were harvested by centrifugation (5000 rpm, 10 min, 4 °C), and the cell pellet was resuspended in 100 mL of binding buffer containing 1% Triton-X-100 (50 mM tris-HCl, 300 mM NaCl, 20 mM imidazole, 10% glycerol, pH = 7.2) and lysed by sonication for a total process time of 2.5 min. Cellular debris was removed by centrifugation (18,500 rpm, 40 min, 4 °C), and the supernatant was filtered through a syringe filter (0.2 µm). The clear lysate was immediately applied to a Ni-NTA affinity column, washed with binding buffer, and eluted with a one-step gradient of 500 mM imidazole. The protein containing fractions were buffer-exchanged into storage buffer (140 mM NaCl, 10 mM Na₂HPO₄, 2.7 mM KCl, 1.8 mM KH₂PO₄ and 10% glycerol (v/v), pH = 7.2), using a PD10 column (GE Healthcare, Little Chalfont, UK) and judged to be pure by SDS-PAGE analysis. Then protein was stored in aliquots at –80 °C in a final concentration of 50 µM.²²

Before SPR streptavidin immobilization CYP121 was biotinylated. For biotinylation, Sulfo-NHS-LC-LC-Biotin (Thermo Science, Waltham, US) was dissolved in storage buffer (140 mM NaCl, 10 mM Na₂HPO₄, 2.7 mM KCl, 1.8 mM KH₂PO₄ and 10% glycerol (v/v)) with CYP121 in 1:1 molar ratio. The solution was incubated on ice for 2 h and mixed carefully every 30 min. The biotinylated CYP121 was purified by size

exclusion chromatography using the storage buffer and subsequently stored at -80 °C at a final concentration of 10 µM.²³

17. In silico binding mode.

In silico studies were performed with the X-ray co-crystal structure of a type II inhibitor and CYP121 (PDB-ID: 4G44) using MOE software package (Chemical Computing Group).²⁴ Prior to modelling, a pharmacophore model was created, placing a feature for an interacting metal on the heme iron (ML2, R = 1) and a second feature for a metal ligand (ML, R = 1) on the iron-coordinating nitrogen of the co-crystallized ligand. Both features were set to be essential and constrained (Atoms/Projections). Before energy minimization with LigX the solvent and the ligand was deleted from the structure. For LigX, an AMBER10:EHT forcefield with the default parameters were used but the solvation model was changed to R-Field as recommended by the manufacturer. For docking experiments the following parameters were used: Protocols = induced fit, Receptor = Receptor+Solvent, Site = Selected Atoms (these consisted of the heme and the surrounding amino acids in 4.5 Å proximity), Pharmacophore = File (as described above), Ligand = MDB File (Database file with **I:47**, energy minimized with MMFF94x), Placement = Pharmacophore, Rescoring 1 = London dG, Refinement = Forcefield, Rescoring 2 = GBVI/WSA dG. 30 poses were retained within the placement and refinement step. The resulting poses were sorted by their *E_refine* score and the first (best) pose was selected for further evaluation.

18. Physicochemical properties.

Physicochemical properties were calculated using ACD/Percepta version 2012 (Build 2203, 29 jan. 2013), ACD/Labs.

19. Cyp121 *in vitro* enzyme inhibition assay.

The enzyme inhibition assay was performed in 200 mL PBS buffer pH 7.2. Compounds were used in a concentration of 100 µM and incubated with 1 µM CYP121 for 30 minutes at 30 °C. The final DMSO concentration did not exceed 2%. After incubation the electron transfer system Arh1_A18G (5 µM), Etp1fd (15 µM) and NADPH+H⁺ (200 µM) was added. The reaction was started with the addition of cYY

6 Supporting information

(50 μM) and stopped after 30 min by addition of 200 μl methanol with internal standard estrone (1 μM final concentration, addition included).

The characterization of CYP121 activity was conducted by a UHPLC-MS/MS analysis carried out on a TSQ Quantum Access Max mass spectrometer equipped with an HESI-II source and a triple quadrupole mass detector (Thermo Scientific, Dreieich, Germany). Compounds were separated on an Accucore RP-MS 150 \times 2.1 mm 2.6 μm column (Thermo Fisher, Waltham, US) by a methanol/water gradient (from 1.4 min - 3.5 min 50% methanol to 3.5 min - 5.0 min 90% methanol) with a flow of 550 $\mu\text{L}/\text{min}$. Compounds were ionized in negative mode by electrospray ionization. Ionization was assisted by a post-column addition of 2 mM ammonia in methanol with an automated syringe at 1.25 $\mu\text{L}/\text{min}$. Monitored ions were (mother ion [m/z], product ion [m/z], scan time [s], scan width [m/z], collision energy [V], tube lens offset [V], polarity): mycocyclosin: 323.101, 111.100, 0.3, 0.7, 28, negative; CYY: 325.129, 113.043, 0.3, 0.7, 29, negative; internal standard (estrone): 269.153, 145.035, 0.3, 0.7, 42, negative. Samples were injected in a volume of 25 μL . Xcalibur software was used for data acquisition. For quantification, the ratios of the area under the curve of the educt and the product were used.

20. Determination MIC_{Mtb} using MABA.

The assay for determination of minimal inhibition concentration against *Mtb* was performed as previously described.⁵

21. MIC_{Eco} *E. coli* ToIC and MIC_{Sa} *S.aureus* Newman

$\text{MIC}_{\text{Eco}} / \text{MIC}_{\text{Sa}}$ values were performed for econazole, **I:16**, **I:47**, **I:48** in *E. coli* ToIC and *S. aureus* Newman. A start OD_{600} of 0.03 was used in a total volume of 200 mL in lysogeny broth (LB) + ACD enrichment containing the compounds predissolved in DMSO. Final compound concentrations were prepared from serial dilutions ranging from 1.56 to 100 μM in duplicates. The maximal DMSO concentration in the experiment was 1%. The recorded OD_{600} values were determined after addition of the compounds and again after incubation for 18 h at 37 $^{\circ}\text{C}$ and 50 rpm in a 96-well plate (Sarstedt, Nümbrecht, Germany) using a FLUOStar Omega (BMG Labtech, Ortenberg, Germany). Given $\text{MIC}_{\text{Eco}} / \text{MIC}_{\text{Sa}}$ values are means of two independent

experiments (two different clones) and are defined as concentrations at which no bacterial growth was detectable.

22. Spectroscopic characterization of enzyme activity.

Recombinant CYP121 from *Mycobacterium tuberculosis* as well as ferredoxin Etp1fd (516-618) and ferredoxin reductase Arh1_A18G from the fission yeast *Schizosaccharomyces pombe* were expressed and purified as described previously.^{25,26}

Functionality of CYP121 and electron transfer were assayed by the occurrence of the characteristic absorbance maximum at $\lambda \cong 450$ nm, related to the reduced, CO-bound heme complex. The assay was conducted following the method of Omura and Sato²⁷ with slight modifications. CYP121 (2 μ M) was reduced through the addition of a few grains of sodium dithionite or incubation with NADPH (100 μ M), ferredoxin Etp1fd(516-618) (40 μ M), and Arh1_A18G ferredoxin reductase (2 μ M) and divided in two cuvettes to record a baseline. One of the samples was saturated with carbon monoxide for 60 s and difference spectra were recorded until the absorbance at $\lambda \cong 450$ nm was constant.

23. References

- (1) Cochrane, J. R., White, J. M., Wille, U., and Hutton, C. A. (2012) Total synthesis of mycrocyclostin. *Organic letters* 14, 2402–2405. DOI: 10.1021/ol300831t.
- (2) Jung, M. E., and Rohloff, J. C. (1985) Organic chemistry of L-tyrosine. 1. General synthesis of chiral piperazines from amino acids. *J. Org. Chem.* 50, 4909–4913. DOI: 10.1021/jo00224a051.
- (3) Franzblau, S. G., DeGroot, M. A., Cho, S. H., Andries, K., Nuermberger, E., Orme, I. M., Mdluli, K., Angulo-Barturen, I., Dick, T., Dartois, V., and Lenaerts, A. J. (2012) Comprehensive analysis of methods used for the evaluation of compounds against *Mycobacterium tuberculosis*. *Tuberculosis* 92, 453–488. DOI: 10.1016/j.tube.2012.07.003.
- (4) Brzostek, A., Dziadek, B., Rumijowska-Galewicz, A., Pawelczyk, J., and Dziadek, J. (2007) Cholesterol oxidase is required for virulence of *Mycobacterium tuberculosis*. *FEMS microbiology letters* 275, 106–112. DOI: 10.1111/j.1574-6968.2007.00865.x.
- (5) Collins, L., and Franzblau, S. G. (1997) Microplate alamar blue assay versus BACTEC 460 system for high-throughput screening of compounds against *Mycobacterium tuberculosis* and *Mycobacterium avium*. *Antimicrob. Agents Chemother.* 41, 1004–1009.
- (6) Hauptenthal, J., Baehr, C., Zeuzem, S., and Piiper, A. (2007) RNase A-like enzymes in serum inhibit the anti-neoplastic activity of siRNA targeting polo-like kinase 1. *Int. J. Cancer* 121, 206–210. DOI: 10.1002/ijc.22665.
- (7) Fonvielle, M., Le Du, M.-H., Lequin, O., Lecoq, A., Jacquet, M., Thai, R., Dubois, S., Grach, G., Gondry, M., and Belin, P. (2013) Substrate and reaction specificity of *Mycobacterium tuberculosis* cytochrome P450

6 Supporting information

- CYP121: insights from biochemical studies and crystal structures. *J. Biol. Chem.* *288*, 17347–17359. DOI: 10.1074/jbc.M112.443853.
- (8) Cochrane, J. R., White, J. M., Wille, U., and Hutton, C. A. (2012) Total synthesis of mycocyclusin. *Org. Lett.* *14*, 2402–2405. DOI: 10.1021/ol300831t.
- (9) Wachall, B. G., Hector, M., Zhuang, Y., and Hartmann, R. W. (1999) Imidazole substituted biphenyls: A new class of highly potent and in vivo active inhibitors of P450 17 as potential therapeutics for treatment of prostate cancer. *Bioorg. Med. Chem.* *7*, 1913–1924. DOI: 10.1016/S0968-0896(99)00160-1.
- (10) Hille, U. E., Zimmer, C., Vock, C. A., and Hartmann, R. W. (2011) First Selective CYP11B1 Inhibitors for the Treatment of Cortisol-Dependent Diseases. *ACS Med. Chem. Lett.* *2*, 2–6. DOI: 10.1021/ml100071j.
- (11) Jagusch, C., Negri, M., Hille, U. E., Hu, Q., Bartels, M., Jahn-Hoffmann, K., Pinto-Bazurco Mendieta, Mariano A E, Rodenwaldt, B., Müller-Vieira, U., Schmidt, D., Lauterbach, T., Recanatini, M., Cavalli, A., and Hartmann, R. W. (2008) Synthesis, biological evaluation and molecular modelling studies of methyleneimidazole substituted biaryls as inhibitors of human 17 α -hydroxylase-17,20-lyase (CYP17). Part I: Heterocyclic modifications of the core structure. *Bioorg. Med. Chem.* *16*, 1992–2010. DOI: 10.1016/j.bmc.2007.10.094.
- (12) Pinto-Bazurco Mendieta, Mariano A E, Negri, M., Hu, Q., Hille, U. E., Jagusch, C., Jahn-Hoffmann, K., Müller-Vieira, U., Schmidt, D., Lauterbach, T., and Hartmann, R. W. (2008) CYP17 inhibitors. Annulations of additional rings in methylene imidazole substituted biphenyls: synthesis, biological evaluation and molecular modelling. *Arch. Pharm.* *341*, 597–609. DOI: 10.1002/ardp.200700251.
- (13) Hille, U. E., Hu, Q., Vock, C., Negri, M., Bartels, M., Müller-Vieira, U., Lauterbach, T., and Hartmann, R. W. (2009) Novel CYP17 inhibitors: synthesis, biological evaluation, structure-activity relationships and modelling of methoxy- and hydroxy-substituted methyleneimidazolyl biphenyls. *Eur. J. Med. Chem.* *44*, 2765–2775. DOI: 10.1016/j.ejmech.2009.01.002.
- (14) Hille, U. E., Zimmer, C., Hauptenthal, J., and Hartmann, R. W. (2011) Optimization of the First Selective Steroid-11 β -hydroxylase (CYP11B1) Inhibitors for the Treatment of Cortisol Dependent Diseases. *ACS Med. Chem. Lett.* *2*, 559–564. DOI: 10.1021/ml100283h.
- (15) Yin, L., Lucas, S., Maurer, F., Kazmaier, U., Hu, Q., and Hartmann, R. W. (2012) Novel imidazol-1-ylmethyl substituted 1,2,5,6-tetrahydropyrrolo[3,2,1-ij]quinolin-4-ones as potent and selective CYP11B1 inhibitors for the treatment of Cushing's syndrome. *J. Med. Chem.* *55*, 6629–6633. DOI: 10.1021/jm3003872.
- (16) Yin, L., Hu, Q., and Hartmann, R. W. (2013) Tetrahydropyrroloquinolinone type dual inhibitors of aromatase/aldosterone synthase as a novel strategy for breast cancer patients with elevated cardiovascular risks. *J. Med. Chem.* *56*, 460–470. DOI: 10.1021/jm301408t.
- (17) Yin, L., Hu, Q., Emmerich, J., Lo, M. M.-C., Metzger, E., Ali, A., and Hartmann, R. W. (2014) Novel pyridyl- or isoquinolinyl-substituted indolines and indoles as potent and selective aldosterone synthase inhibitors. *Journal of medicinal chemistry* *57*, 5179–5189. DOI: 10.1021/jm500140c.
- (18) Hu, Q., Kunde, J., Hanke, N., and Hartmann, R. W. (2015) Identification of 4-(4-nitro-2-phenethoxyphenyl)pyridine as a promising new lead for discovering inhibitors of both human and rat 11 β -Hydroxylase. *Eur. J. Med. Chem.* *96*, 139–150. DOI: 10.1016/j.ejmech.2015.04.013.
- (19) Zimmer, C., Hafner, M., Zender, M., Ammann, D., Hartmann, R. W., and Vock, C. A. (2011) N-(Pyridin-3-yl)benzamides as selective inhibitors of human aldosterone synthase (CYP11B2). *Bioorg. Med. Chem. Lett.* *21*, 186–190. DOI: 10.1016/j.bmcl.2010.11.040.
- (20) Zhu, W., Hu, Q., Hanke, N., van Koppen, Chris J, and Hartmann, R. W. (2014) Potent 11 β -hydroxylase inhibitors with inverse metabolic stability in human plasma and hepatic S9 fractions to promote wound healing. *J. Med. Chem.* *57*, 7811–7817. DOI: 10.1021/jm501004t.
- (21) Hudson, S. A., McLean, K. J., Surade, S., Yang, Y.-Q., Leys, D., Ciulli, A., Munro, A. W., and Abell, C. (2012) Application of fragment screening and merging to the discovery of inhibitors of the Mycobacterium

- tuberculosis cytochrome P450 CYP121. *Angew. Chem., Int. Ed.* 51, 9311–9316. DOI: 10.1002/anie.201202544.
- (22) McLean, K. J., Cheesman, M. R., Rivers, S. L., Richmond, A., Leys, D., Chapman, S. K., Reid, G. A., Price, N. C., Kelly, S. M., Clarkson, J., Smith, W., and Munro, A. W. (2002) Expression, purification and spectroscopic characterization of the cytochrome P450 CYP121 from *Mycobacterium tuberculosis*. *J. Inorg. Biochem.* 91, 527–541. DOI: 10.1016/S0162-0134(02)00479-8.
- (23) Hüsecken, K., Hinsberger, S., Elgaher, Walid A M, Hauptenthal, J., and Hartmann, R. W. (2014) Surface plasmon resonance--more than a screening technology: insights in the binding mode of σ 70:core RNAP inhibitors. *Future Med. Chem.* 6, 1551–1565. DOI: 10.4155/fmc.14.105.
- (24) *Molecular Operating Environment (MOE) (Version 2013.08)* (2015), Chemical Computing Group Inc., 1010 Sherbooke St. West, Suite #910, Montreal, QC, Canada, H3A 2R7.
- (25) Ewen, K. M., Schiffler, B., Uhlmann-Schiffler, H., Bernhardt, R., and Hannemann, F. (2008) The endogenous adrenodoxin reductase-like flavoprotein arh1 supports heterologous cytochrome P450-dependent substrate conversions in *Schizosaccharomyces pombe*. *FEMS Yeast Res.* 8, 432–441. DOI: 10.1111/j.1567-1364.2008.00360.x.
- (26) Müller, J. J., Hannemann, F., Schiffler, B., Ewen, K. M., Kappl, R., Heinemann, U., and Bernhardt, R. (2011) Structural and thermodynamic characterization of the adrenodoxin-like domain of the electron-transfer protein Etp1 from *Schizosaccharomyces pombe*. *J. Inorg. Biochem.* 105, 957–965. DOI: 10.1016/j.jinorgbio.2011.04.001.
- (27) Omura, T., and Sato, R. (1964) THE CARBON MONOXIDE-BINDING PIGMENT OF LIVER MICROSOMES. II. SOLUBILIZATION, PURIFICATION, AND PROPERTIES. *J. Biol. Chem.* 239, 2379–2385.

6 Supporting information

6.7 Supporting information for Publication VII

Supplementary Data

Discovery and Biophysical Evaluation of First Low Nanomolar Hits Targeting CYP125 of *M. tuberculosis*

Christian Brengel,^{a+} Andreas Thomann,^{a+} Alexander Schifrin,^c Jens Eberhard,^a Rolf W. Hartmann^{a,b*}

^a *Helmholtz Institute for Pharmaceutical Research Saarland, Campus E8.1, 66123 Saarbrücken, Germany*

^b *Department of Biochemistry, Saarland University, Campus B2.2, 66123 Saarbrücken, Germany*

^c *Department of Pharmacy, Pharmaceutical and Medicinal Chemistry, Saarland University, Campus C2.3, 66123 Saarbrücken, Germany*

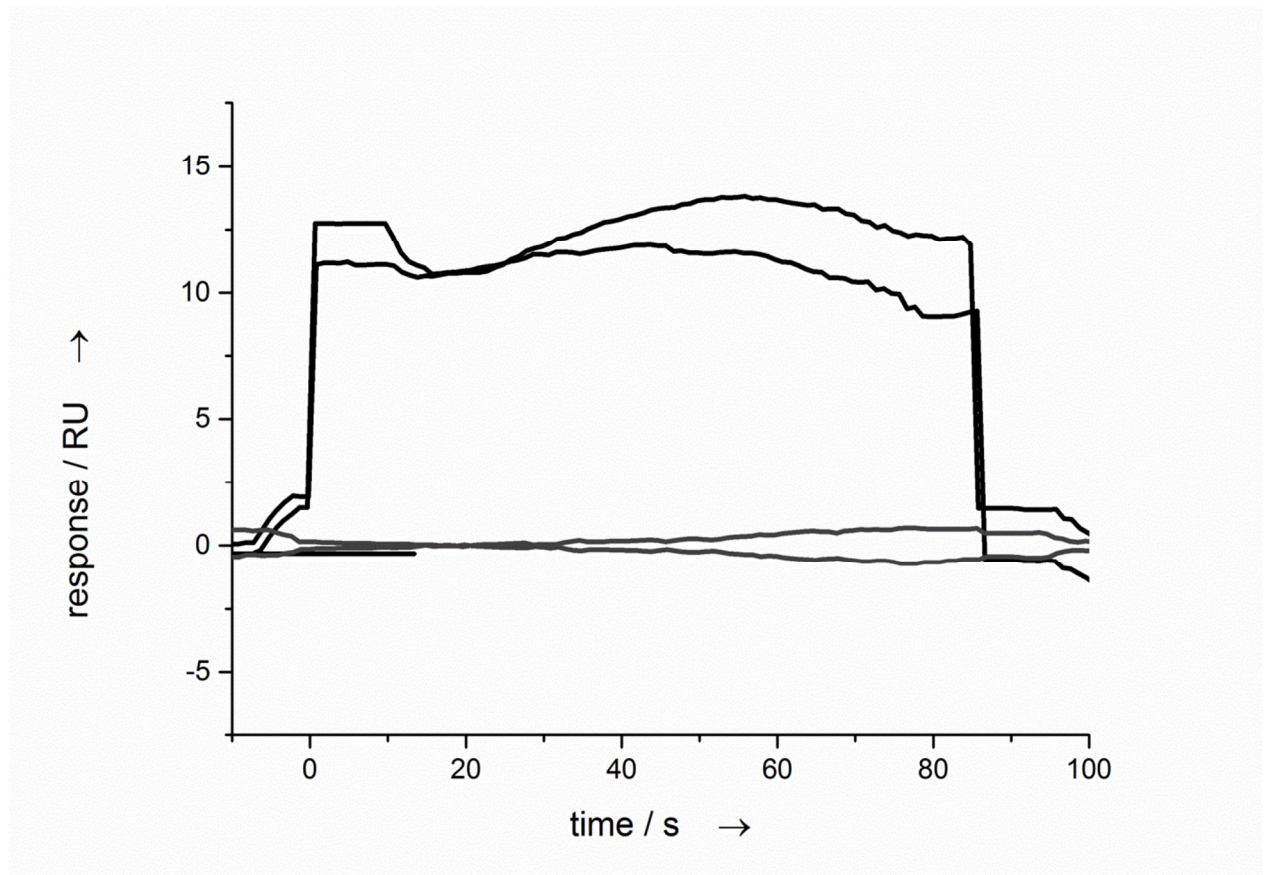
⁺ *These authors contributed equally to this work*

^{*} *Corresponding author: tel: +49 681 98806 2000, fax: +49 681 98806 2009, rolf.hartmann@helmholtz-hzi.de.*

Content

1. **SPR Response Curve of Econazole (positive control)**
2. **Comparison of CYP125 from *M. tuberculosis* and *M. bovis BCG***
3. **Representative K_D Dose Response Curves and Difference Spectra**
4. **Summary of Binding Constants, Profile and Ligand Efficacy Indices of SPR Hits**
5. **Absorbance Maxima in Heme Assay**

1. SPR Response Curve of Econazole (positive control)



SI Figure 1. SPR response curve of 100 μ M econazole (**eco**, black, positive binder) and baseline (grey) recorded against biotin labeled CYP125 immobilized on a streptavidine coated sensorchip.

2. Comparison of CYP125 from *M. tuberculosis* and *M. bovis* BCG

unnamed protein product

Sequence ID: lc|Query_152585 Length: 433 Number of Matches: 1

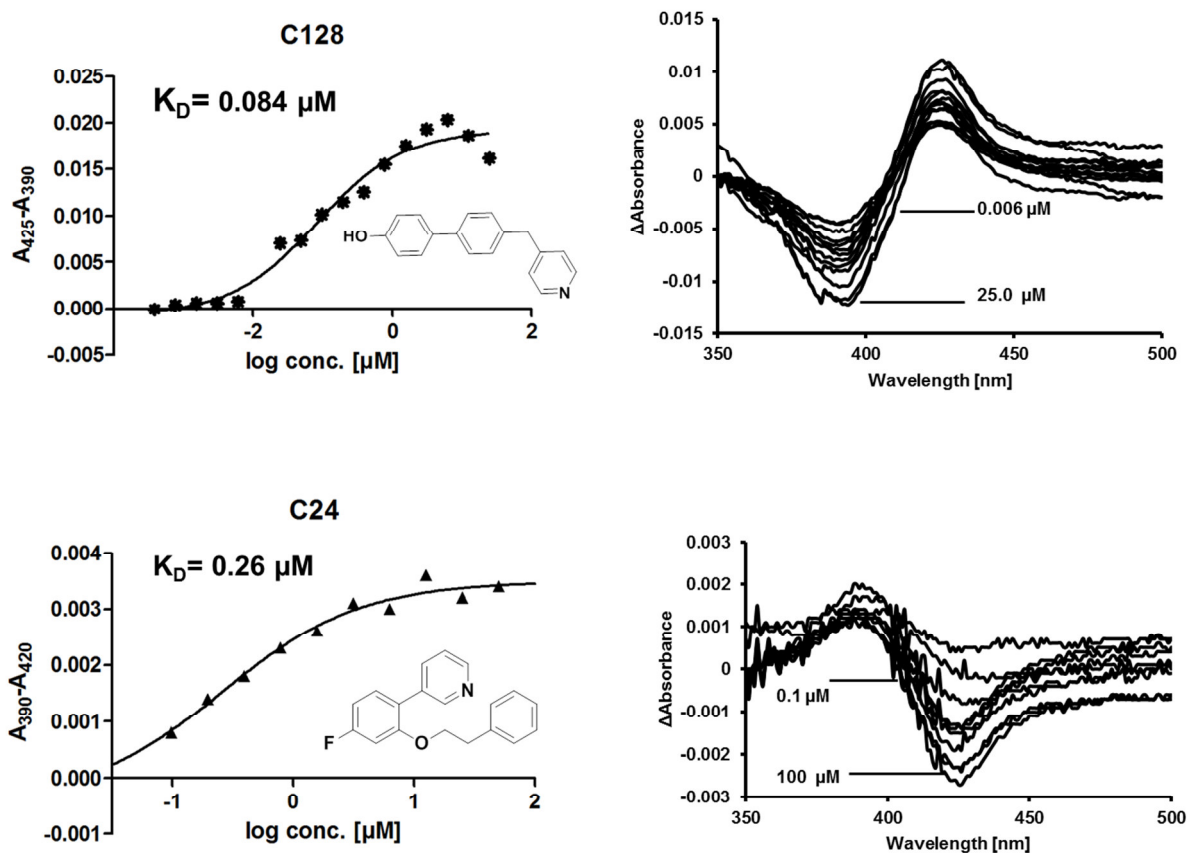
Range 1: 1 to 433 [Graphics](#)

▼ Next Match ▲ Previous Match

Score	Expect	Method	Identities	Positives	Gaps
901 bits(2329)	0.0	Compositional matrix adjust.	433/433(100%)	433/433(100%)	0/433(0%)
Query 1	MSWNHQSV EIAVRRTTVPSNLPPGFDFDTPAIYAERLPVAEFAELRSAAPIWINGQDPG				60
Sbjct 1	MSWNHQSV EIAVRRTTVPSNLPPGFDFDTPAIYAERLPVAEFAELRSAAPIWINGQDPG				60
Query 61	KGGGFHDGGFWAITKLN DVKEISRHSDFVSSYENGVIPRFKNDIARE DIEVQRFVMLNMD				120
Sbjct 61	KGGGFHDGGFWAITKLN DVKEISRHSDFVSSYENGVIPRFKNDIARE DIEVQRFVMLNMD				120
Query 121	APHHTRLRK IISRGFTPRAVGRLHDELQERAQKIAAEAAAAGSGDFVEQVSC ELPLQAIA				180
Sbjct 121	APHHTRLRK IISRGFTPRAVGRLHDELQERAQKIAAEAAAAGSGDFVEQVSC ELPLQAIA				180
Query 181	GLLGVPQEDRGKLFHWSNEMTGNE DPEYAHIDPKASSAELIGYAMKMAEEKAKNPADDIV				240
Sbjct 181	GLLGVPQEDRGKLFHWSNEMTGNE DPEYAHIDPKASSAELIGYAMKMAEEKAKNPADDIV				240
Query 241	TQLIQADIDG EKLSDEDFGFFVVMLAVAGNETTRNSITQGMMAFAEHPDQWEL YKKVRPE				300
Sbjct 241	TQLIQADIDG EKLSDEDFGFFVVMLAVAGNETTRNSITQGMMAFAEHPDQWEL YKKVRPE				300
Query 301	TAADEIVRWATPVTA FQRTALRDYELSGVQIKKGQRVVMFYRSANFDEEVFQDPPTFNIL				360
Sbjct 301	TAADEIVRWATPVTA FQRTALRDYELSGVQIKKGQRVVMFYRSANFDEEVFQDPPTFNIL				360
Query 361	RNP NPHVGFGGTGAHYCIGANLARMTINLIFNAVADHMPDLKPI SAPERLRSGWLN GIKH				420
Sbjct 361	RNP NPHVGFGGTGAHYCIGANLARMTINLIFNAVADHMPDLKPI SAPERLRSGWLN GIKH				420
Query 421	WQVDYTGRC PVAH	433			
Sbjct 421	WQVDYTGRC PVAH	433			

SI Figure 2. Result of the Protein BLAST of CYP125 from *M. tuberculosis* (gene-ID: Rv3545c) and *M. bovis* BCG (gene-ID: BCG_3609c) showing 100% amino acid identity of both proteins.

3. Representative K_D Dose Response Curves and Difference Spectra



SI Figure 3. Representative K_D dose response curves (left) and difference spectra (right) of a type I (C24, lower spectra) and a type II (C128, upper spectra) CYP125 heme ligands.

4. Summary of Binding Constants, Profile and Ligand Efficiency Indices of SPR Hits

SI Table 1. Relative responses of SPR hits (R/R_{pos}) and their respective heme binding profiles, binding affinities (K_D) and Ligand efficiency scores (LE) against CYP125.

Compound	SPR [R/R_{pos}]	Heme assay Binding Type ^c	Heme assay K_D [μM]	Ligand efficiency [kcal/HA]
Econazole (Eco = R_{pos})	1.0	I	0.94	0.36
CHN ^a	-	I	4.6	-
LP10 ^b	-	rl	6.1	0.24
C003	1.3	II	19	0.35
C005	1.0	II	28	0.29
C016	1.1	I	16	0.32
C023	1.0	I	1.5	0.37
C024	1.1	I	0.26	0.42
C025	0.9	no	-	-
C036	2.8	I	1.3	0.46
C037	3	I	1.1	0.49
C042	0.0	no	-	-
C043	1.2	II	13.1	0.26
C052	2.8	no	-	-
C053	0.5	-	-	-
C055	1.2	II	38.7	0.29
C059	0.8	-	-	-
C060	1.1	I	0.28	0.42
C068	1.0	II	38.7	0.34
C080	1.6	II	39.6	0.22
C083	2.9	no	-	-
C087	1.2	no	-	-
C090	1.7	no	-	-
C119	2.0	no	-	-

C126	1.2	II	2.1	0.27
C127	3.1	II	0.85	0.47
C128	1.1	II	0.08	0.50
C129	2.6	II	1.34	0.41
C130	2.4	II	0.174	0.53

^a CHN = Cholest-4-en-3-one; ^b LP10 = α -[(4-methylcyclohexyl)carbonyl amino]-*N*-4-pyridinyl-1*H*-indole-3-propanamide; ^c I = Type I binding profile, II = Type II binding profile, rI = reverse Type II binding profile no = no binding profile observed at the highest tested concentration (100 μ M).

5. Absorbance maximum in Heme assay

SI Table 2. Binding affinities (K_D) and absorbance maxima of selected compounds against CYP125.

Compound	Heme assay K_D [μ M]	Heme assay Absorbance maximum [nm]
LP10	6.1	419
C127	0.85	421
C128	0.08	420
C129	1.34	422
C130	0.17	421

6. Synthesis, analytical and biological data of the screening compounds and their derivatives

C1,^[1] **C2**,^[1] , **C3**,^[2] **C4**,^[1] **C5**,^[3] **C6**,^[1] **C7** - **C10**,^[5] **C11** - **C18**,^[4] **C19** - **C27**,^[5] **C28** - **C29**,^[1] **C30** - **C33**,^[6] **C34** - **C74**,^[7] **C75** - **C121**,^[8] **C122** - **C125**,^[9] **C127** - **C130**.^[10]

[1] C. Zimmer, M. Hafner, M. Zender, D. Ammann, R. W. Hartmann, C. A. Vock, *Bioorganic & medicinal chemistry letters* **2011**, *21*, 186–190.

[2] S. S. Gunatilleke, C. M. Calvet, J. B. Johnston, C.-K. Chen, G. Erenburg, J. Gut, J. C. Engel, Ang, Kenny K H, J. Mulvaney, S. Chen et al., *PLoS neglected tropical diseases* **2012**, *6*, e1736.

6 Supporting information

- [3] M. Balcells, J. Avilla, J. Profitos, R. Canela, *Journal of Agricultural and Food Chemistry* **2000**, *48*, 83–87.
- [4] J. Emmerich, Q. Hu, N. Hanke, R. W. Hartmann, *Journal of medicinal chemistry* **2013**, *56*, 6022–6032.
- [5] Q. Hu, J. Kunde, N. Hanke, R. W. Hartmann, *European journal of medicinal chemistry* **2015**, *96*, 139–150.
- [6] a) R. Heim, S. Lucas, C. M. Grombein, C. Ries, K. E. Schewe, M. Negri, U. Müller-Vieira, B. Birk, R. W. Hartmann, *Journal of medicinal chemistry* **2008**, *51*, 5064–5074; b) S. Lucas, M. Negri, R. Heim, C. Zimmer, R. W. Hartmann, *Journal of medicinal chemistry* **2011**, *54*, 2307–2319; c) Q. Hu, L. Yin, R. W. Hartmann, *Journal of medicinal chemistry* **2012**, *55*, 7080–7089.
- [7] a) U. E. Hille, Q. Hu, C. Vock, M. Negri, M. Bartels, U. Müller-Vieira, T. Lauterbach, R. W. Hartmann, *European journal of medicinal chemistry* **2009**, *44*, 2765–2775; b) U. E. Hille, C. Zimmer, C. A. Vock, R. W. Hartmann, *ACS medicinal chemistry letters* **2011**, *2*, 2–6; c) U. E. Hille, C. Zimmer, J. Hauptenthal, R. W. Hartmann, *ACS medicinal chemistry letters* **2011**, *2*, 559–564.
- [8] a) L. Yin, Q. Hu, R. W. Hartmann, *Journal of medicinal chemistry* **2013**, *56*, 460–470; b) L. Yin, Q. Hu, J. Emmerich, M. M.-C. Lo, E. Metzger, A. Ali, R. W. Hartmann, *Journal of medicinal chemistry* **2014**, *57*, 5179–5189; c) L. Yin, S. Lucas, F. Maurer, U. Kazmaier, Q. Hu, R. W. Hartmann, *Journal of medicinal chemistry* **2012**, *55*, 6629–6633.
- [9] W. Zhu, Q. Hu, N. Hanke, van Koppen, Chris J, R. W. Hartmann, *Journal of medicinal chemistry* **2014**, *57*, 7811–7817.
- [10] Q. Hu, C. Jagusch, U. E. Hille, J. Hauptenthal, R. W. Hartmann, *Journal of medicinal chemistry* **2010**, *53*, 5749–5758.

6.8 Supporting information for Publication VIII

supporting information

Acta Cryst. (2015). E71, o1051–o1052 [doi:10.1107/S2056989015023634]

Crystal structure of 4-methylsulfanyl-2-(2*H*-tetrazol-2-yl)pyrimidine

Andreas Thomann, Volker Huch and Rolf W. Hartmann

S1. Comment

4-tetrazolylpyrimidines are well reported scaffolds in many bioactive entities. Besides synthetic chemistry, tetrazolyl substituted aromatic systems are also of high interest for example, in metal-ligand research (Kim *et al.*, 2008; Stoessel *et al.*, 2010), drug development (Pasternak *et al.*, 2012; Biswas *et al.*, 2015) and polymer discovery (Yu *et al.*, 2008; Sengupta *et al.*, 2010). Thus, the knowledge of the three dimensional structure of these moieties is of crucial importance for the rational design in these fields of research. Recently, we have reported a novel method to synthesize such compounds (Thomann *et al.*, 2014). We have reported the synthesis of 4-(methylthio)-2-(1*H*-tetrazol-1-yl)pyrimidine (**1**). Interestingly, when scaling up the reaction, another product was found in small amounts. NMR analytical characterization revealed the compound to be the 2-tetrazolyl regioisomer (**2**). To determine unequivocally proof of the structure of this compound, we determined its crystal structure.

The title compound (**2**), crystallized with two independent molecules (A and B) in the asymmetric unit (Fig. 1). Interestingly, the two molecules differ in their conformation. While the tetrazole moieties are arranged similarly, with the tetrazole ring is inclined to the pyrimidine ring by 5.48 (7) and 4.24 (7) ° in molecules A and B, respectively, the thio-methyl groups have a difference of the torsion angle about the C_{ar}...S bond of *ca* 180° [for example, torsion angle N5—C4—S1—C6 = 0.89 (12) °, compared to torsion angle N11—C10—S2—C12 = -176.78 (10) °] indicating higher rotational freedom than the tetrazoles (Fig. 1). The latter finding is of importance for computational chemists in medicinal chemistry, as the polarized hydrogen at atom C5 of the tetrazole ring is able to form non-classical hydrogen bonds. Therefore, the results from the crystal structure may favour this conformational isomer for *in silico* predictions.

In the crystal, the A and B molecules are linked *via* a C—H...N hydrogen bond (Table 1 and Fig. 2). They stack along the *b* axis direction forming columns within which there are weak π - π interactions present [shortest inter-centroid distance is Cg2...Cg4ⁱ = 3.6918 (5) Å; Cg2 and Cg4 are the centroids of rings N5/N6/C1—C4 and N11/N12/C7—C10, respectively; symmetry code: (i) *x*, *y* + 1, *z*].

S2. Synthesis and crystallization

The title compound (**2**), was synthesized following a previously reported procedure (Thomann *et al.*, 2014). A mixture of 4-chloro-2-(methylthio)pyrimidine, 1*H*-tetrazole and triethylamine, in the ratio 1:1:1, was stirred under microwave irradiation at 50 W, 353 K for 1 h. The crude product was purified by flash chromatography (hexane:ethyl acetate, 8:2, *R_f* = 1/4) to yield a white solid (9%). Crystals formed at 294 K after 16 h from a saturated solution of **2** in ethyl acetate. ¹H NMR (CDCl₃, 300 MHz) 8.80 (dd, *J* = 5.3, 0.6 Hz, 1 H), 8.77 (s, 1 H), 7.77 (dd, *J* = 5.3, 0.7 Hz, 1 H), 2.69 p.p.m. (d, *J* = 0.7 Hz, 3 H).

S3. Refinement

Crystal data, data collection and structure refinement details are summarized in Table 2. H atoms were located in a difference Fourier map and freely refined.

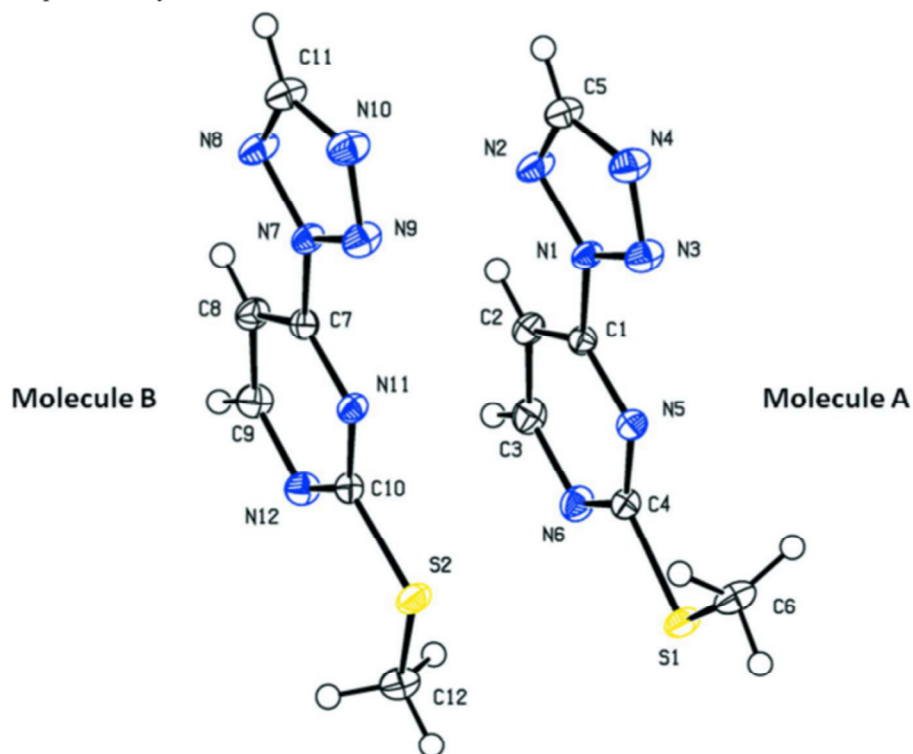


Figure 1

The molecular structure of the two independent molecules (*A* and *B*) of the title compound (2), with atom labelling. Displacement ellipsoids are drawn at the 50% probability level.

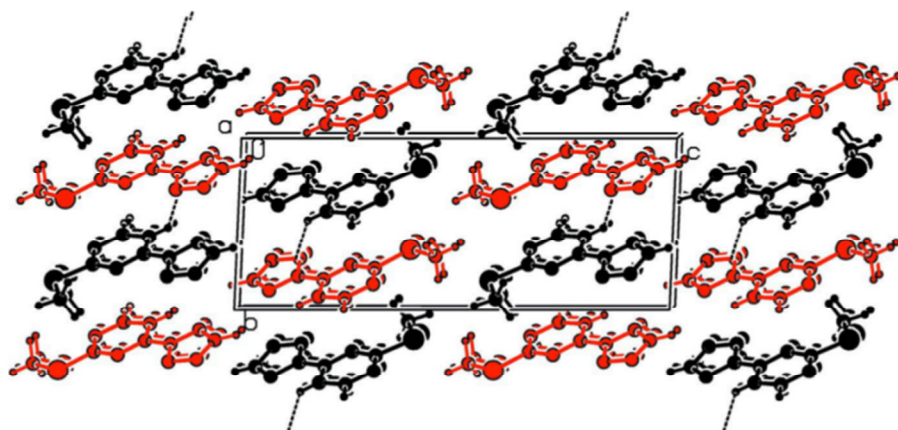


Figure 2

The crystal packing of the two independent molecules (*A* black; *B* red) of the title compound (2), viewed along the *a* axis. Hydrogen bonds are shown as dashed lines (see Table 1).

6 Supporting information

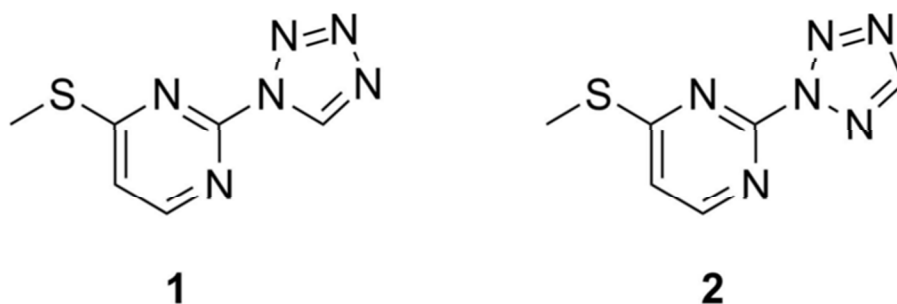


Figure 3

Compounds (1) and (2).

4-Methylsulfanyl-2-(2H-tetrazol-2-yl)pyrimidine

Crystal data

$C_6H_6N_6S$

$M_r = 194.23$

Triclinic, $P\bar{1}$

$a = 6.3001$ (17) Å

$b = 7.393$ (2) Å

$c = 18.159$ (5) Å

$\alpha = 91.407$ (7)°

$\beta = 95.864$ (7)°

$\gamma = 102.695$ (8)°

$V = 819.9$ (4) Å³

$Z = 4$

$F(000) = 400$

$D_x = 1.574$ Mg m⁻³

Mo $K\alpha$ radiation, $\lambda = 0.71073$ Å

Cell parameters from 728 reflections

$\theta = 3.6$ – 24.3 °

$\mu = 0.35$ mm⁻¹

$T = 143$ K

Cuboid, colourless

$0.22 \times 0.22 \times 0.01$ mm

Data collection

Bruker APEXII CCD
diffractometer

φ and ω scans

Absorption correction: multi-scan
(*SADABS*; Bruker, 2010)

$T_{\min} = 0.716$, $T_{\max} = 0.746$

15501 measured reflections

4581 independent reflections

3596 reflections with $I > 2\sigma(I)$

$R_{\text{int}} = 0.028$

$\theta_{\max} = 29.6$ °, $\theta_{\min} = 2.3$ °

$h = -8 \rightarrow 8$

$k = -10 \rightarrow 10$

$l = -24 \rightarrow 25$

Refinement

Refinement on F^2

Least-squares matrix: full

$R[F^2 > 2\sigma(F^2)] = 0.034$

$wR(F^2) = 0.086$

$S = 1.01$

4581 reflections

283 parameters

0 restraints

Hydrogen site location: difference Fourier map

All H-atom parameters refined

$w = 1/[\sigma^2(F_o^2) + (0.0376P)^2 + 0.2718P]$

where $P = (F_o^2 + 2F_c^2)/3$

$(\Delta/\sigma)_{\max} = 0.001$

$\Delta\rho_{\max} = 0.35$ e Å⁻³

$\Delta\rho_{\min} = -0.30$ e Å⁻³

Special details

Geometry. All e.s.d.'s (except the e.s.d. in the dihedral angle between two l.s. planes) are estimated using the full covariance matrix. The cell e.s.d.'s are taken into account individually in the estimation of e.s.d.'s in distances, angles and torsion angles; correlations between e.s.d.'s in cell parameters are only used when they are defined by crystal symmetry. An approximate (isotropic) treatment of cell e.s.d.'s is used for estimating e.s.d.'s involving l.s. planes.

Fractional atomic coordinates and isotropic or equivalent isotropic displacement parameters (\AA^2)

	x	y	z	$U_{\text{iso}}^*/U_{\text{eq}}$
S1	0.84117 (6)	0.83334 (5)	0.58281 (2)	0.01975 (9)
N1	1.04303 (18)	0.69484 (15)	0.84617 (6)	0.0152 (2)
N2	1.00906 (19)	0.60999 (17)	0.90974 (6)	0.0208 (3)
N3	1.24517 (19)	0.79683 (17)	0.84553 (7)	0.0209 (3)
N4	1.3498 (2)	0.77865 (18)	0.91059 (7)	0.0233 (3)
N5	0.93885 (18)	0.76012 (15)	0.72442 (6)	0.0159 (2)
N6	0.56784 (19)	0.65519 (16)	0.66803 (7)	0.0200 (3)
C1	0.8749 (2)	0.67900 (17)	0.78527 (7)	0.0148 (3)
C2	0.6647 (2)	0.58341 (19)	0.79335 (8)	0.0184 (3)
C3	0.5146 (2)	0.5770 (2)	0.73096 (8)	0.0203 (3)
C4	0.7801 (2)	0.74205 (18)	0.66783 (8)	0.0162 (3)
C5	1.2034 (2)	0.6651 (2)	0.94818 (8)	0.0209 (3)
C6	1.1309 (2)	0.9298 (2)	0.60068 (9)	0.0230 (3)
H1	0.629 (3)	0.532 (2)	0.8352 (10)	0.028 (5)*
H2	0.366 (3)	0.512 (2)	0.7313 (9)	0.023 (4)*
H3	1.235 (3)	0.634 (2)	0.9944 (11)	0.030 (5)*
H4	1.204 (3)	0.833 (2)	0.6178 (10)	0.032 (5)*
H5	1.160 (3)	1.037 (2)	0.6366 (10)	0.030 (5)*
H6	1.172 (3)	0.969 (3)	0.5531 (11)	0.040 (5)*
S2	0.91337 (6)	0.35407 (5)	0.59998 (2)	0.02003 (10)
N7	1.07557 (18)	0.19569 (15)	0.85809 (6)	0.0156 (2)
N8	1.0376 (2)	0.11547 (17)	0.92240 (7)	0.0219 (3)
N9	1.28032 (19)	0.29223 (17)	0.85739 (7)	0.0218 (3)
N10	1.3817 (2)	0.27602 (18)	0.92304 (7)	0.0241 (3)
N11	0.97742 (18)	0.26119 (15)	0.73636 (6)	0.0159 (2)
N12	0.60819 (19)	0.16413 (16)	0.67866 (7)	0.0192 (2)
C7	0.9101 (2)	0.18161 (17)	0.79690 (7)	0.0146 (3)
C8	0.6975 (2)	0.08981 (19)	0.80433 (8)	0.0181 (3)
C9	0.5511 (2)	0.0862 (2)	0.74162 (8)	0.0204 (3)
C10	0.8194 (2)	0.24779 (18)	0.67912 (8)	0.0162 (3)
C11	1.2311 (2)	0.1686 (2)	0.96118 (8)	0.0218 (3)
C12	0.6629 (3)	0.3216 (2)	0.53901 (9)	0.0256 (3)
H7	0.658 (3)	0.041 (2)	0.8462 (10)	0.028 (5)*
H8	0.400 (3)	0.022 (2)	0.7410 (10)	0.027 (4)*
H9	1.264 (3)	0.138 (3)	1.0104 (11)	0.035 (5)*
H10	0.564 (3)	0.385 (2)	0.5600 (10)	0.035 (5)*
H11	0.702 (3)	0.373 (3)	0.4949 (11)	0.037 (5)*
H12	0.600 (3)	0.192 (3)	0.5294 (10)	0.038 (5)*

Atomic displacement parameters (\AA^2)

	U^{11}	U^{22}	U^{33}	U^{12}	U^{13}	U^{23}
S1	0.02103 (18)	0.02210 (18)	0.01490 (18)	0.00253 (13)	-0.00004 (13)	0.00614 (13)
N1	0.0152 (5)	0.0167 (5)	0.0130 (5)	0.0007 (4)	0.0036 (4)	0.0040 (4)
N2	0.0216 (6)	0.0250 (6)	0.0152 (6)	0.0020 (5)	0.0040 (5)	0.0078 (5)

6 Supporting information

N3	0.0155 (6)	0.0260 (6)	0.0190 (6)	-0.0011 (5)	0.0024 (5)	0.0049 (5)
N4	0.0203 (6)	0.0295 (7)	0.0186 (6)	0.0031 (5)	0.0005 (5)	0.0046 (5)
N5	0.0166 (5)	0.0159 (5)	0.0149 (6)	0.0028 (4)	0.0030 (4)	0.0019 (4)
N6	0.0182 (6)	0.0193 (6)	0.0212 (6)	0.0019 (4)	0.0009 (5)	0.0034 (5)
C1	0.0155 (6)	0.0138 (6)	0.0150 (6)	0.0030 (5)	0.0025 (5)	0.0011 (5)
C2	0.0186 (7)	0.0180 (7)	0.0181 (7)	0.0012 (5)	0.0057 (5)	0.0042 (5)
C3	0.0168 (7)	0.0200 (7)	0.0232 (8)	0.0008 (5)	0.0039 (6)	0.0026 (5)
C4	0.0181 (6)	0.0149 (6)	0.0157 (7)	0.0034 (5)	0.0026 (5)	0.0020 (5)
C5	0.0221 (7)	0.0251 (7)	0.0153 (7)	0.0044 (6)	0.0022 (6)	0.0045 (5)
C6	0.0203 (7)	0.0305 (8)	0.0190 (7)	0.0053 (6)	0.0042 (6)	0.0093 (6)
S2	0.02219 (18)	0.02074 (18)	0.01648 (18)	0.00230 (13)	0.00321 (14)	0.00600 (13)
N7	0.0134 (5)	0.0181 (5)	0.0149 (6)	0.0015 (4)	0.0037 (4)	0.0045 (4)
N8	0.0203 (6)	0.0281 (7)	0.0170 (6)	0.0028 (5)	0.0044 (5)	0.0090 (5)
N9	0.0152 (6)	0.0265 (6)	0.0213 (6)	-0.0005 (5)	0.0014 (5)	0.0057 (5)
N10	0.0182 (6)	0.0316 (7)	0.0203 (7)	0.0015 (5)	-0.0004 (5)	0.0048 (5)
N11	0.0159 (5)	0.0160 (5)	0.0155 (6)	0.0021 (4)	0.0029 (4)	0.0033 (4)
N12	0.0170 (6)	0.0214 (6)	0.0184 (6)	0.0020 (5)	0.0026 (5)	0.0016 (5)
C7	0.0139 (6)	0.0142 (6)	0.0160 (6)	0.0039 (5)	0.0019 (5)	0.0008 (5)
C8	0.0171 (7)	0.0200 (7)	0.0170 (7)	0.0018 (5)	0.0056 (5)	0.0036 (5)
C9	0.0164 (7)	0.0233 (7)	0.0206 (7)	0.0019 (5)	0.0034 (6)	0.0014 (5)
C10	0.0189 (7)	0.0139 (6)	0.0160 (7)	0.0039 (5)	0.0023 (5)	0.0008 (5)
C11	0.0188 (7)	0.0294 (8)	0.0168 (7)	0.0039 (6)	0.0023 (6)	0.0060 (6)
C12	0.0305 (8)	0.0281 (8)	0.0181 (8)	0.0075 (7)	-0.0006 (6)	0.0034 (6)

Geometric parameters (Å, °)

S1—C4	1.7453 (15)	S2—C10	1.7487 (15)
S1—C6	1.8004 (16)	S2—C12	1.7992 (16)
N1—N3	1.3311 (16)	N7—N9	1.3314 (16)
N1—N2	1.3412 (16)	N7—N8	1.3421 (16)
N1—C1	1.4347 (17)	N7—C7	1.4291 (17)
N2—C5	1.3207 (19)	N8—C11	1.3182 (19)
N3—N4	1.3176 (17)	N9—N10	1.3148 (17)
N4—C5	1.356 (2)	N10—C11	1.3566 (19)
N5—C1	1.3267 (17)	N11—C7	1.3237 (17)
N5—C4	1.3412 (17)	N11—C10	1.3496 (17)
N6—C3	1.3336 (19)	N12—C10	1.3377 (18)
N6—C4	1.3506 (18)	N12—C9	1.3393 (19)
C1—C2	1.3815 (19)	C7—C8	1.3837 (19)
C2—C3	1.393 (2)	C8—C9	1.386 (2)
C2—H1	0.885 (19)	C8—H7	0.886 (19)
C3—H2	0.951 (17)	C9—H8	0.965 (18)
C5—H3	0.891 (19)	C11—H9	0.940 (19)
C6—H4	0.974 (17)	C12—H10	0.955 (19)
C6—H5	0.988 (17)	C12—H11	0.93 (2)
C6—H6	0.96 (2)	C12—H12	0.957 (19)
C4—S1—C6	101.92 (7)	C10—S2—C12	101.37 (8)

6 Supporting information

N3—N1—N2	113.78 (11)	N9—N7—N8	113.63 (11)
N3—N1—C1	123.45 (11)	N9—N7—C7	123.40 (11)
N2—N1—C1	122.75 (11)	N8—N7—C7	122.96 (11)
C5—N2—N1	101.28 (11)	C11—N8—N7	101.34 (12)
N4—N3—N1	105.82 (12)	N10—N9—N7	105.89 (12)
N3—N4—C5	106.17 (12)	N9—N10—C11	106.19 (12)
C1—N5—C4	114.47 (12)	C7—N11—C10	114.67 (12)
C3—N6—C4	115.71 (12)	C10—N12—C9	115.82 (12)
N5—C1—C2	125.31 (12)	N11—C7—C8	125.20 (12)
N5—C1—N1	115.33 (12)	N11—C7—N7	115.25 (12)
C2—C1—N1	119.36 (12)	C8—C7—N7	119.55 (12)
C1—C2—C3	114.59 (13)	C7—C8—C9	114.40 (13)
C1—C2—H1	122.4 (11)	C7—C8—H7	122.5 (11)
C3—C2—H1	123.0 (12)	C9—C8—H7	123.1 (12)
N6—C3—C2	123.19 (13)	N12—C9—C8	123.46 (14)
N6—C3—H2	116.5 (10)	N12—C9—H8	116.1 (11)
C2—C3—H2	120.3 (10)	C8—C9—H8	120.5 (11)
N5—C4—N6	126.72 (13)	N12—C10—N11	126.44 (13)
N5—C4—S1	119.87 (10)	N12—C10—S2	119.96 (10)
N6—C4—S1	113.41 (10)	N11—C10—S2	113.60 (10)
N2—C5—N4	112.96 (13)	N8—C11—N10	112.94 (13)
N2—C5—H3	124.0 (12)	N8—C11—H9	124.6 (12)
N4—C5—H3	123.0 (12)	N10—C11—H9	122.5 (12)
S1—C6—H4	108.9 (11)	S2—C12—H10	109.7 (11)
S1—C6—H5	110.3 (10)	S2—C12—H11	105.7 (12)
H4—C6—H5	112.5 (14)	H10—C12—H11	110.6 (16)
S1—C6—H6	103.5 (11)	S2—C12—H12	110.3 (11)
H4—C6—H6	110.8 (15)	H10—C12—H12	111.9 (16)
H5—C6—H6	110.4 (15)	H11—C12—H12	108.4 (16)

Hydrogen-bond geometry (Å, °)

<i>D</i> —H \cdots <i>A</i>	<i>D</i> —H	H \cdots <i>A</i>	<i>D</i> \cdots <i>A</i>	<i>D</i> —H \cdots <i>A</i>
C2—H1 \cdots N9 ⁱ	0.89 (2)	2.58 (2)	3.203 (2)	129 (2)

Symmetry code: (i) $x-1, y, z$.

6 Supporting information

6.9 Supporting information for Posters

Abstract of Poster I:

Steering the Azido-Tetrazole Equilibrium of 4-Azidopyrimidines via Substituent Variation – Implications for Drug Design

A. Thomann, Saarbrücken/DE, J. Zapp, Saarbrücken/DE, M. Hutter, Saarbrücken/DE, M. Empting, Saarbrücken/DE, R. W. Hartmann, Saarbrücken/DE

Andreas Thomann, Helmholtz Institute for Pharmaceutical Research Saarland, Campus C2.3, 66123 Saarbrücken, Germany

This study focuses on an interesting constitutional isomerism called azido-tetrazole equilibrium which is observed in azido-substituted *N*-heterocycles [1]. We present a systematic investigation on the effect of different substituents on the ratio of the two isomers within a 2-substituted 4-azidopyrimidine model scaffold. To this end, NMR- and IR-spectroscopic as well as X-Ray crystallographic analysis of synthesized derivatives were performed demonstrating the possibility to steer this valence tautomerism towards the isomer of choice by means of substituent variation.

Furthermore, we investigated the impact of this tetrazole-based disguise of the azido group in reactivity regarding copper(I)-catalyzed as well as strain-promoted azide-alkyne cycloadditions (CuAAC and SPAAC, respectively). Substituents stabilized tetrazoles showed a highly decreased or even abolished reactivity in our CuAAC setup whereas the azides and compounds in the equilibrium were directly converted. By use of an pH sensitive derivative, we provide, to our knowledge, the first experimental basis for a possible exploitation of this dynamic isomerism as a pH-dependent azide-protecting motif for selective SPAAC conjugations in aqueous media.

Fragment-based drug design (FBDD) has emerged to be a powerful technique for the discovery of highly effective drug leads. Our tetrazolo[1,5-*c*]pyrimidines display ideal physicochemical properties for the use as potential fragment inhibitors. Furthermore, they share a high degree of similarity with adenosine, a motif occurring frequently in

natural molecules e.g. nucleic acids or Co-enzyme A. To demonstrate the applicability of these tetrazolo[1,5-c]pyrimidines for FBDD we investigated whether they could inhibit PqsD. This anthranoyl-CoA-dependent enzyme mediates a key step in the signal molecule synthesis of the pqs quorum sensing system which regulates virulence of *P. aeruginosa* and biofilm formation [2, 3]. Two fragments from our library inhibited PqsD in micromolar concentrations resulting in high Ligand – and Ligand Lipophilicity Efficiencies (LE and LLE, respectively). Hence, they can be considered as ideal starting points for further fragment growing or merging approaches.

[1] W. E. Hull et al., *Angew. Chem. Int. Ed. Engl.*, 1980, 19, 924. [2] M. P. Storz et al., *JACS*, 2012, 134, 16143. [3] Sahner et al, *J. Med. Chem.*, 2013, 56, 8656.

Steering the Azido-Tetrazole Equilibrium of 4-Azidopyrimidines via Substituent Variation – Implications for Drug Design

Andreas Thomann[†], Josef Zapp[‡], Michael Hutter[§], Martin Empting^{†*} and Rolf W. Hartmann^{†Δ}

[†] Helmholtz-Institute for Pharmaceutical Research Saarland, Department of Drug Design and Optimization, Campus C2.3, 66123 Saarbrücken, Germany.

[‡] Department of Pharmaceutical Biology, Saarland University, Campus C2.2, 66123 Saarbrücken, Germany.

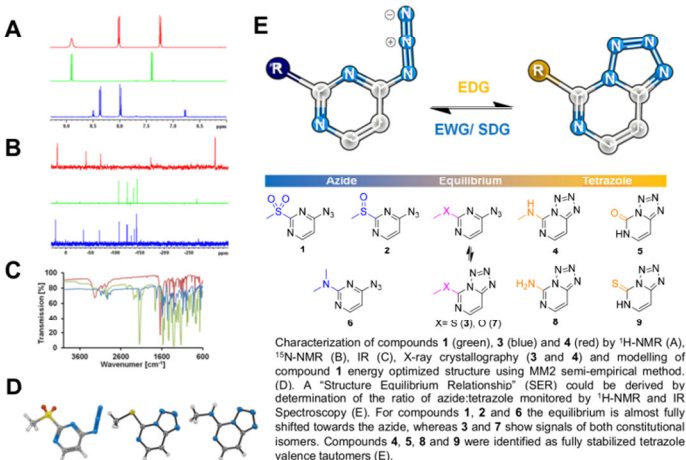
[§] Center for Bioinformatics, Saarland University, Campus E2.1, 66123 Saarbrücken, Germany.

^Δ Department of Pharmaceutical and Medicinal Chemistry, Saarland University, Campus C2.3, 66123 Saarbrücken, Germany.

This study focuses on an interesting constitutional isomerism called azido-tetrazole equilibrium which is observed in azido-substituted *N*-heterocycles [1]. We present a systematic investigation on the effect of different substituents on the ratio of the two isomers within a 2-substituted 4-azidopyrimidine scaffold. To this end, NMR- and IR-spectroscopic as well as X-ray crystallographic analysis of synthesized derivatives were performed demonstrating the possibility to steer this valence tautomerism towards the isomer of choice by means of substituent variation. Furthermore, we investigated the impact of this tetrazolo-based disguise of the azido group in reactivity regarding copper(II)-catalyzed as well as strain-promoted azide-alkyne cycloadditions (CuAAC and SPAAC, respectively). Substituents that stabilize tetrazoles showed a highly decreased or even abolished reactivity in our CuAAC setup whereas the azide valence isomers and compounds in the equilibrium were directly converted. By use of a pH-sensitive derivative, we provide, to our knowledge, the first experimental basis for a possible exploitation of this dynamic isomerism as a pH-dependent azide-protecting motif for selective SPAAC conjugations in aqueous media. Fragment-based drug design (FBDD) has emerged to be a valuable strategy for the discovery of highly effective drug leads. Our tetrazolo[1,5-*c*]pyrimidines display ideal physicochemical properties for the use as potential fragment inhibitors. Furthermore, they share a high degree of similarity with adenosine, a motif occurring frequently in natural molecules, e.g. nucleic acids or Co-enzyme A. To demonstrate the applicability of these tetrazolo[1,5-*c*]pyrimidines for FBDD we investigated whether they could inhibit PqsD. This anthranoyl-CoA-dependent enzyme mediates a key step in the signal molecule synthesis of the pqs quorum sensing system which regulates virulence of *P. aeruginosa* and biofilm formation [2,3]. Two fragments from our library inhibited PqsD in micromolar concentrations resulting in high Ligand- and Ligand Lipophilicity Efficiencies (LE and LLE, respectively). Hence, they can be considered as ideal starting points for further fragment growing or merging approaches.

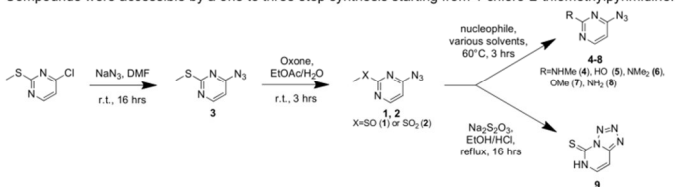
“Structure Equilibrium Relationship” of 4-azido-2-thiomethylpyrimidines

The ratio of azide:tetrazole could be determined by ¹H-NMR, ¹⁵N-NMR, IR and X-ray crystallography. The data indicated that electron-withdrawing groups (EWG) and sterically demanding groups shift the equilibrium to the azide constitutional isomer whereas electron-donors shift towards tetrazole.



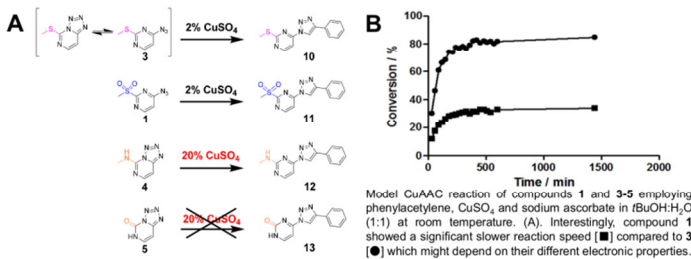
Synthesis of 2-substituted 4-azidopyrimidines

Compounds were accessible by a one to three step synthesis starting from 4-chloro-2-thiomethylpyrimidine.



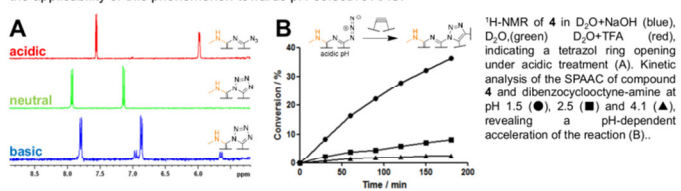
CuAAC of stabilized tetrazolo[1,5-*c*] and 4-azidopyrimidines

Compounds 1 (stabilized azide), 7 (both isomers), 4 (stabilized tetrazole) and 5 (stabilized tetrazole) were employed in a model CuAAC reaction. 1 and 3 were readily transformed to the corresponding click products, whereas 4 and 5 only reacted upon high catalyst load while 5 remained unreacted. Notably, 3 reacted faster than 1 indicating an involvement of an electronic effect on azide reactivity.



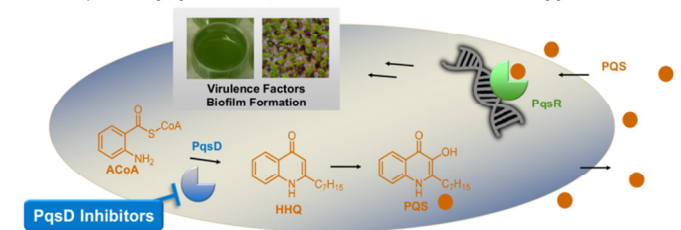
pH-dependent SPAAC of 4 with dibenzocyclooctyne-amine

Könnecke *et al.* [4] showed that tetrazolo[1,5-*c*]pyrimidines can be opened to yield the azide by treatment with TFA. Thus, we hypothesized whether we could use this phenomenon to mask the trapped azide of 4 by acidic treatment. Indeed, we monitored the appearance of new signals under treatment of 4 with TFA in D₂O as indicated by ¹H-NMR. Hence, we designed a pH-dependent SPAAC experiment to demonstrate the applicability of this phenomenon towards pH-selective AAC.



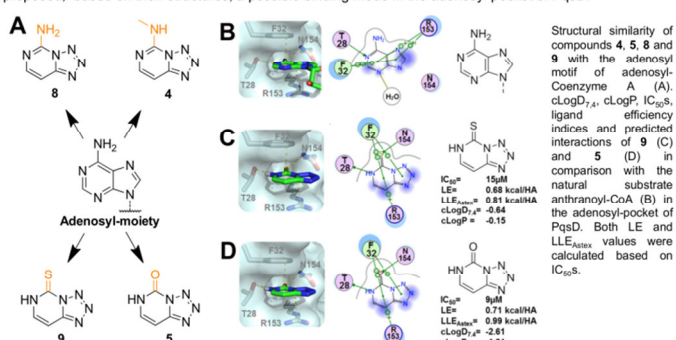
The Pqs quorum sensing system of *P. aeruginosa* - A novel drug target

Quorum sensing is used by *P. aeruginosa* to coordinate group behaviour such as biofilm formation and virulence factor production [2,5]. Furthermore, inhibition was shown to be effective *in vivo* [5].



FBDD of novel fragment-like PqsD inhibitors employing stabilized tetrazolo[1,5-*c*]pyrimidines - Implications for Drug Discovery

Because of the high degree of similarity towards adenosine motifs, (also present in PqsD's natural substrate anthranoyl-Coenzyme A) compounds 4, 5, 8 and 9 were selected for a fragment-based approach towards PqsD. Compounds 5 and 9 displayed an IC₅₀ in low micromolar concentrations, resulting in high Ligand and Ligand Lipophilicity Efficiencies (LE and LLE). Hence, they may serve as ideal starting points for further fragment-based approaches towards antibiofilm and antivirulence agents. Furthermore, we proposed, based on their structures, a possible binding mode in the adenosyl pocket of PqsD.



SUMMARY

In our study we have presented a rational approach to steer the azido-tetrazole equilibrium towards the azide or the tetrazolo form via variations of the substituent at the 2 position of 4-azidopyrimidines. The Structure Equilibrium Relationship (SER) was used to create azide-based compounds which are readily “clickable”, poorly “clickable” and “unclickable” in a prototypical CuAAC reaction. In additional experiments we demonstrated a pH-dependent protecting group characteristic of the acid-sensitive tetrazole for the control of SPAAC reactions. These results may motivate the application towards pH-dependent regioselective couplings or even pH-selective bioconjugation and labeling via bioorthogonal click chemistry in acidic environments e.g. cancer or inflammatory tissue. Finally, the analytical results were used for a fragment-based drug discovery approach towards PqsD. The usefulness of these highly efficient and physicochemically favourable fragments as potential analogues of adenosyl motifs was demonstrated and may lead to further fragment-based drug development campaigns.

OUTLOOK

- Introduce substituents in 6-position of 4 to steer the equilibrium towards pH-dependent tetrazole ring opening at physiological relevant pH
- Further investigate if such a compound could be a probe for the pH-sensitive labelling of cancer or inflammatory cells.
- Fragment-based design of novel PqsD inhibitors based on 5 by either fragment-linking or growing

REFERENCES

- Hull *et al.*, *Angew. Chem. Int. Ed. Engl.*, **1980**, 19, 924.
- Storz *et al.*, *JACS*, **2012**, 134, 16143.
- Sahnor *et al.*, *J. Med. Chem.*, **2013**, 56, 8656.
- Könnecke *et al.*, *Tetrahedron*, **1979**, 35, 1957
- Lu *et al.*, *Angew. Chem. Int. Ed. Engl.*, **2014**, 126, 1127

Abstract of Poster II:

Biological evaluation of an *in vivo*-potent dual target PQS-Quorum Sensing inhibitor that hinders biofilm formation

Andreas Thomann¹, Antonio G. Martins¹, Christian Brengel¹, Elisabeth Weidel¹,
Alberto Plaza¹, Carsten Börger², Martin Empting¹, Rolf W. Hartmann^{1,3*}

¹Helmholtz Institute for Pharmaceutical Research Saarland, Campus C 2.3, 66123 Saarbrücken, Germany;

²PharmBioTec GmbH, Sciencepark 1, Universität des Saarlandes, 66123 Saarbrücken, Germany;

³Department for Pharmaceutical and Medicinal Chemistry, Campus C 2.3, Saarland University, 66123 Saarbrücken, Germany; email: Rolf.Hartmann@helmholtz-hzi.de.

Keywords: *Pseudomonas aeruginosa*, PQS, Dual Target QS Inhibitors, PqsD, PqsR, Drug Discovery

Abstract

Emergence of *Pseudomonas aeruginosa* (PA) as a leading cause of nosocomial infections and morbidity in immunocompromised patients has consolidated it in the race for novel anti-microbial compounds. PA infections are notoriously difficult to eradicate due to intrinsic resistance to a variety of available antibiotics. Its distinguished ability to form biofilms amplifies resistance and promotes immune response evasion.

The PA quorum-sensing (QS) system is a sophisticated network of genome-wide regulation. A major player is the pseudomonas quinolone signal system (PQS-QS) that regulates the production of several non-vital virulence and biofilm-related determinants. Therefore, QS circuitry is an attractive target for anti-virulence therapeutics with lowered resistance development potential^[1,2,3]. We have developed a dual-inhibitor compound (cmpd. A) of low molecular weight and high solubility that targets PQS transcriptional regulator (PqsR) and PqsD, a key enzyme in the biosynthesis of PQS-QS signal molecules (HHQ and PQS).

In this context, cmpd. A markedly reduced virulence factor production without affecting bacterial growth. Additionally, ciprofloxacin co-administration *in vitro* increased susceptibility of PA14 to antibiotic administration under biofilm conditions. Disruption of pathogenicity mechanisms was assessed *in vivo*, with significant increased survival of challenged larvae in an established *Galleria mellonella* infection

6 Supporting information

model. Finally, we observed considerable reduction of biofilm volume and extracellular DNA.

Favourable physicochemical properties and effects on virulence/biofilm establish a promising starting point for further optimization. In particular, interference with biofilm holds great promise in lowering pathogenicity and increasing susceptibility to pharmacological treatment and immune responses in chronic and persistent infections.

References

1. M. P. Storz *et al.*, *J. Am. Chem. Soc.*, 134:16143-16146, 2012, doi: 10.1021/ja3072397;
2. C. Lu *et al.*, *Angew. Chem.*, 126:1127-1130, 2014, doi: 10.1002/ange.201307547;
3. E. Weidel *et al.*, *Future Med Chem*, 6:2057-72, 2014, doi: 10.4155/fmc.14.142

Andreas Thomann^{1,†,‡}, Antonio de Mello Martins^{1,†,‡}, Christian Brengel¹, Elisabeth Weidelt¹, Alberto Plaza², Carsten Börger³, Martin Empting⁴ and Rolf W. Hartmann^{1,Δ,*}

¹ Helmholtz-Institute for Pharmaceutical Research Saarland, Department of Drug Design and Optimization, Campus C2.3, 66123 Saarbrücken, Germany.

² Helmholtz-Institute for Pharmaceutical Research Saarland, Department of Microbial Natural Products, Campus C2.3, 66123 Saarbrücken, Germany.

³ PharmBioTec GmbH, Sciencepark 1, 66123 Saarbrücken, Germany.

⁴ Department of Pharmaceutical and Medicinal Chemistry, Saarland University, Campus C2.3, 66123 Saarbrücken, Germany.

* Authors equally contributed to this work

Emergence of *Pseudomonas aeruginosa* (PA) as a leading cause of nosocomial infections and morbidity in immunocompromised patients has consolidated it in the race for novel antimicrobial compounds.^[1] PA infections are notoriously difficult to eradicate due to intrinsic resistance to a variety of available antibiotics. Its distinguished ability to form biofilms amplifies resistance and promotes immune response evasion. The PA quorum-sensing (QS) system is a sophisticated network of genome-wide regulation triggered in response to population density. A major component is the pseudomonas quinolone signal (PQS) QS system that regulates the production of several non-vital virulence and biofilm-related determinants.^[1] Hence, this QS circuitry is an attractive target for anti-virulence agents with lowered resistance development potential. We have developed a dual-inhibitor compound (cmpd. VI) of low molecular weight and high solubility that targets PQS transcriptional regulator (PqsR) and PqsD, a key enzyme in the biosynthesis of PQS-QS signal molecules (HHQ and PQS).^[2,3] *In vitro*, cmpd. VI markedly reduced virulence factor production and biofilm formation accompanied by a diminished content of extracellular DNA. Additionally, co-administration with ciprofloxacin increased susceptibility of PA14 to antibiotic treatment under biofilm conditions. Finally, disruption of pathogenicity mechanisms was also assessed *in vivo*, with significantly increased survival of challenged larvae in a *Galleria mellonella* infection model.^[4] Favourable physicochemical properties and effects on virulence/biofilm establish a promising starting point for further optimization. In particular, the ability to address two targets of the PQS autoinduction cycle at the same time with a single compound holds great promise in achieving enhanced (synergistic) cellular effects while potentially lowering rates of resistance development.

Disruption of Cell-to-Cell Communication by Hindering Forward Feedback Loops in PQS-Quorum Sensing System

P. aeruginosa group-related acute and chronic infections are regulated by a complex QS-communication network. PQS system is a pivotal link in upstream QS circuitry, as well as in the production of secreted virulence factors, iron assimilation, and biofilm formation.

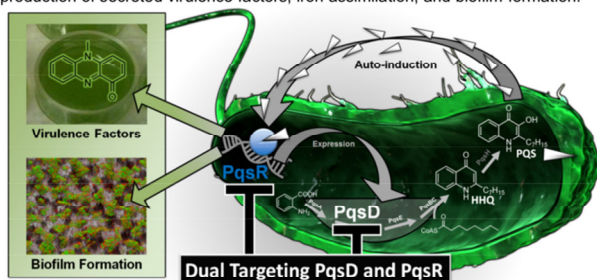


Fig. 1. Overview of *Pseudomonas* quinolone signal (PQS)-quorum sensing system.

Synergistic Effect of a Combined Targeting of PqsD and PqsR on Pyocyanin – Proof of Principle for a Dual Target Approach –

Synergistic activity of dual inhibition leads to a significant, dose-dependent, decrease on PQS-derived pyocyanin production.

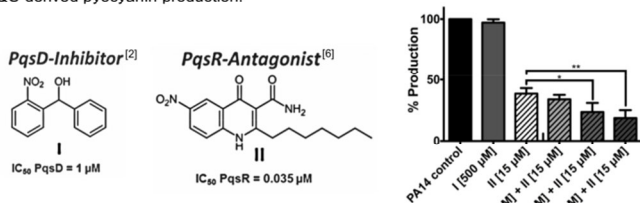


Fig. 2. Synergistic activity of PqsD inhibitor (I) and PqsR antagonist (II) on pyocyanin inhibition in PA14.

Application Towards the Rational Design of a Dual Acting Compound

Matching and merging of structural properties of selective PqsR and PqsD active compounds resulted in a dual-target inhibitor.

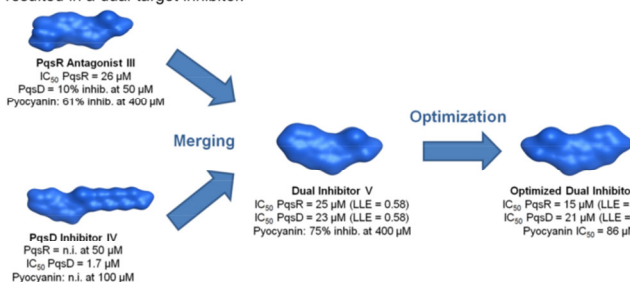


Fig. 3. Matching of PqsR antagonist III and PqsD inhibitor IV resulted in a dual active cmpd. V. Further Ligand Lipophilicity Efficiency Astex (LLE) improvement led to an optimized dual inhibitor VI.

SUMMARY

In this study we have demonstrated that dual(multi)-drug targeting strategies are of particular relevance in complex pathway circuitries driven by autoinducing signalling molecules such as those in the PQS-QS system. Rational design and optimization resulted in dually active compound (VI) and led to increased inhibition of relevant metabolic machinery, achieving a synergistic effect that hinders the production of virulence factors pyocyanin and pyoverdine without affecting bacterial viability. Compound VI also decreased *in cellulo* the formation of biofilm and associated components, while increasing *P. aeruginosa* susceptibility to antibiotic treatment *in vitro*. Antivirulence therapy also had a significant protective effect *in vivo*. Thus, VI is a good starting point for further drug development due to beneficial physico-chemical properties and low propensity to drug resistance development.

Effect of VI on Growth and Virulence Factor Production in *P. aeruginosa*

Virulence factors Pyocyanin and Pyoverdine are key drivers of pathogenicity and biofilm formation.^[5] Dual-inhibition significantly decreased signal molecule formation without affecting bacterial cell growth.

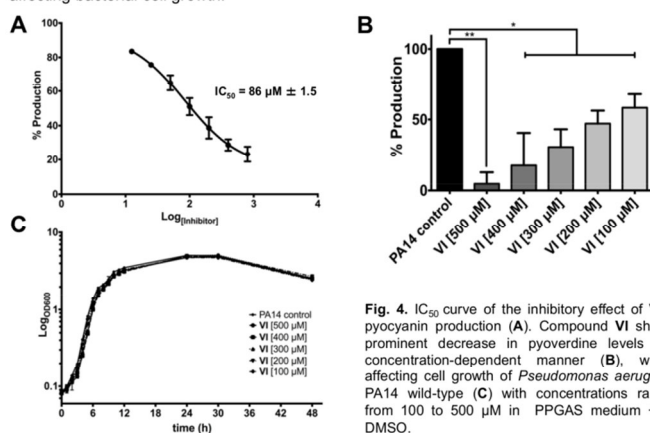


Fig. 4. IC₅₀ curve of the inhibitory effect of VI on pyocyanin production (A). Compound VI showed prominent decrease in pyoverdine levels in a concentration-dependent manner (B), without affecting cell growth of *Pseudomonas aeruginosa* PA14 wild-type (C) with concentrations ranging from 100 to 500 µM in PPGAS medium + 1% DMSO.

Cmpd. VI Disrupts Biofilm Formation and Increases Antibiotic Susceptibility Under Biofilm Conditions

Interference with PQS-QS leads to decrease in biofilm formation and antibiotic tolerance

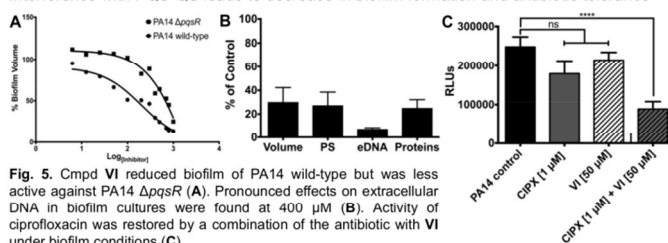


Fig. 5. Cmpd VI reduced biofilm of PA14 wild-type but was less active against PA14 $\Delta pqsR$ (A). Pronounced effects on extracellular DNA in biofilm cultures were found at 400 µM (B). Activity of ciprofloxacin was restored by a combination of the antibiotic with VI under biofilm conditions (C).

Protective Effect on *G. mellonella* Against *P. aeruginosa* Infection with Dual-Inhibitor Treatment

Significant positive correlation with mouse models constitutes *G. mellonella* a powerful tool to investigate mammalian-associated pathogens. Treatment with compound VI increased larvae survival by up to 6-fold.

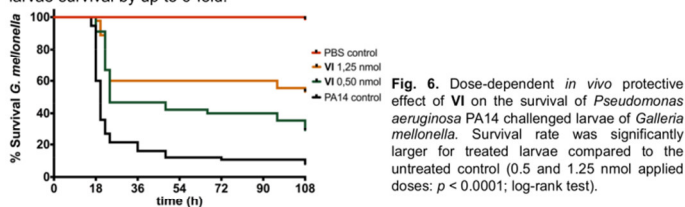


Fig. 6. Dose-dependent *in vivo* protective effect of VI on the survival of *Pseudomonas aeruginosa* PA14 challenged larvae of *Galleria mellonella*. Survival rate was significantly larger for treated larvae compared to the untreated control (0.5 and 1.25 nmol applied doses: $p < 0.0001$; log-rank test).

OUTLOOK

- Generate X-ray co-crystal structures of VI with both targets
- Structure-based design of dual target inhibitors with increased target affinity and *in vivo* efficacy
- eDNA reduction of VI provides the basis for further studies towards increased susceptibility of PA against antimicrobial agents under PQS-QSI treatment

REFERENCES

- [1] Y. Tashiro, Y. Yawata *et al.*, *Microbes Environ.* **2013**, *28*, 13-24.
- [2] M. P. Storz *et al.*, *J. Am. Chem. Soc.* **2012**, *134*, 16143-16146.
- [3] C. Lu *et al.*, *Chem. Biol.* **2012**, *19*, 381-390.
- [4] L. Hill, N. Veli, P. J. Coote, *Int. J. Antimicrob. Agents.* **2014**, *43*, 254-261.
- [5] C. Cézar *et al.*, *Curr. Med. Chem.* **2015**, *22*, 165-186.
- [6] C. Lu, C. K. Maurer *et al.*, *Angew. Chem. Int. Ed.* **2014**, *126*, 1127-1130

Abstract for Poster III:

Biophysical Screening of a Focused Library for the Discovery of Novel Antimycobacterials targeting CYP121

Bregel, Christian⁺¹, Thomann, Andreas⁺¹, Schifrin, Alexander², Bernhardt, Rita², Kamal, Ahmed¹, Cho, Sang Hyun³, Franzblau, Scott G.³ and Hartmann, Rolf W.*¹

¹ Helmholtz Institute for Pharmaceutical Research Saarland, , Department for Drug Development and Optimization, Campus C2.3,66123 Saarbrücken, Germany, E-mail: Rolf.Hartmann@helmholtz-hzi.de

² Biochemie, Universität des Saarlandes, Campus B2.2, 66123 Saarbrücken, Germany

³ Institute for Tuberculosis Research, College of Pharmacy, University of Illinois at Chicago, 833 S. Wood St., Chicago, Illinois 60612-7231, USA

* Corresponding author; + Authors equally contributed to this work

Abstract

Tuberculosis, caused by *Mycobacterium tuberculosis* (Mtb), is still the most deadly bacterial infection worldwide. In 2011 the WHO registered about 1.4 million cases of death related to Mtb infections.^[1] Despite a broad arsenal of available anti-mycobacterial agents, treatment becomes ineffective caused by the increased abundance of multiresistant mutants.^[2] These circumstances underline the urgency for new therapeutic strategies with novel modes of action. The mycobacterial P450 enzyme CYP121, being essential for Mtb growth *in vitro*^[3], is such a promising new drug target for prospective anti-microbial agents. Previous studies revealed azole antifungals (e.g. econazol)^[4] to be nanomolar binders to CYP121 with effectivity against Mtb *in vitro* and *in vivo*.^[5]

To identify new hits against CYP121, we employed a CYP-Inhibitor focused library in a Surface Plasmon Resonance spectroscopic (SPR) screening. The 44 identified hits were validated in a P450 coordination assay resulting in 14 heme type II binders with low micromolar K_D 's. Those compounds displayed single digit $\mu\text{g/ml}$ MIC_{50} 's *in vitro* against *Mycobacterium bovis* BCG. The frontrunner compound I:47 was selected for further evaluation against the human pathogen Mtb and showed significant growth inhibition with a MIC_{90} of 0.28 $\mu\text{g/ml}$. Additionally, I:47 was evaluated in a HEK293 Cell assay for toxicity and displayed a LD_{50} that was 40 times higher than its MIC. Finally, we could demonstrate that I:47 does not only bind to CYP121 but does also inhibit the enzyme reaction *in vitro*.

Promising anti-mycobacterial activity, low toxicity and a novel mode of action together with the low molecular weight make I47 an excellent basis for further drug development.

References

- 1 WHO, *Global Tuberculosis Report*, **2012**.
- 2 ZF Udwadia et al., *Clin. Infect. Dis.*, **2012**, *54*, 579-81.
- 3 KJ McLean et al., *J. Biol. Chem.*, **2008**, *283*, 33406-16.
- 4 KJ. McLean et al., *J. Inorg. Bioch.*, **2002**, *91*, 527-41.
- 5 S. T. Byrne et al, *J. Med. Microbiol.*, **2007**, *56*, 1047-51.

Biophysical Screening of a Focused Library for the Discovery of Novel Antimycobacterials targeting CYP121

Andreas Thomann^{††}, Christian Brengel^{††}, Alexander Schifrin[†], Rita Bernhard[†], Giuseppe Alegretta[†], Ahmed Kamal[†], Jörg Haupenthal[†], Jens Eberhard[†], Sang Hyun Cho[§], Scott G. Franzblau[§] and Rolf W. Hartmann^{†Δ}

[†] Helmholtz-Institute for Pharmaceutical Research Saarland, Department of Drug Design and Optimization, Campus E8.1, 66123 Saarbrücken, Germany.

[†] Biochemie, Universität des Saarlandes, Campus B2.2, 66123 Saarbrücken, Germany.

[§] Institute for Tuberculosis Research, College of Pharmacy, University of Illinois at Chicago, 833 S. Wood St., Chicago, Illinois 60612-7231, USA

^Δ Department of Pharmacy, Pharmaceutical and Medicinal Chemistry, Saarland University, Campus C2.3, 66123 Saarbrücken, Germany.

* Authors equally contributed to this work

Tuberculosis, caused by *Mycobacterium tuberculosis* (Mtb), is still the most deadly bacterial infection worldwide. In 2011 the WHO registered about 1.4 million cases of death related to Mtb infections.^[1] Despite a broad arsenal of available antimycobacterial agents, treatment becomes ineffective caused by the increased abundance of multiresistant mutants.^[2] These circumstances underline the urgency for new therapeutic strategies with novel modes of action. The mycobacterial P450 enzyme CYP121, being essential for Mtb growth *in vitro*,^[3] is such a promising new drug target for prospective antimicrobial agents. Previous studies revealed azole antifungals (e.g. econazole)^[4] to be nanomolar binders to CYP121 with effectivity against Mtb *in vitro* and *in vivo*.^[5]

To identify new hits against CYP121, we employed a CYP-inhibitor focused library in a surface plasmon resonance spectroscopic (SPR) screening. The 44 identified hits were validated in a P450 coordination assay resulting in 14 heme type II binders with low micromolar K_D 's. Those compounds displayed single digit $\mu\text{g/ml}$ MIC₅₀'s *in vitro* against *Mycobacterium bovis* BCG. The frontrunner compound I:47 was selected for further evaluation against the human pathogen Mtb and showed significant growth inhibition with a MIC₅₀ of 0.28 $\mu\text{g/ml}$. Additionally, I:47 was evaluated in a HEK293 cell assay for toxicity and displayed a LD₅₀ that was more than 60 times higher than its MIC value. Finally, we could demonstrate that I:47 does not only bind to CYP121 but does also inhibit the enzyme reaction *in vitro*.

Cytochrome P450 121 - A Novel, Promising Target for the Treatment of Tuberculosis Infections

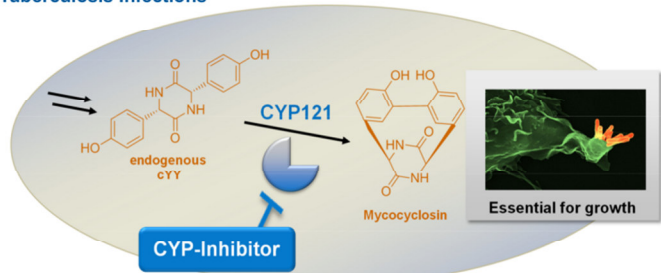


Figure 1. CYP121 catalysis the reaction of cyclo-dithyrosin (cYY) to mycrocyclosin. Knock out studies revealed CYP121 to be essential for survival of Mtb *in vitro*. Thus, CYP121 displays a new target for the treatment of drug resistant Mtb

Screening Procedure for the Discovery of CYP121 Inhibitors With Cellular Effectivity

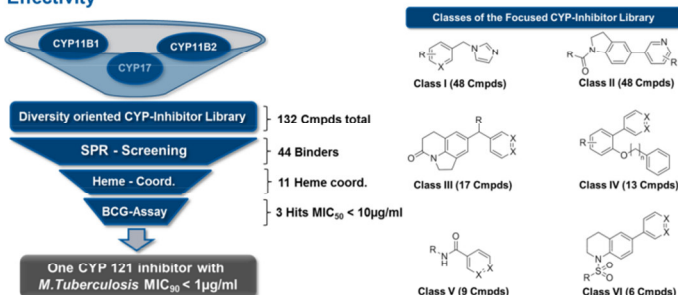


Figure 2. From different in-house libraries targeting human steroidogenic CYP enzymes, a diversity oriented small library of privileged scaffolds was assembled. The library was screened by biophysical (figures 3 & 4). This procedure lead to the discovery of compounds in the ng/ml range.

Initial Biophysical Screening by Surface Plasmon Resonance (SPR) for the Identification of Binders to CYP121

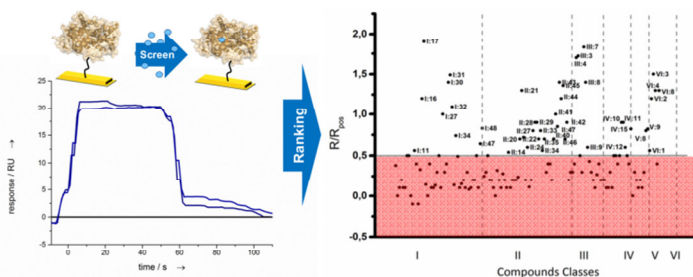


Figure 3. SPR Screening results of the focused library. Compounds that showed binding (left, sensorgram) were ranked against econazole (right, ranking). This ratio (Response_{compound}/Response_{econazole} or R/R_{pos}) allowed rational evaluation of the library compounds for further biophysical evaluation *in vitro*. 44 compounds showed a ratio > 0.5 and were further evaluated.

In vitro Assessment of SPR-Hits Towards Their Binding Profile to CYP121 Heme

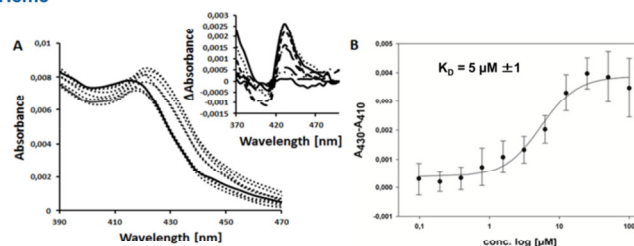


Figure 4. 44 SPR positive binders were evaluated for their ability to bind to the heme iron of CYP121. Therefore, potential binders were initially tested at 100 μM and the respective UV-VIS difference spectra (A) were recorded. As for the positive control econazole, all of the 14 positive heme coordinators showed a type II profile (direct iron interaction, see A upper right difference spectrum). For these compounds K_D 's (B) were determined by titration (A), as shown here for I:47.

Evaluation of Biophysical Hits in a *Mycobacterium bovis* BCG Cellular Assay

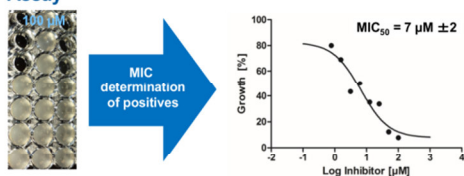


Figure 5. 14 positive heme coordinators were challenged against *Mycobacterium bovis* BCG for their ability to inhibit growth at 100 μM . Compounds which showed over 50 % of growth inhibition were chosen for further MIC₅₀ determination. Three showed MIC₅₀'s in the low $\mu\text{g/ml}$ range. A representative MIC curve in the presence of inhibitor I:48 is shown on the right.

Biological evaluation of the best hit compounds against the human pathogen *M. tuberculosis* and cellular toxicity assessment in HEK293 cells

Cmpd.	SPR (R/R _{pos})	Heme binding type	BCG MIC ₅₀ [μM]	Mtb MIC ₅₀ [μM]	Cytotox LD ₅₀ (HEK293) [μM]
Econazole	1.0	Type II	14	12*	13
I:6	1.2	Type II	5	6	19
I:48	0.8	Type II	7	12	76
I:47	0.6	Type II	2	1	67

Figure 6. The best antimycobacterials were selected for detailed biological evaluation and tested against the human pathogen *Mycobacterium tuberculosis*. Further studies regarding toxicity in Human Embryonic Kidney 293 cells showed compound I:47 to be the frontrunner for further drug discovery efforts and *in vivo* evaluation.

In silico binding mode of I:47 to the active site of CYP121

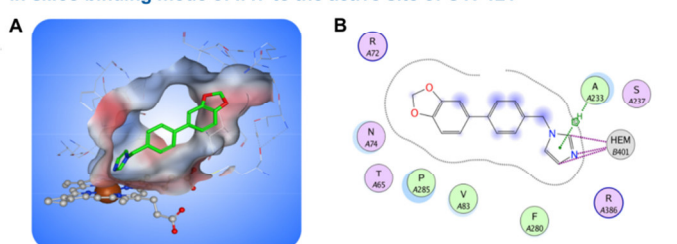


Figure 7. For the frontrunner compound I:47 a molecular modelling study was conducted to reveal further insights into its binding mode. Previously obtained data proving type II binding profile of I:47 were used to generate a pharmacophore model for heme-guided docking. The resulting poses were sorted by score. The best rated score is displayed. The iron interaction (B) as well as the placement of the hydrophobic residue is in good accordance with the active site properties regarding hydrophobicity.

SUMMARY

Biophysical screening of a focused library resulted in cellular active compounds against the human pathogen *Mycobacterium tuberculosis*. These compounds are of favorable physicochemical properties regarding bioavailability as they were designed against human steroidogenic CYP enzymes. The low molecular weight frontrunner I:47 displayed promising antimycobacterial activity, while having reduced cytotoxicity compared to econazole, a reported cellular active CYP121 binder. Furthermore, knowledge of a type II binding profile enabled sophisticated molecular docking studies employing the crystalstructure of CYP121 to generate further insights into the bindingmode of I:47. Promising antimycobacterial activity, low toxicity and a novel mode of action together with the low molecular weight make I:47 an excellent basis for further drug development.

OUTLOOK

- Evaluation of I:47 in macrophage infection models
- Cocrystallisation of I:47 and CYP121 to derive a X-ray structure
- Structure based design based on I:47 to increase on target and cellular potency
- Validation of CYP121 as an antimycobacterial drug target using a small molecule inhibitor *in vivo*

REFERENCES

- [1] WHO, *Global Tuberculosis Report*, 2012.
- [2] ZF Udwadia et al., *Clin. Infect. Dis.*, 2012, 54, 579-81.
- [3] KJ McLean et al., *J. Biol. Chem.*, 2008, 283, 33406-16.
- [4] KJ McLean et al., *J. Inorg. Biochem.*, 2002, 91, 527-41.
- [5] ST Byrne et al., *J. Med. Microbiol.*, 2007, 56, 1047-51.
- [6] SG Franzblau et al., *Tuberculosis*, 2012, 92, 453-488.

7 Appendices

7.1 Curriculum vitae

Personal data

Name	Andreas Thomann
Place of birth	Merzig, Germany
Date of birth	25.06.1984

Scientific experience

- Since 10/2016** Pharmacist Process- & Productvalidation
Pfizer Global Supply Freiburg, Pfizer Manufacturing
Deutschland GmbH
- 01/2016 – 10/2016** Management Trainee (Pharmaceutical Sciences)
Pfizer Global Supply Freiburg, Pfizer Manufacturing
Deutschland GmbH
- 01/2012 – 12/2015** PhD thesis at the Helmholtz-Institute for Pharmaceutical
Research Saarland (HIPS), Department Drug Design and
Optimization (DDOP)
Topic: *"Discovery and development of anti-infectives with novel
modes of action for the treatment of respiratory tract infections"*
- 04/2011 - 09/2011** Diploma thesis at the University of Cambridge, UK, Department
of Chemistry with a scholarship of the Studienstiftung Saar,
Topic: *"Structure-based design of small molecule probes for the
Van Hippel Lindau protein (VHL)"*
- 08/2010** Research student at the Department of Clinical and Experimental
Toxicology, University Hospital Homburg
Topic: *"HPLC-MS and GC-MS analysis of metabolites of 4-
Fluoramphetamin in rat urine and human liver microsomes"*
- 04/2008 – 06/2010** Assistent research student at the Department of Medicinal and
Pharmaceutical Chemistry, Saarland University
Topic: *"Synthesis and characterization of allosteric inhibitors of
PKC ζ "*
- 10/2006 – 09/2010** Studies of pharmaceutical science at Saarland University

7 Appendices

7.2 Conference contributions

7.2.1 Oral presentations

Title: „**Moleküle als Sonden – Ein neuer Ansatz zur Arzneistoffentwicklung**“,
Absolventenfeier der Naturwissenschaftlich Technischen Fakultät III, June **2012**,
Saarbrücken, Germany.

7.2.2 Poster presentations

The posters listed below are shown in section 6.9 Supporting Information for Posters.

Andreas Thomann, Josef Zapp, Martin Empting, Michael Hutter and Rolf W. Hartmann

Steering the Azido-Tetrazole Equilibrium of 4-Azidopyrimidines via Substituent Variation – Implications for Drug Design,

Frontiers in Medicinal Chemistry, March **2015**, Marburg, Germany.

Andreas Thomann,⁺ Antonio G. Martins,⁺ Christian Brengel, Elisabeth Weidel, Alberto Plaza, Carsten Börger, Martin Empting, Rolf W. Hartmann

Biological evaluation of an in vivo-potent dual target PQS-Quorum Sensing inhibitor that hinders biofilm formation,

First International Symposium on Quorum Sensing Inhibition and Satellite meeting on Novel anti-fouling strategies, June **2015**, Santiago de Compostela, Spain.

⁺These authors contributed equally to this work.

Brengel, Christian,⁺ Thomann, Andreas,⁺ Schiffrin, Alexander, Bernhardt, Rita, Kamal, Ahmed, Cho, Sang Hyun, Franzblau, Scott G. and Hartmann, Rolf W.

Biophysical Screening of a Focused Library for the Discovery of Novel Antimycobacterials Targeting CYP121,

5th International HIPS Symposium, July **2015**, Saarbrücken, Germany.

⁺These authors contributed equally to this work.

Andreas Thomann,⁺ Antonio G. Martins,⁺ Christian Brengel, Elisabeth Weidel, Alberto Plaza, Carsten Börger, Martin Empting¹, Rolf W. Hartmann

Biological evaluation of an in vivo-potent dual target PQS-Quorum Sensing inhibitor that hinders biofilm formation,

5th International HIPS Symposium, July **2015**, Saarbrücken, Germany.

⁺These authors contributed equally to this work.

Andreas Thomann, Josef Zapp, Martin Empting, Michael Hutter and Rolf W. Hartmann

Steering the Azido-Tetrazole Equilibrium of 4-Azidopyrimidines via Substituent Variation – Implications for Drug Design,

IV. Symposium of the Interdisciplinary Graduate School of Natural Products Research, August **2015**, Saarbrücken, Germany.

7.3 Publications

Dissecting fragment-based lead discovery at the von Hippel-Lindau protein:hypoxia inducible factor 1 α protein-protein interface

Inge Van Molle, Andreas Thomann, Dennis L. Buckley, Ernest C. So, Steffen Lang, Craig M. Crews and Alessio Ciulli

Chem. Biol.; **2012**; 19; 1300-1312; DOI: 10.1016/j.chembiol.2012.08.015.

Microwave-Assisted Synthesis of 4-Substituted 2-Methylthiopyrimidines

Andreas Thomann, Carsten Börger; Martin Empting and Rolf W. Hartmann

Synlett; **2014**; 25; 935-938; DOI: 10.1055/s-0033-1340860.

Steering the Azido-Tetrazole Equilibrium of 4-Azidopyrimidines via Substituent Variation – Implications for Drug Design and Azide-Alkyne Cycloadditions

Andreas Thomann, Josef Zapp, Michael C. Hutter, Martin Empting and Rolf W. Hartmann

Org. Biomol. Chem.; **2015**; 13; 10620-10630; DOI: 10.1039/C5OB01006C.

Mild and Catalyst-free Microwave-assisted Synthesis of 4,6-Disubstituted 2-Methylthiopyrimidines – Exploiting Tetrazole as an Efficient Leaving Group

Andreas Thomann, Jens Eberhard, Giuseppe Allegretta, Martin Empting and Rolf W. Hartmann

Synlett; **2015**; 26; 2606-2610; DOI: 10.1055/s-0035-1560577.

Application of Dual Inhibition Concept Within Looped Autoregulatory Systems Towards Anti-virulence Agents Against *Pseudomonas aeruginosa* Infections

Andreas Thomann,^Δ Antonio G. G. de M. Martins,^Δ Christian Brengel, Martin Empting, and Rolf W. Hartmann

ACS Chem. Biol.; 2016, **11**, 1279–1286, DOI: 10.1021/acscchembio.6b00117;

^ΔThese authors contributed equally to this work.

Crystal structure of 4-methylsulfanyl-2-(2H-tetrazol-2-yl)pyrimidine

Andreas Thomann, Volker Huch and Rolf W. Hartmann

Acta Cryst.; **2016**; E76; o1051-o1052; DOI: 10.1107/S2056989015023634.

Discovery and Biophysical Evaluation of First Low Nanomolar Hits Targeting CYP125 of *M. tuberculosis*

Christian Brengel,^Δ Andreas Thomann,^Δ Jens Eberhard, Alexander Schifrin, and Rolf W. Hartmann

ChemMedChem; just accepted, DOI: 10.1002/cmdc.201600361

^ΔThese authors contributed equally to this work.

Structure-activity Relationships of 2-Sufonylpyrimidines as Quorum Sensing Inhibitors to Tackle Biofilm Formation and eDNA Release of *Pseudomonas aeruginosa*

Andreas Thomann, Christian Brengel, Carsten Börger, Dagmar Kail, Anke Steinbach, Martin Empting and Rolf W. Hartmann

ChemMedChem; just accepted, DOI: 10.1002/cmdc.201600419

8 Acknowledgements

An erster Stelle möchte ich meinem Doktorvater Herrn Prof. Dr. Rolf W. Hartmann danken für die Möglichkeit in seinem Arbeitskreis diese Arbeit anfertigen zu dürfen. Im Besonderen dafür, dass Sie mir das Vertrauen und den Spielraum gaben auch in Gebieten zu forschen die am Rande der Medizinischen Chemie lagen. Ohne diesen Freiraum wären einige meiner Arbeiten sicherlich nicht möglich gewesen. Herzlichen Dank auch an Herrn Prof Dr. Dr. h.c. Hans H. Maurer für die Übernahme des Zweitgutachtens und die durchweg sehr gute Betreuung über die gesamte Zeit, sowie seine Fürsprache für meine Reserveposition in der Bundeswehr. Herrn Dr. Josef Zapp möchte ich dafür danken, dass er die Position des akademischen Beirates übernommen hat.

Des Weiteren möchte ich mich bei den Post-Docs des Arbeitskreises bedanken die mir über die letzten Jahre mit viel Rat, Hilfe und ihrem Fachwissen zu Seite standen. Dr. Martin Empting in allen Belangen der Medizinischen Chemie, des Modelings, Erstellung von Grafiken und dem Verfassen von Manuskripten. Dr. Jens Burkhart für die lehrreiche und witzige Zeit im Synthese Labor. Dr. Jens Eberhard für die unermüdlichen Bemühungen im Labor und beim CYP Projekt. Dr. Carsten Börger für die Hilfe bei meinem ersten Synthese Paper und allen massenspektrometrischen Problemen. Dr. Josef Zapp für sein enormes Wissen über das NMR, die tollen Spektren und weil er einfach immer Zeit für mich hatte. Dr. Anke Steinbach für ihre Hilfe beim Verfassen von Manuskripten und ihrem unerschütterlichen Optimismus. Dr. Stefan Böttcher für die Hilfe am Massenspektrometer, sowie die tolle Zeit in der Toskana. Dr. Jörg Haupenthal für sein biologisches Fachwissen, Unterstützung beim humanen Zell-Assay und seine unglaubliche Ruhe in allen Forschungslagen.

Ein ganz besonderer Platz in dieser Danksagung gehört dem „Carré d’amour“ mit seinen alten Mitglieder: Jan-Henning „Age“ Sahner, Christian „der Coach“ Brengel, Michael „Mize/Mike“ Zender und natürlich dem neuen Mitglied: Andreas „der 2 Meter-Kany“ Kany. Wieviel Spaß ich im Büro, wie auch im Labor und in der Mensa hatte, kann ich gar nicht in Stunden beziffern. Danke für die tolle, lockere und witzige Zeit; auch außerhalb der Arbeit.

Weiterhin möchte ich außerdem Lorenz Siebenbürger, Marius Wirth, Alex Kiefer, Phillip Barbie, Daniel Wiegmann, Ole Schneemann und allen weiteren neuen und

alten Mitgliedern des Spritwoch-Teams für die unvergesslichen, gediegenen Mittwochabende danken.

Ein großer Dank auch an das Sekretariat (May Küffner und Katrin Schmitt) des Arbeitskreises für die durchweg sehr gute Organisation und Hilfe bei allen bürokratischen Hürden.

Des Weiteren sei hier besonders Lothar Jager erwähnt, der mit seinen technischen Fähigkeiten fast jedes Gerät wieder zum Laufen brachte.

Vielen Dank an meine Mitdoktoranden Christine Maurer, Juliette Emerich, Elisabeth „Lilli“ Weidel, Martina Fruth, Benjamin „Doc“ Kirsch, Walid Elgaher, Ahmed Kamal, Kristina Hüsecken, Stefan Hinsberger, Michael Storz, Friedrich „Fritz“ Cenbin Lu, Giuseppe Allegretta, Isabel Schnorr. und Antonio „Alberto“ Martins für den Zusammenhalt und die tolle Arbeitsatmosphäre.

Meinen Studenten die mich in ihren Vertiefungs- und Wahlpflichtpraktika unterstützt haben: Nadja Klippel, Isabel Schnorr, Theresa Manz, Phil Servatius, Melissa Mang Sebastian Schardon und Kathrin Voos.

Auch an die fleißigen Helferlein im Arbeitskreis sei hier gedacht. Vielen Dank an Simone Amann, Jeannine Ludwig, Jeannine Jung, Aline Kirchhoff, Isabella Mang, und Carina Scheidt. Ohne eure Unterstützung hätte diese Arbeit mit Sicherheit nicht entstehen können.

Ein herzliches Dankeschön gebührt auch den Freunden aus dem AK Kazmaier, organische Chemie für die höchst gastliche Bewirtung mit verschiedensten Sorten Bier zu jeder Tages- und Nachtzeit. Im Einzelnen waren hierbei die prominentesten Vertreter: Phillip Barbie und Alexander Kiefer.

Dem gesamten Team der Blumen Apotheke, in der ich seit meinem Praktischen Jahr arbeiten durfte. Vielen herzlichen Dank für die tolle Zusammenarbeit und das immer leckere Frühstück am Samstagmorgen. An dieser Stelle besonderen Dank an meinen „Chefapotheker“ Jörg Schulze für die Möglichkeit ihn vertreten, mein pharmazeutisches Wissen anwenden und erweitern zu dürfen. Allen Patienten und Kunden der Blumen-Apotheke danke ich für ihr Vertrauen und die große Wertschätzung meiner Arbeit, welche mich immer während bestärkt den richtigen Beruf gewählt zu haben.

8 Acknowledgements

Auch sei an dieser Stelle meinen Kammeraden am ZinstSanBW in München gedankt, welche mich, während meinen Wehrübungen, in die Tiefen der Qualitätskontrolle von Arzneimitteln einführten.

Einen riesen Dank an Simon „Nerd“ Pähler, meinem Mitbewohner und langjährigen Freund für die tolle Zeit in unserer WG.

Dankeschön Jannick „Jank“ Altherr für deine unersetzliche Freundschaft seit der 2. Klasse.

Danke auch an meinen guten, lieben Freund Artem „Gerb“ Gerbershagen für die vielen interessanten Gesprächsrunden und lustigen Abende bei einer guten Tasse heißen Tee.

Meiner Mutter Margit, meinem Vater Christian sowie meinem Bruder Holger vielen Dank für die vielen Stunden des Zuspruchs und Anhörens meiner Klagen.

Meiner Katharina für deine Liebe und Marina für die Vermittlung der Nachhilfestunde.